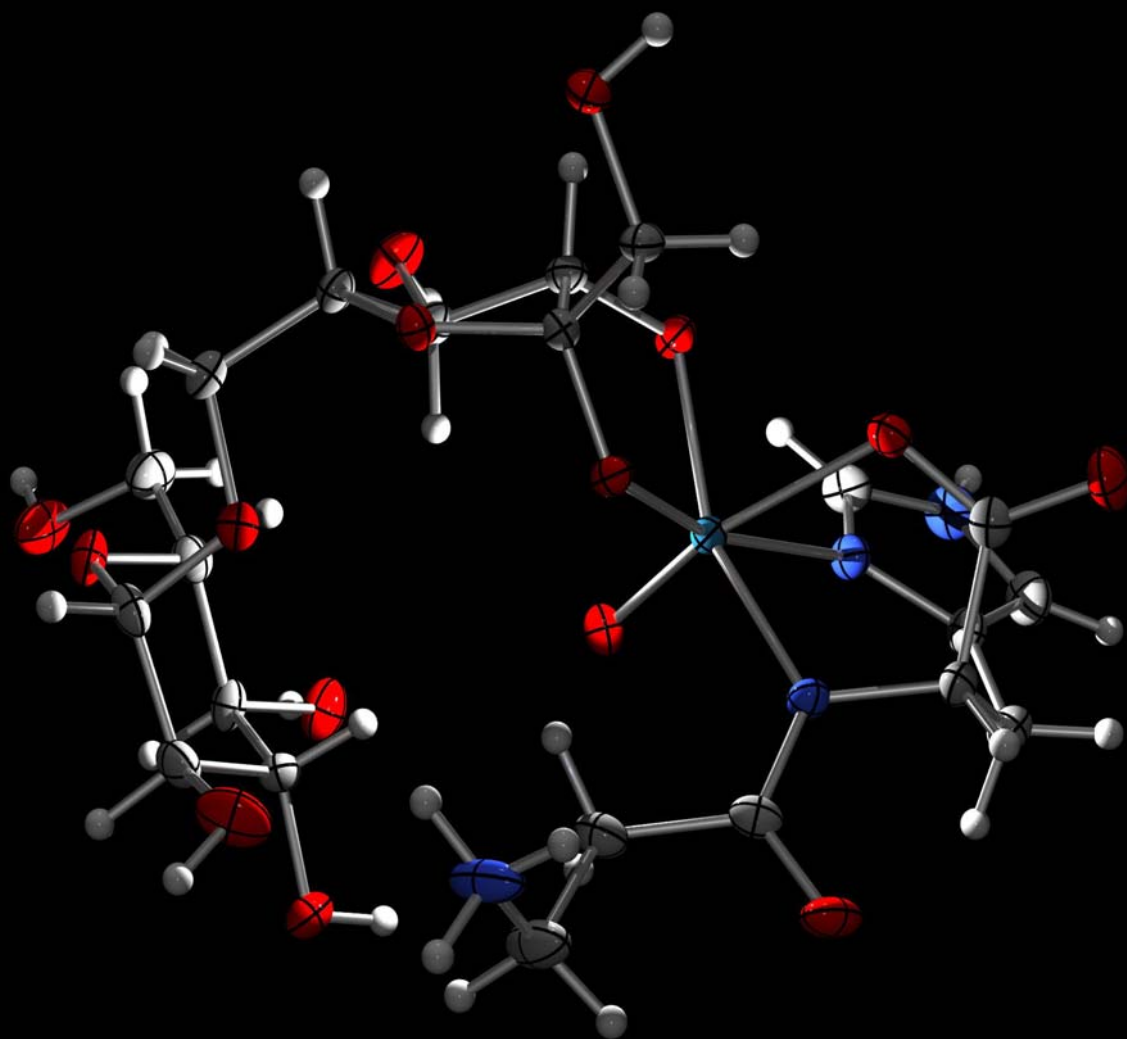


Rhenium(V)–Carbohydrate Complexes with Amino Acids



Dissertation
von
Philipp Grimminger
2009

Dissertation zur Erlangung des Doktorgrades
der Fakultät für Chemie und Pharmazie
der Ludwig-Maximilians-Universität München

Rhenium(V)–Carbohydrate Complexes with Amino Acids

Philipp Grimminger
aus
München

2009

Erklärung:

Diese Dissertation wurde im Sinne von § 13 Abs. 3 der Promotionsordnung vom 29. Januar 1998 von Prof. Dr. Peter Klüfers betreut.

Ehrenwörtliche Versicherung:

Diese Dissertation wurde selbständig, ohne unerlaubte Hilfe erarbeitet.

München, am 11.5.2009

A handwritten signature in black ink, appearing to read 'P. Guler'.

Dissertation eingereicht am 11.5.2009

1. Gutachter: Prof. Dr. P. Klüfers

2. Gutachter: Prof. Dr. T. M. Klapötke

Mündliche Prüfung am 3.7.2009

Für Christine Grimminger und Beatrice Brandfaß

Contents

1	Introduction	1
1.1	Carbohydrates and amino acids	1
1.2	Coordination compounds with rhenium(V)	3
1.3	Radiopharmaceutical compounds	6
1.4	Aims of this work	10
2	Results	11
2.1	Compounds of rhenium(V) with diethylenetriamine	11
2.1.1	The reaction of $[\text{ReO}_2(\text{PPh}_3)_2\text{I}]$ with dien and cytidine	13
2.1.2	The reaction of $[\text{ReO}_2(\text{PPh}_3)_2\text{I}]$ with dien and uridine	19
2.1.3	The reaction of $[\text{ReOCl}_3(\text{PPh}_3)_2]$ with dien and other nucleosides	23
2.1.4	The reaction of $[\text{Re}(\text{NPh})\text{Cl}_3(\text{PPh}_3)_2]$ with dien and anhydroerythritol	26
2.1.5	The reaction of $[\text{Re}(\text{NPh})\text{Cl}_3(\text{PPh}_3)_2]$ with dien and ethanol	32
2.2	Compounds of rhenium(V) with <i>rac</i> -2,3-diaminopropionic acid	35
2.2.1	The reaction of $[\text{ReOCl}_3(\text{PPh}_3)_2]$ with <i>rac</i> -2,3-diaminopropionic acid and 1,2-ethanediol	37
2.2.2	The reaction of $[\text{ReOCl}_3(\text{PPh}_3)_2]$ with <i>rac</i> -2,3-diaminopropionic acid and anhydroerythritol	40
2.2.3	The reaction of $[\text{ReOCl}_3(\text{PPh}_3)_2]$ with <i>rac</i> -2,3-diaminopropionic acid and pyrimidine nucleosides	45
2.3	Compounds of rhenium(V) with L-histidine	50
2.3.1	The reaction of $[\text{ReOCl}_3(\text{PPh}_3)_2]$ with L-histidine and oxalic acid	53
2.3.2	The reaction of $[\text{ReOCl}_3(\text{PPh}_3)_2]$ with L-histidine and 1,2-ethanediol	57
2.3.3	The reaction of $[\text{ReOCl}_3(\text{PPh}_3)_2]$ with L-histidine and anhydroerythritol	62
2.3.4	The reaction of $[\text{ReOCl}_3(\text{PPh}_3)_2]$ with L-histidine and uridine	66

Contents

2.3.5	The reaction of [ReO(L-his)(ox)] with cytidine	71
2.3.6	The reaction of [ReOCl ₃ (PPh ₃) ₂] with L-histidine and methyl α-D-mannopyranoside	75
2.3.7	The reaction of [ReOCl ₃ (PPh ₃) ₂] with L-histidine and methyl β-D-ribofuranoside	79
2.3.8	The reaction of [ReOCl ₃ (PPh ₃) ₂] with L-histidine and other carbohydrates	84
2.4	Compounds of rhenium(V) with L-carnosine	85
2.4.1	The reaction of [ReOCl ₃ (PPh ₃) ₂] with L-carnosine and oxalic acid	88
2.4.2	The reaction of [ReOCl ₃ (PPh ₃) ₂] with L-carnosine and 1,2-ethanediol	92
2.4.3	The reaction of [ReOCl ₃ (PPh ₃) ₂] with L-carnosine and adenosine	95
2.4.4	The reaction of [ReOCl ₃ (PPh ₃) ₂] with L-carnosine and D-ribose	100
2.4.5	The reaction of [ReOCl ₃ (PPh ₃) ₂] with L-carnosine and D-mannose	105
2.4.6	The reaction of [ReOCl ₃ (PPh ₃) ₂] with L-carnosine and D-fructose	109
2.4.7	The reaction of [ReOCl ₃ (PPh ₃) ₂] with L-carnosine and D-isomaltulose	114
2.4.8	The reaction of [ReOCl ₃ (PPh ₃) ₂] with L-carnosine and other carbohydrates	120
2.5	Other compounds with rhenium	121
2.5.1	The reaction of [ReOCl ₃ (PPh ₃) ₂] with oxalic acid	121
2.5.2	The reaction of [Re(NPh)Cl ₃ (PPh ₃) ₂] with oxalic acid	124
2.5.3	The reaction of [ReOCl ₃ (PPh ₃) ₂] with anhydroerythritol	127
2.5.4	The reaction of [ReOCl ₃ (PPh ₃) ₂] with L-threonine and anhydroerythritol	129
2.5.5	The reaction of [ReOCl ₃ (PPh ₃) ₂] with iminodiacetic acid and erythromycin	132
2.5.6	The reaction of [ReO(L-his)(ox)] with Cu ²⁺ and phen	138
2.5.7	The reaction of [ReOCl ₃ (PPh ₃) ₂] and other amino acids	141
3	Discussion	142
3.1	Selectivity of the reactions	142

3.2	NMR spectroscopy	148
3.3	Structural observations	150
4	Summary	154
5	Experimental Part	159
5.1	Common working techniques	159
5.2	Analytical methods	159
5.3	Reagents and solvents	161
5.4	Preparation of the precursor compounds	163
5.4.1	Iodido-dioxido-bis(triphenylphosphane)-rhenium(V)	163
5.4.2	Trichlorido-oxido- <i>trans</i> -bis(triphenylphosphane)-rhenium(V)	163
5.4.3	Trichlorido-phenylimido- <i>trans</i> -bis(triphenylphosphane)- rhenium(V)	164
5.5	Preparation of the crystalline compounds	165
5.5.1	[ReO(<i>fac</i> -dien)(<i>syn</i> -Cyd2',3'H ₋₂)]I (1)	165
5.5.2	[ReO(<i>fac</i> -dien)(<i>syn</i> -Urd2',3'H ₋₂)]BPh ₄ · MeOH (2)	165
5.5.3	[Re(NPh)(<i>fac</i> -dien)(<i>syn</i> -AnErytH ₋₂)]BPh ₄ (3)	166
5.5.4	[Re(NPh)(<i>fac</i> -dien)(<i>anti</i> -AnErytH ₋₂)] [ReO(<i>fac</i> -dien)(<i>anti</i> - AnErytH ₋₂)] [BPh ₄]Cl (4)	167
5.5.5	[Re(NPh)(<i>mer</i> -dien)(OEt)(PPh ₃)] [ReO ₄]Cl · EtOH · 0.5 Me ₂ CO (5)	167
5.5.6	[ReO(<i>rac</i> -dap)(EthdH ₋₂)] · MeOH (6)	168
5.5.7	[ReO(<i>rac</i> -dap)(<i>syn</i> -AnErytH ₋₂)] · H ₂ O (7)	168
5.5.8	[ReO(<i>rac</i> -dap)(<i>anti</i> -Cyd2',3'H ₋₂)] · 2 H ₂ O (8)	169
5.5.9	[ReO(L-his)(ox)] (9)	170
5.5.10	[ReO(L-his)(EthdH ₋₂)] · 4.5 H ₂ O (10)	171
5.5.11	[ReO(L-his)(<i>syn</i> -AnErytH ₋₂)] · 2 H ₂ O (11)	171
5.5.12	[ReO(L-his)(<i>syn</i> -Urd2',3'H ₋₂)] · 1.5 H ₂ O (12)	172
5.5.13	[ReO(L-his)(<i>anti</i> -Cyd2',3'H ₋₂)] · 5 H ₂ O (13)	173
5.5.14	[ReO(L-his)(<i>syn</i> -Me- α -D-Manp2,3H ₋₂)] · 2 MeOH (14)	174
5.5.15	[ReO(L-his)(<i>syn</i> -Me- β -D-Ribp3,4H ₋₂)] · 0.5 MeOH (15)	174
5.5.16	[ReO(L-car)(ox)] · 2 H ₂ O (16)	175
5.5.17	[ReO(L-car)(EthdH ₋₂)] · MeOH · H ₂ O (17)	176
5.5.18	[ReO(L-car)(<i>syn</i> -AdoH2',3'H ₋₂)] · 3 MeOH · 2 H ₂ O (18)	177
5.5.19	[ReO(L-car)(<i>syn</i> - α -D-Ribf1,2H ₋₂)] · 3 MeOH (19)	177
5.5.20	[ReO(L-car)(<i>anti</i> - α / β -D-Manp2,3H ₋₂)] · MeOH (20)	178

Contents

5.5.21	[ReO(L-car)(<i>anti</i> - β -D-Fruf _{2,3} H ₋₂)] · MeOH (21)	179
5.5.22	[ReO(L-car)(<i>syn</i> -6-O- α -D-Glcp- β -D-Fruf _{2,3} H ₋₂)] · 3 H ₂ O (22)	180
5.5.23	(HNEt ₃)[ReO(ox) ₂ (PPh ₃)] (23)	182
5.5.24	[Re(NPh)(ox)(PPh ₃) ₂ Cl] · MeOH (24)	182
5.5.25	[ReO(<i>syn</i> -AnErytH ₋₂)(MeOH)(PPh ₃)Cl] (25)	182
5.5.26	[ReO(L-thr)(<i>syn</i> -AnErytH ₋₂)(PPh ₃)] (26)	183
5.5.27	[ReO(<i>fac</i> -ida)(Emy _{11,12} H ₋₂)] · MeOH · H ₂ O (27)	183
5.5.28	[Cu ₂ (phen) ₂ (ox)(ReO ₄) ₂] _n (28)	184
6	Appendix	185
6.1	Packing diagrams of the crystal structures	185
6.2	Crystallographic tables	214
6.3	Summary of rhenium coordination geometries	225
	Bibliography	228

List of Figures

1.1	Scheme of rhenium(V) diolato complexes	4
1.2	Scheme of rhenium(V) complexes with amino acids	5
1.3	Design of targeted radiopharmaceuticals	7
1.4	Coordination of rhenium(V) to octreotide	9
1.5	General composition of the compounds in this work	10
2.1	Scheme of the reactions with diethylenetriamine	11
2.2	Scheme of the observed binding modes with rhenium and diethylenetriamine	12
2.3	ORTEP presentation of 1a	13
2.4	MERCURY presentation of the furanose rings in cytidine, 1a and 1b	14
2.5	MERCURY presentation of hydrogen bonds in 1	15
2.6	Scheme of 1	17
2.7	ORTEP presentation of 2	19
2.8	MERCURY presentation of hydrogen bonds in 2	21
2.9	Scheme of 2	22
2.10	Scheme of the nucleosides used in this work	24
2.11	¹³ C NMR spectra of the nucleosides	25
2.12	ORTEP presentation of 3	26
2.13	MERCURY presentation of hydrogen bonds in 3	28
2.14	Scheme of possible isomers with anhydroerythritol	29
2.15	¹³ C NMR spectrum of the reaction mixture of 3	29
2.16	ORTEP presentation of 4	30
2.17	MERCURY presentation of hydrogen bonds in 4	31
2.18	ORTEP presentation of 5	33
2.19	MERCURY presentation of hydrogen bonds in 5	34
2.20	Scheme of the D- and L-enantiomers of <i>rac</i> -2,3-diaminopropionic acid	35
2.21	Scheme of the pH-dependent forms of <i>rac</i> -2,3-diaminopropionic acid	36
2.22	Scheme of complexes with <i>rac</i> -2,3-diaminopropionic acid	36
2.23	Scheme of the general reaction route	37
2.24	ORTEP presentation of 6	37

List of Figures

2.25	MERCURY presentation of hydrogen bonds in 6	38
2.26	Scheme of 6	39
2.27	ORTEP presentation of 7	41
2.28	MERCURY presentation of hydrogen bonds in 7	42
2.29	Scheme of 7	43
2.30	¹³ C NMR spectra of 7	44
2.31	ORTEP presentation of 8	45
2.32	MERCURY presentation of hydrogen bonds in 8	46
2.33	Scheme of 8	48
2.34	Scheme of L-histidine	50
2.35	Complexes with tridentate L-histidine	50
2.36	ORTEP presentation of L-histidine and a related structure	51
2.37	Scheme of the general reaction route	52
2.38	Scheme of the pH-dependent forms of L-histidine	52
2.39	ORTEP presentation of 9	53
2.40	MERCURY presentation of hydrogen bonds in 9	55
2.41	Scheme of 9	56
2.42	ORTEP presentation of 10	57
2.43	MERCURY presentation of hydrogen bonds in 10	60
2.44	Scheme of 10	61
2.45	ORTEP presentation of 11	62
2.46	MERCURY presentation of hydrogen bonds in 11	64
2.47	Scheme of 11	65
2.48	ORTEP presentation of 12	66
2.49	MERCURY presentation of the furanose rings in free uridine and in 12	67
2.50	MERCURY presentation of hydrogen bonds in 12	68
2.51	Scheme of 12	70
2.52	ORTEP presentation of 13	71
2.53	MERCURY presentation of hydrogen bonds in 13	73
2.54	Scheme of 13	74
2.55	ORTEP presentation of 14	75
2.56	MERCURY presentation of hydrogen bonds in 14	77
2.57	Scheme of 14	78
2.58	ORTEP presentation of 15	79
2.59	MERCURY presentation of hydrogen bonds in 15	81
2.60	Scheme of 15	82
2.61	Scheme of L-carnosine	85

List of Figures

2.62	Complexes with L-carnosine	85
2.63	Scheme of the pH-dependent forms of carnosine	86
2.64	ORTEP presentation of the free form of L-carnosine	86
2.65	Scheme of the reaction route by <i>Tessier et al.</i>	87
2.66	Scheme of the general reaction route	87
2.67	ORTEP presentation of 16	88
2.68	MERCURY presentation of hydrogen bonds in 16	90
2.69	Scheme of 16	91
2.70	ORTEP presentation of 17	92
2.71	MERCURY presentation of hydrogen bonds in 17	94
2.72	Scheme of 17	94
2.73	ORTEP presentation of 18	96
2.74	MERCURY presentation of free adenosine and disordered parts in 18	97
2.75	MERCURY presentation of hydrogen bonds in 18	98
2.76	Scheme of 18	99
2.77	ORTEP presentation of 19	101
2.78	MERCURY presentation of hydrogen bonds in 19	103
2.79	Scheme of 19 and possible binding sites of D-ribose	104
2.80	ORTEP presentation of 20	106
2.81	MERCURY presentation of hydrogen bonds in 20	107
2.82	Scheme of 20	108
2.83	ORTEP presentation of 21	110
2.84	MERCURY presentation of hydrogen bonds in 21	111
2.85	Scheme of 21	112
2.86	ORTEP presentation of 22	115
2.87	Scheme of 22	118
2.88	HPLC radiochromatogram of 22	119
2.89	Scheme of compounds related to 23	121
2.90	ORTEP presentation of 23	122
2.91	MERCURY presentation of hydrogen bonds in 23	123
2.92	Scheme of compounds with an imido-rhenium(V) core	124
2.93	ORTEP presentation of 24	125
2.94	MERCURY presentation of hydrogen bonds in 24	126
2.95	ORTEP presentation of 25	127
2.96	MERCURY presentation of hydrogen bonds in 25	128
2.97	Scheme of <i>rac</i> -dapH and L-thrH	129
2.98	ORTEP presentation of 26	130

List of Figures

2.99	MERCURY presentation of hydrogen bonds in 26	131
2.100	Scheme of idaH ₂ and a complex with ida	132
2.101	Scheme of the erythromycins A–F	132
2.102	Scheme of the acid- and base-catalyzed degradations of erythromycin A	134
2.103	ORTEP presentation of 27	135
2.104	Structures of erythromycin	136
2.105	MERCURY presentation of hydrogen bonds in 27	137
2.106	Scheme of the reaction route for bimetallic complexes	138
2.107	ORTEP presentation of 28	139
2.108	Scheme of related compounds with copper(II)	139
2.109	MERCURY presentation of weak interactions in 28	140
3.1	Competing reactions of the “3 + 2” approach	142
3.2	Torsion angles in 1–27	146
3.3	Diolate substitution reactions	147
3.4	CIS values of coordinated diols	149
3.5	Mean bond distances of the compounds	151
6.1	SCHAKAL packing diagram of 1	186
6.2	SCHAKAL packing diagram of 2	187
6.3	SCHAKAL packing diagram of 3	188
6.4	SCHAKAL packing diagram of 4	189
6.5	SCHAKAL packing diagram of 5	190
6.6	SCHAKAL packing diagram of 6	191
6.7	SCHAKAL packing diagram of 7	192
6.8	SCHAKAL packing diagram of 8	193
6.9	SCHAKAL packing diagram of 9	194
6.10	SCHAKAL packing diagram of 10	195
6.11	SCHAKAL packing diagram of 11	196
6.12	SCHAKAL packing diagram of 12	197
6.13	SCHAKAL packing diagram of 13	198
6.14	SCHAKAL packing diagram of 14	199
6.15	SCHAKAL packing diagram of 15	200
6.16	SCHAKAL packing diagram of 16	201
6.17	SCHAKAL packing diagram of 17	202
6.18	SCHAKAL packing diagram of 18	203
6.19	SCHAKAL packing diagram of 19	204

List of Figures

6.20	SCHAKAL packing diagram of 20	205
6.21	SCHAKAL packing diagram of 21	206
6.22	SCHAKAL packing diagram of 22	207
6.23	SCHAKAL packing diagram of 23	208
6.24	SCHAKAL packing diagram of 24	209
6.25	SCHAKAL packing diagram of 25	210
6.26	SCHAKAL packing diagram of 26	211
6.27	SCHAKAL packing diagram of 27	212
6.28	SCHAKAL packing diagram of 28	213

List of Tables

2.1	Hydrogen bonds in 1	16
2.2	¹³ C NMR chemical shifts of 1	18
2.3	¹ H NMR chemical shifts and ³ J _{HH} coupling of 1	18
2.4	Hydrogen bonds in 2	20
2.5	¹³ C NMR chemical shifts of 2	22
2.6	¹ H NMR chemical shifts and ³ J _{HH} coupling of 2	23
2.7	¹³ C NMR chemical shifts of the compounds with adenosine, guanosine, inosine	24
2.8	Hydrogen bonds in 3	27
2.9	Hydrogen bonds in 4	32
2.10	Hydrogen bonds in 5	34
2.11	Hydrogen bonds in 6	39
2.12	¹³ C NMR chemical shifts of 6	40
2.13	Hydrogen bonds in 7	42
2.14	¹³ C NMR chemical shifts of 7	44
2.15	Hydrogen bonds in 8	47
2.16	¹³ C NMR chemical shifts of 8	49
2.17	Hydrogen bonds in 9	54
2.18	¹³ C NMR chemical shifts of 9	56
2.19	Hydrogen bonds in 10	59
2.20	¹³ C NMR chemical shifts of 10	61
2.21	Hydrogen bonds in 11	63
2.22	¹³ C NMR chemical shifts of 11	65
2.23	Hydrogen bonds in 12	69
2.24	¹³ C NMR chemical shifts of 12	70
2.25	Hydrogen bonds in 13	72
2.26	¹³ C NMR chemical shifts of 13	74
2.27	Hydrogen bonds in 14	76
2.28	¹³ C NMR chemical shifts of 14	78
2.29	Hydrogen bonds in 15	80

List of Tables

2.30	¹³ C NMR chemical shifts of 15	83
2.31	Hydrogen bonds in 16	89
2.32	¹³ C NMR chemical shifts of 16	91
2.33	Hydrogen bonds in 17	93
2.34	¹³ C NMR chemical shifts of 17	95
2.35	Hydrogen bonds in 18	99
2.36	¹³ C NMR chemical shifts of 18	100
2.37	Hydrogen bonds in 19	102
2.38	¹³ C NMR chemical shifts of 19	104
2.39	Hydrogen bonds in 20	107
2.40	¹³ C NMR chemical shifts of 20	108
2.41	Hydrogen bonds in 21	111
2.42	¹³ C NMR chemical shifts of 21	113
2.43	Hydrogen bonds in 22	116
2.44	¹³ C NMR chemical shifts of 22	117
2.45	Hydrogen bonds in 23	123
2.46	Hydrogen bonds in 24	126
2.47	Hydrogen bonds in 25	129
2.48	Hydrogen bonds in 26	131
2.49	Hydrogen bonds in 27	137
2.50	Weak interactions in 28	140
3.1	Structural observations	152
6.1	Archive codes	214
6.2	Crystallographic tables of 1, 2 and 3	215
6.3	Crystallographic tables of 4, 5 and 6	216
6.4	Crystallographic tables of 7, 8 and 9	217
6.5	Crystallographic tables of 10, 11 and 12	218
6.6	Crystallographic tables of 13, 14 and 15	219
6.7	Crystallographic tables of 16, 17 and 18	220
6.8	Crystallographic tables of 19, 20 and 21	221
6.9	Crystallographic tables of 22, 23 and 24	222
6.10	Crystallographic tables of 25, 26 and 27	223
6.11	Crystallographic table of 28	224
6.12	Selected geometrical parameters	225

Listing of the numbered compounds

- 1 [ReO(*fac*-dien)(*syn*-Cyd2',3'H₋₂)]I
- 2 [ReO(*fac*-dien)(*syn*-Urd2',3'H₋₂)]BPh₄ · MeOH
- 3 [Re(NPh)(*fac*-dien)(*syn*-AnErytH₋₂)]BPh₄
- 4 [Re(NPh)(*fac*-dien)(*anti*-AnErytH₋₂)] [ReO(*fac*-dien)(*anti*-AnErytH₋₂)] [BPh₄]Cl
- 5 [Re(NPh)(*mer*-dien)(OEt)(PPh₃)] [ReO₄]Cl · EtOH · 0.5 Me₂CO
- 6 [ReO(*rac*-dap)(EthdH₋₂)] · MeOH
- 7 [ReO(*rac*-dap)(*syn*-AnErytH₋₂)] · H₂O
- 8 [ReO(*rac*-dap)(*anti*-Cyd2',3'H₋₂)] · 2 H₂O
- 9 [ReO(L-his)(ox)]
- 10 [ReO(L-his)(EthdH₋₂)] · 4.5 H₂O
- 11 [ReO(L-his)(*syn*-AnErytH₋₂)] · 2 H₂O
- 12 [ReO(L-his)(*syn*-Urd2',3'H₋₂)] · 1.5 H₂O
- 13 [ReO(L-his)(*anti*-Cyd2',3'H₋₂)] · 5 H₂O
- 14 [ReO(L-his)(*syn*-Me-α-D-Manp2,3H₋₂)] · 2 MeOH
- 15 [ReO(L-his)(*syn*-Me-β-D-Ribp3,4H₋₂)] · 0.5 MeOH
- 16 [ReO(L-car)(ox)] · 2 H₂O
- 17 [ReO(L-car)(EthdH₋₂)] · MeOH · H₂O
- 18 [ReO(L-car)(*syn*-AdoH2',3'H₋₂)] · 3 MeOH · 2 H₂O
- 19 [ReO(L-car)(*syn*-α-D-Ribf1,2H₋₂)] · 3 MeOH
- 20 [ReO(L-car)(*anti*-α/β-D-Manp2,3H₋₂)] · MeOH
- 21 [ReO(L-car)(*anti*-β-D-Fruf2,3H₋₂)] · MeOH
- 22 [ReO(L-car)(*syn*-6-O-α-D-Glcp-β-D-Fruf2,3H₋₂)] · 3 H₂O
- 23 (HNEt₃)[ReO(ox)₂(PPh₃)]
- 24 [Re(NPh)(ox)(PPh₃)₂Cl] · MeOH
- 25 [ReO(*syn*-AnErytH₋₂)(MeOH)(PPh₃)Cl]
- 26 [ReO(L-thr)(*syn*-AnErytH₋₂)(PPh₃)]
- 27 [ReO(*fac*-ida)(Emy11,12H₋₂)] · MeOH · H₂O
- 28 [Cu₂(phen)₂(ox)(ReO₄)₂]_n

Abbreviations

Ado	adenosine
amiH	bis(1-ethanolaminomethyl)-1-methylimidazole
AMP	adenosine monophosphate
AnEryt	anhydroerythritol, <i>cis</i> -oxolane-3,4-diol
bdmpza	bis(3,5-dimethylpyrazol-1-yl)acetate
bicine	<i>N,N</i> -bis(2-hydroxyethyl)glycine
bpy	2,2'-bipyridine
carH	carnosine, β -alanyl-histidine
catH ₂	benzene-1,2-diol, catechol
CIS	<i>coordination-induced shift</i>
Cp*	pentamethylcyclopentadienyl anion
CT	computed tomography
Cyd	cytidine
cysH	cysteine
dapH	2,3-diaminopropionic acid, 3-amino-alanine
dien	diethylenetriamine
DMSO	dimethylsulfoxide
dppe	1,2-bis(diphenylphosphino)ethane
dppm	1,2-bis(diphenylphosphino)methane
en	ethylenediamine
Emy	erythromycin
Ethd	ethanediol
<i>fac</i>	facial
Fru	fructose
Guo	guanosine
Glc	glucose
hisH	histidine
HPLC	high-performance liquid chromatography
idaH ₂	iminodiacetic acid
Ino	inosine
leuH	leucine

Man	mannose
<i>mer</i>	meridional
metH	methionine
MS	mass spectrometry
NADH	nicotinamide adenine dinucleotide
NBA	3-nitrobenzyl alcohol
NMR	nuclear magnetic resonance
ox	oxalate
PET	positron emission tomography
phen	1,10-phenanthroline
proH	proline
pz	pyrazole
<i>rac</i>	racemic
Rib	ribose
SPECT	single photon emission computed tomography
tacn	1,4,7-triazacyclononane
thrH	threonine
tpa	tris(2-pyridylmethyl)amine
tpb	hydridotris(pyrazolyl)borate
tricine	<i>N</i> -[tris(hydroxymethyl)methyl]glycine
Urd	uridine
thrH	threonine
XRD	X-ray diffraction

Abstract

This thesis is about the coordination chemistry of rhenium(V) with small biomolecules. Such rhenium complexes may be of medical significance in the field of radiopharmacy, since radioactive isotopes such as ^{186}Re or ^{188}Re are used for the diagnosis or treatment of tumors. But fundamental research is still necessary for the attachment of radiometals to biologically active molecules. Most rhenium(V)-based radiopharmaceuticals lack stability (at physiological conditions) or selectivity (in terms of targeting cells, or in terms of preparing an exactly defined agent).

In order to meet these requirements, a library of ligands was scanned to synthesize kinetically inert mixed-ligand rhenium(V) complexes. Most of the prepared complexes (22 out of 28) were built with tri- and bidentate chelating ligands ("3 + 2" approach). They were studied by means of single-crystal X-ray diffraction, NMR spectroscopy, mass spectrometry, elemental analysis and other methods. As tridentate chelators, nitrogen containing compounds such as diethylenetriamine, *rac*-2,3-diaminopropionic acid, L-histidine, L-carnosine and other ligands based on amino acids were used. As bidentate chelators, an oxygen donor library was used, covering simple diols such as ethanediol or anhydroerythritol, and more complex molecules such as nucleosides, pyranosides, mono- and disaccharides or glycoside antibiotics.

The optimum was found for a compound derived from the reducing disaccharide D-isomaltose and the dipeptide L-carnosine. It was possible to transfer the synthesis from standard laboratory conditions (millimolar concentration range, methanol as solvent, alkaline pH) to labeling experiments with ^{188}Re (nanomolar concentration range, water as solvent, physiological pH).

With this work, the chemistry of coordination compounds with rhenium(V) is extended to physiological conditions and the synthesized compounds are promising candidates for prospective works in the field of radiopharmacy.

1 Introduction

1.1 Carbohydrates and amino acids

This work deals with two important substance classes in biochemistry: carbohydrates and amino acids. Since the discovery of DNA, it has been shown that all processes in living organisms are based on the following major classes of organic compounds: nucleic acids, proteins, lipids and carbohydrates. Until today, biochemical research focused mainly on nucleic acids (the genome) and proteins (the proteome). These biopolymers were identified as the basis for storage and transfer of biological information.

Although carbohydrates are the most predominant form of biomolecules on earth, they have not been taken into account in this context for a long time. Up to the present the main topic about them is their role as energy source in most living organisms. They play an important role in the storage and transport of energy (such as starch in plants, glycogen in animals) or as structural and protective component in cells (such as cellulose in plants, chitin in animals). Roughly 75 % of the annually renewable biomass on earth ($2 \cdot 10^{11}$ tons) consists of carbohydrates^[1]. During evolution, the carbohydrate D-ribose was selected as the exclusive sugar component of nucleic acids^[2]. But in addition to these important roles, carbohydrates are involved in many other metabolic processes. Glycoconjugates are carbohydrates attached to other molecules such as lipids (glycolipids), or proteins (glycoproteins). A study on a protein database showed that more than half of all known proteins are glycosylated^[3]. Such glycoconjugates take part in recognition processes on a molecular level. They are destination labels for proteins or other molecules. It has been shown that they have an influence on cell growth and development, tumor growth and metastasis, anticoagulation, the immune system, fertilization, cell-cell communication and microbial pathogenesis^[4]. Today, carbohydrates are considered to be a third type of information-encoding biological macromolecules, after nucleic acids and proteins^[5, 6]. They are worthwhile to study, as the full complexity of cellular life cannot be directly explained solely by genome and proteome^[7]. The reason for this late awareness is the complexity of the glycoconjugates, which are much more difficult to study than proteins or nu-

1 Introduction

cleic acids. This complexity is caused by the chemical features of carbohydrates. By definition, carbohydrates are “hydrates of carbon”, but not all of them fit into the formula $(C \cdot H_2O)_n$. More generally, they can be regarded as aldehydes or ketones with two or more hydroxyl groups. Optionally, they may contain other elements such as sulfur, nitrogen or phosphorus. All functional groups can be linked to other molecules, giving an immense variety of structures. Monosaccharides, the smallest unit of carbohydrates, contain at least one chiral carbon atom and each stereogenic center may double the amount of isomeric forms. Moreover, many monosaccharides are mixtures in solution, as they are able to adopt α -, β - furanoidic, pyranoidic and open-chain isomers. For all these reasons, the chemistry of carbohydrates is varied and complicated. It is difficult to predict which functional groups may interact with other reacting agents, such as metal ions. Furthermore, saccharides containing an aldehyde function (aldoses) or other reactive groups show reducing properties toward some metal ions in analogy to Fehling’s solution with copper(II). But despite the configurational lability and potentially unfavorable redox properties, carbohydrates provide manifold oxygen-donor functions in particular for the coordination of metals. An increase in structural information of such metallated compounds has been observed in recent years^[8].

Amino acids are molecules containing both acidic and alkaline functional groups. They show chirality and their properties vary with attached side chains. These side chains may be hydrophobic and nonpolar, or polar and variably charged. Except for glycine, all standard (proteinogenic) amino acids contain an asymmetric α -carbon atom, which bears one carboxy and one amino function. For historical reasons related to the molecule L-glyceraldehyde, their configuration is assigned by the stereodescriptor L. Amino acids are able to polymerize via peptide bonds; the polymers are called peptides (if below ca. 100 units) and proteins (if more). As found in nature for metalloproteins, amino acids are excellent chelators for metal ions. Between one-quarter to one-third of all proteins are thought to need metals as co-factors such as zinc, iron, copper, cobalt, nickel, manganese, magnesium and calcium^[9]. In such metalloproteins and -enzymes, the metals are bonded via the nitrogen, oxygen or sulfur atoms of the amino acid side chains. But even much smaller subunits of these polymers, individual amino acids and peptides, have been known as chelating ligands for metals for a long time^[10, 11]. In these coordination compounds, amino acids are mostly bidentate (N,O)-chelates, or tridentate in the presence of suitable side chains.

1.2 Coordination compounds with rhenium(V)

Rhenium was the last stable, naturally occurring element to be discovered. In 1925 it was isolated and verified by *W. Noddack, I. Tacke* and *O. Berg* from fractions of the manganese containing minerals columbite, tantalite and gadolinite^[12]. After rhodium and ruthenium, it is among the rarest metals on earth. Like its lighter homologue manganese, rhenium covers a wide range of oxidation states: from –III to VII (configurations d^{10} to d^0). While higher and intermediate oxidation states are dominated by oxides and halides (like ReO_4^-), carbon monoxide extends this series to lower oxidation states (I and below)^[12]. The most stable oxidation states in water are IV and VII^[13]. This holds true for the occurrence of rhenium in nature, where it is widely distributed in concentrations of parts-per-billion, but never elemental. It occurs as ReO_2 and $\text{Re}(\text{OH})_4$ under reductive/anaerobic conditions, and as ReO_4^- in oxidizing environments^[14–16].

Concerning the chemistry of coordination compounds, the oxidation state with the most reported complexes is V^[17]. Rhenium(V) tends to disproportionate^a to rhenium(VII) and rhenium(IV), but it is possible to stabilize it with a variety of ligands. Examples are multiply bonded oxido-, nitrido- or imido-groups, which are good π -donor ligands. Such complexes are diamagnetic (d^2 configuration) and the coordination geometry is mostly octahedral, but also square-pyramidal or trigonal-bipyramidal are known for pentavalent complexes. For the $\{\text{ReO}\}^{3+}$ core, there are mainly three strategies for the design of stable complexes. The so-called “2 + 2”, “3 + 1” and “3 + 2” approaches^[19, 20] were developed for complexes with mixed-ligand donor atom sets. The numbers refer to the denticities of the ligands entering the coordination sphere of rhenium, in addition to the multiply bonded oxido ligand. Five-coordinated square-pyramidal complexes are the result of the “2 + 2” and “3 + 1” systems. But many of these 16-electron species are not substitution inert in a biological milieu^[19]. Octahedral complexes derived from the “3 + 2” approach are 18-electron species^b. They are built with tri- and bidentate chelating ligands, and due to this closed shell, seem to be more substitution inert^[20].

But which ligands are suitable? As reported in the previous chapter, carbohydrates and amino acids may be used as oxygen- and nitrogen-donor ligands. According to literature, structures of complexes with each of these two substance classes are known. But as of today, not for both combined.

^a The following hydrolysis equation was reported for a rhenium(V) compound by *Cotton et al.*:^[18]
 $2 \text{ReOCl}_4^- + n \text{H}_2\text{O} \longrightarrow \text{ReO}_2 \cdot n \text{H}_2\text{O} + \text{ReO}_4^- + 8 \text{Cl}^-$

^b only for an alternative notation of the multiple bond: $\text{Re}\equiv\text{O}|^+$ instead of $\text{Re}=\text{O}$

1 Introduction

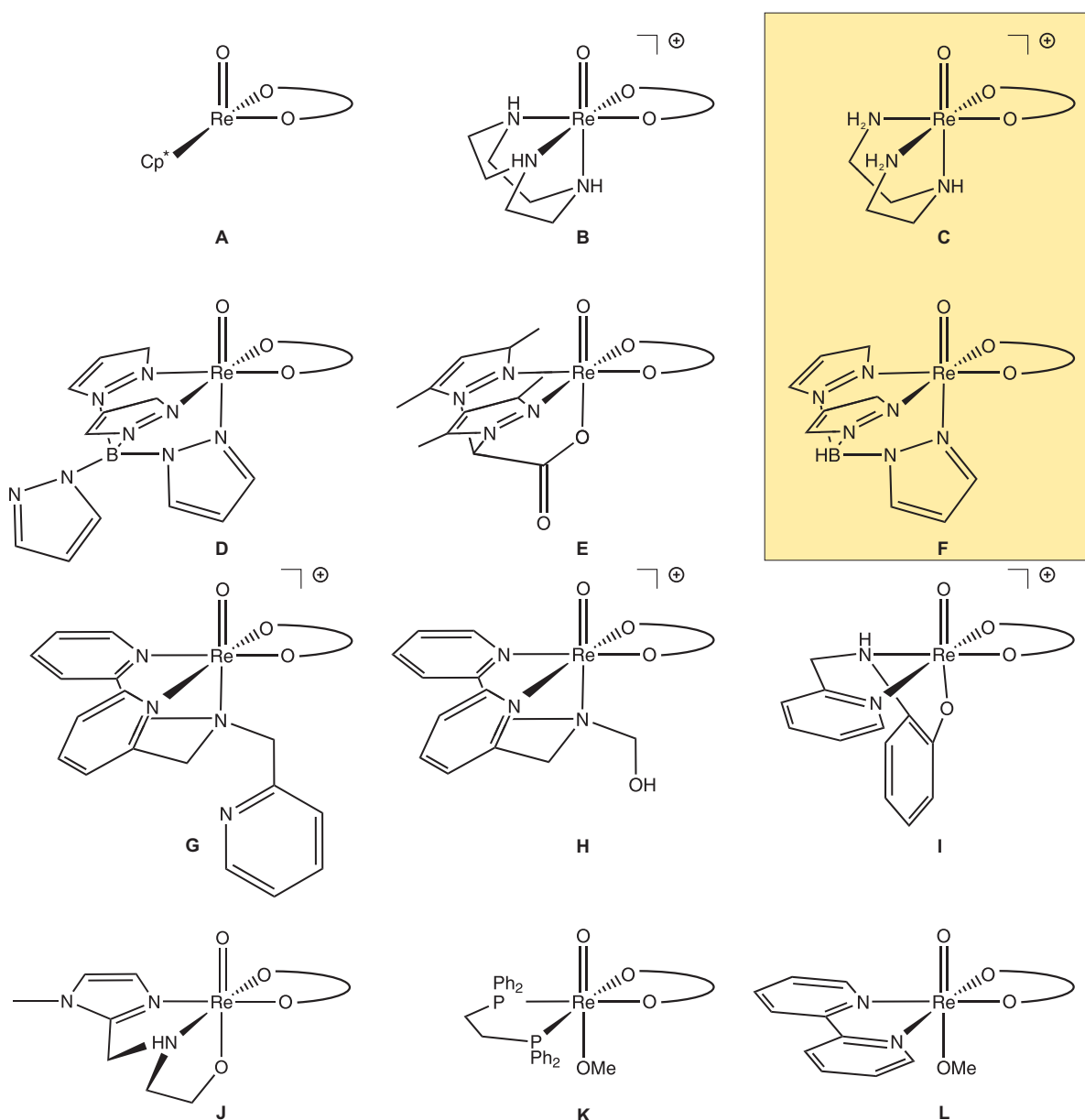


Figure 1.1 Scheme of rhenium(V) diolato complexes. **A:** $[\text{ReO}(\text{Cp}^*)(\text{diolH}_{-2})]$ with ethanediol^[21], **B:** $[\text{ReO}(\text{tacn})(\text{diolH}_{-2})]^+$ with ethanediol^[22], **C:** $[\text{ReO}(\text{dien})(\text{diolH}_{-2})]^+$ with several carbohydrates^[23, 24], **D:** $[\text{ReO}(\text{B}(\text{pz})_4)(\text{diolH}_{-2})]$ with ethanediol^[25], **E:** $[\text{ReO}(\text{bdmpza})(\text{diolH}_{-2})]$ with ethanediol^[26] and other diols^[27], **F:** $[\text{ReO}(\text{tpb})(\text{diolH}_{-2})]$ with ethanediol^[28], propanediol^[29], oxalate^[30] and several carbohydrates^[23, 31, 32], **G:** $[\text{ReO}(\text{tpa})(\text{diolH}_{-2})]$ with ethanediol and catechol^[33], **H:** $[\text{ReO}(\text{bpen})(\text{diolH}_{-2})]^+$ with ethanediol^[34], **I:** $[\text{ReO}(\text{L})(\text{diolH}_{-2})]$ with catechol^[35], **J:** $[\text{ReO}(\text{ami})(\text{diolH}_{-2})]$ with oxalate^[36], **K:** $[\text{ReO}(\text{dppe})(\text{OMe})(\text{diolH}_{-2})]$ with oxalate^[37], **L:** $[\text{ReO}(\text{bipy})(\text{OMe})(\text{diolH}_{-2})]$ with oxalate^[37].

For carbohydrates, mainly structures with the co-ligands dien^[23, 24] and tpb^[23, 31, 32] are known, as illustrated in Figure 1.1 (yellow box). But as shown there too, many other compounds were reported since 1987 for simple diols like ethanediol. They can be regarded as model compounds for carbohydrate complexes in prospective

works. In all cases, a bidentate (*O,O*) binding mode was observed for the diols, while mostly tridentate nitrogen-donor ligands complete the octahedral coordination. Figure 1.2 shows complexes with single amino acids that were structurally characterized since 1999. Bi- and tridentate binding modes via the thiol-, amine- and carboxylate-functions of the amino acids were observed. Most of the compounds depicted in the Figures 1.1 and 1.2 are built in analogy to the previously mentioned “3 + 2” approach. The affinity of these compounds raises the question, whether it is possible to combine both ligand types (carbohydrates and amino acids) complementarily in one complex. With regard to pharmacology, such compounds that are related to biological molecules might have promising features.

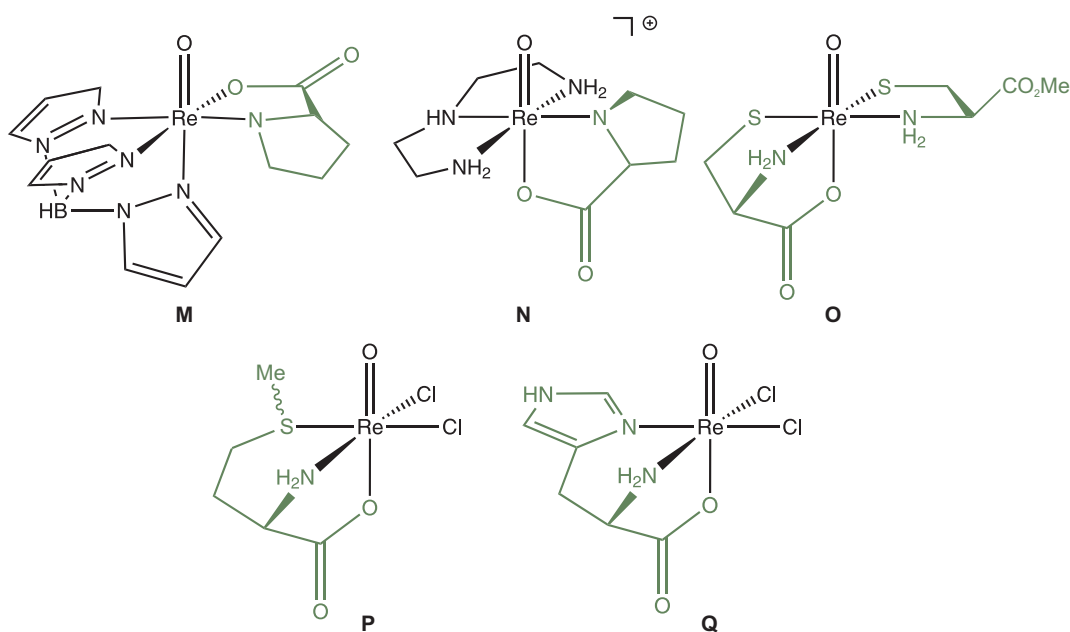


Figure 1.2 Scheme of rhenium(V) complexes with amino acids. **M**: [ReO(tpb)(L-pro)] with L-proline^[38], **N**: [ReO(dien)(L-pro)]⁺ with L-proline or L-leucine (not depicted)^[39], **O**: [ReO-(L-cys)(L-cysMe)] with L-cysteine^[40], **P**: [ReO(D,L-met)Cl₂] with L-methionine^[41], **Q**: [ReO-(L-his)Cl₂] with L-histidine^[42].

1.3 Radiopharmaceutical compounds

Radiopharmaceuticals are radioactive drugs for the diagnosis or treatment of diseases. Depending on their purpose, they contain different radioactive nuclides.

Imaging agents

The term “medical imaging” implies all techniques used in medicine to diagnose or examine diseases by images. For the imaging of internal organs, compounds are used with short-lived isotopes, which are γ -ray or positron emitting. Widely used isotopes are metals such as ^{99m}Tc , ^{67}Ga , ^{111}In (γ -ray emitters) and $^{61,62,64}\text{Cu}$, ^{68}Ga , ^{94m}Tc , ^{89}Zr (positron emitters), but also non-metallic isotopes are used (such as ^{18}F or ^{123}I)^[43]. Diagnostic agents labeled with these isotopes are administered to patients in low and non-toxic doses, with a total radiation dose comparable with conventional X-ray radiography^[44]. In the case of γ -emitters, the radiation emerging from inside the body is detected by scintigraphic cameras, giving images of internal organs with computerized tomography techniques (SPECT)^c. In the case of β^+ -emitters, the energetic particles are detected indirectly via pairs of γ -photons, originating from electron-positron annihilation (PET)^d. SPECT and PET are methods of functional imaging, as they show the biochemical activity in living organisms, and not their morphology (as in X-ray tomography). It is possible, however, to combine both imaging types in modern diagnostics.

The most developed branch of radiopharmaceuticals are compounds with ^{99m}Tc . In 2004, this isotope was used for 80 % of the diagnostic studies in routine nuclear medicine^[17, 43]. It is readily available from $^{99}\text{Mo}/^{99m}\text{Tc}$ generators and commercially “instant kits” have been developed for the preparation of imaging agents^e. The “radiolabeling” of these compounds is generally done with the following methods^[43]:

- direct labeling: the disulfide linkages of large biomolecules (like antibodies) are converted by reducing agents to free thiols, which bind strongly to the metal.
- pre-labeling approach (preformed chelate approach): at first, stable metal-chelate species are formed, that are conjugated to a biomolecule in a second step.
- post-labeling approach (indirect labeling): a reactive functional group is attached to a biomolecule, and in a second step this chelator is coordinated to a metal core.

^c Single Photon Emission Computed Tomography

^d Positron Emission Tomography

^e Widely-used compounds are $[\text{}^{99m}\text{Tc}^{\text{I}}(\text{MIBI})_6]^+$ (Cardiolite[®], a complex with the carbon bonded ligand 2-methoxy-isobutyl-isocyanide for the imaging of the heart), $[\text{}^{99m}\text{Tc}^{\text{V}}\text{O}_2(\text{tetrafosmin})_2]^+$ (Myoview[®], a complex with the ligand bis(2-ethoxyethyl)phosphino-ethane for the imaging of the heart) or $[\text{}^{99m}\text{Tc}^{\text{V}}\text{O}(\text{DMSA})_2]^-$ (a complex with dimercapto succinic acid for the imaging of the kidneys)

First generation or *metal essential* agents are simple compounds such as $[^{99m}\text{TcO}_4]^-$. Their biodistribution depends solely on the size and charge of the compounds, which means their allocation in the body is not very specific. For *second generation* agents, chelated metals are linked to biologically active molecules (such as antibodies or small peptides) which are able to interact with specific biological targets (Figure 1.3). As the ligands in these complexes contain two different units (a chelating and a bioactive site), this design is called the bifunctional chelate approach (BFC). As another strategy, these two sites may even be located coincidentally in one bioactive molecule (integrated approach). An example is given later in this text (Figure 1.4).

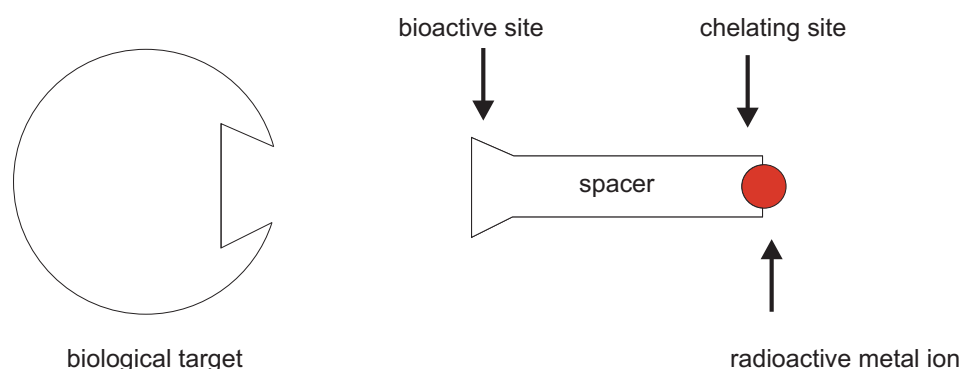


Figure 1.3 Design of targeted radiopharmaceuticals according to the bifunctional approach.

Radio-therapy

The above holds true for therapeutic radiopharmaceuticals, but the radionuclides differ. Mostly β^- -radiating isotopes are used for cancer therapy, and the radiation doses are higher and more toxic. Due to the cell-damaging properties of β^- -radiating isotopes, such pharmaceuticals must be high-selectively harmful for tumor cells and minimally harmful to the entire organism. This goal seems to be reachable by the conjunction of radiometals with biologically active molecules. Like a Trojan horse, these pharmaceuticals are designed to bind to certain receptors of tumor cells, resulting in a selective apoptosis. For such applications, the most widely used radionuclides are ^{90}Y and ^{177}Lu . Although ^{188}Re is conveniently purchased from a $^{188}\text{W}/^{188}\text{Re}$ generator, it has not been commonly accepted for medical use so far. The physical properties^f are attractive for diagnostics and therapy, but its chemical properties have been, so far, the major draw-back for its use. Much of the knowledge about imaging agents with technetium is transferable to rhenium, as these elements are very similar due to the lanthanide contraction. But there are important discrepancies, in particular in the

^f The following isotopes might be useful for scintigraphic imaging (γ -radiation) and therapeutic application (β^- -radiation): ^{186}Re ($\beta_{\text{max}}^- = 1.07$ MeV, $t_{1/2} = 3.8$ d, $E_\gamma = 137$ keV) and ^{188}Re ($\beta_{\text{max}}^- = 2.1$ MeV, $t_{1/2} = 17$ h, $E_\gamma = 155$ keV)

redox properties. Rhenium complexes are harder to reduce (and easier to oxidize)^[44]. But during the last decade, many efforts have been made in the chemistry of rhenium to develop an application to radiopharmacy^[43, 45–48]. At present, some compounds have reached the status of clinical application:

- ¹⁸⁸Re-HEDP, a radiopharmaceutical compound derived from hydroxy-ethylene-diphosphonate, is utilized for the pain therapy of skeletal metastases (palliative care). In spite of its simple composition (it is a *first generation* agent, see previous page) and its unknown oxidation state, charge or geometry, it has been classified as “bone seeking”. This may be caused by the tendency of hydroxylapatite surfaces to adsorb diphosphonates^[49].

- In 1997 the first antibody for cancer therapy was approved by the FDA^g. *Rituximab* is a monoclonal antibody against the protein CD20^h found on the surface of B cells, a kind of lymphocytes. Since then, more and more monoclonal antibodies have been used for radio immunotherapy (RIT) of cancer^[50]. Mainly antibodies labeled with ¹³¹I and ⁹⁰Y have been accepted for clinical use. But recent research focused also on compounds with ¹⁸⁸Re^[46]. In 2004, clinical trials of ¹⁸⁸Re-labeled antibodies against the protein tenascin were reported by the Department of Nuclear Medicine of the LMU Munichⁱ. The protein tenascin is expressed by degenerated cells showing symptoms of malignant glioma, a kind of brain cancer. For such a radio-immune therapy, the labeled monoclonal antibodies show high target-specific activity.

- The following example shows the successful transfer of knowledge obtained from technetium imaging agents to therapy with rhenium isotopes. Octreotid is a synthetic analogon of the peptide hormone somatostatin. Some of its functions are to inhibit other hormones, such as the growth hormone (GH) and hormones of carbohydrate metabolism (glucagon and insulin). It is an even more potent inhibitor than natural somatostatin. Certain tumors have an increased number of receptors for these hormones (receptor overexpressing tumors), which is useful for the diagnosis. Imaging agents containing ^{99m}Tc-labeled octreotide showed a high affinity toward these tumors^[51]. The analog ¹⁸⁸Re-labeled compounds would be suitable for therapy. As shown in Figure 1.4, this cyclic eight-amino-acid peptide offers two chelating sites for rhenium(V) after cleavage of the disulfide bridge. Depending on the acylation of

^g U.S. Food and Drug Administration

^h cluster of differentiation 20, an immunological surface characteristics of cells

ⁱ M. Decker, F. J. Gildehaus, C. Götz, K. Hahn, A. Hischa, G. Jung, G. Pöpperl, W. Rächinger, H. J. Reulen, P. Riva, O. Schnell, S. Stocker, K. Tatsch, J.C. Tonn, T.A. Yousry, [link](#).

1 Introduction

the *N*-terminus, two coordination modes of rhenium(V) were detected. In both complexes, octreotide is recycled by the metal core and both show even higher affinities against target receptors. Although so far only preclinical studies were reported for these compounds, animal studies showed its therapeutic potential^[46].

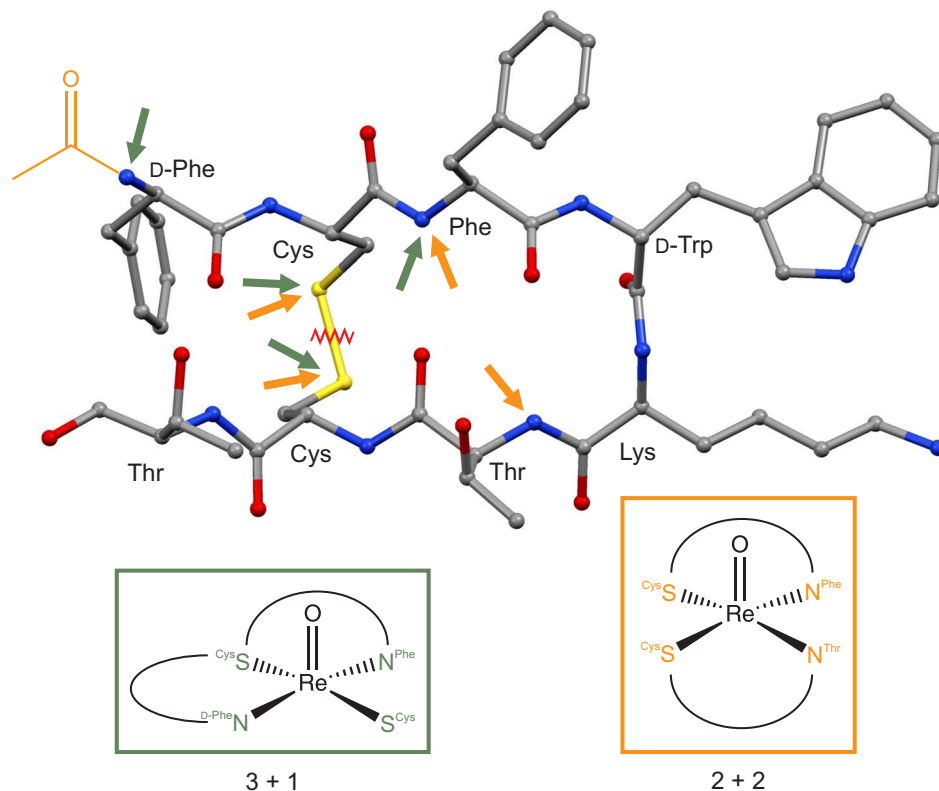


Figure 1.4 Coordination of rhenium(V) to octreotide, a derivative of the bioactive peptide somatostatin^[52]. The observed binding sites (green: 3 + 1) after cleavage of the disulfide bridge are overlaid to the structure of free octreotide reported by *Sheldrick et al.*^[53]. The second coordination mode (orange: 2 + 2) was observed for the same reaction with *N*-acetylated octreotide.

1.4 Aims of this work

As shown on the previous pages, the most selective radiopharmaceuticals are involved with peptides. Rhenium compounds with carbohydrates have not been taken into account for this purpose so far. Carbohydrates labeled with the isotope ^{18}F are known solely as diagnostic agents^j, but not for therapy. Compounds containing both carbohydrates and amino acids show interesting properties in view of biochemistry. Glycopeptides^[54, 55], for example, or sugar amino acids (SAA)^[56, 57] are research fields of increasing interest for drug design.

Fundamental research is still necessary for the attachment of radiometals such as ^{188}Re to biologically active molecules. Most rhenium-based radiopharmaceuticals lack stability (at physiological conditions) or selectivity (in terms of targeting cells, or in terms of preparing an exactly defined therapeutic agent). This work focuses on the interaction of non-radioactive^k rhenium(V) species with carbohydrates and amino acids in solution and in the solid state. In this work, three basic building blocks were varied around a rhenium(V) core in the search for stable rhenium complexes. As illustrated in Figure 1.5, an oxido- or phenylimido-rhenium(V) unit (A) may be connected with two further molecules. One of these molecules may be a carbohydrate with a diol function (B). The other molecule, a nitrogen-containing co-ligand (C), completes the octahedral coordination of the rhenium core. The following chapters are grouped by these co-ligands: diethylenetriamine (chapter 2.1), amino-alanine (chapter 2.2), L-histidine (chapter 2.3), L-carnosine (chapter 2.4) and other ligands (chapter 2.5).

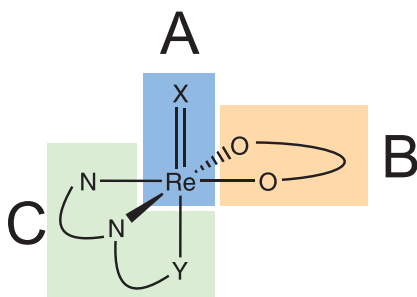


Figure 1.5 General composition of the compounds in this work. A: the rhenium(V) core with an oxido or phenylimido ligand. B: a carbohydrate with a diol function. C: a nitrogen containing co-ligand.

^j FDG: 2-fluoro-2-deoxy-D-glucose is most commonly used for medical imaging, as it shows the regional glucose uptake of cells.

^k Naturally occurring rhenium consists of the isotopes ^{185}Re (37 %) and ^{187}Re (63 %). ^{185}Re is non-radioactive, ^{187}Re is weakly radioactive with a long half-life (β^- -radiation, $t_{1/2} = 4.3 \cdot 10^{10}$ years)^[12].

2 Results

2.1 Compounds of rhenium(V) with diethylenetriamine

Diethylenetriamine (dien) is a common chelating ligand for transition metals. In the chemistry of rhenium(V), complexes with dien in bi- and tridentate binding modes are known. Whereas in the compound $[\text{ReO}_2(\text{dien})_2]\text{I}$ reported by *Kremer et al.*^[58] the third nitrogen atom of dien remains non-bonded, tridentate binding modes are observed in compounds bearing a $\{\text{ReO}\}^{3+}$ core. For example, in the compounds $[\text{ReO}(\text{dien})(\text{L-leu})]\text{I}$ and $[\text{ReO}(\text{dien})(\text{L-pro})]\text{ReO}_4$ with the amino acids L-leucine and L-proline (also reported by *Kremer et al.*^[39]), dien is part of an $(N,N,N)(N,O)$ donor atom set.

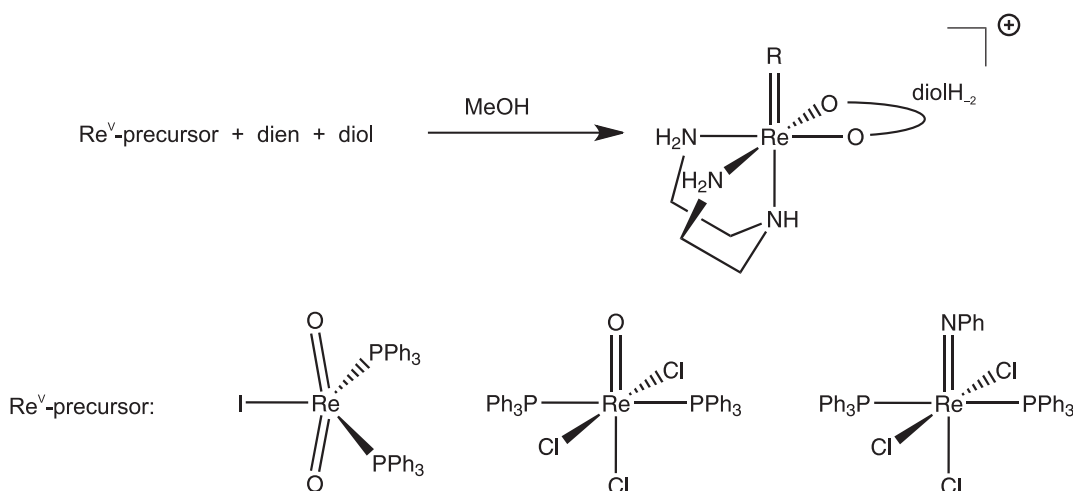


Figure 2.1 Scheme of the reactions with diethylenetriamine (dien) in this chapter. **R** may be an oxido or phenylimido ligand depending on the precursor, **diol** denotes a carbohydrate with a *cis*-vicinal diol function.

In this chapter mixed-ligand compounds with rhenium(V), dien and carbohydrates are presented. The preparations start from different rhenium(V) precursors, dien and carbohydrates with a *cis*-vicinal diol function (see Figure 2.1). Different binding modes are observed: Figure 2.2 shows *fac*/*mer* coordination of dien and *syn*/*anti* isomerism of the diol. According to the “3 + 2” approach^[19], these new compounds are built with tri- and bidentate ligands in the coordination sphere of a distorted octa-

2 Results

hedral complex with an $\{\text{ReO}\}^{3+}$ or $\{\text{ReNPh}\}^{3+}$ core. This $(N,N,N)(O,O)$ donor set is also to be found in compounds reported by M. Oßberger^[23]. The first two compounds in this chapter were made in analogy to this work.

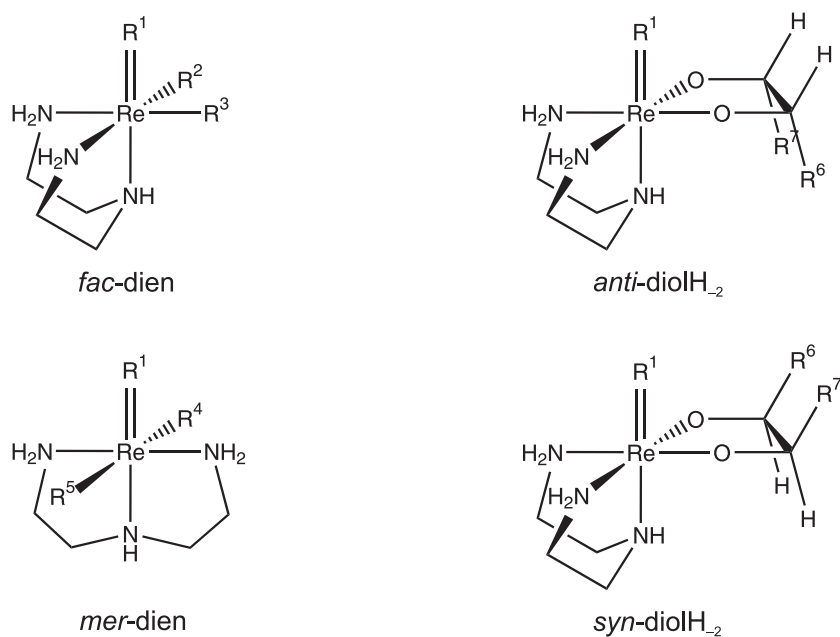


Figure 2.2 Scheme of the observed binding modes with rhenium and diethylenetriamine. R¹ implies for an oxido or phenylimido ligand, **diol** with R⁶ and R⁷ represents a carbohydrate with a *cis*-vicinal diol function.

To synthesize these new compounds the diols must be deprotonated. If the starting material is iodido-dioxido-bis(triphenylphosphane)-rhenium(V), no further base is needed for deprotonation as one of the leaving groups acts as a built-in base: an oxido ligand. The geometry of the complexes changes from five-coordinate trigonal-bipyramidal to six-coordinate octahedral. With this reactive precursor, reactions at room temperature are possible, but the solutions are not very stable.

The other precursors *trans*-trichlorido-oxido-bis(triphenylphosphane)-rhenium(V) and *trans*-trichlorido-phenylimido-bis(triphenylphosphane)-rhenium(V) are less reactive. They require higher temperatures and a base like triethylamine must be added to start the reaction.

2.1.1 The reaction of $[\text{ReO}_2(\text{PPh}_3)_2\text{I}]$ with dien and cytidine

The rhenium(V) precursor $[\text{ReO}_2(\text{PPh}_3)_2\text{I}]$ reacts with diethylenetriamine and cytidine in methanol at room temperature to give a lilac compound, from which the complex $[\text{ReO}(\text{fac-dien})(\text{syn-Cyd}2',3'\text{H}_-)]\text{I}$ (**1**) was recrystallized (Figure 2.3).

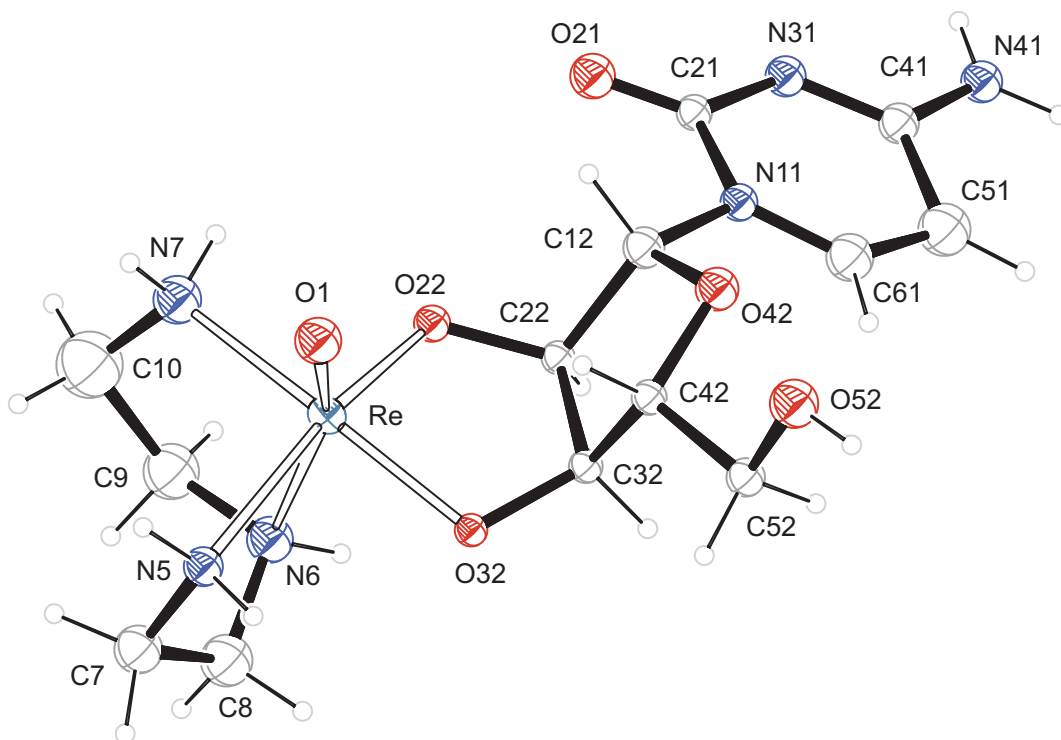


Figure 2.3 ORTEP presentation of **1a** in crystals of $[\text{ReO}(\text{fac-dien})(\text{syn-Cyd}2',3'\text{H}_-)]\text{I}$.

Ellipsoids are drawn at 20 % probability level. Distances [\AA] and angles [$^\circ$]: Re-O1 1.658(16), Re-O22 1.936(12), Re-O32 1.928(12), Re-N5 2.197(15), Re-N6 2.29(2), Re-N7 2.18(2); O1-Re-O22 112.3(6), O1-Re-O32 109.7(7), O1-Re-N5 88.8(7), O1-Re-N6 160.1(7), O1-Re-N7 94.1(8), O22-Re-O32 82.0(5), O22-Re-N5 158.9(6), O22-Re-N6 85.1(6), O22-Re-N7 81.8(6), O32-Re-N5 90.6(6), O32-Re-N6 81.2(6), O32-Re-N7 155.0(7), N5-Re-N6 74.1(6), N5-Re-N7 97.6(7), N6-Re-N7 78.5(7), furanose torsion angle O22-C22-C32-O32: 24(2), puckering parameters^[59] for O42-C12-C22-C32-C42: $Q_2 = 0.30(2)$ \AA , $\phi_2 = 327(4)^\circ$, conformation E_4 . **Distances [\AA] and angles [$^\circ$] of the other molecule **1b** in the asymmetric unit (with same atom numbering):** Re-O1 1.624(17), Re-O22 1.931(14), Re-O32 1.945(13), Re-N5 2.219(15), Re-N6 2.257(16), Re-N7 2.193(17); O1-Re-O22 112.3(7), O1-Re-O32 110.0(7), O1-Re-N5 89.6(7), O1-Re-N6 155.8(7), O1-Re-N7 91.0(7), O22-Re-O32 81.0(5), O22-Re-N5 157.4(6), O22-Re-N6 87.2(6), O22-Re-N7 85.3(6), O32-Re-N5 86.5(5), O32-Re-N6 86.3(5), O32-Re-N7 158.1(6), N5-Re-N6 73.2(6), N5-Re-N7 100.3(6), N6-Re-N7 76.0(6), furanose torsion angle O22-C22-C32-O32: 4(2), puckering parameters^[59] for O42-C12-C22-C32-C42: $Q_2 = 0.25(2)$ \AA , $\phi_2 = 349(5)^\circ$, conformation oT_4 .

The asymmetric unit of the crystals in the monoclinic space group $P2_1$ contains two slightly different molecules (**1a** and **1b**). The charge of these cationic complexes is counterbalanced with two iodide ions. Diethylenetriamine acts as a tridentate chelator in *facial* coordination while the deprotonated ribofuranosyl ligand is connected via

O2' and O3' in *syn*-position respective to the $\{\text{ReO}\}^{3+}$ core forming a five-membered chelate ring. The diols' torsion angles for the two molecules (24° and 4°) are smaller than the corresponding angle in free cytidine^[60] (44.4°) and the *N*-glycosidic torsion angles χ for both molecules (-126.4° and -154.4°) are determining according to the JCBN^[61] an *anti* conformation of the pyrimidine part, like the free form of cytidine (*anti* with -162.6°).

Figure 2.3 shows **1a** of the two molecules in the asymmetric unit. **1b** is very similar, the main difference between them is illustrated in Figure 2.4. The free form of cytidine being in 3T_2 conformation, in this case the ribofuranosyl residues are in E_4 or ${}^{\circ}T_4$ conformation including a different hydrogen bond environment.

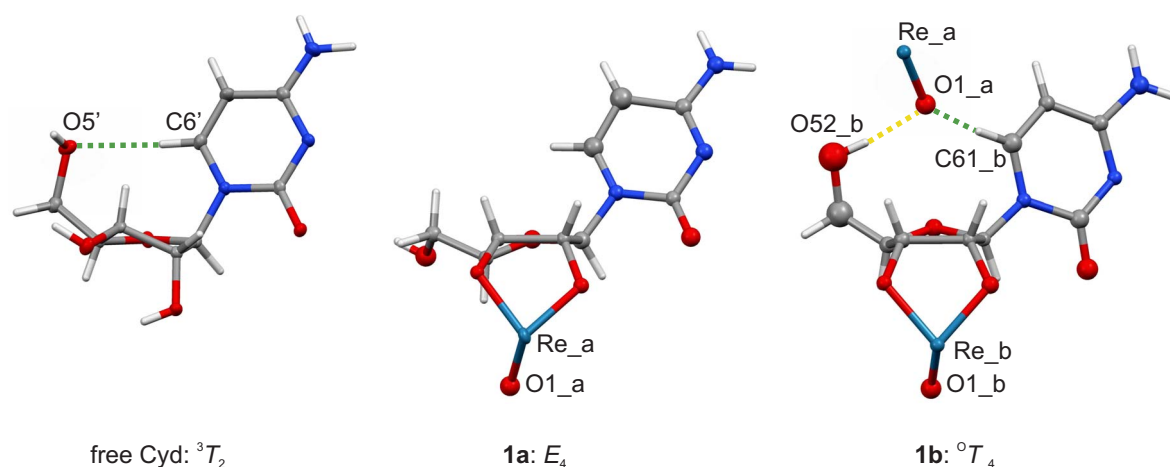


Figure 2.4 MERCURY presentation of the furanose rings in cytidine, **1a** and **1b**. The atoms of the dien ligand are not shown. Yellow and green dashed lines: classical hydrogen bonds and weak interactions of the type C-H \cdots O.

Another difference to the free form is the absence of an intramolecular interaction of the type C-H \cdots O from the pyrimidine's H61 to O52 of the ribose part. In lieu of this, an intermolecular bonding is observed: there is a hydrogen bond and a C-H \cdots O interaction from **1b** to the $\{\text{ReO}\}^{3+}$ core of **1a**. The distances and angles for these interactions are listed in Table 2.1 including the values of the intramolecular C-H \cdots O interaction in free cytidine. All the remaining hydrogen bonds are illustrated in Figure 2.5. Along $[\bar{1}00]$ there are iodide-connected sheets of hydrogen-bond-connected chains of complex molecules. These chains are built of the two different molecules of the asymmetric unit in two orientations. Each chain consists of one sort of molecule connected to each other with two hydrogen bonds. The above-mentioned C-H \cdots O contact from the pyrimidine's C6-H6 of **1b** to O1 of **1a** completes the hydrogen bond environment of the molecules: together with the hydrogen bond from the ribofuranose's O52 to O1, the **1a** chain is cross-linked to the **1b** chain.

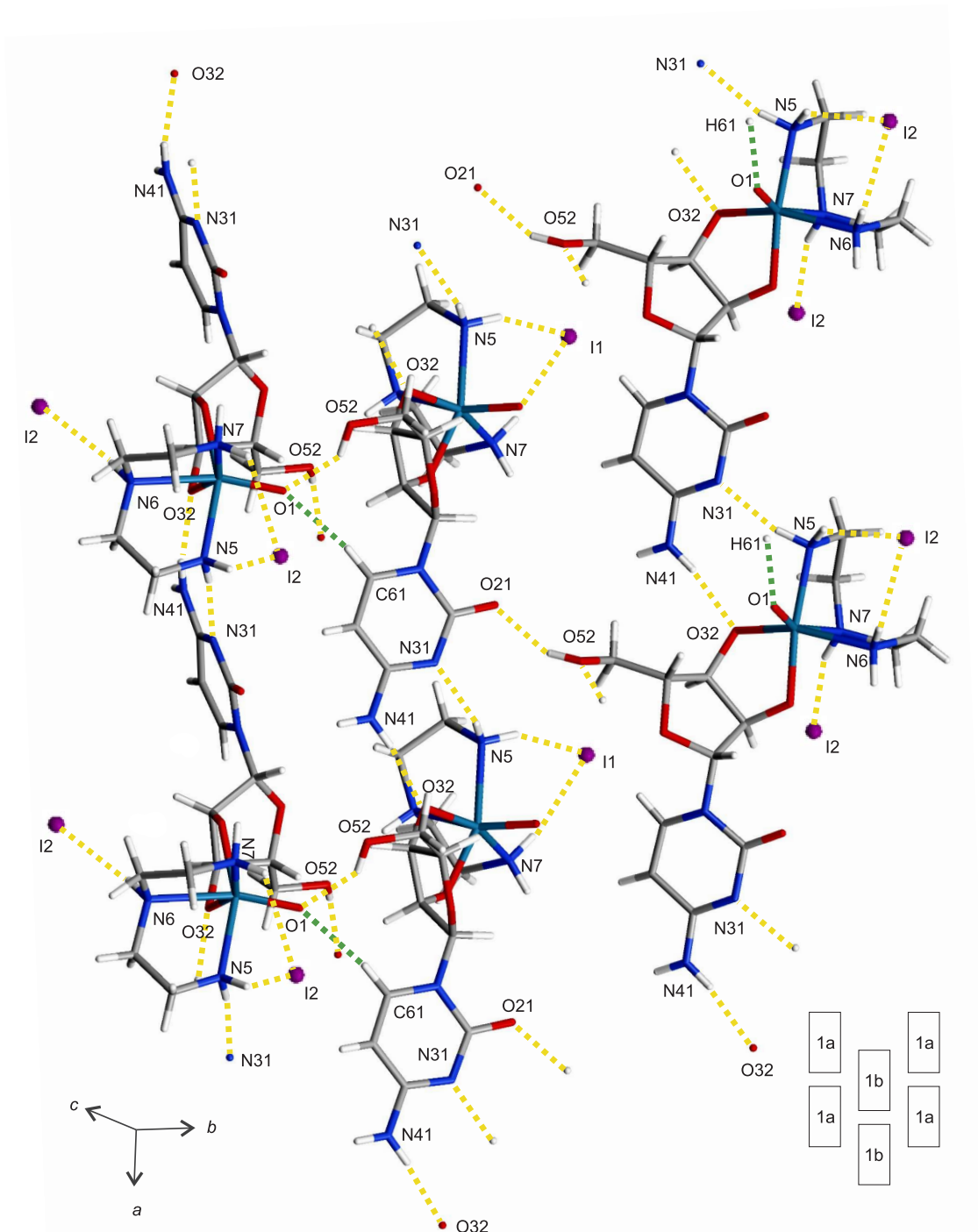


Figure 2.5 MERCURY presentation of hydrogen bonds (yellow dashed lines) and C-H...O contacts (green dashed lines) in **1**. The rectangles with "1a" and "1b" refer to the two independent molecules in the asymmetric unit. For symmetry codes see Table 2.1.

2 Results

Table 2.1 Distances [\AA] and angles [$^\circ$] of hydrogen bonds in **1**. As there are two molecules in the asymmetric unit, the following suffixes are attached to the atoms' names: "_a" and "_b". I1 and I2 are from the anionic part of the structure. Values without standard deviation are related to hydrogen atoms at calculated positions. For atom numbering see Figure 2.3. In the last row the values of an intramolecular C-H \cdots O interaction in a published structure of free cytidine are listed^[60]. D: donor, A: acceptor, x : difference of (H \cdots A) and the sum of the van-der-Waals radii^[62].

D	H	A	D \cdots A	D-H	H \cdots A	x	D-H \cdots A
O52_b	H852_b	O1_a	3.18(5)	0.84	2.47	-0.25	143
N41_b	H741_b	O32_b ⁱ	2.85(2)	0.88	1.97	-0.75	174
N5_b	H751_b	N31_b ⁱⁱ	3.08(2)	0.92	2.23	-0.52	152
N5_b	H752_b	I1 ⁱⁱⁱ	3.746(17)	0.92	3.00	-0.18	140
N6_b	H76_b	O52_a	2.99(2)	0.93	2.20	-0.52	142
N7_b	H771_b	I1 ⁱⁱⁱ	3.595(17)	0.92	2.69	-0.49	167
O52_a	H852_a	O21_b ^{iv}	2.69(2)	0.84	1.92	-0.81	154
N41_a	H741_a	O32_a ⁱⁱ	2.97(2)	0.88	2.11	-0.61	167
N5_a	H751_a	N31_a ⁱ	2.98(2)	0.92	2.08	-0.67	166
N5_a	H752_a	I2 ^v	3.77(2)	0.92	2.96	-0.22	148
N6_a	H76_a	I2	3.50(2)	0.93	2.60	-0.58	162
N7_a	H771_a	I2 ^v	3.55(2)	0.92	2.80	-0.38	139
C61_b	H61_b	O1_a	3.18(3)	0.95	2.28	-0.44	157
C6'	H6'	O5'	3.246(5)	0.94(3)	2.35(3)	-0.38	161(3)

Symmetry codes: ⁱ $1 + x, y, z$; ⁱⁱ $1 + x, y, z$; ⁱⁱⁱ $2 - x, \frac{1}{2} + y, -z$; ^{iv} $1 - x, -\frac{1}{2} + y, -z$; ^v $1 - x, \frac{1}{2} + y, -1 - z$.

According to NMR spectroscopy, there should not be a difference between the signals of the very similar molecules of **1a** and **1b** of the XRD study. *Syn/anti* isomerism has a much greater effect. Both diastereomeric forms should be present in solution (see Figure 2.6), but only one major species was observed in spectra of the crude reaction mixture as well as in solutions of the redissolved lilac compound. Most of the signals of the minor species were below the limit of detection for ^{13}C NMR. But ^1H NMR experiments showed a ratio of 90:10 for major to minor isomer. The free form of the nucleoside was not detected.

Table 2.2 presents the ^{13}C NMR data of the major species from the redissolved lilac compound in MeOH- d_4 . The signals of C2' and C3' are moved on the NMR scale by +28 ppm compared with the free form of cytidine. This coordination-induced shift (CIS, $\delta_{\text{complex}} - \delta_{\text{freeligand}}$) shows a connection of the nucleoside to the rhenium center via O2' and O3'. Contrariwise, the small CIS of C5' confirms that O5' is not metalated. Except for the signals of C2' and C3', the influence of the rhenium core on most

2 Results

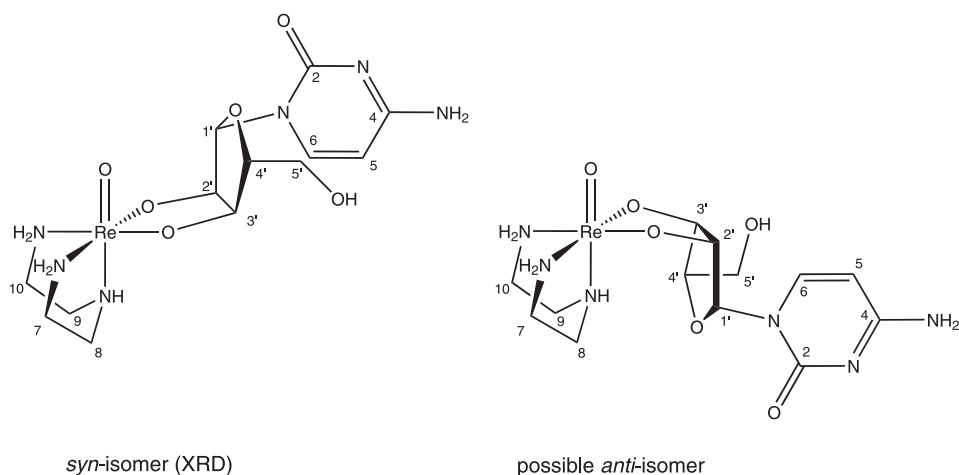


Figure 2.6 Scheme of the diastereomeric forms of **1** and atom numbering used in the ^{13}C NMR study according to the recommendations of the JCBN^[61]. XRD: result of the structure determination.

of the signals is only small. Therefore the assignment of the signals is possible by comparing with the reported data of the free form^[63]. But due to the large CIS of up to +28 ppm an exact assignment of C2' and C3' is only possible by 2D NMR and ^1H NMR experiments. In Table 2.3 the $^3J_{\text{HH}}$ couplings of the protons of **1** are listed. The identical values for the couplings attest to the correct assignment. A cross-check with the H-C-C-H angles of the X-ray structure determination is possible by the *Karplus* relation, adopted by *Haasnoot et al.*^[64]. Obviously the structure of the solid state is similar to the species in solution. The other ligand in this complex, dien, loses symmetry caused by the distorted octahedral coordination. Four signals, instead of two for the free form, are observed in the ^{13}C NMR spectra (Table 2.2). Only small CIS values are observed, despite the fact that the distance to the rhenium center is similar to C2' and C3' bearing a much larger CIS.

Table 2.2 ^{13}C NMR chemical shifts (in ppm) of **1** in MeOH- d_4 (101 MHz, 25 °C) and comparison with the free ligands under the same conditions. The signal of the deuterated solvent ($\delta = 49.00$ ppm) was used as an internal secondary reference^[65] for the chemical shift. For atom numbering see Figure 2.6. $\Delta\delta$ values indicating a diolate coordination are in boldface. Assignment of free cytidine according to literature^[63].

		C7/C10	C8/C9							
dien	δ	40.40	49.84							
1	δ	44.66, 44.53	50.60, 50.42							
	$\Delta\delta$	4.23, 4.13	0.76, 0.58							
		C1'	C2'	C3'	C4'	C5'	C2	C4	C5	C6
Cyd	δ	91.93	75.89	70.63	85.49	61.87	158.36	167.47	96.29	142.93
1	δ	93.42	104.18	99.02	86.59	62.94	158.22	167.47	96.75	143.58
	$\Delta\delta$	1.49	28.29	28.39	1.10	1.07	-0.14	0.00	0.46	0.65

Table 2.3 ^1H NMR chemical shifts and $^3J_{\text{HH}}$ coupling (in Hz) of **1** in MeOH- d_4 (400 MHz, 25 °C) and comparison with calculated values. The signal of the deuterated solvent ($\delta = 3.31$ ppm) was used as an internal secondary reference^[65] for the chemical shift. For atom numbering see Figure 2.6. Assignment was controlled with HMQC and HMBC experiments. The torsion angles H-C-C-H for the calculated^[64] values derive from **1a** and **1b** of the structure determination.

		H1'	H2'	H3'	H4'/H5'
1	δ	5.71	5.26	5.30	3.79–3.86 ^a
	multipl.	d	dd	dd	m
	$^3J_{\text{HH}}$	4.0	4.0, 6.6	6.6, 4.8	a
		$^3J(\text{H1}, \text{H2})$	$^3J(\text{H2}, \text{H3})$	$^3J(\text{H3}, \text{H4})$	$^3J(\text{H4}, \text{H5ab})$
calc. 1a		4.7	6.7	6.5	0.5, 5.2
calc. 1b		3.2	6.0	7.3	11.0, 2.5

^a signal overlap

2.1.2 The reaction of $[\text{ReO}_2(\text{PPh}_3)_2\text{I}]$ with dien and uridine

A modification of the preparation in the previous section leads to a new compound. Uridine, another pyrimidine nucleoside, reacts with the precursor $[\text{ReO}_2(\text{PPh}_3)_2\text{I}]$ and diethylenetriamine in methanol to give a lilac raw compound. Crystals were obtained with a different anion: $[\text{ReO}(\text{fac-dien})(\text{syn-Urd}2',3'\text{H}_-)]\text{BPh}_4 \cdot \text{MeOH}$ (**2**) was recrystallized from methanol after addition of equimolar amounts of sodium tetraphenylborate.

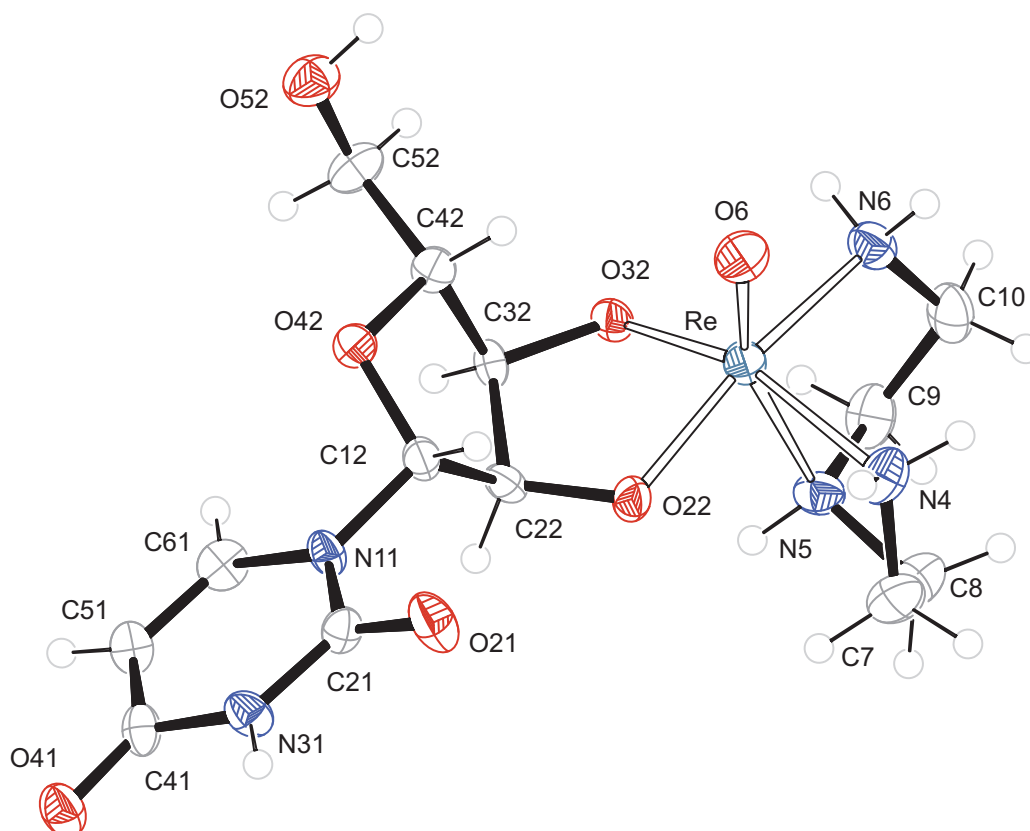


Figure 2.7 ORTEP presentation of **2** in crystals of $[\text{ReO}(\text{fac-dien})(\text{syn-Urd}2',3'\text{H}_-)]\text{BPh}_4 \cdot \text{MeOH}$. Ellipsoids are drawn at 50 % probability level. Distances [\AA] and angles [$^\circ$]: Re-O6 1.684(4), Re-O22 1.936(4), Re-O32 1.965(4), Re-N4 2.159(6), Re-N5 2.279(5), Re-N6 2.189(5); O6-Re-O22 109.1(2), O6-Re-O32 108.62(19), O6-Re-N4 92.5(2), O6-Re-N5 160.7(2), O6-Re-N6 91.8(2), O22-Re-O32 82.47(17), O22-Re-N4 84.7(2), O22-Re-N5 85.08(18), O22-Re-N6 158.89(18), O32-Re-N4 158.0(2), O32-Re-N5 85.69(19), O32-Re-N6 87.87(18), N4-Re-N5 75.5(2), N4-Re-N6 98.1(2), N5-Re-N6 75.47(18), furanose torsion angle O22-C22-C32-O32: 15.9(7), puckering parameters^[59] for O42-C12-C22-C32-C42: $Q_2 = 0.364(6)$ \AA , $\phi_2 = 335.1(10)^\circ$, conformation oT_4 .

The asymmetric unit in the orthorhombic space group $P2_12_12_1$ contains an anionic part (one molecule of tetraphenylborate), a cationic part (one molecule of the complex with rhenium) and a neutral part (one molecule of methanol). Figure 2.7 shows the

cationic part. Diethylenetriamine forms a tridentate chelator in *facial* coordination and uridine is connected in *syn*-position with the deprotonated hydroxy functions (O2' and O3') as a five-membered-ring chelator. Due to this chelate, the torsion angle O2'-C2'-C3'-O3' is smaller (15.9°) than in free uridine (46.7° and 52.1°)^[66]. In free uridine the furanose ring is in ³T₂ or ³E conformation whereas in this compound it is in ⁰T₄ conformation. The conformation about the *N*-glycosidic bond is *anti* (torsion angle $\chi = -133.1^\circ$) and not far from the one of free uridine (-153.0° and -164.4°).

With their classical donor and acceptor functions like N(H) or O(H), the dien and uridine ligands of the cationic part build sheets of polar cationic areas in the crystal, that are connected with typical hydrogen bonds (Table 2.4). The anion tetraphenylborate fills up the space between these sheets along the *ab* plane. These charge-separated areas are also visible in the packing diagram of the crystal structure (Figure 6.2 on page 187). In Figure 2.8 weak interactions of tetraphenylborate with the dien ligands are illustrated, as well as the hydrogen bonds of the polar section. Compared with the crystal structure of free uridine^[66] there is a similar intermolecular interaction of the type C-H...O from the pyrimidine's C51-H51 as donor (see Table 2.4). But the acceptors differ: O41 of the neighboring pyrimidine part instead of O4 of the neighboring ribosyl moiety.

Table 2.4 Distances [Å] and angles [°] of hydrogen bonds in 2. O99 is affiliated to methanol. In the last row the values of an intermolecular C-H...O interaction in free uridine are listed^[66]. D: donor, A: acceptor, *x*: difference of (H...A) and the sum of the van-der-Waals radii^[62].

D	H	A	D...A	D-H	H...A	<i>x</i>	D-H...A
N31	H31	O32 ⁱ	2.890(6)	0.88	2.01	-0.71	177
N5	H75	O99	2.875(10)	0.93	1.98	-0.74	162
N6	H761	O21 ⁱⁱ	2.922(7)	0.92	2.03	-0.69	164
N6	H762	O52 ⁱⁱⁱ	2.898(7)	0.92	2.06	-0.66	150
O52	H852	O41 ^{iv}	2.868(6)	0.84	2.17	-0.55	141
C7	H72	Cg1 ^v	3.444(8)	0.99	2.52	-0.12 ^a	156
N4	H741	C91 ^{vi}	3.377(10)	0.92	2.52	-0.38	155
N4	H742	Cg2 ^v	3.160(7)	0.92	2.31	-0.41 ^b	154
O99	H899	Cg3 ^{vii}	3.284(7)	0.84	2.44	-0.16 ^c	178
C51	H51	O42 ^{viii}	3.364(8)	0.95	2.53	-0.19	147
C5	H5	O4	3.258	0.95	2.42	-0.30	150

Symmetry codes: ⁱ $-1 + x, y, z$; ⁱⁱ $1 + x, y, z$; ⁱⁱⁱ $2 - x, -\frac{1}{2} + y, \frac{1}{2} - z$; ^{iv} $1 - x, -\frac{1}{2} + y, \frac{1}{2} - z$; ^v $x, -1 + y, z$; ^{vi} $1 + x, -1 + y, z$; ^{vii} x, y, z ; ^{viii} $1 - x, \frac{1}{2} + y, \frac{1}{2} - z$.

Calculated centroids Cg1: C82–C87, Cg2: C70–C75, Cg3: C76–C81. ^a contact of H72 to C87 of Cg1, ^b contact of H742 to C72 of Cg2, ^c contact of H899 to C79 of Cg3.

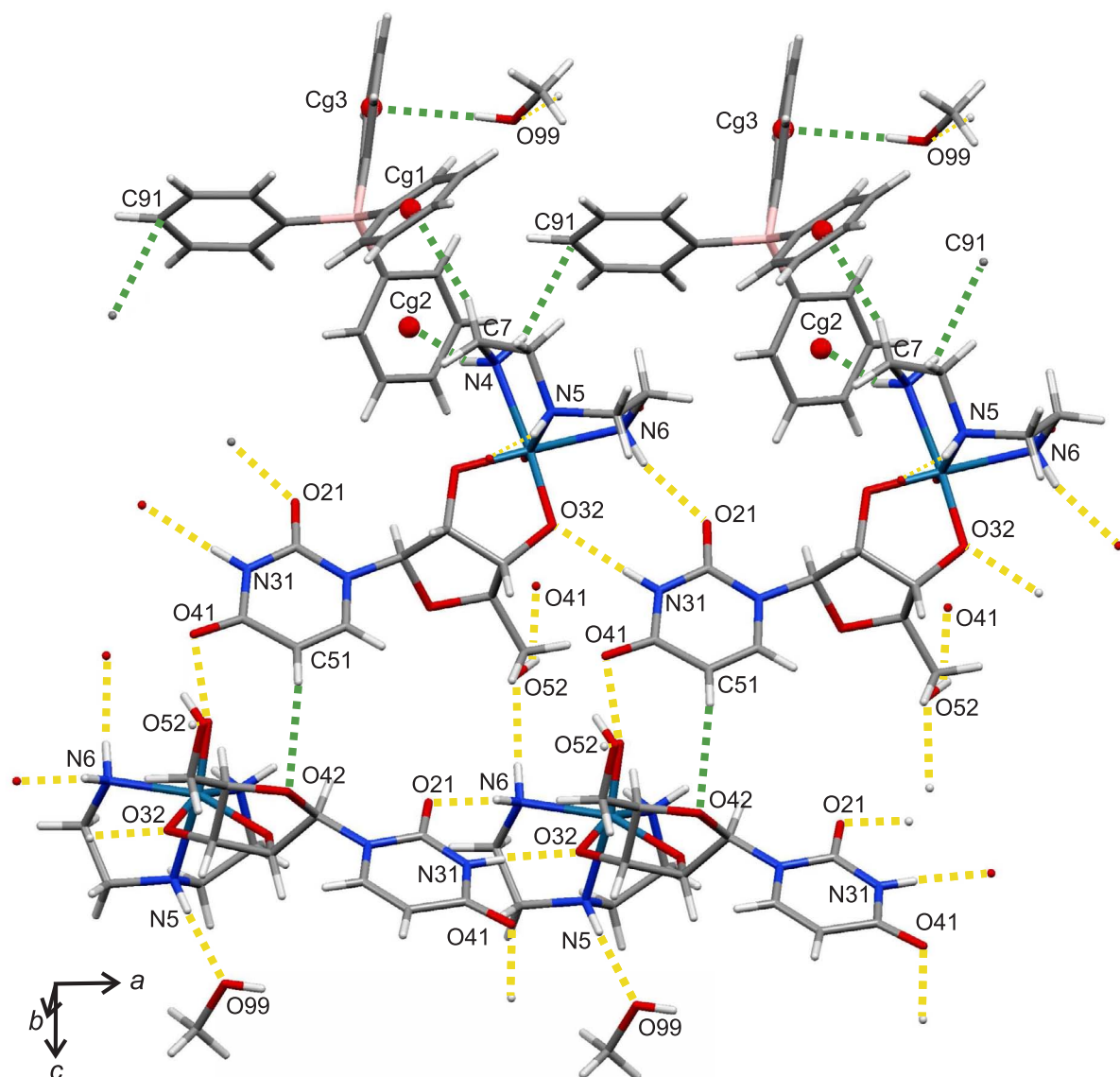


Figure 2.8 MERCURY presentation of hydrogen bonds (yellow dashed lines) and weak interactions (green dashed lines) in **2** forming sheets along the *ab* plane. For symmetry codes and centroid definition see Table 2.4.

The ^{13}C NMR spectrum of the redissolved lilac raw compound shows mainly signals of one of the two possible isomers of this compound (Figure 2.9), while the other one seems to be below the detection limit. Integration of ^1H NMR signals showed a ratio of ca. 90:10. In Table 2.5 signals of the major isomer of a solution of **2** in D_2O are listed. Most of them are similar to the signals of free uridine^[67]. Depending on the distance to the rhenium center they are more or less shifted, except for the signals of C2' and C3'. Their large CIS of up to 28.10 ppm indicates a chelate via O2' and O3' to the metal. The signals of the other chelating ligand, dien, are shifted up

2 Results

to 3.1 ppm. Table 2.6 shows the $^3J_{\text{HH}}$ couplings of the protons of **2** and calculated couplings according to the *Karplus* relation, adopted by *Haasnoot et al.*^[64]. The values for the couplings around the diol group attest a similar conformation in solution compared with the structure determination.

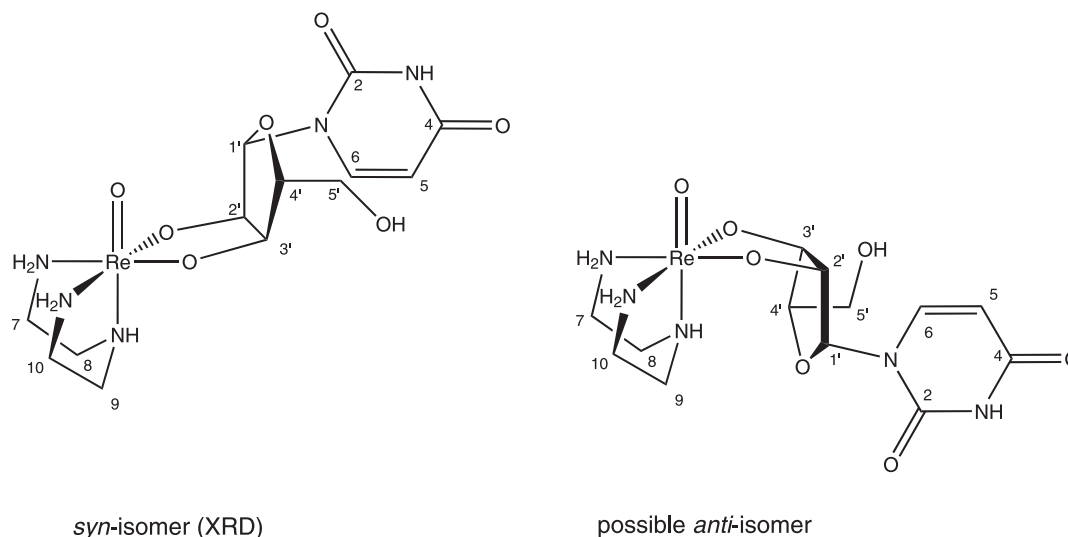


Figure 2.9 Scheme of the diastereomeric forms of **2** and atom numbering used in the ^{13}C NMR study according to the recommendations of the JCBN^[61]. XRD: result of the structure determination.

Table 2.5 ^{13}C NMR chemical shifts (in ppm) of **2** in D_2O (101 MHz, 25 °C) and comparison with the free ligands under the same conditions. The signal of a drop of methanol ($\delta = 49.50$ ppm in D_2O) was used as an internal secondary reference^[65] for the chemical shift. For atom numbering see Figure 2.9. $\Delta\delta$ values indicating a diolate coordination are in boldface. Assignment of free uridine according to literature^[67].

		C7/C10	C8/C9							
dien	δ	40.89	50.06							
2	δ	44.09, 44.01	50.04							
	$\Delta\delta$	3.20, 3.12	-0.02							
		C1'	C2'	C3'	C4'	C5'	C2	C4	C5	C6
Urd	δ	89.98	74.27	70.03	84.82	61.33	152.17	166.64	102.88	142.44
2	δ	91.66	101.64	98.13	85.93	62.19	152.25	166.82	103.28	143.28
	$\Delta\delta$	1.68	27.37	28.10	1.11	0.86	0.08	0.18	0.40	0.84

Table 2.6 ^1H NMR chemical shifts and $^3J_{\text{HH}}$ coupling (in Hz) of **2** in D_2O (400 MHz, 25 °C) and comparison with calculated values. The signal of the deuterated solvent ($\delta = 4.79$ ppm) was used as an internal secondary reference^[65] for the chemical shift. For atom numbering see Figure 2.9. Assignment was controlled with HMQC experiments. The torsion angles H-C-C-H for the calculated^[64] values derive from the result of the structure determination of **2**.

		H1'	H2'	H3'	H4'	H5'
2	δ	5.73	5.38	5.31	3.88	3.97
	multipl.	d	dd	dd	dt	d
	$^3J_{\text{HH}}$	4.4	4.4, 6.6	6.6, 5.5	5.5, 3.3	3.3
		$^3J(\text{H1}, \text{H2})$	$^3J(\text{H2}, \text{H3})$	$^3J(\text{H3}, \text{H4})$	$^3J(\text{H4}, \text{H5ab})$	
calc.		3.8	6.3	7.5	2.5, 11.0	

2.1.3 The reaction of $[\text{ReOCl}_3(\text{PPh}_3)_2]$ with dien and other nucleosides

The following pyrimidine- and purine-type nucleosides were tested with the less reactive precursor *trans*-trichlorido-oxido-bis(triphenylphosphane)-rhenium(V): cytidine, uridine, adenosine, guanosine and inosine (Figure 2.10). Three equivalents of triethylamine were added to the mixtures of one equivalent of the precursor and dien and two equivalents of the nucleosides in methanol. They were stirred for three hours at 60 °C. Although no crystals were obtained, the spectra of the crude reaction mixtures in methanol were promising (Figure 2.11). The signals in the spectra of the reactions with uridine and cytidine showing a coordination to the metal (marked orange) are identical to the spectra of redissolved crystals of **1** and **2** from the previous chapters. Partially (at small intensities, not tagged in the figure), the spectra show a second signal set indicating *syn/anti* isomerism. Table 2.7 shows the signals of the major isomers of the mixtures with the purine nucleosides adenosine, guanosin and inosine. The signals of C2' and C3' are shifted up to 28 ppm compared with the free nucleosides. This indicates a coordination via O2' and O3' to the rhenium center.

2 Results

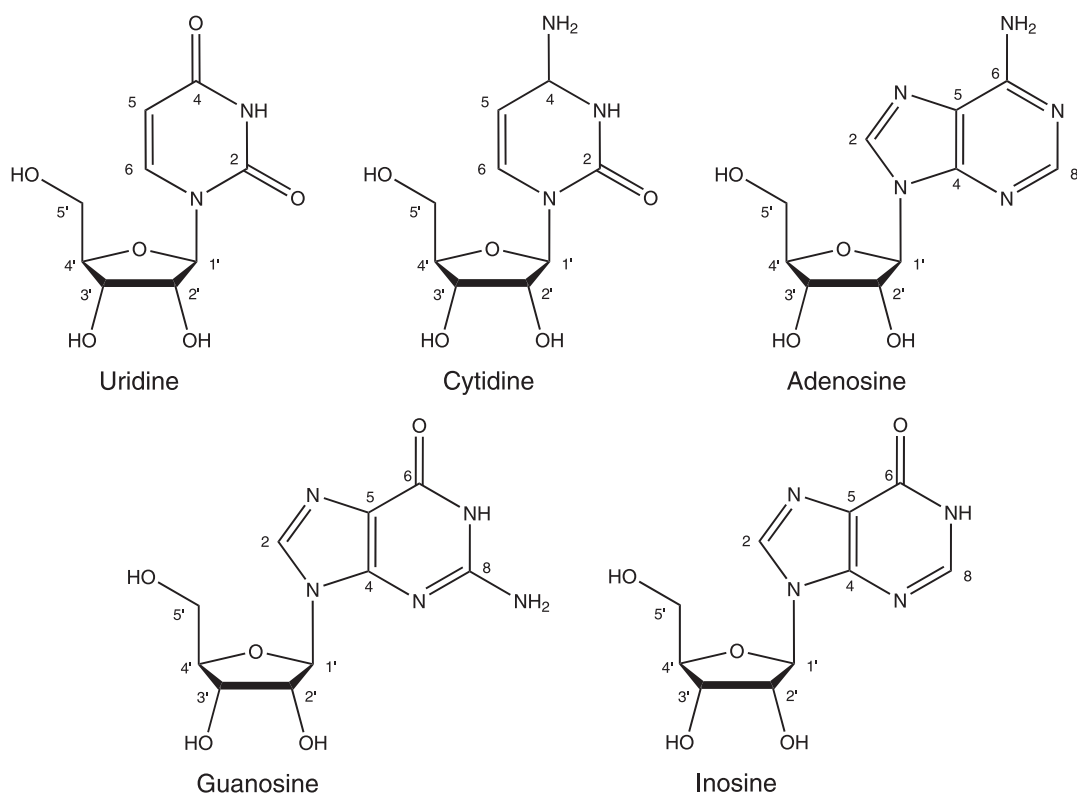


Figure 2.10 Scheme of the nucleosides used in this work and atom numbering for the ^{13}C NMR study according to the recommendations of the JCBN^[61].

Table 2.7 ^{13}C NMR chemical shifts (in ppm) of non-crystalline compounds of adenosine, guanosine, inosine with dien in MeOH-d_4 and comparison with the free ligands under the same conditions. The signal of the deuterated solvent ($\delta = 49.00$ ppm) was used as an internal secondary reference^[65] for the chemical shift. $\Delta\delta$ values indicating a diolate coordination are in boldface. Assignment according to literature: adenosine^[68], guanosine^[69], inosine^[69].

Compound with adenosine										
adenosine	C1'	C2'	C3'	C4'	C5'	C2	C4	C5	C6	C8
free δ	90.88	75.34	72.47	87.93	63.32	153.30	149.77	120.77	157.20	141.80
cmp. δ	91.78	102.80	100.85	88.20	63.72	153.48	149.86	120.45	157.06	141.51
$\Delta\delta$	0.90	27.46	28.38	0.27	0.40	0.18	0.09	-0.32	-0.14	-0.29
Compound with guanosine										
guanosine	C1'	C2'	C3'	C4'	C5'	C2	C4	C5	C6	C8
free δ	88.65	74.44	71.40	86.23	62.26	154.68	152.00	117.25	159.65	138.67
cmp. δ	89.87	101.47	99.20	86.79	62.82	154.78	152.09	117.25	159.69	138.76
$\Delta\delta$	1.22	27.03	27.80	0.56	0.56	0.10	0.09	0.00	0.04	0.09
Compound with inosine										
inosine	C1'	C2'	C3'	C4'	C5'	C2	C4	C5	C6	C8
free δ	90.44	76.08	72.06	87.45	62.94	146.82	149.49	125.80	158.75	140.85
cmp. δ	91.57	103.65	100.44	87.93	63.55	146.87	149.53	125.61	158.75	140.85
$\Delta\delta$	1.13	27.57	28.38	0.48	0.61	0.05	0.04	-0.19	0.00	0.00

2 Results

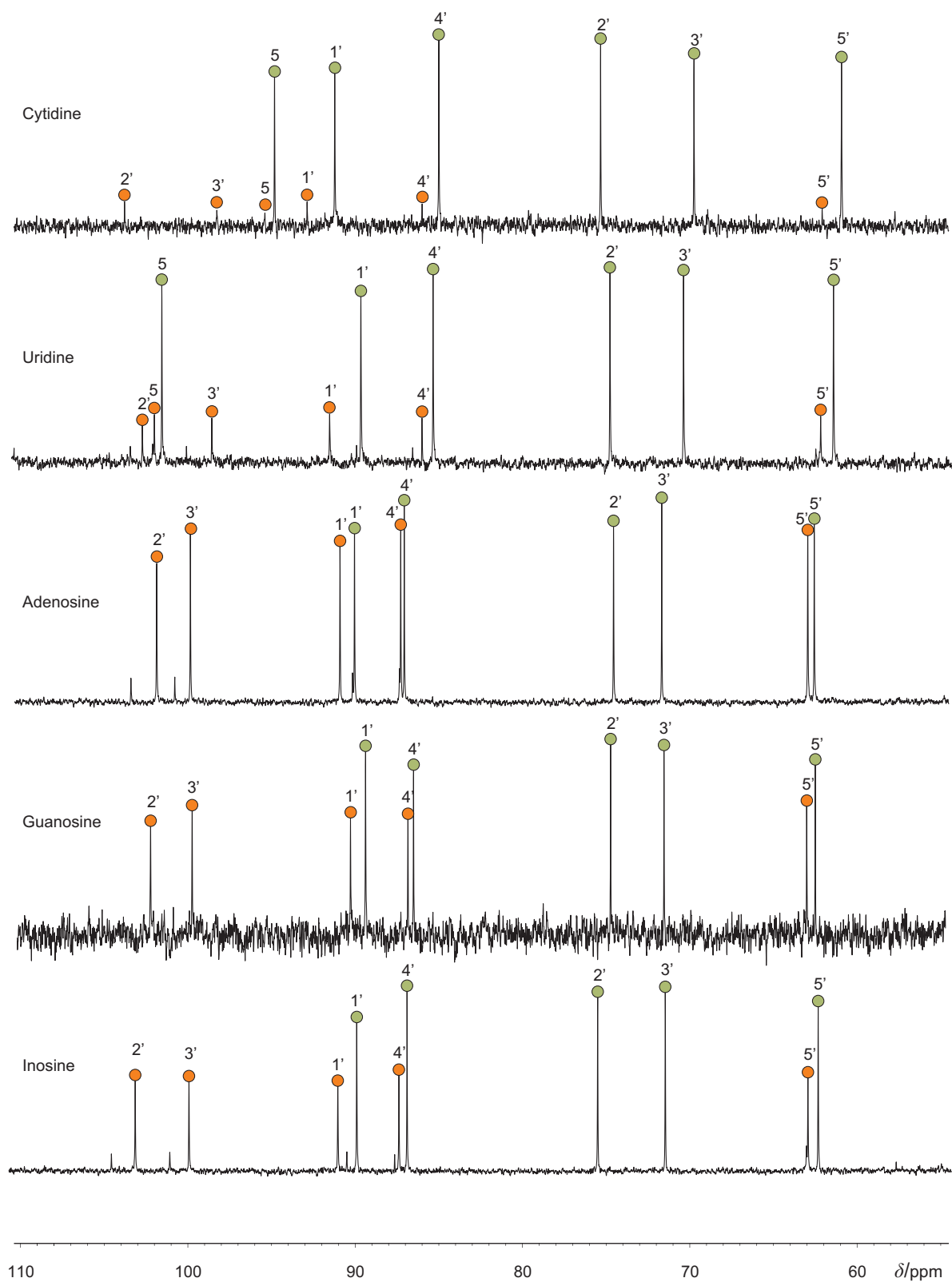


Figure 2.11 ^{13}C NMR spectra of crude reaction mixtures with the nucleosides cytidine, uridine, adenosine, guanosine and inosine in methanol. Green: free nucleoside, orange: complex with oxidorhenium and dien. For atom numbering see Figure 2.10.

2.1.4 The reaction of $[\text{Re}(\text{NPh})\text{Cl}_3(\text{PPh}_3)_2]$ with dien and anhydroerythritol

2.1.4.1 The *syn*-isomer

In this section a different rhenium(V) precursor was chosen. The oxygen atom of the $\{\text{ReO}\}^{3+}$ core was replaced by the isoelectronic motif phenylimine giving the phenylimidorhenium core. First, the reaction with a simple diol was investigated. Harsher conditions were necessary: the rhenium(V) precursor $[\text{Re}(\text{NPh})\text{Cl}_3(\text{PPh}_3)_2]$ reacted with diethylenetriamine and anhydroerythritol in methanol only after addition of triethylamine at 50 °C to give a green solution. By evaporation and addition of equimolar amounts of sodium tetraphenylborate, the complex $[\text{Re}(\text{NPh})(\text{fac-dien})\text{-}(\text{syn-AnErytH}_{-2})]\text{BPh}_4$ (**3**) was recrystallized (Figure 2.12).

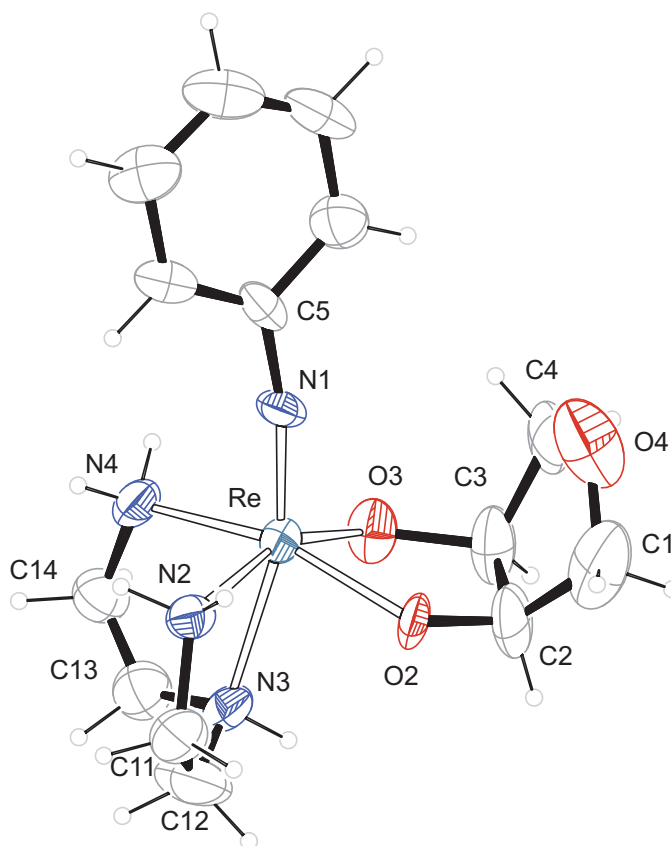


Figure 2.12 ORTEP presentation of **3** in crystals of $[\text{Re}(\text{NPh})(\text{fac-dien})(\text{syn-AnErytH}_{-2})]\text{BPh}_4$. Ellipsoids are drawn at 20 % probability level. Distances [Å] and angles [°]: Re-O2 1.961(6), Re-O3 1.937(8), Re-N1 1.720(8), Re-N2 2.075(9), Re-N3 2.239(10), Re-N4 2.144(10); O2-Re-O3 82.3(3), O2-Re-N1 107.0(3), O2-Re-N2 86.8(3), O2-Re-N3 85.6(3), O2-Re-N4 159.2(3), O3-Re-N1 107.1(4), O3-Re-N2 157.4(3), O3-Re-N3 84.3(4), O3-Re-N4 87.7(3), N1-Re-N2 95.0(4), N1-Re-N3 163.8(4), N1-Re-N4 93.3(4), N2-Re-N3 75.1(4), N2-Re-N4 95.9(4), N3-Re-N4 75.3(4), Re-N1-C5 170.6(8), diol torsion angle O2-C2-C3-O3: $-20.8(18)$, puckering parameters^[59] for O4-C1-C2-C3-C4: $Q_2 = 0.32(2)$ Å, $\phi_2 = 34(4)^\circ$, conformation E_1 .

2 Results

The green crystals in the monoclinic space group $P2_1/n$ have four formula units in the unit cell and one in the asymmetric unit with an anionic (tetraphenylborate) and a cationic part. Figure 2.12 shows the cationic part, a phenylimidorhenium(V) complex in distorted octahedral coordination. The phenylimidorhenium unit is not exactly linear. Similarly to the precursor compound (172.6°)^[70] the angle of Re-N-C5 is diminished to $170.6(8)^\circ$. The tridentate chelator dien coordinates in *facial* binding mode and the diol anhydroerythritol gives a five-membered chelate in *syn*-position respective to the phenylimido ligand. The furanose ring adopts an envelope conformation on C1 and the torsion angle O2-C2-C3-O3 (-20.8°) is similar to a structure based on the oxidorhenium core (Ofberger^[23]: 29.7°).

Only one classical hydrogen bond can be found in **3**. It is of the type N-H \cdots O (from N2 of dien to O2 of the diol) and connects two molecules of **3**. In addition there is a weak interaction of the type C-H \cdots N (from C11 of dien to N1 of the phenylimido group) assisting the connection between these molecules. Figure 2.13 illustrates the classical and non-classical hydrogen bonds between these dimeric units including other contacts with the surrounding phenyl groups listed in Table 2.8.

Table 2.8 Distances [\AA] and angles [$^\circ$] of hydrogen bonds in **3**. Values without standard deviation are related to hydrogen atoms at calculated positions. For atom numbering see Figure 2.12. D: donor, A: acceptor, x : difference of (H \cdots A) and the sum of the van-der-Waals radii^[62].

D	H	A	D \cdots A	D-H	H \cdots A	x	D-H \cdots A
N2	H721	O2 ⁱ	2.856(11)	0.90	2.03	-0.68	151
C11	H111	N1 ⁱ	3.493(17)	0.97	2.58	-0.17	156
N3	H73	C36 ⁱⁱ	3.375(17)	0.91	2.54	-0.36	154
N4	H742	Cg ⁱⁱⁱ	3.177(10)	0.90	2.39	-0.35 ^a	146

Symmetry code: ⁱ $1 - x, -y, 1 - z$; ⁱⁱ $-\frac{1}{2} + x, \frac{1}{2} - y, \frac{1}{2} + z$; ⁱⁱⁱ x, y, z .
 Calculated centroid Cg: C15-C20. ^a contact of H742 to C18 of Cg.

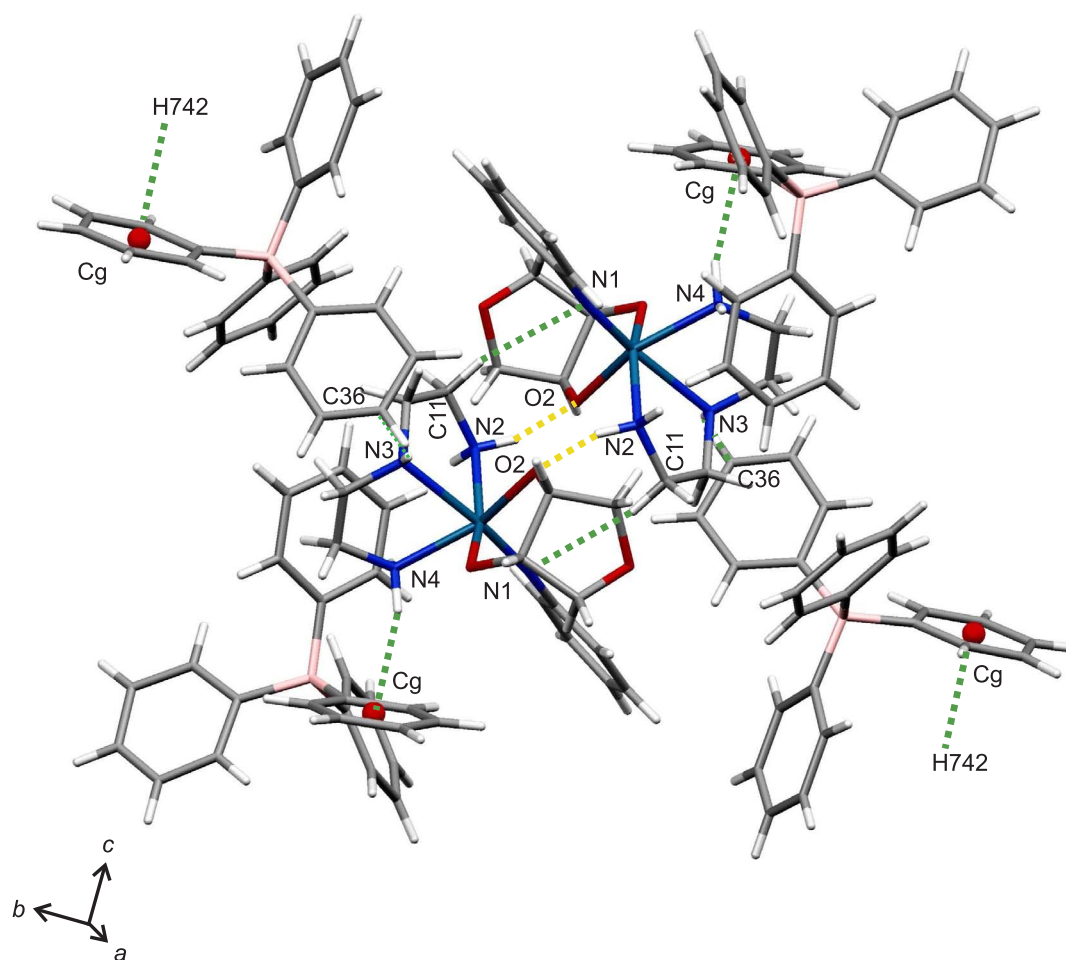


Figure 2.13 MERCURY presentation of hydrogen bonds (yellow dashed lines) and weak interactions (green dashed lines) in **3** forming units of two molecules.

2 Results

This structure determination shows the *syn*-isomer, but a hint to another isomer (Figure 2.14) can be found in the ^{13}C NMR spectrum of the reaction mixture (Figure 2.15). With different settings it was possible to obtain the other isomer with anhydroerythritol in *anti*-position (see next paragraph).

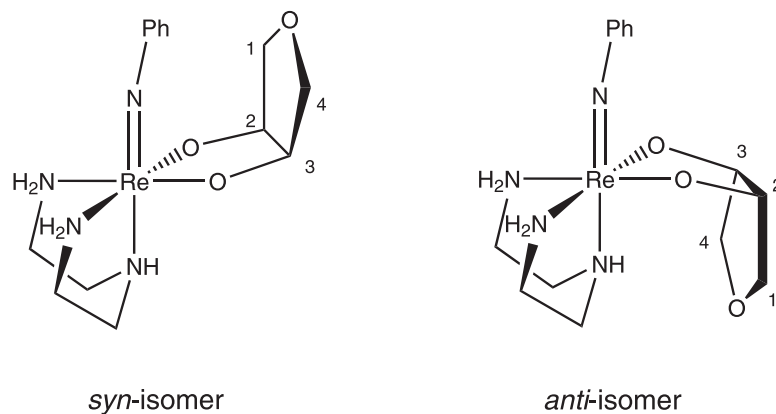


Figure 2.14 Scheme of possible isomers with anhydroerythritol. Left: *syn*-isomer, Right: *anti*-isomer.

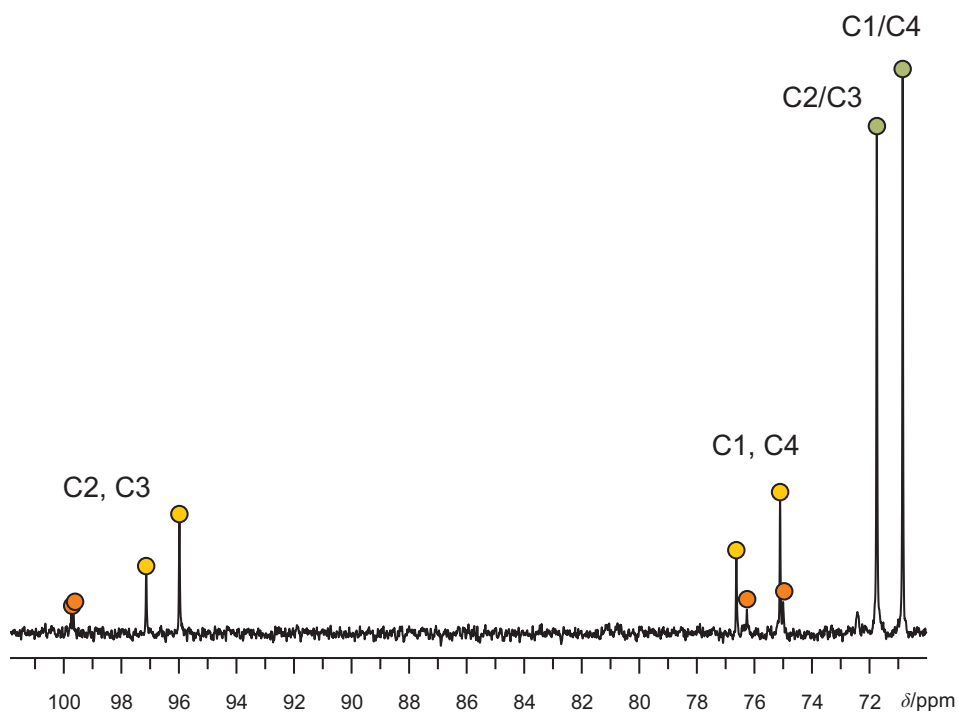


Figure 2.15 ^{13}C NMR spectrum of the reaction mixture of **3**. Green: free anhydroerythritol, yellow: major isomer, orange: minor isomer. For atom numbering see Figure 2.14.

2.1.4.2 The *anti*-isomer

In order to crystallize the *anti*-isomer of **3**, the following mixed crystal approach was chosen. The two rhenium(V) precursors $[\text{Re}(\text{NPh})\text{Cl}_3(\text{PPh}_3)_2]$ and $[\text{ReOCl}_3(\text{PPh}_3)_2]$ were heated with diethylenetriamine, anhydroerythritol and triethylamine in methanol. From this mixture, crystals in the monoclinic space group $P2_1/c$ were obtained.

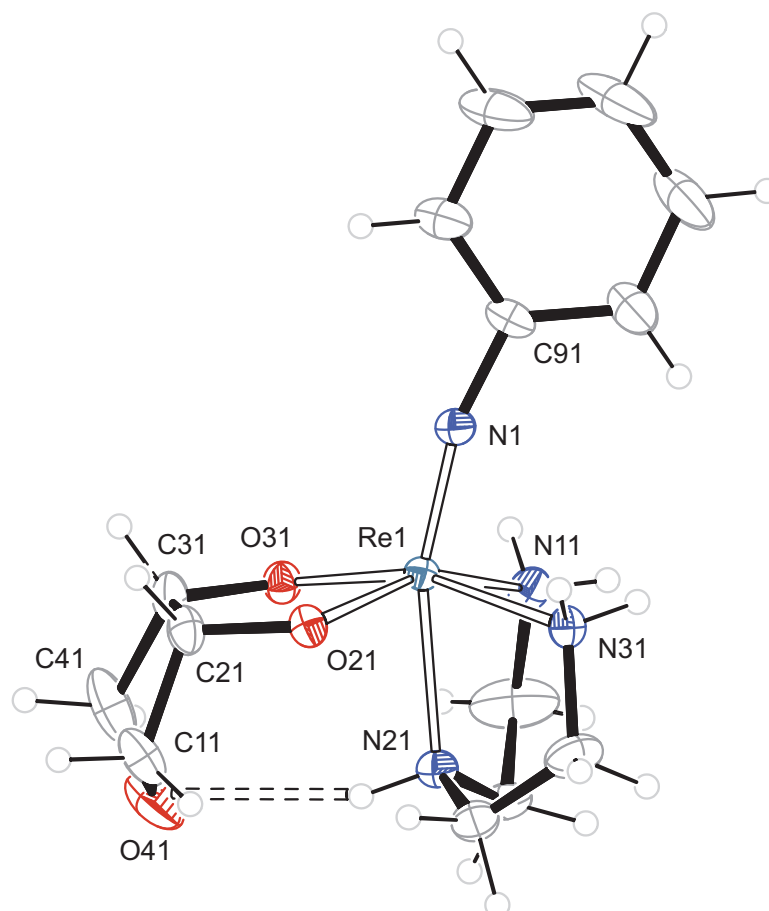


Figure 2.16 ORTEP presentation of the phenylimido-complex **4** in crystals of $[\text{Re}(\text{NPh})(\text{fac-dien})(\text{anti-AnErytH}_{-2})][\text{ReO}(\text{fac-dien})(\text{anti-AnErytH}_{-2})][\text{BPh}_4]\text{Cl}$. Ellipsoids are drawn at 50 % probability level. The minor parts (occupancy ca. 40 %) of the disordered atoms C611/C612 and C711/C712 are not depicted. Distances [\AA] and angles [$^\circ$]: Re1-O21 1.964(2), Re1-O31 1.962(2), Re1-N1 1.723(3), Re1-N11 2.157(3), Re1-N21 2.240(3), Re1-N31 2.185(3); O21-Re1-O31 82.14(9), O21-Re1-N1 109.81(11), O21-Re1-N11 156.14(10), O21-Re1-N21 81.80(9), O21-Re1-N31 89.98(9), O31-Re1-N1 108.01(11), O31-Re1-N11 88.17(10), O31-Re1-N21 85.68(10), O31-Re1-N31 160.98(9), N1-Re1-N11 93.90(11), N1-Re1-N21 162.80(13), N1-Re1-N31 90.93(11), N11-Re1-N21 75.75(10), N11-Re1-N31 92.33(10), N21-Re1-N31 76.04(10), Re1-N1-C91 165.9(3), diol torsion angle O21-C21-C31-O31: 5.4(4), donor-acceptor distance of intramolecular hydrogen bond: N21 \cdots O41 3.255(5), puckering parameters^[59] for O41-C11-C21-C31-C41: $Q_2 = 0.423(4) \text{ \AA}$, $\phi_2 = 354.4(6)^\circ$, conformation $^{\text{O}}E$. The values for the other molecule in the asymmetric unit $[\text{ReO}(\text{fac-dien})(\text{anti-AnErytH}_{-2})]^+$, are very similar to a reported structure^[23].

There are four formula units in the unit cell and one in the asymmetric unit with an anionic (tetraphenylborate and chloride) and a cationic part (one phenylimidorhenium complex and one oxidorhenium complex). Figure 2.16 shows the phenylimido-rhenium complex of the cationic part. The oxidorhenium complex is not shown as it is similar to a known structure^[23]. In both complexes anhydroerythritol is connected in *anti* position respective to the phenylimido- or oxido-rhenium core and the torsion angles of the chelating diol are small (5.4° and -3.2°). The furanose rings are both in envelope conformation (${}^{\circ}E$). The tridentate ligand diethylenetriamine (*facial* binding mode) is disordered on two atoms: C611/C612 and C711/C712. Figure 2.16 shows the atoms of the major part (occupancy ca. 60 %). The bond angle of the phenylimido ligand to the metal (165.9°) deviates more from linearity than in the precursor compound (172.6°)^[70].

In respect to the hydrogen bond connections, the phenylimido- and oxido-rhenium complexes in this crystal are different: the oxido-rhenium complexes (above in Figure 2.17) are connected only via one classical hydrogen bond to their environment, while the phenylimido-complexes (bottom in Figure 2.17) form chains along [010] with stronger hydrogen bonds (see Table 2.9).

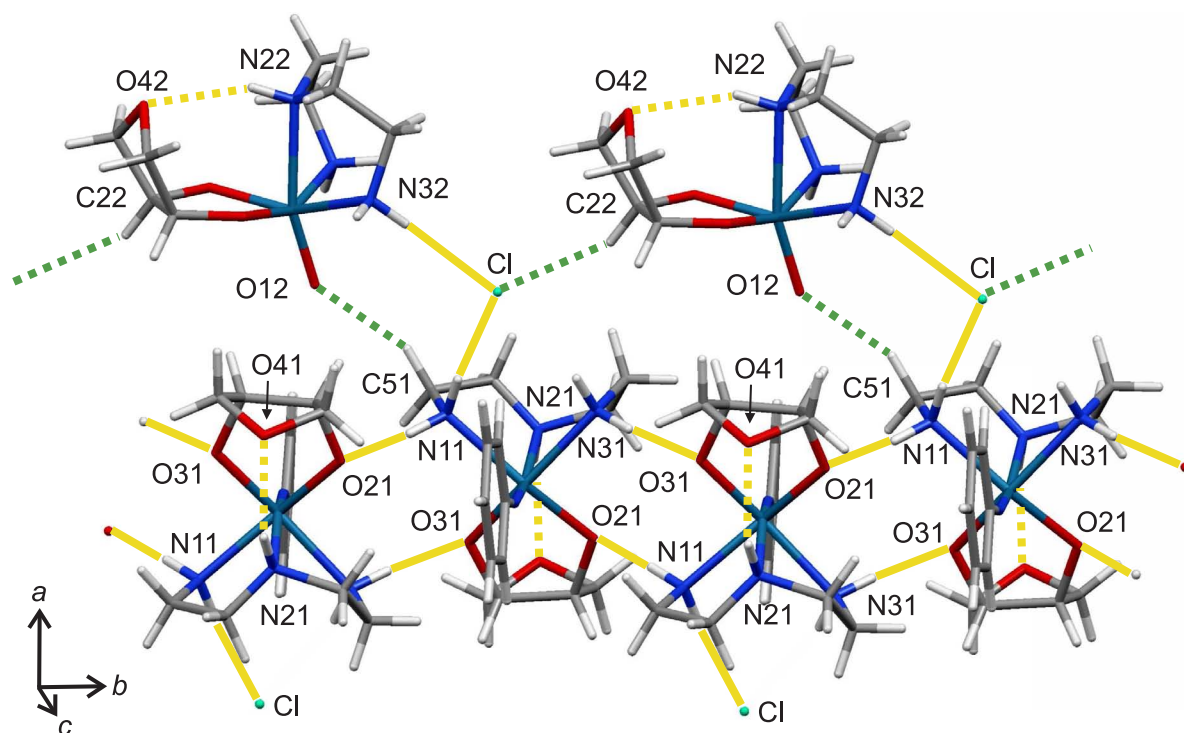


Figure 2.17 MERCURY presentation of hydrogen bonds (yellow: intermolecular, yellow dashed: intramolecular) and weak interactions (green dashed lines) in **4**.

Table 2.9 Distances [Å] and angles [°] of hydrogen bonds in **4**. Values without standard deviation are related to hydrogen atoms at calculated positions. For atom numbering see Figure 2.16. D: donor, A: acceptor, x : difference of (H...A) and the sum of the van-der-Waals radii^[62].

D	H	A	D...A	D-H	H...A	x	D-H...A
N11	H112	O21 ⁱ	2.798(3)	0.92	1.90	-0.82	166
N11	H113	Cl	3.179(3)	0.92	2.27	-0.68	171
N21	H211	O41	3.225(5)	0.93	2.35	-0.37	156
N31	H311	Cl	3.357(3)	0.92	2.49	-0.46	158
N31	H312	O31 ⁱⁱ	2.905(3)	0.92	1.99	-0.73	174
N32	H322	Cl	3.246(3)	0.92	2.41	-0.54	151
N22	H722	O42	3.231(4)	0.93	2.37	-0.35	154
C22	H22	Cl ⁱⁱⁱ	3.451(4)	1.00	2.74	-0.21	128
C51	H511	O12	3.364(5)	0.99	2.46	-0.26	152

Symmetry codes: ⁱ $-x, -\frac{1}{2} + y, \frac{1}{2} - z$; ⁱⁱ $-x, \frac{1}{2} + y, \frac{1}{2} - z$; ⁱⁱⁱ $x, -1 + y, z$.

2.1.5 The reaction of [Re(NPh)Cl₃(PPh₃)₂] with dien and ethanol

In analogy to the behavior of the {ReO}³⁺ core, the phenylimidorhenium(V) moiety is able to build complexes with alcoholic solvents. This reaction is observed in cases where a proper diol is missing. In these cases methanol or ethanol act as oxygen donor ligands. The crystalline compound [Re(NPh)(*mer*-dien)(OEt)(PPh₃)] [ReO₄]Cl · EtOH · 0.5 Me₂CO (**5**) was obtained starting from the phenylimidorhenium(V) precursor [Re(NPh)Cl₃(PPh₃)₂] with diethylenetriamine in boiling ethanol.

Its unit cell in the triclinic space group $P\bar{1}$ contains nine independent ions and molecules that can be merged to the moiety formula: 2(C₃₀H₃₈N₄OPRe), 2(C₂H₆O), C₃H₆O, 2(ReO₄), 2(Cl). In the asymmetric unit there are four and a half different species. They are separated in a cationic rhenium complex with the charge 2+, an anionic part (perrhenate and chloride) and a neutral part (half occupied acetone and disordered ethanol). Figure 2.18 shows the phenylimidorhenium complex of the cationic part. The bond angle of the phenylimido ligand to the metal is close to linearity (173.7°), like the angle found in the precursor compound (172.6°)^[70]. Contrary to the compounds so far described, dien is coordinated in a meridional binding mode. The fourth position is occupied by triphenylphosphane, a ligand remaining from the precursor (see Figure 2.1). A deprotonated ethanol molecule is connected to the rhenium center with a typical Re-O distance (1.935 Å) compared with the distances of the diolato-structures in the previous sections. This ethoxido ligand is oriented *trans* to the phenylimido ligand.

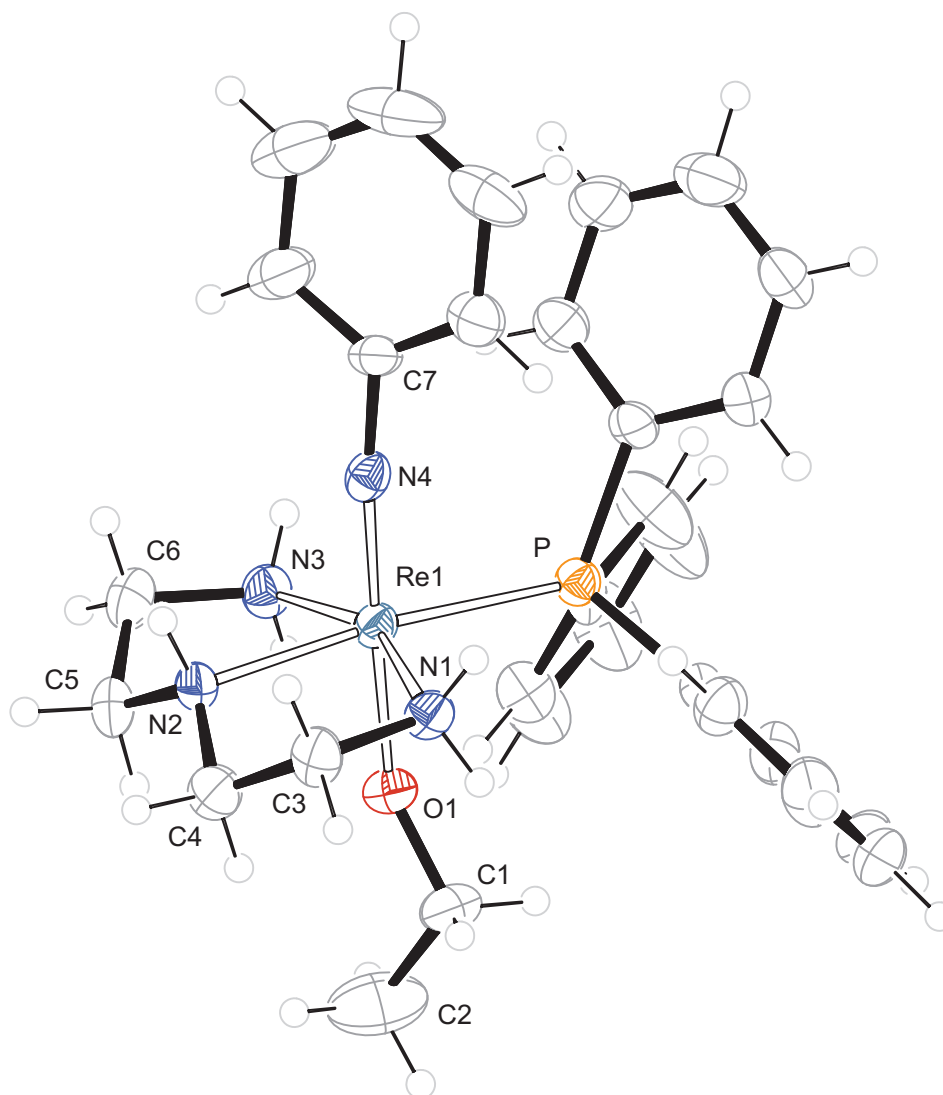


Figure 2.18 ORTEP presentation of **5** in crystals of $[\text{Re}(\text{NPh})(\text{mer-dien})(\text{OEt})(\text{PPh}_3)] [\text{ReO}_4]\text{Cl} \cdot \text{EtOH} \cdot 0.5 \text{Me}_2\text{CO}$. Ellipsoids are drawn at 50 % probability level. Distances [\AA] and angles [$^\circ$]: Re1-P1 2.4349(16), Re1-O1 1.935(4), Re1-N1 2.165(5), Re1-N2 2.148(5), Re1-N3 2.158(5), Re1-N4 1.733(5); P1-Re1-O1 86.61(14), P1-Re1-N1 102.01(13), P1-Re1-N2 171.53(15), P1-Re1-N3 96.05(13), P1-Re1-N4 91.66(16), O1-Re1-N1 84.77(19), O1-Re1-N2 85.34(19), O1-Re1-N3 82.78(19), O1-Re1-N4 178.2(2), N1-Re1-N2 79.86(19), N1-Re1-N3 157.4(2), N1-Re1-N4 95.3(2), N2-Re1-N3 80.35(19), N2-Re1-N4 96.4(2), N3-Re1-N4 97.7(2), Re1-N4-C7 173.7(4), torsion angle of N1-C3-C4-N2: $-52.7(7)$, N2-C5-C6-N3: $57.7(7)$, puckering parameters^[59] for Re1-N1-C3-C4-N2: $Q_2 = 0.451(7) \text{\AA}$, $\phi_2 = 107.9(7)^\circ$, for Re1-N2-C5-C6-N3: $Q_2 = 0.473(7) \text{\AA}$, $\phi_2 = 267.7(6)^\circ$.

The NH and NH₂ groups of the dien ligand act as donors in intermolecular hydrogen bonding. With their bonds to the oxygen atoms of perchlorate and the chloride ions, the cationic complexes form chains along the *a* axis (Figure 2.19).

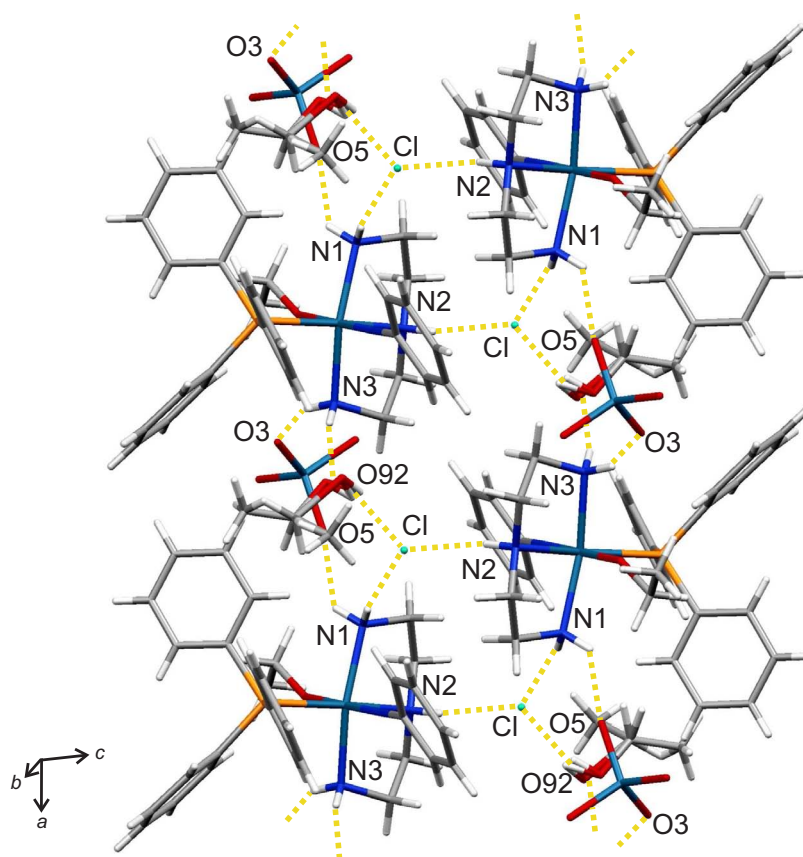


Figure 2.19 MERCURY presentation of hydrogen bonds (yellow dashed lines) in **5** forming chains along the *a* axis.

Table 2.10 Distances [Å] and angles [°] of hydrogen bonds in **5**. O921 is affiliated to the major part of disordered isopropanol. Values without standard deviation are related to hydrogen atoms at calculated positions. For atom numbering see Figure 2.18. D: donor, A: acceptor, *x*: difference of (H···A) and the sum of the van-der-Waals radii^[62].

D	H	A	D···A	D-H	H···A	<i>x</i>	D-H···A
N2	H72	Cl ⁱ	3.145(5)	0.93	2.25	−0.70	160
N1	H711	O5 ⁱⁱ	2.938(8)	0.92	2.21	−0.51	136
N1	H712	Cl ⁱⁱ	3.204(6)	0.92	2.35	−0.60	154
N3	H731	O921	2.871(19)	0.92	1.98	−0.74	162
N3	H732	O3	3.022(8)	0.92	2.20	−0.52	149
O921	H925	Cl	3.121(18)	0.84	2.31	−0.64	162

Symmetry codes: ⁱ $-x, -\frac{1}{2} + y, \frac{1}{2} - z$; ⁱⁱ $-x, \frac{1}{2} + y, \frac{1}{2} - z$.

2.2 Compounds of rhenium(V) with *rac*-2,3-diaminopropionic acid

In contrast to the cationic complexes described in the previous section, this chapter deals with neutral compounds of rhenium(V) with racemic 2,3-diaminopropionic acid (*rac*-dapH), a derivative of the amino acid alanine (Figure 2.20). *rac*-dapH is a non-proteinogenic amino acid and a common plant metabolite. In 1999, for example, it was discovered to be the direct precursor of the neurotoxin β -*N*-oxalyl-L- α,β -diaminopropionic acid (ODAP) in *lathyrus sativus*^[71] that causes human neuro-lathyrism, a neurone disease.

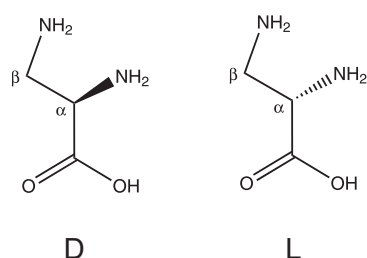


Figure 2.20 Scheme of the D- and L-enantiomers of *rac*-2,3-diaminopropionic acid.

In organometallic chemistry, most of the complexes known are of the deprotonated form *rac*-dap with transition metals such as copper(II), nickel(II), mercury(II) or cobalt(III) but rarely with rhenium. In most of the reported complexes *rac*-dap binds as a bidentate chelate to the metal via two of the three potential binding sites: N_{α} , N_{β} and the carboxylate oxygen. Depending on the pH of the solution, these potential binding sites are variably protonated. Figure 2.21 shows these species with the abbreviations dapH_3 , dapH_2 , dapH and dap . To a certain degree this protonation has an influence on which donor atoms are used for metal-binding. The copper complex depicted in Figure 2.22 with the deprotonated form (dap) was prepared at pH 10 while at lower pH other protonated species are apparent in solution^[72]. On the other hand the cobalt(III) complex (on the left) was prepared at pH 2. Apart from the pH of the solutions, the metal itself and the ligand-to-metal ratio have a significant influence on the complexes formed in solution.

2 Results

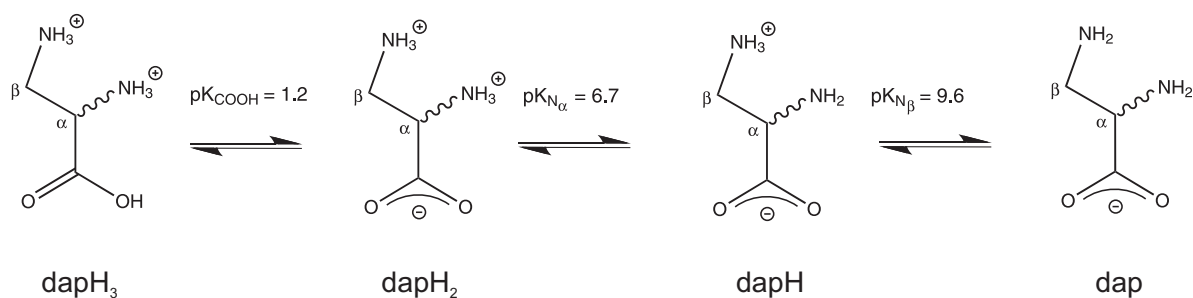


Figure 2.21 Scheme of the pH-dependent forms of *rac*-2,3-diaminopropionic acid. The abbreviations dapH_3 , dapH_2 , dapH and dap correspond to the different protonated forms in water^[72, 73].

The sole example in the literature concerning a complex of dap with rhenium is the carbonyl compound $[\text{Re}(\text{L-dap})(\text{CO})_3]$ reported by *Alberto et al.*^[74] (see on the right in Figure 2.22). It was prepared at pH 7. This complex with rhenium at the low oxidation state I is a rare example with dap in a tridentate binding mode.

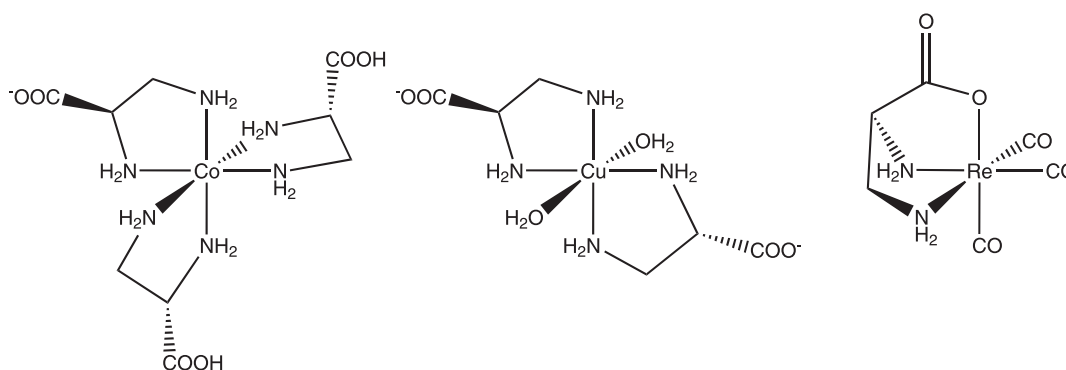


Figure 2.22 Scheme of complexes with *rac*-2,3-diaminopropionic acid. From left to right: Compound with cobalt(III)^[75], copper(II)^[76] and rhenium(I)^[74].

In contrast to this, the following complexes in this work were prepared with rhenium at the oxidation state V. They are built in analogy to the “3 + 2” approach^[19], as with the complexes in the previous section. Figure 2.23 shows the general route. The reactions were carried out in methanol at 65 °C in the presence of triethylamine starting from the rhenium(V) precursor $[\text{ReOCl}_3(\text{PPh}_3)_2]$, *rac*- dapH and an excess of a diol with a *cis*-vicinal diol function. pH values of 9–10 were observed for samples of the reaction mixtures after addition of water. In the resulting complexes, *rac*- dap serves as a tridentate (N_β, N_α, O)-chelate and the deprotonated diol as an (O, O)-chelate. Both enantiomeric forms of *rac*- dap are able to bind to the rhenium center and the carboxylate group in these new compounds is oriented exclusively in *trans* position to the oxido ligand of the $\{\text{ReO}\}^{3+}$ core.

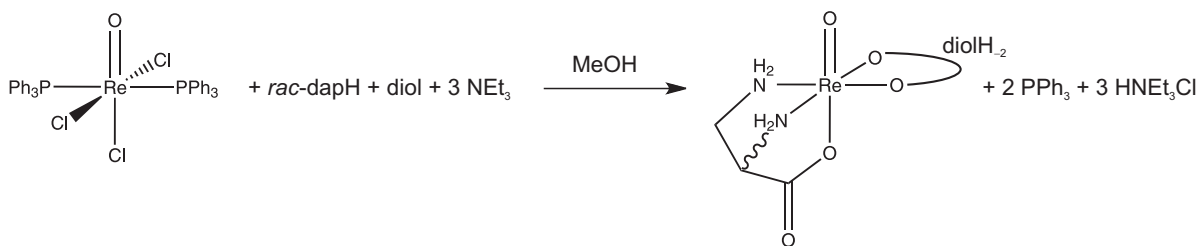


Figure 2.23 Scheme of the general reaction route with *rac*-dap in this chapter. **diol** represents a carbohydrate with a *cis*-vicinal diol function. The wavy bond denotes that both the D- and L-enantiomeric forms of *rac*-dap were detected as chelators.

2.2.1 The reaction of [ReOCl₃(PPh₃)₂] with *rac*-2,3-diaminopropionic acid and 1,2-ethanediol

To explore this system, first the simplest diol was chosen: 1,2-ethanediol. It was stirred with [ReOCl₃(PPh₃)₂], *rac*-dapH and triethylamine in methanol for 3 hours at 65 °C. Over night, dark violet crystals of [ReO(*rac*-dap)(EthdH₂)] (**6**) were obtained from this solution.

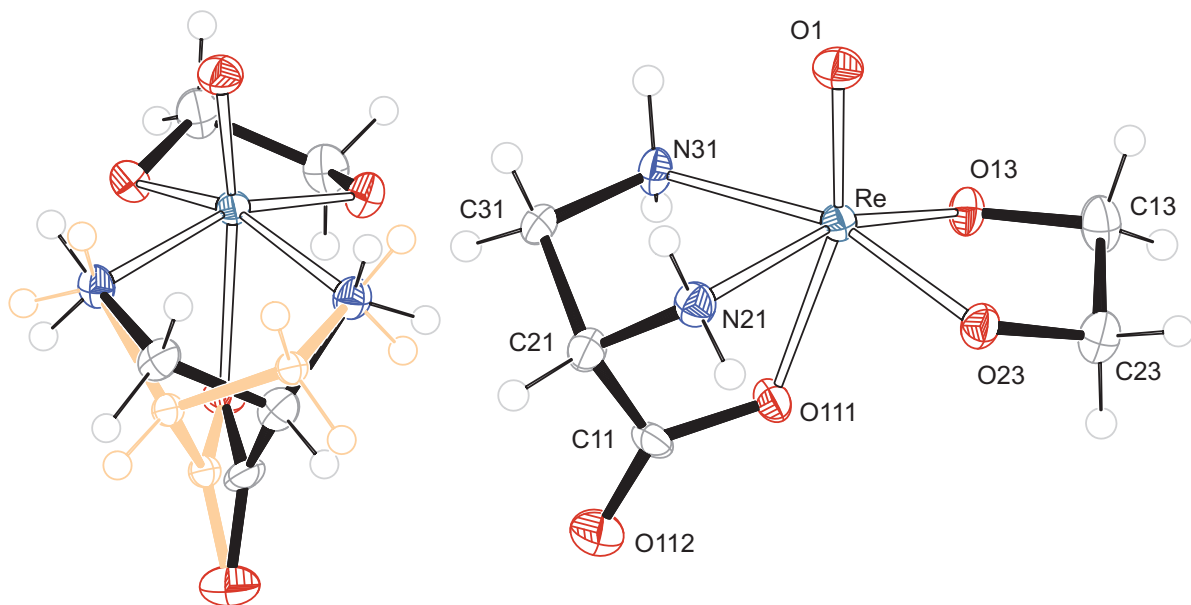


Figure 2.24 ORTEP presentation of both isomers (on the left) and in detail of the isomer [ReO(D-dap)(EthdH₂)] (on the right) in crystals of **6**. The atoms C12, C22, C32 of the other disordered part (L-dap, occupancy ca. 19 %) were omitted for lucidity in the presentation on the right side. Ellipsoids are drawn at 50 % probability level. Distances [Å] and angles [°]: Re-O1 1.686(4), Re-O13 1.976(4), Re-O23 1.943(3), Re-O111 2.118(3), Re-N21 2.151(5), Re-N31 2.186(5); O1-Re-O13 104.01(18), O1-Re-O23 109.81(17), O1-Re-O111 160.97(15), O1-Re-N21 96.2(2), O1-Re-N31 87.99(18), O13-Re-O23 82.13(15), O13-Re-O111 86.05(14), O13-Re-N21 159.82(16), O13-Re-N31 100.25(16), O23-Re-O111 87.32(15), O23-Re-N21 91.46(18), O23-Re-N31 161.07(19), O111-Re-N21 74.51(17), O111-Re-N31 74.19(16), N21-Re-N31 79.88(18), diol torsion angle O13-C13-C23-O23: -40.7(6).

6 crystallizes in the monoclinic space group $P2_1/n$ with four formula units in the unit cell. The asymmetric unit contains the rhenium complex (Figure 2.24) and one molecule of methanol. The aminoalanine part of the complex consists of both the D- and the L-enantiomer at disordered positions: the ratio is about 80:20 or 20:80, respectively. Figure 2.24 shows on the right the isomer with D-dap. As the synthesis started from the racemic compound *rac*-dapH, these crystals of **6** are a true racemate with an overall ratio of 1:1 for the enantiomers. Strictly speaking, these two isomeric complexes are not exactly mirror images of each other (see left presentation in Figure 2.24). But these small differences are, however, negligible in solution.

Classical hydrogen bonds mainly of the type $\text{NH} \cdots \text{O}$ are listed in Table 2.11. They are formed between the amino functions of dap as donor and the rhenium-bonded oxygen atoms of 1,2-ethanediol as acceptor. The molecules of **6** form infinite layers parallel to the (101) plane. In between these layers there are molecules of methanol as donors and acceptors for hydrogen bonds with O112 of the carboxylato groups and N_β of the amino functions (Figure 2.25). The SCHAKAL packing diagram (Figure 6.6 on page 191) viewed along $[0\bar{1}0]$ shows non-polar areas (with CH_2 and CH_3 groups) in the crystal embedded in a matrix of polar parts with hydrogen bonds.

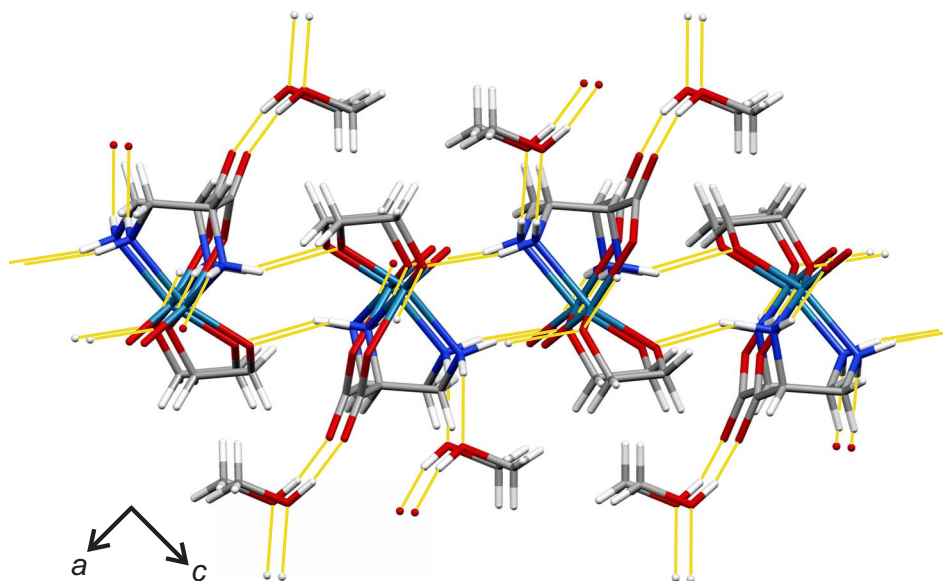


Figure 2.25 MERCURY presentation of hydrogen bonds (yellow lines) in **6** forming layers parallel to the (101) plane.

2 Results

Table 2.11 Distances [Å] and angles [°] of hydrogen bonds in **6**. O99 is affiliated to methanol. Values without standard deviation are related to hydrogen atoms at calculated positions. For atom numbering see Figure 2.24. D: donor, A: acceptor, x : difference of (H···A) and the sum of the van-der-Waals radii^[62].

D	H	A	D···A	D-H	H···A	x	D-H···A
N21	H211	O23 ⁱ	3.001(6)	0.92	2.15	-0.57	154
N21	H212	O13 ⁱⁱ	3.004(6)	0.92	2.13	-0.59	157
N31	H313	O13 ⁱⁱⁱ	2.975(6)	0.92	2.07	-0.65	166
N31	H314	O99	2.917(7)	0.92	2.10	-0.62	148
O99	H899	O112 ^v	2.731(7)	0.84	1.99	-0.73	146

Symmetry codes: ⁱ $1 - x, 1 - y, -z$; ⁱⁱ $x, 1 + y, z$; ⁱⁱⁱ $\frac{1}{2} - x, \frac{1}{2} + y, \frac{1}{2} - z$;
^{iv} $\frac{1}{2} - x, -\frac{1}{2} + y, \frac{1}{2} - z$; ^v $\frac{3}{2} - x, -\frac{1}{2} + y, \frac{1}{2} - z$.

As mentioned above, in solution (with a non-chiral solvent like D₂O) the difference between the two complex species with D- and L-dap are not resolved by NMR spectroscopy in achiral solvents. Only one signal set is observed in spectra of the reaction mixture as well as of the redissolved product in D₂O (Table 2.12). As a chelator, 1,2-ethanediol has a lowered symmetry and two signals are observed for C1/C2, shifted 21 ppm to lower field. Although air-stable, **6** decomposes in water within several hours to give a brown solution with solely free 1,2-ethanediol detectable by NMR spectroscopy.

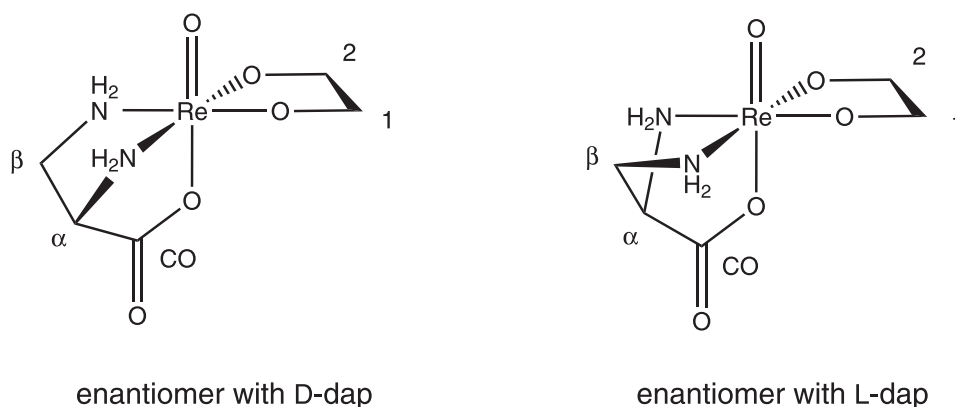


Figure 2.26 Scheme of the enantiomeric forms of **6** and atom numbering used in the ¹³C NMR study.

Table 2.12 ^{13}C NMR chemical shifts (in ppm) of **6** in D_2O (101 MHz, 25 °C) and comparison with the free ligands under the same conditions (pH 4.7). The signal of a drop of methanol ($\delta = 49.50$ ppm in D_2O) was used as an internal secondary reference^[65] for the chemical shift. For atom numbering see Figure 2.26. $\Delta\delta$ values indicating a diolate coordination are in boldface. Assignment of free dap according to the literature^[73].

		dap			ethanediol
		C_{CO}	C_α	C_β	C1/C2
free	δ	171.48	50.83	39.42	63.18
6	δ	177.85	67.02	50.63	84.26, 84.02
	$\Delta\delta$	6.37	16.19	11.21	21.08, 20.84

2.2.2 The reaction of $[\text{ReOCl}_3(\text{PPh}_3)_2]$ with *rac*-2,3-diaminopropionic acid and anhydroerythritol

The analog reaction of $[\text{ReOCl}_3(\text{PPh}_3)_2]$ with *rac*-dapH, anhydroerythritol and triethylamine in methanol leads to the new compound $[\text{ReO}(\text{rac-dap})(\text{syn-AnErytH}_{-2})] \cdot \text{H}_2\text{O}$ (**7**), presented in Figure 2.25. The diol anhydroerythritol can be regarded as a model compound for furanoidic carbohydrates with a *cis*-vicinal diol function.

7 crystallizes in the orthorhombic space group *Pbcn* with eight formula units in the unit cell. The asymmetric unit contains one molecule of the rhenium complex and one half-occupied molecule of water. Related to the previous compound **6**, the aminoalanine part of the complex consists of both the D- and the L-enantiomer of dap on disordered positions with a ratio of about 37:63 or 63:37, respectively. Figure 2.27 shows both forms (above) and in detail the enantiomer with L-dap (below). The deprotonated diol is connected in *syn* orientation with respect to the oxido ligand of the oxidorhenium(V) unit having a typical torsion angle (11°) for a chelating diolato(2-) group. The furanose ring of anhydroerythritol is twisted on the C41-O41 bond having a conformation close to ${}^{\text{O}}T_4$.

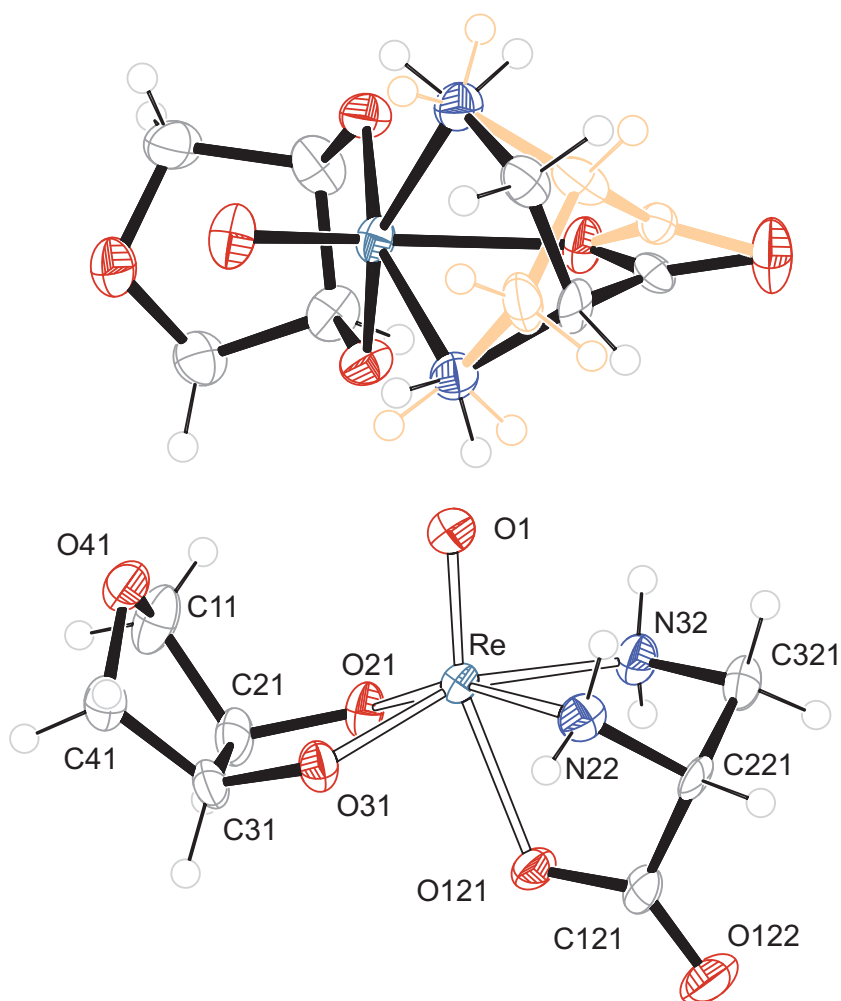


Figure 2.27 ORTEP presentation of both enantiomers (above) and in detail of the enantiomer $[\text{ReO}(\text{L-dap})(\text{syn-AnErytH}_{-2})]$ (below) in crystals of **7**. The atoms C122, C222, C322 of the other disordered part (D-dap, occupancy ca. 37 %) were omitted for lucidity in the presentiaion below. Ellipsoids are drawn at 50 % probability level. Distances [\AA] and angles [$^{\circ}$]: Re-O1 1.677(4), Re-O21 1.938(3), Re-O31 1.939(3), Re-O121 2.167(3), Re-N22 2.150(4), Re-N32 2.164(4); O1-Re-O21 106.99(15), O1-Re-O31 108.83(15), O1-Re-O121 161.00(13), O1-Re-N22 92.34(15), O1-Re-N32 91.54(15), O21-Re-O31 82.12(13), O21-Re-O121 87.31(13), O21-Re-N22 160.44(14), O21-Re-N32 95.77(13), O31-Re-O121 85.07(12), O31-Re-N22 94.68(13), O31-Re-N32 159.29(14), O121-Re-N22 73.17(13), O121-Re-N32 74.25(12), N22-Re-N32 80.41(14), diol torsion angle O21-C21-C31-O31: 10.8(5), puckering parameters^[59] for O41-C11-C21-C31-C41: $Q_2 = 0.401(5) \text{ \AA}$, $\phi_2 = 345.8(7)^{\circ}$, conformation ${}^{\circ}T_4$.

In view of intermolecular hydrogen bonding, the formation of chains along the c axis is observed. Figure 2.28 shows the repetitive pattern of hydrogen bonds listed in Table 2.13. As already observed in **6**, they are mostly of the type $\text{NH} \cdots \text{O}$, connecting the amino functions of dap as donor and the rhenium-bonded oxygen atoms of

anhydroerythritol as acceptor. Molecules of water are part of the hydrogen bonding in these chains. Affiliated to these hydrogen bonds of the type OH \cdots O, only H99 is listed in Table 2.13, the second hydrogen atom of the water molecule is symmetry-generated.

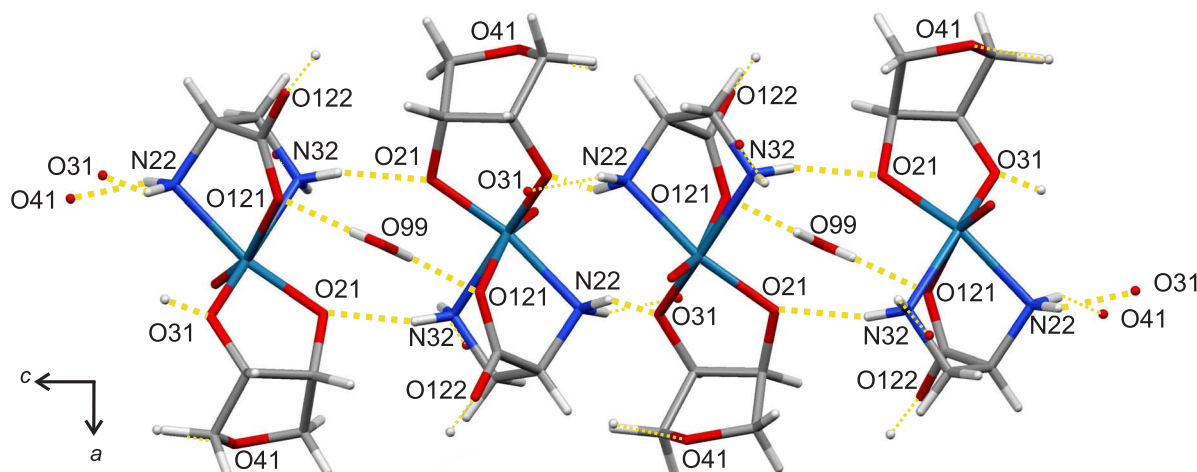


Figure 2.28 MERCURY presentation of hydrogen bonds (yellow dashed lines) in **7** forming chains along the *c* axis.

Table 2.13 Distances [Å] and angles [°] of hydrogen bonds in **7**. O99 is affiliated to water. Values without standard deviation are related to hydrogen atoms at calculated positions. For atom numbering see Figure 2.27. D: donor, A: acceptor, *x*: difference of (H \cdots A) and the sum of the van-der-Waals radii^[62].

D	H	A	D \cdots A	D-H	H \cdots A	<i>x</i>	D-H \cdots A
O99	H99	O121 ⁱ	2.882(5)	0.78(4)	2.10(4)	-0.61	178(7)
N22	H221	O41 ⁱⁱ	2.958(5)	0.92	2.08	-0.65	160
N22	H222	O31 ⁱⁱⁱ	2.917(5)	0.92	2.04	-0.68	159
N32	H321	O21 ^{iv}	2.929(5)	0.92	2.03	-0.69	165
N32	H322	O122 ^v	2.912(5)	0.92	2.17	-0.55	137

Symmetry codes: ⁱ $\frac{1}{2} + x, -\frac{1}{2} + y, \frac{1}{2} - z$; ⁱⁱ $\frac{1}{2} + x, \frac{1}{2} - y, -z$; ⁱⁱⁱ $-x, 1 - y, -z$; ^{iv} $-x, y, \frac{1}{2} - z$; ^v $\frac{1}{2} - x, -\frac{1}{2} + y, z$.

Syn/anti isomerism is observed in spectra of the reaction mixture as well as of **7** dissolved in water. The ¹³C NMR spectra in Figure 2.30 show two signal sets: one for the major species (the two enantiomers of *syn-7* found in the structure determination and not differentiated by NMR spectroscopy) and one of lower intensity for the minor species (the enantiomers of the *anti*-isomer). All species are depicted in Figure 2.29

2 Results

and the signals are listed in Table 2.14. Similarly to **6** the signals of C2/C3 and C1/C4 indicate that anhydroerythritol loses symmetry as chelate, and four signals instead of two appear for each signal set. The signals of C2/C3 are shifted up to 25 ppm to lower field, but the other signals are also remarkably shifted under the influence of the metal.

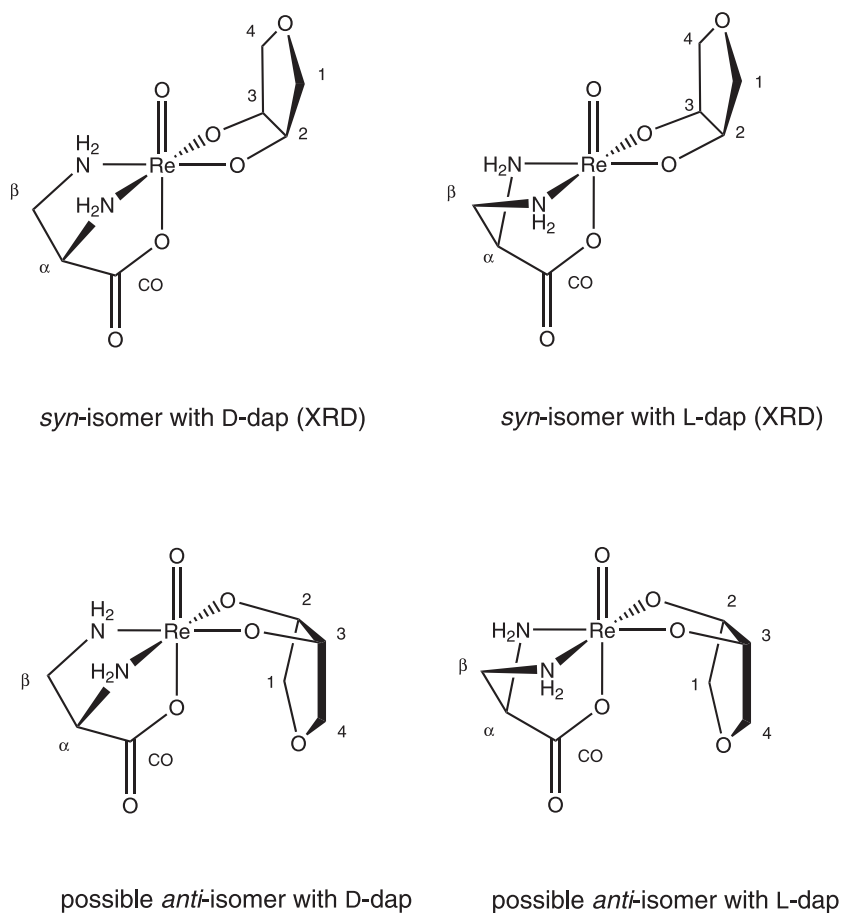


Figure 2.29 Scheme of the enantiomeric (D,L) and diastereomeric (*syn*, *anti*) forms of **7** and atom numbering used in the ^{13}C NMR study. XRD: result of the structure determination.

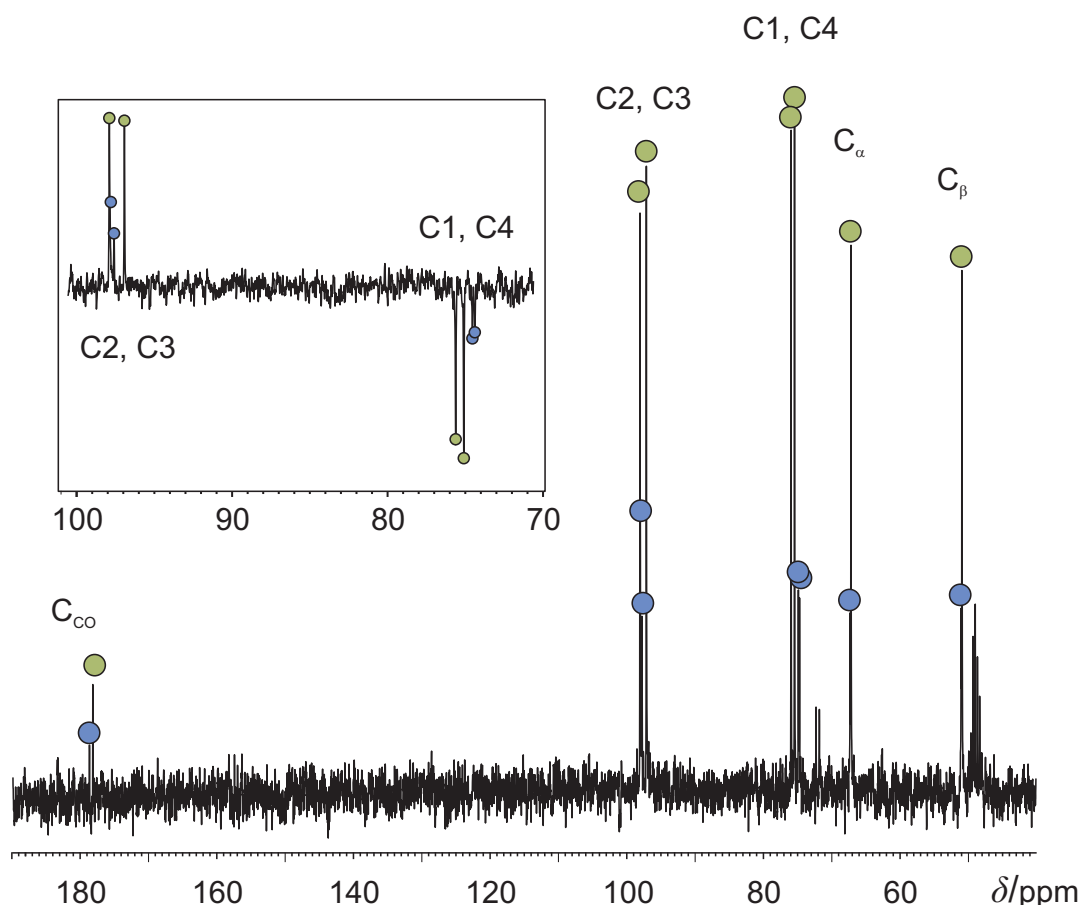


Figure 2.30 ^{13}C NMR spectrum of **7** dissolved in D_2O and close-up of the region of C1/C4 C2/C3 with a DEPT-135 experiment. For atom numbering see Figure 2.29. green: major isomer, blue: minor isomer (ratio ca. 84:16 according to ^1H NMR).

Table 2.14 ^{13}C NMR chemical shifts (in ppm) of **7** in D_2O (67.9 MHz, 25 °C) and comparison with the free ligands under the same conditions (pH 6.5). The signal of a drop of methanol ($\delta = 49.50$ ppm in D_2O) was used as an internal secondary reference^[65] for the chemical shift. For atom numbering see Figure 2.29. Assignment of the free forms according to the literature: dap^[73], AnEryt^[77]. $\Delta\delta$ values indicating a diolate coordination are in boldface.

		dap			AnEryt		
		C_{CO}	C_α	C_β	C2/C3	C1/C4	
free	δ	171.48	50.83	39.42	72.02	71.47	
7	a	δ	177.73	66.84	50.65	97.75, 96.87	75.63, 75.15
	b	δ	178.22	66.97	50.75	97.46, 96.59	74.60, 74.42
	a	$\Delta\delta$	6.25	16.01	11.23	25.73, 24.85	4.16, 3.68
	b	$\Delta\delta$	6.74	16.14	11.33	25.44, 24.57	3.13, 2.96

a: major isomer (ca. 84 %), b: minor isomer.

2.2.3 The reaction of $[\text{ReOCl}_3(\text{PPh}_3)_2]$ with *rac*-2,3-diaminopropionic acid and pyrimidine nucleosides

The nucleosides cytidine and uridine include the structural motifs of 1,2-ethane-1,2-diol and anhydroerythritol used for the compounds **6** and **7**, but also provide the possibility of different coordination modes via the 1,3-diol function of the ribose part or via the nitrogen atoms of pyrimidine. Nevertheless, exclusively 1,2-diol-coordination was observed. While the reaction of $[\text{ReOCl}_3(\text{PPh}_3)_2]$ with *rac*-dapH, triethylamine and uridine in methanol seemed to be successful only according to NMR spectroscopy, it was possible to obtain dark violet crystals of $[\text{ReO}(\text{rac-dap})(\text{anti-Cyd}2',3'\text{H}_{-2})] \cdot 2 \text{H}_2\text{O}$ (**8**) from the analog reaction with cytidine.

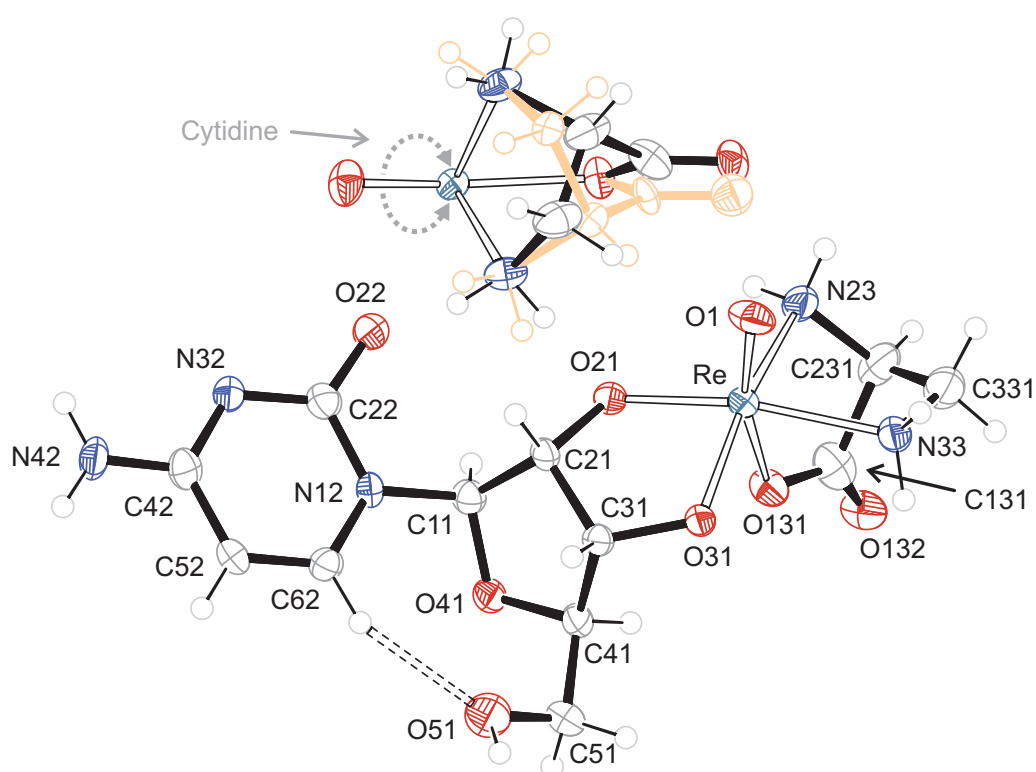


Figure 2.31 ORTEP presentation of both diastereomers (above) and exclusively the main diastereomer $[\text{ReO}(\text{D-dap})(\text{anti-Cyd}2',3'\text{H}_{-2})]$ (below) in crystals of **8**. The atoms O133, C132, C232, C332 of the disordered minor part (L-dap, occupancy ca. 46 %) were omitted for lucidity in the presentation below. Ellipsoids are drawn at 50 % probability level. Distances [Å] and angles [°]: Re-O1 1.677(3), Re-O21 1.952(2), Re-O31 1.938(2), Re-O131 2.131(3), Re-N23 2.169(3), Re-N33 2.151(3); O1-Re-O21 105.47(14), O1-Re-O31 108.33(12), O1-Re-O131 162.66(12), O1-Re-N23 90.59(14), O1-Re-N33 92.96(15), O21-Re-O31 82.23(10), O21-Re-O131 85.47(13), O21-Re-N23 96.49(12), O21-Re-N33 160.98(14), O31-Re-O131 86.16(10), O31-Re-N23 160.74(13), O31-Re-N33 96.59(10), O131-Re-N23 74.59(13), O131-Re-N33 75.51(14), N23-Re-N33 78.36(12), furanose torsion angle O21-C21-C31-O31: 24.5(4), donor-acceptor distance of intramolecular C-H \cdots O interaction: C62 \cdots O51 3.200(5), puckering parameters^[59] for O41-C11-C21-C31-C41: $Q_2 = 0.232(4)$ Å, $\phi_2 = 294.5(9)^\circ$, conformation 3E .

2 Results

The crystals of **8** in the orthorhombic space group $P2_12_12_1$ have four formula units in the unit cell. The asymmetric unit contains one molecule of the rhenium complex and two molecules of water of which one is disordered. Also on disordered positions, both the D- and the L-enantiomers of dap are present in the complex. These enantiomeric ligands build, with uridine, two diastereomeric forms of **8**. Figure 2.31 shows both diastereomers (above) found in the structure determination and solely the major diastereomer with D-dap (ca. 54 %, below). The ribofuranosyl moiety of the cytidine part is connected via O21 and O31 in *anti*-position to the oxido ligand of the rhenium core. Its torsion angle (24.5° for O21-C21-C31-O31) is diminished compared with the free form of cytidine (44.4°)^[60], and the conformation of the furanose ring has changed from 3T_2 to 3E with a smaller puckering amplitude (0.232 \AA vs. 0.378 \AA). The 3E conformation is also predominantly found in base-paired rRNAs^[78]. In **8** the glycosidic torsion angle χ (-161.1° for O4'-C1'-N1-C2) is close to the angle of the free form (-162.6°) and defines an *anti* orientation of the pyrimidine part. Although con-

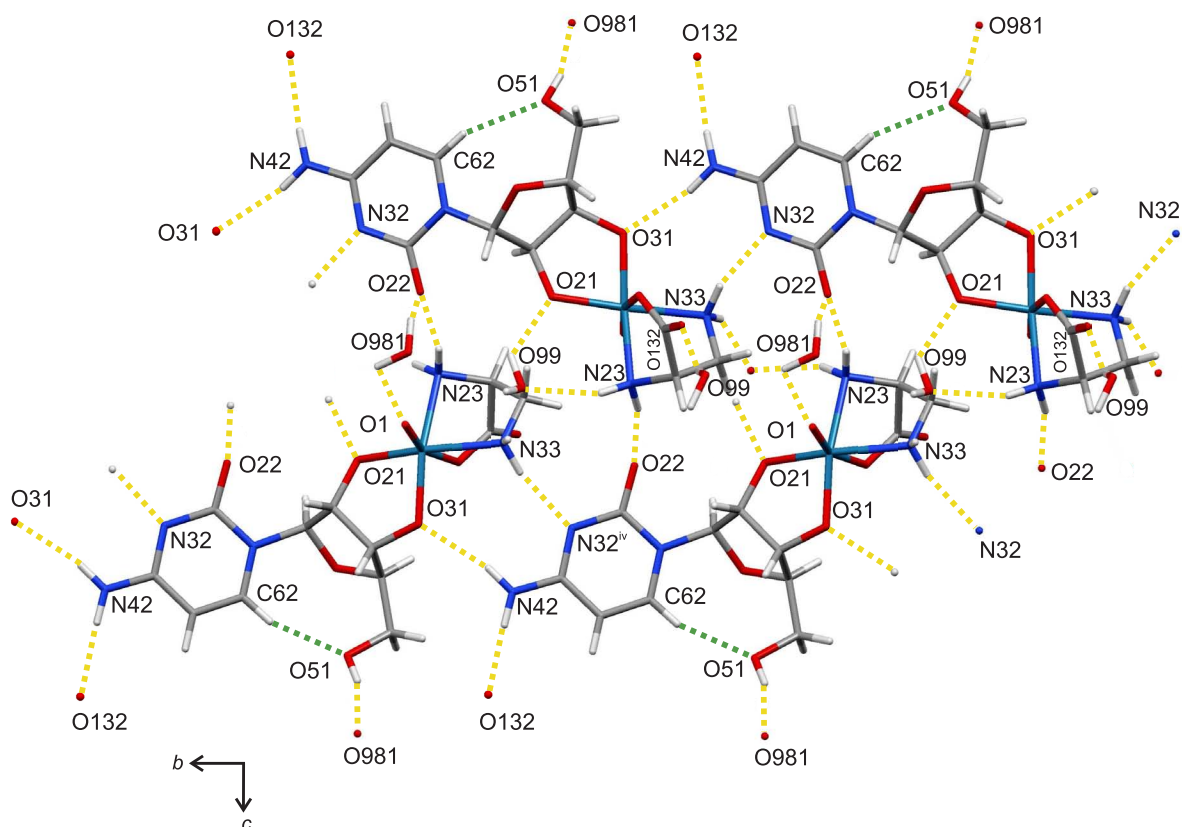


Figure 2.32 MERCURY presentation of hydrogen bonds (yellow dashed lines) and C-H...O contacts (green dashed lines) in **8** forming double-strand molecule chains along the *b* axis.

taining the nucleoside cytidine, in **8** no typical hydrogen bondings of RNA base pairs are observed in this structure, but there are similarities to the C:C base-pair group^[78].

Figure 2.32 shows hydrogen bonds forming eight-membered rings (N32-C42-N42-H421 \cdots O31-Re-N33-H336 \cdots). Instead of connecting two cytosine moieties, they are formed between the nitrogen atoms of cytosine, N $_{\alpha}$ of D-dap and the metal-bonded O3' of the ribose part. These bonds connect the molecules of 8 to infinite chains along the [010] direction. Water molecules assist the cross-link of these chains (see also SCHAKAL packing diagram on page 193). These hydrogen bonds of the water molecules are also listed in Table 2.15 although their angles are partially unfavorable due to disorder/data quality. Similarly to the free form of cytidine^[60], there is an intramolecular contact of the type C-H \cdots O from H61 to O52 forcing the torsion angle χ of the glycosidic bond very close to the angle of the free form, as mentioned above.

Table 2.15 Distances [Å] and angles [°] of hydrogen bonds in 8. O99 is affiliated to water, O981/O982 to disordered water. Hydrogen bonds of the minor disordered part of dap are not listed. Values without standard deviation are related to hydrogen atoms at calculated positions. In the last row the values of an intramolecular C-H \cdots O interaction in a published^[60] structure of free cytidine are listed. D: donor, A: acceptor, x : difference of (H \cdots A) and the sum of the van-der-Waals radii^[62].

D	H	A	D \cdots A	D-H	H \cdots A	x	D-H \cdots A
O51	H851	O981 ⁱ	2.529(12)	0.84	1.72	-1.00	162.5
O51	H851	O982 ⁱ	2.782(12)	0.84	1.96	-0.76	164.3
N42	H421	O31 ⁱⁱ	3.016(4)	0.88	2.15	-0.57	168.2
N42	H422	O132 ⁱ	3.026(8)	0.88	2.17	-0.56	166.0
N23	H233	O99	2.939(5)	0.92	2.09	-0.63	152.9
N23	H234	O22 ⁱⁱⁱ	3.010(5)	0.92	2.11	-0.61	165.9
N33	H335	O99 ⁱⁱⁱ	2.904(6)	0.92	2.10	-0.62	145.4
N33	H336	N32 ^{iv}	2.892(4)	0.92	2.00	-0.75	161.8
O981	H982	O22	2.875(17)	0.95(4)	2.09(12)	-0.63	139(14)
O981	H981	O1 ^{vii}	2.892(12)	0.94(4)	2.49(19)	-0.23	106(13)
O982	H983	O99 ^{vi}	2.863(14)	0.95(5)	2.21(15)	-0.51	126(14)
O982	H984	O133 ⁱⁱ	2.898(16)	0.94(4)	2.10(10)	-0.62	142(13)
O99	H991	O132 ^{vi}	2.776(8)	0.93(4)	1.96(5)	-0.76	145(6)
O99	H992	O21	2.790(5)	0.94(4)	2.09(6)	-0.63	130(6)
C62	H62	O51	3.200(5)	0.95	2.31	-0.41	155.3
C6'	H6'	O5'	3.246(5)	0.94(3)	2.35(3)	-0.34	161(3)

Symmetry codes: ⁱ $x - \frac{1}{2}, -y + \frac{1}{2}, -z$; ⁱⁱ $x, y + 1, z$; ⁱⁱⁱ $-x + 1, y - \frac{1}{2}, -z + \frac{1}{2}$; ^{iv} $x, y - 1, z$; ^v $-x + 2, y - \frac{1}{2}, -z + \frac{1}{2}$; ^{vi} $-x + 2, y + \frac{1}{2}, -z + \frac{1}{2}$; ^{vii} $-x + 1, y + \frac{1}{2}, -z + \frac{1}{2}$.

2 Results

Table 2.16 shows the ^{13}C NMR data of **8** and the residue obtained from the analog reaction with uridine (both solved in D_2O). Altogether there are four signal sets with different intensities in each spectrum. They are consistent with the result of the structure determination as the large CIS values for $\text{C}2'$ and $\text{C}3'$ attest to a coordination via $\text{O}2'$ and $\text{O}3'$ to the rhenium center. It is likely that in the case of cytidine the two major sets correspond to the two diastereomeric forms of *anti*-**8** and the other two sets to *syn*-**8**, as illustrated in Figure 2.33. These four species are observed in spectra of the reaction mixtures as well as in spectra of the compounds redissolved in water. A further enrichment of any diastereomeric species in solution was not successful. Solutions of **8** in water (pH 5.5) are stable for several days whereas decomposition within hours was observed for the previous compounds **6** and **7**.

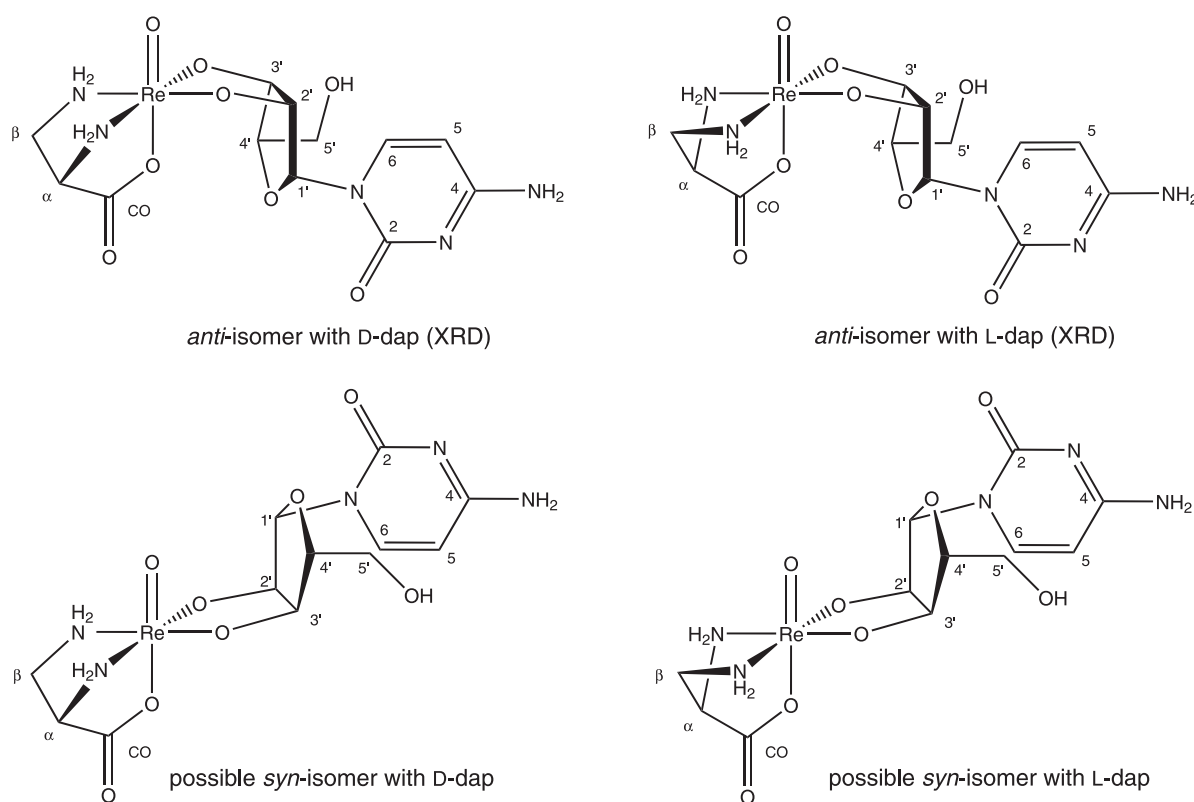


Figure 2.33 Scheme of the diastereomeric forms of **8** and atom numbering used in the ^{13}C NMR study according to the recommendations of the JCBN^[61, 79]. XRD: result of the structure determination.

Table 2.16 ^{13}C NMR chemical shifts (in ppm) of **8**, free cytidine, the related compound with uridine and free uridine in D_2O (101 MHz, 25 °C) under the same conditions (pH 5.5). The signal of a drop of methanol ($\delta = 49.50$ ppm in D_2O) was used as an internal secondary reference^[65] for the chemical shift. For atom numbering see Figure 2.33. $\Delta\delta$ values indicating a diolate coordination are in boldface. Assignment of free cytidine^[63] and uridine^[67] according to the literature.

Cyd		C1'	C2'	C3'	C4'	C5'	C2	C4	C5	C6
free	δ	90.69	74.51	69.77	84.47	61.21	155.08	164.49	96.37	142.91
8 in D_2O :										
a	δ	91.94*	100.44*	95.97	85.52	62.13	154.79*	164.41	96.69*	143.72
b	δ	91.94*	100.44*	95.85	84.88	62.30	154.79*	164.37	96.69*	143.85
c	δ	91.57	99.21	94.51	85.86	62.39	154.14	164.30	96.60	143.97
d	δ	91.19	100.34	95.81	86.27	62.50	153.56	164.18	96.55	144.01
a	$\Delta\delta$	1.25	25.93	26.20	1.05	0.92	-0.29	-0.08	0.32	0.81
b	$\Delta\delta$	1.25	25.93	26.08	0.41	1.09	-0.29	-0.12	0.32	0.94
c	$\Delta\delta$	0.88	24.70	24.74	1.39	1.18	-0.94	-0.19	0.23	1.06
d	$\Delta\delta$	0.50	25.83	26.04	1.80	1.29	-1.72	-0.31	0.18	1.10
Urd		C1'	C2'	C3'	C4'	C5'	C2	C4	C5	C6
free	δ	89.93	74.24	70.04	84.83	61.37	152.19	166.69	102.84	142.42
compound with uridine in D_2O :										
a	δ	90.42	100.02	96.23	85.70	62.38	152.16	166.73*	103.06	143.32*
b	δ	91.32	100.10	96.21	85.02	62.20	152.03	166.73*	103.16	143.32*
c	δ	91.19	98.82*	94.87*	86.36	62.46	152.11	166.73*	103.16	143.36
d	δ	90.82	98.82*	94.87*	85.96	62.54	152.13	166.73*	103.16	143.13
a	$\Delta\delta$	0.49	25.78	26.19	0.87	1.01	-0.03	0.04	0.22	0.90
b	$\Delta\delta$	1.39	25.86	26.17	0.19	0.83	-0.16	0.04	0.32	0.90
c	$\Delta\delta$	1.26	24.58	24.83	1.53	1.09	-0.08	0.04	0.32	0.94
d	$\Delta\delta$	0.89	24.58	24.83	1.13	1.17	-0.06	0.04	0.32	0.71

Signals of four species in solution were observed, according to the intensities, there was distinguished between: a (major isomer) > b > c > d (minor isomer).

* signal overlap

2.3 Compounds of rhenium(V) with L-histidine

As one of the 20 proteinogenic amino acids, L-histidine is present as subunit in most of the naturally occurring proteins. Furthermore its side chain is a preferred ligand for transition metals in many metalloproteins and enzymes. But even the free form of L-histidine occurs in many organisms. It was detected as a metal chelator in plants accumulating nickel from the soil^[80], or even in human blood as a part of the copper transport system^[81]. Though being an essential trace element for organisms, free copper is also toxic. Therefore, it exists only in bound form, such as histidinato complexes.

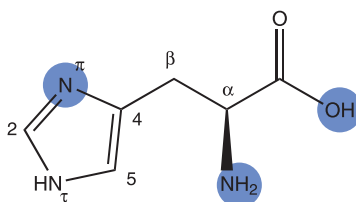


Figure 2.34 Scheme of L-histidine and observed binding sites (blue: N,N,O with rhenium(V)). Atom numbering according to the recommendations of the JCBN^[79].

As a chelating ligand, L-histidine provides up to three potential binding sites (Figure 2.34). There are many reported compounds with transition metals—well characterized are complexes with nickel(II)^[82, 83], chromium(III)^[84], cobalt(III)^[85], molybdenum(V)^[86], vanadium(IV)^[87], copper(II)^[81] and rhenium at low and high oxidation states. Figure 2.35 shows the latter two examples with histidine in a tridentate binding mode reported by *Alberto et al.*^[88] and *Tessier et al.*^[42].

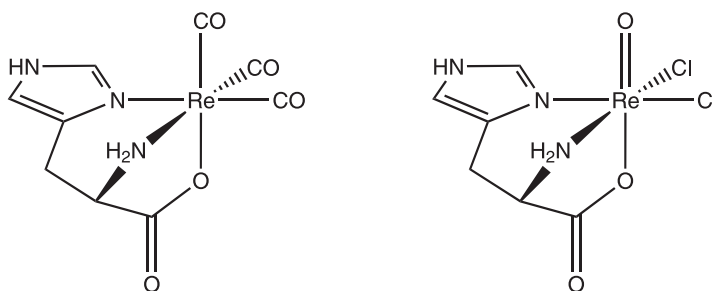


Figure 2.35 Complexes with tridentate L-histidine. Left: $[\text{Re}(\text{CO})_3(\text{L-his})]$ ^[88] with rhenium(I), right: $[\text{ReO}(\text{L-his})\text{Cl}_2]$ ^[42] with rhenium(V).

The rhenium(I) complex $[\text{Re}(\text{CO})_3(\text{L-his})]$ ^[88] was prepared from $[\text{Re}(\text{CO})_3(\text{H}_2\text{O})_3]^+$ in water at pH 1, whereas the rhenium(V) complex $[\text{ReO}(\text{L-his})\text{Cl}_2]$ ^[42] was prepared from $[\text{ReOCl}_3(\text{OPPh}_3)(\text{Me}_2\text{S})]$ in acetonitrile at neutral conditions. While the former is stable in water, decomposition occurs for the latter with rhenium(V). Figure 2.36

shows a detailed presentation (including distances and angles) of the free form of L-histidine (L-hisH) as well as of the structure with rhenium(V) for comparison with the following structures in this chapter. Basically, the torsion angles of histidine are affected by the coordination. The change of the bond distances is only minimal. The acid group and the aromatic imidazole ring remain planar and the metal is placed with deviations of 0.014 Å and 0.183 Å within these planes.

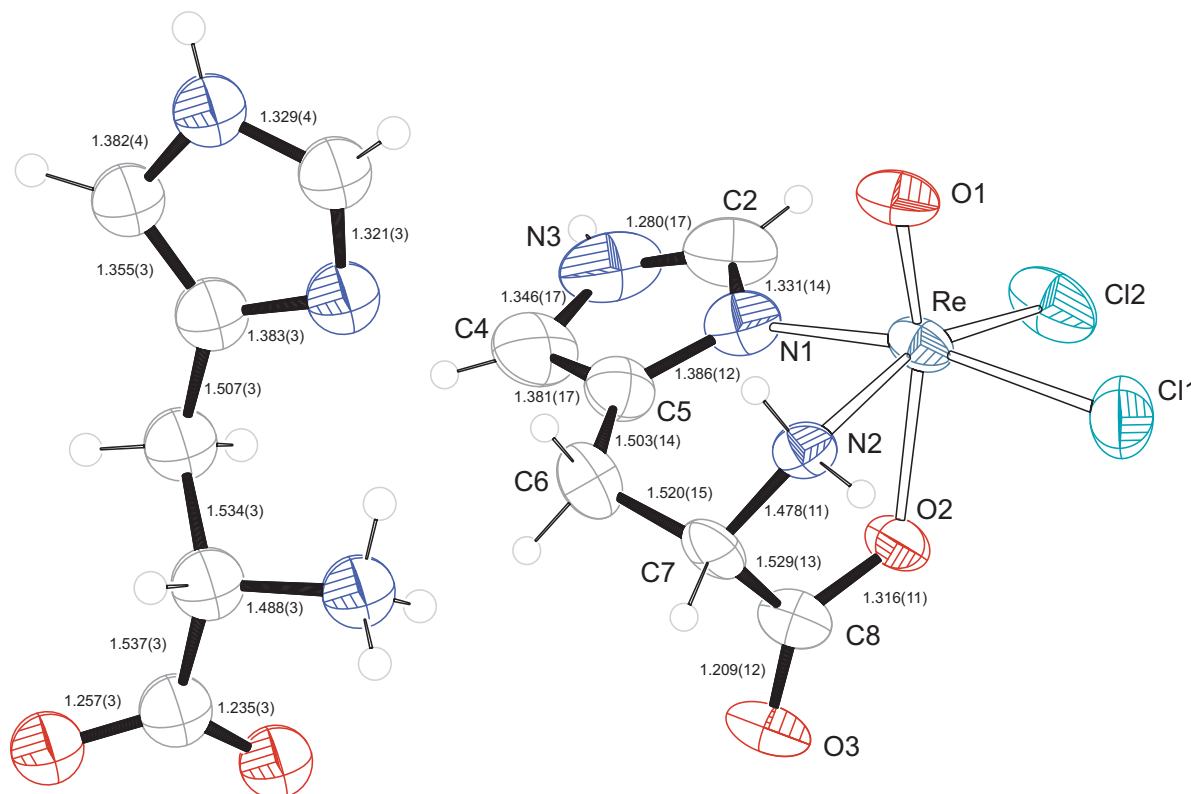


Figure 2.36 ORTEP presentation of the free form of L-histidine^[89] and $[\text{ReO}(\text{L-his})\text{Cl}_2]$ ^[42] Atoms are drawn at 50 % probability level. Distances [Å] and angles [°] of the compound with rhenium: Re-Cl1 2.351(4), Re-Cl2 2.334(3), Re-O1 1.660(7), Re-O2 2.081(6), Re-N1 2.099(9), Re-N2 2.146(6); Cl1-Re-Cl2 86.95(11), Cl1-Re-O1 99.4(3), Cl1-Re-O2 87.2(2), Cl1-Re-N1 167.0(2), Cl1-Re-N2 89.32(18), Cl2-Re-O1 108.7(2), Cl2-Re-O2 87.44(15), Cl2-Re-N1 90.4(2), Cl2-Re-N2 160.40(18), O1-Re-O2 162.8(3), O1-Re-N1 93.6(3), O1-Re-N2 90.9(3), O2-Re-N1 80.0(3), O2-Re-N2 73.2(2), N1-Re-N2 88.9(3), Re-O2-C8 121.2(5), Re-N1-C2 126.0(7), Re-N1-C5 127.3(6), Re-N2-C7 109.4(4); torsion angle of the coordinated acid group Re-O2-C8-O3 171.4(8).

The compounds in this chapter were prepared starting from the rhenium(V) precursor $[\text{ReOC}_3(\text{PPh}_3)_2]$, L-histidine and, additionally, a carbohydrate with a *cis*-vicinal diol function. Figure 2.37 shows the general reaction route. The resulting octahedral complexes are built according to the “3 + 2” approach^[19] with an (N,N,N)(O,O) donor set. In contrast to the compound reported by *Tessier et al.*^[42], these new compounds are stable in aqueous media.

2 Results

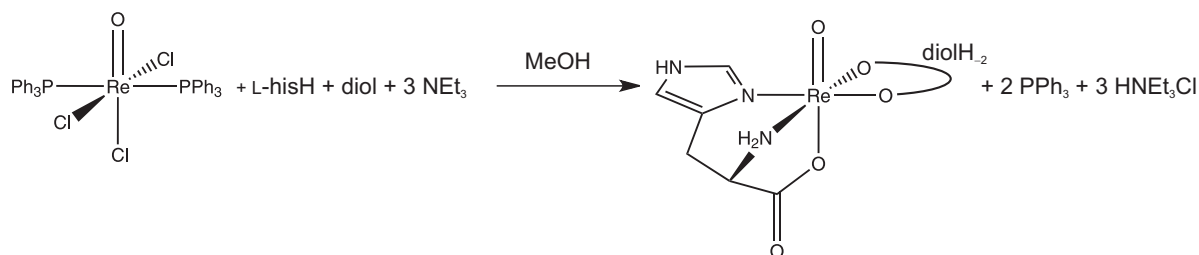


Figure 2.37 Scheme of the general reaction route with L-histidine in this chapter. **diol** represents a carbohydrate with a *cis*-vicinal diol function.

There are various species of L-histidine in solution depending on the pH (Figure 2.38). At physiological pH the major form is L-hisH and the isoelectric point is $\text{pH(I)} = 7.47^{[90]}$. The reactions in this chapter were carried out in the solvent methanol, but it is likely that the deprotonated form L-his was available, as pH 9 was observed for samples of the crude reaction mixture after addition of water.

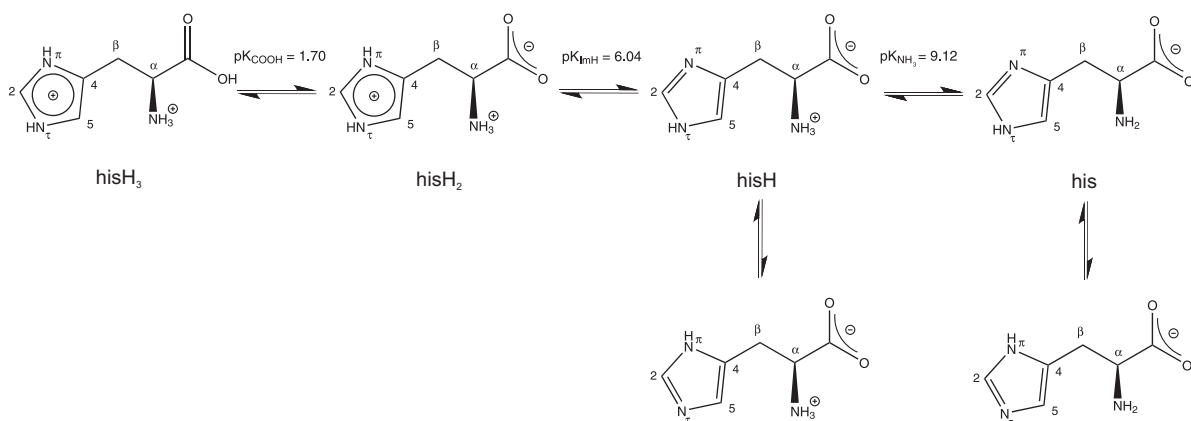


Figure 2.38 Scheme of the pH-dependent forms of L-histidine and tautomeric equilibria of the imidazole ring. hisH_3 , hisH_2 , hisH and his correspond to the different protonated forms in aqueous solution from pH 1.0 to 10^[91].

2.3.1 The reaction of $[\text{ReOCl}_3(\text{PPh}_3)_2]$ with L-histidine and oxalic acid

Oxalic acid (ethanedioic acid) is the smallest of the dicarboxylic acids. It was chosen to explore the rhenium-histidine system, as its anion is known as ligand for metals. In 1992, *Brown et al.*^[30] reported of a first oxalato complex with rhenium(V) and the co-ligand *tpb*, and in the following decade similar complexes with the co-ligands *ami*^[36], *dppe* and *bipy*^[37] were reported.

The reaction of a methanolic solution of the rhenium(V) precursor $[\text{ReOCl}_3(\text{PPh}_3)_2]$ with L-histidine and sodium oxalate in excess at 65 °C yielded the electroneutral complex $[\text{ReO}(\text{L-his})(\text{ox})]$ (**9**). Crystals suitable for X-ray diffraction were obtained from a saturated solution in methanol/water.

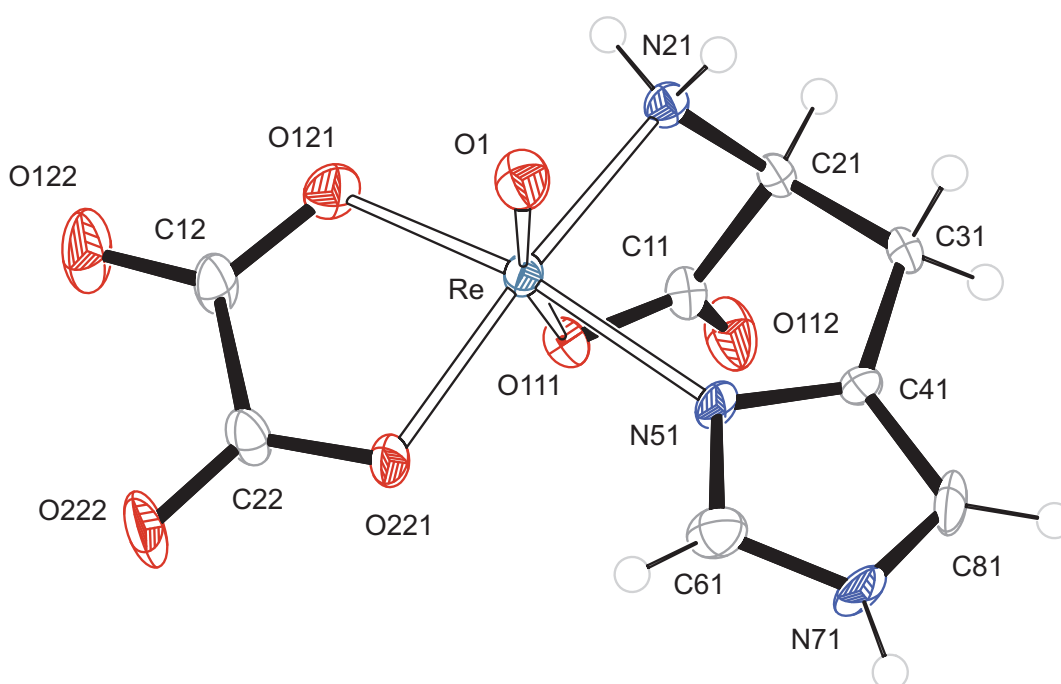


Figure 2.39 ORTEP presentation of $[\text{ReO}(\text{L-his})(\text{ox})]$ (**9**). Ellipsoids are drawn at 50 % probability level. Distances [Å] and angles [°]: Re-O1 1.676(5), Re-O111 2.113(6), Re-O121 2.034(5), Re-O221 2.019(6), Re-N21 2.128(7), Re-N51 2.071(5); O1-Re-O111 163.7(3), O1-Re-O121 101.3(2), O1-Re-O221 108.6(3), O1-Re-N21 90.5(3), O1-Re-N51 97.9(2), O111-Re-O121 80.7(2), O111-Re-O221 87.8(2), O111-Re-N21 73.2(2), O111-Re-N51 81.5(2), O121-Re-O221 81.3(2), O121-Re-N21 93.5(2), O121-Re-N51 160.7(2), O221-Re-N21 160.9(2), O221-Re-N51 90.8(2), N21-Re-N51 88.2(2), torsion angle of O121-C12-C22-O221: $-4.4(11)$, torsion angle of the coordinated acid group Re-O111-C11-O112: $173.7(6)$.

The unit cell in the orthorhombic space group $P2_12_12_1$ contains four formula units of the rhenium complex illustrated in Figure 2.39. The monoanionic tridentate histidinato ligand is connected as an (*N,N,O*)-donor to the metal via N21, N51 in *cis*

position and O111 of the carboxylato group *trans* to the oxido ligand O1. With small deviations the rhenium core is in-plane with all sp^2 -hybridized molecule parts: the aromatic imidazole ring (deviation 0.075 Å), the carboxylato group (0.201 Å) and the oxalato ligand (0.040 Å). The latter forms as a dianionic (O,O)-donor a five membered chelate ring with approximately planar geometry (torsion angle O121-C12-C22-O221: -4.4°). Together with the $\{\text{ReO}\}^{3+}$ core these ligands build a distorted octahedral complex with a non-linear O1-Re-O111 axis (163.7°), similar to a compound reported by Tessier *et al.* (Figure 2.36 on page 51).

There are mainly classical hydrogen bonds of the type N-H...O between the NH- and NH₂-functions of the amino acid and the carboxylato oxygen atoms of oxalate and histidine (Table 2.17). A weak intermolecular interaction of the type C-H...O at C61 of the imidazole ring to O112 of the acid group should also be mentioned, as it is part of the bonds connecting four molecules of **9**. Figure 2.40 illustrates the ring formation of these four molecules. There are tunnels along $[\bar{1}00]$ with a diameter of about 7.5 Å, but no solvent molecules were found in them (the maximal remaining electron density is located close to the rhenium atom, see Table 6.4 on page 217).

Table 2.17 Distances [Å] and angles [$^\circ$] of hydrogen bonds in **9**. Values without standard deviation are related to hydrogen atoms at calculated positions. For atom numbering see Figure 2.39. D: donor, A: acceptor, x : difference of (H...A) and the sum of the van-der-Waals radii^[62].

D	H	A	D...A	D-H	H...A	x	D-H...A
N21	H211	O222 ⁱ	2.875(8)	0.92	2.00	-0.72	159
N21	H212	O112 ⁱⁱ	2.857(9)	0.92	1.99	-0.73	157
N71	H71	O222 ⁱⁱⁱ	2.956(9)	0.88	2.22	-0.50	141
N71	H71	O122 ⁱⁱⁱ	3.155(10)	0.88	2.39	-0.33	145
C61	H61	O112 ^{iv}	3.142(10)	0.95	2.28	-0.44	150

Symmetry codes: ⁱ $x + 1, y, z$; ⁱⁱ $-x + 1, y - \frac{1}{2}, -z + \frac{1}{2}$; ⁱⁱⁱ $-x - \frac{1}{2}, -y + 1, z - \frac{1}{2}$; ^{iv} $-x, -\frac{1}{2} + y, \frac{1}{2} - z$.

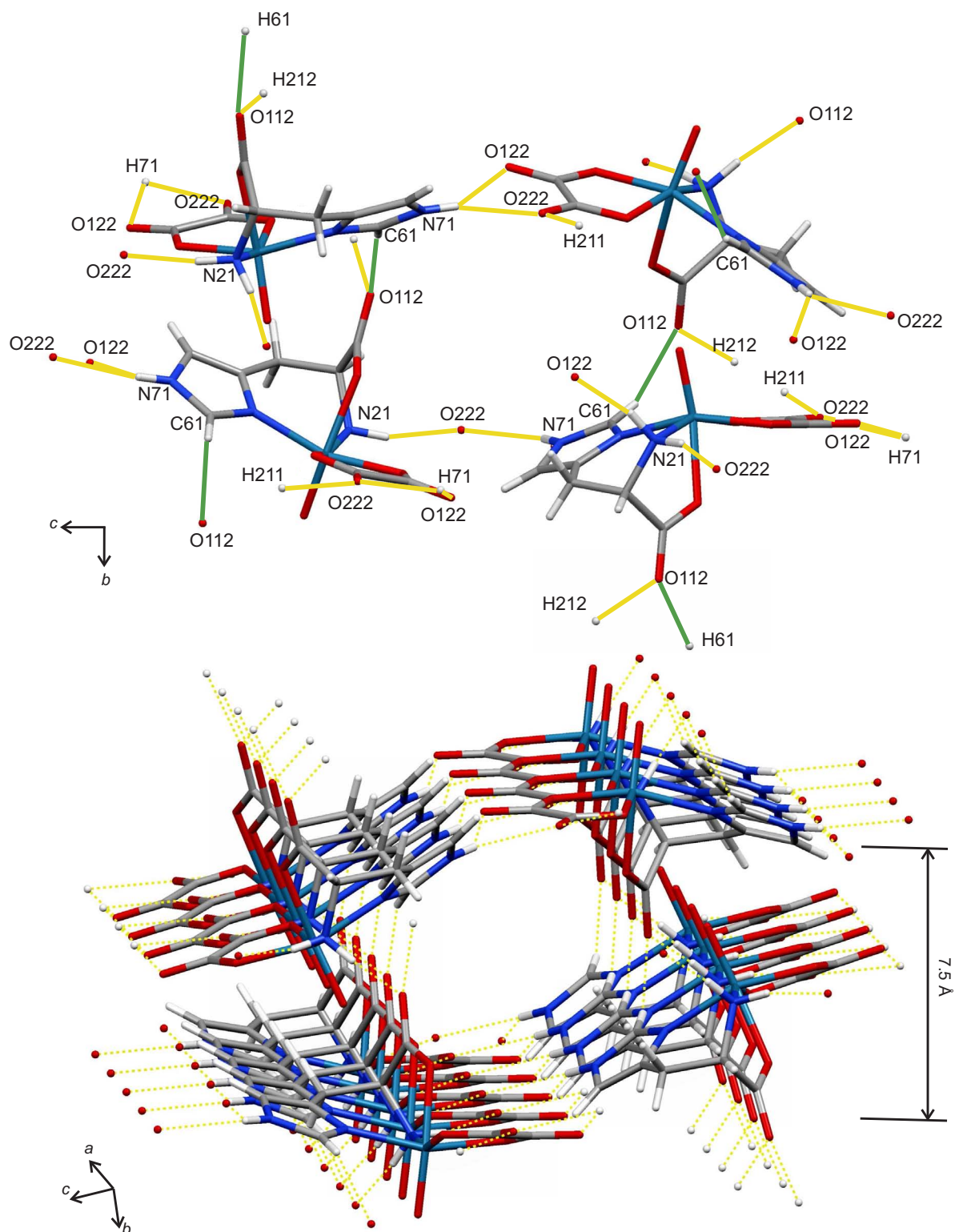


Figure 2.40 MERCURY presentation of hydrogen bonds (yellow lines) and C-H...O contacts (green lines) in **9**. Above only a frame is illustrated and below the repetitive pattern forming tunnels along $[100]$.

2 Results

Solutions of **9** in water were acidic (see experimental part chapter 5.5.9 on page 170) and stable for several days. But due to its limited solubility in water, ^{13}C NMR spectra of **9** were recorded in DMSO- d_6 . These signals are listed in Table 2.18. As opposed to coordinated diolato functions with sp^3 carbon atoms, the signals of the oxalato ligand (sp^2) were shifted only by -0.84 ppm (instead of up to $+28$ ppm) to lower field. Only one signal was observed for C1/C2 in spite of the distorted octahedral geometry of the complex. Depending on the distance to the metal center, the signals of the histidinato ligand were shifted up to 11 ppm.

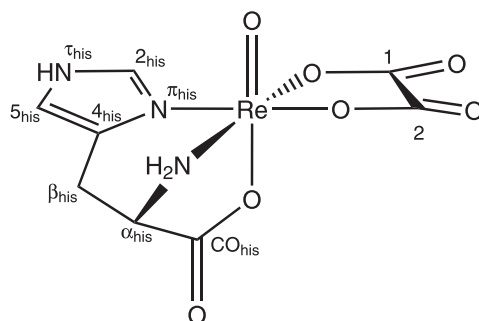


Figure 2.41 Scheme of **9** and atom numbering used in the ^{13}C NMR study according to the recommendations of the JCBN^[79].

Table 2.18 ^{13}C NMR chemical shifts (in ppm) of **9** in DMSO- d_6 (67.9 MHz, 25 °C) and comparison with the free ligands under the same conditions. The signal of the deuterated solvent ($\delta = 39.52$ ppm) was used as an internal secondary reference^[65] for the chemical shift. For atom numbering see Figure 2.41. Assignment of free L-histidine according to the literature^[91].

		L-histidine					sodium oxalate	
		C_{CO}	C_{α}	C_{β}	C_2	C_4	C_5	C1/C2
free	δ	169.98	51.62	25.63	134.59	127.61	118.13	161.94
9	δ	174.55	59.00	26.65	145.55	137.49	117.78	161.10
	$\Delta\delta$	4.57	7.38	1.02	10.96	9.88	-0.35	-0.84

2.3.2 The reaction of $[\text{ReOCl}_3(\text{PPh}_3)_2]$ with L-histidine and 1,2-ethanediol

After recrystallization from water, crystals of $[\text{ReO}(\text{L-his})(\text{EthdH}_{-2})] \cdot 4.5 \text{ H}_2\text{O}$ (**10**) were obtained from the reaction of $[\text{ReOCl}_3(\text{PPh}_3)_2]$, L-histidine, 1,2-ethanediol and triethylamine in methanol. The asymmetric unit in the monoclinic space group $P2_1$ contains eleven molecules: two rhenium complexes and nine molecules of water. Two of water molecules are disordered and were refined without hydrogen atoms (O911/O912, O921/O922). The two rhenium complexes are very similar, Figure 2.42 shows one of them.

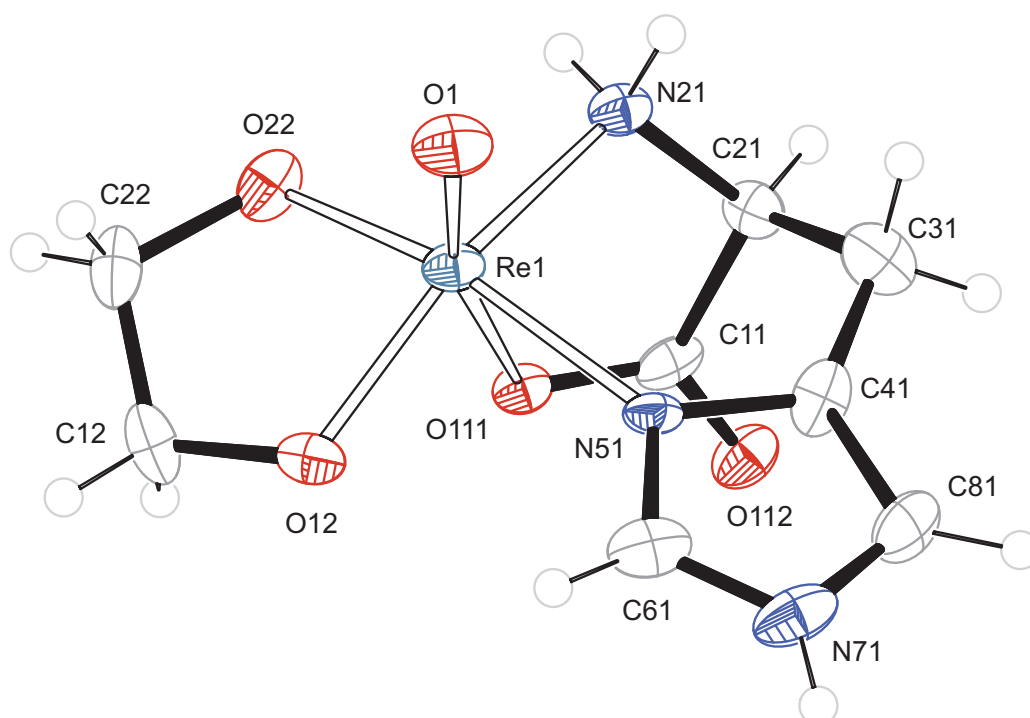


Figure 2.42 ORTEP presentation of **10** in crystals of $[\text{ReO}(\text{L-his})(\text{EthdH}_{-2})] \cdot 4.5 \text{ H}_2\text{O}$. Ellipsoids are drawn at 50 % probability level. Distances [Å] and angles [°]: Re1-O1 1.689(6), Re1-O12 1.950(5), Re1-O22 1.945(6), Re1-O111 2.187(5), Re1-N21 2.143(6), Re1-N51 2.105(6); O1-Re1-O12 111.2(3), O1-Re1-O22 103.9(3), O1-Re1-O111 163.6(2), O1-Re1-N21 93.6(3), O1-Re1-N51 95.1(3), O12-Re1-O22 83.2(3), O12-Re1-O111 84.0(2), O12-Re1-N21 155.2(3), O12-Re1-N51 88.4(2), O22-Re1-O111 83.3(2), O22-Re1-N21 90.5(3), O22-Re1-N51 160.9(3), O111-Re1-N21 71.4(3), O111-Re1-N51 78.9(3), N21-Re1-N51 90.1(2), diol torsion angle O12-C12-C22-O22: 43.5(10), torsion angle of the coordinated acid group Re1-O111-C11-O112: 155.1(6). **Distances [Å] and angles [°] of the other molecule in the asymmetric unit:** Re2-O2 1.685(6), Re2-O14 1.954(5), Re2-O24 1.958(6), Re2-O131 2.198(5), Re2-N23 2.151(6), Re2-N53 2.115(6); O2-Re2-O14 110.5(3), O2-Re2-O24 103.8(3), O2-Re2-O131 163.4(2), O2-Re2-N23 93.6(3), O2-Re2-N53 96.2(3), O14-Re2-O24 82.2(2), O14-Re2-O131 85.3(2), O14-Re2-N23 155.9(3), O14-Re2-N53 88.5(3), O24-Re2-O131 82.8(2), O24-Re2-N23 91.0(2), O24-Re2-N53 159.9(3), O131-Re2-N23 70.9(3), O131-Re2-N53 78.7(3), N23-Re2-N53 90.4(2), diol torsion angle O14-C14-C24-O24: 44.1(9), torsion angle of the coordinated acid group Re2-O131-C13-O132: 153.9(6).

The deprotonated form of L-histidine is in the tridentate binding mode as an (*N,N,O*)-donor with O111 of the carboxylato-group *trans* to the oxido ligand O1. Compared with **9** and the compound reported by *Tessier et al.* (Figure 2.36 on page 51), this complex is more severely distorted octahedral: the imidazole ring is still planar, but the rhenium center is shifted 0.172 Å out of its plane and the carboxylato group is tilted (torsion angle of Re1-O111-C11-O112: 155.1°). Unlike the previous compound, the chelating diolato moiety is non-planar with a torsion angle of 43.5° for O12-C12-C22-O22. The same holds true for the other molecule in the asymmetric unit (see text of Figure 2.42).

Concerning the crystal packing, there are sheets of rings parallel to the ($\bar{1}01$) plane connected by hydrogen bonds of the type N-H \cdots O. In between there are sheets of water molecules with hydrogen bonds of the type O-H \cdots O (Table 2.19 and Figure 2.43). With a view along [010], the imidazole rings are staggered parallel with distances of 3.21 Å and 3.26 Å. But they are not exactly lying upon each other: they are shifted and approximately only two of the five atoms of imidazole are stacked (see Figure 2.43).

Table 2.19 Distances [\AA] and angles [$^\circ$] of hydrogen bonds in **10**. Values without standard deviation are related to hydrogen atoms at calculated positions. For atom numbering see Figure 2.42. Hydrogen atoms of two disordered water molecules (O911/O912, O921/O922) were not included, but in five further water molecules (O93 to O97) they were accounted in calculation. D: donor, A: acceptor, x : difference of ($\text{H} \cdots \text{A}$) and the sum of the van-der-Waals radii^[62].

D	H	A	D \cdots A	D-H	H \cdots A	x	D-H \cdots A
N21	H211	O1 ⁱ	2.996(10)	0.92	2.15	-0.57	153
N21	H212	O22 ⁱⁱ	2.822(11)	0.92	1.97	-0.75	154
N23	H231	O2 ^{iv}	3.051(9)	0.92	2.20	-0.52	154
N23	H232	O24 ^v	2.811(10)	0.92	1.96	-0.76	153
N71	H771	O131	2.834(8)	0.88	2.07	-0.65	145
N71	H771	O132	3.165(8)	0.88	2.53	-0.19	130
N73	H773	O111 ^{vi}	2.808(8)	0.88	2.07	-0.65	141
O93	H931	O14 ⁱⁱⁱ	2.903(10)	0.80(7)	2.14(8)	-0.58	161(7)
O93	H932	O99 ^{vii}	2.878(11)	0.80(5)	2.42(9)	-0.30	118(8)
O94	H941	O911	2.895(18)	0.80(4)	2.36(7)	-0.36	126(8)
O94	H941	O912	2.739(18)	0.80(4)	2.03(5)	-0.69	148(9)
O94	H942	O98	2.760(11)	0.80(8)	2.00(7)	-0.72	160(7)
O95	H951	O94 ^v	2.775(12)	0.79(6)	2.05(6)	-0.67	152(6)
O95	H952	O98 ^{iv}	2.775(11)	0.79(6)	2.05(8)	-0.67	152(8)
O96	H961	O94 ^v	2.802(11)	0.80(6)	2.06(7)	-0.66	155(8)
O96	H962	O99	2.825(11)	0.80(7)	2.09(7)	-0.63	154(9)
O97	H971	O93	2.767(11)	0.79(6)	2.02(5)	-0.71	159(8)
O97	H972	O95	2.814(11)	0.80(7)	2.16(7)	-0.56	140(8)
O98	H981	O132	2.762(9)	0.79(5)	2.04(6)	-0.68	151(7)
O98	H982	O921	2.75(2)	0.79(7)	2.00(8)	-0.73	159(7)
O98	H982	O922	2.85(3)	0.79(7)	2.12(6)	-0.61	155(7)
O99	H991	O97	2.755(11)	0.80(7)	2.17(7)	-0.54	130(7)
O99	H992	O112 ^{viii}	2.766(8)	0.80(8)	2.04(8)	-0.68	152(7)

Symmetry codes: ⁱ $-x, y - \frac{1}{2}, -z$; ⁱⁱ $-x, y + \frac{1}{2}, -z$; ⁱⁱⁱ $x, y - 1, z$; ^{iv} $-x + 1, y - \frac{1}{2}, -z + 1$;
^v $-x + 1, y + \frac{1}{2}, -z + 1$; ^{vi} $x, y + 1, z$; ^{vii} $-x + 1, y - \frac{1}{2}, -z$; ^{viii} $-x + 1, y + \frac{1}{2}, -z$.

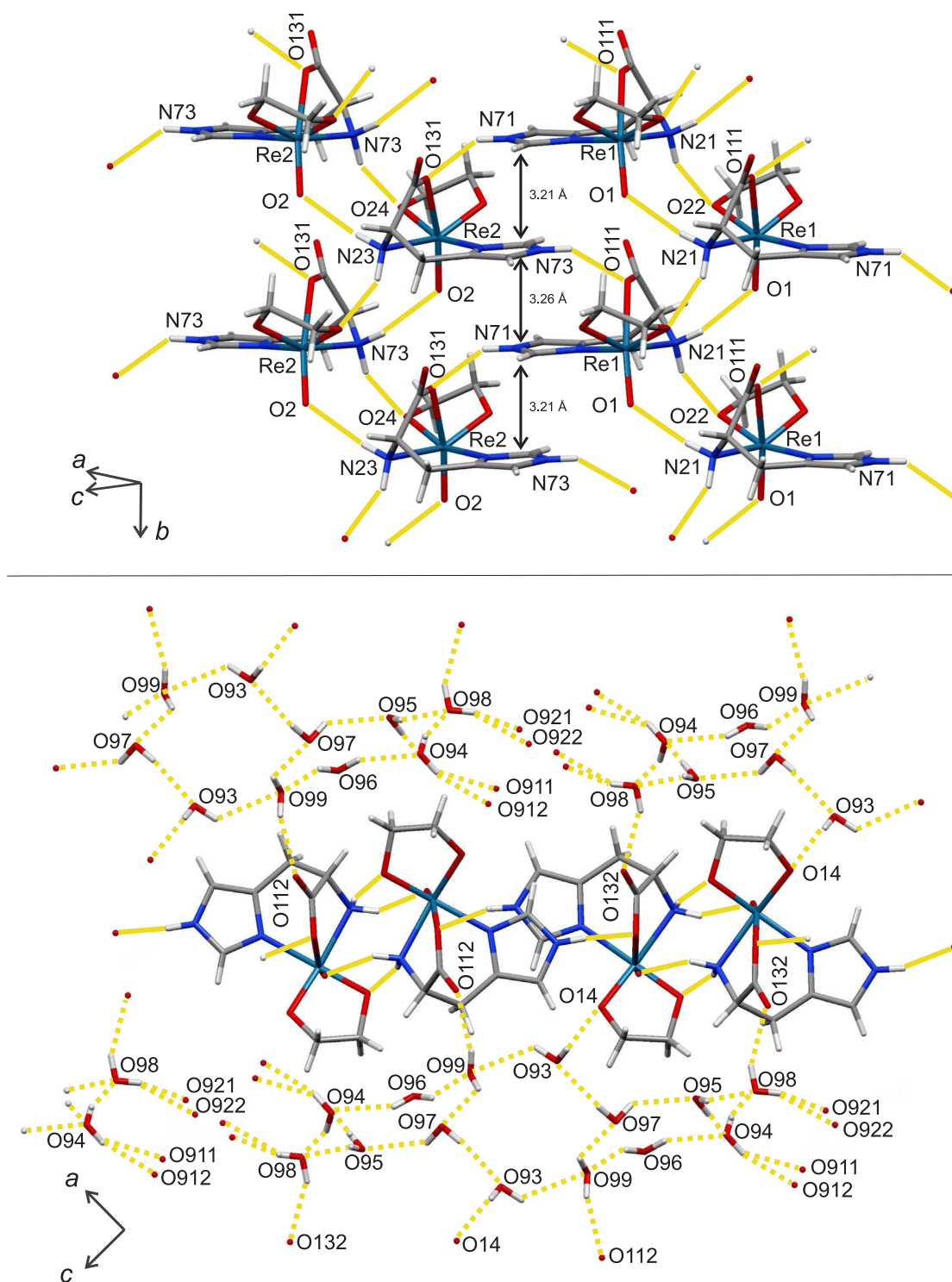


Figure 2.43 MERCURY presentation of hydrogen bonds in **10**. Top: π -stacking of the imidazole groups and hydrogen bond chains (yellow lines) along the b axis presented without water molecules. Below: view along the b axis including hydrogen bonds (yellow dashed lines) of the water molecules.

2 Results

For solutions of **10**, only one signal set was observed. Table 2.20 shows the ^{13}C NMR chemical shifts in D_2O . As C1 and C2 of the ethanediolato ligand are not chemically equivalent, two signals are observed. They are shifted 20–21 ppm due to the coordination of the diol. The signals of L-histidine are shifted up to 7.9 ppm to lower field.

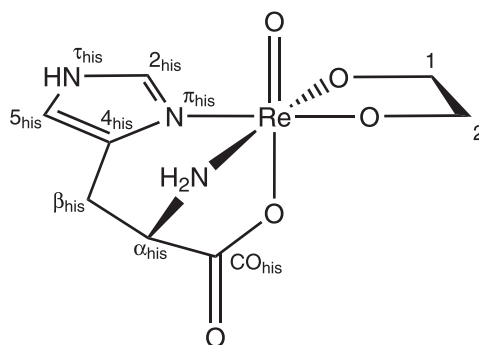


Figure 2.44 Scheme of **10** and atom numbering used in the ^{13}C NMR study according to the recommendations of the JCBN^[79].

Table 2.20 ^{13}C NMR chemical shifts (in ppm) of **10** in D_2O (67.9 MHz, 25 °C) and comparison with the free ligands under the same conditions (pH 5.8). The signal of a drop of methanol ($\delta = 49.50$ ppm in D_2O) was used as an internal secondary reference^[65] for the chemical shift. For atom numbering see Figure 2.44. $\Delta\delta$ values indicating a diolate coordination are in boldface. Assignment of free L-histidine according to the literature^[91].

		L-histidine					ethanediol	
		C_{CO}	C_{α}	C_{β}	C2	C4	C5	C1/C2
free	δ	174.24	55.40	28.67	136.72	132.62	117.44	63.20
10	δ	180.32	59.00	27.78	144.60	138.80	118.10	83.51, 84.24
	$\Delta\delta$	6.08	3.60	-0.89	7.88	6.18	0.66	20.31, 21.04

2.3.3 The reaction of $[\text{ReOCl}_3(\text{PPh}_3)_2]$ with L-histidine and anhydroerythritol

To explore the reactions of more complex carbohydrates with the $\{\text{ReO}\}^{3+}$ core and L-histidine, anhydroerythritol was chosen as a model compound for furanoidic carbohydrates. Starting from the rhenium(V) precursor $[\text{ReOCl}_3(\text{PPh}_3)_2]$, L-histidine, anhydroerythritol (AnEryt) and triethylamine in refluxing methanol, blue crystals of $[\text{ReO}(\text{L-his})(\text{syn-AnErytH}_2)] \cdot 2 \text{H}_2\text{O}$ (**11**) were recrystallized from water.

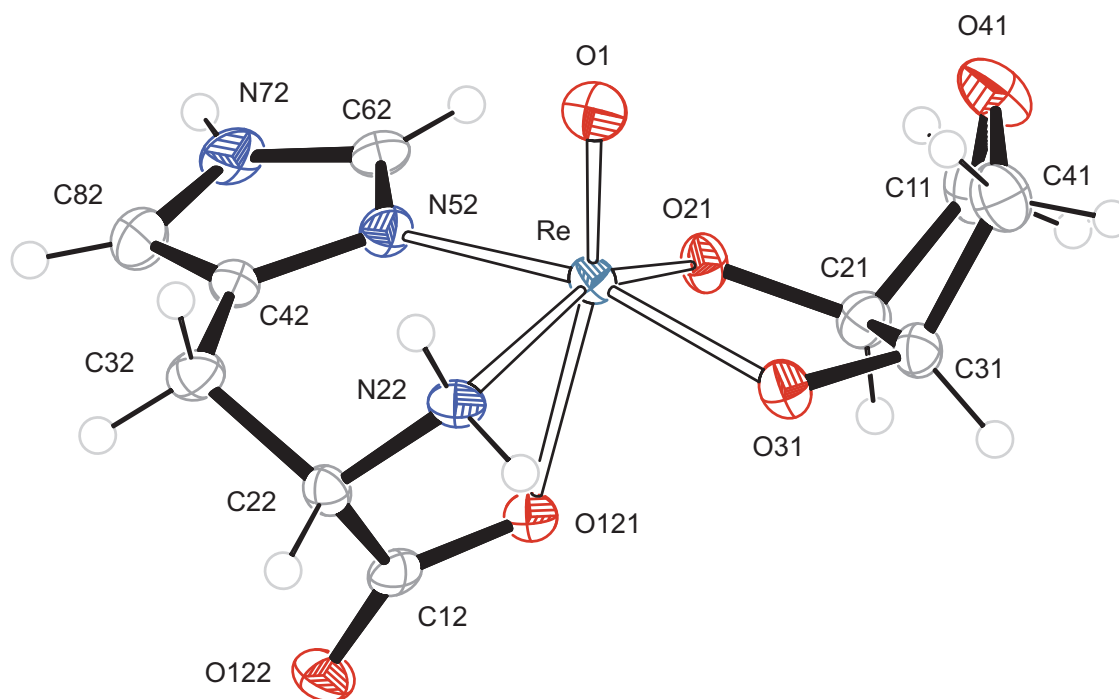


Figure 2.45 ORTEP presentation of **11** in crystals of $[\text{ReO}(\text{L-his})(\text{syn-AnErytH}_2)] \cdot 2 \text{H}_2\text{O}$. Ellipsoids are drawn at 50 % probability level. Distances [Å] and angles [°]: Re-O1 1.682(3), Re-O21 1.924(3), Re-O31 1.959(3), Re-O121 2.205(3), Re-N22 2.169(3), Re-N52 2.102(3); O1-Re-O21 112.78(17), O1-Re-O31 104.17(15), O1-Re-O121 162.64(16), O1-Re-N22 93.0(2), O1-Re-N52 96.4(2), O21-Re-O31 82.47(13), O21-Re-O121 83.87(13), O21-Re-N22 154.2(2), O21-Re-N52 86.95(15), O31-Re-O121 82.17(13), O31-Re-N22 91.11(15), O31-Re-N52 159.21(19), O121-Re-N22 70.5(2), O121-Re-N52 78.94(17), N22-Re-N52 90.71(14), diol torsion angle O21-C21-C31-O31: 28.2(5), torsion angle of the coordinated acid group Re-O121-C12-O122: 157.6(3), puckering parameters^[59] for O41-C11-C21-C31-C41: $Q_2 = 0.345(6)$ Å, $\phi_2 = 218.1(10)^\circ$, conformation 1E .

The asymmetric unit contains one molecule of the rhenium complex (Figure 2.45) and two molecules of water while there are two of these formula units in the unit cell of the monoclinic space group $P2_1$. In analogy to **9** and **10**, the deprotonated form of L-histidine is connected as an (N,N,O)-donor to the metal with O121 of the carboxylate group *trans* to the oxido ligand O1. The (O,O)-donor AnErytH₂ completes

the distorted octahedral coordination in *syn* orientation to O1. The torsion angle of the diol (28.2°) is smaller than the corresponding angle in **10** of the previous chapter, but normal for an oxolanediolato ligand (see also **3** and **7**). The closest pucker descriptor^[59] for the five membered ring C11-C21-C31-C41-O41 describes an envelope conformation on C11.

In analogy to the isostructural crystal packing of **10**, the imidazole rings are stacked along [010] with a distance of 3.25 Å. Hydrogen-bonded eight membered rings are forming chains in this direction, as illustrated in Figure 2.46 (above). The figure in the middle shows the crystal packing including the water molecules linked between these sheets parallel to the (010) plane. Among the hydrogen bonds listed in Table 2.21, two weak interactions of the type C-H···O were also accounted for, as they are part of the hydrogen bonding of the water chains along [010] (see below in Figure 2.46).

Table 2.21 Distances [Å] and angles [°] of hydrogen bonds in **11**. Values without standard deviation are related to hydrogen atoms at calculated positions. For atom numbering see Figure 2.45. O98 and O99 are affiliated to water molecules. D: donor, A: acceptor, x : difference of (H···A) and the sum of the van-der-Waals radii^[62].

D	H	A	D···A	D-H	H···A	x	D-H···A
N72	H72	O121 ⁱⁱⁱ	2.872(5)	0.88	2.08	-0.64	149
N22	H221	O1 ⁱ	3.051(6)	0.92	2.21	-0.51	152
N22	H222	O31 ⁱⁱ	2.779(7)	0.92	1.93	-0.79	152
O98	H981	O41	2.924(8)	0.82(5)	2.13(4)	-0.59	163(5)
O98	H982	O99 ^{iv}	2.740(8)	0.83(4)	1.92(4)	-0.80	172(4)
O99	H991	O98	2.776(8)	0.83(4)	1.96(4)	-0.76	171(4)
O99	H992	O122 ^v	2.769(6)	0.82(4)	1.96(4)	-0.76	167(4)
C62	H62	O99 ^{iv}	3.600(7)	0.95	2.66	-0.06	171
C82	H82	O98 ^{vi}	3.408(7)	0.95	2.61	-0.11	142

Symmetry codes: ⁱ $-x + 1, y + \frac{1}{2}, -z$; ⁱⁱ $-x + 1, y - \frac{1}{2}, -z$; ⁱⁱⁱ $-x, y - \frac{1}{2}, -z$;
^{iv} $-x, y + \frac{1}{2}, -z + 1$; ^v $x, y - 1, z + 1$; ^{vi} $-x, y + \frac{1}{2}, -z$.

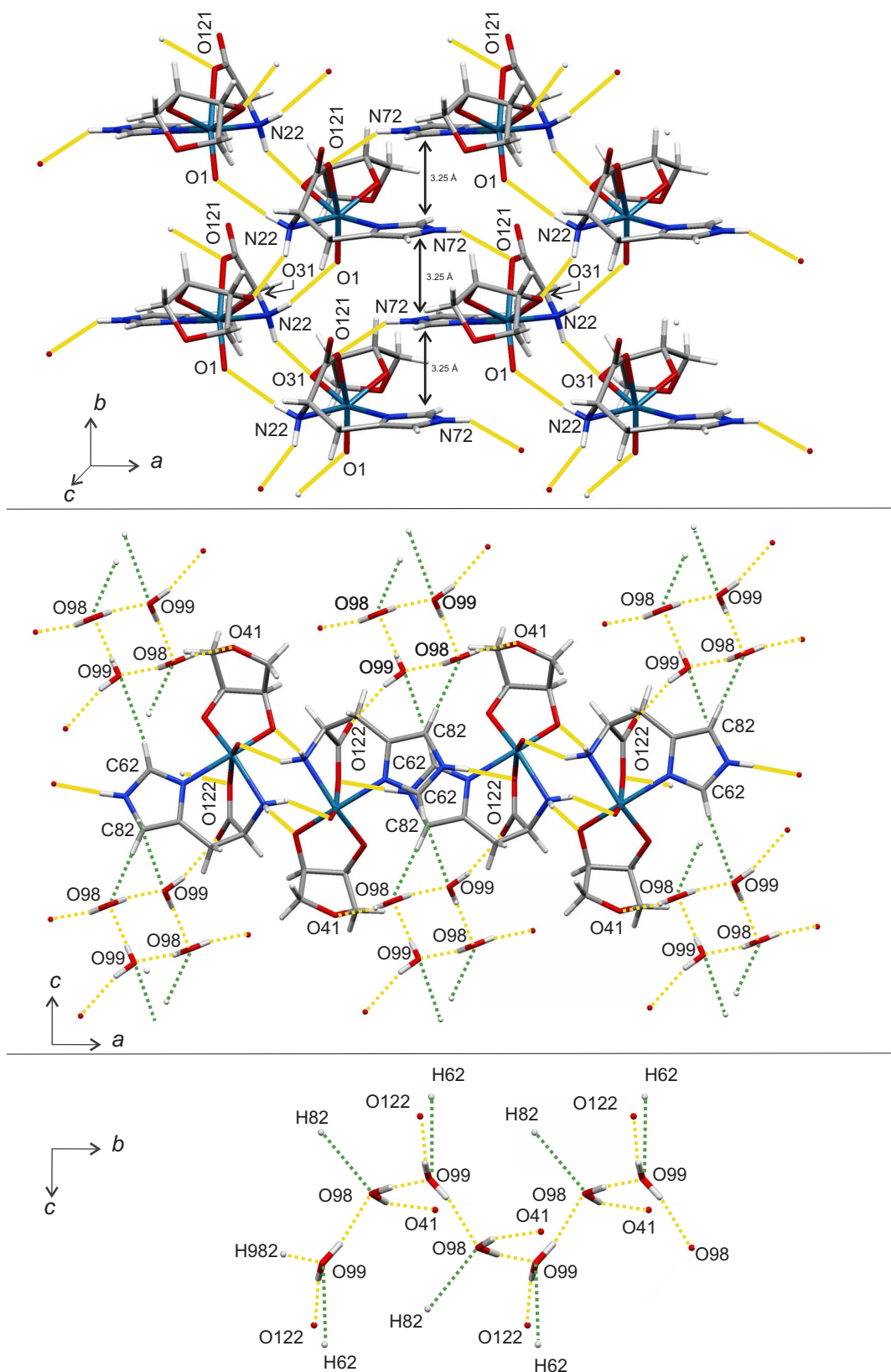


Figure 2.46 MERCURY presentation of hydrogen bonds and weak interactions in **11**. Top: π - π interactions of the imidazole groups and hydrogen bond chains (yellow lines) along the *b* axis without water molecules. Middle: view along the *b* axis including hydrogen bonds (yellow dashed lines) and C-H \cdots O contacts (green dashed lines) affecting the water molecules. Below: infinite water chain along the *b* axis.

2 Results

As mentioned above, the result of the structure determination shows the oxolane-diolato ligand in *syn* orientation to the oxido ligand. The possible presence of *syn/anti* isomerism (Figure 2.47) was not observed in spectra of the crude reaction mixture or of redissolved crystals. These spectra showed only one signal set of *syn*-**11**, the signals of the possible *anti*-isomer were below detection limit. In Table 2.21 the ^{13}C NMR chemical shifts of redissolved crystals of **11** in D_2O are listed. The signals of C2/C3 of the coordinated diol gain a low-field shift of up to 26.2 ppm and are observed as separated signals due to the lack of chemical equivalence in this distorted octahedral coordination. The same is observed for the signals of C1/C4, but these are shifted only by up to 4.6 ppm. This relation of a large/small shift and the distance to the rhenium core is also observed for the histidinato ligand: the signals of C_{CO} , C_α , C2 and C4 are shifted up to 7.9 ppm to lower field, while the signals of C_β and C5 are shifted less than 0.9 ppm.

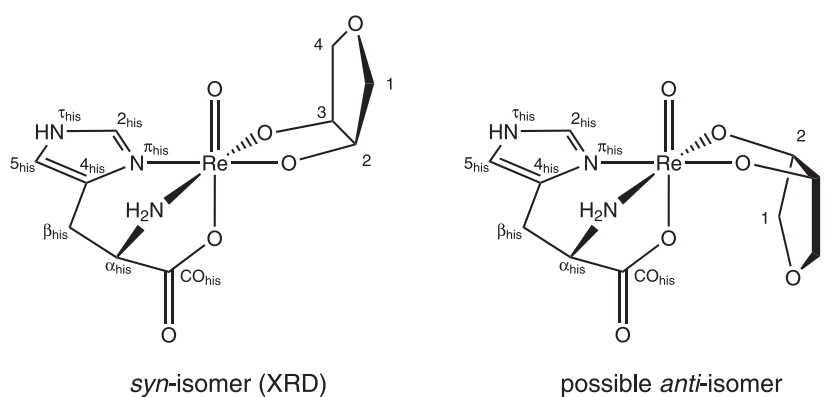


Figure 2.47 Scheme of the diastereomeric forms of **11** and atom numbering used in the ^{13}C NMR study according to the recommendations of the JCBN^[79]. XRD: result of the structure determination.

Table 2.22 ^{13}C NMR chemical shifts (in ppm) of **11** in D_2O (67.9 MHz, 25 °C) and comparison with the free ligands under the same conditions (pH 6.5). The signal of a drop of methanol ($\delta = 49.50$ ppm in D_2O) was used as an internal secondary reference^[65] for the chemical shift. For atom numbering see Figure 2.47. $\Delta\delta$ values indicating a diolate coordination are in boldface. Assignment according to the literature: L-histidine^[91], anhydroerythritol^[77].

		L-histidine			AnEryt				
		C_{CO}	C_α	C_β	C2	C4	C5	C2/C3	C1/C4
free	δ	173.66	55.38	28.67	136.65	133.12	117.40	72.06	71.04
11	δ	179.75	58.83	27.87	144.27	139.05	117.96	98.25, 95.84	76.08, 74.74
	$\Delta\delta$	6.09	3.45	-0.96	7.62	5.93	0.56	26.19, 23.78	4.66, 3.32

2.3.4 The reaction of $[\text{ReOCl}_3(\text{PPh}_3)_2]$ with L-histidine and uridine

The successful preparation of the oxolanediolato complex **11** in the previous chapter gave rise to the question of whether it is possible to coordinate a more complex furanoidic carbohydrate derivative. Uridine (Urd), a pyrimidine nucleoside, offers among its functions the structural motifs of the diols used so far in this section (ethanediol, anhydroerythritol). The reaction of $[\text{ReOCl}_3(\text{PPh}_3)_2]$ with L-histidine, uridine and triethylamine in methanol yielded a blue powder, from which $[\text{ReO}(\text{L-his})(\text{syn-Urd}_{2',3'\text{H}_-2})] \cdot 1.5 \text{H}_2\text{O}$ (**12**) was recrystallized from water.

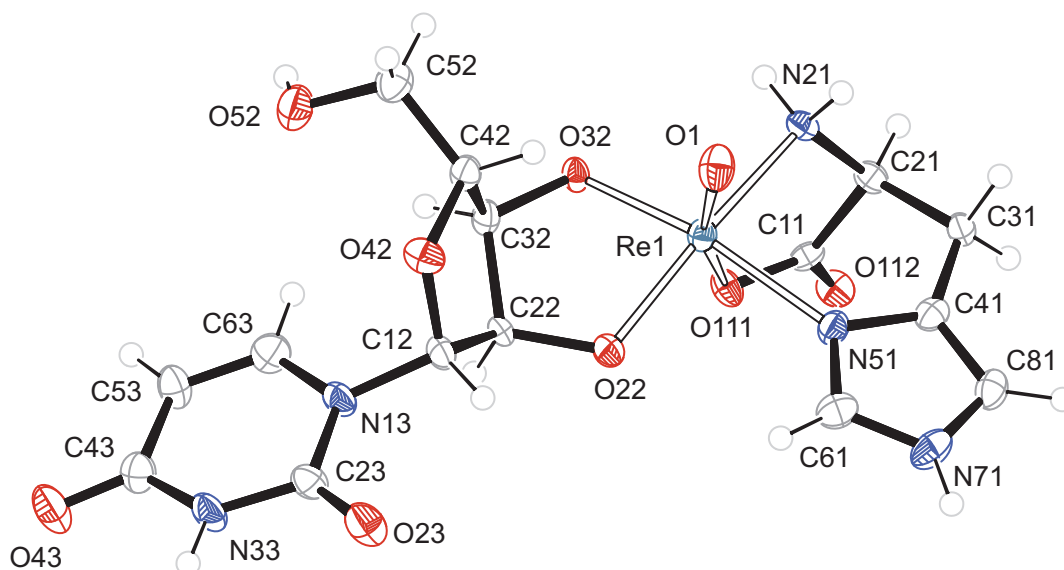


Figure 2.48 ORTEP presentation of **12a** in crystals of $[\text{ReO}(\text{L-his})(\text{syn-Urd}_{2',3'\text{H}_-2})] \cdot 1.5 \text{H}_2\text{O}$. Ellipsoids are drawn at 50 % probability level. Distances [Å] and angles [°]: Re1-O1 1.676(3), Re1-O22 1.962(3), Re1-O32 1.972(3), Re1-O111 2.142(3), Re1-N21 2.156(3), Re1-N51 2.117(3), O1-Re1-O22 109.37(15), O1-Re1-O32 101.99(15), O1-Re1-O111 160.12(14), O1-Re1-N21 87.60(14), O1-Re1-N51 94.69(15), O22-Re1-O32 81.27(13), O22-Re1-O111 90.13(13), O22-Re1-N21 163.00(13), O22-Re1-N51 92.31(13), O32-Re1-O111 84.31(12), O32-Re1-N21 94.54(13), O32-Re1-N51 163.28(13), O111-Re1-N21 73.02(13), O111-Re1-N51 80.26(12), N21-Re1-N51 87.11(13), furanose torsion angle O22-C22-C32-O32: 28.6(5), torsion angle of the coordinated acid group Re1-O111-C11-O112: 172.3(3), puckering parameters^[59] for O42-C12-C22-C32-C42: $Q_2 = 0.266(5) \text{ \AA}$, $\phi_2 = 283.0(10)^\circ$, conformation 3E . **Distances [Å] and angles [°] of the other molecule **12b** in the asymmetric unit:** Re2-O2 1.688(3), Re2-O26 1.934(3), Re2-O36 1.971(3), Re2-O141 2.139(3), Re2-N24 2.170(4), Re2-N54 2.092(4), O2-Re2-O26 110.99(16), O2-Re2-O36 103.31(15), O2-Re2-O141 163.20(15), O2-Re2-N24 92.01(17), O2-Re2-N54 93.26(17), O26-Re2-O36 81.94(13), O26-Re2-O141 84.62(13), O26-Re2-N24 156.92(16), O26-Re2-N54 88.52(15), O36-Re2-O141 84.48(13), O36-Re2-N24 94.98(15), O36-Re2-N54 162.96(16), O141-Re2-N24 72.30(15), O141-Re2-N54 80.58(15), N24-Re2-N54 88.27(16), furanose torsion angle O26-C26-C36-O36: 1.6(5), torsion angle of the coordinated acid group Re2-O141-C14-O142: 171.9(4), puckering parameters^[59] for O46-C16-C26-C36-C46: $Q_2 = 0.395(5) \text{ \AA}$, $\phi_2 = 358.4(8)^\circ$, conformation 0E .

12 crystallizes in the orthorhombic space group $P2_12_12_1$ with eight formula units in the unit cell. The asymmetric unit contains two similar rhenium complexes (Figure 2.48 shows one of them) and three molecules of water. Two of these water molecules are disordered (O992/O993 and O994/O995). In both neutral rhenium complexes the double deprotonated uridine ligands are connected as (*O,O*)-donor ligands via O2' and O3' of the ribosyl moiety (for general carbohydrate numbering see Figure 2.51) to the metal, namely O22, O32 and O26, O36. The orientation of these Urd2',3'H₋₂ ligands is *syn* to the respective oxido ligands O1/O2. Due to this chelate formation the diol's torsion angles (28.6° and 1.6°) deviate from the angles found in the free form of uridine^[66] (46.7° and 52.1°). The torsion angles for O4'-C1'-N1-C2 about the *N*-glycosidic bond ($\chi = -106.8^\circ$ and -154.7°) differ from the ones in free uridine (-153.0° and -164.4°), though they are still defining an *anti* conformation. The monoanionic histidinato ligands are both in an (*N,N,O*) binding mode with O111/O141 of the carboxylato groups in *trans* position to the oxido ligands O1/O2.

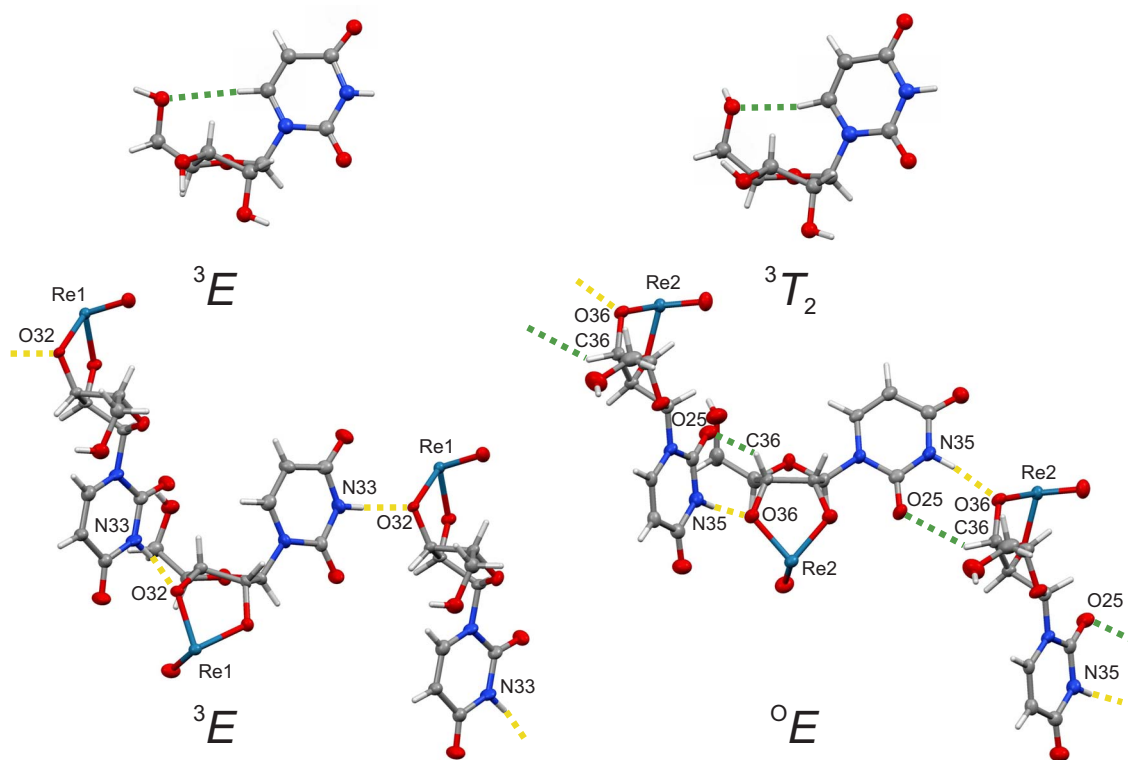


Figure 2.49 MERCURY presentation of the furanose rings in free uridine^[66] (above) and in **12a**, **12b** (below). The atoms of the histidinato ligand are not shown. Yellow and green dashed lines: classical hydrogen bonds (N-H \cdots O) and weak interactions (C-H \cdots O).

In the structure of free uridine^[66], an intramolecular weak interaction of the type C-H \cdots O from the pyrimidine's C6 to O5' of the ribose part is found. No such intramolecular, but rather intermolecular interactions are to be found in the structure of **12**.

Figure 2.49 illustrates the furanose rings of **12** being in 3E and 0E conformation with different hydrogen-bond/short-contact environments. Among the various other hydrogen bonds (Table 2.23) only the stronger ones (shorter than $\text{svdW} - 0.5 \text{ \AA}$) were accounted for Figure 2.50. Parallel to the (100) plane, hydrogen bonds of the type $\text{N-H} \cdots \text{O}$ and $\text{O-H} \cdots \text{O}$ connect the pyrimidine and ribosyl parts to sheets of **12a** and **12b**. Although no typical hydrogen bondings of RNA base pairs are observed, in this case eight-membered rings ($\text{O43-C43-N33-H733} \cdots \text{O32-Re1-N21-H721} \cdots$) are linking the uracil parts with neighboring molecules (similar to the U:U base-pair group^[78]). Above in Figure 2.50 the formation of such a sheet of **12a** is illustrated (the sheets of **12b** are not shown). They are linked by hydrogen bonds from the amino functions to the carboxylate oxygens of the histidinato ligands in [100] direction.

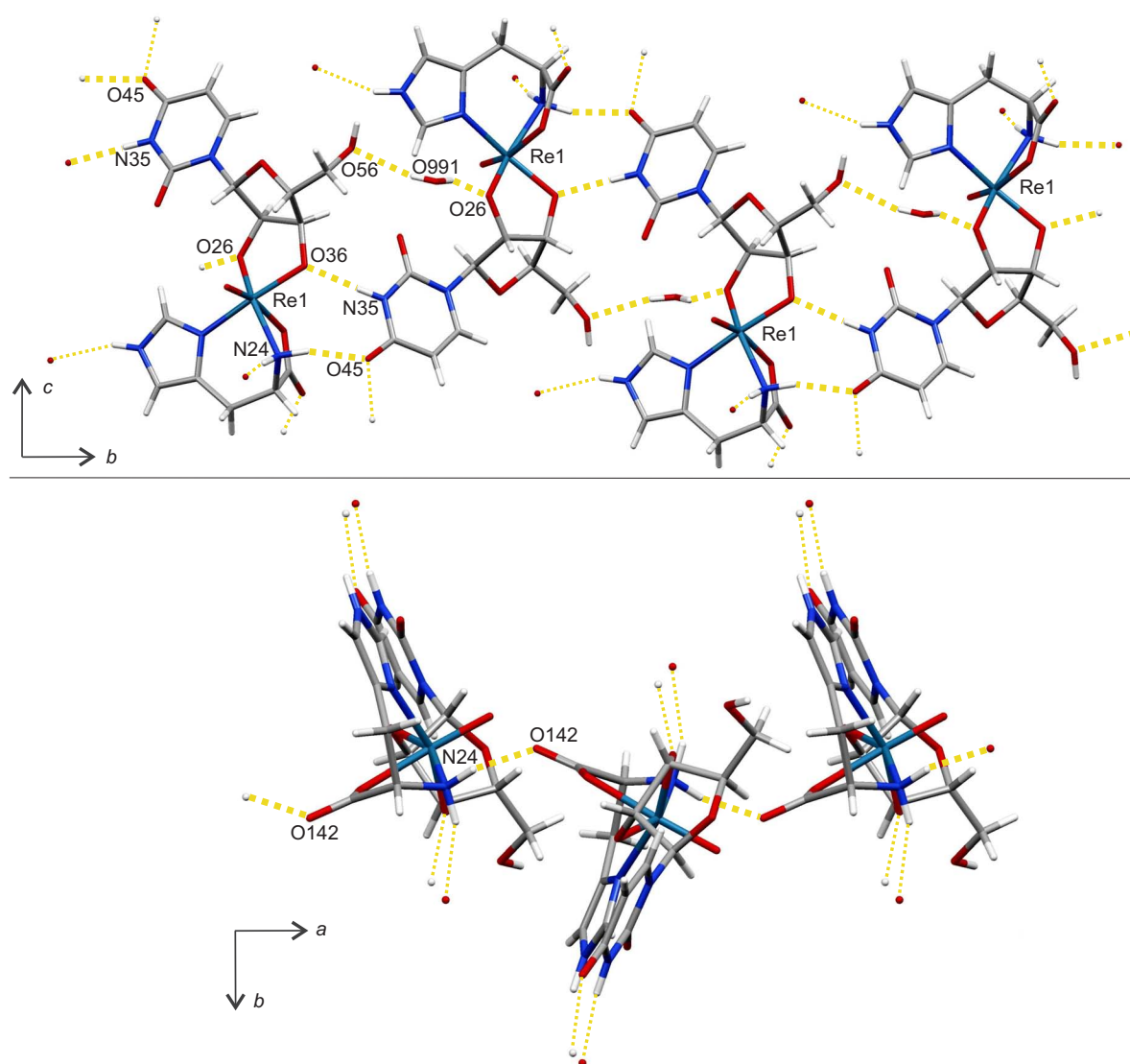


Figure 2.50 MERCURY presentation of hydrogen bonds (yellow lines) in **12**.

2 Results

Table 2.23 Distances [Å] and angles [°] of hydrogen bonds in **12**. Values without standard deviation are related to hydrogen atoms at calculated positions. O991 as well as O992/O993 and O994/O995 are affiliated to three water molecules. D: donor, A: acceptor, x: difference of (H···A) and the sum of the van-der-Waals radii^[62].

D	H	A	D···A	D-H	H···A	x	D-H···A
N21	H721	O43 ⁱ	2.863(5)	0.92	2.00	-0.72	155
N21	H722	O112 ⁱⁱ	2.954(5)	0.92	2.04	-0.68	171
N71	H771	O52 ⁱⁱⁱ	2.938(5)	0.88	2.18	-0.54	144
O52	H852	O994	2.771(17)	0.84	1.94	-0.79	174
O52	H852	O995	2.784(16)	0.84	2.01	-0.71	152
N33	H733	O32 ^v	2.768(5)	0.88	1.89	-0.83	173
N24	H241	O45 ^{vi}	2.852(6)	0.92	1.99	-0.73	155
N24	H242	O142 ^{vii}	2.825(5)	0.92	1.92	-0.80	168
N74	H774	O112 ^{viii}	2.894(5)	0.88	2.20	-0.52	136
N35	H735	O36 ^{ix}	2.772(5)	0.88	1.90	-0.82	172
O56	H856	O993 ^v	3.00(2)	0.84	2.21	-0.52	157
O991	H991	O26 ^x	2.986(7)	0.80(3)	2.21(3)	-0.51	164(6)
O991	H992	O56 ⁱ	2.931(7)	0.80(3)	2.16(3)	-0.56	162(6)
O992	H993	O22 ⁱ	2.806(7)	0.80(3)	2.10(4)	-0.62	148(7)
O992	H994	O45 ^{viii}	2.738(7)	0.80(3)	1.95(3)	-0.77	170(7)
O993	H995	O22 ⁱ	3.03(2)	0.80(3)	2.4(2)	-0.29	132(26)
O993	H996	O45 ^{viii}	3.10(2)	0.80(3)	2.41(16)	-0.31	145(25)
O994	H997	O991	3.06(2)	0.80(3)	2.34(7)	-0.38	151(12)
O994	H998	O23 ⁱ	2.80(2)	0.80(3)	2.23(8)	-0.49	129(9)
O995	H999	O992	2.72(2)	0.80(3)	2.06(8)	-0.66	139(12)
O995	H990	O141 ^x	3.13(4)	0.80(3)	2.73(11)	-0.01	113(10)
C36	H36	O25 ^{vi}	3.324(6)	1.00	2.49	-0.23	141

Symmetry codes: ⁱ $-x + 1, y - \frac{1}{2}, -z + \frac{1}{2}$; ⁱⁱ $x + \frac{1}{2}, -y + \frac{1}{2}, -z + 1$; ⁱⁱⁱ $-x + \frac{3}{2}, -y + 1, z + \frac{1}{2}$; ^{iv} $-x + \frac{1}{2}, -y + 1, z + \frac{1}{2}$; ^v $-x + 1, y + \frac{1}{2}, -z + \frac{1}{2}$; ^{vi} $-x, y + \frac{1}{2}, -z + \frac{1}{2}$; ^{vii} $x + \frac{1}{2}, -y + \frac{1}{2}, -z$; ^{viii} $-x + \frac{1}{2}, -y, z - \frac{1}{2}$; ^{ix} $-x, y - \frac{1}{2}, -z + \frac{1}{2}$; ^x $x + 1, y, z$.

In view of NMR spectroscopy the small differences of **12a** and **12b** are negligible in solution. Both ribosyl parts are in *syn* orientation to the oxido ligands and one signal set is to be expected for this complex species in terms of NMR spectroscopy. The possible *trans* isomeric form is shown in Figure 2.51, though it was not detected by NMR spectroscopy, not even in spectra of the crude reaction mixture. Due to the limited solubility of **12** in water or methanol, the spectra of the signals given in Table 2.24 were recorded in DMSO- d_6 . They show only one signal set for the *syn* form. While the signals of the histidinato ligand are shifted to lower field by up to 11.5 ppm depending on the distance to rhenium, only the signals of C2' and C3' of Urd2',3'H $_2$ gain a low field shift of up to 27.0 ppm.

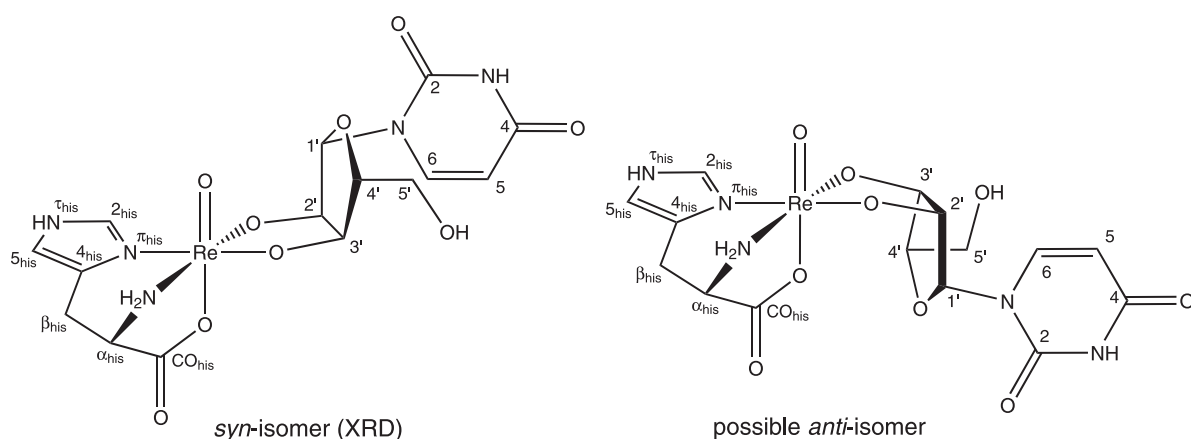


Figure 2.51 Scheme of the diastereomeric forms of **12** and atom numbering used in the ^{13}C NMR study according to the recommendations of the JCBN^[61, 79]. XRD: result of the structure determination.

Table 2.24 ^{13}C NMR chemical shifts (in ppm) of **12** in DMSO- d_6 (67.9 MHz, 25 °C) and comparison with the free ligands under the same conditions. The signal of the deuterated solvent ($\delta = 39.52$ ppm) was used as an internal secondary reference^[65] for the chemical shift. For atom numbering see Figure 2.51. $\Delta\delta$ values indicating a diolate coordination are in boldface. Assignment according to the literature: L-histidine^[91], uridine^[67].

		C_{CO}	C_{α}	C_{β}	C2	C4	C5				
L-Histidine	δ	169.98	51.62	25.63	134.59	127.61	118.13				
12	δ	175.95	58.42	27.31	143.59	139.15	116.91				
	$\Delta\delta$	5.97	6.80	1.68	9.00	11.54	-1.22				
		C1'	C2'	C3'	C4'	C5'	C2	C4	C5	C6	
Uridine	δ	87.93	73.76	70.05	85.01	61.02	150.93	163.44	101.88	140.89	
12	δ	90.56	100.75	94.44	84.55	61.78	150.71	163.35	101.95	141.93	
	$\Delta\delta$	2.63	26.99	24.39	-0.46	0.76	-0.22	-0.09	0.07	1.04	

2.3.5 The reaction of [ReO(L-his)(ox)] with cytidine

All the reactions so far in this work were carried out in methanol or ethanol. But a substantial requirement for the handling of biologically active molecules at physiological conditions is aqueous chemistry. The compounds so far presented meet this requirement: they are soluble in water and, to a certain degree, stable against hydrolysis. But the preparation of such a compound in aqueous media has not been explored yet, as the rhenium(V) precursor [ReOCl₃(PPh₃)₂] is insoluble. Unlike this, the complex [ReO(L-his)(ox)] (see 9 in section 2.3.1 on page 53) is soluble in water. With this new precursor it is possible to substitute another carbohydrate for the oxalato group. 9 reacts with an excess of cytidine (Cyd) in water to form a new complex, while oxalate decomposes. From such an aqueous solution, crystals of [ReO(L-his)(*anti*-Cyd2',3'H₋₂)] · 5 H₂O (13) were obtained within one day. The unit cell of the

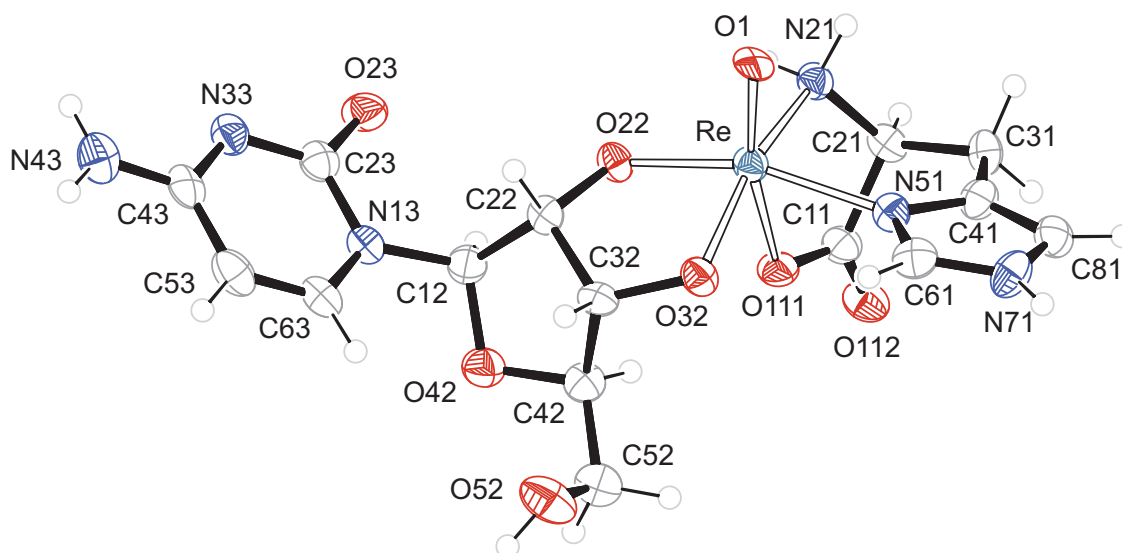


Figure 2.52 ORTEP presentation of **13** in crystals of [ReO(L-his)(*anti*-Cyd2',3'H₋₂)] · 5 H₂O. Ellipsoids are drawn at 50 % probability level. Distances [Å] and angles [°]: Re-O1 1.704(5), Re-O22 1.979(5), Re-O32 1.936(5), Re-O111 2.198(5), Re-N21 2.179(6), Re-N51 2.073(6), O1-Re-O22 103.7(2), O1-Re-O32 109.8(2), O1-Re-O111 163.7(2), O1-Re-N21 91.8(2), O1-Re-N51 95.3(3), O22-Re-O32 82.2(2), O22-Re-O111 83.67(18), O22-Re-N21 94.9(2), O22-Re-N51 160.7(2), O32-Re-O111 85.5(2), O32-Re-N21 158.4(2), O32-Re-N51 88.2(2), O111-Re-N21 72.9(2), O111-Re-N51 78.9(2), N21-Re-N51 87.9(2), furanose torsion angle O22-C22-C32-O32: 30.0(7), torsion angle of the coordinated acid group Re-O111-C11-O112: 176.1(5), puckering parameters^[59] for O42-C12-C22-C32-C42: $Q_2 = 0.382(8)$ Å, $\phi_2 = 317.1(12)^\circ$, conformation E_4 .

crystals in the orthorhombic space group $P2_12_12_1$ contains four formula units while there is one molecule of the neutral rhenium complex (Figure 2.52) and five molecules of water in the asymmetric unit. In analogy to the previous structure with the nucleoside uridine, the deprotonated form of histidine is in an (*N,N,O*) binding mode

with O111 of the carboxylato group *trans* to the oxido ligand O1. Cyt2',3'H₋₂, the dianionic form of the nucleoside cytidine, is also connected via O22 and O32 to the metal, but in *anti* position to the oxido ligand O1. The torsion angle of this diolato group (30.0°) is diminished, compared with the corresponding angle of the free form (44.4°^[60]) and the furanose conformation has changed from ³T₂ to E₄. Moreover, the torsion angle about the *N*-glycosidic bond ($\chi = -154.0^\circ$ for O42-C12-N13-C23) deviates from that of free cytidine (-162.6°), but still defines an *anti* conformation.

At first glance the hydrogen bonding of **13** seems to be complex (see Table 2.25 and SCHAKAL packing diagram on page 198). But if the solvent molecules are omitted, patterns are apparent: Figure 2.53 shows (above) the crystal packing without water molecules. Hydrogen bonds of the type N-H \cdots O link the cytosine and histidine parts of neighboring molecules and build an infinite network with tunnels in [100] direction. In these tunnels are hydrogen bonded water molecules.

Table 2.25 Distances [Å] and angles [°] of hydrogen bonds in **13**. O91 to O95 are affiliated to five water molecules. D: donor, A: acceptor, *x*: difference of (H \cdots A) and the sum of the van-der-Waals radii^[62].

D	H	A	D \cdots A	D-H	H \cdots A	<i>x</i>	D-H \cdots A
N21	H211	O91	2.953(10)	0.92	2.22	-0.50	136
N21	H211	O93 ⁱ	3.214(10)	0.92	2.62	-0.10	123
N21	H212	O112 ⁱⁱ	3.010(8)	0.92	2.13	-0.59	160
N71	H71	O23 ⁱⁱⁱ	2.743(9)	0.88	1.87	-0.85	172
N43	H431	O95	2.908(11)	0.88	2.11	-0.61	150
N43	H432	O112 ^{iv}	3.011(9)	0.88	2.14	-0.58	167
O52	H852	O94 ^v	2.743(10)	0.84	1.93	-0.79	163
O91	H911	O95 ⁱ	2.757(11)	0.85(6)	1.92(7)	-0.80	165(9)
O91	H912	O22	2.752(9)	0.85(7)	2.22(10)	-0.49	121(8)
O92	H921	O93 ⁱ	2.756(10)	0.85(7)	1.95(6)	-0.77	158(9)
O92	H922	O22	3.017(9)	0.84(7)	2.23(6)	-0.50	157(8)
O93	H931	N33	3.071(10)	0.84(8)	2.26(7)	-0.49	165(9)
O93	H932	O52 ^{vi}	2.894(11)	0.83(7)	2.06(8)	-0.66	175(10)
O94	H941	O92 ⁱⁱⁱ	2.717(11)	0.84(6)	1.93(7)	-0.79	155(8)
O94	H942	O111	3.058(9)	0.83(4)	2.24(3)	-0.49	169(9)
O95	H951	O94 ⁱⁱ	2.822(12)	0.85(3)	2.07(6)	-0.65	148(9)
O95	H952	O23 ^{vii}	2.924(10)	0.84(3)	2.23(7)	-0.50	141(8)
C31	H312	O91 ⁱⁱ	3.347(10)	0.99	2.70	-0.03	124
C61	H61	O92 ⁱⁱⁱ	3.145(11)	0.95	2.82	-0.10	101

Symmetry codes: ⁱ $-x, y - \frac{1}{2}, -z + \frac{1}{2}$; ⁱⁱ $x + \frac{1}{2}, -y + \frac{1}{2}, -z + 1$; ⁱⁱⁱ $x + \frac{1}{2}, -y - \frac{1}{2}, -z + 1$; ^{iv} $-x, y + \frac{1}{2}, -z + \frac{3}{2}$; ^v $-x + \frac{1}{2}, -y, z + \frac{1}{2}$; ^{vi} $x - \frac{1}{2}, -y + \frac{1}{2}, -z + 1$; ^{vii} $-x, y + \frac{1}{2}, -z + \frac{1}{2}$.

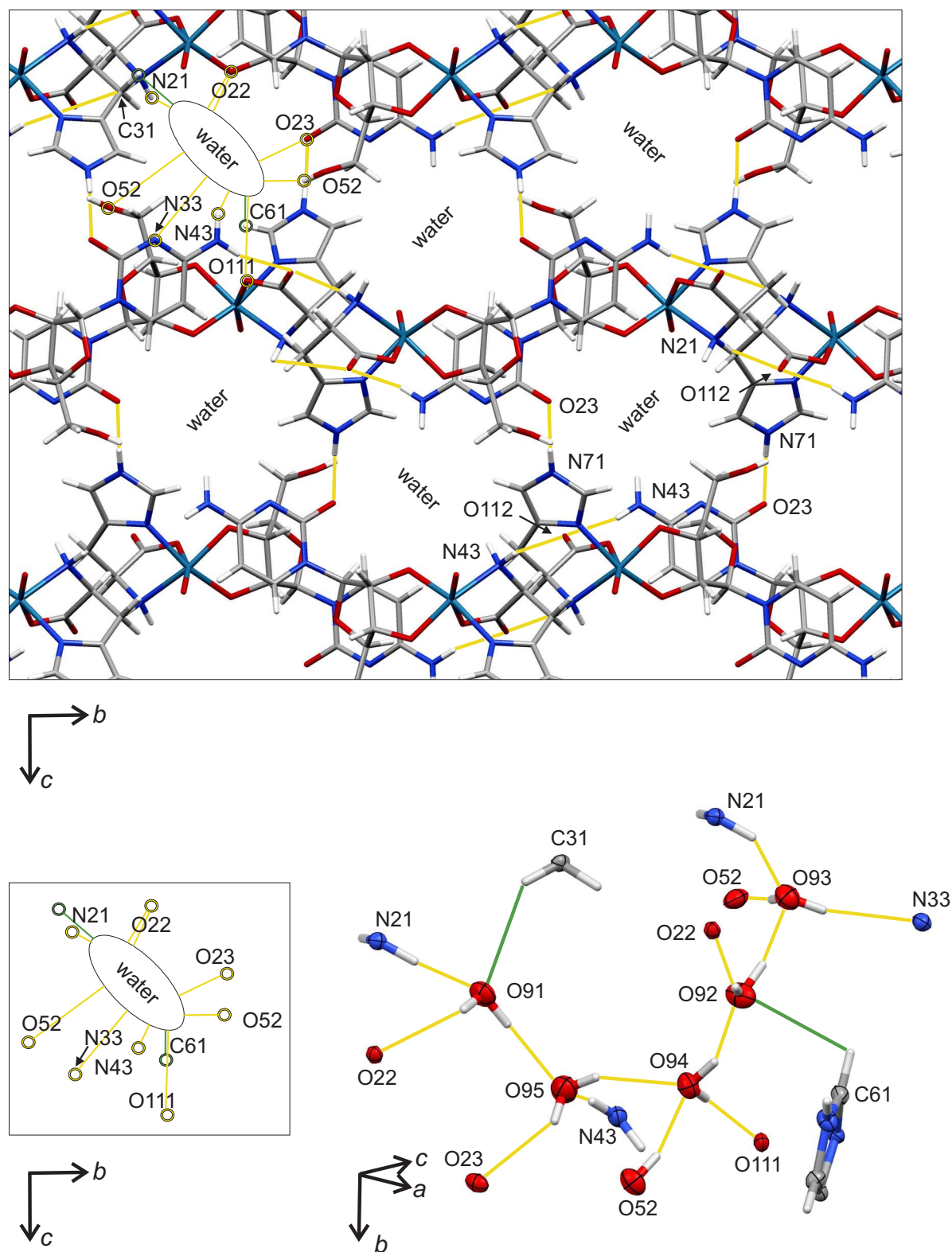


Figure 2.53 MERCURY presentation of hydrogen bonds (yellow lines) and C-H...O contacts in **13**. Above: the crystal packing with tunnels in [100] direction, below: a close-up of the hydrogen bond environment of the water molecules within these tunnels.

2 Results

The ^{13}C NMR chemical shifts of **13** in D_2O are given in Table 2.26. Two signal sets at different intensities were observed, as there are two possible orientations for $\text{Cyd}2',3'\text{H}_2$ being connected to the oxidorhenium core. Figure 2.53 illustrates this *syn/anti* isomerism. Surprisingly, this isomerism was observed in spectra of the reaction mixture as well as of redissolved crystals of **13**, although the result of the structure determination showed only the *anti* isomer. In view of NMR spectroscopy, the signals of both of these diastereomeric species are very similar, both show a coordination via $\text{O}2'$ and $\text{O}3'$ as the signals of $\text{C}2'$ and $\text{C}3'$ are shifted to lower field by up to 26.4 ppm.

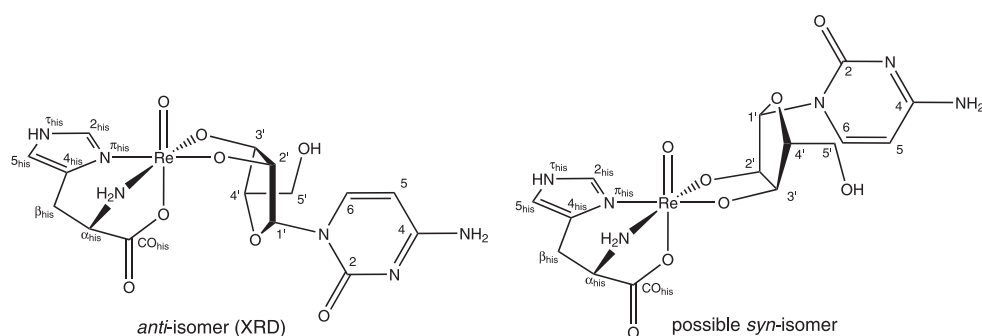


Figure 2.54 Scheme of the diastereomeric forms of **13** and atom numbering used in the ^{13}C NMR study. XRD: result of the structure determination.

Table 2.26 ^{13}C NMR chemical shifts (in ppm) of **13** in D_2O (67.9 MHz, 25 °C) and comparison with the free ligands under the same conditions (pH 6.4). The signal of a drop of methanol ($\delta = 49.50$ ppm in D_2O) was used as an internal secondary reference^[65] for the chemical shift. For atom numbering see Figure 2.54. $\Delta\delta$ values indicating a diolate coordination are in boldface. Assignment according to the literature: L-histidine^[91], cytidine^[63].

		C_{CO}	C_{α}	C_{β}	$\text{C}2$	$\text{C}4$	$\text{C}5$			
L-his	δ	173.66	55.38	28.83	136.65	133.12	117.40			
13	δ	180.48 ^a	62.03 ^a	27.62 ^a	144.68 ^a	138.11 ^a	118.09			
		180.13 ^b	62.18 ^b	27.70 ^b	144.91 ^b	138.22 ^b				
	$\Delta\delta$	6.82 ^a	6.65 ^a	-1.21 ^a	8.03 ^a	4.99 ^a	0.69			
		6.47 ^b	6.75 ^b	-1.13 ^b	8.26 ^b	5.10 ^b				
		$\text{C}1'$	$\text{C}2'$	$\text{C}3'$	$\text{C}4'$	$\text{C}5'$	$\text{C}2$	$\text{C}4$	$\text{C}5$	$\text{C}6$
Cyd	δ	90.76	74.54	69.70	84.49	61.13	153.97	163.64	96.23	143.18
13	δ	93.23	99.92 ^a	92.22 ^a	85.64	62.03 ^a	153.76 ^a	163.34	96.10 ^a	144.19
			100.95 ^b	92.71 ^b		62.18 ^b	153.69 ^b		96.52 ^b	
	$\Delta\delta$	2.47	25.38^a	22.52^a	1.15	0.90 ^a	-0.21 ^a	-0.30	-0.13 ^a	1.01
			26.41^b	23.01^b		1.05 ^b	-0.28 ^b		0.29 ^b	

In the case of two signals observed: ^a major isomer, ^b minor isomer.

2.3.6 The reaction of $[\text{ReOCl}_3(\text{PPh}_3)_2]$ with L-histidine and methyl α -D-mannopyranoside

So far in this work only simple diols and furanoidic carbohydrates were investigated, as these ligands seem to be flexible enough to adopt the torsion angle of the affected hydroxy groups suitable for chelation. At this point the ability of pyranoidic carbohydrates had not been tested yet. Methyl α -D-mannopyranoside (Me- α -D-Manp), a methylated derivative of D-mannose, was chosen to react with the oxidorhenium core. Although it is polyfunctional like its parent saccharide, it is conformationally stable and provides among its functions only one *cis*-vicinal diol function. The reaction of this pyranoside with $[\text{ReOCl}_3(\text{PPh}_3)_2]$ and L-histidine in boiling methanol yielded a blue powder from which crystals of $[\text{ReO}(\text{L-his})(\text{syn-Me-}\alpha\text{-D-Manp}_{2,3\text{H}_{-2}})] \cdot 2 \text{ MeOH}$ (**14**) were recrystallized from water.

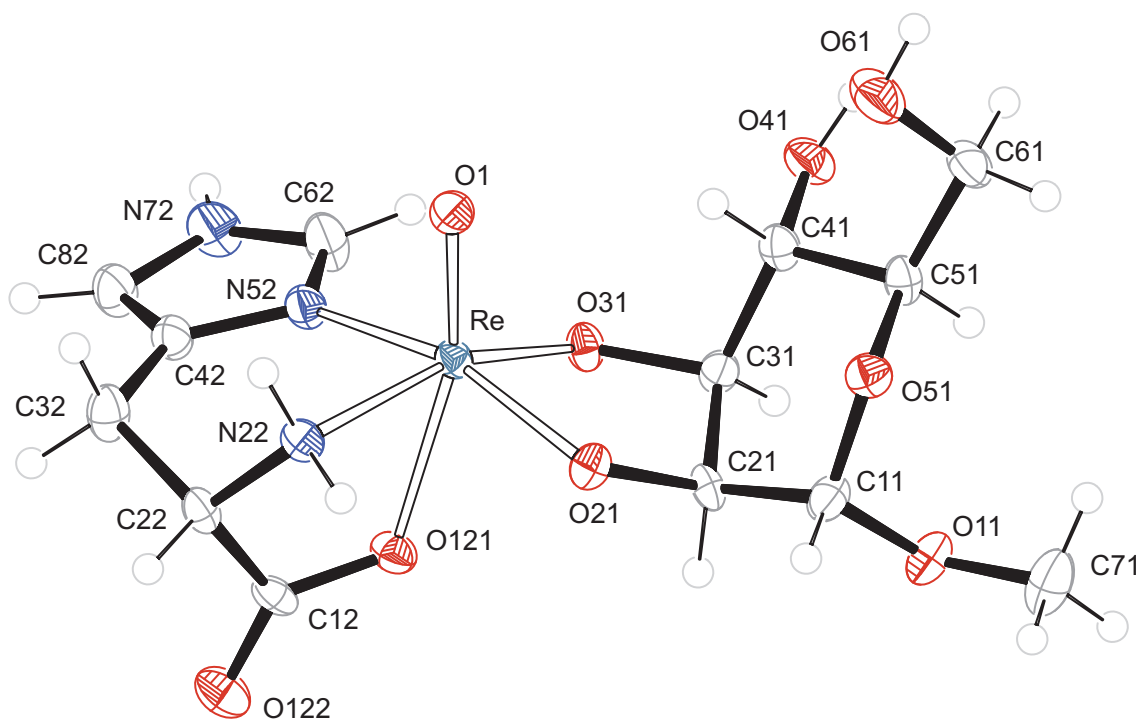


Figure 2.55 ORTEP presentation of **14** in crystals of $[\text{ReO}(\text{L-his})(\text{syn-Me-}\alpha\text{-D-Manp}_{2,3\text{H}_{-2}})] \cdot 2 \text{ MeOH}$. Ellipsoids are drawn at 50 % probability level. Distances [\AA] and angles [$^\circ$]: Re-O1 1.688(3), Re-O21 1.955(2), Re-O31 1.937(3), Re-O121 2.183(3), Re-N22 2.179(4), Re-N52 2.098(3); O1-Re-O21 106.12(14), O1-Re-O31 107.62(13), O1-Re-O121 161.78(14), O1-Re-N22 91.62(14), O1-Re-N52 95.20(13), O21-Re-O31 82.75(10), O21-Re-O121 81.83(13), O21-Re-N22 90.98(12), O21-Re-N52 158.64(13), O31-Re-O121 89.45(12), O31-Re-N22 160.73(13), O31-Re-N52 89.62(12), O121-Re-N22 71.58(13), O121-Re-N52 78.17(11), N22-Re-N52 89.75(12), pyranose torsion angle O21-C21-C31-O31: $-40.8(5)$, torsion angle of the coordinated acid group Re-O121-C12-O122: $169.6(3)$, puckering parameters^[59] for O51-C11-C21-C31-C41-C51: $Q = 0.527(5) \text{ \AA}$, $\theta = 14.4(5)^\circ$, $\phi = 319(2)^\circ$, conformation 4C_1 .

2 Results

The asymmetric unit in the monoclinic space group $C2$ contains one molecule of the rhenium complex (Figure 2.55) and two molecules of methanol while there are four of these formulas in the unit cell. The histidinato ligand is in a tridentate (N,N,O) binding mode with O121 of the carboxylato-group *trans* to the oxido ligand O1. With a deviation of 0.092 Å the rhenium core is in-plane with the imidazole ring but not with the planar carboxylato group (torsion angle Re-O121-C12-O122: 169.6°). The (O,O)-donor Me- α -D-Manp_{2,3H}-₂ is coordinated via O21 and O31 in *syn* orientation to O1. Although having a diminished torsion angle for O21-C21-C31-O31 (-40.8°) compared with the free form (-55.5°), the pyranoside ring is still in ⁴ C_1 conformation (Puckering parameters^[59] of the free form^[92]: $Q = 0.556$ Å, $\theta = 0.51^\circ$). Hydrogen bonds of the type N-H...O are to be found between the amino functions of the histidinato ligand and the oxygen acceptor atoms of the carboxylato group and the oxido ligand O1. Assisted by hydrogen bonds of the type O-H...O involving methanol solvent molecules, sheets are formed parallel to the (100) plane. In Figure 2.56 a lateral cut of such a sheet is shown. In between these sheets there are no classical hydrogen bonds, as the SCHAKAL packing diagram (Figure 6.14 on page 199) also exhibits. Instead, weak interactions of the type C-H...O link the Me- α -D-Manp moieties (see below in Figure 2.56).

Table 2.27 Distances [Å] and angles [°] of hydrogen bonds in 14. Values without standard deviation are related to hydrogen atoms at calculated positions. For atom numbering see Figure 2.55. O98 and O99 are affiliated to methanol molecules. D: donor, A: acceptor, x : difference of (H...A) and the sum of the van-der-Waals radii^[62].

D	H	A	D...A	D-H	H...A	x	D-H...A
N22	H221	O61 ⁱ	2.910(5)	0.92	2.02	-0.70	161
N22	H222	O1 ⁱ	2.974(4)	0.92	2.21	-0.51	139
N72	H772	O122 ⁱⁱ	2.766(5)	0.88	1.93	-0.79	158
O41	H841	O98 ⁱⁱⁱ	2.720(6)	0.84	1.92	-0.80	158
O61	H861	O99 ^{iv}	2.686(7)	0.84	1.90	-0.82	156
O98	H898	O121	2.768(6)	0.84	1.93	-0.79	175
O99	H899	O21 ^v	2.718(5)	0.84	1.93	-0.80	157
C22	H22	O21 ⁱ	3.309(5)	1.00	2.32	-0.40	169
C31	H31	O11 ^{vi}	3.481(5)	1.00	2.54	-0.18	156
C51	H51	O41 ^{vi}	3.515(7)	1.00	2.58	-0.14	156

Symmetry codes: ⁱ $\frac{1}{2} - x, -\frac{1}{2} + y, -z$; ⁱⁱ $\frac{1}{2} - x, \frac{1}{2} + y, 1 - z$; ⁱⁱⁱ $x, 1 + y, z$; ^{iv} $x, 1 + y, -1 + z$; ^v $x, y, 1 + z$; ^{vi} $-x, y, -z$.

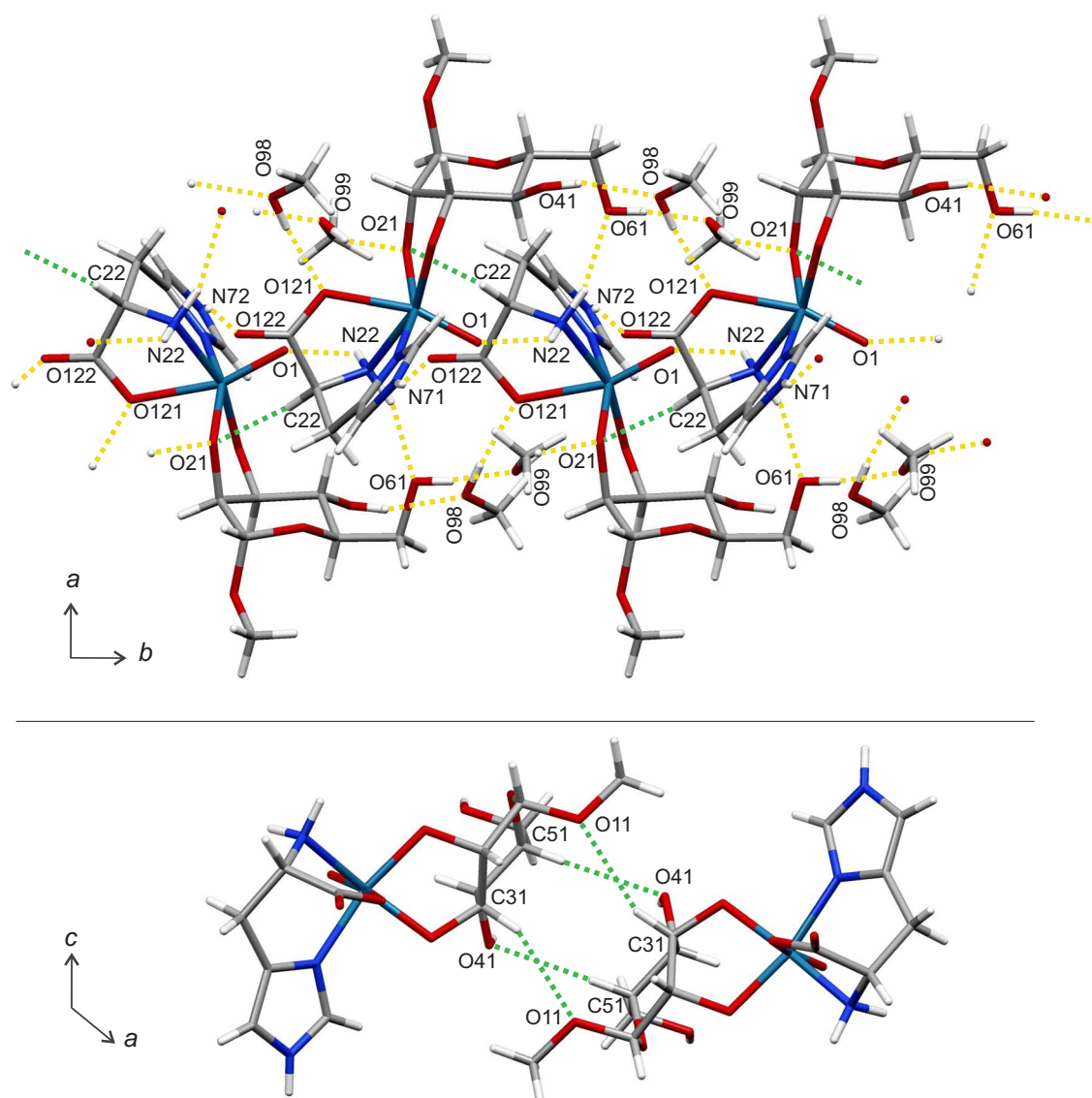


Figure 2.56 MERCURY presentation of the hydrogen bonds (yellow dashed lines) and weak interactions (green dashed lines) forming sheets parallel to the bc plane in the structure of **14**. Below: view along the b axis, weak interactions of the carbohydrate moieties.

The ^{13}C NMR spectra of redissolved crystals of **14** in D_2O showed two signal sets at different intensities (Table 2.28, the same was observed for the reaction mixture). The signals of C2 and C3 are shifted up to 23.6 ppm to lower field, while the signal of C4 in both signal sets is shifted less than 1 ppm, indicating that O4 is not bonded to the metal. This demonstrates the preference of *cis*-vicinal diol functions for a coordination to rhenium(V). No coordination of the *trans*-vicinal diol function O3-C3-C4-O4 was observed, not even in spectra of the reaction mixture. As there are two possible orientations for Me- α -D-Manp2,3H $_2$ with respect to the oxido ligand (*syn/anti* iso-

2 Results

merism: see Figure 2.57), two signal sets were observed. In view of the result of the structure determination, *syn*-**14** can be regarded as the major species in solution.

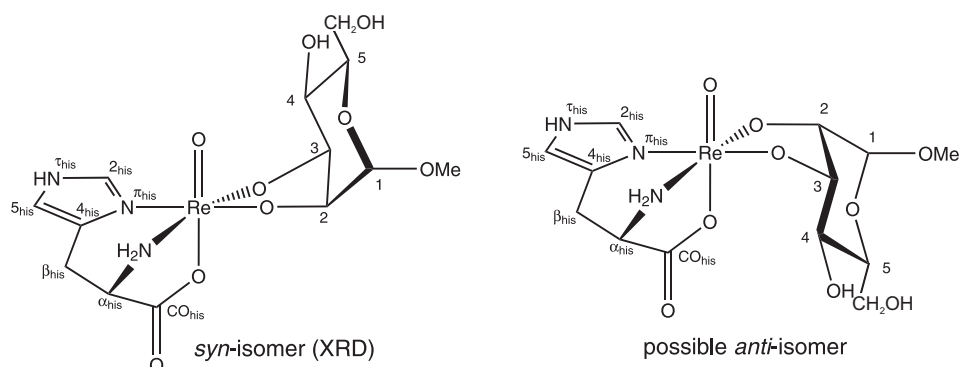


Figure 2.57 Scheme of the diastereomeric forms of **14** and atom numbering used in the ^{13}C NMR study. XRD: result of the structure determination.

Table 2.28 ^{13}C NMR chemical shifts (in ppm) of **14** in D_2O (67.9 MHz, 25 °C) and comparison with the free ligands under the same conditions (pH 3.2). The signal of a drop of methanol ($\delta = 49.50$ ppm in D_2O) was used as an internal secondary reference^[65] for the chemical shift. For atom numbering see Figure 2.57. $\Delta\delta$ values indicating a diolate coordination are in boldface. Assignment according to the literature: L-histidine^[91], Me- α -D-manp^[93].

		C_{CO}	C_α	C_β	C2	C4	C5		
L-Histidine	δ	174.37	55.50	28.86	136.86	132.94	117.37		
14	δ	180.31 ^a	59.51	27.94	145.64 ^a	138.57 ^a	117.91		
		180.88 ^b			145.18 ^b	138.73 ^b			
14	$\Delta\delta$	5.94 ^a	4.01	-0.92	8.78 ^a	5.63 ^a	0.54		
		6.50 ^b			8.32 ^b	5.79 ^b			
		C1	C2	C3	C4	C5	C6	OMe	
Me- α -D-Manp	δ	101.51	70.62	71.26	67.42	73.23	61.60	55.26	
14	δ	101.62	90.48 ^a	91.02 ^a	68.26 ^a	71.81 ^a	61.74	55.49	
			91.63 ^b	94.84 ^b	68.11 ^b	72.28 ^b			
14	$\Delta\delta$	0.11	19.86^a	19.76^a	0.84 ^a	-1.42 ^a	0.14	0.23	
			21.01^b	23.58^b	0.69 ^b	-0.95 ^b			

In the case of two observed signals: ^a major isomer, ^b minor isomer.

2.3.7 The reaction of $[\text{ReOCl}_3(\text{PPh}_3)_2]$ with L-histidine and methyl β -D-ribose

As opposed to the pyranoside used in the previous chapter, methyl β -D-ribose (Me- β -D-Rib p) provides a chelating ligand with two possible *cis*-vicinal diol binding sites at O2, O3 and O3, O4. Its reaction with $[\text{ReOCl}_3(\text{PPh}_3)_2]$, L-histidine and triethylamine in methanol gave a blue solid from which crystals of $[\text{ReO}(\text{L-his})(\text{syn-Me-}\beta\text{-D-Ribp3,4H}_{-2})] \cdot 0.5 \text{ MeOH}$ (**15**) in the monoclinic space group $P2_1$ were obtained.

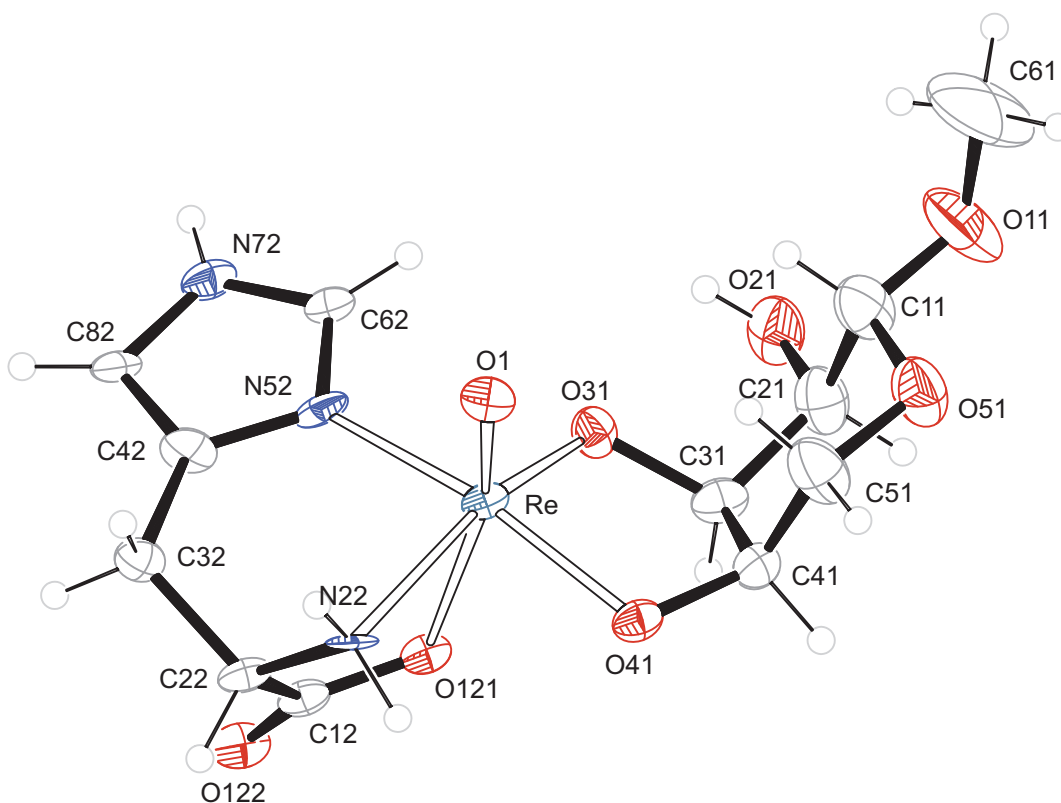


Figure 2.58 ORTEP presentation of **15** in crystals of $[\text{ReO}(\text{L-his})(\text{syn-Me-}\beta\text{-D-Ribp3,4H}_{-2})] \cdot 0.5 \text{ MeOH}$. Ellipsoids are drawn at 50 % probability level. Distances [\AA] and angles [$^\circ$]: Re-O1 1.684(7), Re-O31 1.926(6), Re-O41 1.960(5), Re-O121 2.194(5), Re-N22 2.179(6), Re-N52 2.115(7), O1-Re-O31 111.6(3), O1-Re-O41 104.5(3), O1-Re-O121 162.5(3), O1-Re-N22 92.6(4), O1-Re-N52 96.7(4), O31-Re-O41 82.8(2), O31-Re-O121 85.0(2), O31-Re-N22 155.9(4), O31-Re-N52 87.0(3), O41-Re-O121 82.6(2), O41-Re-N22 91.2(3), O41-Re-N52 158.6(4), O121-Re-N22 71.0(4), O121-Re-N52 77.8(4), N22-Re-N52 90.5(3), pyranose torsion angle O31-C31-C41-O41: 41.3(10), torsion angle of the coordinated acid group Re-O121-C12-O122: 154.5(7), puckering parameters^[59] for O51-C11-C21-C31-C41-C51: $Q = 0.554(14) \text{ \AA}$, $\theta = 17.9(13)^\circ$, $\phi = 35(5)^\circ$, conformation 4C_1 .

There are two formula units in the unit cell while the asymmetric unit contains one molecule of the rhenium complex (Figure 2.58) and a half-occupied methanol

2 Results

site. This distorted octahedral complex contains the doubly deprotonated form of the pyranoside (Me- β -D-Ribp3,4H₂) connected via O3 and O4 in *syn* position to the oxido ligand O1. Compared with the structure of free methyl β -D-ribose[94], the diol's torsion angle O3-C3-C4-O4 changes from 54.3° to 41.3°, and the pyranose ring conformation from ¹C₄ to approximate ⁴C₁ (Puckering parameters^[59] of the free form for O5-C1-C2-C3-C4-C5: $Q = 0.569 \text{ \AA}$, $\theta = 176.5^\circ$, $\phi = 55^\circ$). The histidinato ligand is in an (*N,N,O*) binding mode with O121 of the carboxylato group being *trans* to the oxido ligand O1. The above-mentioned distortion towards the histidinato ligand is visible in the angle of the *trans* O=Re–O unit differing from 180° (O1-Re-O121 162.5°).

As far as hydrogen bonds and crystal packing, this structure is very similar to 14. Mainly hydrogen bonds of the type N-H \cdots O link the amino functions of histidine with the oxygen-acceptor atoms in this compound. Together with hydrogen bonds of the type O-H \cdots O involving the carbohydrate part (O21) and methanol solvent molecules, all these bondings form sheets parallel to the (001) plane (see Figure 2.59 or for a larger overview the SCHAKAL packing diagram Figure 6.15 on page 200). Among the classical hydrogen bonds in Table 2.29, two weak interactions of the type C-H \cdots O are listed additionally. Although the angles are not very favorable for bonding, they were exclusively found as the only interaction between the above-mentioned sheets (see below in Figure 2.59).

Table 2.29 Distances [\AA] and angles [$^\circ$] of hydrogen bonds in 15. Values without standard deviation are related to hydrogen atoms at calculated positions. For atom numbering see Figure 2.58. O99 is affiliated to methanol. D: donor, A: acceptor, x : difference of (H \cdots A) and the sum of the van-der-Waals radii^[62].

D	H	A	D \cdots A	D-H	H \cdots A	x	D-H \cdots A
O21	H821	O99	2.830(18)	0.84	2.10	−0.62	145
N22	H221	O1 ⁱ	3.030(11)	0.92	2.17	−0.56	156
N22	H222	O41 ⁱⁱ	2.790(13)	0.92	1.94	−0.78	153
N72	H772	O121 ⁱⁱⁱ	2.850(9)	0.88	2.12	−0.60	140
O99	H899	O122 ⁱⁱⁱ	2.795(13)	0.84	1.96	−0.76	172
C61	H611	O11 ^v	3.39(2)	0.98	2.55	−0.17	144
C61	H611	O21 ^v	3.46(2)	0.98	2.69	−0.03	136

Symmetry codes: ⁱ $-x, y - \frac{1}{2}, -z$; ⁱⁱ $-x, y + \frac{1}{2}, -z$; ⁱⁱⁱ $-x + 1, y + \frac{1}{2}, -z$; ^{iv} $x, y + 1, z$;
^v $1 - x, y + \frac{1}{2}, 1 - z$.

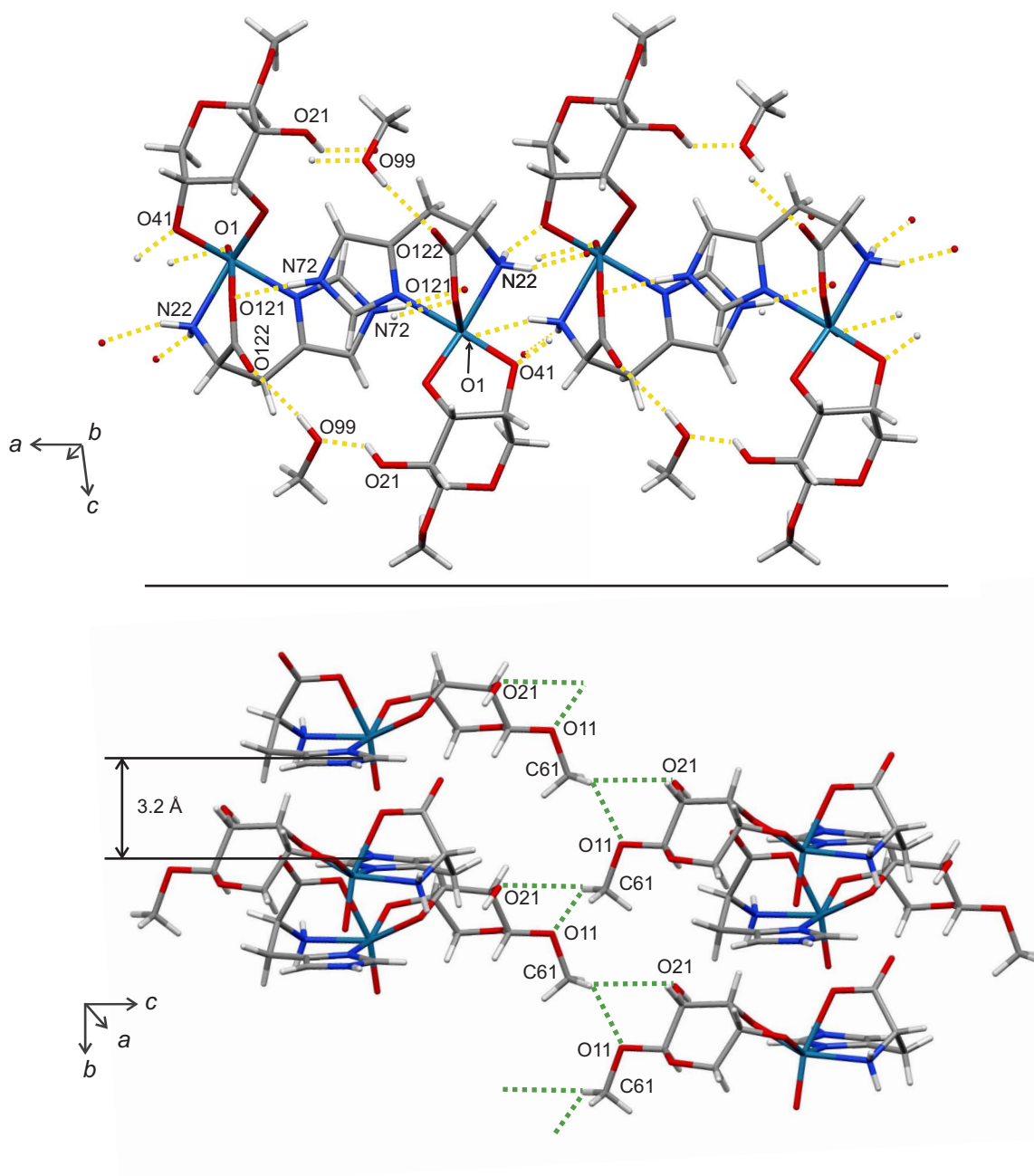


Figure 2.59 MERCURY presentation of hydrogen bonds (yellow dashed lines), π - π interactions and C-H \cdots O contacts (green dashed lines) in **15**.

2 Results

The two potential *cis*-vicinal diol binding sites of methyl β -D-ribofuranoside adopt in the structure of the free form^[94] angles of 54.3° (O2-C2-C3-O3) and 61.9° (O3-C3-C4-O4). Surprisingly, the second one occurs in the structure determination as a chelating unit, its angle diminishes to 41.3° . But the first one has to be accounted for as a chelate species in solution, too. Due to the *syn/anti* isomerism of each of these two complexes, four species are to be expected in solution. Figure 2.60 illustrates these four diastereomeric forms. In agreement with this, ^{13}C NMR spectra of the reaction mixture showed four signal sets at different intensities. Surprisingly, the same was observed in spectra of the crystalline product. Even as pure compound, **15** seems to isomerize in water to the species given in Figure 2.60. Table 2.29 lists the chemical shifts in D_2O . Depending on the coordination via (O2,O3) or (O3,O4) the signals of C2, C3 and C4 are shifted up to 25.6 ppm to lower field.

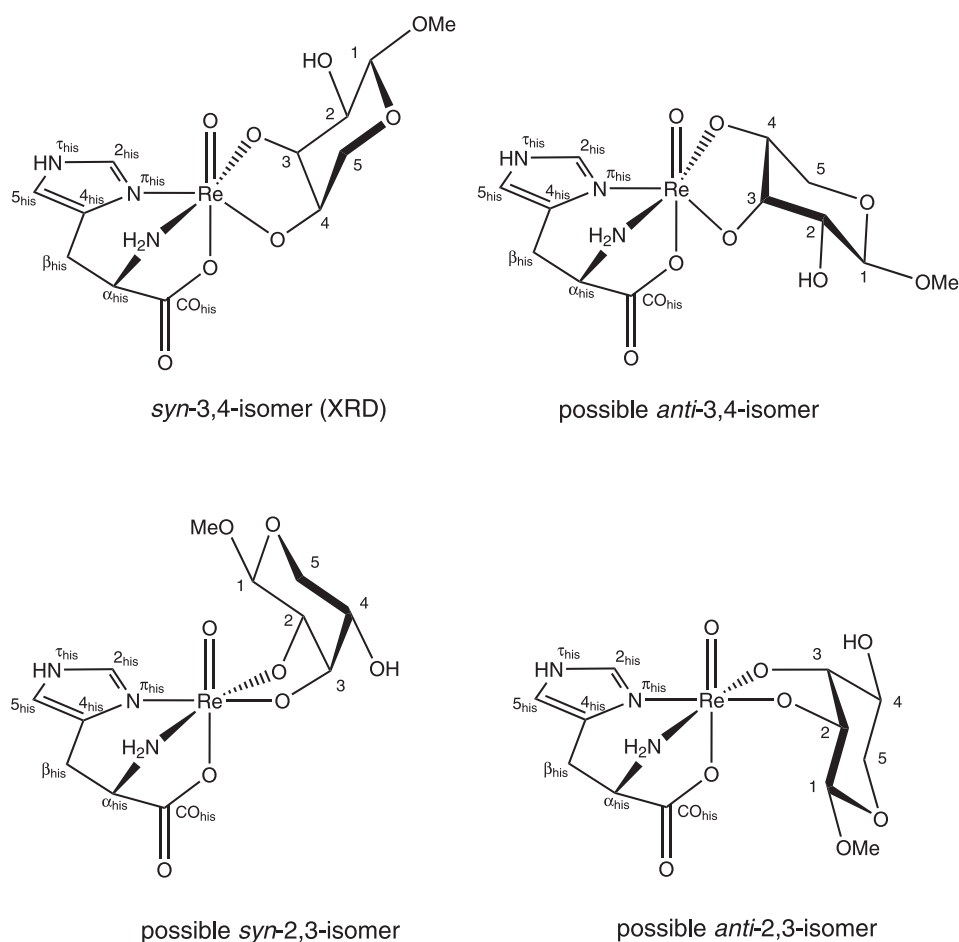


Figure 2.60 Scheme of the diastereomeric forms of **15** and atom numbering used in the ^{13}C NMR study according to the recommendations of the JCBN^[79, 95]. XRD: result of the structure determination.

2 Results

Table 2.30 ^{13}C NMR chemical shifts (in ppm) of **15** in D_2O (101 MHz, 25 °C) and comparison with the free ligands under the same conditions (pH 6.6). The signal of a drop of methanol ($\delta = 49.50$ ppm in D_2O) was used as an internal secondary reference^[65] for the chemical shift. For atom numbering see Figure 2.60. $\Delta\delta$ values indicating a diolate coordination are in boldface. Assignment according to the literature: L-histidine^[91], Me- β -D-ribp^[93].

			C_{CO}	C_{α}	C_{β}	C2	C4	C5
L-Histidine		δ	174.57	56.69	28.89	136.96	132.94	117.41
15	a	δ	180.41	58.72	27.67	145.05	138.49	118.06
	b	δ	180.35	59.29	27.98	145.55	138.77	118.06
	c	δ	180.55	58.78	27.78	144.73	138.85	118.23
	d	δ	180.52	58.76	27.91	145.80	138.63	117.90
	a	$\Delta\delta$	5.84	2.03	-1.22	8.09	5.55	0.65
	b	$\Delta\delta$	5.78	2.60	-0.91	8.59	5.83	0.65
	c	$\Delta\delta$	5.98	2.09	-1.11	7.77	5.91	0.82
	d	$\Delta\delta$	5.95	3.07	-0.98	8.84	5.69	0.49
			C1	C2	C3	C4	C5	OMe
Me- β -D-Ribp		δ	102.00	70.76	68.35	68.30	63.68	55.50
15	a	δ	102.42	93.31	85.71	67.17	64.84	57.23
	b	δ	102.14	71.41	90.39	93.66	64.03	57.57
	c	δ	102.52	94.05	88.64	67.55	63.70	57.47
	d	δ	103.02	70.18	89.12	90.62	64.22	57.34
	a	$\Delta\delta$	0.42	25.55	17.36	-1.13	1.16	1.73
	b	$\Delta\delta$	1.14	0.65	22.04	25.36	0.35	2.07
	c	$\Delta\delta$	0.52	23.29	20.29	-0.75	0.02	1.97
	d	$\Delta\delta$	1.02	-0.58	20.77	22.32	0.54	1.84

Signals of four species in solution were observed, according to the intensities there was distinguished between: a(major isomer) > b > c > d(minor isomer).

2.3.8 The reaction of $[\text{ReOCl}_3(\text{PPh}_3)_2]$ with L-histidine and other carbohydrates

So far, in this chapter complexes of the rhenium(V)-histidine system were presented with simple diols and carbohydrates like glycosides and nucleosides. Many other carbohydrates were tested for this system, but the findings of these reactions were limited to ^{13}C NMR spectra of the crude reaction mixtures, as it was not possible to precipitate a product of these reactions.

Among the glycosides, nucleosides and their derivatives, methyl α -D-galactopyranoside, methyl α -D-glucopyranoside, methyl β -D-xylopyranoside, adenosine, AMP and NADH showed a coordination.

Although the reaction mixtures with the monosaccharides D-erythrose, D-glucose, D-mannose, D-galactose, D-arabinose, D-xylose, D-ribose and D-fructose were unstable (they showed decomposition even at 4 °C), the spectra of the latter four reactions in this series showed small signals at low intensities of complex species for some hours.

Even spectra of reactions with disaccharides and oligosaccharides (D-turanose, D-iso-maltulose, D-raffinose, D-stachyose, α -, β -, γ -cyclodextrin) showed hints of a coordination. With these saccharides decomposition did not occur, but it was not possible to precipitate a product from the mixtures.

Finally, spectra of reaction mixtures with the antibiotics lincomycin and clindamycin showed hints of a coordination.

2.4 Compounds of rhenium(V) with L-carnosine

The dipeptide L-carnosine (L-carH) consists of the amino acids histidine and β -alanine. In the year 1900 *Gulewitsch* and *Amiradzibi* were the first who isolated it from meat extract^[96]. In the following century it was found in muscle and nerve tissues, although its function is not fully understood until today. Its ability to buffer protons^[97], chelate metals^[98] and scavenge radicals^[99] or reactive sugars^[100], presumably is why it protects cells against oxidative stress^[101].

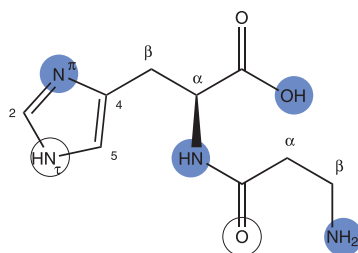


Figure 2.61 Scheme of L-carnosine and reported binding sites with metals (blue: observed for rhenium). Atom numbering according to the recommendations of the JCBN^[79].

L-Carnosine provides up to six different binding sites for metal ions, as shown in Figure 2.61. In analogy to L-histidine, there are many reported compounds with copper(II), zinc(II), cobalt(II,III), vanadium(IV) and other transition metals^[102]. But until today, there are only three structurally characterized metal complexes with L-carnosine (Figure 2.62). In all three cases the imidazole ring, the deprotonated acid group and the deprotonated amide group are coordinated to the metal with their respective oxygen or nitrogen donor atoms.

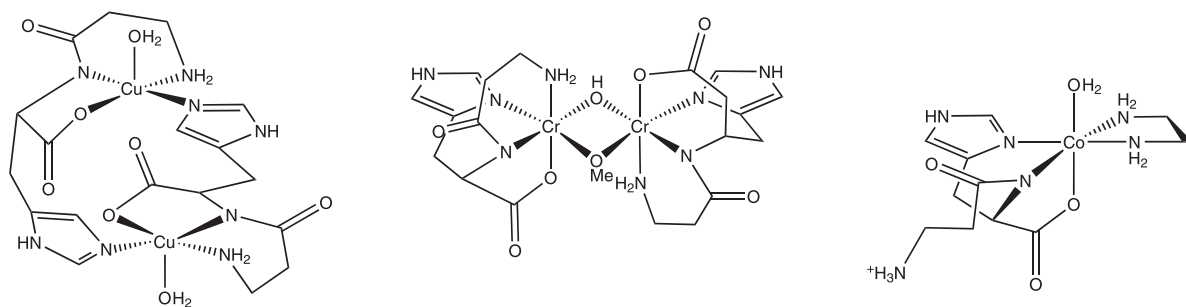


Figure 2.62 Complexes with L-carnosine that were characterized by X-ray crystal structure analyses. From left to right: $[\text{Cu}_2(\text{L-carH}_{-1})_2]$ with copper(II)^[103], $[\text{Cr}_2(\text{L-carH}_{-1})_2(\text{OH})(\text{OMe})]$ with chromium(III)^[104] and $[\text{Co}(\text{L-car})(\text{en})(\text{OH}_2)]\text{Cl}_2$ with cobalt(III)^[105].

Much work has been done on the system copper(II)-carnosine^[106], as these complexes depend not only on temperature and stoichiometry, but also on the pH of the solution. The pH-dependent forms of carnosine are illustrated in Figure 2.63. Its iso-

electric point ($\text{pH(I)} = 8.17$) is weakly shifted to alkaline conditions, compared with histidine ($\text{pH(I)} = 7.47$)^[90]. Figure 2.64 shows the structure of the neutral form of carnosine (carH) that was crystallized from a water/ethanol mixture. It contains the N_τ -protonated tautomer of imidazole, and the torsion angle of the peptide bond is close to 180° , which defines a typical *trans* configuration as in most peptides.

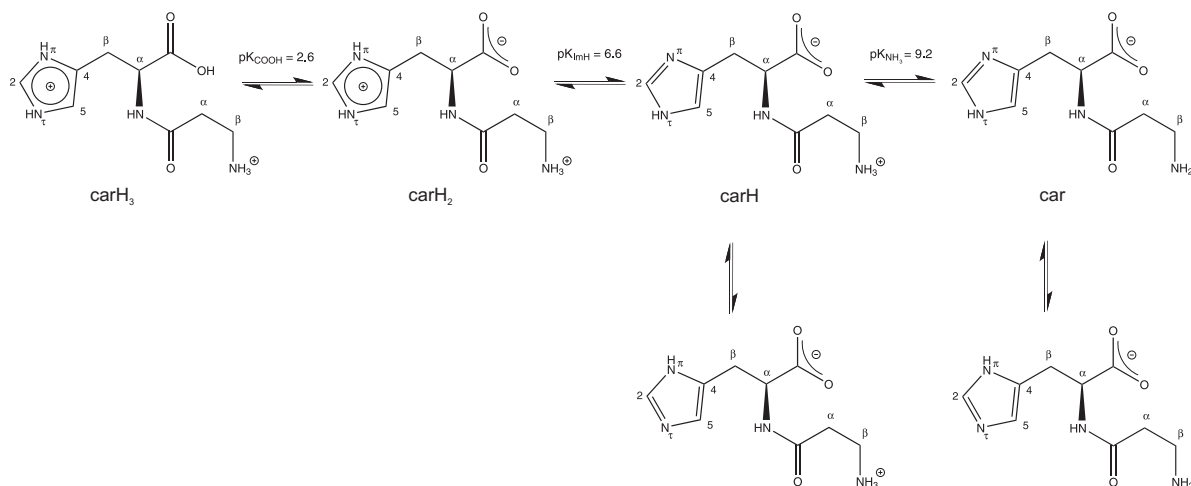


Figure 2.63 Scheme of the pH-dependent forms of L-carnosine and tautomeric equilibria of the imidazole ring. The abbreviations carH₃, carH₂, carH and car correspond to the various protonated forms in aqueous solution from pH 1 to 10. The deprotonation of the amide group HN_α becomes important only at pH values in which the hydrolysis of the dipeptide is relevant or in the presence of metal cations^[102].

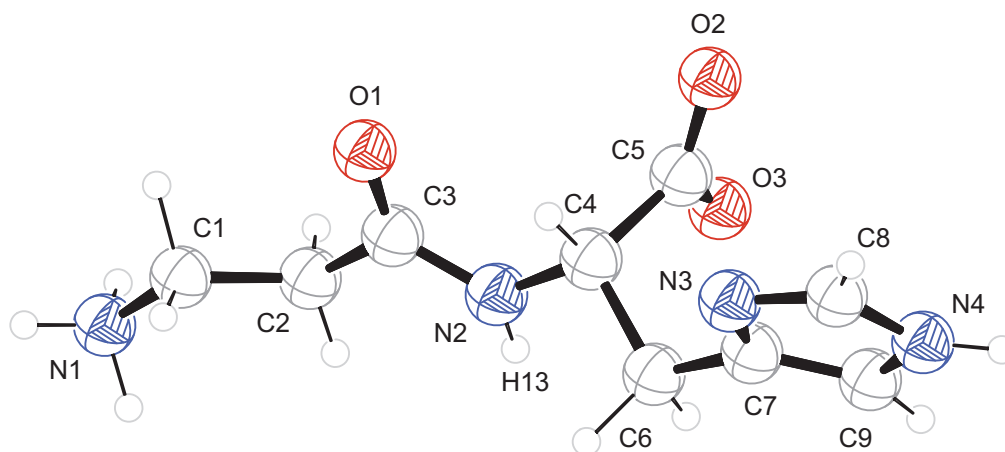


Figure 2.64 ORTEP presentation of the free form of L-carnosine^[107]. Atoms are drawn at 50 % probability level. Distances [Å] and angles [°]: O1-C3 1.233, O2-C5 1.257, O3-C5 1.250, N1-C1 1.476, N2-C3 1.333, N2-C4 1.455, N3-C7 1.383, N3-C8 1.326, N4-C8 1.331, N4-C9 1.377, C1-C2 1.489, C2-C3 1.500, C4-C5 1.535, C4-C6 1.539, C6-C7 1.485, C7-C9 1.356; peptide torsion angle C2-C3-N2-C4: 174.9, O1-C3-N2-H13: 175.0.

The information available for the chemistry of rhenium and dipeptides is scant and nothing at all is found for rhenium and carnosine. But a similar system was presented by *Tessier et al.* in 2004. They isolated complexes with the dipeptide his-ala^[41]. In contrast to carnosine, his-ala consists of *N*-terminal histidine and α -alanine. As depicted in Figure 2.65, the peptide is coordinated via N_π of the imidazole ring, the carbonyl oxygen of the peptide bond and the terminal amino function.

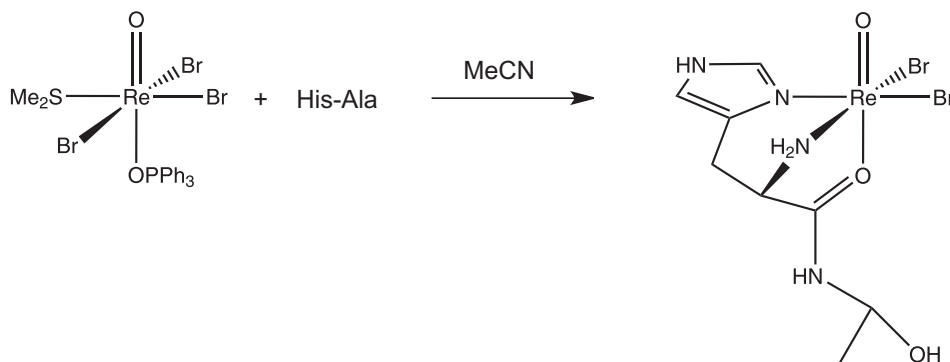


Figure 2.65 Scheme of the reaction route by *Tessier et al.* with dipeptides^[41].

The general reaction route with L-carnosine in this chapter is shown in Figure 2.66. In analogy to the reactions with L-histidine, they start from $[\text{ReOCl}_3(\text{PPh}_3)_2]$ in methanol with an excess of a diol. Triethylamine was used to deprotonate the amide group $N_\alpha\text{H}$ and the hydroxy functions of the diol. pH values of about 10 were measured for samples of the reaction mixtures after addition of water. The resulting octahedral complexes were built according to the “3 + 2” approach^[19] with a mixed-ligand set. The diols were connected as an (*O,O*)-donor to the metal and in most cases (7 out of 8) the histidine moiety of carnosine served as an (*N,N,O*)-donor. Only in one case was N_β of the alanyl moiety metallated instead of N_π of the imidazole ring. Unlike the complexes in the Figures 2.62 and 2.65, a metallation of N_τ or of the amide oxygen atom was never observed.

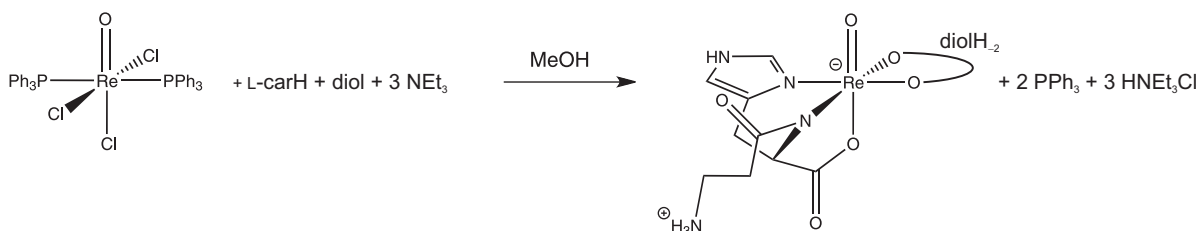


Figure 2.66 Scheme of the general reaction route with L-carnosine in this chapter. **diol** represents a carbohydrate with a *cis*-vicinal diol function.

2.4.1 The reaction of $[\text{ReOCl}_3(\text{PPh}_3)_2]$ with L-carnosine and oxalic acid

In analogy to the preparation of $[\text{ReO}(\text{L-his})(\text{ox})]$ (see **9** in section 2.3.1 on page 53), L-carnosine should react with the rhenium(V) precursor $[\text{ReOCl}_3(\text{PPh}_3)_2]$, sodium oxalate and triethylamine in methanol. Indeed, it was possible to precipitate a product from the reaction mixture. The blue powder was dissolved in water/methanol and crystals in the orthorhombic space group $P2_12_12_1$ were obtained from this saturated solution. Figure 2.67 shows the result of the structure determination, the electroneutral complex $[\text{ReO}(\text{L-car})(\text{ox})] \cdot 2 \text{H}_2\text{O}$ (**16**).

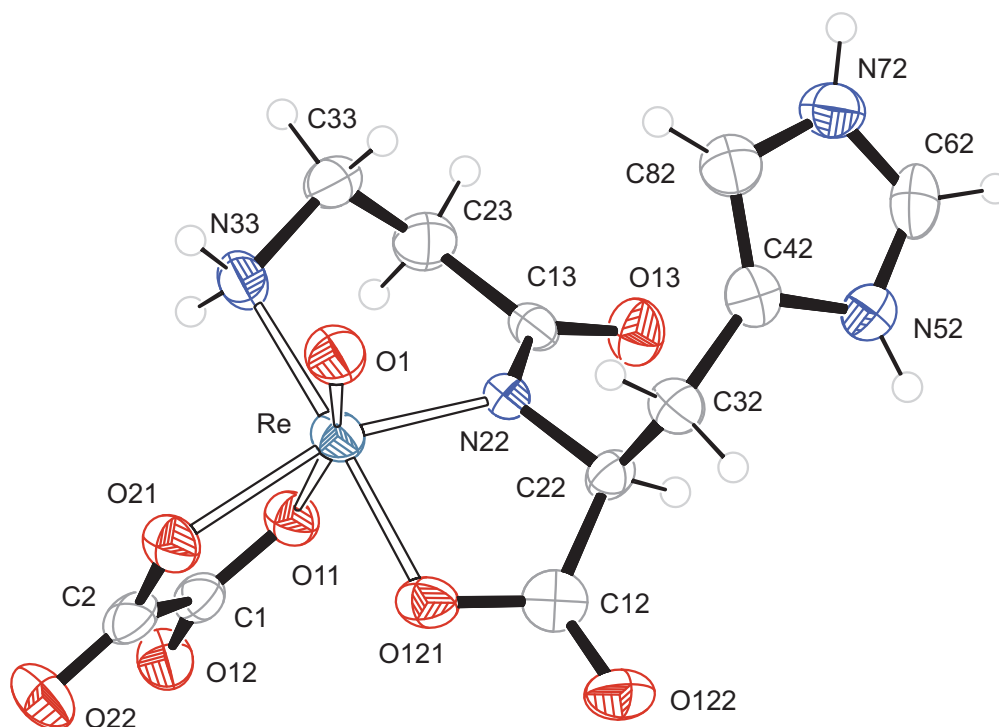


Figure 2.67 ORTEP presentation of **16** in crystals of $[\text{ReO}(\text{L-car})(\text{ox})] \cdot 2 \text{H}_2\text{O}$. Ellipsoids are drawn at 50 % probability level. Distances [Å] and angles [°]: Re-O1 1.660(6), Re-O11 2.131(6), Re-O21 2.082(5), Re-O121 2.004(7), Re-N22 1.968(7), Re-N33 2.111(7); O1-Re-O11 164.9(3), O1-Re-O21 97.1(3), O1-Re-O121 105.7(3), O1-Re-N22 104.7(3), O1-Re-N33 89.1(3), O11-Re-O21 74.7(2), O11-Re-O121 86.3(3), O11-Re-N22 85.9(2), O11-Re-N33 79.2(3), O21-Re-O121 83.8(3), O21-Re-N22 156.2(2), O21-Re-N33 95.2(3), O121-Re-N22 81.2(3), O121-Re-N33 165.2(3), N22-Re-N33 94.6(3), oxalic acid torsion angle O11-C1-C2-O21: 6.2(11), peptide torsion angle C23-C13-N22-C22: $-178.9(7)$, O13-C13-N22-Re: $-162.1(6)$, torsion angle of the coordinated acid group Re-O121-C12-O122: 176.3(7).

The asymmetric unit contains the rhenium complex and two molecules of water, of which one is disordered. There are four of these formulas in the unit cell. Compared to **9** with histidine in *facial* coordination, **16** shows a different binding mode: the

imidazole ring in this new compound is not metallated, it is protonated. The amino function of the alanyl part binds as a donor to the metal center and carnosine is in a *mer*-(*N,N,O*) binding mode via N33, N22 and O121. While in **9** the carboxylato group of histidine binds *trans* to the oxido ligand, in this case O11 of oxalate binds *trans* to the oxido ligand O1 (these two possibilities for coordination are illustrated in Figure 2.69). The chelating oxalate ligand is connected as an (*O,O*)-donor to the metal via O11 and O21 with a small torsion angle (6.2°). As in **9**, the rhenium core is, with small deviations, in-plane with all sp²-hybridized molecule parts (except for the non-coordinated imidazole ring): the oxalato group (0.04 Å) and the carboxylato group (0.02 Å). The torsion angle about the peptide bond (C23-C13-N22-C22: -178.9°) is closer to the ideal value of 180° than in the free form of carnosine (174.9°)^[107].

Table 2.31 Distances [Å] and angles [°] of hydrogen bonds and contacts in **16**. O99 is affiliated to water, O981/O982 to disordered water. D: donor, A: acceptor, *x*: difference of (H···A) and the sum of the van-der-Waals radii^[62].

D	H	A	D···A	D-H	H···A	<i>x</i>	D-H···A
N33	H333	O12 ⁱ	3.070(9)	0.92	2.26	-0.46	147
N33	H334	O11 ⁱⁱ	3.307(10)	0.92	2.43	-0.29	159
N33	H334	O12 ⁱⁱ	3.247(9)	0.92	2.56	-0.16	132
N52	H752	O99 ⁱⁱⁱ	2.829(11)	0.88	2.04	-0.68	149
N52	H752	O122 ⁱⁱⁱ	2.989(10)	0.88	2.46	-0.26	119
N72	H772	O981 ^{iv}	2.776(18)	0.88	1.97	-0.75	151
N72	H772	O982 ^{iv}	2.66(2)	0.88	1.79	-0.93	168
O981	H981	O22 ⁱⁱ	2.747(14)	0.84(10)	2.02(10)	-0.70	145(10)
O981	H982	O21	2.933(16)	0.83(14)	2.35(19)	-0.37	129(14)
O981	H982	O22	3.041(14)	0.83(14)	2.31(11)	-0.41	148(15)
O99	H991	O981 ^v	3.05(2)	0.84(7)	2.23(7)	-0.49	168(7)
O99	H992	O121	2.799(10)	0.84(7)	2.05(8)	-0.67	149(7)
C62	H62	O122 ⁱⁱⁱ	3.022(12)	0.95	2.51	-0.21	114
C82	H82	O13 ⁱⁱ	3.538(12)	0.95	2.60	-0.12	169
O1		C12 ⁱⁱ	2.782(11)			-0.44	
Cg		O12 ⁱ	2.769			^a	

Symmetry codes: ⁱ $-\frac{1}{2} + x, \frac{1}{2} - y, -z$; ⁱⁱ $-1 + x, y, z$; ⁱⁱⁱ $2 - x, \frac{1}{2} + y, \frac{1}{2} - z$; ^{iv} $x, 1 + y, z$; ^v $1 + x, y, z$; Calculated centroid Cg: C1-C2. ^a contact of O12 to C1: -0.42, O12 to C2: -0.27.

Mainly hydrogen bonds of the type N-H···O link the molecules to sheets parallel to the (100) plane. They are given in Table 2.31. Even all the hydrogen atoms of imidazole are integrated in hydrogen bondings, if one regards also weak interactions of the type C-H···O (see below in Figure 2.68). The hydrogen-bonded sheets are con-

nected in [100] direction by two intermolecular contacts between the oxalate ligands ($O12 \cdots Cg$) and between the oxido ligand O1 and the coordinated carboxylato group of the amino acid ($O1 \cdots C12$).

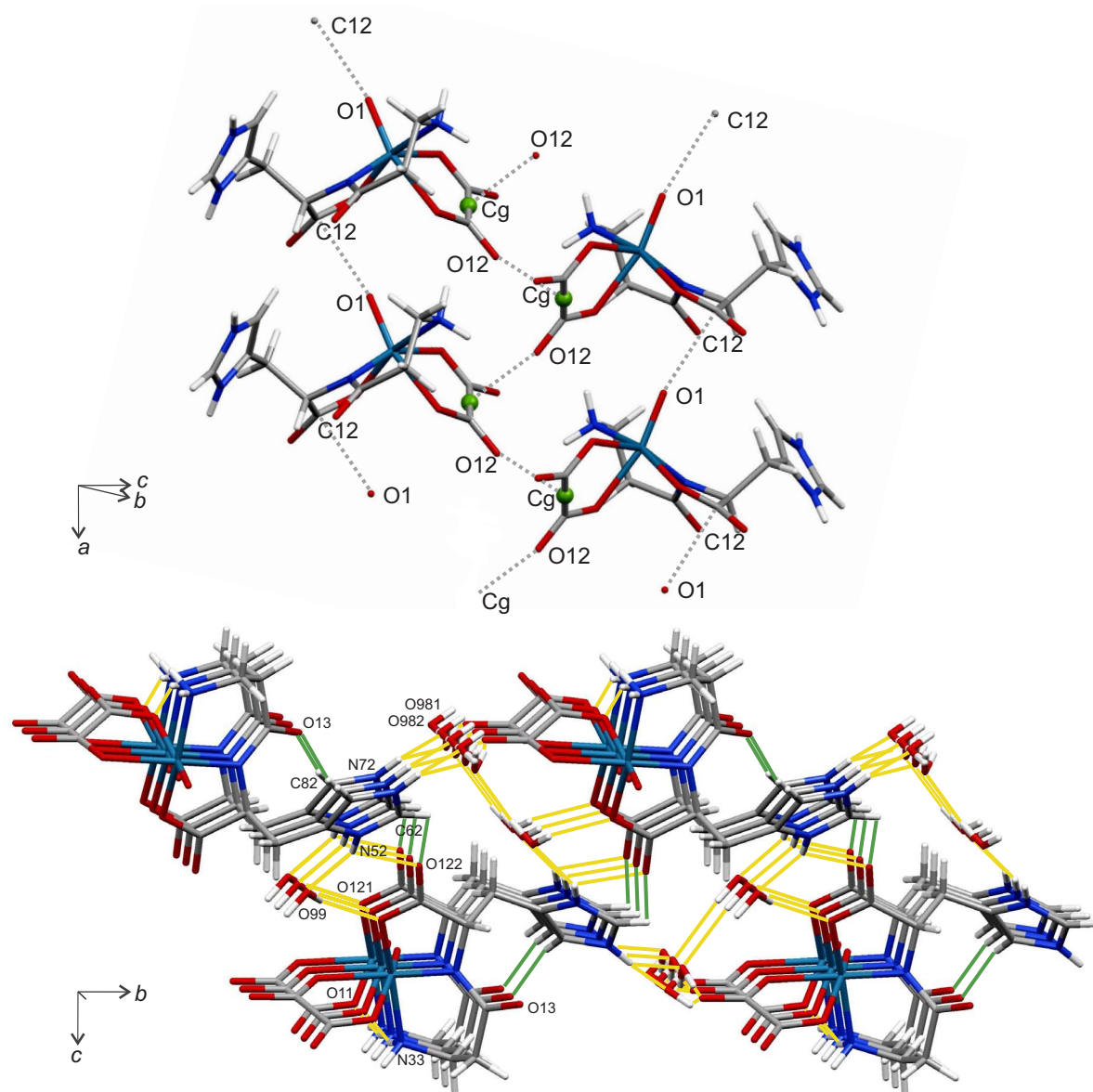


Figure 2.68 MERCURY presentation of hydrogen bonds (yellow lines), C-H \cdots O contacts (green lines) and C \cdots O contacts (grey dashed lines) in **16**. Above, a close-up of weak interactions, water molecules and hydrogen bonds omitted. The centroids of the C=C double bond of oxalate are marked green. Below: a view along [100] including water molecules.

^{13}C NMR spectra of **16** in D_2O showed two signal sets at different intensities (ca. 3:1). The complex found in the structure determination is obviously not the only species in solution. The minor species can be regarded as the primarily expected product of this reaction (Figure 2.69). Compared to **9** with histidine in *facial* coordination,

N_{π} of the imidazole ring is connected to the metal and not N_{β} of the alanyl part. This different metallation has an impact on the signals of these species in solution. As shown in Table 2.32, notably the signals of the alanine and oxalate parts are different for these two isomers, while the signals of the histidine parts are similar. Remarkably, the signal of C_{β} from the alanine part is shifted 14.5 ppm or -1.0 ppm to lower or higher field depending on the metallation of N_{β} .

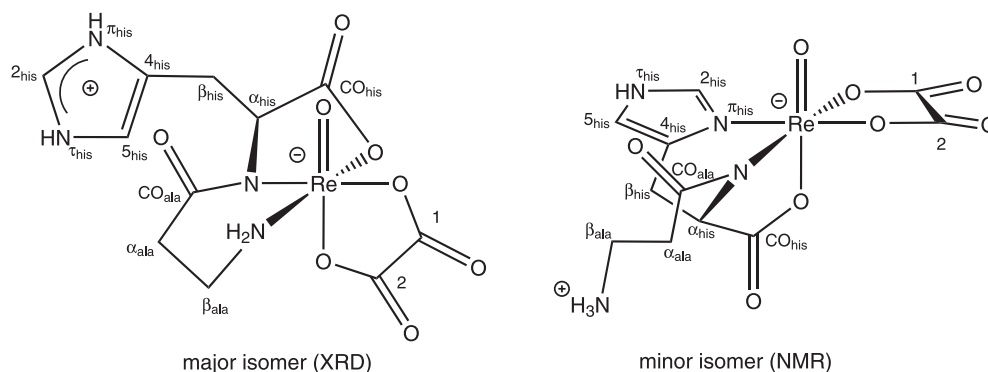


Figure 2.69 Scheme of the isomeric forms of **16** with different binding modes of L-carnosine. Left: result of the structure determination with *mer*-(N,N,O). Right: species detected in solution with *fac*-(N,N,O).

Table 2.32 ^{13}C NMR chemical shifts (in ppm) of **16** in D_2O (101 MHz, 25 °C) and comparison with the free ligands under the same conditions (pH 4.3). The signal of a drop of methanol ($\delta = 49.50$ ppm in D_2O) was used as an internal secondary reference^[65] for the chemical shift. For atom numbering see Figure 2.69. Assignment according to the literature: L-carnosine^[108].

			L-carnosine					
			C_{COhis}	$\text{C}_{\alpha\text{his}}$	$\text{C}_{\beta\text{his}}$	$\text{C}_{2\text{his}}$	$\text{C}_{4\text{his}}$	$\text{C}_{5\text{his}}$
free		δ	176.76	54.57	27.59	133.85	130.19	117.28
16	a	δ	191.89	68.03	27.48	133.86	128.98	117.70
	b	δ	192.73	68.80	26.92	132.34	129.90	117.48
	a	$\Delta\delta$	15.13	13.46	-0.11	0.01	-1.21	-0.42
	b	$\Delta\delta$	15.97	14.23	-0.67	-1.51	-0.29	-0.20
			L-carnosine			sodium oxalate		
			C_{COala}	$\text{C}_{\alpha\text{ala}}$	$\text{C}_{\beta\text{ala}}$	C1/C2		
free		δ	172.17	32.53	36.35	161.91		
16	a	δ	187.27	37.75	50.87	165.43, 162.94		
	b	δ	186.81	32.45	35.30	174.86, 171.88		
	a	$\Delta\delta$	15.10	5.22	14.52	3.52, 0.76		
	b	$\Delta\delta$	14.64	-0.08	-1.05	12.95, 9.97		

a: major isomer, b: minor isomer.

2.4.2 The reaction of $[\text{ReOCl}_3(\text{PPh}_3)_2]$ with L-carnosine and 1,2-ethanediol

The reaction of $[\text{ReOCl}_3(\text{PPh}_3)_2]$ with ethanediol, L-carnosine and triethylamine in methanol yielded the compound $[\text{ReO}(\text{L-car})(\text{EthdH}_{-2})] \cdot \text{MeOH} \cdot \text{H}_2\text{O}$ (**17**) after recrystallization from methanol/water. The unit cell of the crystals in the triclinic space group $P1$ contains the rhenium complex (Figure 2.70), one molecule of methanol and one molecule of water.

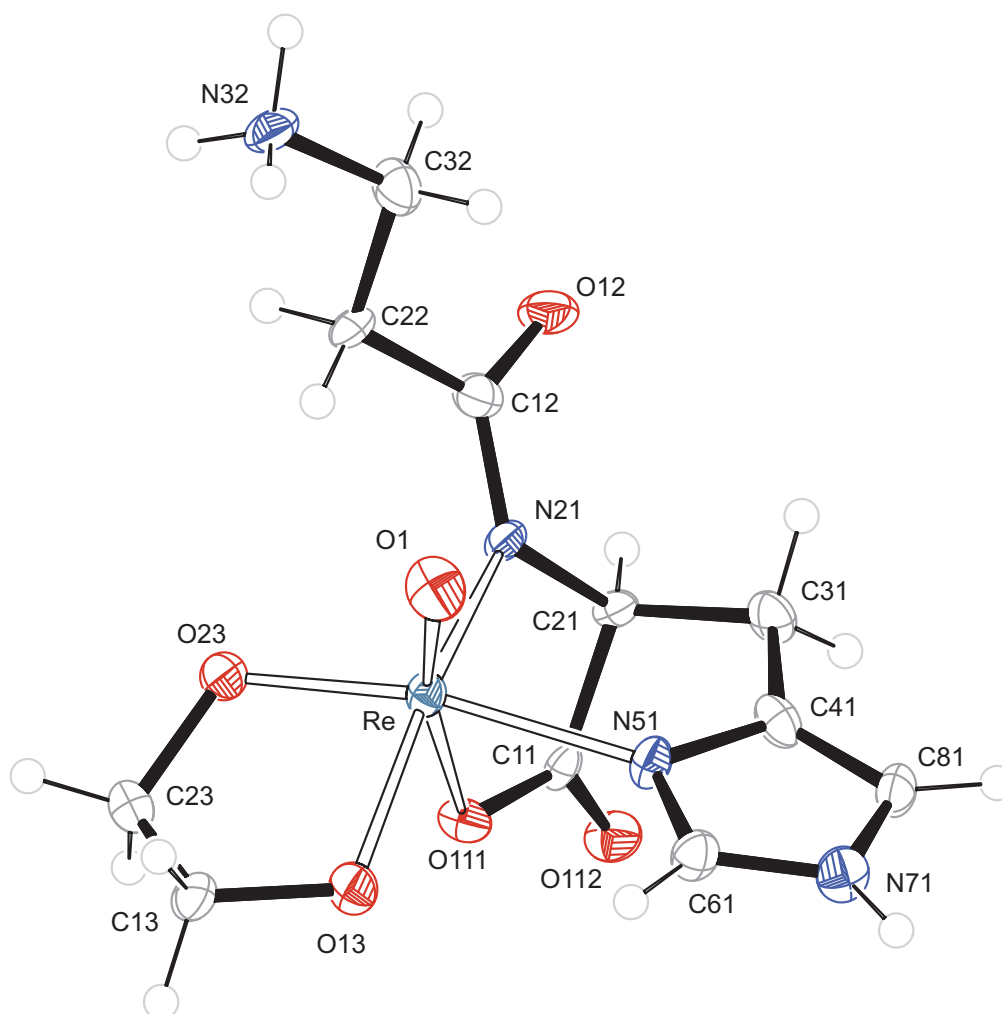


Figure 2.70 ORTEP presentation of **17** in crystals of $[\text{ReO}(\text{L-car})(\text{EthdH}_{-2})] \cdot \text{MeOH} \cdot \text{H}_2\text{O}$. Ellipsoids are drawn at 50 % probability level. Distances [Å] and angles [°]: Re-O1 1.679(4), Re-O13 1.946(3), Re-O23 1.946(4), Re-O111 2.171(3), Re-N21 2.105(3), Re-N51 2.120(4); O1-Re-O13 106.08(17), O1-Re-O23 106.81(18), O1-Re-O111 167.70(16), O1-Re-N21 99.98(17), O1-Re-N51 91.29(19), O13-Re-O23 82.21(13), O13-Re-O111 80.58(13), O13-Re-N21 153.92(12), O13-Re-N51 91.67(14), O23-Re-O111 84.12(15), O23-Re-N21 91.31(13), O23-Re-N51 161.86(12), O111-Re-N21 73.62(13), O111-Re-N51 78.02(16), N21-Re-N51 86.73(14), diol torsion angle O13-C13-C23-O23: $-36.7(5)$, peptide torsion angle C21-N21-C12-C22: $173.3(3)$, O12-C12-N21-Re: $169.9(3)$, torsion angle of the coordinated acid group Re-O111-C11-O112: $167.9(3)$.

2 Results

Contrary to the oxalate ligand in **16**, ethanediol does not offer further carboxylato groups in competition with the carboxylato group of the amino acid. As shown in Figure 2.70, O111 of the amino acid binds *trans* to the oxido ligand O1, a feature observed in the structures with L-histidine of the previous section. L-Carnosine is coordinated *facial* via N21, N71 and O111 of the histidine part, and the protonated amino function N32 of the alanine part is left dangling. The peptide bond is nearly planar, its torsion angle ($\omega = 173.3^\circ$ for C21-N21-C12-C22) is close to the angle found in the free form (174.9°)^[107]. Except for the negative sign the diol torsion angle (-36.7° for O13-C13-C23-O23) is similar to the corresponding angles found in **10** with histidine and ethanediol ($+43.5^\circ$ and $+44.1^\circ$).

The hydrogen bonds found in **17** are given in Table 2.33. The first three bonds in the table are not involved with solvent molecules, they define a backbone of sheets orthogonal to the [110] axis (Figure 2.71). The solvent molecules (water, methanol) are placed within these sheets with strong hydrogen bonds (favorable angles $>170^\circ$ and distances about 2.8 Å). Together, with an interaction of the type C-H...O from C61 of imidazole to O112 of the carboxylate function, they connect the sheets.

Table 2.33 Distances [Å] and angles [$^\circ$] of hydrogen bonds in **17**. Values without standard deviation are related to hydrogen atoms at calculated positions. O98 is affiliated to water, O99 to methanol. D: donor, A: acceptor, x : difference of (H...A) and the sum of the van-der-Waals radii^[62].

D	H	A	D...A	D-H	H...A	x	D-H...A
N71	H771	O23 ^{iv}	2.743(6)	0.88	1.94	-0.78	150
N32	H324	O13 ⁱⁱ	2.848(5)	0.91	2.18	-0.54	130
N32	H324	O111 ⁱⁱ	2.874(5)	0.91	2.10	-0.62	143
N32	H323	O99 ⁱ	2.797(6)	0.91	1.90	-0.82	170
N32	H325	O98 ⁱⁱⁱ	2.740(7)	0.91	1.85	-0.87	164
O99	H899	O12	2.813(6)	0.84	1.98	-0.74	172
O98	H981	O12 ^v	2.795(6)	0.83(6)	1.97(6)	-0.75	173(5)
O98	H982	O112 ^{vi}	2.868(5)	0.82(5)	2.05(5)	-0.67	172(6)
C61	H61	O112 ⁱⁱⁱ	3.100(6)	0.95	2.15	-0.57	175

Symmetry codes: ⁱ $x, -1 + y, z$; ⁱⁱ $x, y, -1 + z$; ⁱⁱⁱ $-1 + x, -1 + y, z$; ^{iv} $-1 + x, 1 + y, z$; ^v $x, 1 + y, z$; ^{vi} $x, 1 + y, -1 + z$.

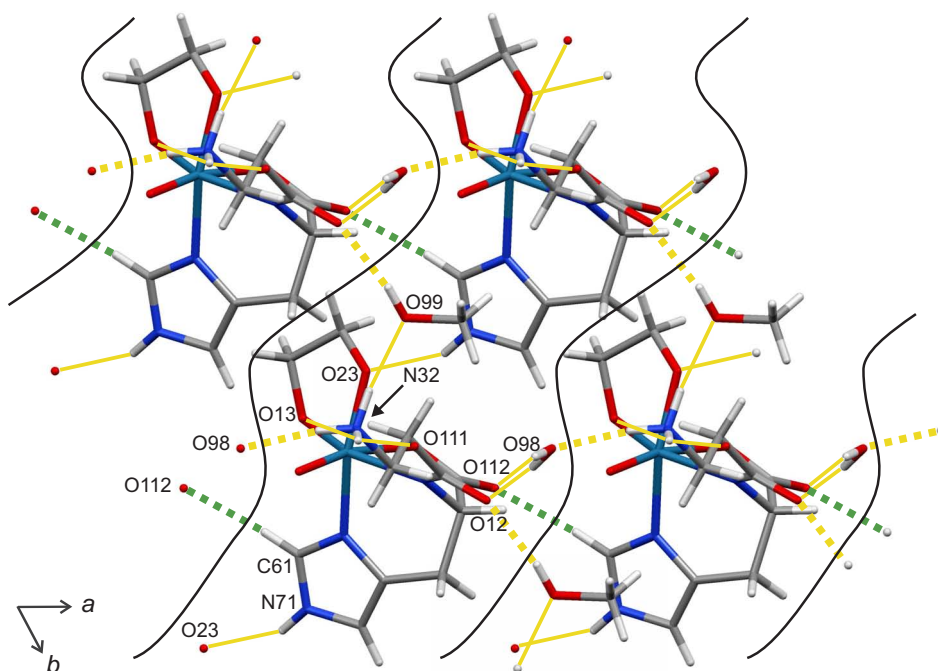


Figure 2.71 MERCURY presentation of hydrogen bonds (yellow) and C-H...O contacts (green) in **17**. Dashed bonds: connections between sheets orthogonal to the [110] axis.

Only one signal set was observed in spectra of the reaction mixture and of dissolved product in water. The ^{13}C NMR chemical shifts of **17** in D_2O are listed in Table 2.34. Due to the distorted octahedral coordination, two signals are observed for C1/C2 of ethanediol with a shift to lower field of up to 21.5 ppm. The values were close to the data for **10**, the analog compound with L-histidine. But for **17**, the influence of the rhenium core on the signals of the histidine part is stronger: the signals of C_{CO} , C_{α} , C2 and C4 are shifted 7.8–11.6 ppm to lower field, while for **10** they are shifted 3.6–7.9 ppm (see Table 2.20 on page 61).

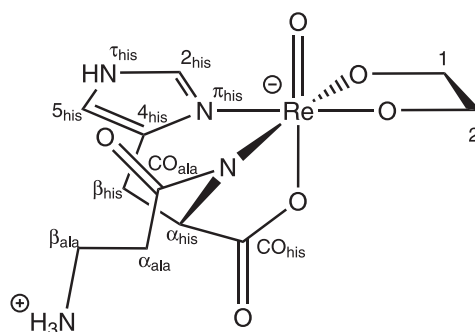


Figure 2.72 Scheme of **17** and atom numbering used in the ^{13}C NMR study according to the recommendations of the JCBN^[79].

Table 2.34 ^{13}C NMR chemical shifts (in ppm) of **17** in D_2O (67.9 MHz, 25 °C) and comparison with the free ligands under the same conditions (pH 4.3). The signal of a drop of methanol ($\delta = 49.50$ ppm in D_2O) was used as an internal secondary reference^[65] for the chemical shift. For atom numbering see Figure 2.72. $\Delta\delta$ values indicating a diolate coordination are in boldface. Assignment of free L-carnosine according to the literature^[108].

		L-carnosine					
		C_{COhis}	$\text{C}_{\alpha\text{his}}$	$\text{C}_{\beta\text{his}}$	$\text{C}_{2\text{his}}$	$\text{C}_{4\text{his}}$	$\text{C}_{5\text{his}}$
free	δ	176.76	54.57	27.59	133.85	130.19	117.28
17	δ	184.59	63.42	28.34	145.48	138.86	117.32
	$\Delta\delta$	7.83	8.85	0.75	11.63	8.67	0.04
		L-carnosine			ethanediol		
		C_{COala}	$\text{C}_{\alpha\text{ala}}$	$\text{C}_{\beta\text{ala}}$	$\text{C}_{1/2}$		
free	δ	172.17	32.53	36.35	63.16		
17	δ	177.45	34.68	38.36	82.34, 84.65		
	$\Delta\delta$	5.28	2.15	2.01	19.18, 21.49		

2.4.3 The reaction of $[\text{ReOCl}_3(\text{PPh}_3)_2]$ with L-carnosine and adenosine

In the previous sections some structures of complexes with pyrimidine nucleosides were presented (**1**, **2**, **8**, **12**, **13**), but none, so far, with a purine nucleoside. Generally, compounds with rhenium and nucleosides are hardly found in the literature.

M. Oßberger^[23] reported on a complex with adenosine (Ado) with the postulated formula $[\text{ReO}(\text{dien})(\text{AdoH}_{-2})]\text{I}$. But crystal-structure determinations are known so far only with nucleobases, the subunit of nucleosides. *Beauchamp et al.*^[109] reported in 1998 structures with *N*6,*N*6-dimethyladenine and rhenium(IV,V) and *Alberto et al.*^[110] with 7-methylguanine and rhenium(I) in 2005.

The reactions of the co-ligands presented in this work so far (dien, aminoalanine, histidine) with rhenium(V) and purine nucleosides showed hints of successful coordination according to NMR spectroscopy. But the yields were unsatisfying and a crystal-structure determination was not possible. In contrast to this, the reaction of $[\text{ReOCl}_3(\text{PPh}_3)_2]$ with L-carnosine, adenosine and triethylamine in methanol yielded blue crystals of $[\text{ReO}(\text{L-car})(\text{syn-AdoH}_{2',3'\text{H}_{-2}})] \cdot 3 \text{ MeOH} \cdot 2 \text{ H}_2\text{O}$ (**18**). With four formula units in the unit cell of the monoclinic space group C2, the asymmetric unit contains one molecule of the rhenium complex (Figure 2.73), three molecules of methanol and two molecules of water.

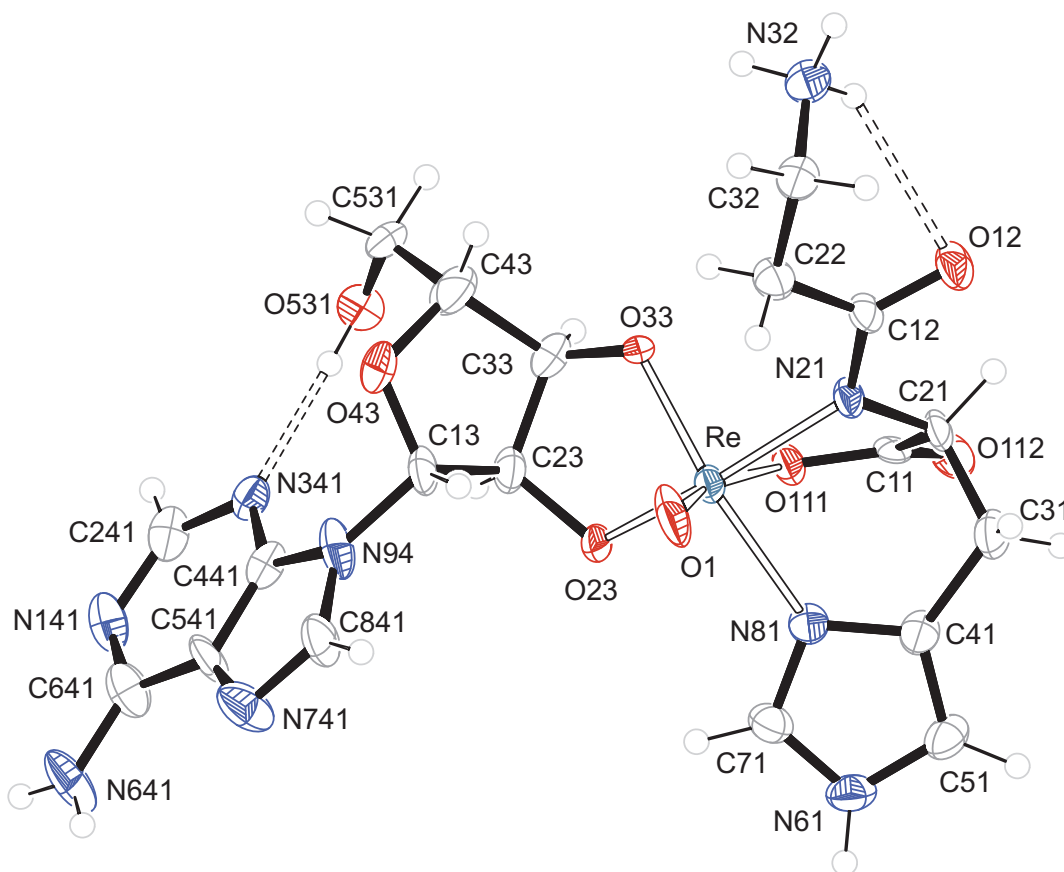


Figure 2.73 ORTEP presentation of **18** in crystals of $[\text{ReO}(\text{L-car})(\text{syn-AdoH2}',3'\text{H}_{-2})] \cdot 3 \text{ MeOH} \cdot 2 \text{ H}_2\text{O}$. The atoms N142, C242, N342, C442, C542, C642, N642, N742, C842 of the minor disordered adenine moiety (occupancy ca. 34 %) were omitted for lucidity. Ellipsoids are drawn at 50 % probability level. Distances [Å] and angles [°]: Re-O1 1.646(8), Re-O23 1.977(4), Re-O33 1.947(7), Re-O111 2.177(7), Re-N21 2.066(5), Re-N81 2.131(8), O1-Re-O23 105.8(3), O1-Re-O33 107.7(3), O1-Re-O111 167.4(3), O1-Re-N21 100.9(3), O1-Re-N81 92.6(4), O23-Re-O33 81.3(2), O23-Re-O111 80.2(2), O23-Re-N21 153.28(18), O23-Re-N81 93.2(2), O33-Re-O111 84.0(3), O33-Re-N21 88.9(2), O33-Re-N81 159.7(3), O111-Re-N21 74.1(2), O111-Re-N81 75.8(3), N21-Re-N81 87.5(3), furanose torsion angle O23-C23-C33-O33: $-32.1(7)$, peptide torsion angle C22-C12-N21-C21: $179.5(6)$, O12-C12-N21-Re: $-176.8(5)$, torsion angle of the coordinated acid group Re-O111-C11-O112: $167.5(7)$, puckering parameters^[59] for O43-C13-C23-C33-C43: $Q_2 = 0.296(8)$ Å, $\phi_2 = 67.3(14)^\circ$, conformation 2E , donor-acceptor distances in intramolecular hydrogen bonds: N32 \cdots O12 3.010(8), O531 \cdots N341 2.787(17).

The deprotonated form of L-carnosine binds *facial* via N81, N21 and O111 to the metal with O111 of the carboxylate group *trans* to the oxido ligand O1. An intramolecular hydrogen bond is formed between the protonated amino function N32 as donor and O12 of the peptide bond as acceptor. The torsion angle of the peptide bond ($\omega = 179.5^\circ$ for C22-C12-N21-C21) is even closer to the ideal value of 180° than in the free form of L-carnosine ($\omega = 174.9^\circ$)^[107]. With a deviation of 0.023 Å the rhenium center is in-plane with the planar peptide bond.

Adenosine binds as a double-deprotonated (*O,O*)-donor via O23 and O33 to the rhenium core in *syn* orientation to the oxido ligand O1. Due to this chelate, the diol's torsion angle (O23-C23-C33-O33) diminishes to -32.1° compared with the angle found in the free form ($+45.4^\circ$)^[111] and the conformation of the ribofuranosyl ring changes from 3T_2 to 2E . Except for N94, all the atoms of the adenine moiety and CH₂OH of the ribose moiety are disordered (occupancy of the major part ca. 66 %, see Figure 2.74). For both disordered parts an intramolecular hydrogen bond is correlated with deviating torsion angles at the glycosidic bond. Their conformation is *syn* ($\chi = 61.9^\circ$ for O43-C13-N94-C441 and $\chi = 50.4^\circ$ for O43-C13-N94-C442), while for the free form it is *anti* ($\chi = -172.7^\circ$).

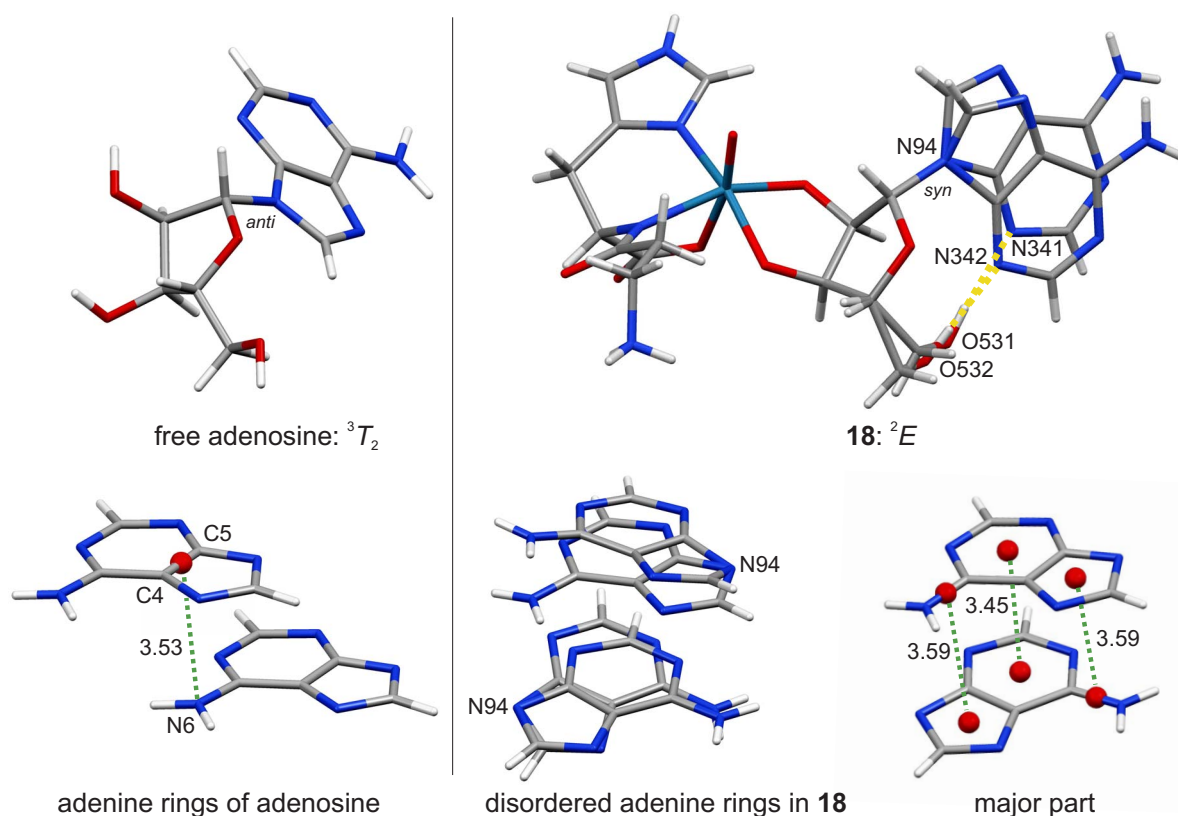


Figure 2.74 MERCURY presentation of free adenosine^[111] (left) and disordered parts in **18** (right). Top: intramolecular hydrogen bond of adenosine (yellow dashed lines). Below: π - π interactions of adenine, green dashed lines: distances between selected centroids.

The hydrogen bonds in **18** are given in Table 2.35. They connect the hydrophilic parts in **18** and the solvent molecules to sheets parallel to the *bc* plane. In between, there are π - π interactions of the adenine moieties (Figure 2.75). In analogy to the free form of adenosine, π -stacking of adenine rings is observed with an interplanar spacing of 3.45–3.59 Å. All hydrogen atoms of the protonated amino function N34 take part in hydrogen bonding.

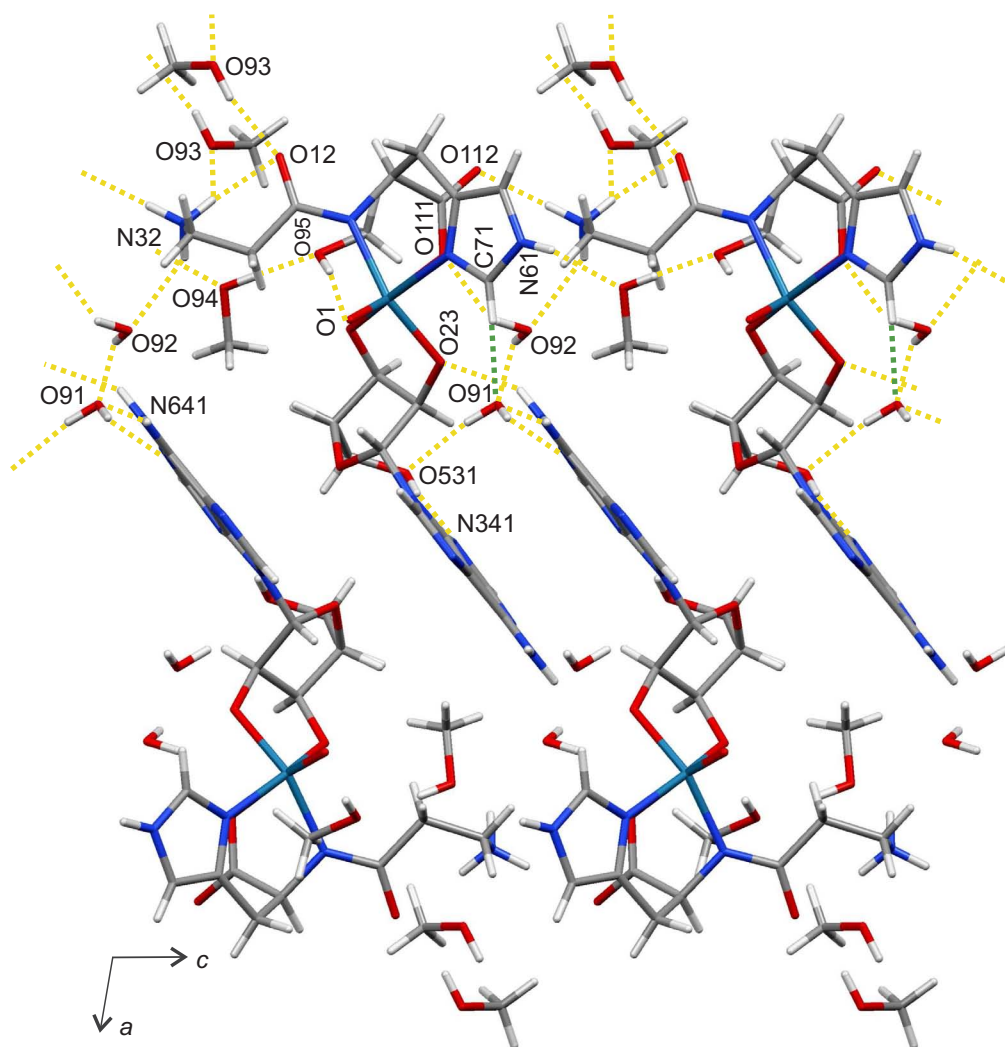


Figure 2.75 MERCURY presentation of hydrogen bonds (yellow dashed lines) and C-H...O contacts (green dashed lines) in **18**.

Figure 2.76 illustrates the possible binding modes of adenosine. In accordance with the other nucleoside-containing compounds in this work, *syn/anti* isomerism was observed in ^{13}C NMR spectra, but limited to protic solvents. Spectra of the crude reaction mixture (methanol), or redissolved product in water, showed two signal sets at a ratio of 2:1 but with poor intensities. However, spectra of **18** in DMSO-d_6 showed clearly only one signal set for the *syn* isomer. The chemical shifts listed in Table 2.36 show a coordination of the histidine residue of carnosine via N_{π} , N_{α} , O_{CO} and of the nucleoside via $\text{O}2'$ and $\text{O}3'$. The signals of the C-atoms directly neighboring these donor atoms (C_{CO} , C_{α} , $\text{C}2$, $\text{C}4$, C_{CO}) are shifted, as expected, 6.9–10.2 ppm to lower field. The signals of the corresponding atoms $\text{C}2'$ and $\text{C}3'$ of the nucleoside are shifted noticeably to lower field (24.5 ppm and 26.4 ppm) compared with the values for $\text{C}1$, $\text{C}2$ in **17** (19.2 ppm and 21.5 ppm).

2 Results

Table 2.35 Distances [Å] and angles [°] of hydrogen bonds in **18**. Values without standard deviation are related to hydrogen atoms at calculated positions. O91, O92 are affiliated to water and O93, O94, O95 to methanol. D: donor, A: acceptor, x : difference of (H···A) and the sum of the van-der-Waals radii^[62].

D	H	A	D···A	D-H	H···A	x	D-H···A
N32	H323	O93 ⁱ	2.879(11)	0.91	2.23	−0.49	128
N32	H324	O112 ⁱⁱ	2.776(7)	0.91	1.89	−0.83	165
N32	H325	O92 ⁱⁱ	2.873(10)	0.91	2.17	−0.55	134
N32	H325	O94	3.178(9)	0.91	2.47	−0.25	134
N641	H641	O23 ⁱⁱⁱ	2.900(12)	0.88	2.10	−0.62	151
N641	H642	O91 ^{iv}	3.058(14)	0.88	2.33	−0.39	140
N61	H761	O94 ^v	2.771(8)	0.88	1.95	−0.77	154
O531	H853	N341	2.787(17)	0.84	1.95	−0.80	170
O532	H854	N342	2.68(3)	0.84	1.89	−0.87	158
O93	H893	O12 ^{vi}	2.742(7)	0.84	1.98	−0.74	150
O94	H894	O95	2.646(9)	0.84	1.81	−0.91	177
O95	H895	O33	2.720(9)	0.84	1.91	−0.81	163
O91	H911	N142 ⁱⁱⁱ	3.140(19)	0.83(7)	2.41(8)	−0.34	148(8)
O91	H912	O531	2.770(12)	0.83(8)	2.07(8)	−0.65	141(8)
O91	H912	O532	2.91(2)	0.83(8)	2.17(8)	−0.55	148(7)
O92	H921	O91	2.827(11)	0.83(6)	2.07(7)	−0.66	152(8)
O92	H922	O111	2.879(10)	0.84(6)	2.12(7)	−0.60	151(7)
C71	H71	O91 ^{vii}	3.290(10)	0.95	2.44	−0.28	148

Symmetry codes: ⁱ $\frac{1}{2} - x, \frac{1}{2} + y, 1 - z$; ⁱⁱ $x, y, 1 + z$; ⁱⁱⁱ $-x, y, -z$; ^{iv} $-x, -1 + y, -z$;
^v $x, -1 + y, -1 + z$; ^{vi} $x, y, -1 + z$; ^{vii} $x, -1 + y, z$.

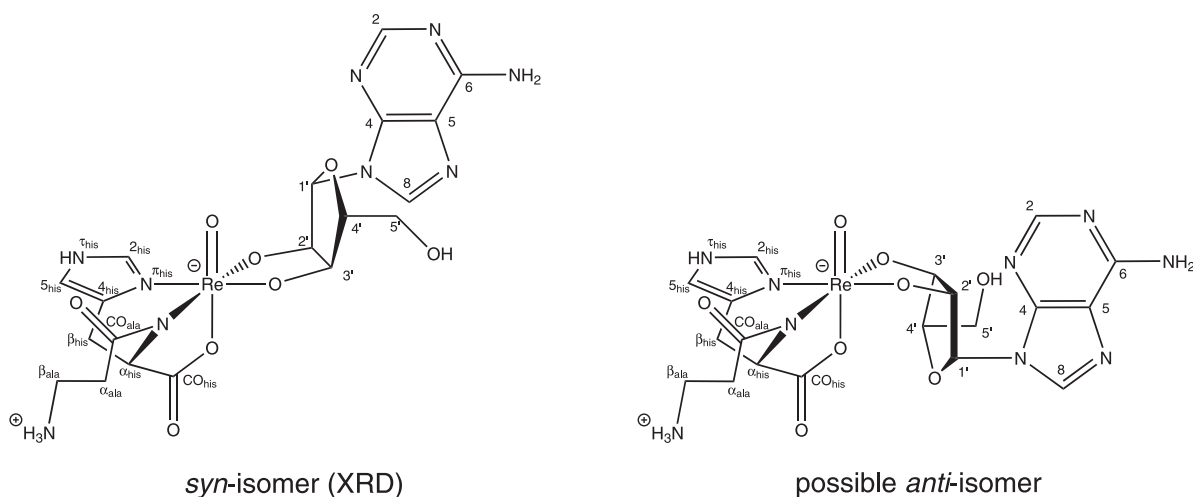


Figure 2.76 Scheme of the diastereomeric forms of **18** and atom numbering used in the ¹³C NMR study according to the recommendations of the JCBN^[61, 79]. XRD: result of the structure determination.

Table 2.36 ^{13}C NMR chemical shifts (in ppm) of **18** in DMSO- d_6 (101 MHz, 25 °C) and comparison with the free ligands under the same conditions. The signal of the deuterated solvent ($\delta = 39.52$ ppm) was used as an internal secondary reference^[65] for the chemical shift. For atom numbering see Figure 2.76. $\Delta\delta$ values indicating a diolate coordination are in boldface. Assignment according to the literature: adenosine^[68], L-carnosine^[108].

		C_{COhis}	$\text{C}_{\alpha\text{his}}$	$\text{C}_{\beta\text{his}}$	$\text{C}_{2\text{his}}$	$\text{C}_{4\text{his}}$	$\text{C}_{5\text{his}}$	C_{COala}	$\text{C}_{\alpha\text{ala}}$	$\text{C}_{\beta\text{ala}}$	
L-car	δ	172.90	52.47	27.61	134.67	132.23	115.70	169.59	31.98	35.44	
18	δ	180.36	61.86	28.28	144.31	138.55	115.69	176.53	33.30	37.59	
	$\Delta\delta$	7.40	9.40	0.67	9.64	6.32	-0.01	6.94	1.32	2.15	
		$\text{C}1'$	$\text{C}2'$	$\text{C}3'$	$\text{C}4'$	$\text{C}5'$	$\text{C}2$	$\text{C}4$	$\text{C}5$	$\text{C}6$	$\text{C}8$
Ado	δ	87.98	73.50	70.71	85.95	61.73	152.44	149.11	119.40	156.21	139.98
18	δ	88.30	97.98	97.12	86.38	62.67	152.58	149.45	119.23	156.17	139.86
	$\Delta\delta$	0.32	24.48	26.41	0.43	0.94	0.14	0.34	-0.17	0.14	-0.12

2.4.4 The reaction of $[\text{ReOCl}_3(\text{PPh}_3)_2]$ with L-carnosine and D-ribose

The complex with adenosine in the previous chapter showed a coordination of the ribofuranosyl residue to the rhenium(V) core. Keeping in mind that adenosine is an *N*-glycoside of the monosaccharide D-ribose, the question arises if it is possible to build a complex with rhenium(V) and D-ribose. This aldopentose provides several different binding sites for coordination due to the isomerism of the furanose and pyranose anomers. Structurally characterized coordination compounds with D-ribose are rare, but they are known for both anomeric forms. They have been reported for the furanose anomer (with calcium^[112], silicon^[113]) and for the pyranose anomer (with palladium^[114] and some elements of the lanthanoid series: lanthanum^[115], cerium^[115], praseodymium^[116], neodymium^[117], samarium^[118]).

Among the aldopentoses, D-ribose offers the largest percentage of furanose anomers in aqueous solution (α : 7.4 %, β : 13.3 %)^[119], while the pyranose anomers are predominant as for all aldopentoses (α : 20.3 %, β : 58.9 %). But this flexibility in view of possible binding sites may also lead to non-selective product mixtures. Moreover, solutions of reducing sugars are prone to react with oxidizing agents like rhenium(V) in analogy to Fehling's solution. Only compounds with non-reducing O1-methylated derivatives of D-aldopentoses were prepared successfully up to now: $[\text{ReO}(\text{dien})(\text{syn-Me-}\beta\text{-L-Arap3,4H}_2)]\text{I}^{[24]}$, $[\text{ReO}(\text{dien})(\text{Me-}\beta\text{-D-Xylp2,3H}_2)]\text{I}^{[24]}$ and $[\text{ReO}(\text{L-his})(\text{syn-Me-}\beta\text{-D-Ribp3,4H}_2)]$ (**15**). Decomposition to rhenium(IV) occurred

for all reactions of free D-aldopentoses with rhenium(V) and the co-ligands phen^[23], tpb^[23], dien, *rac*-dap and L-histidine.

A similar behavior was observed for reactions with L-carnosine. The mixtures with D-aldopentoses showed a tendency to decompose within hours, but it was possible to precipitate a blue raw product from the reaction of $[\text{ReOCl}_3(\text{PPh}_3)_2]$, L-carnosine, D-ribose and triethylamine in methanol. This hygroscopic precipitate was recrystallized from methanol. Figure 2.77 shows the result of the structure determination, $[\text{ReO}(\text{L-car})(\text{syn-}\alpha\text{-D-Ribf1,2H}_2)] \cdot 3 \text{ MeOH}$ (**19**).

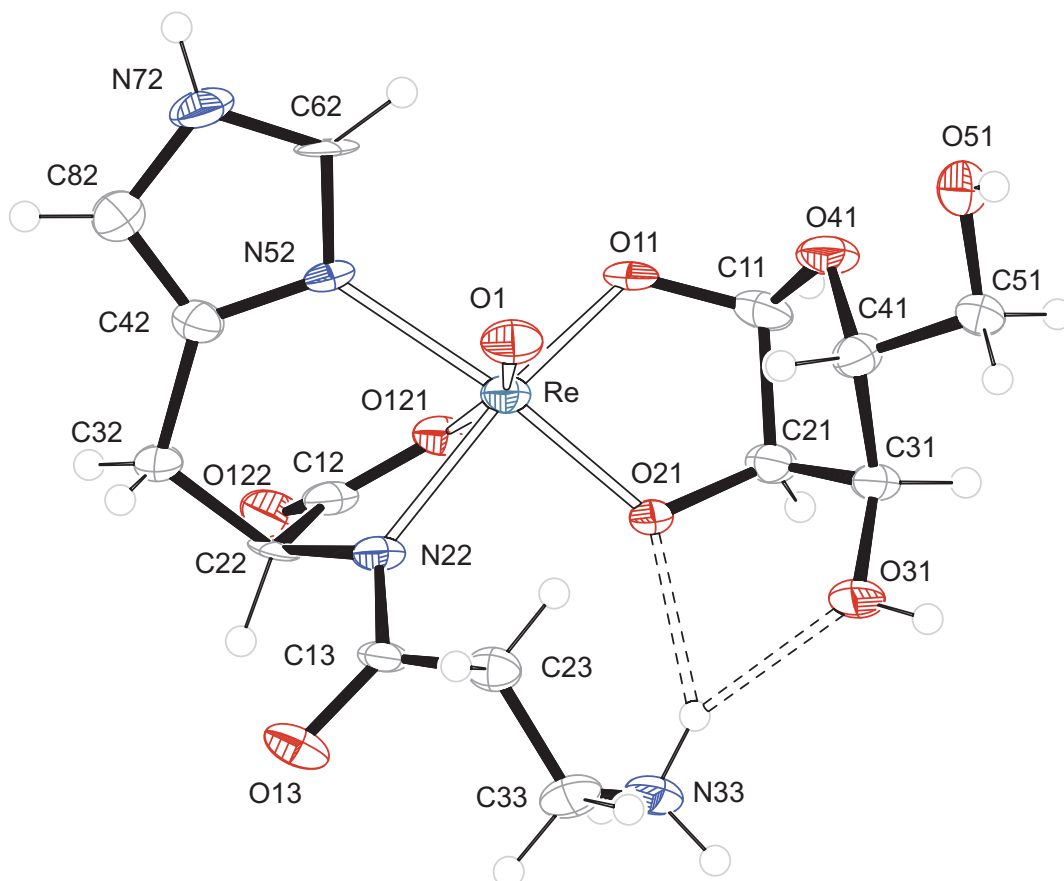


Figure 2.77 ORTEP presentation of **19** in crystals of $[\text{ReO}(\text{L-car})(\text{syn-}\alpha\text{-D-Ribf1,2H}_2)] \cdot 3 \text{ MeOH}$. Ellipsoids are drawn at 50 % probability level. Distances [Å] and angles [°]: Re-O1 1.689(7), Re-O11 2.003(8), Re-O21 1.951(6), Re-O121 2.165(7), Re-N22 2.073(7), Re-N52 2.158(8); O1-Re-O11 104.6(3), O1-Re-O21 107.9(3), O1-Re-O121 163.4(3), O1-Re-N22 101.0(3), O1-Re-N52 85.5(3), O11-Re-O21 80.4(3), O11-Re-O121 81.4(3), O11-Re-N22 154.2(3), O11-Re-N52 99.3(3), O21-Re-O121 88.3(3), O21-Re-N22 89.2(3), O21-Re-N52 166.3(3), O121-Re-N22 74.8(3), O121-Re-N52 78.2(3), N22-Re-N52 85.5(3), furanose torsion angle O11-C11-C21-O21: $-18.7(10)$, peptide torsion angle C23-C13-N22-C22: $176.7(8)$, O13-C13-N22-Re: $179.3(7)$, torsion angle of the coordinated acid group Re-O121-C12-O122: $171.4(8)$, puckering parameters^[59] for O41-C11-C21-C31-C41: $Q_2 = 0.353(10) \text{ \AA}$, $\phi_2 = 300.1(16)^\circ$, conformation 3T_0 , donor-acceptor distances in intramolecular hydrogen bonds: N33 \cdots O21 2.951(10), N33 \cdots O31 2.913(10).

Compound **19** crystallizes in the monoclinic space group $P2_1$ with two formula units in the unit cell. The asymmetric unit contains one molecule of the rhenium complex and two molecules of methanol. Different to **15**, not the β -pyranose anomer of D-ribose is to be found in this complex, although this anomer is the main species of free D-ribose in solution. Similarly to the silicon compound $[K([18]\text{crown-6})][\text{PhSi}(\alpha\text{-D-Ribf1,2H}_{-2})_2]$ ^[113] the α -furanose anomer of D-ribose is coordinated to the central atom. But in **19** the conformation of the ribofuranose ring is 3T_O (*vs.* close to E_4)^[113] and the torsion angle of the deprotonated *cis*-vicinal diol function (O11, O21) is -18.7° (*vs.* -5.4°)^[113]. The chelating dianionic α -D-Ribf1,2H $_{-2}$ ligand is oriented *syn* to the oxido ligand O1. Its remaining hydroxy groups (O31-H and O51-H) are left dangling, they are not deprotonated and take part in hydrogen bonding. L-Carnosine binds as monoanionic co-ligand *facial* via N22, N51 and O121 to the metal. O121 is in *trans* position to the oxido ligand O1. The torsion angle of the peptide bond (C23-C13-N22-C22: 176.7°) is close to the value found in the free form of L-carnosine ($\omega = 174.9^\circ$)^[107]. The protonated amino function of the β -alanyl residue takes part in an intramolecular bifurcated hydrogen bond to the acceptor atoms O21 and O31. Further hydrogen bonds in **19** are listed in Table 2.37. Only two of the intermolecular hydrogen bonds are without the participation of the solvent molecules. They build an infinite two-dimensional network parallel to the *ab*-plane, which is extended in all dimensions by the hydrogen bonding of the solvent molecules (Figure 2.78).

Table 2.37 Distances [\AA] and angles [$^\circ$] of hydrogen bonds in **19**. Values without standard deviation are related to hydrogen atoms at calculated positions. O97, O98, O99 are affiliated to methanol. D: donor, A: acceptor, x : difference of ($\text{H} \cdots \text{A}$) and the sum of the van-der-Waals radii^[62].

D	H	A	D \cdots A	D-H	H \cdots A	x	D-H \cdots A
N33	H333	O98 ⁱ	2.794(13)	0.91	1.89	-0.83	174
N33	H334	O51 ⁱⁱ	2.876(9)	0.91	2.03	-0.69	154
N33	H335	O21	2.951(10)	0.91	2.21	-0.51	138
N33	H335	O31	2.913(10)	0.91	2.11	-0.61	146
N72	H772	O122 ⁱⁱⁱ	2.802(13)	0.88	1.99	-0.73	153
O31	H831	O99	2.664(10)	0.84	1.84	-0.88	166
O51	H851	O97 ^{iv}	2.74(2)	0.84	2.03	-0.69	142
O97	H897	O121 ^v	2.89(2)	0.84	2.16	-0.56	145
O98	H898	O11 ^{vi}	2.700(11)	0.84	1.86	-0.86	177
O99	H899	O13 ⁱ	2.646(12)	0.84	2.05	-0.67	127

Symmetry codes: ⁱ $1 - x, -\frac{1}{2} + y, 1 - z$; ⁱⁱ $1 + x, y, z$; ⁱⁱⁱ $-x, \frac{1}{2} + y, 2 - z$; ^{iv} $-1 + x, y, z$;
^v $1 - x, \frac{1}{2} + y, 1 - z$; ^{vi} $-x, \frac{1}{2} + y, 1 - z$.

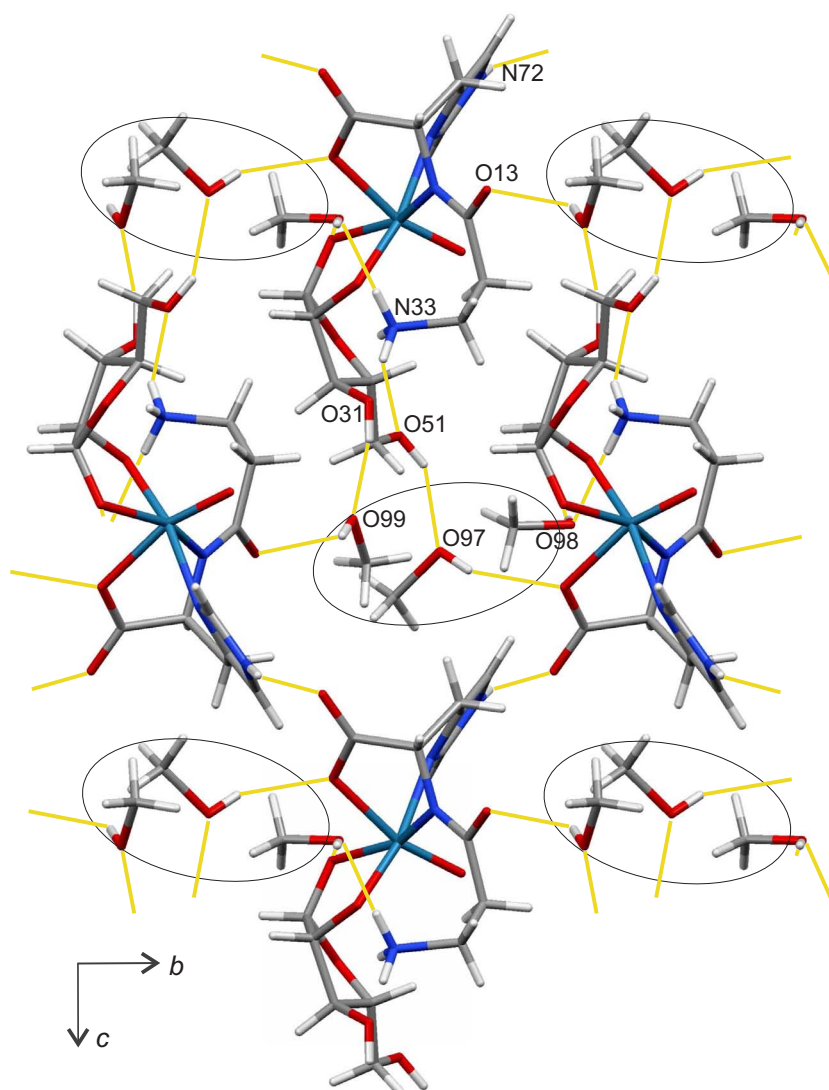


Figure 2.78 MERCURY presentation of hydrogen bonds (yellow lines) in **19**.

2.4.4.1 NMR spectroscopy and reactions with other aldopentoses

The result of the structure determination shows a coordination of the α -ribofuranose anomer. But in analogy to **15**, a related structure with methyl β -D-ribofuranoside, the pyranose anomer of D-ribose has to be considered as a chelating species, too. As illustrated in Figure 2.79, D-ribose provides many different binding sites for coordination to rhenium. Although not all of them may be favorable, a mixture of isomers is to be expected for the reaction mixture. Even more species result from the presence of *syn/anti* isomerism. ^{13}C NMR spectra of the reaction mixture were hard to interpret as they showed many small signals at low intensities. But even spectra of redissolved product in water or methanol showed more than one species and the so-

lutions decomposed within hours. In Table 2.38 only the signals of the main species are listed. The large shifts of C1 and C2 are consistent with the result of the structure determination.

According to NMR spectroscopy, reactions with D-arabinose, D-xylose, D-lyxose showed hints of a coordination to the metal, but the solutions were not stable. Even at 4 °C decomposition occurred after several hours.

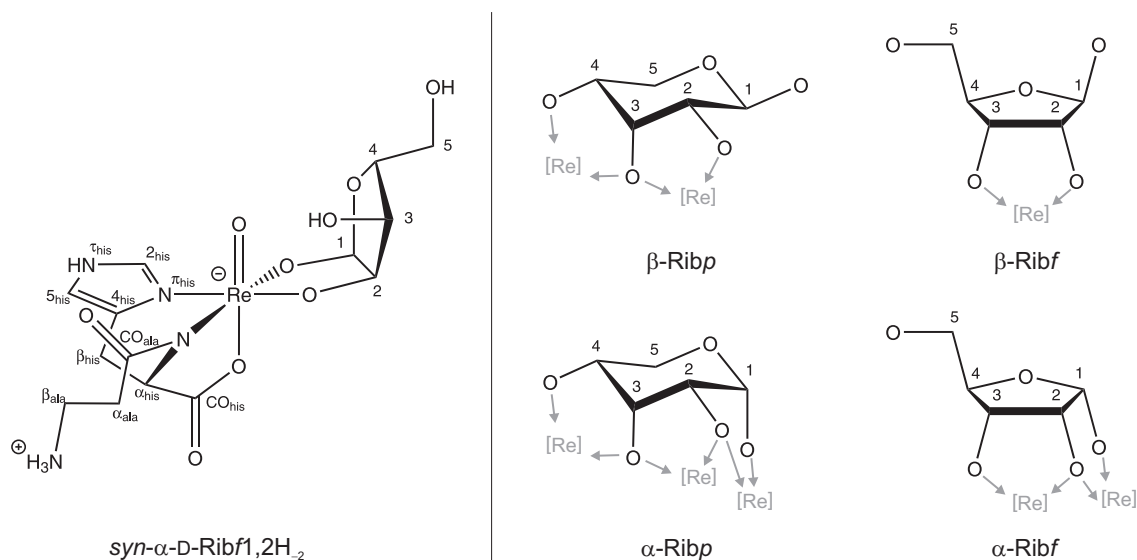


Figure 2.79 Scheme of **19** (on the left) and possible binding sites of D-ribose with *cis*-vicinal diol functions (on the right). For the pyranose forms only the 4C_1 conformation is depicted. The open-chain anomers of D-ribose were not considered.

Table 2.38 ${}^{13}\text{C}$ NMR chemical shifts (in ppm) of **19** in D_2O (101 MHz, 25 °C) and comparison with the free ligands under the same conditions (pH 3.6). The signal of a drop of methanol ($\delta = 49.50$ ppm in D_2O) was used as an internal secondary reference^[65] for the chemical shift. For atom numbering see Figure 2.79. $\Delta\delta$ values indicating a diolate coordination are in boldface. Assignment according to the literature: D-ribose^[119], L-carnosine^[108].

		C_{COhis}	$\text{C}_{\alpha\text{his}}$	$\text{C}_{\beta\text{his}}$	$\text{C}_{2\text{his}}$	$\text{C}_{4\text{his}}$	$\text{C}_{5\text{his}}$	C_{COala}	$\text{C}_{\alpha\text{ala}}$	$\text{C}_{\beta\text{ala}}$
L-car	δ	177.83	55.42	28.92	135.28	132.54	117.80	172.07	32.61	36.34
19	δ	184.76	63.04	28.49	145.67	138.34	117.34	177.93	34.58	38.28
	$\Delta\delta$	6.93	7.62	-0.43	10.39	5.80	-0.46	5.86	1.97	1.94
		C1	C2	C3	C4	C5				
α -Ribf	δ	96.90	70.36	69.50	83.65	61.98				
19	δ	117.14	96.08	74.25	86.61	64.22				
	$\Delta\delta$	20.24	25.72	4.75	2.96	2.24				

2.4.5 The reaction of $[\text{ReOCl}_3(\text{PPh}_3)_2]$ with L-carnosine and D-mannose

According to the results so far presented, furanoidic carbohydrates seem to be preferred for coordination to rhenium(V). To test the reaction of a carbohydrate with mainly pyranose species in solution, D-mannose was chosen. Aside from D-glucose, D-mannose provides among the aldohexoses in aqueous solution, one of the lowest percentages of furanose forms^[120] (α : 0.64 %, β : 0.24 %), while the dominating species are the pyranose forms (α : 66.23 %, β : 32.85 %). This also holds true for the solid state: D-mannose crystallizes as α -D-mannopyranose^[121]. Only few crystal-structure determinations have been reported up to the present for metal complexes with D-mannose. They contain the pyranose anomer (with palladium^[114], copper^[122]), but also the furanose anomer (with calcium^[123]), as metal ions can enrich anomeric species^[113]. With rhenium(V), only structures with non-reducing O1-methylated derivatives of the pyranose anomer were prepared successfully, so far, with the co-ligands dien^[23] and L-histidine (**14**). In both compounds methyl α -D-mannopyranoside is coordinated via O2 and O3 to the metal.

A similar coordination mode is to be expected for free D-mannose. Its reaction with the rhenium(V) precursor $[\text{ReOCl}_3(\text{PPh}_3)_2]$, L-carnosine and triethylamine in methanol yielded a blue solid, which is far less soluble in water or methanol than related compounds in this chapter (**19**, **21**, **22**). It was redissolved in a hot mixture of water/methanol, from which crystals of $[\text{ReO}(\text{L-car})(\textit{anti}\text{-}\alpha/\beta\text{-D-Manp}_{2,3}\text{H}_{-2})] \cdot \text{MeOH}$ (**20**) grew in the orthorhombic space group $P2_12_12_1$. The asymmetric unit contains the rhenium complex and one molecule of methanol, while there are four of these formulas in the unit cell.

As depicted in Figure 2.80, both the α - and the β -form of D-mannopyranose are present in the structure (slightly more α : occupancy ca. 58 %). This disorder of the hydroxy group on position 1 of the pyranose ring (atoms O111/O112) affects also the CH_2OH group (atoms C611-O611/C612-O612) at the same ratio. As in **14**, both pyranose anomers are connected via O21 and O31 to the rhenium core, but in *anti* orientation to the oxido ligand O1. The remaining hydroxy groups are not metallated. As mentioned above, they are disordered (O111/O112 and O611/O612) and take part in hydrogen bonding (see Figure 2.81). Further hydrogen bonds are listed in Table 2.39). In analogy to the above-mentioned compounds with methyl α -D-mannopyranoside, the torsion angle of the chelating diolato group (O21-C21-C31-O31: -46.0°) is diminished compared with the angle found in the free form (-61°)^[121], but in all three cases the pyranose ring is in ${}^4\text{C}_1$ chair conformation.

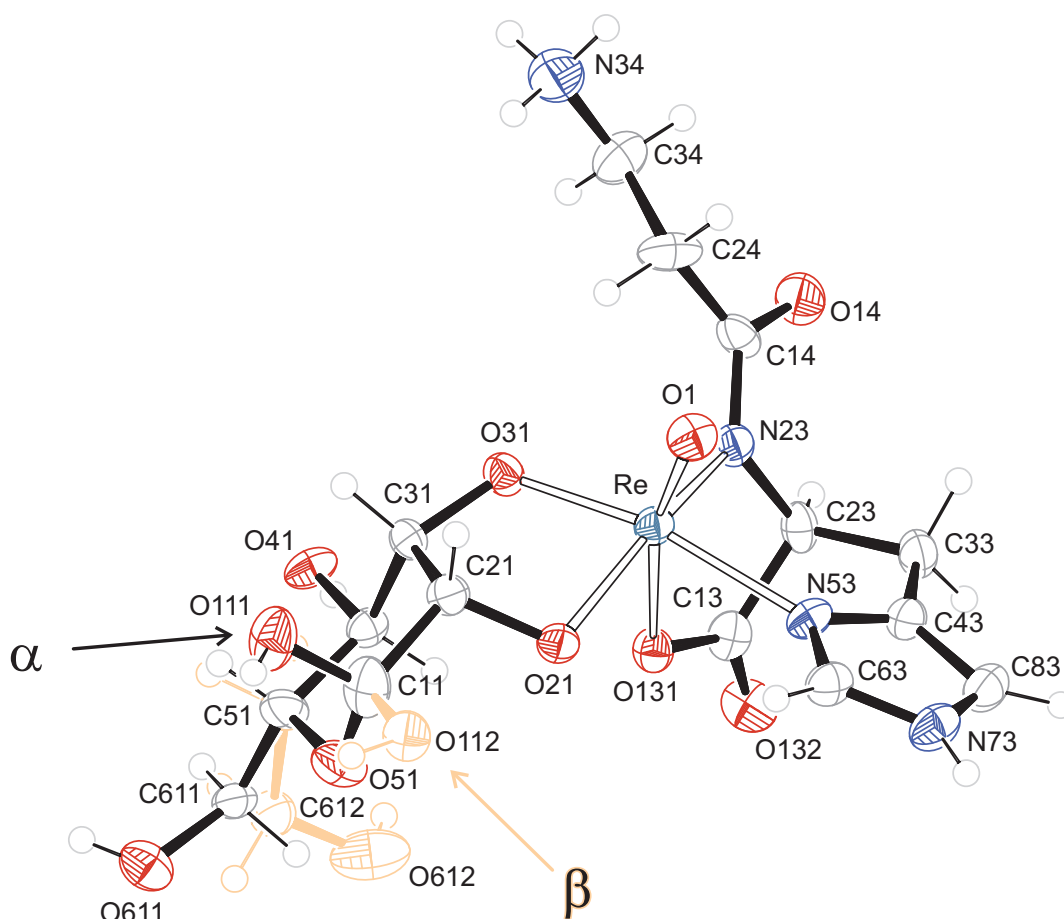


Figure 2.80 ORTEP presentation of **20** in crystals of $[\text{ReO}(\text{L-car})(\text{anti-}\alpha/\beta\text{-D-Manp2,3H}_2)] \cdot \text{MeOH}$. The atoms of the minor disordered part (occupancy ca. 42 %) are drawn in orange. Ellipsoids represent 50 % probability level. Distances [Å] and angles [°]: Re-O1 1.679(4), Re-O21 1.982(4), Re-O31 1.972(3), Re-O131 2.166(4), Re-N23 2.075(4), Re-N53 2.139(4); O1-Re-O21 104.39(17), O1-Re-O31 107.13(16), O1-Re-O131 164.82(15), O1-Re-N23 99.86(17), O1-Re-N53 88.90(15), O21-Re-O31 81.57(13), O21-Re-O131 81.94(14), O21-Re-N23 155.72(15), O21-Re-N53 93.70(14), O31-Re-O131 87.30(14), O31-Re-N23 90.31(13), O31-Re-N53 163.94(14), O131-Re-N23 74.82(13), O131-Re-N53 76.81(14), N23-Re-N53 87.84(14), pyranose torsion angle O21-C21-C31-O31: $-46.0(5)$, peptide torsion angle C24-C14-N23-C23: $178.3(4)$, O14-C14-N23-Re: $173.3(4)$, torsion angle of the coordinated acid group Re-O131-C13-O132: $171.5(4)$, puckering parameters^[59] for O51-C11-C21-C31-C41-C51: $Q = 0.542(5)$ Å, $\theta = 9.8(5)^\circ$, $\phi = 319(3)^\circ$, conformation 4C_1 .

The histidine part of the carnosine ligand is in a *facial* (*N,N,O*) binding mode with O131 of the acid group *trans* to the oxido ligand O1. The β -amino function of the alanyl residue is protonated and takes part in hydrogen bonding. With a small deviation (<0.06 Å) the rhenium core is in-plane with the imidazole ring. The torsion angle of the peptide bond (C24-C14-N23-C23 178.3°) is closer to 180° than the angle found in the free form of L-carnosine ($\omega = 174.9^\circ$)^[107].

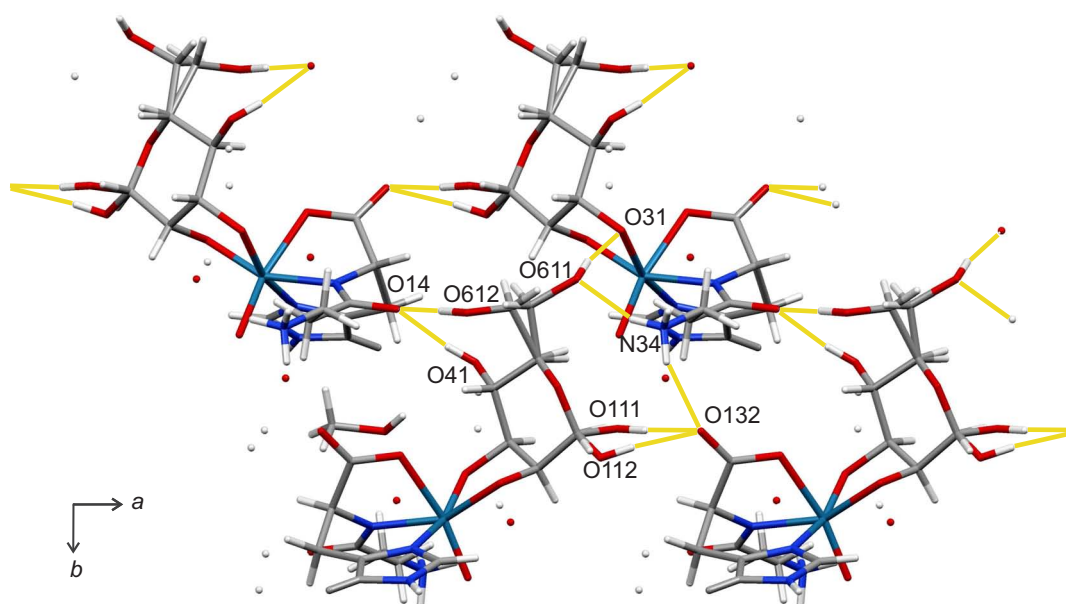


Figure 2.81 MERCURY presentation of selected hydrogen bonds (yellow lines) in **20**.

Table 2.39 Distances [Å] and angles [°] of hydrogen bonds in **20**. Values without standard deviation are related to hydrogen atoms at calculated positions. O99 is affiliated to methanol. D: donor, A: acceptor, x : difference of (H···A) and the sum of the van-der-Waals radii^[62].

D	H	A	D···A	D-H	H···A	x	D-H···A
O99	H99	O41	3.203(6)	0.84	2.44	-0.28	151
O111	H113	O132 ⁱ	2.675(8)	0.84	1.84	-0.88	175
O112	H114	O132 ⁱ	2.732(9)	0.84	1.91	-0.81	165
N34	H341	O611 ⁱⁱ	2.962(9)	0.91	2.10	-0.63	159
N34	H342	O21 ⁱⁱⁱ	2.864(7)	0.91	2.01	-0.71	157
N34	H343	O612 ⁱⁱⁱ	3.223(11)	0.91	2.48	-0.24	139
N34	H343	O132 ^{iv}	2.966(7)	0.91	2.17	-0.55	145
N73	H573	O41 ^v	2.796(6)	0.88	1.94	-0.78	165
O611	H611	O31 ^{vi}	2.998(7)	0.84	2.17	-0.55	170
O612	H612	O14 ^{vii}	2.856(10)	0.84	2.04	-0.68	163
O41	H841	O14 ^{vii}	2.689(5)	0.84	1.87	-0.85	164

Symmetry codes: ⁱ $1 + x, y, z$; ⁱⁱ $2 - x, \frac{1}{2} + y, \frac{1}{2} - z$; ⁱⁱⁱ $\frac{3}{2} - x, 1 - y, \frac{1}{2} + z$; ^{iv} $1 - x, \frac{1}{2} + y, \frac{1}{2} - z$; ^v $\frac{3}{2} - x, 1 - y, -\frac{1}{2} + z$; ^{vi} $2 - x, -\frac{1}{2} + y, \frac{1}{2} - z$; ^{vii} $1 - x, -\frac{1}{2} + y, \frac{1}{2} - z$.

¹³C NMR spectra of dissolved product in DMSO-*d*₆ showed two signal sets, as given in Table 2.40. The large shifts of C2 and C3 show a coordination of α - and β -D-Manp2,3H₂ to the metal via O2 and O3. *Syn/anti* isomerism, or a coordination via O1 and O2 was not observed. The presence of these phenomenons for the crude

reaction mixture could not be approved due to the limited solubility of the product in methanol.

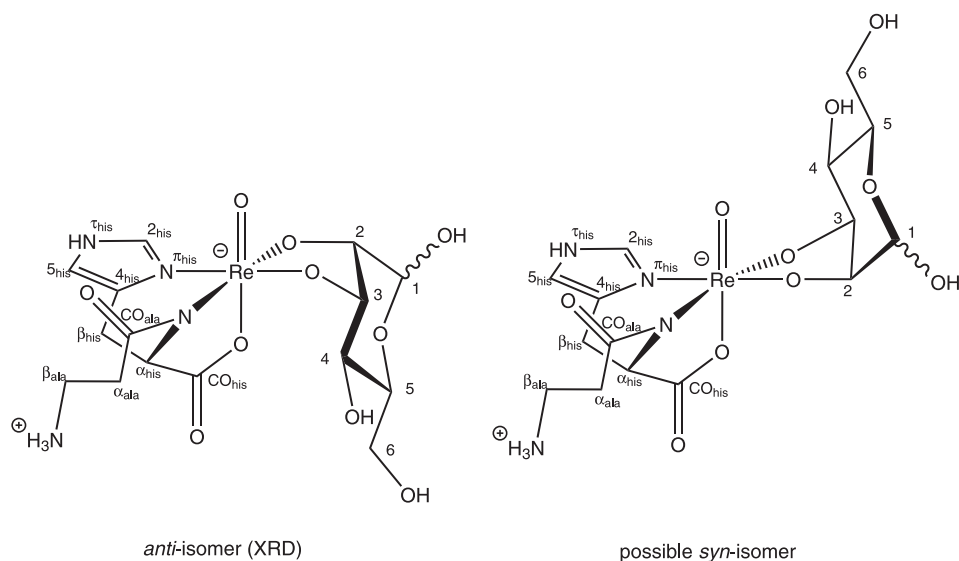


Figure 2.82 Scheme of the diastereomeric forms of **20** and atom numbering used in the ^{13}C NMR study according to the recommendations of the JCBN^[79, 95]. XRD: result of the structure determination.

Table 2.40 ^{13}C NMR chemical shifts (in ppm) of **20** in DMSO- d_6 (126 MHz, 25 °C) and comparison with the free ligands under the same conditions. The signal of the deuterated solvent ($\delta = 39.52$ ppm) was used as an internal secondary reference^[65] for the chemical shift. For atom numbering see Figure 2.82. $\Delta\delta$ values indicating a diolate coordination are in boldface. Assignment according to the literature: D-mannose^[120], L-carnosine^[108].

		C_{COhis}	$\text{C}_{\alpha\text{his}}$	$\text{C}_{\beta\text{his}}$	$\text{C}_{2\text{his}}$	$\text{C}_{4\text{his}}$	$\text{C}_{5\text{his}}$	C_{COala}	$\text{C}_{\alpha\text{ala}}$	$\text{C}_{\beta\text{ala}}$	
L-car	δ	172.90	52.47	27.61	134.67	132.23	115.70	169.59	31.98	35.44	
20	a	δ	181.40	61.61	28.47	144.10	138.55	115.88	176.50	34.82	37.21
	b	δ	181.18	61.90	28.59	144.66	138.66	115.86	176.46	34.52	37.24
	a	$\Delta\delta$	8.50	9.14	0.86	9.43	6.32	0.18	6.91	2.84	1.77
	b	$\Delta\delta$	8.28	9.43	0.98	9.99	6.43	0.16	6.87	2.54	1.80
		C1	C2	C3	C4	C5	C6				
$\alpha\text{-Manp}$	δ	94.09	71.52	70.70	67.46	73.24	61.66				
$\beta\text{-Manp}$	δ	94.24	71.71	73.93	67.13	77.09	61.53				
20	a	δ	94.38	95.32	92.94	67.85	71.93	62.26			
	b	δ	93.68	93.45	95.74	67.61	77.04	62.38			
	a	$\Delta\delta$	0.29	23.80	22.24	0.39	-1.31	0.60			
	b	$\Delta\delta$	-0.70	21.74	21.81	0.48	-0.05	0.85			

a: major isomer (*anti*-isomer with $\alpha\text{-manp}$), b: minor isomer (*anti*-isomer with $\beta\text{-manp}$).

2.4.6 The reaction of $[\text{ReOCl}_3(\text{PPh}_3)_2]$ with L-carnosine and D-fructose

Like the monosaccharides of the previous chapters, the ketohexose D-fructose exists in aqueous solution at 20 °C in an equilibrium of pyranose (α : 2.3 %, β : 72.5 %) and furanose anomers (α : 5.2 %, β : 20.0 %)^[124]. Crystalline D-fructose solely occurs as β -D-fructopyranose, the above given main anomer in solution^[125, 126]. It is also found in some of the few structurally characterized metal complexes (with strontium^[127] and calcium^[128]). Complexes with β -D-fructofuranose are even more rare, as only one structure with silicon^[113] is known so far. Metal ions are able to change the equilibrium composition of the anomers in solution, for example palladium(II)^[129]. The reaction of rhenium(V) with D-ribose in chapter 2.4.4 showed a similar behavior where the resulting complex contained the minor anomer of D-ribose. On the other hand, the compound of chapter 2.4.5 was built with the major anomers of D-mannose.

The reaction of the rhenium(V) precursor $[\text{ReOCl}_3(\text{PPh}_3)_2]$ with L-carnosine, D-fructose and triethylamine in methanol yielded a blue powder from which crystals in the orthorhombic space group $P2_12_12_1$ were recrystallized. As shown in Figure 2.83, the β -furanose anomer is coordinated to rhenium. The resulting compound is $[\text{ReO}(\text{L-car})(\textit{anti}\text{-}\beta\text{-D-Fruf2,3H}_{-2})] \cdot \text{MeOH}$ (**21**).

The asymmetric unit of the crystals contains one molecule of the rhenium complex and one molecule of methanol, which is disordered. The same holds true for the hydroxy-function on C11 of the fructose moiety. Both take part in hydrogen bonding. As in the above-mentioned silicate $[\text{PhSi}(\beta\text{-D-Fruf2,3H}_{-2})_2]^-$, the furanose is coordinated via O2 and O3 (here: O21 and O31) in *anti* orientation to the oxidorhenium unit. But in **21**, the torsion angle of the chelating diol group is increased (-28.4° vs. 13.1° and 16.1°) and the ring adopts an envelope conformation close to 3E (vs. 4T_3 and E_3). No intra-, but intermolecular hydrogen bonds are found for the remaining hydroxy groups of the ribosyl moiety.

The tridentate co-ligand L-carnosine binds *facial* via N22, N52 and O121 to the metal. Between the protonated β -amino function of the alanyl part and O13 of the peptide bond an intramolecular hydrogen bond is established, although it is not very strong due to an unfavorable angle (126°). It forms a six-membered ring (N33-H333...O13-C13-C23-C33-). In analogy to the other compounds in this section, the peptide bond is closer to planarity than in the free form of L-carnosine ($\omega = 177.5^\circ$ vs. 174.9° ^[107]). With small deviations, the rhenium core is in-plane with the imidazole ring ($<0.08 \text{ \AA}$) and the peptide bond ($<0.02 \text{ \AA}$), but not with the acid group. The latter one is tilted toward the imidazole group.

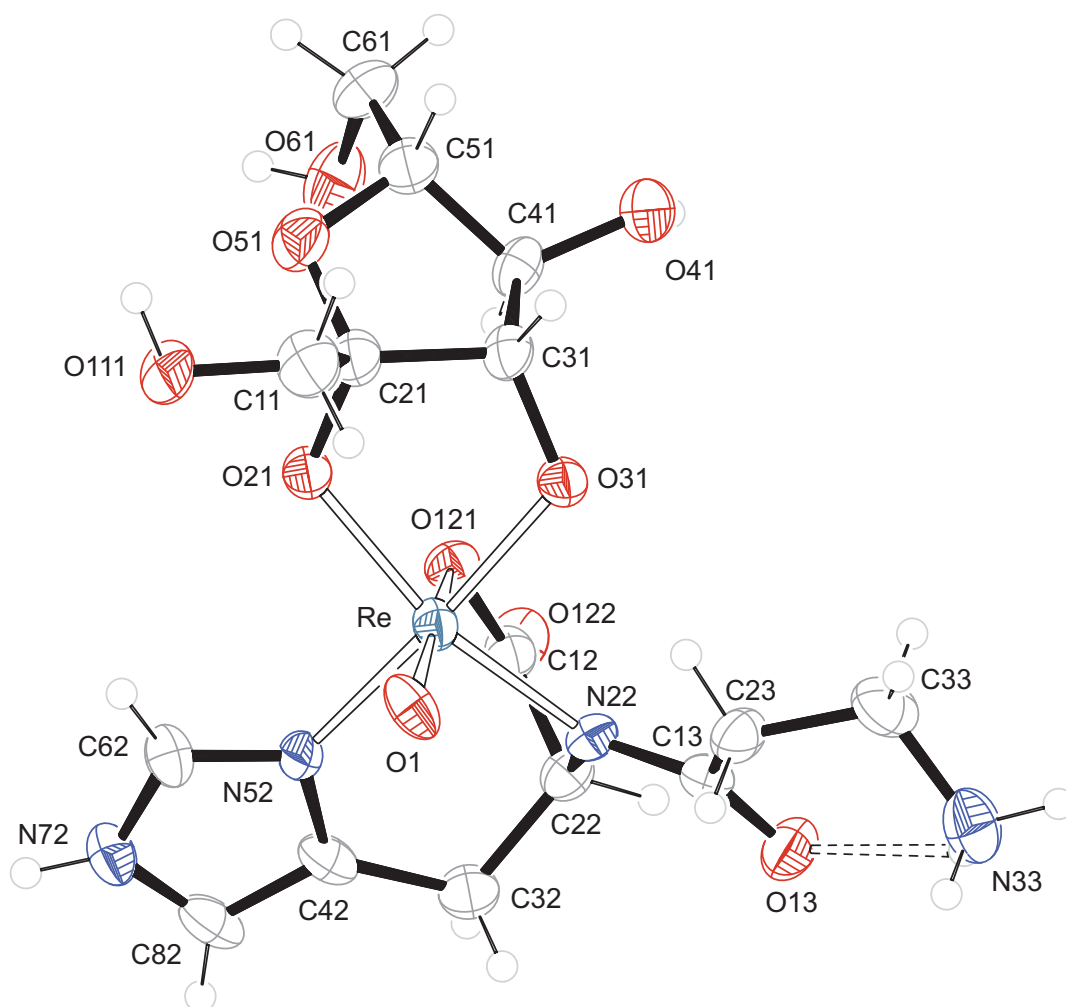


Figure 2.83 ORTEP presentation of **21** in crystals of $[\text{ReO}(\text{L-car})(\text{anti-}\beta\text{-D-Fruf}_{2,3}\text{H}_{-2})] \cdot \text{MeOH}$. Atom O112 of the disordered atom pair O111/O112 was omitted for lucidity. Ellipsoids are drawn at 50 % probability level. Distances [\AA] and angles [$^\circ$]: Re-O1 1.680(5), Re-O21 1.985(5), Re-O31 1.944(5), Re-O121 2.226(5), Re-N22 2.090(5), Re-N52 2.112(5); O1-Re-O21 106.3(2), O1-Re-O31 107.2(2), O1-Re-O121 165.3(2), O1-Re-N22 99.3(2), O1-Re-N52 89.6(2), O21-Re-O31 82.0(2), O21-Re-O121 81.5(2), O21-Re-N22 154.3(2), O21-Re-N52 93.8(2), O31-Re-O121 85.97(19), O31-Re-N22 88.54(19), O31-Re-N52 163.1(2), O121-Re-N22 74.02(19), O121-Re-N52 77.2(2), N22-Re-N52 88.3(2), furanose torsion angle O21-C21-C31-O31: $-28.4(8)$, peptide torsion angle C23-C13-N22-C22: $177.5(6)$, O13-C13-N22-Re: $177.8(5)$, torsion angle of the coordinated acid group Re-O121-C12-O122: $173.6(5)$, puckering parameters^[59] for O51-C21-C31-C41-C51: $Q_2 = 0.401(8)$ \AA , $\phi_2 = 285.0(11)^\circ$, conformation 3E , donor-acceptor distance of the intramolecular hydrogen bond N33 \cdots O13 2.709(9).

The hydrogen bonds in **21** are given in Table 2.41. All the bonds noted so far are illustrated in Figure 2.84. Although the hydroxy function on C11 is disordered, a strong hydrogen-bonded chain is formed along [100]. A typical feature of the imidazole ring from the histidine part is the occurrence of weak interactions of the type C-H \cdots O, in this case from C62 to O98 of methanol.

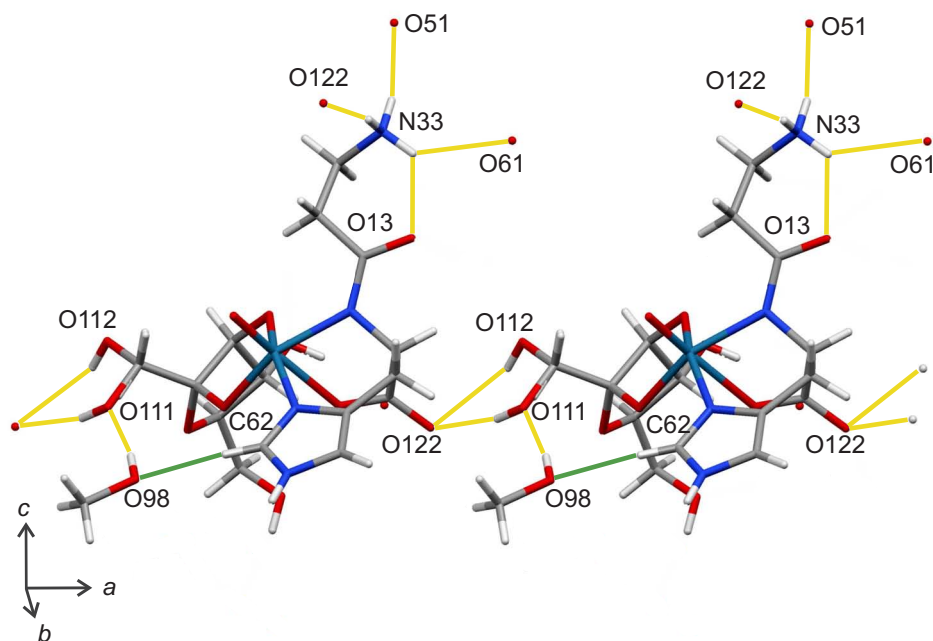


Figure 2.84 MERCURY presentation of selected hydrogen bonds (yellow lines) and C-H \cdots O contacts (green lines) in **21**.

Table 2.41 Distances [Å] and angles [°] of hydrogen bonds in **21**. Values without standard deviation are related to hydrogen atoms at calculated positions. O98/O99 is affiliated to disordered methanol. D: donor, A: acceptor, x : difference of (H \cdots A) and the sum of the van-der-Waals radii^[62].

D	H	A	D \cdots A	D-H	H \cdots A	x	D-H \cdots A
O111	H115	O122 ⁱ	2.730(12)	0.84	1.91	-0.81	166
N33	H331	O122 ⁱⁱ	2.866(9)	0.91	1.97	-0.75	167
N33	H332	O51 ⁱⁱⁱ	2.859(8)	0.91	1.98	-0.74	161
N33	H333	O13	2.709(9)	0.91	2.08	-0.64	126
N33	H333	O61 ⁱⁱ	3.112(9)	0.91	2.39	-0.33	137
N72	H772	O41 ^{iv}	2.789(7)	0.88	1.95	-0.77	159
O41	H841	O13 ^v	2.698(7)	0.84	1.89	-0.83	160
O61	H861	O122 ^{vi}	2.764(7)	0.84	1.93	-0.79	170
O98	H898	O111 ^{vii}	2.76(2)	0.84	1.92	-0.80	170
C62	H62	O98 ^{viii}	3.282(18)	0.95	2.33	-0.39	176

Symmetry codes: ⁱ $-1 + x, y, z$; ⁱⁱ $1 - x, -\frac{1}{2} + y, \frac{1}{2} - z$; ⁱⁱⁱ $\frac{1}{2} - x, 1 - y, \frac{1}{2} + z$;
^{iv} $\frac{1}{2} - x, 1 - y, -\frac{1}{2} + z$; ^v $1 - x, \frac{1}{2} + y, \frac{1}{2} - x$; ^{vi} $-\frac{1}{2} + x, \frac{3}{2} - y, -z$; ^{vii} $\frac{1}{2} + x, \frac{1}{2} - y, -x$;
^{viii} $-\frac{1}{2} + x, \frac{1}{2} - y, -z$.

As detected by NMR spectroscopy, different complex species of **21** are apparent in solution (Figure 2.85). Depending on the solvent, one or two signal sets were observed. Two signal sets due to *syn/anti* isomerism were observed in spectra of the reaction mixture (solvent: methanol) and of **21** redissolved in D₂O. ¹H NMR spectra showed a ratio of about 1:4. Contrarily in DMSO-d₆, an aprotic solvent, only one species was observed. In accordance with the structure determination, β-D-Fruf2,3H₂ can be regarded as connected in *anti* orientation to the Re=O unit. In all these solvents the signals of C2 and C3 are shifted up to 26 ppm, indicating a coordination via (O2, O3). A possible coordination via (O1, O2) or of the pyranose form was not detected.

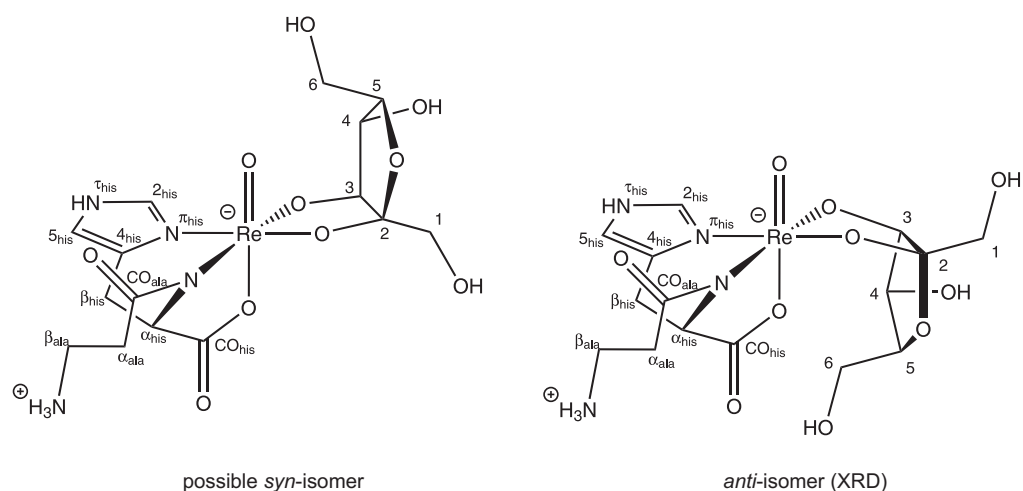


Figure 2.85 Scheme of the diastereomeric forms of **21** and atom numbering used in the ¹³C NMR study according to the recommendations of the JCBN^[79, 95]. XRD: result of the structure determination.

2 Results

Table 2.42 ^{13}C NMR chemical shifts (in ppm) of **21** in DMSO- d_6 and D_2O (each 67.9 MHz, 25 °C) and comparison with the free ligands under the same conditions. The signal of the deuterated solvent ($\delta = 39.52$ ppm for DMSO- d_6) or a drop of methanol ($\delta = 49.50$ ppm in D_2O) was used as an internal secondary reference^[65] for the chemical shift. For atom numbering see Figure 2.85. $\Delta\delta$ values indicating a diolate coordination are in boldface. Assignment according to the literature: D-fructose^[130], L-carnosine^[108].

DMSO- d_6		C_{COhis}	$\text{C}_{\alpha\text{his}}$	$\text{C}_{\beta\text{his}}$	$\text{C}_{2\text{his}}$	$\text{C}_{4\text{his}}$	$\text{C}_{5\text{his}}$	C_{COala}	$\text{C}_{\alpha\text{ala}}$	$\text{C}_{\beta\text{ala}}$
L-car	δ	172.83	52.37	28.33	134.67	132.54	116.71	169.56	32.09	35.49
21	δ	180.54	62.10	28.26	144.49	138.38	115.65	176.20	33.06	37.41
	$\Delta\delta$	7.71	9.73	-0.07	9.82	5.84	-1.06	6.64	0.97	1.92
DMSO- d_6		C1	C2	C3	C4	C5	C6			
β -Fruf	δ	64.55	102.14	75.93	75.50	82.04	63.06			
21	δ	63.20	123.65	102.21	77.41	85.45	62.96			
	$\Delta\delta$	-1.35	21.51	26.28	1.91	3.41	-0.10			
D_2O		C_{COhis}	$\text{C}_{\alpha\text{his}}$	$\text{C}_{\beta\text{his}}$	$\text{C}_{2\text{his}}$	$\text{C}_{4\text{his}}$	$\text{C}_{5\text{his}}$	C_{COala}	$\text{C}_{\alpha\text{ala}}$	$\text{C}_{\beta\text{ala}}$
L-car	δ	178.26	55.72	29.41	135.97	133.46	118.03	172.08	32.69	36.38
21	a δ	185.06	63.48	28.31	145.66	138.35	117.22	177.50	34.80	38.30
	b δ	184.73	63.25	c	145.50	138.55	117.31	177.44	35.11	c
	a $\Delta\delta$	6.80	7.76	-1.10	9.69	4.89	-0.81	5.42	2.11	1.92
	b $\Delta\delta$	6.47	7.53	c	9.53	5.09	-0.72	5.36	2.42	c
D_2O		C1	C2	C3	C4	C5	C6			
β -Fruf	δ	63.30	102.01	76.00	75.04	81.17	62.93			
21	a δ	64.22	124.01	101.99	77.48	85.50	62.58			
	b δ	64.14	123.47	99.88	76.82	84.26	c			
	a $\Delta\delta$	0.92	22.00	25.99	2.44	4.33	-0.35			
	b $\Delta\delta$	0.84	21.46	23.88	1.78	3.09	c			

a: major isomer (80 %), b: minor isomer (20 %), c: broad signal.

2.4.7 The reaction of $[\text{ReOCl}_3(\text{PPh}_3)_2]$ with L-carnosine and D-isomaltulose

The reducing disaccharide D-isomaltulose is composed of glucose (Glc) and fructose (Fru) units with an *O*-glycosidic $\alpha(1\rightarrow6)$ linkage. Its commercial name Palatinose[®] derives from *palatinum*, the Latin name of the region where it was first isolated by Weidenhagen and Lorenz^[131] in 1957. D-Isomaltulose is a natural constituent of honey and sugar cane, although commercially it is produced from sucrose^[132, 133]. By enzymatical rearrangement, the $\alpha(1\leftrightarrow2)$ linkage of sucrose changes to $\alpha(1\rightarrow6)$, which causes the reducing properties of the fructose moiety. As 6-*O*-glycosylated fructose it is restricted to adopt furanoidic forms of the fructose ring. At 20 °C in water the equilibrium composition consists of 80 % β - and 20 % α -anomer, while the open-chain form is only relevant in the solvent DMSO^[134].

Coordination compounds with D-isomaltulose are discussed with silicon^[135] and palladium^[129], but no structural information is available as yet. Crystals of the free form of this disaccharide were characterized in 1973 as 6-*O*- α -D-Glcp- β -D-Fruf^[136], which is also the main anomer in solution. It contains a β -fructofuranose motif, that was also found in **21** of the previous chapter.

The reaction of $[\text{ReOCl}_3(\text{PPh}_3)_2]$ with L-carnosine, D-isomaltulose and triethylamine in methanol was conducted at an even higher rate of yield than the reaction with D-fructose. The result of the structure determination is depicted in Figure 2.86.

$[\text{ReO}(\text{L-car})(\text{syn-6-O-}\alpha\text{-D-Glcp-}\beta\text{-D-Fruf2,3H}_{-2})] \cdot 3 \text{H}_2\text{O}$ (**22**) crystallizes in the orthorhombic space group $P2_12_12_1$ with four formula units in the unit cell. The asymmetric unit contains one molecule of the rhenium complex and three molecules of water. The free dangling, and not-metallated β -amino function (N341/N342) of the alanine part is disordered (occupancies ca. 30:70). An intramolecular hydrogen bond is established between this amino function and O21 of the glucopyranose part forming a molecule ring. As in **21**, β -D-fructofuranose is coordinated via O22 and O32 to the metal. The torsion angle of this chelating diolato group (-32.1°) is close to the angle found in **21** (-28.4°) or in the free form (-36.3°). The conformation of the furanose ring in **22** is in between 3E and 3T_2 , while it is in between 3T_2 and E_2 for the free form. The pyranose ring is in typical 4C_1 conformation, which is also to be found in the free form. L-Carnosine is connected *facial* with the donor atoms N23, N53 and O131 of the histidine part to the metal. The peptide bond is close to planarity, although its torsion angle (C24-C14-N23-C23: -176.3°) differs by 8.8° to the angle found in the free form ($+174.9^\circ$)^[107]. With a deviation of only 0.005 Å the rhenium core is in-plane with the atoms of the peptide bond.

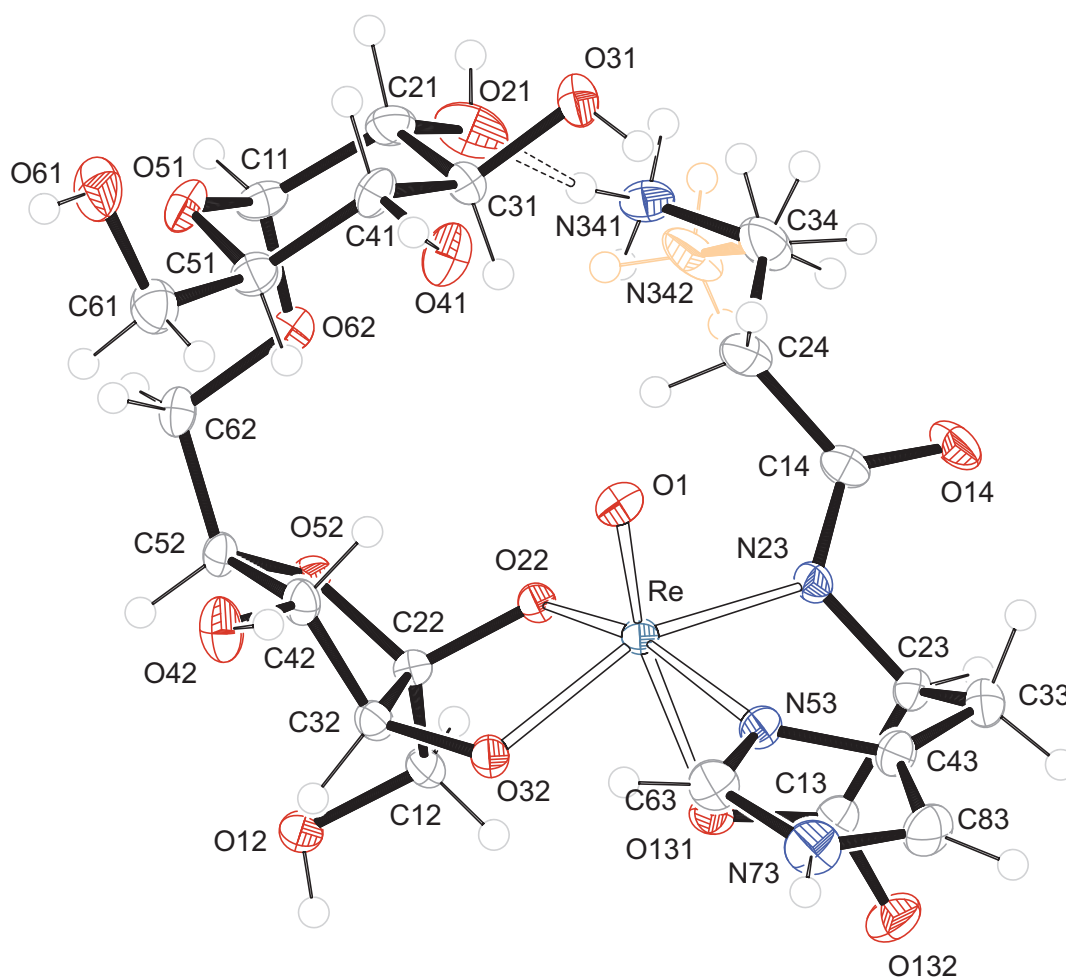


Figure 2.86 ORTEP presentation of **22** in crystals of $[\text{ReO}(\text{L-car})(\text{syn-6-O-}\alpha\text{-D-Glup-}\beta\text{-D-Fruf2,3H}_2)] \cdot 3 \text{H}_2\text{O}$. The atom pair N341/N342 is disordered (occupancies ca. 30:70). Ellipsoids are drawn at 50 % probability level. Distances [Å] and angles [°]: Re-O1 1.678(2), Re-O22 1.984(2), Re-O32 1.968(2), Re-O131 2.198(2), Re-N23 2.073(3), Re-N53 2.120(3); O1-Re-O22 107.41(11), O1-Re-O32 106.32(11), O1-Re-O131 166.16(11), O1-Re-N23 100.44(12), O1-Re-N53 89.78(12), O22-Re-O32 81.73(9), O22-Re-O131 85.24(8), O22-Re-N23 89.86(10), O22-Re-N53 162.78(10), O32-Re-O131 80.57(9), O32-Re-N23 153.24(10), O32-Re-N53 92.58(10), O131-Re-N23 73.42(10), O131-Re-N53 77.77(10), N23-Re-N53 88.03(11), chelating fructofuranose's torsion angle O22-C22-C32-O32: $-32.1(3)$, peptide torsion angle C24-C14-N23-C23: $-176.3(3)$, O14-C14-N23-Re: $178.7(2)$, torsion angle of the coordinated acid group Re-O131-C13-O132: $171.2(3)$, puckering parameters^[59] for O52-C22-C32-C42-C52: $Q_2 = 0.414(4)$ Å, $\phi_2 = 278.7(4)^\circ$, conformation in between 3E and 3T_2 , for O51-C11-C21-C31-C41-C51: $Q = 0.587(4)$ Å, $\theta = 6.8(4)^\circ$, $\phi = 298(3)^\circ$, conformation 4C_1 , donor-acceptor distance of the intramolecular hydrogen bond N341...O21 2.664(18).

The hydrogen bonds of **22** are listed in Table 2.43. The molecules are connected by a complex system of hydrogen bonds, as illustrated in the SCHAKAL packing diagram (Figure 6.22 on page 207). They form sheets parallel to the *ab* plane. All of the remaining hydroxy groups take part in hydrogen bonding, even all metallated and ether-type oxygen atoms (as acceptors). Exceptions are O62 of the glycosidic bond

and O1, the oxido ligand of rhenium. No hydrogen bonds were to be found here. Among the nitrogen atoms, only the protonated atoms N73 and N341/N342 take part as donors in hydrogen bonding.

Table 2.43 Distances [Å] and angles [°] of hydrogen bonds in **22**. Values without standard deviation are related to hydrogen atoms at calculated positions. O97, O98, O99 are affiliated to water. D: donor, A: acceptor, x : difference of (H···A) and the sum of the van-der-Waals radii^[62].

D	H	A	D···A	D-H	H···A	x	D-H···A
N73	H73	O97 ⁱ	2.906(4)	0.88	2.05	-0.67	164
N341	H345	O131 ⁱⁱ	2.764(12)	0.91	1.90	-0.82	159
N341	H347	O12 ⁱⁱⁱ	2.745(13)	0.91	2.13	-0.59	124
N341	H346	O21	2.664(18)	0.91	1.77	-0.95	168
N342	H340	O131 ⁱⁱ	2.903(6)	0.91	2.07	-0.65	152
N342	H348	O12 ⁱⁱⁱ	2.806(7)	0.91	1.97	-0.75	151
N342	H349	O61 ^{iv}	2.735(7)	0.91	2.01	-0.71	136
O12	H812	O52 ^v	2.792(3)	0.84	2.05	-0.67	147
O21	H821	O32 ⁱⁱ	2.759(4)	0.84	1.99	-0.73	153
O31	H831	O97 ^{vi}	2.768(4)	0.84	1.98	-0.74	155
O41	H841	O14 ^{vii}	2.737(4)	0.84	1.95	-0.77	157
O42	H842	O98	2.828(5)	0.84	2.01	-0.71	163
O61	H861	O22 ^{vii}	3.014(4)	0.84	2.18	-0.54	170
O97	H971	O99 ^{iv}	2.744(4)	0.91(3)	1.85(3)	-0.87	168(3)
O97	H972	O14 ^{viii}	2.673(4)	0.89(3)	1.83(3)	-0.89	158(4)
O98	H981	O41	3.320(5)	0.89(3)	2.58(3)	-0.14	141(3)
O98	H982	O132 ^{vii}	2.834(4)	0.89(2)	1.96(2)	-0.76	166(4)
O99	H991	O31 ^{viii}	2.880(4)	0.91(3)	1.97(3)	-0.74	174(3)
O99	H992	O132 ^{vii}	2.867(4)	0.90(3)	1.98(3)	-0.74	166(3)

Symmetry codes: ⁱ $-x, 1/2 + y, 1/2 - z$; ⁱⁱ $1 + x, y, z$; ⁱⁱⁱ $1/2 + x, 1/2 - y, -z$; ^{iv} $x, -1 + y, z$; ^v $-1/2 + x, 1/2 - y, -z$; ^{vi} $1 - x, 1/2 + y, 1/2 - z$; ^{vii} $x, 1 + y, z$; ^{viii} $-1 + x, y, z$.

The ¹³C NMR spectrum of crystals of **22** redissolved in water showed only one signal set, as given in Table 2.44. In accordance to the spectra of the previous chapters, the signals of L-carnosine are shifted up to 8 ppm. The large CIS values for C2 and C3 prove a coordination of the fructofuranose moiety to the rhenium core, while the signals of the glycopyranosyl moiety are shifted only marginally. After one week, a second signal set appeared at small intensities, consistent with spectra of the crude reaction mixture. These two signal sets reflect the different populations of the two possible isomeric forms (see Figure 2.87) in solution at a ratio of about 5:1 according to ¹H NMR.

2 Results

Table 2.44 ^{13}C NMR chemical shifts (in ppm) of **22** in D_2O (67.9 MHz, 25 °C) and comparison with the free ligands under the same conditions (pH 5.8). The signal of a drop of methanol ($\delta = 49.50$ ppm in D_2O) was used as an internal secondary reference^[65] for the chemical shift. For atom numbering see Figure 2.87. $\Delta\delta$ values indicating a diolate coordination are in boldface. Assignment according to the literature: D-isomaltulose^[137], L-carnosine^[108].

		C_{COhis}	$\text{C}_{\alpha\text{his}}$	$\text{C}_{\beta\text{his}}$	$\text{C}_{2\text{his}}$	$\text{C}_{4\text{his}}$	$\text{C}_{5\text{his}}$	C_{COala}	$\text{C}_{\alpha\text{ala}}$	$\text{C}_{\beta\text{ala}}$	
L-car	δ	178.26	55.72	29.41	135.97	133.46	118.03	172.08	32.69	36.38	
22	a	δ	184.59	63.56	28.35	145.41	138.59	117.28	177.48	35.24	38.48
	b	δ	184.93	63.76	27.86	145.64	138.43	117.11	177.36	34.82	38.48
	a	$\Delta\delta$	6.33	7.84	-0.43	9.44	5.13	-0.75	5.40	2.55	1.95
	b	$\Delta\delta$	6.67	8.04	-0.49	9.67	4.97	-0.92	5.28	2.13	2.10
		$\text{C}1'$	$\text{C}2'$	$\text{C}3'$	$\text{C}4'$	$\text{C}5'$	$\text{C}6'$				
$\alpha\text{-D-Glcp}$	δ	98.92	72.07	72.53	70.24	73.72	61.27				
22	a	δ	98.70	72.11	72.71	70.30	73.72	61.11			
	b	δ	99.11	72.34	72.57	70.17	73.29	61.16			
	a	$\Delta\delta$	-0.22	0.04	0.18	0.06	0.00	-0.16			
	b	$\Delta\delta$	-0.19	0.27	0.04	-0.07	-0.43	-0.11			
		$\text{C}1$	$\text{C}2$	$\text{C}3$	$\text{C}4$	$\text{C}5$	$\text{C}6$				
$\beta\text{-D-Fruf}$	δ	63.31	102.35	75.97	75.20	79.60	68.43				
22	a	δ	64.38	123.07	99.54	75.54	81.88	66.52			
	b	δ	64.21	124.11	101.36	75.26	83.33	67.73			
	a	$\Delta\delta$	1.07	20.72	23.57	0.34	2.28	-1.91			
	b	$\Delta\delta$	0.90	21.76	25.39	0.06	3.73	-0.70			

a: major isomer, b: minor isomer appears after one week at a ratio of 1:5.

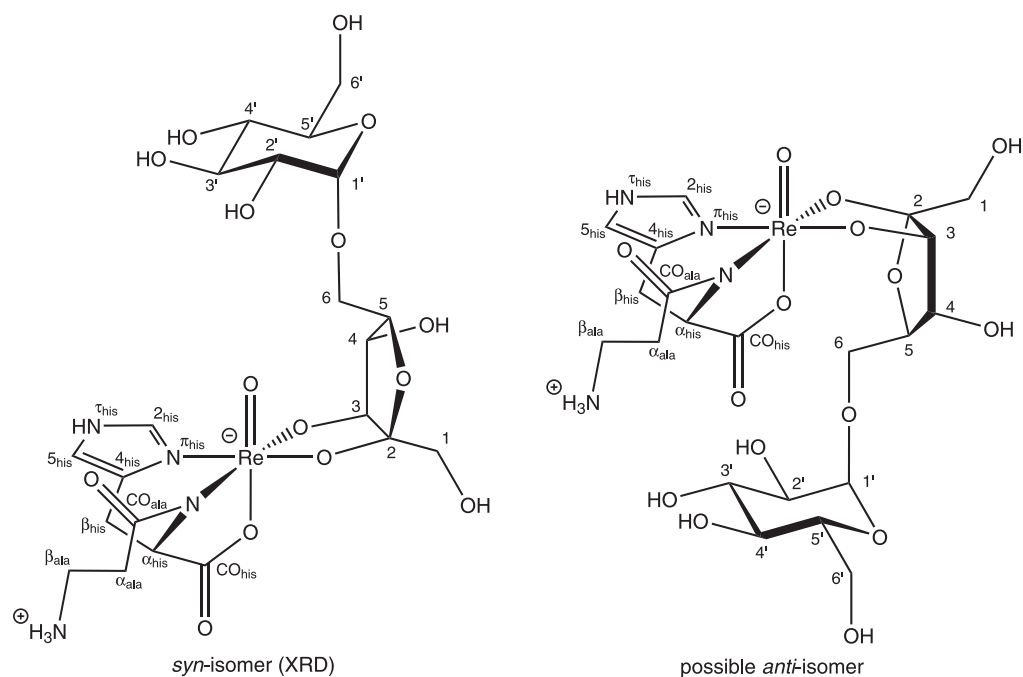


Figure 2.87 Scheme of the diastereomeric forms of **22** and atom numbering used in the ^{13}C NMR study according to the recommendations of the JCBN^[79, 95]. XRD: result of the structure determination.

2.4.7.1 Application to aqueous chemistry

All the syntheses in this section, so far, were carried out in methanol due to the insolubility of the rhenium(V) precursor $[\text{ReOCl}_3(\text{PPh}_3)_2]$. But in analogy to the preparation of **13** from $[\text{ReO}(\text{L-his})(\text{ox})]$ and cytidine in water (see chapter 2.3.5 on page 71), it should be possible to start the reactions from $[\text{ReO}(\text{L-car})(\text{ox})]$ (see **16** in chapter 2.4.1 on page 88). One handicap may be the different binding modes of oxalate and L-carnosine found in the structure determination of **16**. But at least a complex species with a similar binding mode to L-histidine was detected in aqueous solution (see Table 2.32 on page 91).

The crystalline complex **16** was stirred in water with a twofold excess of D-isomaltulose (see Route 2 on page 180 of the experimental part). The ^{13}C NMR spectrum of this mixture showed many species. But on closer inspection, the signals of free and metallated D-isomaltulose (Table 2.44) and of the minor species of **16** (Table 2.32) were present. It was possible to grow crystals from this mixture, their cell parameters (orthorhombic, length / Å: $a = 9.024$, $b = 10.806$, $c = 30.378$) were close to the data of the already presented structure in this chapter (see **22** in Table 6.9 on page 222).

2.4.7.2 Application to radiolabeling with ^{188}Re

All the compounds presented so far in this work were prepared from precursor compounds derived from commercially available ammonium perrhenate, which consists of the naturally occurring isotopes ^{185}Re and ^{187}Re . The perrhenate of the radioactive isotope ^{188}Re is available as elution from a $^{188}\text{W}/^{188}\text{Re}$ generator with saline solution. To adopt the reactions so far presented in this work, first, a one-pot-synthesis must be found starting from an aqueous perrhenate solution. Second, the volume of the reaction medium must be downscaled drastically, as the amounts of the radioactive isotope are in nanomolar range. To meet the first requirement, a reducing agent for a one-pot-synthesis has to be found. According to the literature, tin(II) is capable of reducing rhenium(VII) to rhenium(IV) if used in 100fold excess at pH 2 for a 0.5 mM perrhenate solution^[138]. But it is also used to generate radiopharmaceutical compounds with rhenium in the oxidation state V^[48].

In a first step, non-radioactive ammonium perrhenate was stirred in water with L-carnosine, D-isomaltulose and tin(II) oxalate (see Route 3 on page 181 of the experimental part). Surprisingly the ^{13}C NMR spectrum of this mixture did not show a complex mixture as reported in the paragraph before. The signals were consistent to the data in Table 2.44, *syn/anti* isomerism was observed. A convenient one-pot synthesis for aqueous media was found.

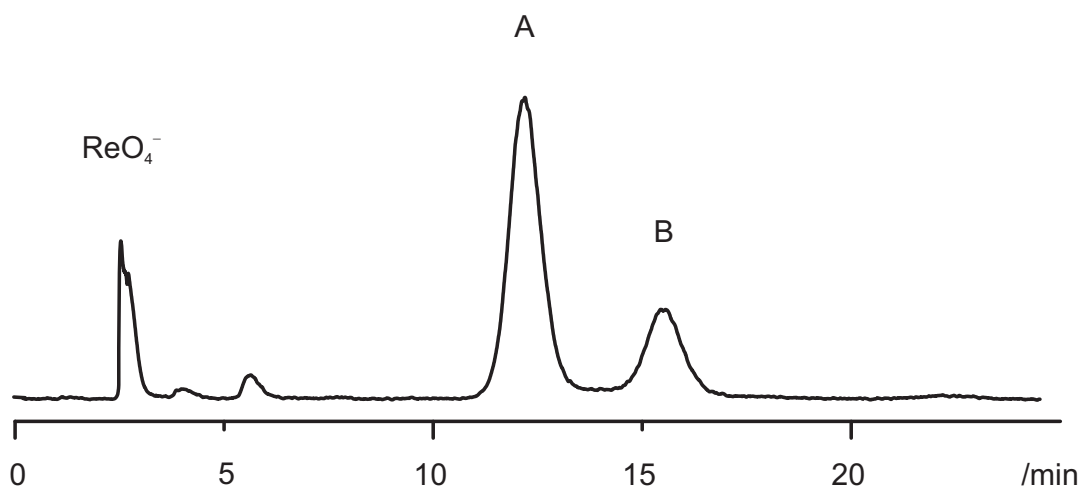


Figure 2.88 HPLC radiochromatogram of **22** with the isotope ^{188}Re . The products are marked with A (12.1 min, 63 %) and B (15.5 min, 23 %), free perrhenate with ReO_4^- (2.4 min, 11 %).

In the second step, the reaction volume was downscaled and the amounts of the reactants were adopted to a range typically found for radiopharmaceutical preparations with ^{188}Re (see Route 4 on page 181 of the experimental section). A possible problem was the limited solubility of the reactants, but the best results were obtained

from a reaction of L-carnosine, D-isomaltulose and tin(II) oxalate with a stoichiometry of 1:15:20 in a range of 10–200 μmol and only 0.5 mL solvent, giving a white suspension. After filtration, up to 97 % of the total activity was recovered in solution and further purification was done by HPLC. The radiochromatogram (Figure 2.88) shows free $^{188}\text{ReO}_4^-$ (11 %), but also two radiometallated species (63 %, 23 %). All in all, the radiochemical purity of this labelling experiment was 86 %.

A control HPLC experiment with redissolved crystals of the already presented (non-radioactive) compound **22** was done with an UV/VIS detector at 220 nm. First, a freshly prepared solution showed only peak A, but after one week both peaks were detected. As already observed for NMR spectroscopy of aqueous solutions of **22**, these two complex species can be regarded as the two diastereomers of **22** due to *syn/anti* isomerism.

2.4.8 The reaction of $[\text{ReOCl}_3(\text{PPh}_3)_2]$ with L-carnosine and other carbohydrates

Apart from the carbohydrates that were presented as ligands in this section, there were hints of a successful coordination to the rhenium core with further carbohydrates. According to NMR spectroscopy, the reaction mixtures of the following carbohydrates with rhenium(V) and L-carnosine showed the presence of complex species:

Among the glycosides, methyl α -D-galactopyranoside, methyl β -D-galactopyranoside, methyl α -D-glucopyranoside, methyl β -D-xylopyranoside, methyl α -D-mannopyranoside and D-salicin were tested positive.

Among the nucleosides and their derivatives, cytidine, uridine, guanosine, inosine, 5-methyl-uridine, AMP and NADH showed a coordination.

Among the monosaccharides, reactions with D-erythrose, D-threose, D- and L-arabinose, D- and L-xylose, D- and L-lyxose, D-allose, D-glucose, D-fucose showed decomposition, but small signals of complex species were detectable for several hours with D-arabinose, D-xylose, D-lyxose and D-galactose.

Spectra of the reaction mixtures with the disaccharides D-turanose, D-melibiose, D-trehalose, D-lactose, D-lactulose and D-maltose showed signals of coordinated species at small intensities, but not D-leucrose, D-saccharose or D-lactobionic acid. Even spectra of reactions with the trisaccharides D-maltotriose, D-melezitose and D-raffinose and the tetrasaccharide D-stachyose were promising, but complex.

Finally, the following antibiotics with amino sugar moieties showed a reaction: lincomycin, clindamycin and erythromycin.

2.5 Other compounds with rhenium

The first three paragraphs in this chapter deal with compounds that were obtained without any further addition of a co-ligand. They were prepared from various rhenium(V) precursors and carbohydrates such as oxalate and anhydroerythritol. These preparations are, however, limited to simple diols and acids. The remaining paragraphs deal with complexes that were prepared with various co-ligands in accordance to the “3 + 2” approach^[19].

2.5.1 The reaction of $[\text{ReOCl}_3(\text{PPh}_3)_2]$ with oxalic acid

Apart from the oxalato complexes so far presented in this work (**9** and **16** with the co-ligands L-histidine and L-carnosine), there have been other mononuclear complexes reported in the recent years with rhenium(V) and the co-ligands ami^[36], tpb^[30], phen and dppe^[37] (see Figure 1.1 on page 4). They are all built with one oxalato ligand and a nitrogen-containing co-ligand. Complexes with two oxalate ligands are only known for rhenium(IV). Generally, rhenium complexes with two (*O,O*)-donor chelate ligands are rare. Figure 2.89 shows two complexes with catecholates, a similar (*O,O*)-donor chelate ligand. Even though these complexes are in dissimilar oxidation states, their geometry resembles a new compound that is to be presented in this chapter^[139].

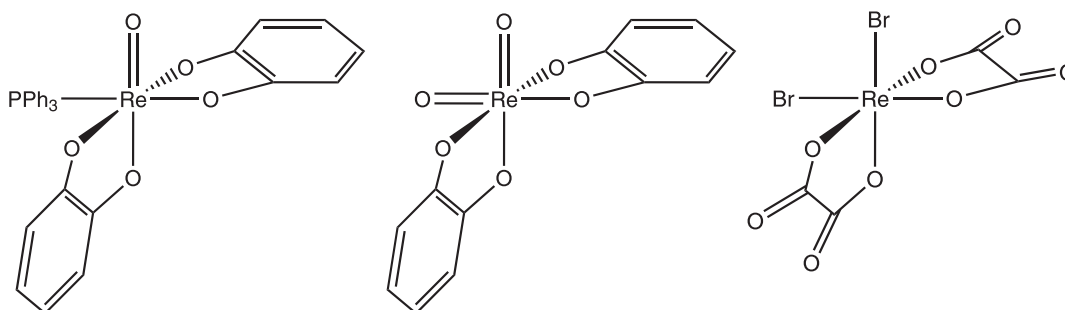


Figure 2.89 Scheme of compounds related to **23** with catecholates and oxalate. From left to right: $[\text{ReO}(\text{cat})_2(\text{PPh}_3)]^-$ with rhenium(V)^[140], $[\text{ReO}_2(\text{cat})_2(\text{PPh}_3)]^-$ with rhenium(VII)^[141] and $[\text{Re}(\text{ox})_2\text{Br}_2]^{2-}$ with rhenium(IV)^[142].

$(\text{HNEt}_3)[\text{ReO}(\text{ox})_2(\text{PPh}_3)]$ (**23**) was obtained from the reaction of $[\text{ReOCl}_3(\text{PPh}_3)_2]$ with a fourfold excess of oxalic acid and triethylamine in methanol. The crystals in the orthorhombic space group *Pbca* contain eight formula units in the cell. The asymmetric unit is separated in two charged parts: the anionic rhenium complex (Figure 2.90) and one molecule of protonated triethylamine as counterion. One triphenylphosphane and two oxalate ligands are connected to a $\{\text{ReO}\}^{3+}$ core. The distances of the oxygen donor atoms to the metal vary from 2.00 to 2.09 Å, but they do

not deviate much from the values observed for the previously mentioned compound $[\text{Re}(\text{ox})_2\text{Br}_2]^{2-}$ with rhenium(IV) (2.02 to 2.05 Å)^[142]. The longest bond is *trans* to the oxido ligand. With small deviations, the chelating oxalate ligands are planar: the torsion angle of the oxalate ligand with the shorter distances to the metal is 1.4°, and the torsion angle of the oxalate ligand with the longer distances to the metal is 4.4°.

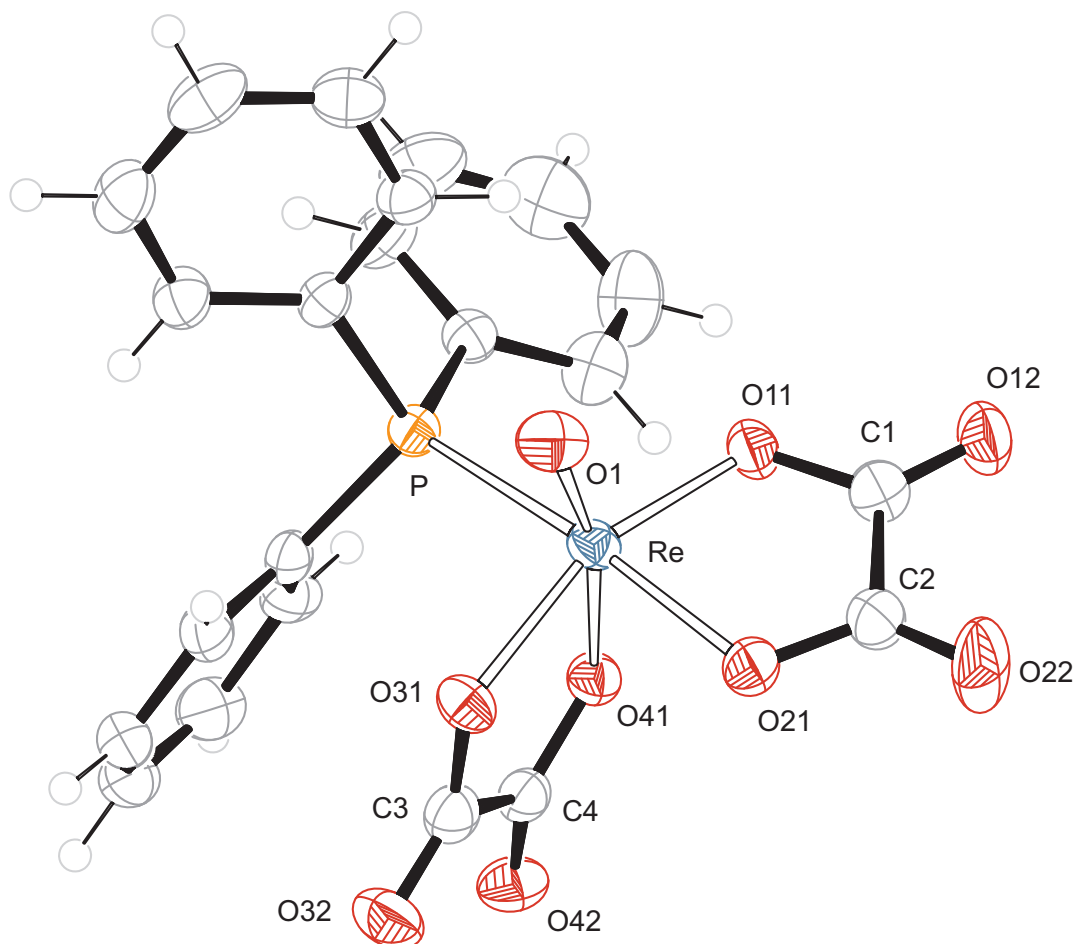


Figure 2.90 ORTEP presentation of **23** in crystals of $(\text{HNEt}_3)[\text{ReO}(\text{ox})_2(\text{PPh}_3)]$. Ellipsoids are drawn at 50 % probability level. Distances [Å] and angles [°]: Re-P 2.4626(11), Re-O1 1.685(3), Re-O11 2.003(3), Re-O21 2.031(3), Re-O31 2.046(3), Re-O41 2.092(3); P-Re-O1 89.94(10), P-Re-O11 94.51(9), P-Re-O21 165.22(9), P-Re-O31 94.11(8), P-Re-O41 80.59(8), O1-Re-O11 105.32(12), O1-Re-O21 104.84(13), O1-Re-O31 94.51(12), O1-Re-O41 166.23(12), O11-Re-O21 81.40(11), O11-Re-O31 158.35(12), O11-Re-O41 85.50(11), O21-Re-O31 85.24(11), O21-Re-O41 84.92(11), O31-Re-O41 76.38(11), oxalate torsion angle O11-C1-C2-O21: 1.4(6), O31-C3-C4-O41: 4.4(5).

Due to a lack of hydrogen donors, there is only one classical hydrogen bond in **23** (Table 2.45). This bifurcated bond is established between the NH donor of triethylammonium and the oxygen acceptors of the oxalato ligand with the longer distances to the metal. A weak interaction of the type C-H \cdots O,O between C25-H251 of the triethylammonium molecule and the other oxalate ligand is established with similar geometry. As shown in Figure 2.90, these bonds connect the anions and cations in the crystal packing of **23**.

Table 2.45 Distances [Å] and angles [°] of hydrogen bonds in **23**. Values without standard deviation are related to hydrogen atoms at calculated positions. N is affiliated to triethylammonium. D: donor, A: acceptor, x : difference of (H \cdots A) and the sum of the van-der-Waals radii^[62].

D	H	A	D \cdots A	D-H	H \cdots A	x	D-H \cdots A
N	H71	O32	3.030(5)	0.93	2.29	-0.43	136
N	H71	O42	3.022(5)	0.93	2.25	-0.47	140
C25	H251	O12 ⁱ	3.268(6)	0.99	2.53	-0.19	131
C25	H251	O22 ⁱ	3.376(6)	0.99	2.43	-0.29	160

Symmetry codes: ⁱ 1 - x , 1 - y , 1 - z .

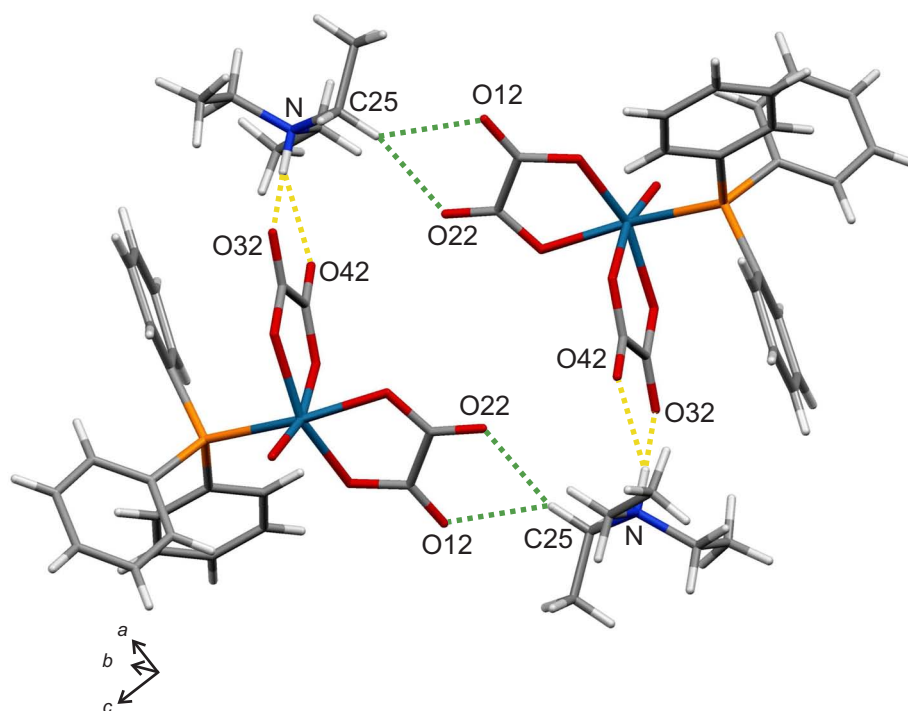


Figure 2.91 MERCURY presentation of hydrogen bonds (yellow dashed lines) and C-H \cdots O contacts (green dashed lines) in **23**.

2.5.2 The reaction of $[\text{Re}(\text{NPh})\text{Cl}_3(\text{PPh}_3)_2]$ with oxalic acid

As shown in chapter 2.1.4, it is possible to build rhenium-diolato complexes with the phenylimido-rhenium(V) precursor $[\text{Re}(\text{NPh})\text{Cl}_3(\text{PPh}_3)_2]$. The nitrogen atom of the phenylimido unit is formally isoelectronic with the oxido ligand of $[\text{ReOCl}_3(\text{PPh}_3)_2]$, and a similar complex to **23** of the previous chapter was expected for the reaction with oxalate. According to the literature, there were, so far, only some imido-rhenium(V) complexes reported with oxalate or catechol and the co-ligands tacn and PNP (Figure 2.92).

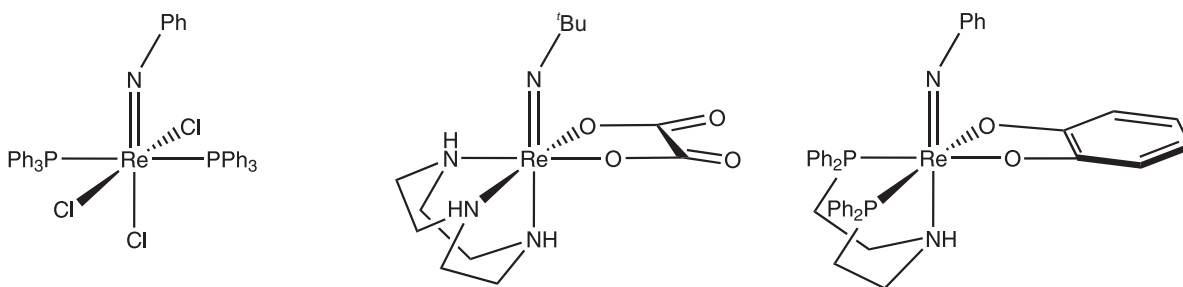


Figure 2.92 Scheme of compounds with an imido-rhenium(V) core. From left to right: $[\text{Re}(\text{NPh})\text{Cl}_3(\text{PPh}_3)_2]$ ^[70], $[\text{Re}(\text{N}^t\text{Bu})(\text{tacn})(\text{ox})]$ ^[143], $[\text{Re}(\text{NPh})(\text{PNP})(\text{cat})]\text{Cl}$ ^[144],

But first, a modification of the preparation in analogy to **23** was necessary, as the phenylimido-rhenium precursor decomposed in the presence of base. For this reason, the disodium salt of oxalic acid was used. $[\text{Re}(\text{NPh})\text{Cl}_3(\text{PPh}_3)_2]$ was refluxed in methanol with a twofold excess of oxalic acid disodium salt. Green crystals were formed over night.

Figure 2.93 shows the result of the structure determination, the electroneutral complex $[\text{Re}(\text{NPh})(\text{ox})(\text{PPh}_3)_2\text{Cl}] \cdot \text{MeOH}$ (**24**). It crystallizes in the monoclinic space group $P2_1/n$ with four formula units in the unit cell. The asymmetric unit contains the rhenium complex and one disordered molecule of methanol. Compared to the precursor (see left in Figure 2.92), only two chlorido ligands are replaced by oxalate and all other ligands are still present. The phenylimido-rhenium unit is almost linear (angle Re-N-C3: 171.5°) as in the precursor compound (172.6°)^[70] or the compounds of chapter 2.1: **3** (170.6°), **4** (165.9°) and **5** (173.7°). But among all these compounds, the shortest Re-N bond length is found for **24**: 1.709 Å (precursor: 1.726 Å, **3**: 1.720 Å, **4**: 1.723 Å, **5**: 1.733 Å). The oxalate ligand is almost planar, its chelating unit adopts a torsion angle of 2.6° . This angle and the bond lengths to the metal are close to the values for the oxido-rhenium(V) complex of the previous chapter. Strictly speaking, they are close to the values of the oxalate ligand with O41 in *trans* orientation to the Re=O unit (see Figure 2.90 on page 122).

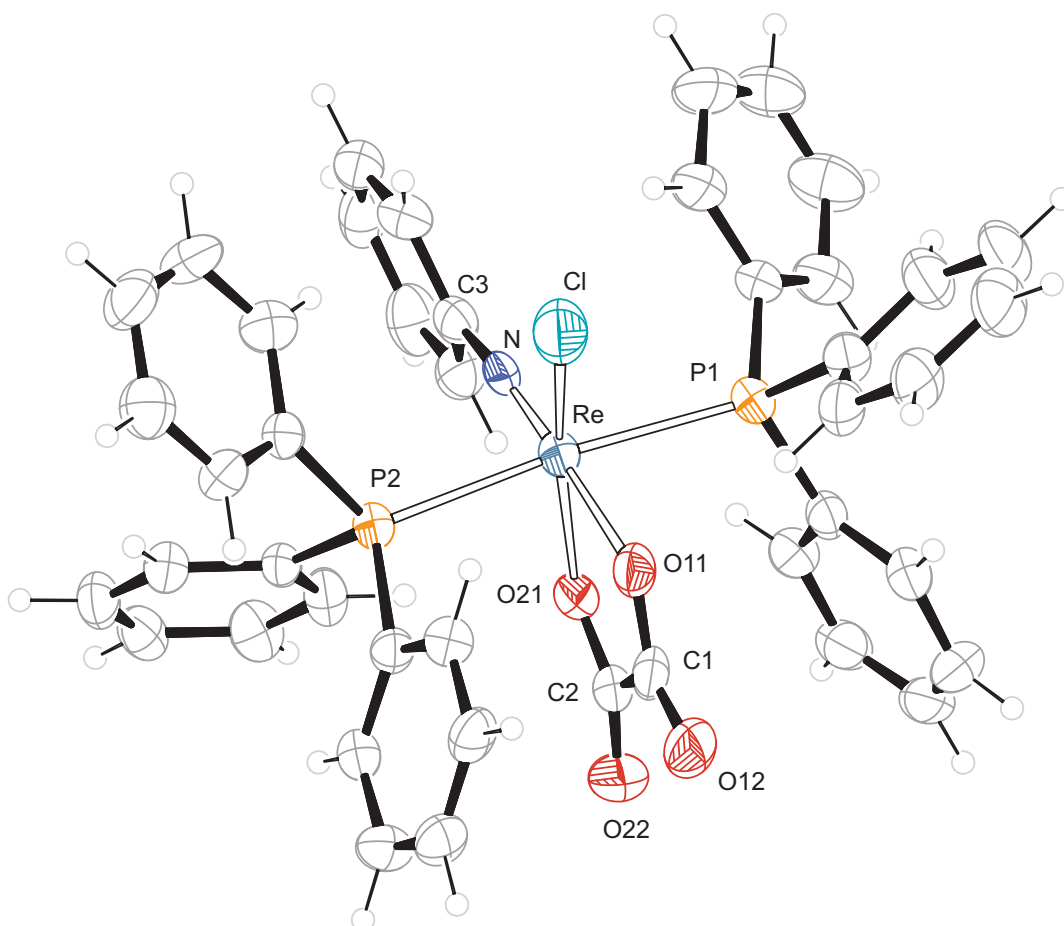


Figure 2.93 ORTEP presentation of **24** in crystals of $[\text{Re}(\text{NPh})(\text{ox})(\text{PPh}_3)_2\text{Cl}] \cdot \text{MeOH}$. Ellipsoids are drawn at 50 % probability level. Distances [\AA] and angles [$^\circ$]: Re-Cl 2.360(3), Re-P1 2.466(2), Re-P2 2.479(2), Re-O11 2.059(5), Re-O21 2.090(5), Re-N 1.709(7); Cl-Re-P1 89.82(8), Cl-Re-P2 90.35(8), Cl-Re-O11 87.25(17), Cl-Re-O21 162.24(19), Cl-Re-N 102.5(2), P1-Re-P2 173.25(7), P1-Re-O11 83.54(17), P1-Re-O21 90.09(13), P1-Re-N 94.8(2), P2-Re-O11 89.72(17), P2-Re-O21 87.71(13), P2-Re-N 91.7(2), O11-Re-O21 75.1(2), O11-Re-N 170.2(3), O21-Re-N 95.2(3), Re-N-C3 171.5(6), oxalic acid torsion angle O11-C1-C2-O21: 2.6(10).

Similar to the previous compound **23**, there is a lack of classical hydrogen donors in **24**. Only two classical hydrogen bonds are to be found in **24**. Donors for both bonds are O98/O99 of the disordered molecule of methanol (Table 2.46). But in view of intermolecular bonding, weak interactions of the type C-H \cdots O and C-H \cdots Cl should be accounted for, too. The donor-acceptor distances of these contacts (and the comparison with the van-der-Waals radii^[62]) deviate not much from classical hydrogen bonds. All these bonds build a two-dimensional network parallel to the *ac* plane (Figure 2.94).

Table 2.46 Distances [Å] and angles [°] of hydrogen bonds and contacts in **24**. Values without standard deviation are related to hydrogen atoms at calculated positions. O98/O99 is affiliated to disordered methanol. D: donor, A: acceptor, x : difference of $(H \cdots A)$ and the sum of the van-der-Waals radii^[62].

D	H	A	D \cdots A	D-H	H \cdots A	x	D-H \cdots A
O98	H898	O21	2.91(2)	0.84	2.22	-0.50	139
O99	H899	O12 ⁱ	3.08(3)	0.84	2.52	-0.20	125
C37	H37	O12 ⁱⁱ	3.196(14)	0.95	2.25	-0.47	172
C44	H44	O21	3.090(10)	0.95	2.23	-0.49	149
C98		Cl ⁱⁱⁱ	3.06(2)			-0.39	

Symmetry codes: ⁱ $x - 1, y, z$; ⁱⁱ $-\frac{1}{2} + x, \frac{1}{2} - y, -\frac{1}{2} + z$; ⁱⁱⁱ $-\frac{1}{2} + x, \frac{1}{2} - y, \frac{1}{2} + z$.

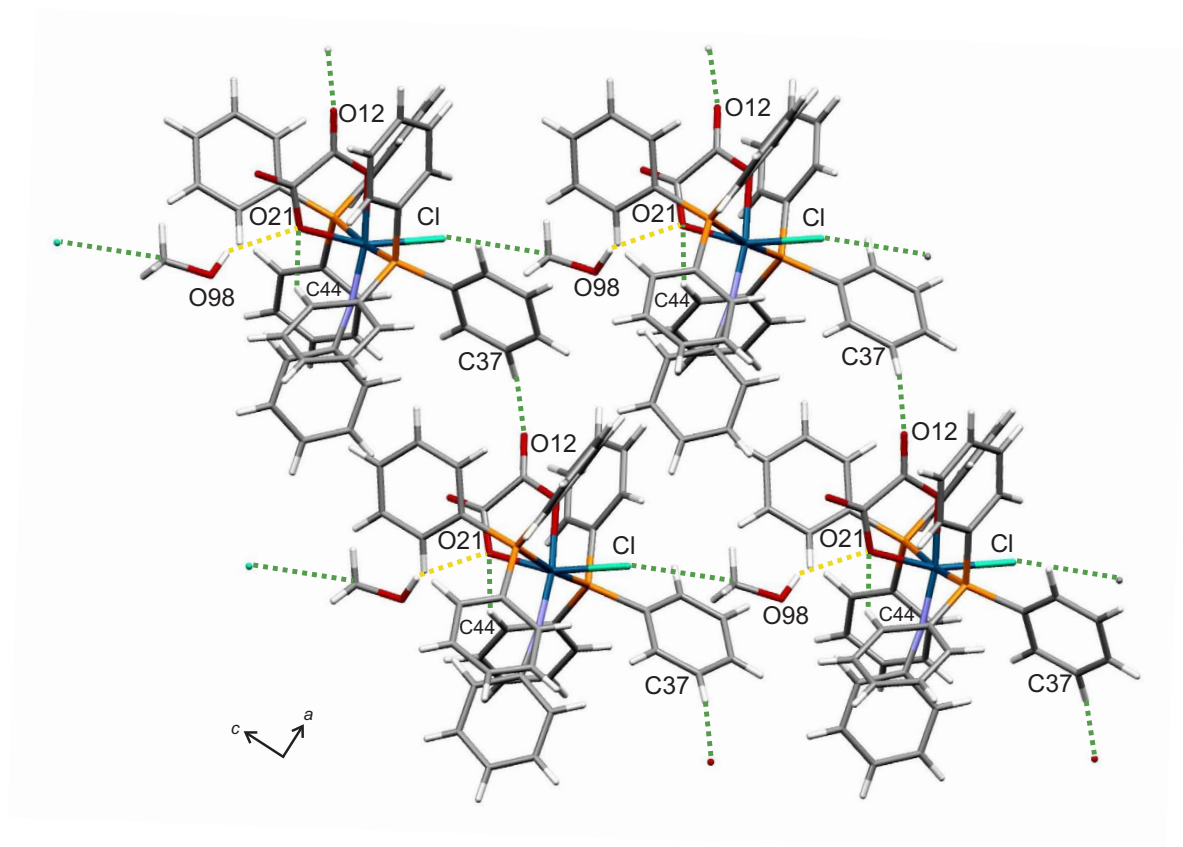


Figure 2.94 MERCURY presentation of hydrogen bonds (yellow dashed lines) and weak interactions (green dashed lines) in **24**.

2.5.3 The reaction of $[\text{ReOCl}_3(\text{PPh}_3)_2]$ with anhydroerythritol

Most of the reported diolato complexes with rhenium(V) contain nitrogen donor ligands (see Figure 1.1 on page 4). Rare exceptions are $[\text{ReO}(\text{Cp}^*)(\text{EthdH}_{-2})]$, $[\text{ReO}(\text{dppe})(\text{ox})]$ or $[\text{ReO}(\text{cat})_2(\text{PPh}_3)]^-$ derived from ethanediol^[21], oxalic acid^[37] or catechol^[140].

The following compound, $[\text{ReO}(\text{syn-AnErytH}_{-2})(\text{MeOH})(\text{PPh}_3)\text{Cl}]$ (**25**), is another example of these rare species. **25** was prepared by heating $[\text{ReOCl}_3(\text{PPh}_3)_2]$ with anhydroerythritol and methanol. It crystallizes in the triclinic space group $P\bar{1}$ with one molecule in the asymmetric unit. The molecular structure of **25** is shown in Figure 2.95.

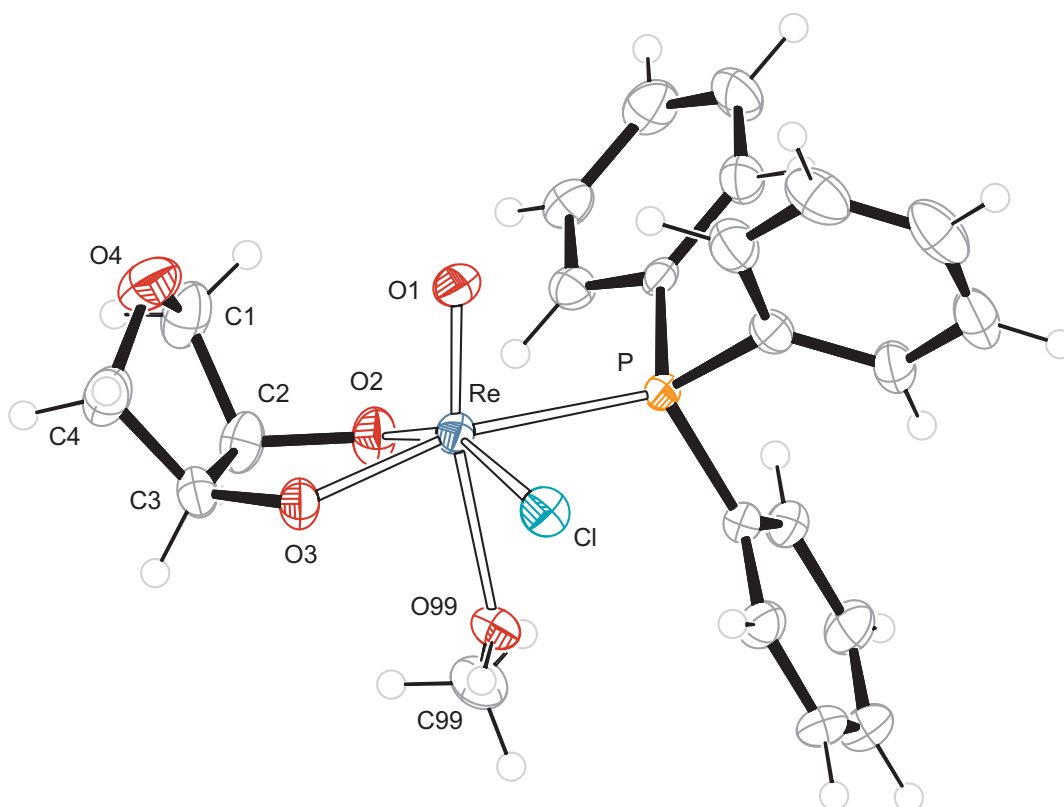


Figure 2.95 ORTEP presentation of **25** in crystals of $[\text{ReO}(\text{syn-AnErytH}_{-2})(\text{MeOH})(\text{PPh}_3)\text{Cl}]$. Ellipsoids are drawn at 50 % probability level. Distances [Å] and angles [°]: Re-Cl 2.3833(10), Re-P 2.4850(9), Re-O1 1.670(3), Re-O2 1.928(3), Re-O3 1.955(3), Re-O99 2.255(3); Cl-Re-P 90.49(3), Cl-Re-O1 97.07(10), Cl-Re-O2 157.89(9), Cl-Re-O3 87.96(9), Cl-Re-O99 79.01(8), P-Re-O1 85.07(9), P-Re-O2 94.93(8), P-Re-O3 166.83(8), P-Re-O99 83.74(7), O1-Re-O2 104.73(13), O1-Re-O3 108.10(12), O1-Re-O99 168.10(11), O2-Re-O3 81.90(11), O2-Re-O99 80.30(11), O3-Re-O99 83.13(11), Re-O99-C99 127.5(2), diol torsion angle O2-C2-C3-O3: 7.3(5), puckering parameters^[59] for O4-C1-C2-C3-C4: $Q_2 = 0.364(5)$ Å, $\phi_2 = 348.0(8)^\circ$, conformation ${}^{\circ}T_4$.

One molecule of methanol is coordinated to the metal in *trans* position to the oxido ligand O1. With rhenium(V), complexes of protonated^[145] and deprotonated^[37, 146] methanol ligands are known, their Re-O distances vary from 1.859–2.289 Å. The value found in this structure (2.255 Å) is typical for the protonated form, it is 21 % longer than the bond length for a methoxido ligand to the rhenium core. The remaining hydrogen atom takes part in hydrogen bonding (Table 2.47). The dianionic chelating ligand AnErytH₂ is coordinated via O2 and O3 to the metal in *syn* orientation to the oxido ligand O1. The diol torsion angle and the conformation of the oxolane ring (^oT₄) are similar to other rhenium(V) complexes with anhydroerythritol^[31].

In the crystal packing of **25**, only one classical hydrogen bond is established from H899 of the protonated methanol ligand to O3 of AnErytH₂. This hydrogen bond and its centrosymmetric counterpart form dimers of **25**. As illustrated in the SCHAKAL packing diagram (Figure 6.25 on page 210), these polar molecule parts seem to be isolated between bulky triphenylphosphane ligands. But a closer inspection of weak C-H...Cl and C-H...O interactions shows a formation of chains of dimers along [100] (Figure 2.96).

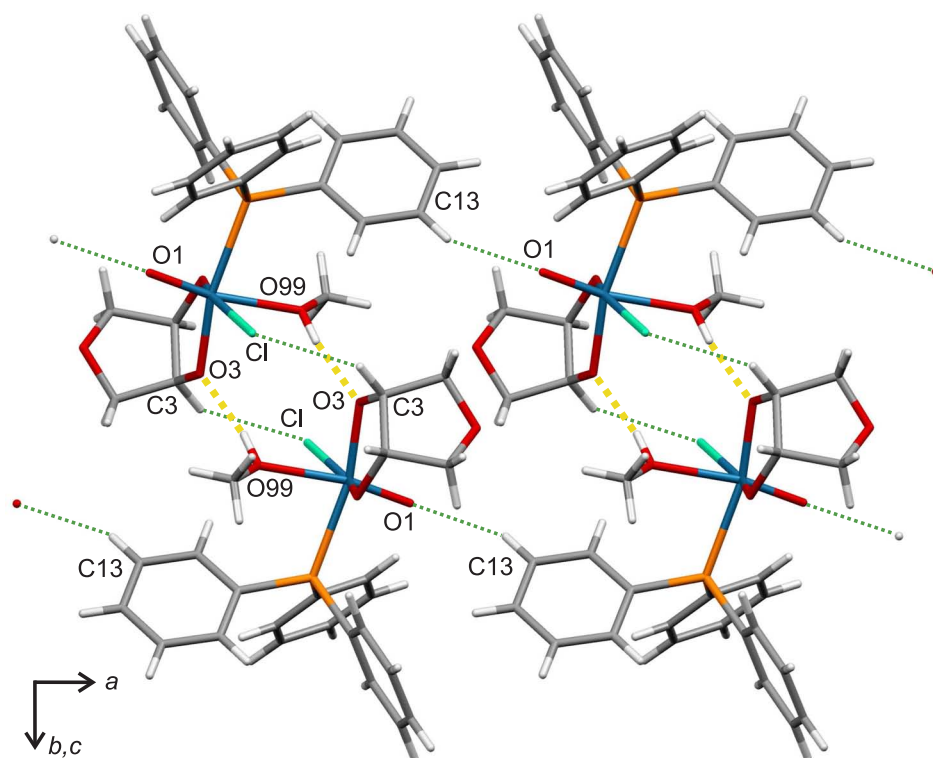


Figure 2.96 MERCURY presentation of hydrogen bonds (yellow dashed lines) and intermolecular interactions shorter than [svdW – 0.3 Å] (green dashed lines) in **25** forming chains of dimers along [100]. svdW: sum of the van-der-Waals radii^[62].

Table 2.47 Distances [Å] and angles [°] of hydrogen bonds in **25**. Values without standard deviation are related to hydrogen atoms at calculated positions. D: donor, A: acceptor, x : difference of (H···A) and the sum of the van-der-Waals radii^[62].

D	H	A	D···A	D-H	H···A	x	D-H···A
O99	H899	O3 ⁱ	2.708(4)	0.84	1.88	-0.84	170
C3	H3	Cl ⁱ	3.421(5)	1.00	2.65	-0.30	134
C10	H10	O1	3.149(5)	0.95	2.37	-0.35	139
C13	H13	O1 ⁱⁱ	3.208(5)	0.95	2.39	-0.33	145
C22	H22	O2	3.119(5)	0.95	2.36	-0.36	137
C4	H42	O4 ⁱⁱⁱ	3.477(6)	0.99	2.59	-0.14	150

Symmetry codes: ⁱ $1 - x, 1 - y, 1 - z$; ⁱⁱ $1 + x, y, z$; ⁱⁱⁱ $-x, 1 - y, 1 - z$.

2.5.4 The reaction of $[\text{ReOCl}_3(\text{PPh}_3)_2]$ with L-threonine and anhydroerythritol

The amino acid L-threonine (L-thrH) offers up to three binding sites for coordination to metals, although so far, threoninato complexes with rhenium are unknown in the literature. Similarly to the compounds in chapter 2.2 with racemic 2,3-diaminopropionic acid (*rac*-dapH), a tridentate binding mode was expected (Figure 2.97).

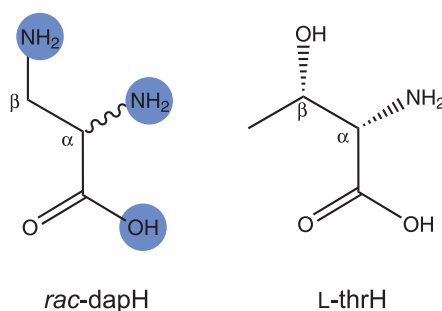


Figure 2.97 Scheme of *rac*-dapH and L-thrH.

The analog reactions of the rhenium(V) precursor $[\text{ReOCl}_3(\text{PPh}_3)_2]$ with L-threonine and the diols ethanediol, anhydroerythritol, methyl α -D-galactopyranoside and cytidine showed a coordination to the metal in view of NMR spectroscopy, but with numerous complex species. Only the reaction with anhydroerythritol yielded a small amount of crystals in the orthorhombic space group $P2_12_12_1$. Figure 2.98 shows the result of the structure determination: $[\text{ReO}(\text{L-thr})(\text{syn-AnErytH}_{-2})(\text{PPh}_3)]$ (**26**).

In this electroneutral complex, L-threonine binds bidentately to the rhenium core via the α -amino and carboxylate functions, while the β -hydroxy function is left dangling.

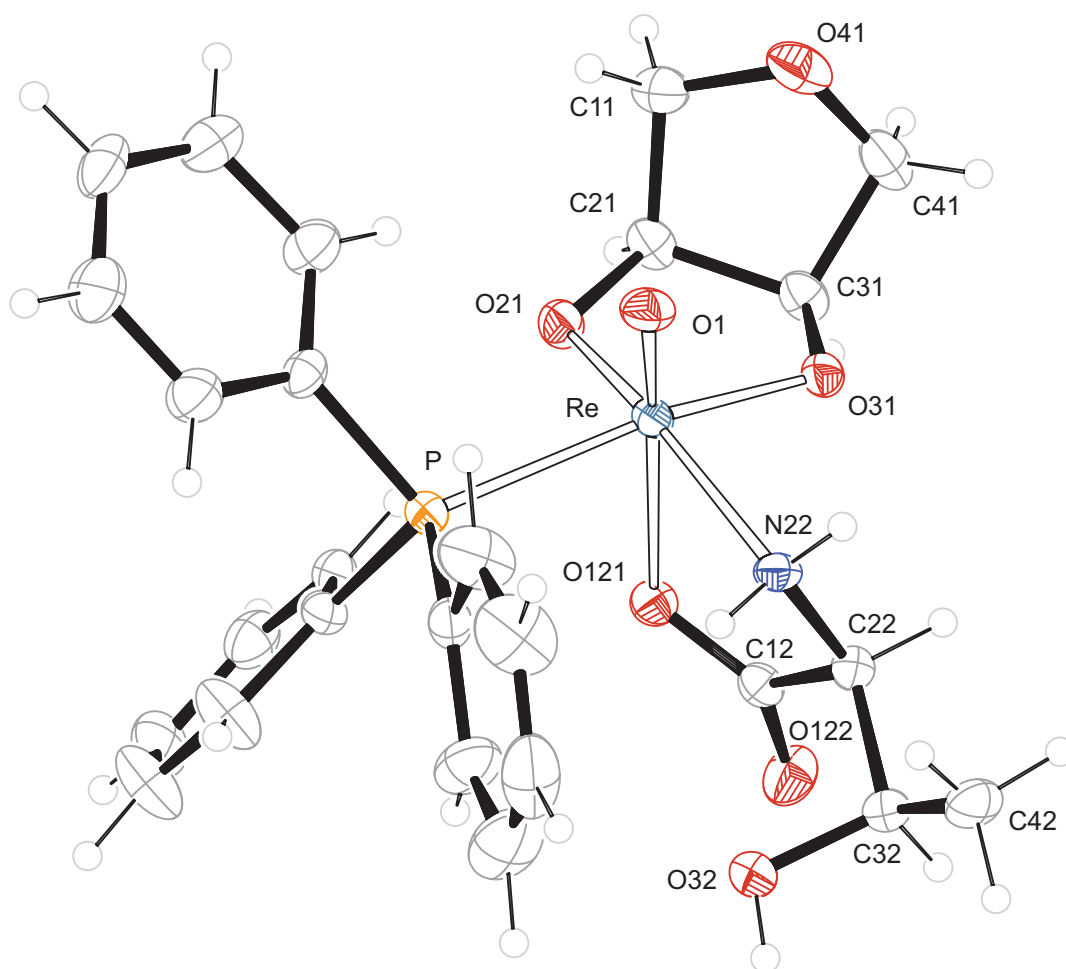


Figure 2.98 ORTEP presentation of **26** in crystals of $[\text{ReO}(\text{L-thr})(\text{syn-AnErytH}_{-2})(\text{PPh}_3)]$. Ellipsoids are drawn at 50 % probability level. Distances [Å] and angles [°]: Re-P1 2.4666(13), Re-O1 1.680(3), Re-O21 1.948(4), Re-O31 1.965(3), Re-O121 2.117(3), Re-N22 2.196(4); P1-Re-O1 87.13(12), P1-Re-O21 91.25(10), P1-Re-O31 164.67(10), P1-Re-O121 82.66(9), P1-Re-N22 93.82(11), O1-Re-O21 108.33(17), O1-Re-O31 108.12(15), O1-Re-O121 161.16(17), O1-Re-N22 91.59(17), O21-Re-O31 82.56(15), O21-Re-O121 87.75(14), O21-Re-N22 159.67(14), O31-Re-O121 83.10(12), O31-Re-N22 87.52(15), O121-Re-N22 73.43(15), diol torsion angle O21-C21-C31-O31: $-20.4(5)$, torsion angle of the coordinated acid group Re-O121-C12-O122: $-161.6(4)$, puckering parameters^[59] for O41-C11-C21-C31-C41: $Q_2 = 0.401(6)$ Å, $\phi_2 = 156.8(9)^\circ$, conformation 4T_O .

Although it is similarly acidic to the diol functions of anhydroerythritol, it is non-deprotonated and takes part in hydrogen bonding. As observed for other amino acids in this work, O121 of the acid group binds *trans* to the oxido group O1. The other bidentate ligand in this complex, the deprotonated diol AnErytH₋₂, is coordinated via O2 and O3 to the metal in *syn* orientation to the oxido ligand O1. Compared to the previous compound **25**, the diol torsion angle in **26** differs (-20° vs. 7°) as well as the conformation of the oxolane ring (4T_O vs. 0T_4). But both the angles and the conformations, were observed for other rhenium(V) complexes with anhydroerythritol^[31].

The hydrogen bonds in **26** are listed in Table 2.48. The intermolecular hydrogen bonds are formed between the dangling β -hydroxy function and O31 of the chelating diol, and between the α -amino function and O122 of the acid function. They connect the molecules of **26** to chains along [010], as illustrated in Figure 2.98. The intramolecular hydrogen bond N22-H222 \cdots O32 is not depicted in the figure due to its unfavorable angle (106°).

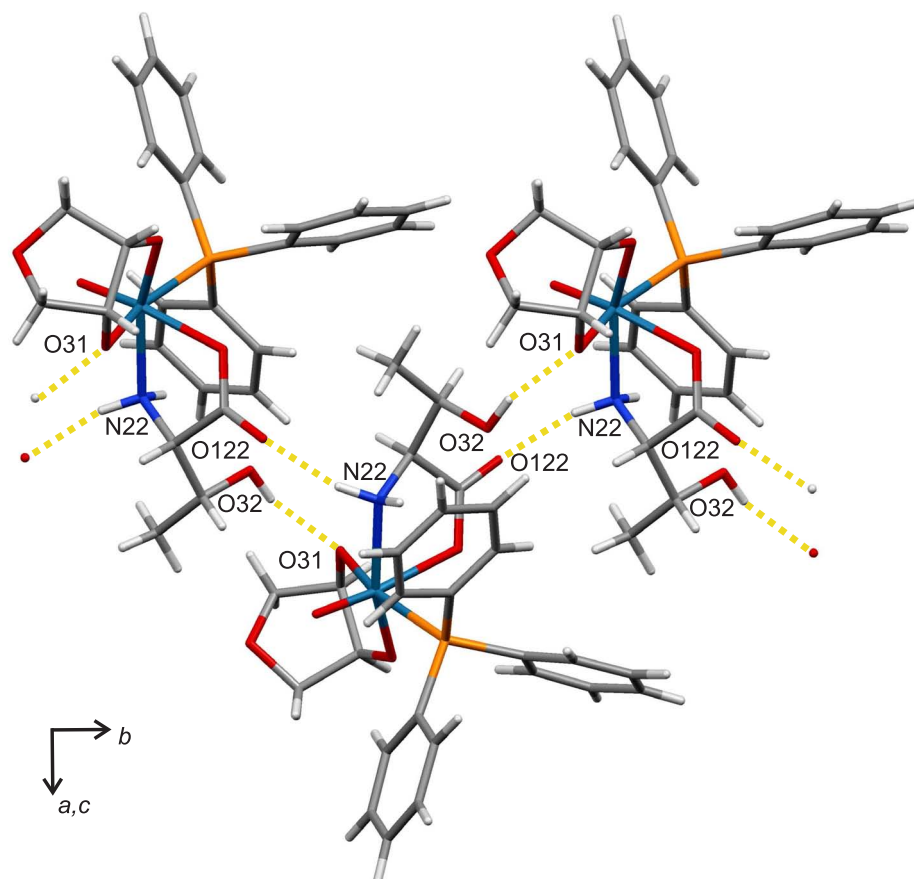


Figure 2.99 MERCURY presentation of hydrogen bonds (yellow dashed lines) in **26**.

Table 2.48 Distances [\AA] and angles [$^\circ$] of hydrogen bonds in **26**. Values without standard deviation are related to hydrogen atoms at calculated positions. D: donor, A: acceptor, x : difference of $(\text{H}\cdots\text{A})$ and the sum of the van-der-Waals radii^[62].

D	H	A	D \cdots A	D-H	H \cdots A	x	D-H \cdots A
N22	H221	O122 ⁱ	3.112(6)	0.92	2.25	-0.47	157
N22	H222	O32	2.893(6)	0.92	2.50	-0.22	106
O32	H832	O31 ⁱⁱ	2.745(5)	0.84	1.94	-0.78	160

Symmetry codes: ⁱ $2 - x, -\frac{1}{2} + y, \frac{1}{2} - z$; ⁱⁱ $2 - x, \frac{1}{2} + y, \frac{1}{2} - z$.

2.5.5 The reaction of $[\text{ReOCl}_3(\text{PPh}_3)_2]$ with iminodiacetic acid and erythromycin

Iminodiacetic acid (idaH_2) is well known as chelating ligand in various complexes with metal cores such as copper(II), nickel(II), chromium(III) or cadmium(II) but scarcely with rhenium. In 2005 the compound $[\text{Re}(\text{NO})(\text{CO})_2(\text{fac-ida})]$ with rhenium(I) was reported by *Schibli et al.*, but complexes with rhenium(V) have not been reported so far. As illustrated in Figure 2.100, *ida* offers a tridentate O,N,O donor atom set. In analogy to the compounds with *dien* in this work (chapter 2.1), *ida* was tested as co-ligand for reactions of carbohydrates with a diol function and $[\text{ReOCl}_3(\text{PPh}_3)_2]$. In view of NMR spectroscopy, reactions with ethanediol, anhydroerythritol, adenosine, uridine and cytidine seemed to be successful, but it was not possible to precipitate a product from these mixtures. Surprisingly, this was possible for the reaction with a larger molecule: erythromycin, a polyhydroxy-lactone.

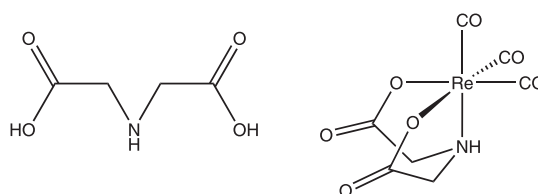


Figure 2.100 Scheme of idaH_2 and a complex with *ida*: $[\text{Re}(\text{NO})(\text{CO})_2(\text{fac-ida})]$ ^[147].

Erythromycin is one of the oldest and best studied antibiotics of the macrolide class. Discovered in 1952 (with the name *Ilotycin*^[148]), it is still used today for the treatment of bacterial infections. It is produced by fermentation from *streptomyces erythreus* as a mixture of the homologous erythromycins A – F (see Figure 2.101).

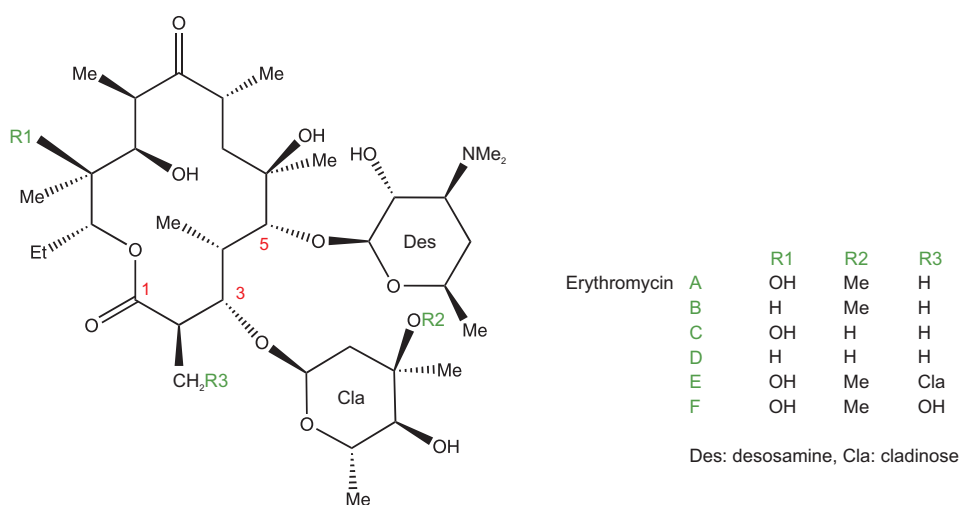


Figure 2.101 Scheme of the erythromycins A – F^[149].

The A form is the major component of commercial-grade erythromycin. It consists of a 14-membered lactone ring and two sugar moieties, α -L-cladinose (a hexose deoxy sugar) and β -D-desosamine (an aminosugar), linked glycosidic on C3 and C5. It inhibits protein synthesis in bacteria by reversibly binding to the large ribosomal subunit. The transpeptidation reactions are blocked, as it binds to the exit tunnel for the nascent peptides^[150–152]. Structure-activity relationship studies showed that the lactone ring and the desosamine sugar are involved with hydrogen-bond interactions to the ribosome, while the cladinose unit seems to be dispensable (see blue marked regions of erythromycin A in Figure 2.104). In a newer class of antibiotics, the ketolides, the cladinose is replaced by a keto group.

The major drawback of erythromycin is its chemical instability. Acid and base catalyzed degradations are known. Well explored is the decomposition in acidic aqueous solution, given in Figure 2.102. The ketone and enol-ether forms are in equilibrium and decompose under acidic conditions irreversible to the anhydro-form, which has no antibiotic activity. The enol-ether causes gastrointestinal distress, as it is a mimic of the peptide hormone motilin^[153]. In alkaline media, transesterification occurs for the lactone ring. The resulting pseudoerythromycins have no antibiotic activity, either. All these processes are observed in aqueous media, whereas in methanol erythromycin is reported to be more stable. *Kanfer et al.* reported only 5 % degradation in methanol over a period of 168 h, but the influence of a base like triethylamine was not investigated^[154].

The available information on the interaction of metals with erythromycin is scant. An iron complex of erythromycin for scavenging radicals was reported by *Muranaka et al.* in 1997, but without any information about its structure or binding mode^[155]. The sole structurally characterized coordination compound of erythromycin was reported in 1986 by *Oliver et al.* They reported of $[\text{Zn}(\text{C}_2\text{H}_3\text{O}_2)_2(\text{C}_{37}\text{H}_{67}\text{NO}_{13})(\text{H}_2\text{O})]$, a zinc(II) acetate complex where erythromycin is coordinated via the desosamine moiety as (N,O)-donor^[156].

The rhenium(V) complex, that is to be presented in this chapter, shows a different binding mode of erythromycin. As illustrated in Figure 2.103, the enol ether of erythromycin A is coordinated via the vicinal hydroxy functions on C11 and C12 of the lactone ring to the oxido-rhenium core. A tridentate ida ligand in *facial* binding mode completes the distorted octahedral coordination sphere. The resulting compound, $[\text{ReO}(\text{fac-ida})(\text{E}_{\text{my}11,12\text{H}_{-2}})] \cdot \text{MeOH} \cdot \text{H}_2\text{O}$ (**27**), was obtained from the reaction of $[\text{ReOCl}_3(\text{PPh}_3)_2]$ with iminodiacetic acid, erythromycin and triethylamine in methanol. Despite the presence of base and a temperature of 60 °C, degradation of erythromycin to anhydro- or pseudo-erythromycin did not occur.

2 Results

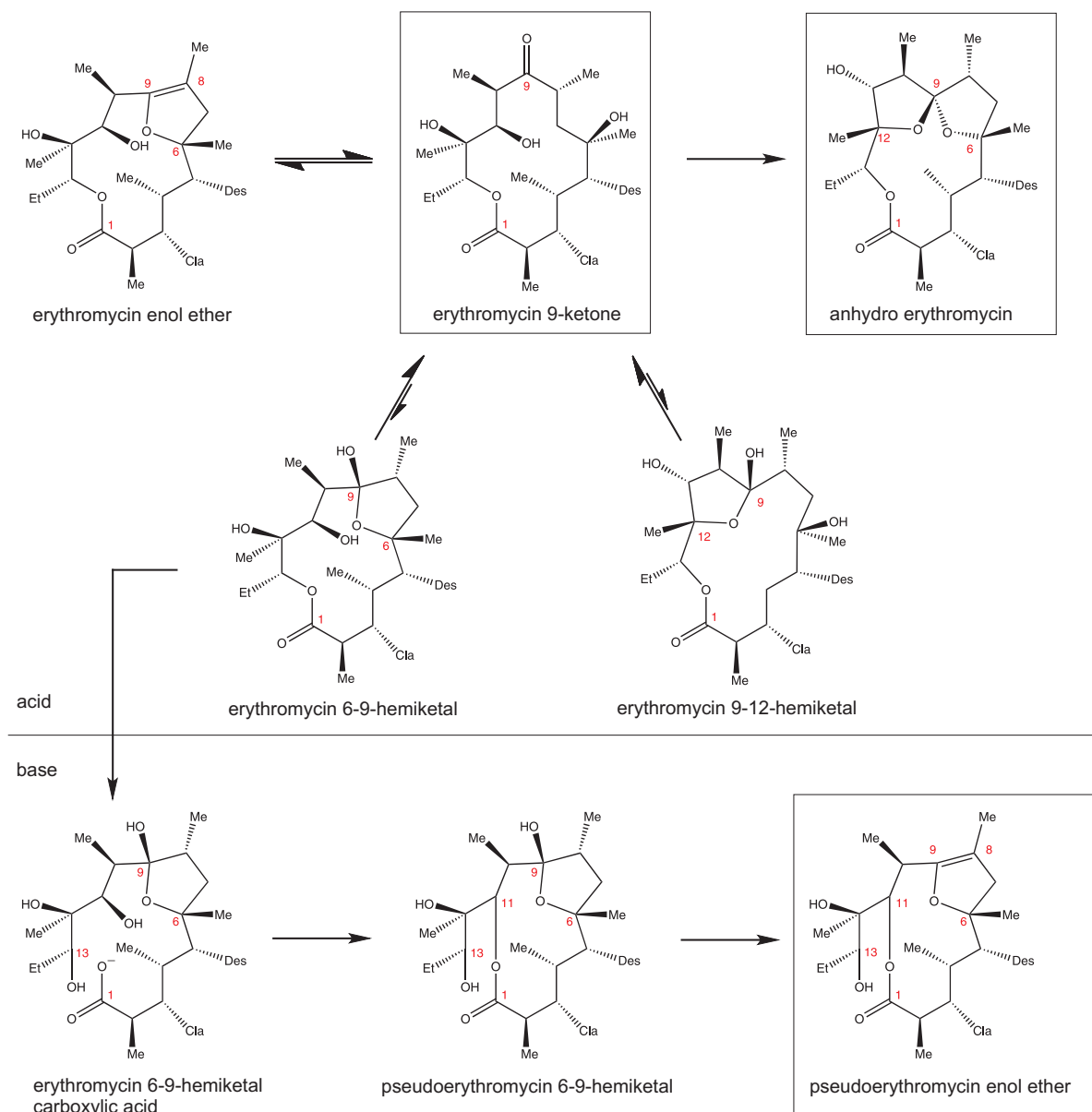


Figure 2.102 Scheme of the acid and base catalyzed degradations of erythromycin A. Starting point is erythromycin 9-ketone. In acidic media it decomposes to the anhydro form^[157, 158], in alkaline media to pseudoerythromycin enol ether^[159–161]. Des: desosamine, Cla: cladinose.

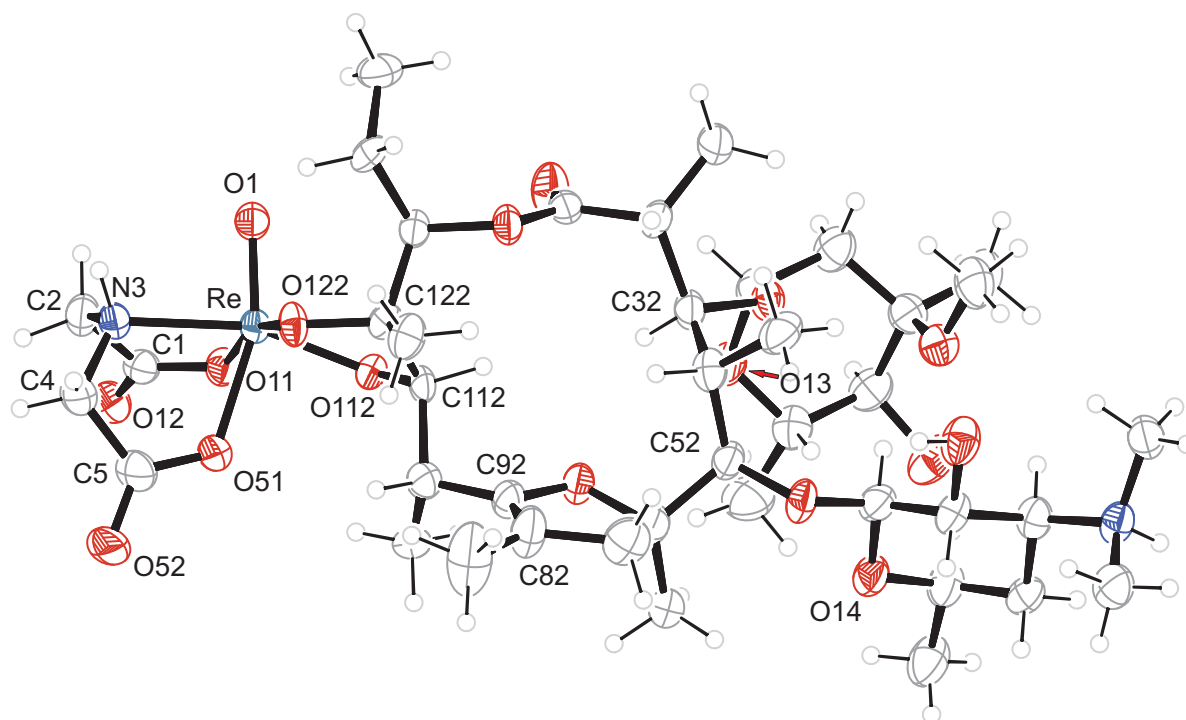


Figure 2.103 ORTEP presentation of **27** in crystals of $[\text{ReO}(\text{fac-ida})(\text{E}my_{11,12}\text{H}_{-2})] \cdot \text{MeOH} \cdot \text{H}_2\text{O}$. Hydrogen atoms were omitted for lucidity. Ellipsoids are drawn at 50 % probability level. Distances [Å] and angles [°]: Re-O1 1.671(5), Re-O11 2.069(5), Re-O51 2.101(5), Re-O112 1.949(5), Re-O122 1.955(5), Re-N3 2.185(6), double bond C82-C92 1.307(11); O1-Re-O11 94.8(2), O1-Re-O51 161.0(2), O1-Re-O112 110.7(2), O1-Re-O122 102.0(2), O1-Re-N3 87.0(2), O11-Re-O51 79.3(2), O11-Re-O112 90.52(19), O11-Re-O122 162.9(2), O11-Re-N3 80.0(2), O51-Re-O112 87.52(19), O51-Re-O122 85.7(2), O51-Re-N3 74.2(2), O112-Re-O122 80.55(19), O112-Re-N3 160.6(2), O122-Re-N3 104.0(2), diol torsion angle O112-C112-C122-O122: 41.3(7), torsion angle of the axial coordinated acid group Re-O51-C5-O52: 174.0(7), puckering parameters^[59] for O72-C62-C72-C82-C92: $Q_2 = 0.185(9)$ Å, $\phi_2 = 40(3)^\circ$, for O14-C14-C24-C34-C44-C54: $Q = 0.613(9)$ Å, $\theta = 2.9(8)^\circ$, $\phi = 133(16)^\circ$, conformation 4C_1 , for O13-C13-C23-C33-C43-C53: $Q = 0.531(9)$ Å, $\theta = 173.2(10)^\circ$, $\phi = 38(8)^\circ$, conformation 1C_4 .

27 crystallizes in the orthorhombic space group $P2_12_12_1$ with four formula units in the unit cell. The asymmetric unit contains the rhenium complex (Figure 2.103) and two solvent molecules (methanol and water), which are disordered. The torsion angle of the chelating diol moiety O112-C112-C122-O122 (41.3°) is similar to the angles found for complexes with ethanediol in this work (**6**: -40.7° , **10**: 43.5° , **17**: -36.7°). The two sugar moieties, α -L-cladinose and β -D-desosamine, are in chair conformations (1C_4 and 4C_1) which also holds true for the three related structures with erythromycin depicted in Figure 2.104. As shown there, the geometry of the lactone ring in **27** is close to a structure of a derivative of erythromycin enol ether^[162]. This derivative was chosen for comparison, as the structure of free erythromycin enol ether has not been reported yet. But for **27**, the length of the C8-C9 double bond is

closer to the expected value of 1.33 Å^[163] (1.31 Å *vs.* 1.17 Å). In addition to the structure of **27**, in this figure all available structures of erythromycin, the enol ether and the anhydro-compound from the Cambridge Structural Database^[164] are presented.

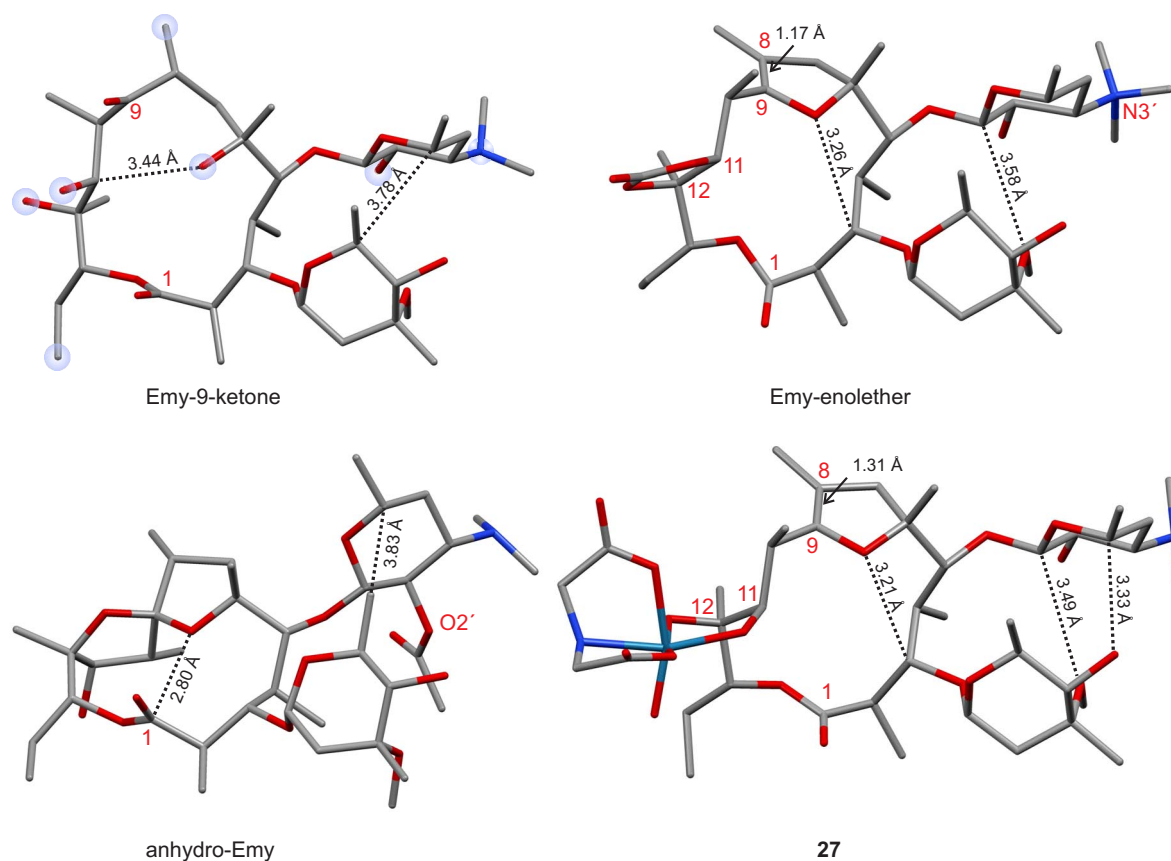


Figure 2.104 Structures of free erythromycin A^[165], the enol-ether (as cyclic carbonate ester on O11/O12, methylated on N3')^[162], the anhydride (acetylated on O2')^[166] and **27** (from top left to down right). The shortest intramolecular distances are given as dotted lines. The interacting groups of erythromycin A with the peptidyl transferase cavity are marked blue^[152].

The hydrogen bonds in **27** are listed in Table 2.49. As illustrated in Figure 2.105, chains are formed along [100] by strong intermolecular hydrogen bonds between the donor and acceptor functions of the ida-ligand. Noteworthy is also an interaction of the type C-H \cdots O from the methylene unit of ida (C2-H22) to the rhenium-bonded oxido ligand (O1) as the distance is markedly shorter than the sum of the van-der-Waals radii^[62] and the angle is typical for a classical hydrogen bond. Although there are many functional groups in this molecule, no intramolecular hydrogen bonds are established. But on closer inspection, two other weak interactions of the type C-H \cdots O are found between the α -L-cladinose and β -D-desosamine parts. These two sugar moieties are closer to each other than in the related structures in Figure 2.104.

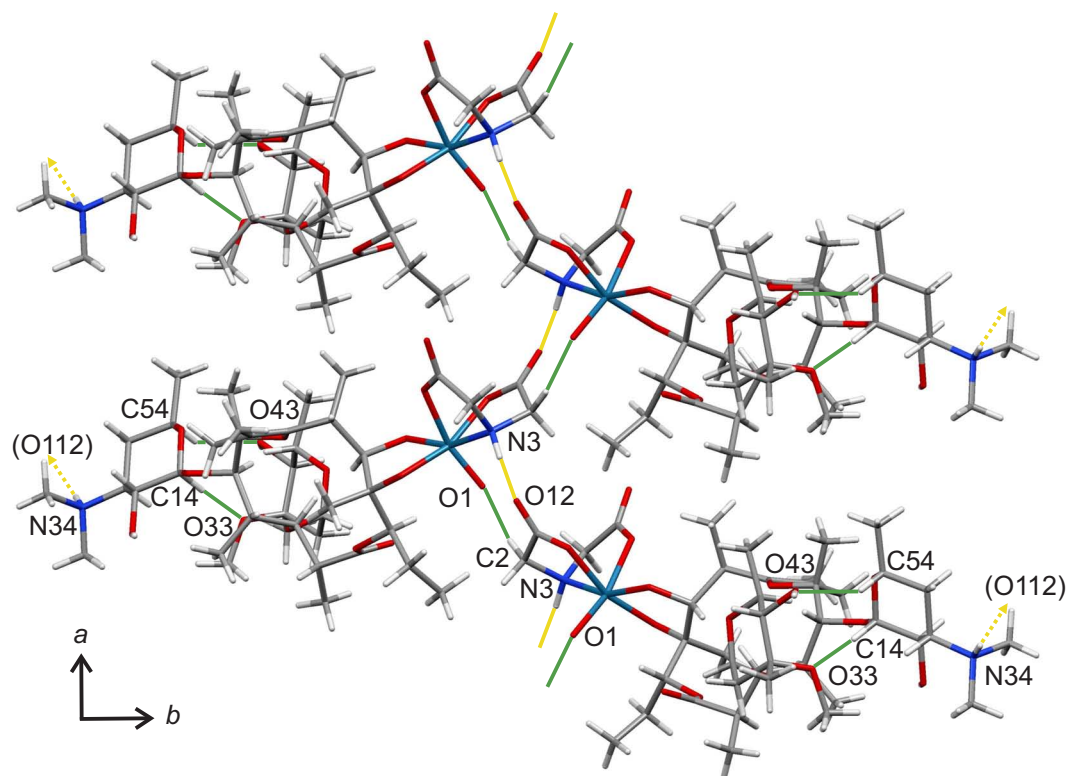


Figure 2.105 MERCURY presentation of selected hydrogen bonds (yellow lines) and C-H...O contacts (green lines) in **27** forming chains along [100]. Disordered solvent molecules are not shown.

Table 2.49 Distances [Å] and angles [°] of hydrogen bonds in **27**. Values without standard deviation are related to hydrogen atoms at calculated positions. O997 is affiliated to disordered water, O990 to disordered methanol. D: donor, A: acceptor, x : difference of (H...A) and the sum of the van-der-Waals radii^[62].

D	H	A	D...A	D-H	H...A	x	D-H...A
N3	H73	O12 ⁱ	2.805(8)	0.93	1.89	-0.83	167
N34	H734	O112 ⁱⁱ	2.720(8)	0.93	1.80	-0.92	168
O24	H824	O997 ⁱⁱⁱ	2.83(3)	0.84	2.12	-0.60	142
O43	H843	O52 ^{iv}	2.683(8)	0.84	1.90	-0.82	155
O990	H990	O122 ^v	2.93(3)	0.84	2.27	-0.45	135
C2	H22	O1 ^{vi}	3.394(10)	0.99	2.41	-0.31	170
C14	H14	O33	3.492(11)	1.00	2.54	-0.18	160
C54	H54	O43	3.327(11)	1.00	2.43	-0.29	149

Symmetry codes: ⁱ $-\frac{1}{2} + x, -\frac{1}{2} - y, 1 - z$; ⁱⁱ $1 - x, \frac{1}{2} + y, \frac{1}{2} - z$; ⁱⁱⁱ $1 - x, -\frac{1}{2} + y, 1\frac{1}{2} - z$;
^{iv} $\frac{3}{2} - x, -y, -\frac{1}{2} + z$; ^v $\frac{3}{2} - x, 1 - y, -\frac{1}{2} + z$; ^{vi} $\frac{1}{2} + x, -\frac{1}{2} - y, 1 - z$.

2.5.6 The reaction of [ReO(L-his)(ox)] with Cu²⁺ and phen

Faus et al. reported in 2001 on a heterobimetallic complex with rhenium(IV) and copper(II). The tetranuclear anion [Ni{ReCl₄(ox)}₃]⁴⁻ was prepared starting from a rhenium(IV)-oxalato complex^[167]. As shown in Figure 2.106, an adaption of this reaction route to rhenium(V) was intended.

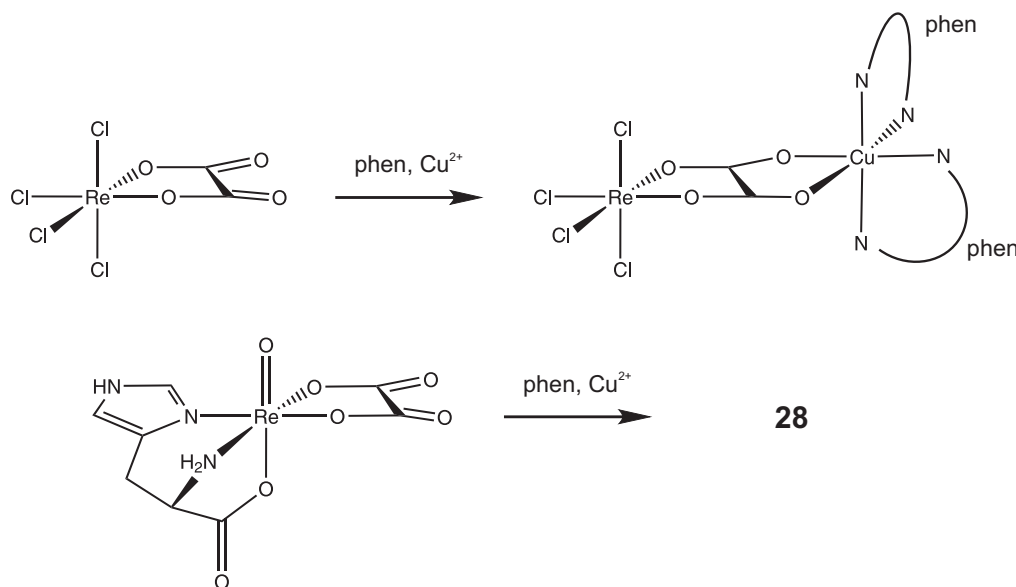


Figure 2.106 Scheme of the reaction route for bimetallic complexes with rhenium(IV) and copper(II) reported by *Faus et al.* and intended adaption to rhenium(V).

Instead, a change of the oxidation state of rhenium was observed. The oxalato-rhenium(V) complex **9** (see section 5.5.9 on page 170) was heated with 1,10-phenanthroline and Cu(NO₃)₂ · 3 H₂O in acetonitrile. From this green solution, crystals of a coordination polymer compound with rhenium(VII) and copper(II) were obtained with the formula [Cu₂(phen)₂(ox)(ReO₄)₂]_n (**28**). They crystallized in the monoclinic space group C2/c with eight formula units in the unit cell. The asymmetric unit contains the smallest subunit of the polymeric chain with the sum formula C₁₃H₈CuN₂O₆Re. Six of these subunits are depicted in Figure 2.107, they form three repetitive units of the polymeric chains in **28**. As shown there, perrhenate ions connect binuclear oxalato-bridged copper moieties. Despite the linkages to the copper cores, the Re-O distances vary only from 1.71 to 1.74 Å. This is close to the observed values for uncombined perrhenate ions: the distances in the perrhenate anion of **5** (chapter 2.1.5, page 32) vary from 1.70 to 1.73 Å. The distances of the perrhenate-oxygen atoms to the copper cores are long, but within a range reported in the PhD thesis of *G. Kramer* (see Figure 2.108).

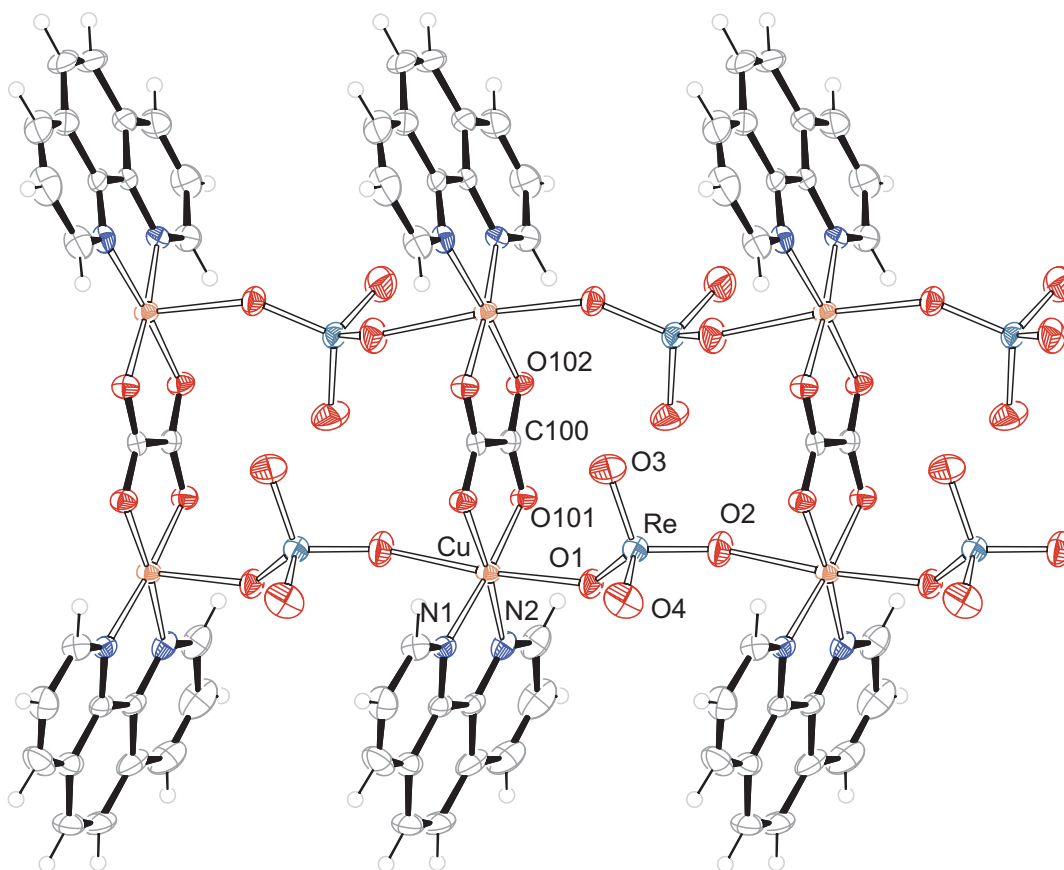


Figure 2.107 ORTEP presentation of 3 units of the polymeric chain of **28** in crystals of $[\text{Cu}_2(\text{phen})_2(\text{ox})(\text{ReO}_4)_2]_n$. Ellipsoids are drawn at 50 % probability level. Distances [\AA] and angles [$^\circ$]: Re-O1 1.738(2), Re-O2 1.718(3), Re-O3 1.705(3), Re-O4 1.723(3), Cu-O1 2.295(2), Cu-O101 1.972(3), Cu-N1 1.989(3), Cu-N2 1.997(3), Cu-O2ⁱ 2.433(2), Cu-O102ⁱⁱⁱ 1.974(2); O1-Re-O2 108.06(12), O1-Re-O3 111.02(13), O1-Re-O4 108.92(14), O2-Re-O3 110.62(15), O2-Re-O4 108.55(15), O3-Re-O4 109.61(16), O1-Cu-O101 91.14(10), O1-Cu-N1 94.47(11), O1-Cu-N2 96.11(10), O1-Cu-O2ⁱ 174.60(10), O1-Cu-O102ⁱⁱⁱ 89.41(9), O101-Cu-N1 174.35(11), O101-Cu-N2 95.80(12), O101-Cu-O2ⁱ 84.54(10), O101-Cu-O102ⁱⁱⁱ 85.86(11), N1-Cu-N2 82.98(13), N1-Cu-O2ⁱ 89.90(12), N1-Cu-O102ⁱⁱⁱ 94.83(11), N2-Cu-O2ⁱ 87.56(11), N2-Cu-O102ⁱⁱⁱ 174.20(11), O2ⁱ-Cu-O102ⁱⁱⁱ 87.07(10), Re-O1-Cu 139.48(12), Re-O2-Cuⁱⁱ 137.41(17), oxalate torsion angle O101-C100-C100ⁱⁱⁱ-O102ⁱⁱⁱ: $-3.1(4)$, phen torsion angle N1-C5-C6-N2: $0.4(4)$. ⁱ $x, -1+y, z$; ⁱⁱ $x, 1+y, z$; ⁱⁱⁱ $2-x, y, \frac{1}{2}-z$.

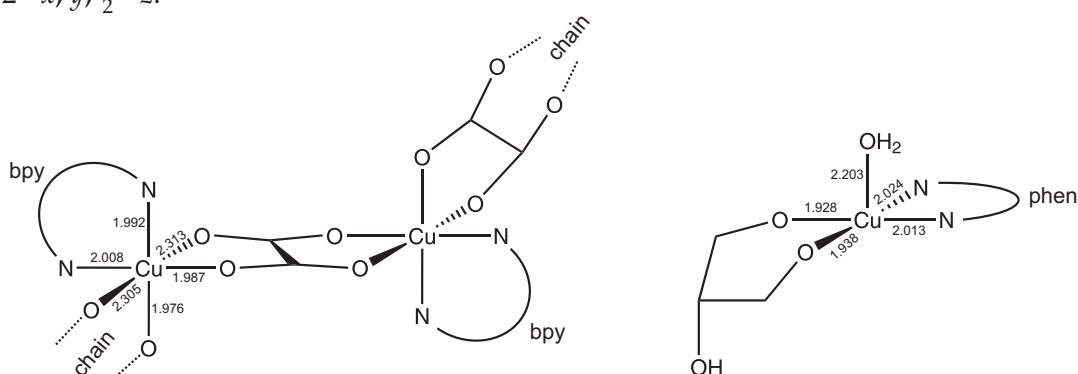


Figure 2.108 Scheme of related compounds with copper(II) reported by G. Kramer with oxalate/bipy and tartronic acid/phen^[168]. Left: $[\text{Cu}(\text{bipy})(\text{ox})]_n$, right: $[\text{Cu}(\text{phen})(\text{C}_3\text{H}_2\text{O}_5)(\text{H}_2\text{O})]$.

No classic hydrogen bonds are established in this structure due to missing hydrogen donors. But apart from the van-der-Waals interactions, the only interaction between the polymeric chains are C-H \cdots O contacts between the phen and perrhenate moieties. As given in Table 2.50, the distances of four interactions are more than 0.25 Å shorter than the sum of the van-der-Waals radii^[62]. Figure 2.108 shows the interaction of two adjacent chain-link moieties.

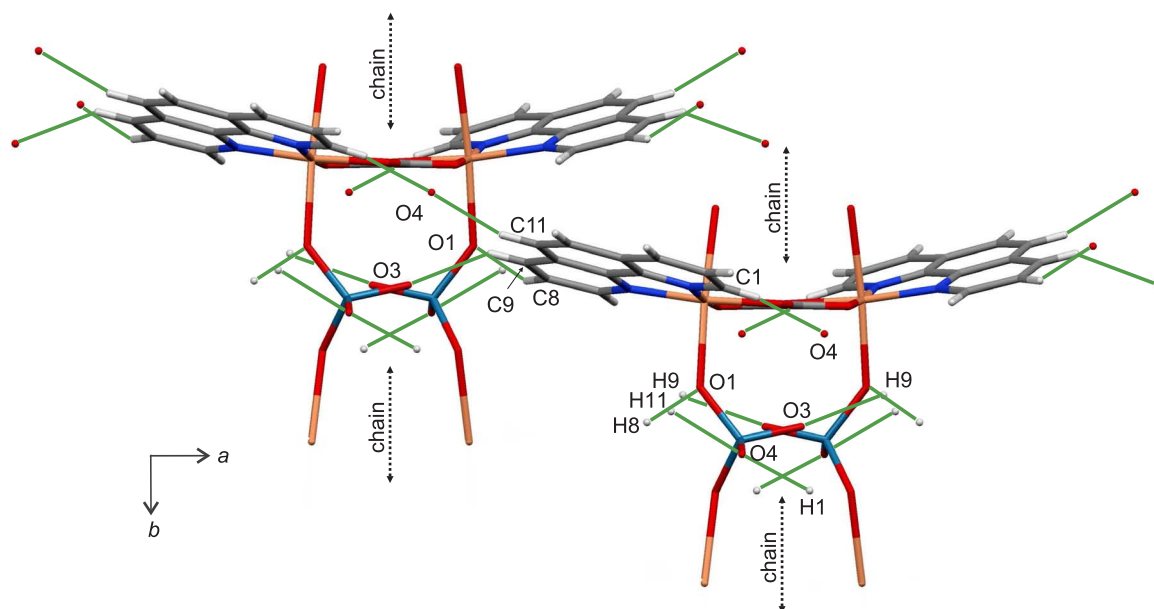


Figure 2.109 MERCURY presentation of C-H \cdots O contacts (green lines) between the phen and perrhenate moieties in 28.

Table 2.50 Distances [Å] and angles [°] of C-H \cdots O contacts in 28. D: donor, A: acceptor, x : difference of (H \cdots A) and the sum of the van-der-Waals radii^[62].

D	H	A	D \cdots A	D-H	H \cdots A	x	D-H \cdots A
C1	H1	O4 ⁱ	3.212(5)	0.95	2.47	-0.25	135
C8	H8	O1 ⁱⁱ	3.349(6)	0.95	2.47	-0.25	155
C9	H9	O3 ⁱⁱⁱ	3.179(5)	0.95	2.38	-0.34	141
C11	H11	O4 ^{iv}	3.340(6)	0.95	2.47	-0.25	153

Symmetry codes: ⁱ $2 - x, 1 - y, -z$; ⁱⁱ $\frac{3}{2} - x, -\frac{1}{2} + y, \frac{1}{2} - z$; ⁱⁱⁱ $-\frac{1}{2} + x, -\frac{1}{2} + y, z$;
^{iv} $\frac{3}{2} - x, \frac{1}{2} - y, -z$.

2.5.7 The reaction of $[\text{ReOCl}_3(\text{PPh}_3)_2]$ and other amino acids

In this work, mixed-ligand complexes were presented with the amino acid derivative *rac*-dap, the amino acids L-histidine and L-threonine, and the dipeptide L-carnosine. But the following combinations of amino acids (or derivatives thereof) and diols should be mentioned, too, as the NMR spectra of the reaction mixtures were promising. The reaction mixtures of $[\text{ReOCl}_3(\text{PPh}_3)_2]$ in methanol with three equivalents triethylamine and the following standard proteinogenic amino acids (in brackets the respective diols) showed complex species:

L-alanine (cytidine), L-arginine (cytidine), L-asparagine (ethanediol, methyl α -D-galactopyranoside, adenosine), L-aspartic acid (ethanediol, anhydroerythritol, methyl α -D-galactopyranoside, cytidine), L-cysteine (cytidine), L-glycine (cytidine), L-isoleucine (cytidine), L-leucine (cytidine), L-proline (cytidine).

The same holds true for the following amino acid derivatives and peptides: β -aspartame (anhydroerythritol, adenosine, cytidine, uridine, D-isomaltulose), BICINE (anhydroerythritol, methyl α -D-galactopyranoside, cytidine, uridine), TRICINE (cytidine), 4-hydroxy-L-proline (cytidine), and the dipeptide L-gly-his (uridine). The latter system was investigated in the MSc thesis of M. Korth^[169].

3 Discussion

3.1 Selectivity of the reactions

Most of the compounds in this work are built according to the “3 + 2” approach^[19]. But what is so special about this approach? As shown in the previous chapters, it is possible to synthesize stable mixed-ligand complexes with carbohydrates containing a diolato function and tridentate co-ligands like dien (chapter 2.1), *rac*-dap (chapter 2.2), L-histidine (chapter 2.3) and L-carnosine (chapter 2.4). At first glance, the “3 + 2” approach seems to be only a simple methodology to synthesize complexes with tri- and bidentate ligands, with the chelate effect as the only driving force. But these reactions also showed a high chemo- and regioselectivity and the products were more stable against hydrolysis than possible side products. Figure 3.1 illustrates the possible reaction routes, that may compete with the “3 + 2” reactions in this work.

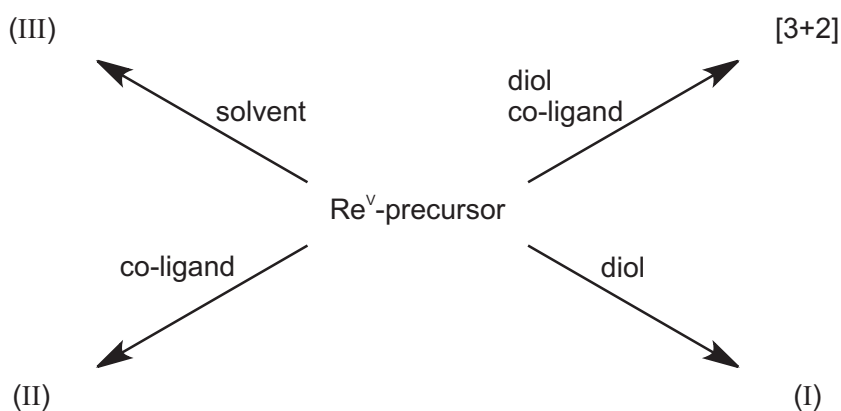


Figure 3.1 Competing reactions of the “3 + 2” approach.

(I)

It is possible to synthesize homoleptic complexes with simple diols and rhenium(V). *Zubieta et al.* reported in 1994 on an air-sensitive compound of oxido-rhenium(V) with two ligands of catechol (benzene-1,2-diol)^[140]. The anionic complex $[\text{ReO}(\text{cat})_2]^-$ was prepared under nitrogen in the presence of base from the rhenium(V) precursor

[ReOCl₃(PPh₃)₂] in anhydrous methanol. The same reaction in air yielded a complex with dioxido-rhenium(VII), as reported in 1990 by *Dilworth et al.*^[141]. Obviously rhenium(V) was oxidized to rhenium(VII) by air. Three compounds in this work were also obtained without the addition of a co-ligand (chapter 2.5). The oxalate-substituted derivatives **23** and **24** of the precursors [ReOCl₃(PPh₃)₂] and [Re(NPh)Cl₃(PPh₃)₂] are stable against air. A third compound in this series, the oxalatediolato-substituted derivative **25** contains additionally a coordinated molecule of methanol. But all these compounds were insoluble in aqueous media and it was not possible to synthesize such complexes with more complex diols. Furthermore, in the presence of one of the above mentioned tridentate co-ligands, these products were not detectable in the reaction mixtures, not even as side-products.

(II)

It is possible to build complexes with rhenium(V) that contain the above-mentioned co-ligands, but not a diolato moiety. Complexes with dien and L-histidine are structurally characterized. The hygroscopic compound [ReO₂(dien)₂]I was reported by *Kremer et al.* in 2001^[58]. In addition to this compound, *Oßberger* observed [ReO(OMe)(dien)(PPh₃)₂]I₂ as a further side product of the reaction with diols in methanol^[23]. *Tessier et al.* reported in 2002 the structure of [ReO(L-his)Cl₂] with L-histidine^[42]. Within the scope of this work, the hydrolytic stability of this compound was tested: in water, decomposition within minutes was observed for this complex. Moreover, this complex was not detected in the presence of diols. Potentially related compounds with *rac*-dap or L-carnosine were not detected, irrespective of the presence of diols.

(III)

A third possibility is the reaction with the solvent. The widely used precursors [ReO₂(PPh₃)₂] and [ReOCl₃(PPh₃)₂] react with alcohols to alkoxido complexes. Structurally characterized are compounds with the formula [ReO(OR)X₂(PPh₃)₂] (X = Cl, Br, I) for methanol^[146, 170] and ethanol^[171, 172]. But not till 2007, was any hydroxido complex reported. As shown by *Gerber et al.*^[173], [ReO(OH)Cl₂(PPh₃)₂] was obtained from [ReOCl₃(PPh₃)₂] in acetone containing 1 % water and an imidazole derivative. The product of the reaction of [ReOCl₃(PPh₃)₂] with DMSO was tentatively reported^[174] to be [ReOCl₃(Me₂SO)(PPh₃)], though later analyses showed that the correct formula is [ReOCl₃(Me₂S)(OPPh₃)]^[175]. In the course of this work, the known compound [ReO(OMe)Cl₂(PPh₃)₂]^[170] was crystallized repeatedly, but only for reactions where NMR spectroscopy did not show a coordination of the diols or co-ligands.

In addition to the routes I–III, further reactions may compete with the “3 + 2” approach as some oxido-rhenium(V) compounds were reported to have catalytic properties. Generally, transition-metal-oxo species like permanganate or osmiumtetroxide have been long known as stoichiometric or catalytic oxidants^[12]. In the chemistry of rhenium, mainly compounds such as methyl rhenium(VII) trioxide (MTO) are known as catalysts for the oxidation and epoxidation of organic compounds^[176]. But in the last decade many oxido-rhenium(V) complexes were also reported to have catalytic properties^a, too. They all have in common the presence of a phosphane or phosphaneoxide ligand. These catalytic reactions were not included in Figure 3.1, as they were not observed for the reactions in this work. A reason for this may be the use of methanol or water as solvents, while the reported catalytic properties were observed mainly in aprotic solvents.

All these competing reactions were not observed for the “3 + 2” reactions with the nitrogen-containing co-ligands and the diols in this work. In particular, the combination of amino acids and diols showed a strong tendency to bind to oxido-rhenium(V). The reactions with L-histidine and L-carnosine (paragraphs 5.5.9 to 5.5.22 of the experimental part) were carried out with 1 mmol of a rhenium(V) precursor in 10 to 500 mL methanol or water, but it was also possible to operate in 2500 mL solvent. The molar concentration range was 0.4 to 100 mM or even only in a nanomolar range with the isotope ¹⁸⁸Re (see page 181 of the experimental part). For the reactions in methanol, it was possible to use various rhenium(V) precursors like [ReOCl₃(PPh₃)₂]^[172], [ReO₂(PPh₃)₂I]^[146], [ReOCl₃(SMe₂)(OPPh₃)]^[174] or [BzNEt₃][ReOCl₄]^[187] with similar findings, as the resulting complexes were mainly determined by the incoming ligands and not by the precursors^[17]. But the reactions in water were only possible starting from the oxalato complexes **9** and **16** with L-histidine and L-carnosine, or with *in-situ*-prepared rhenium(V) species by the reduction of perrhenate with tin(II). Such flexibility as to the choice of precursor, reaction volume or solvent, was not observed for the reactions with dien. The reactions with dien in water were not successful at all, only decomposition to rhenium(IV) was observed.

^a The oxidation of thiols to disulfides was reported to be catalyzed by [ReOCl₃(PPh₃)₂] and [ReOCl₃(SMe₂)(OPPh₃)]^[177]. [ReOCl₃(PPh₃)₂] catalyzes in presence of DMSO the oxidation of primary/secondary alcohols to aldehydes/ketones^[178, 179]. The reduction of aldehydes and ketones via hydrosilylation, is also reported for [ReO₂(PPh₃)₂I] and [ReOCl₃(PPh₃)₂] in the presence of silanes^[180, 181]. [ReOCl₂(CNbox)(OPPh₃)] catalyzes an enantioselective reduction of imines with silanes^[182]. Even carbon-carbon bond forming reactions are catalyzed by oxido-rhenium(V) compounds. A mild aromatic propargylation reaction in analogy to Friedel-Crafts reactions was reported for [ReOCl₃(dppm)]^[183]. Aldehyde-olefination reactions in analogy to Wittig reactions are catalyzed by [ReOCl₃(PPh₃)₂]^[184, 185]. Concerning the chemistry of carbohydrates, a catalyzed O-glycosylation was reported for 2-deoxyglycosides with [ReOCl₃(SMe₂)(OPPh₃)]^[186].

These observations substantiate a tendency to large association constants of the “3 + 2” compounds in equilibrium, in particular with amino acids. Furthermore, these reactions showed a high selectivity towards the attendant functional groups in terms of chemo- and regio-selectivity.

The $\{\text{ReO}\}^{3+}$ core shows a high regioselectivity toward *cis*-vicinal diolato functions of furanoses and pyranoses. Up to now, the sole exception to this observation is a hydrolytically unstable complex with dien and methyl β -D-xylopyranoside^[24]. The torsion angle of the chelating *trans*-diolato moiety in $[\text{ReO}(\text{dien})(\text{Me-}\beta\text{-D-Xylp2,3H}_{-2})\text{I}]$ is the largest so far observed (47.2°) for diols connected to the rhenium(V) core. As illustrated in Figure 3.2 (page 146), most of the torsion angles are much smaller. In all cases where amino acids were used as co-ligands, the carboxylato functions were connected as preferred binding sites to the metal. They were connected exclusively in *trans*-position to the $\{\text{ReO}\}^{3+}$ core. This holds true for compounds with *rac*-dap, L-histidine, L-carnosine, L-threonine and generally for co-ligands with carboxylic acid functions^[27, 32, 169, 188, 189]. In this work, an exception to this rule was observed for the oxalato complex **16** with L-carnosine (chapter 2.4.1, page 88). The carboxylato-groups of the amino acid and of the oxalate ligand seem to compete for the *trans* position, as the two complex species in solution attested. The analog compound with L-histidine did not show this behavior.

Almost all “3 + 2” complexes in this work are chiral. The stereocenters (if present) of the diols and co-ligands were not affected by the reactions, and both reactants retained their configurations. But in most cases, the presence of more than one diastereomeric complex species was detected in solution.

- On the one hand, two signal sets were observed in many cases due to *syn/anti* isomerism, as there are two possible orientations for coordinated diols towards the $\text{Re}=\text{O}$ axis. In cases where *syn/anti* isomerism was observed, equilibrium adjustment was rapid in protic solvents such as water or methanol, and slow in an aprotic solvent such as DMSO, as shown for the spectra of **21** and **22** (pages 113 and 117). But in most cases, steric restrictions seemed to reduce the observed number of all these species or they were below the detection limit of NMR spectroscopy.
- On the other hand, this may be caused by the presence of more than one *cis*-vicinal diolato function, as any further suitable diolato moiety may compete for coordination. This was observed for the ribose-derived compounds **15** and **19**. For **15**, the result of the structure determination showed a coordination via (O3,O4), whereas in solution additionally (O2,O3)-coordinated minor species were observed (page 83). Various minor species were observed for **19** in solution (page 104), whereas the structure determination showed only a coordination of the furanose anomer via (O1,O2).

But in the cases of **20**, **21** and **22**, no coordination was detected in solution other than the (O2,O3)-coordination found in the structure, although there were other suitable hydroxy functions. This even holds true for naturally raw sugar materials, where carbohydrates occur as mixtures^b.

But which diolato functions are suitable for chelation? The above used criterion, the availability of a *cis*-vicinal diolato function, is sufficient for furanoses and pyranoses, but not for open-chain diols or acids. A closer look on the torsion angles of all coordinated diols that were observed so far in this and other works is given in Figure 3.2. Values were observed from -46.0° to $+47.2^\circ$, the absolute values cover a range from 1.2° to 47.2° . In general, small values are observed for acids and large values for pyranoses. Open-chain diols also adopt wide angles, which can be explained by the *Pitzer* strain of an eclipsed conformation. Due to their flexibility, furanoses cover the largest range within this interval from 1.2° to 32.1° . Although 51 structures are not a reliable basis for statistics, a furanose-preference for rhenium(V) becomes apparent (21 out of 51 structures). In the chemistry of silicon, a preference of furanoses has already been reported yet^[77]. Though, in the chemistry of rhenium, such an effect could not be confirmed in solution. Experiments with oxido-rhenium(V) precursor compounds, dien and equal amounts of two types of diols did not show a preference for furanoses over pyranoses^c.

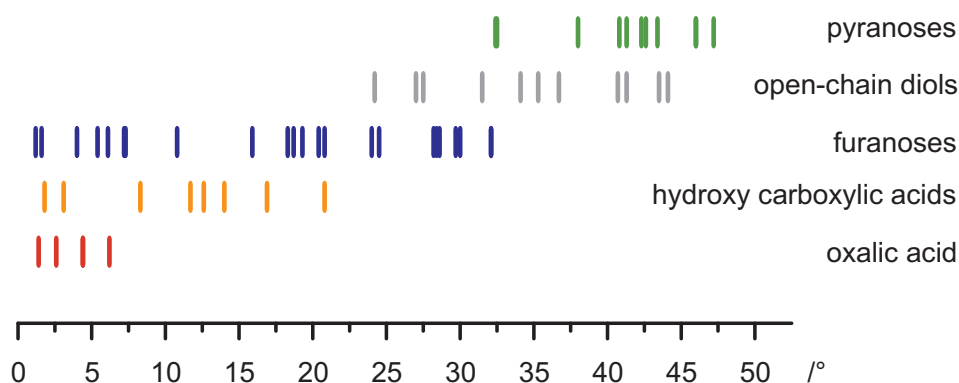


Figure 3.2 Absolute values of the torsion angles in **1** – **27** and 24 other reported structures with rhenium(V) and pyranoses, open-chain diols, furanoses, hydroxy carboxylic acids and oxalic acid^[23, 24, 32, 169, 188, 189].

^b A great quantity of sugars was detected by NMR techniques in naturally raw honeys^[190]. Apart from the well known main components D-fructose (ca. 35 %) and D-glucose (ca. 25 %), they contained up to 10 % of several di- and trisaccharides. It was even possible to adopt the reaction 5.5.21 (page 179) to honey. The NMR spectra showed the same species as for the reaction with pure D-fructose, despite the presence of other carbohydrates.

^c tested combinations: methyl α -D-galactopyranoside and adenosine or uridine

However, substitution reactions of rhenium-bonded diolato ligands were observed. As illustrated in Figure 3.3, it is possible to substitute ethanediolato or oxalato ligands with furanoidic diolates. In particular, the oxalate-based compounds $[\text{ReO}(\text{L-his})(\text{ox})]$ and $[\text{ReO}(\text{L-car})(\text{ox})]$ showed a high tendency for substitution with furanoidic carbohydrates. The substitution reactions with cytidine (chapter 2.3.5, page 71) and D-isomaltulose (chapter 2.4.7.1, page 118) were quantitative, even at a ratio of 1:1. To a smaller extent, and only at temperatures above 50°C , substitution with nucleosides was also observed for $[\text{ReO}(\text{L-his})(\text{EthdH}_{-2})]$ and $[\text{ReO}(\text{L-car})(\text{EthdH}_{-2})]$, if provided in excess. Substitution with pyranoidic carbohydrates or open-chain diols was not observed. The driving force of these reactions seems to involve the law of mass action, the different strains of the chelate rings, or, in the case of ethanediol, the various acidities of the diols. The following observations appear to support the

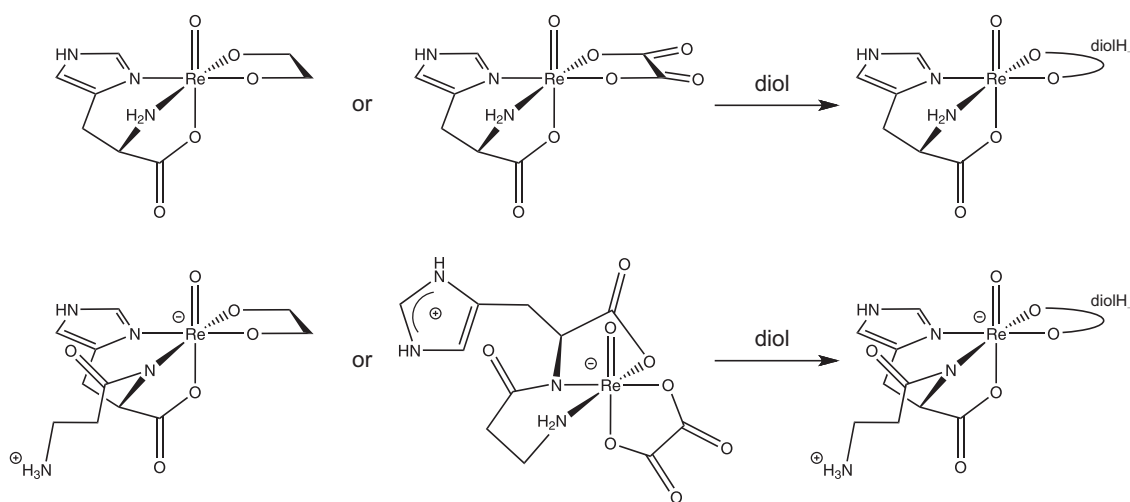


Figure 3.3 Diolate substitution reactions. Above: reactions based on $[\text{ReO}(\text{L-his})(\text{EthdH}_{-2})]$ or $[\text{ReO}(\text{L-his})(\text{ox})]$ (chapter 2.3.5). Below: reactions based on $[\text{ReO}(\text{L-car})(\text{EthdH}_{-2})]$ or $[\text{ReO}(\text{L-car})(\text{ox})]$ (chapter 2.4.7.1). *diol* denotes a furanoidic carbohydrate.

ring-strain as origin of this behavior. As shown on the previous page, the torsion angle range for diols is 1.2° to 47.2° (absolute values). The angles for the ethanediolato and oxalato ligands are near the extreme values of this range ($4-6^\circ$ for oxalate, $37-44^\circ$ for ethanediol), and the successfully substituted ligands adopt values in the mid region: 30° for cytidine and 32° for D-isomaltulose. The torsion angles adopted by furanoses might result in more thermodynamically stable products. The observed hydrolytic stabilities of diolato complexes support this thesis. The diolato ligands of the hydrolytically most stable compounds in this work, **18** and **22**, are both furanoses, and they both adopt a torsion angle of -32.1° . In contrast to this, a pyranose with a torsion angle of 47.2° was found in the compound $[\text{ReO}(\text{dien})(\text{Me-}\beta\text{-D-Xylp}_{2,3\text{H}_{-2}})]\text{I}$, which decomposes in water within minutes^[24].

3.2 NMR spectroscopy

As shown on the previous pages, NMR spectroscopy is a useful tool to study the *syn/anti* isomerism of coordinated diols. In the past, *syn/anti* isomerism was even found for amines connected to the Re=O unit. As reported in 1996, the amino side chains of two diastereomeric aminothiols complexes^[191] were directed toward or away from an Re=O core, and the ¹³C NMR signals differed by up to 10.7 ppm. But generally, there are not many data in the literature about ¹³C NMR shifts of oxido-rhenium(V) complexes, although they are useful for gathering information about the binding mode of the ligands to the metal. The coordination induced shift (CIS, $\delta_{\text{complex}} - \delta_{\text{ligand}}$) of such signals was first reported in 1992 for the catecholato complex [ReO(cat)(PPh₃)₂Cl]^[145]. For this compound, a downfield shift of ca. 20 ppm was found for the signals of the carbon atoms that are adjacent to the coordinated oxygen atoms. Much smaller values were reported for aminothiols complexes^[192]. The signals for the adjacent carbon atoms of coordinated sulfur atoms were shifted 4.9 to 6.8 ppm, while this effect was even smaller in the case of coordinated nitrogen atoms (1.0 to 2.4 ppm). The reason for all these shifts is the deshielding of the carbon atoms caused by the removal of electron density from the adjacent donor atoms to the metal, which is a powerful indicator of the molecular and electronic structure^[145, 192, 193].

In this work, CIS values were observed in a wide range. From -0.8 ppm (for the oxalato complex **9**) to +28.4 ppm (for **1** with cytidine), which is consistent with other reported values for diols^d in a range from +1.1 ppm^e to +31.4 ppm^f. Figure 3.4 illustrates all these data for the adjacent carbon atoms of (O,O) coordinated diols. Separate ranges are to be found for alkoxides (with a CIS of more than ca. 14 ppm) and carboxylates (with a CIS of less than ca. 14 ppm). α -Hydroxy carboxylic acids combine both types, and their signals are roughly in the mid region. Although the origin of this effect is unclear, the electron density and the magnetic shielding of these atoms must be affected. The carbon atoms in question differ in oxidation state and geometry (planar *vs.* tetrahedral).

^d reported by Filser^[189], Grimmingier^[24], Korth^[169], Labisch^[32], Oßberger^[23], Tremaggi^[188].

^e for [(ReO)₂(tpb)₂(Xy1,5A₂H₋₄)] reported by Labisch^[32]

^f for [ReOCl(AnErytH₋₂)(phen)] reported by Oßberger^[23]

3 Discussion

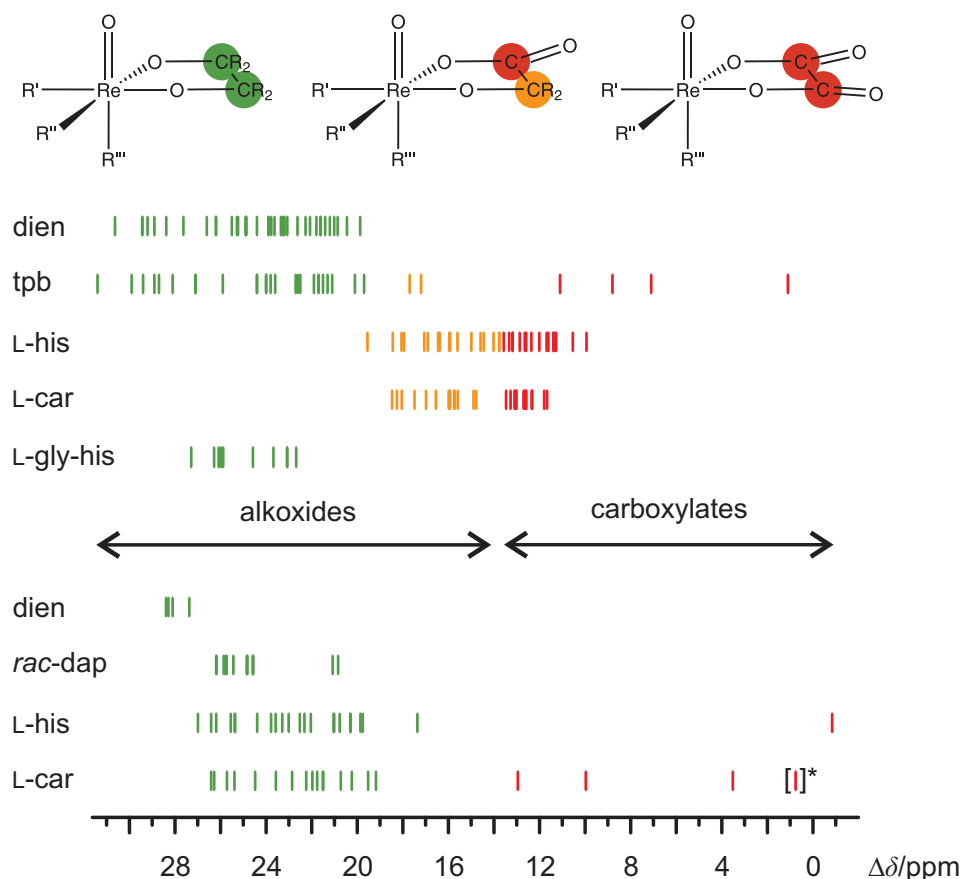


Figure 3.4 ¹³C NMR coordination induced shift values $\Delta\delta = \delta_{\text{complex}} - \delta_{\text{ligand}}$ [ppm] of coordinated diolato groups in oxido-rhenium(V) compounds. On top: the main geometry of all “3 + 2” compounds and reported values for complexes with dien and diols [23, 24], tpb and diols [23, 32] and α -hydroxy carboxylic acids [32], L-his and α -hydroxy carboxylic acids [188], L-car and α -hydroxy carboxylic acids [189], L-gly-his and diols [169]. Below, the respective values for the complexes in this work are shown: dien and diols (chapter 2.1), *rac*-dap and diols (chapter 2.2), L-his with diols and oxalic acid (chapter 2.3), L-car with diols and oxalic acid (chapter 2.4). CIS values of alkoxido carbon atoms are marked green, of α -hydroxy carbon atoms orange and of carboxylic acid carbon atoms red. *differing coordination geometry in the major isomer of **16** in this work: oxygen atom in *trans*-position to the Re=O unit.

All these observations so far correspond to diols that are coordinated in *cis*-position to the Re=O unit. As will be presented in the next chapter, there is a difference in *cis*- and *trans*-positions with respect to the Re=O unit. It is likely that the CIS-values are smaller for ligands in *trans*-position. But the data in the literature are even more scarce for diols or alkoxides in *trans*-position. CIS-values of 8.4 and 9.5 ppm were reported for methoxido ligands in *trans*-position [194, 195]. Most of the “3 + 2” complexes in this work bear the diolato moiety in *cis*-position to the Re=O unit, aside from the oxalato complex [ReO(L-car)(ox)] (**16**). The two species observed in solution showed two coordination modes of oxalate: (*cis*-O,*trans*-O) and (*cis*-O,*cis*-O). The CIS-values of the former coordination mode were much smaller than the values for the latter

mode (3.5/0.8 ppm *vs.* 13.0/10.0 ppm). But strictly speaking, these values are not comparable, as the amino-acid moieties are coordinated via different binding sites. But another functional group was observed repeatedly in *trans*-position. The carboxylato functions of *rac*-dap, L-histidine and L-carnosine were connected *trans* to the Re=O unit. The CIS values for the carbon atoms of these amino acids were in a range from 4.6 to 8.5 ppm. Once again, the values of the above-mentioned isomers of the oxalato complex (**16**) were outstanding from this range (15.1 and 16.0 ppm).

In analogy to the shifts of the oxygen-coordinated groups, the nitrogen-adjacent carbon atoms of the amino acids showed characteristic shifts to lower field, too. The CIS-values were even larger than for the carboxylato functions in *trans*-position. For *rac*-dap, these signals were shifted up to 16.2 ppm, for L-histidine up to 11.5 ppm and for L-carnosine up to 11.6 ppm.

3.3 Structural observations

The main geometrical parameters of the rhenium(V) compounds in this work are summarized in Figure 3.5. The bond distances vary in narrow ranges and all complexes are (distorted) octahedral^g. The atoms of the main molecular axis, defined by the Re=O or Re=NPh units, form an angle of 164° (X-Re-Y, averaged over all). The mean Re=O distances for the complexes with dien (1.66 Å), *rac*-dap (1.68 Å), L-his (1.69 Å) and L-car (1.68 Å) are very similar; they are in a typical range observed for oxido-rhenium(V) complexes^h. They can be regarded as multiple bonds with the participation of strong *dπ-pπ* bonding^[146]. The same holds true for the Re=N bond of the phenylimido-rhenium(V) complexes (1.73 Å). Quantum chemical analyses of the electronic structures of oxido-rhenium(V) complexes showed that the multiple bonds are strongly covalent and the σ - and π -contributions are strongly polarized toward the oxygen atom^[198]. The following distances were proposed in the 1960s, adopted from *Pauling's* radii tableⁱ for typical single, double and triple bonds [Å]: 2.04, 1.86, 1.75 for oxygen^[199] and 2.08, 1.90, 1.79 for nitrogen^[200]. According to these values, the Re=O and Re=N bonds in this work are triple bonds. But they are drawn as double bonds in all schemes in this work, as this presentation is commonly accepted in the literature.

^g Table 6.12 in the Appendix on page 225 gives more details.

^h A statistical study^[196] of metal-oxygen multiple bonds reported for rhenium(V) mono-oxido d^2 complexes a mean value of 1.691(11) Å, and quantum chemical calculations^[197] a value of 1.653 Å.

ⁱ L. Pauling: *The Nature of the Chemical Bond*, 1960, Cornell University Press.

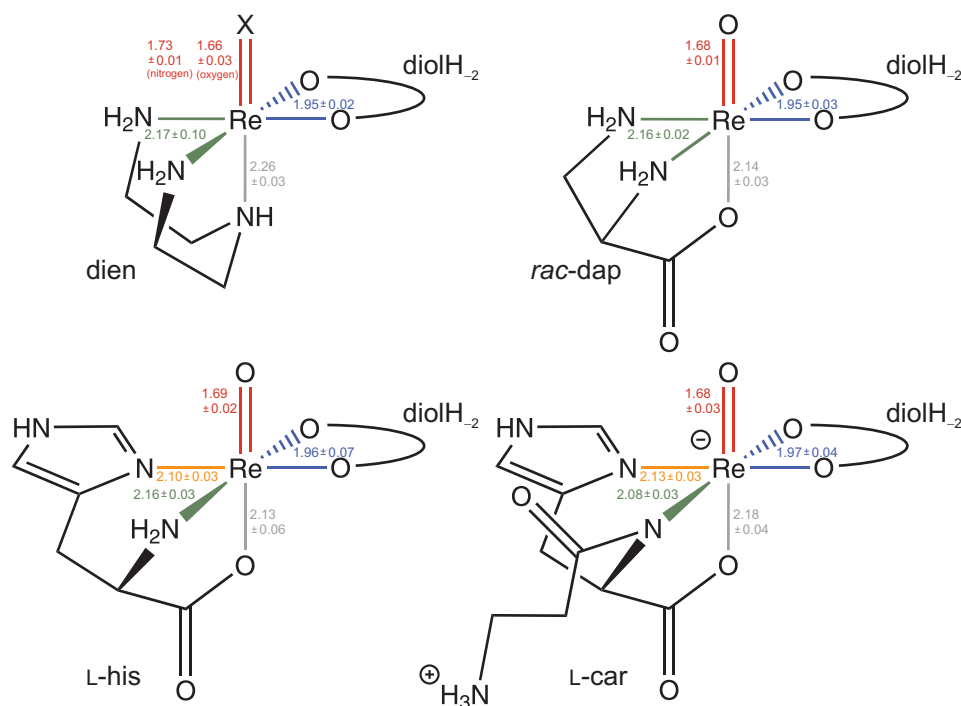


Figure 3.5 Mean bond distances [Å] of the “3 + 2” complexes in this work with the co-ligands dien (1–4), *rac*-dap (6–8), L-his (9–15) and L-car (17–22). The mean values were calculated for the color-coded bonds. X denotes an oxido or phenylimido ligand. [ReO(L-car)(ox)] (16) was excluded due to a different coordination mode.

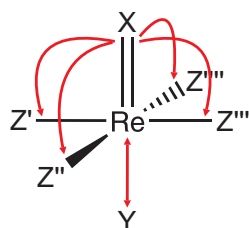
The remaining bonds to the ligands (Re-O and Re-N) are distorted away from the Re=O and Re=N units with angles $> 90^\circ$ (see Table 3.1). The Re-O distances of the diols are in a range from 1.95 to 1.97 Å. As reported in chapter 3.1, the torsion angles of these diols adopt values from -46.0° to $+47.2^\circ$. For symmetrical co-ligands such as *tpb* or *dien*, the distribution of these angles should be statistical. But a tendency for these angles in complexes with enantiopure amino acids was observed. Positive values were observed for L-histidine, negative values for L-carnosine (Table 6.12 on page 225). The reason for this may be a steric hindrance of the side chain or the peptide bond for L-carnosine.

The nitrogen-donor atoms of the co-ligands are connected to the metal cores in a range from 2.08 to 2.16 Å. On closer inspection, a difference between the complexes with L-histidine and L-carnosine becomes apparent. Although this amino acid and its β -alanyl-derivative seem to have similar properties as chelators, their α -amino functions are different. While for complexes with L-histidine, the primary amine is bonded more weakly than the imidazole-nitrogen to the rhenium core, the complexes with L-carnosine differ. The secondary amine of the peptide bond is bonded more strongly to the metal than the imidazole-nitrogen.

3 Discussion

Table 3.1 Structural observations on the compounds in this work. The angles [°] around the oxido ligands (X: O) and the phenylimido ligands (X: NPh) show a distortion of the *cis* ligands away from the Re=O or Re=NPh units, respectively. To illustrate the *trans* influence, the Re-Y distances [Å] of the ligands in *trans* position were compared with compounds, where the ligands are in *cis* position, given as difference [Å].

		X-Re-Z	Re-Y _{trans}	Δ(lit.)
with dien:	1a	112, 110, 94, 89 ^a	2.29(2)	0.2–0.4 ^d
	1b	112, 110, 91, 90 ^a	2.26(2)	0.1–0.4 ^d
	2	109, 109, 93, 92 ^a	2.279(5)	0.14–0.39 ^d
	3	107, 107, 95, 93 ^a	2.239(10)	0.09 ^e
	4	110, 108, 94, 91 ^a	2.240(3)	0.09 ^e
with <i>rac</i> -dap:	6	110, 104, 96, 88 ^a	2.118(3)	0.03–0.11 ^f
	7	109, 107, 92, 92 ^a	2.167(3)	0.08–0.16 ^f
	8	108, 105, 93, 91 ^a	2.131(3)	0.05–0.13 ^f
with L-his:	9	109, 101, 98, 91 ^a	2.113(6)	0.03–0.11 ^f
	10a	111, 104, 95, 94 ^a	2.187(5)	0.10–0.18 ^f
	10b	111, 104, 96, 94 ^a	2.198(5)	0.11–0.19 ^f
	11	113, 104, 96, 93 ^a	2.205(3)	0.12–0.20 ^f
	12a	109, 102, 95, 88 ^a	2.142(3)	0.06–0.14 ^f
	12b	111, 103, 93, 92 ^a	2.092(4)	0.06–0.14 ^f
	13	110, 104, 95, 92 ^a	2.198(5)	0.01–0.09 ^f
	14	108, 106, 95, 92 ^a	2.183(3)	0.10–0.18 ^f
	15	112, 105, 97, 93 ^a	2.194(5)	0.11–0.19 ^f
	with L-car:	16	106, 105, 97, 89 ^a	2.131(6)
17		106, 107, 100, 92 ^b	2.171(3)	0.09–0.17 ^f
18		108, 106, 101, 93 ^b	2.177(7)	0.09–0.17 ^f
19		108, 105, 101, 86 ^b	2.165(7)	0.08–0.16 ^f
20		107, 104, 99, 90 ^b	2.166(4)	0.08–0.16 ^f
21		107, 106, 99, 90 ^b	2.226(5)	0.14–0.22 ^f
22		107, 106, 100, 90 ^b	2.198(2)	0.11–0.19 ^f
other:		26	108, 108, 92, 87 ^c	2.117(3)
	27	111, 102, 95, 87 ^a	2.101(5)	0.02–0.10 ^f



X: O, N
 Y: O_{trans}, N_{trans}
 Z: O_{cis}, N_{cis}

^a smallest angle: X is directed to the amino ligand. ^b smallest angle: X is directed to the imidazole ligand. ^c smallest angle: X is directed to the phosphane ligand. ^d compared with values found in the literature in a range from 1.89–2.14 Å^[20, 23, 39]. ^e compared with **5**. ^f compared with **16** and values found in the literature in a range from 2.00–2.09 Å^[201–203].

The *trans* effect

As a kinetic phenomenon, the *trans* effect was originally observed for square planar complexes (like Cisplatin or its *trans* isomer), where ligands in *trans* position to a certain group are substituted more rapidly. But this effect was also observed for octahedral complexes^[204]. At first glance, the distances of the atoms in *trans*-position to the oxido- (or phenylimido-) ligands in this work seem to be markedly longer than the distances of *cis*-bonded atoms. But as these complexes are heteroleptic, and the atoms belong to different chemical groups (alkoxy *vs.* carboxylato function, primary *vs.* secondary amine), these distances can not be compared directly. Therefore, Table 3.1 gives a correlation with values of ligands of the same type, found in the literature. Even in comparison with these values, a more or less distinctive *trans*-bond elongation is found for the compounds in this work. These observations manifest a structural *trans* influence for the compounds in this work. The reported *trans* influence order for imido and oxido ligands (imido < oxido)^[204] seems to be confirmed. But are these positions bonded more weakly to the metal? Such a kinetic *trans* effect was reported by Cerda *et al.* in 2002 for cyclic voltammetry experiments of glycine, alanine and valine complexes, where the acid groups of these amino acids were reported to behave as left dangling^[205]. But a bond-weakening in terms of a higher substitution rate was not found for the compounds in this work. The sole substitution of a ligand in *trans* position was observed for the substitution reactions with [ReO(L-car)(ox)] (see Figure 3.3 on page 147).

4 Summary

This work deals with coordination compounds of rhenium(V). The combination of an oxido- or phenylimido-rhenium(V) unit with tri- and bidentate chelating ligands resulted in kinetically inert complexes. This so-called “3 + 2” approach^[19] was originally invented by *Chiotellis et al.* in 1999 for oxido-rhenium(V) complexes with amine-dithiol- and phosphanephenol-ligands, forming a $(S,N,S)(P,O)$ donor set connected to a $\{\text{ReO}\}^{3+}$ unit. As presented in this work, alternative donor sets are capable of building stable complexes even with polyfunctional amino acids and carbohydrates.

The first part of this work deals with complexes derived from an $(N,N,N)(O,O)$ donor set (chapter 2.1). (N,N,N) denotes the tridentate co-ligand dien, and (O,O) a carbohydrate with a diolato moiety. In methanol, both oxido-rhenium(V) precursors $[\text{ReO}_2(\text{PPh}_3)_2\text{I}]$ and $[\text{ReOCl}_3(\text{PPh}_3)_2]$ were successfully used to coordinate dien in a *facial* binding mode and the 2',3'-diolato moiety of several nucleosides (adenosine, guanosine, inosine, cytidine, uridine). The complexes were characterized in solution by 2D NMR techniques and in the solid state by X-ray diffraction (**1** with cytidine, **2** with uridine). The isoelectronic phenylimido-rhenium(V) unit is less known for such complexes. Compounds with this motif were investigated starting from the precursor $[\text{Re}(\text{NPh})\text{Cl}_3(\text{PPh}_3)_2]$, which is less reactive than the latter two oxido-rhenium(V) precursors. It was possible, however, to prepare complexes with anhydroerythritol (**3**, **4**) and ethanol (**5**). Generally, the geometry of all these cationic complexes is distorted octahedral and the ligand dien is coordinated *facial* to the rhenium(V) central atom. The latter compound with ethanol is a rare example of a *meridional* binding mode of dien. For all diolato complexes with dien, a strong selectivity towards *cis*-vicinal diolato functions was observed, even in the presence of other functional groups, as they are found in nucleosides. A more-or-less distinctive *syn/anti* isomerism was observed in protic solvents, as there are two possible orientations for coordinated carbohydrates with respect to the main molecule axis. While for the nucleoside complexes **1** and **2** this kind of isomerism was hardly observed, it was possible to crystallize both species with anhydroerythritol (**3**, **4**).

The subsequent chapters deal with compounds derived from (*N,N,O*)(*O,O*) donor sets. The coordination geometry is still distorted-octahedral, but in contrast to the complexes with dien, the overall charge is neutral, as the co-ligands bear an additional negative charge.

In chapter 2.2, complexes are presented with the co-ligand *rac*-dap, which serves as (*N,N,O*) donor. dap is an derivative of the amino acid alanine. It is capable of binding to the rhenium core via the α -, β -amino and carboxylato functions. As the racemic form was used, the reactions with carbohydrates resulted in mixtures of isomeric complexes. The reaction with ethanediol yielded crystals of **6**, in which the two enantiomeric complexes [ReO(D-dap)(EthdH₋₂)] and [ReO(L-dap)(EthdH₋₂)] were both present. A similar result showed the reaction with anhydroerythritol. The crystals of **7** contained the enantiomers [ReO(D-dap)(*syn*-AnErytH₋₂)] and [ReO(L-dap)(*syn*-AnErytH₋₂)]. In addition to these enantiomers, *syn/anti* isomerism was observed in protic solvents, even for redissolved crystals. All in all, these solutions contained four species due to the enantiomeric (D, L) and diastereomeric (*syn*, *anti*) forms. But as non-chiral NMR solvents were used, only two signal sets for the diastereomeric forms were detected in solution at a ratio of about 80:20. Depending on the chirality of the diol, all these species may even be diastereomers. The reaction with the nucleoside cytidine yielded crystals of **8**, containing [ReO(D-dap)(*anti*-Cyd2',3'H₋₂)] and [ReO(L-dap)(*anti*-Cyd2',3'H₋₂)] at about the same ratio. As expected, four signal sets were detected for crystals of **8** in solution.

All the compounds presented so far with the co-ligands dien and *rac*-dap decompose in water within hours or days. A similar behavior was reported for related compounds with dien and other diols^[23,24]. A substantial requirement for the use of such compounds in the field of radiopharmacy, is the hydrolytic stability at physiological conditions, which these compounds only partially meet. A much higher stability was observed for a new class of compounds derived from amino acids and carbohydrates. The chapters 2.3 and 2.4 deal with complexes derived from the amino acid L-histidine and the dipeptide L-carnosine. With this system, it was possible to operate even in aqueous media.

Seven crystalline compounds were prepared which were derived from the amino acid L-histidine and a carbohydrate. The yields were reasonable (in most cases above 50 %) and most of these water soluble complexes were stable against hydrolysis for more than two months. The compounds [ReO(L-his)(ox)] (**9**), [ReO(L-his)(EthdH₋₂)] · 4.5 H₂O (**10**) and [ReO(L-his)(*syn*-AnErytH₋₂)] · 2 H₂O (**11**) were obtained from the reactions with simple diols such as oxalic acid, ethanediol and anhydroerythritol. But even with more complex diols, such as the nucleosides uridine and cytidine,

or the glycosides methyl α -D-mannopyranoside and methyl β -D-ribose, the following compounds were obtained: $[\text{ReO}(\text{L-his})(\text{syn-Urd}2',3'\text{H}_{-2})] \cdot 1.5 \text{ H}_2\text{O}$ (**12**), $[\text{ReO}(\text{L-his})(\text{anti-Cyd}2',3'\text{H}_{-2})] \cdot 5 \text{ H}_2\text{O}$ (**13**), $[\text{ReO}(\text{L-his})(\text{syn-Me-}\alpha\text{-D-Man}p2,3\text{H}_{-2})] \cdot 2 \text{ MeOH}$ (**14**) and $[\text{ReO}(\text{L-his})(\text{syn-Me-}\beta\text{-D-Rib}p3,4\text{H}_{-2})] \cdot 0.5 \text{ MeOH}$ (**15**). In all these chiral compounds (the stereocenters of the ligands were not affected by the reactions), L-histidine is coordinated via N_α of the amino function, N_π of the imidazole ring and O_{CO} of the carboxylato function to the rhenium core. In analogy to the compounds with *rac*-dap, O_{CO} is oriented *trans* to the oxido ligand of the $\{\text{ReO}\}^{3+}$ unit. Apart from **9**, **10** and **11**, all these complexes showed *syn/anti* isomerism in protic solvents. Solely for the ribose-derived compound **15**, even more species were detected in solution. Both *cis*-vicinal diolato functions ($\text{O}2,\text{O}3$ and $\text{O}3,\text{O}4$) were able to coordinate to the metal and an equilibrium was established in solution with **15** as the main species. The most convenient route to prepare all these histidine-based complexes started with the oxido-rhenium(V) precursor $[\text{ReOCl}_3(\text{PPh}_3)_2]$ in methanol at alkaline conditions, similar to the preparations of the complexes with dien or *rac*-dap. An alternative route was developed to synthesize rhenium(V) diolato complexes as well. Starting from **9** and **10**, it was possible to substitute more complex furanoidic carbohydrates for simple ligands like oxalate or ethanediol, even in aqueous media at a pH value of 5. The cytidine complex **13** was prepared according to this approach from the oxalato complex **9**.

The dipeptide L-carnosine is a derivative of the amino acid L-histidine with β -alanine. In analogy to the above given reactions with L-histidine, in a first step the following complexes were prepared with simple diols or nucleosides. Structurally characterized were: $[\text{ReO}(\text{L-car})(\text{ox})] \cdot 2 \text{ H}_2\text{O}$ (**16**) with oxalic acid, $[\text{ReO}(\text{L-car})(\text{EthdH}_{-2})] \cdot \text{MeOH} \cdot \text{H}_2\text{O}$ (**17**) with ethanediol and $[\text{ReO}(\text{L-car})(\text{syn-AdoH}2',3'\text{H}_{-2})] \cdot 3 \text{ MeOH} \cdot 2 \text{ H}_2\text{O}$ (**18**) with adenosine. L-Carnosine was deprotonated on N_α and, as in the free form, the peptide bonds were still planar. In **17** and **18**, it was coordinated via N_α , N_π and O_{CO} to the metal, similar to the complexes with L-histidine. The alanyl moieties were not involved in any bonding to the metal and the β -amino functions were protonated and left dangling. At first glance, these complexes were only a simple variation of the complexes with L-histidine. But in **16**, a different binding mode via N_β of the alanyl part instead of N_π was found in the structure determination. The expected binding mode (like in the histidine complex **9**) was detected only for a minor species in solution. Moreover, the Re-N bond lengths in **17** and **18** deviated from the mean values found for the histidine complexes. The nitrogen atoms N_α at the peptide bonds were about 0.1 Å closer to the central metal than the respective distances for the α -amino functions of L-histidine.

In a second step, the capability of this system to build stable complexes with reducing carbohydrates was tested. At present, the information on coordination compounds with reducing sugars is sparse, which may be caused by the reactivity of these carbohydrates. They are sensitive against oxidation, unstable in alkaline media and overall, they occur as elaborate mixtures of isomeric forms^[8]. Previous work on rhenium(V) with the co-ligands phen, tpb and dien showed that the reactions with monosaccharides do not yield stable compounds, although there were indications for the existence of such complexes^[23, 32]. As shown in this work, the same holds true for reactions with the co-ligand L-histidine. Decomposition was observed for the reactions with monosaccharides, and only in some cases^a the presence of complex species was detected in solution for several hours. Surprisingly, some of these reactions with the co-ligand L-carnosine behaved differently. The reactions with the monosaccharides D-ribose, D-mannose, D-fructose, and even with D-isomaltulose, a disaccharide, yielded crystalline compounds. The resulting complexes, [ReO(L-car)(*syn*- α -D-Ribf1,2H₋₂)] · 3 MeOH (**19**), [ReO(L-car)(*anti*- α / β -D-Manp2,3H₋₂)] · MeOH (**20**), [ReO(L-car)(*anti*- β -D-Fruf2,3H₋₂)] · MeOH (**21**), [ReO(L-car)(*syn*-6-O- α -D-Glcp- β -D-Fruf2,3H₋₂)] · 3 H₂O (**22**), showed, in the cases of **21** and **22**, a high hydrolytic stability at physiological pH. Merely, *syn/anti* isomerism was observed in protic solvents. For **22**, the most stable compound in this series, two alternative reaction routes were developed. As with the previously given substitution reaction of the histidine complex **13** from **9**, it is possible to prepare **22** from **16** in water. But even this route might be disadvantageous for an application to radioactive rhenium, as it requires several reaction steps starting from ¹⁸⁸ReO₄⁻. For this reason, a facile one-pot synthesis was developed for aqueous perrhenate solutions. Usually, tin(II) compounds reduce rhenium(VII) in water directly to rhenium(IV). But in the presence of L-carnosine and D-isomaltulose, intermediate rhenium(V) species seem to be intercepted as **22**. A radiolabeling experiment with the isotope ¹⁸⁸Re showed a radiochemical purity of 86 %, two radiometallated species were detected by HPLC techniques (63 % *syn*-**22** and 23 % *anti*-**22**). Even in this nanomolar concentration range, *syn/anti* isomerism was detected for the product.

The last part of this work deals with compounds that are built with other donor sets. As presented for (HNEt₃)[ReO(ox)₂(PPh₃)] (**23**) and [Re(NPh)(ox)(PPh₃)₂Cl] · MeOH (**24**) with oxalate or [ReO(*syn*-AnErytH₋₂)(MeOH)(PPh₃)Cl] (**25**) with anhydroerythritol, it is possible to prepare carbohydrate complexes without the addition of a co-ligand, but these syntheses are limited to simple diols and require harsh conditions with temperatures of 60 °C and higher. The same holds true for [ReO(L-thr)-

^a D-arabinose, D-xylose, D-ribose and D-fructose

4 Summary

(*syn*-AnErytH₂)(PPh₃)] (**26**). In this complex, the amino acid L-threonine is coordinated bidentately to rhenium(V), while the potential third donor function is left dangling. All these complexes are insoluble in water, as they still contain triphenylphosphane ligands remaining from the precursor compounds. Finally, with a mass of 1.05 kDa the largest complex in this work, [ReO(*fac*-ida)(Ery11,12H₂)] · MeOH · H₂O (**27**), was obtained from iminodiacetic acid and erythromycin, a macrolide antibiotic. As with the compounds with dien, *rac*-dapH, L-histidine and L-carnosine, this complex is built in analogy to the “3 + 2” approach^[19] with iminodiacetate as tridentate (O,N,O) donor and erythromycin enolether as (O,O) donor.

It is concluded that the concomitant coordination of amino acids and carbohydrates on a rhenium(V) core is a very flexible and versatile approach. The compounds in this work are promising candidates for future work in the field of radiopharmacy. In particular, the reactions with the dipeptide L-carnosine showed some as yet unknown attributes of the chemistry of rhenium(V) including a high regioselectivity. They resulted in thermodynamic stable complexes, even with reducing carbohydrates in aqueous media.

5 Experimental Part

5.1 Common working techniques

Reactions with non-radioactive rhenium were carried out with magnetic stirring under normal air conditions and standard laboratory glassware. Preparative work with the radioactive isotope ^{188}Re was done in collaboration with M. Coporda and F.-J. Gildehaus at the Department of Nuclear Medicine at the Klinikum Großhadern of the LMU Munich. ^{188}Re was purchased from ITM (Isotopen Technologien München AG) in Garching.

5.2 Analytical methods

NMR spectroscopy:

The spectra were recorded on the following machines by Jeol: Eclipse 270, ECX 400, Eclipse 400, Eclipse 500. Data processing was done with the Jeol Delta^[206] Software. ^1H NMR and ^{13}C NMR signals were assigned by routine ^1H - ^1H -COSY45, DEPT135, ^1H - ^{13}C -HMQC and ^1H - ^{13}C -HMBC experiments.

Mass spectroscopy: Jeol JMS 700, method: FAB⁺, matrix: NBA or glycerine

IR spectroscopy: Nicolet 520 FT-IR

pH measurement: Mettler Toledo MP 220

HPLC: Agilent 1100 Liquid Chromatograph. Column: Nucleosil[®] 100-5 C18 4.0 · 250 mm with pre-column 4.0 · 20 mm, eluent: acetonitrile/water, pressure: 190–240 bar, detector: Berthold gamma ray counter.

X-ray diffraction:

Crystals suitable for X-ray diffraction were selected using a microscope (Leica MZ6 with polarization filters), covered with liquid paraffin and mounted on the tip of a glass fiber with Lithelen[®] grease. The measurements were done with the following diffractometers: Enraf-Nonius Kappa-CCD with rotating anode or STOE-IPDS with imaging plate technology and sealed tube anode. Both are equipped with Oxford-Cryostream cooling system and graphite-monochromated Mo- K_α radiation. One measurement was done on an Oxford XCalibur 3 diffractometer. The structures were

5 Experimental Part

solved using direct methods with the program SIR-97^[207]. SHELXL-97^[208] was used to refine them by full-matrix, least-squares refinement against $F_o^2 - F_c^2$. Distances and angles were calculated with the program PLATON^[209]. Intermolecular contacts were analyzed with the programs PLATON^[209] and MERCURY^[210]. Molecular graphics were performed with the programs ORTEP^[211], SCHAKAL^[212] and MERCURY^[210]. Further details on the structures are listed in the Appendix, Tables 6.2–6.11. The values given there are defined as follows:

$$R(F) = \frac{\sum ||F_o| - |F_c||}{\sum |F_o|} \quad (5.1)$$

$$R_{\text{int}} = \frac{\sum |F_o^2 - \langle F_o \rangle^2|}{\sum F_o^2} \quad (5.2)$$

$$wR(F^2) = \sqrt{\frac{\sum w(F_o^2 - F_c^2)^2}{\sum w(F_o^2)^2}} \quad (5.3)$$

$$S = \sqrt{\frac{\sum \frac{w(F_o^2 - F_c^2)^2}{N_{\text{hkl}} - N_{\text{parameter}}}}{N_{\text{hkl}} - N_{\text{parameter}}}} \quad (5.4)$$

the weighting factors w and P are defined as follows:

$$w = \frac{1}{\sigma^2(f_o^2) + (xP)^2 + yP} \quad (5.5)$$

$$P = \frac{\max(F_o^2, 0) + 2F_c^2}{3} \quad (5.6)$$

In analogy to SHELXL-97^[208], the values of the parameters x and y were adopted to minimize the variance of $w(F_c^2/F_o^2)$ for several (intensity-ordered) groups of reflexes.

The coefficient U_{eq} is defined as:

$$U_{\text{eq}} = \frac{1}{3} \left(\sum_{i=1}^3 \sum_{j=1}^3 U_{ij} a_i a_j a_i^* a_j^* \right) \quad (5.7)$$

5.3 Reagents and solvents

acetone	≥ 99.5 %	Fluka
acetic acid	99.8 %	Riedel-de Haën
adenosine	99.0 %	Fluka
ammonium perrhenate	99+ %	ABCR
anhydroerythritol	-	[213, 214]
aniline	99+ %	Acros
benzene	≥ 99.5 %	Merck
L-carnosine	≥ 99 %	Fluka
copper(II) nitrate trihydrate	> 98 %	Fluka
cytidine	≥ 99.0 %	Fluka
<i>rac</i> -2,3-diaminopropionic acid monohydrochloride	≥ 99.0 %	Fluka
deuterium oxide	99.9 %	Aldrich
diethylenetriamine	≥ 97.0 %	Fluka
diethyl ether	≥ 99 %	Fluka
dimethylsulfoxide-d ₆	99.8 %	euriso-top
erythromycin hydrate	96 %	Aldrich
1,2-ethanediol	≥ 99.5 %	Fluka
ethanol	≥ 99.8 %	Fluka
D-fructose	≥ 99.8 %	Fluka
L-histidine	≥ 99.0 %	Fluka
hydrochloric acid	37 %	Merck
hydroiodic acid	55–58 %	Fluka
iminodiacetic acid	> 99 %	Fluka
D-isomaltulose	-	Südzucker
D-mannose	> 99 %	Fluka
methanol	≥ 99.9 %	Biesterfeld Graën
methanol-d ₄	99.8+ %	Aldrich
methyl α-D-mannopyranoside	≥ 99.0 %	Fluka
methyl β-D-ribosepyranoside	99.1 %	Glycon
oxalic acid	≥ 99.0 %	Fluka
1,10-phenanthroline	99+ %	Aldrich
D-ribose	≥ 99.0 %	Fluka

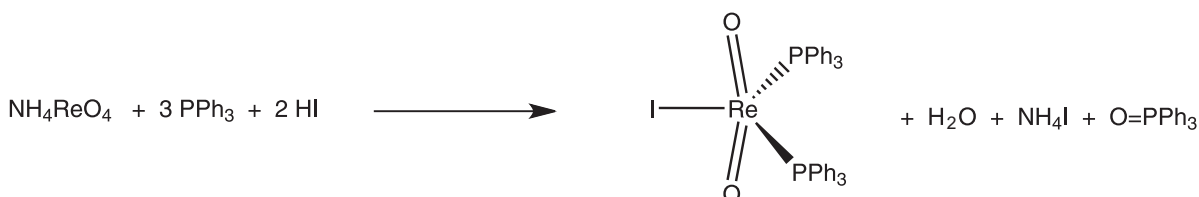
5 Experimental Part

sodium oxalate	≥ 99.0 %	Fluka
sodium tetraphenylborate	≥ 99.0 %	Fluka
L-threonine	98 %	Aldrich
tin(II) oxalate	95 %	ABCR
toluene	≥ 99.0 %	Fluka
triethylamine	≥ 99.5 %	Fluka
triphenylphosphane	~ 99.0 %	Fluka
uridine	≥ 99.0 %	Fluka
water	de-ionized ^a	

^ahouse installation with ion exchange resin

5.4 Preparation of the precursor compounds

5.4.1 Iodido-dioxido-bis(triphenylphosphane)-rhenium(V)

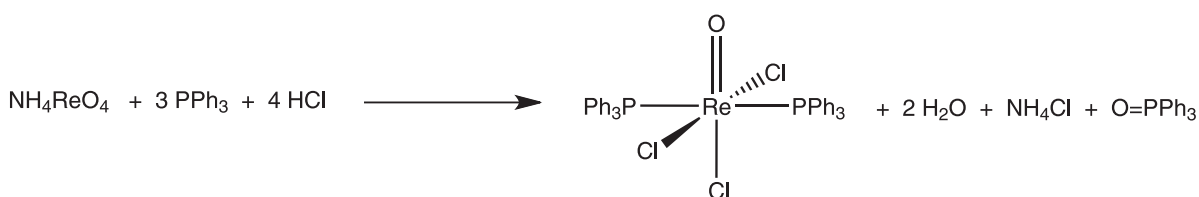


Literature: G. F. Ciani, G. D'Alfonso, P. Romiti, A. Sironi, M. Freni, *Inorg. Chim. Acta* **1983**, 72, 29–37.

At room temperature ammonium perrhenate (1.00 g, 3.73 mmol) and triphenylphosphane (5.24 g, 20.00 mmol) were stirred in ethanol (50 mL). 56 % hydroiodic acid (5.00 mL, 37.88 mmol) was added carefully and the brown mixture was heated under reflux for 1/2 h. The obtained olive-green solid was filtered off and washed twice with ethanol and diethylether. Without further drying this compound and a mixture of water (6 mL) and acetone (150 mL) were stirred in an ice bath for 1 h. A violet compound deposited, which was filtered off and dried *in vacuo*.

Yield:	2.53 g (78 %) of a dark-violet solid
Empirical formula, M_r/gmol⁻¹:	C ₃₆ H ₃₀ IO ₂ P ₂ Re, 869.69
IR (KBr, cm⁻¹):	$\nu = 921$ (s, Re=O)
Elemental analysis (%):	
calcd. for C ₃₆ H ₃₀ IO ₂ P ₂ Re, 869.69:	C 49.72, H 3.48
found:	C 49.13, H 3.45

5.4.2 Trichlorido-oxido-*trans*-bis(triphenylphosphane)-rhenium(V)



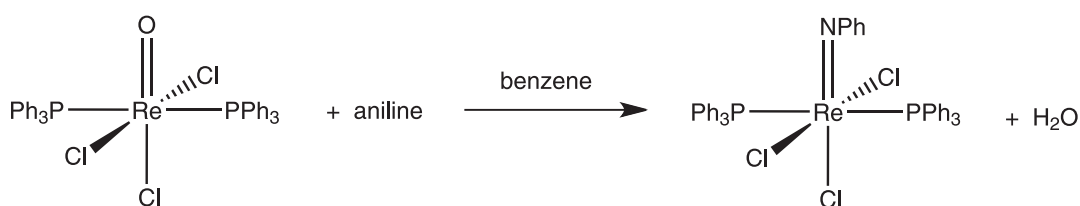
Literature: J. Chatt, G. A. Rowe, *J. Chem. Soc.* **1962**, 4019–4033.

Ammonium perrhenate (2.68 g, 10.00 mmol) and 37 % hydrochloric acid (20 mL) were heated in ethanol (100 mL) under reflux until the perrhenate was dissolved. A solution of triphenylphosphane (15.74 g, 60.00 mmol) in hot ethanol (40 mL at 60 °C)

was added and immediately the clear solution turned into a green-yellow suspension. After 1/2 h of reflux, a yellow solid was filtered off and washed twice with hot ethanol and acetone.

Yield:	7.50 g (90 %) of a yellow solid
Empirical formula, M_r/gmol⁻¹:	C ₃₆ H ₃₀ Cl ₃ O ₂ P ₂ Re, 833.15
Elemental analysis (%)	
calcd. for C ₃₆ H ₃₀ Cl ₃ OP ₂ Re, 833.15:	C 51.90, H 3.63, Cl 12.77
found:	C 52.02, H 3.66, Cl 12.35

5.4.3 Trichlorido-phenylimido-*trans*-bis(triphenylphosphane)-rhenium(V)



Literature: J. Chatt, J. D. Garforth, N. P. Johnson, G. A. Rowe, *J. Chem. Soc.* **1964**, 1012–1020.

Trichlorido-oxido-*trans*-bis(triphenylphosphane)-rhenium(V) (8.33 g, 10.00 mmol, see 5.4.2 on page 163) and aniline (1.00 g, 10.08 mmol) were refluxed in benzene (500 mL) for 18 h. The brown solution was evaporated to 50 mL. Addition of aqueous acetic acid (1:1, 100 mL) gave a green solid, which was recrystallized from benzene.

Yield:	4.60 g (53 %) of a green solid
Empirical formula, M_r/gmol⁻¹:	C ₄₂ H ₃₅ Cl ₃ N ₂ P ₂ Re, 908.26
Elemental analysis (%)	
calcd. for C ₄₈ H ₄₁ Cl ₃ NP ₂ Re =	
[M + C ₆ H ₆]:	C 58.45, H 4.19, N 1.42
found:	C 58.41, H 4.22, N 1.41
MS (FAB⁺, NBA) m/z	
calcd. for C ₄₂ H ₃₅ Cl ₃ NP ₂ Re:	907.1 [M] ⁺ , 872.1 [M – Cl] ⁺
found:	906.9, 872.0
	(each with a characteristic Re ₁ pattern)

5.5 Preparation of the crystalline compounds

5.5.1 [ReO(*fac*-dien)(*syn*-Cyd2',3'H₋₂)]I (1)



At room temperature cytidine (243 mg, 1.00 mmol) and iodido-dioxido-bis(triphenylphosphane)-rhenium(V) (348 mg, 0.40 mmol) were stirred in methanol (50 mL). After addition of diethylenetriamine (41 mg, 0.40 mmol) in methanol (5 mL) within 5 min, the mixture was kept stirring for 2 h. The solution was evaporated to 5 mL and a lilac compound was filtered off. **1** was recrystallized from methanol within two days at room temperature.

Yield, properties:

52 % of a lilac solid. A solution of 50 mg in 5 mL water (pH 6.5 at 23.9 °C) decomposes within 2 h.

IR (KBr, cm⁻¹):

$\nu = 973.2$ (s, Re=O)

Elemental analysis (%)

calcd. for C₁₃H₂₄IN₆O₆Re = [M + I]:

C 23.18, H 3.59, N 12.48, I 18.84

found:

C 23.09, H 3.82, N 12.29, I 19.07

MS (FAB⁺, NBA) *m/z*

calcd. for C₁₃H₂₄N₆O₆Re = [M]⁺:

547.1

found:

547.2 with a characteristic Re₁ pattern

NMR (MeOH-d₄):

¹³C NMR: Table 2.2 on page 18,

¹H NMR: Table 2.3 on page 18.

5.5.2 [ReO(*fac*-dien)(*syn*-Urd2',3'H₋₂)]BPh₄ · MeOH (2)



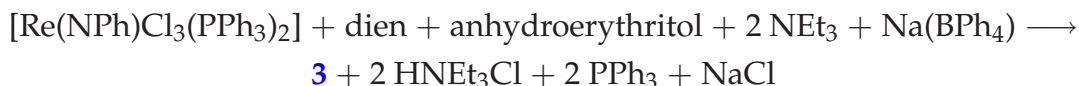
A suspension of uridine (244 mg, 1.00 mmol) and iodido-dioxido-bis(triphenylphosphane)-rhenium(V) (348 mg, 0.40 mmol) was stirred at room temperature in methanol (50 mL). Then a solution of diethylenetriamine (41 mg, 0.40 mmol) in methanol

5 Experimental Part

(5 mL) was added within 5 min and the mixture was stirred for 2 h. The solution was evaporated to 5 mL, the lilac raw product was filtered off and recrystallized from methanol. Suitable crystals of **2** for X-ray diffraction were obtained within one week at 4 °C by addition of sodium tetraphenylborate (136 mg, 0.40 mmol).

Yield:	55 % of a lilac solid
IR (KBr, cm^{-1}):	$\nu = 969.6$ (s, Re=O)
Elemental analysis (%)	
calcd. for $\text{C}_{13}\text{H}_{23}\text{IN}_5\text{O}_7\text{Re} = [\text{M} + \text{I}]$:	C 23.15, H 3.44, N 10.38, I 18.82
found:	C 23.31, H 3.49, N 10.39, I 19.01
MS (FAB ⁺ , NBA) m/z	
calcd. for $\text{C}_{13}\text{H}_{23}\text{N}_5\text{O}_7\text{Re} = [\text{M}]^+$:	548.1
found:	548.2 with a characteristic Re_1 pattern
NMR (D_2O):	^{13}C NMR: Table 2.5 on page 22, ^1H NMR: Table 2.6 on page 23.

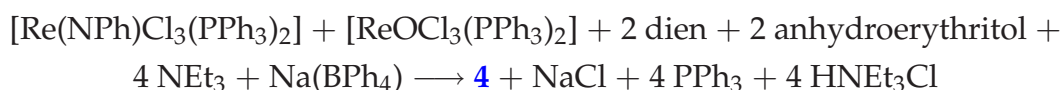
5.5.3 [Re(NPh)(*fac*-dien)(*syn*-AnErytH₋₂)]BPh₄ (**3**)



Over the course of 3 h the phenylimido-rhenium complex trichlorido-phenylimido-*trans*-bis(triphenylphosphane)-rhenium(V) (364 mg, 0.40 mmol) was stirred with anhydroerythritol (84 mg, 1.60 mmol), diethylenetriamine (82 mg, 0.80 mmol) and triethylamine (212 mg, 1.60 mmol) in ethanol (250 mL) at 50 °C. Within this period of time the suspension turned into a greenish solution. Then the volume was evaporated to 20 mL and sodium tetraphenylborate (136 mg, 0.40 mmol) was added. Over night at room temperature green crystals of **3** were obtained.

Yield:	<1 % of green platelets
MS (FAB ⁺ , NBA) m/z	
calcd. for $\text{C}_{14}\text{H}_{24}\text{N}_4\text{O}_3\text{Re} = [\text{M}]^+$:	483.1
found:	483.4 with a characteristic Re_1 pattern

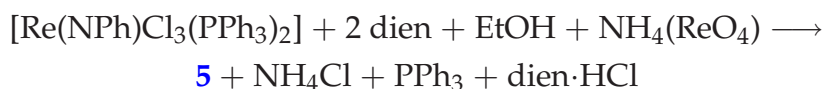
5.5.4 [Re(NPh)(*fac*-dien)(*anti*-AnErytH₋₂)] [ReO(*fac*-dien)(*anti*-AnErytH₋₂)] [BPh₄]Cl (4)



The rhenium(V) precursor compounds trichlorido-phenylimido-*trans*-bis(triphenylphosphane)-rhenium(V) (364 mg, 0.40 mmol) and trichlorido-oxido-*trans*-bis(triphenylphosphane)-rhenium(V) (333 mg, 0.40 mmol) were stirred under reflux with anhydroerythritol (84 mg, 1.60 mmol), diethylenetriamine (82 mg, 0.80 mmol) and triethylamine (212 mg, 1.60 mmol) in methanol (250 mL). After stirring for 3 h at 65 °C the suspension turned into a greenish-brown solution. The reaction mixture was evaporated to 20 mL and sodium tetraphenylborate (340 mg, 1.00 mmol) was added. Within one month at room temperature green crystals of **4** were obtained.

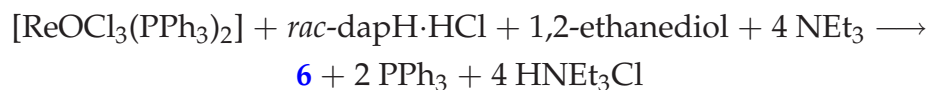
Yield: <1 % of green platelets

5.5.5 [Re(NPh)(*mer*-dien)(OEt)(PPh₃)] [ReO₄]Cl · EtOH · 0.5 Me₂CO (5)



The phenylimido-rhenium(V) precursor trichlorido-phenylimido-*trans*-bis(triphenylphosphane)-rhenium(V) (908 mg, 1.00 mmol) was stirred with diethylenetriamine (102 mg, 1.00 mmol) in ethanol (250 mL). The green mixture turned into a green-brown solution while stirring for 3 h at 60 °C. Then the mixture was concentrated *in vacuo* to 50 mL and ammonium perrhenate (268 mg, 1.00 mmol) was added. Overlaying with acetone provided green crystals of **5** at room temperature over night.

Yield: <1 % of green platelets

5.5.6 [ReO(*rac*-dap)(EthdH₋₂)] · MeOH (6)

Under reflux trichlorido-oxido-*trans*-bis(triphenylphosphane)-rhenium(V) (833 mg, 1.00 mmol) was stirred with 1,2-ethanediol (124 mg, 2.00 mmol), *rac*-2,3-diaminopropionic acid monohydrochloride (141 mg, 1.00 mmol) and triethylamine (405 mg, 4.00 mmol) in methanol (250 mL). While stirring for 3 h at 65 °C the yellow suspension turned into a brown solution which then was evaporated to 30 mL. Over night at room temperature dark-violet crystals of **6** were obtained.

Yield, properties:

48 mg (13 %) of dark-violet crystals. A solution of 25 mg in 2 mL water (pH 4.7 at 27.4 °C) decomposes within 3 h.

Elemental analysis (%)

calcd. for C₆H₁₅N₂O₆Re = [M + MeOH]: C 18.13, H 3.80, N 7.05

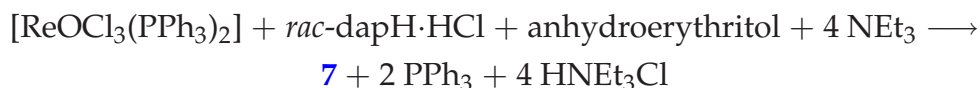
found: C 18.09, H 3.78, N 7.03

MS (FAB⁺, glycerine) *m/z*

calcd. for C₅H₁₂N₂O₅Re = [M + H]⁺: 367.0

found: 367.2 with a characteristic Re₁ pattern

¹³C NMR (101 MHz, D₂O): see Table 2.12 on page 40

5.5.7 [ReO(*rac*-dap)(*syn*-AnErytH₋₂)] · H₂O (7)

Trichlorido-oxido-*trans*-bis(triphenylphosphane)-rhenium(V) (833 mg, 1.00 mmol), anhydroerythritol (208 mg, 2.00 mmol), *rac*-2,3-diaminopropionic acid monohydrochloride (141 mg, 1.00 mmol) and triethylamine (405 mg, 4.00 mmol) were stirred under reflux in methanol (250 mL). After 3 h at 65 °C the yellow suspension turned

into a brown solution, which was concentrated *in vacuo* to 30 mL. Over night at ambient temperature a dark-violet powder was obtained and recrystallized from methanol/water (10:1) to give crystals of **7**.

Yield, properties: 220 mg (54 %) of dark-violet crystals. A solution in pure water decomposes within 3 h.

Elemental analysis (%)

calcd. for $C_7H_{13}N_2O_6Re$, 407.40: C 20.64, H 3.22, N 6.88

found: C 20.55, H 3.02, N 6.77

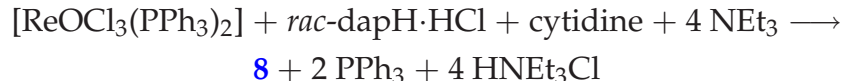
MS (FAB⁺, NBA) *m/z*

calcd. for $C_7H_{14}N_2O_6Re = [M + H]^+$: 409.0

found: 409.3 with a characteristic Re_1 pattern

¹³C NMR (67.9 MHz, D₂O): see Table 2.14 on page 44

5.5.8 [ReO(*rac*-dap)(*anti*-Cyd2',3'H₋₂)] · 2 H₂O (**8**)

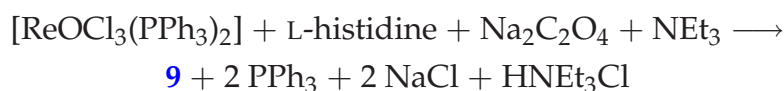


A suspension of cytidine (486 mg, 2.00 mmol), *rac*-2,3-diaminopropionic acid monohydrochloride (141 mg, 1.00 mmol), triethylamine (405 mg, 4.00 mmol) and trichlorido-oxido-*trans*-bis(triphenylphosphane)-rhenium(V) (833 mg, 1.00 mmol) was stirred in methanol (250 mL). After 3 h at 65 °C the yellow suspension turned into a brown solution, which was concentrated *in vacuo* to 30 mL. Dark-violet crystals of **8** were obtained over night at room temperature.

Yield, properties: 98 mg (18 %) of dark-violet crystals. A solution of 50 mg in 5 mL water (pH 5.5 at 24.4 °C) is stable for several days.

Elemental analysis (%)calc. for C₁₂H_{20.3}N₅O_{9.15}Re =[M + 1.15 H₂O]: C 25.41, H 3.61, N 12.35

found: C 25.58, H 3.76, N 12.15

MS (FAB⁺, NBA) *m/z*calc. for C₁₂H₁₉N₅O₈Re = [M + H]⁺: 548.1found: 548.3 with a characteristic Re₁ pattern¹³C NMR (101 MHz, D₂O): see Table 2.16 on page 49**5.5.9 [ReO(L-his)(ox)] (9)**

A suspension of trichlorido-oxido-*trans*-bis(triphenylphosphane)-rhenium(V) (833 mg, 1.00 mmol), sodium oxalate (268 mg, 2.0 mmol), L-histidine (155 mg, 1.0 mmol) and triethylamine (505 mg, 5.00 mmol) in methanol (250 mL) was stirred under reflux for 1 h. The yellow suspension turned into a blue suspension. The blue raw product was filtered off and washed with methanol/water (1:1) and acetone. **9** was recrystallized from boiling methanol/water.

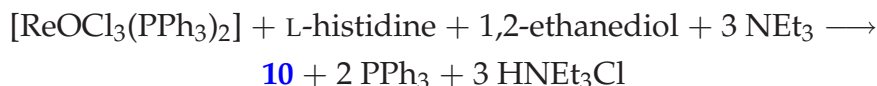
Yield, properties:

401 mg (90 %) of a blue solid. A solution of 50 mg in 5 mL water (pH 2.8 at 23.4 °C) is stable for several days.

Elemental analysis (%)calc. for C_{9.5}H₁₁N₃O_{7.5}Re =[M + 0.5 C₃H₆O]: C 24.10, H 2.34, N 8.88

found: C 24.29, H 2.20, N 9.43

MS (FAB⁺, NBA) *m/z*calc. for C₈H₉N₃O₇Re = [M + H]⁺: 446.0found: 446.3 with a characteristic Re₁ pattern¹³C NMR (67.9 MHz, DMSO-d₆): see Table 2.18 on page 56

5.5.10 [ReO(L-his)(EthdH₋₂)] · 4.5 H₂O (10)

1,2-ethanediol (124 mg, 2.00 mmol), L-histidine (155 mg, 1.00 mmol), triethylamine (303 mg, 3.00 mmol) and trichlorido-oxido-*trans*-bis(triphenylphosphane)-rhenium(V) (833 mg, 1.00 mmol) were stirred in methanol (250 mL). After heating under reflux for 4 h at 50 °C the yellow suspension turned into a blue solution, which was evaporated to dryness. The remaining blue solid was redissolved in water (10 mL) and blue crystals of **10** formed within one night at room temperature.

Yield, properties:

246 mg (59 %) of a blue solid. A solution of 50 mg in 5 mL water (pH 5.8 at 23.8 °C) is stable for more than a week.

Elemental analysis (%)

calc. for C₈H₁₂N₃O₅Re, 416.41:

C 23.08, H 2.90, N 10.09

found:

C 23.36, H 3.05, N 9.99

MS (FAB⁺, NBA) *m/z*

calc. for C₈H₁₃N₃O₅Re = [M + H]⁺:

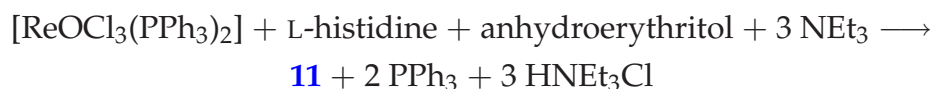
418.0

found:

418.1 with a characteristic Re₁ pattern

¹³C NMR (67.9 MHz, D₂O):

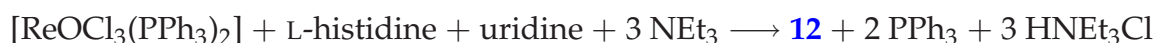
see Table 2.20 on page 61

5.5.11 [ReO(L-his)(*syn*-AnErytH₋₂)] · 2 H₂O (11)

A mixture of anhydroerythritol (208 mg, 2.00 mmol), L-histidine (155 mg, 1.00 mmol) and triethylamine (303 mg, 3.00 mmol) was stirred with trichlorido-oxido-*trans*-bis(triphenylphosphane)-rhenium(V) (833 mg, 1.00 mmol) in methanol (250 mL). After 2 h at 60 °C the yellow suspension turned into a blue solution, which was evaporated to dryness. The remaining blue solid was redissolved in water (10 mL). At room temperature blue crystals of **11** formed within one night.

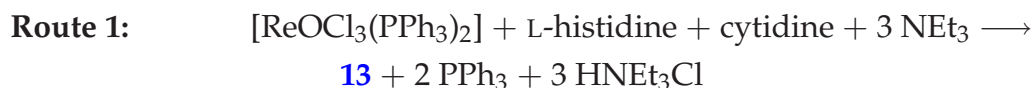
Yield, properties:	142 mg (31 %) of a blue solid. A solution of 25 mg in 2 mL water (pH 6.8 at 24.1 °C) is stable for more than two months.
Elemental analysis (%)	
calc. for C ₁₀ H ₁₄ N ₃ O ₆ Re, 458.4:	C 26.20, H 3.08, N 9.17
found:	C 26.31, H 3.14, N 9.12
MS (FAB⁺, glycerine) <i>m/z</i>	
calc. for C ₁₀ H ₁₅ N ₃ O ₆ Re = [M + H] ⁺ :	460.1
found:	460.3 with a characteristic Re ₁ pattern
¹³ C NMR (67.9 MHz, D ₂ O):	see Table 2.22 on page 65

5.5.12 [ReO(L-his)(*syn*-Urd2',3'H₋₂)] · 1.5 H₂O (12)



Uridine (488 mg, 2.0 mmol), L-histidine (155 mg, 1.00 mmol), triethylamine (303 mg, 3.00 mmol) and trichlorido-oxido-*trans*-bis(triphenylphosphane)-rhenium(V) (833 mg, 1.00 mmol) were stirred in methanol (250 mL). The yellow suspension turned into a blue solution after 2 h at 50 °C. The solution was evaporated to dryness and the remaining blue powder was washed with acetone and stirred with water (10 mL) at 50 °C for 5 min. After filtration blue crystals of **12** formed within one night at room temperature.

Yield, properties:	293 mg (49 %) of a blue solid. A solution of 50 mg in 5 mL water (pH 5.2 at 22.3 °C) is stable for more than two months.
Elemental analysis (%)	
calc. for C ₁₅ H ₂₁ N ₅ O _{10.5} Re = [M + 1.5 H ₂ O]:	C 28.80, H 3.38, N 11.19
found:	C 28.68, H 3.40, N 11.16
MS (FAB⁺, glycerine) <i>m/z</i>	
calc. for C ₁₅ H ₁₉ N ₅ O ₉ Re = [M + H] ⁺ :	600.1
found:	600.3 with a characteristic Re ₁ pattern
¹³ C NMR (67.9 MHz, DMSO-d ₆):	see Table 2.24 on page 70

5.5.13 [ReO(L-his)(*anti*-Cyd2',3'H₋₂)] · 5 H₂O (**13**)

Cytidine (486 mg, 2.0 mmol), L-histidine (155 mg, 1.00 mmol), triethylamine (303 mg, 3.00 mmol) and trichlorido-oxido-*trans*-bis(triphenylphosphane)-rhenium(V) (833 mg, 1.00 mmol) were stirred in methanol (250 mL) for 3 h at 50 °C. After the yellow suspension turned into a blue solution, the solvent was removed *in vacuo*. The remaining blue powder was washed with acetone and recrystallized from boiling methanol.

Yield, properties: 335 mg (56 %) of a blue solid. A solution of 50 mg in 5 mL water (pH 6.4 at 21.7 °C) is stable for more than two months.

Elemental analysis (%)

calc. for C₁₇H₂₇N₆O₁₀Re =

[M + 2 MeOH]: C 30.86, H 4.11, N 12.70

found: C 31.23, H 3.96, N 12.88

MS (FAB⁺, glycerine) *m/z*

calc. for C₁₅H₂₀N₆O₈Re = [M + H]⁺: 599.1

found: 599.3 with a characteristic Re₁ pattern

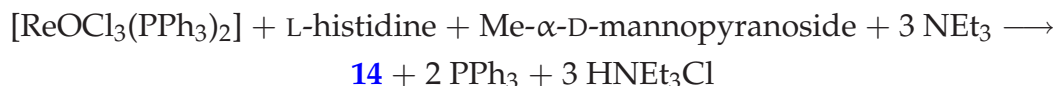
¹³C NMR (67.9 MHz, D₂O): see Table 2.26 on page 74



The rhenium(V) compound [ReO(L-his)(ox) (444 mg, 1.00 mmol, see section 5.5.9 on page 170) was stirred with cytidine (486 mg, 2.00 mmol) in water (10 mL). After 30 min at room temperature the suspension was heated within 1 min. to 60 °C and filtrated. The blue solution was stored at room temperature and within 1 day blue crystals of **13** were formed.

Yield: <1 % of blue crystals

cell data of X-ray analysis and ¹³C NMR data are consistent with the data of Route 1.

5.5.14 [ReO(L-his)(*syn*-Me- α -D-Manp2,3H₋₂)] · 2 MeOH (14)

A mixture of methyl α -D-mannopyranoside (388 mg, 2.0 mmol), L-histidine (155 mg, 1.00 mmol), triethylamine (303 mg, 3.00 mmol) and trichlorido-oxido-*trans*-bis(triphenylphosphane)-rhenium(V) (833 mg, 1.00 mmol) was stirred in methanol (250 mL). After heating for 2 h at 50 °C the yellow suspension turned into a blue solution. Then the volume was reduced *in vacuo* to 30 mL. A blue powder of **14** was filtered off and recrystallized from methanol.

Yield, properties:

340 mg (62 %) of a blue solid. A solution of 50 mg in 5 mL water (pH 3.2 at 25.3 °C) is stable for more than two months.

Elemental analysis (%)

calc. for C₁₄H₂₄N₃O₁₀Re = [M + MeOH]: C 28.96, H 4.17, N 7.24

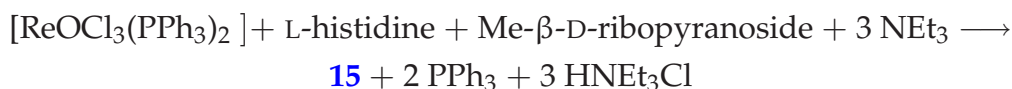
found: C 29.13, H 4.23, N 7.46

MS (FAB⁺, glycerine) *m/z*

calc. for C₁₃H₂₁N₃O₉Re = [M + H]⁺: 550.1

found: 550.4 with a characteristic Re₁ pattern

¹³C NMR (67.9 MHz, D₂O): see Table 2.28 on page 78

5.5.15 [ReO(L-his)(*syn*-Me- β -D-Ribp3,4H₋₂)] · 0.5 MeOH (15)

Methyl β -D-ribosepyranoside (328 mg, 2.00 mmol), L-histidine (155 mg, 1.00 mmol), triethylamine (303 mg, 3.00 mmol) and trichlorido-oxido-*trans*-bis(triphenylphosphane)-rhenium(V) (833 mg, 1.00 mmol) were stirred in methanol (100 mL). After 3 h at 60 °C the yellow suspension turned into a blue solution. The solvent was removed *in vacuo* and the remaining blue solid was recrystallized from a mixture of methanol (10 mL) and water (1 mL). At room temperature blue crystals of **15** formed within 3 days.

Yield, properties: 21 mg (4 %) of a blue solid. A solution of 25 mg in 2 mL water (pH 6.8 at 25.0 °C) is stable for more than two months.

Elemental analysis (%)

calc. for $C_{12}H_{22}N_3O_{10}Re =$

$[M + 2 H_2O]:$

C 25.99, H 4.00, N 7.58

found:

C 26.02, H 4.01, N 7.61

MS (FAB⁺, NBA) *m/z*

calc. for $C_{12}H_{19}N_3O_8Re = [M + H]^+:$

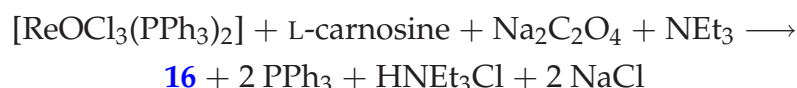
520.1

found:

520.3 with a characteristic Re_1 pattern

¹³C NMR (101 MHz, D₂O):

see Table 2.30 on page 83

5.5.16 [ReO(L-car)(ox)] · 2 H₂O (16)

Sodium oxalate (268 mg, 2.00 mmol), L-carnosine (226 mg, 1.00 mmol), triethylamine (101 mg, 1.00 mmol) and trichlorido-oxido-*trans*-bis(triphenylphosphane)-rhenium(V) (833 mg, 1.00 mmol) were stirred in methanol (500 mL). After 2 h at 50 °C the yellow suspension turned into a blue-violet solution, which was filtered to remove any remaining reactants. The filtrate was evaporated to dryness and the remaining blue powder was washed with methanol/water (1:1) and acetone at room temperature. **16** was recrystallized from boiling methanol/water (1:1).

Yield, properties: 247 mg (48 %) of a blue solid. A solution of 21 mg in 2.5 mL water (pH 4.1 at 23.0 °C) is stable for months.

Elemental analysis (%)calc. for C₁₁H₁₃N₄O₈Re, 515.45:

C 25.63, H 2.54, N 10.87

found:

C 25.64, H 2.74, N 10.87

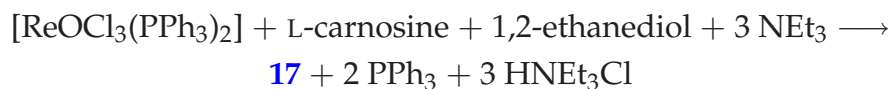
MS (FAB⁺, glycerine) *m/z*calc. for C₁₁H₁₄N₄O₈Re = [M + H]⁺:

517.0

found:

517.4 with a characteristic Re₁ pattern¹³C NMR (101 MHz, D₂O):

see Table 2.32 on page 91

5.5.17 [ReO(L-car)(EthdH₋₂)] · MeOH · H₂O (17)

1,2-Ethanediol (124 mg, 2.00 mmol), L-carnosine (226 mg, 1.00 mmol), triethylamine (303 mg, 3.00 mmol) and trichlorido-oxido-*trans*-bis(triphenylphosphane)-rhenium(V) (833 mg, 1.00 mmol) were stirred in methanol (100 mL). After 3 h at 50 °C the yellow suspension turned into a blue solution. Any remaining reactants were filtered off and the solution was evaporated to dryness. The blue solid was washed with boiling acetone and recrystallized in a mixture of methanol (10 mL) and water (1 mL). At room temperature blue crystals of **17** formed within two days.

Yield, properties:

<1 % of blue crystals. A solution of 15 mg in 2.5 mL water (pH 4.3 at 23.0 °C) decomposes within 1 day.

Elemental analysis (%)calc. for C₁₄H₂₅N₄O₇Re =[M + *i*-propanol]:

C 30.71, H 4.60, N 10.23

found:

C 30.63, H 4.60, N 10.49

MS (FAB⁺, NBA) *m/z*calc. for C₁₁H₁₈N₄O₆Re = [M + H]⁺:

489.1

found:

489.0 with a characteristic Re₁ pattern¹³C NMR (67.9 MHz, D₂O):

see Table 2.34 on page 95

5.5.18 [ReO(L-car)(*syn*-AdoH_{2'},3'H₋₂)] · 3 MeOH · 2 H₂O (18)

A suspension of adenosine (534 mg, 2.0 mmol), L-carnosine (226 mg, 1.00 mmol), triethylamine (303 mg, 3.00 mmol) and trichlorido-oxido-*trans*-bis(triphenylphosphane)-rhenium(V) (833 mg, 1.00 mmol) was stirred in methanol (250 mL). After 2 h at 50 °C the yellow suspension turned into a blue solution. The volume was reduced *in vacuo* to 30 mL and water (5 mL) was added. At ambient temperature blue crystals of **18** formed within one night.

Yield, properties:

173 mg (25 %) of a blue solid. A solution of 50 mg in 5 mL water (pH 5.3 at 23.8 °C) is stable for more than two months.

Elemental analysis (%)

calc. for C_{19.7}H₂₉N₉O_{9.8}Re =

[M + 1.1 H₂O + 0.7 MeOH]:

C 32.20, H 3.98, N 17.15

found:

C 32.19, H 3.97, N 17.16

MS (FAB⁺, NBA) *m/z*

calc. for C₁₉H₂₅N₉O₈Re = [M + H]⁺:

694.1

found:

693.6 with a characteristic Re₁ pattern

¹³C NMR (101 MHz, DMSO-d₆):

see Table 2.36 on page 100

5.5.19 [ReO(L-car)(*syn*-α-D-Ribf_{1,2}H₋₂)] · 3 MeOH (19)

A suspension of D-ribose (300 mg, 2.00 mmol), L-carnosine (226 mg, 1.00 mmol), triethylamine (303 mg, 3.00 mmol) and trichlorido-oxido-*trans*-bis(triphenylphosphane)-rhenium(V) (833 mg, 1.00 mmol) was stirred in methanol (500 mL). After continued stirring for 2 days at room temperature, the yellow suspension turned partially into a blue solution. The remaining reactants were filtered off and the volume was reduced *in vacuo* to 50 mL. To obtain the raw product, *iso*-propanol (50 mL) was added and a

grey deposit was filtered off and recrystallized from methanol. At room temperature blue crystals of **19** formed within three days on the surface of a filter paper projecting outside the liquid.

Yield, properties: <1 % of blue crystals. A solution of 25 mg in 2.5 mL water (pH 3.6 at 23.2 °C) decomposes within hours.

Elemental analysis (%)

calc. for C₁₆H₂₉N₄O₁₁Re =

[M + 2 MeOH]:

C 30.04, H 4.57, N 8.76

found:

C 30.20, H 4.40, N 8.71

MS (FAB⁺, glycerine) *m/z*

calc. for C₁₄H₂₂N₄O₉Re = [M + H]⁺:

577.1

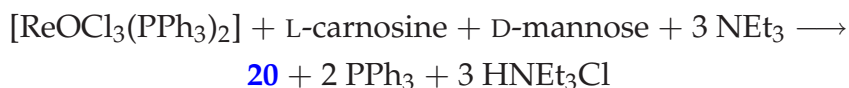
found:

577.0 with a characteristic Re₁ pattern

¹³C NMR (101 MHz, D₂O):

see Table 2.38 on page 104

5.5.20 [ReO(L-car)(*anti*-α/β-D-Manp2,3H₂)] · MeOH (**20**)



D-Mannose (360 mg, 2.00 mmol), L-carnosine (226 mg, 1.00 mmol), triethylamine (303 mg, 3.00 mmol) and trichlorido-oxido-*trans*-bis(triphenylphosphane)-rhenium(V) (833 mg, 1.00 mmol) were stirred in methanol (250 mL). Over night at room temperature the yellow suspension turned blue. A blue powder was filtered off and recrystallized in MeOH/H₂O (10 mL).

Yield, properties: 448 mg (74 %) of a blue solid. A solution of 28 mg in 5 mL water (pH 5.3 at 22.4 °C) decomposes within one week.

Elemental analysis (%)

calc. for $C_{16}H_{27}N_4O_{11}Re = [M + MeOH]$: C 30.14, H 4.27, N 8.79

found: C 29.94, H 4.34, N 8.73

MS (FAB⁺, glycerine) *m/z*

calc. for $C_{15}H_{24}N_4O_{10}Re = [M + H]^+$: 607.1

found: 607.6 with a characteristic Re_1 pattern

¹³C NMR (126 MHz, DMSO-d₆): see Table 2.40 on page 108

5.5.21 [ReO(L-car)(*anti*-β-D-Fruf_{2,3}H₋₂)] · MeOH (21)

D-Fructose (360 mg, 2.00 mmol) was stirred with L-carnosine (226 mg, 1.00 mmol), triethylamine (303 mg, 3.00 mmol) and trichlorido-oxido-*trans*-bis(triphenylphosphane)-rhenium(V) (833 mg, 1.00 mmol) in methanol (250 mL). Over night at room temperature the yellow suspension turned into a blue solution. The solvent was removed *in vacuo* and the remaining blue powder was redissolved in MeOH/H₂O (10 mL). At room temperature blue crystals of **21** formed within three days on the surface of a filter paper projecting outside the liquid.

Yield, properties:

230 mg (38 %) of a blue solid. A solution of 27 mg in 2.5 mL water (pH 7.3 at 22.3 °C) is stable for more than a week.

Elemental analysis (%)

calc. for $C_{16}H_{27}N_4O_{11}Re = [M + MeOH]$: C 30.14, H 4.27, N 8.79

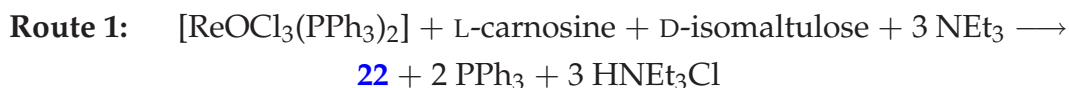
found: C 30.19, H 4.23, N 8.70

MS (FAB⁺, glycerine) *m/z*

calc. for $C_{15}H_{24}N_4O_{10}Re = [M + H]^+$: 607.1

found: 607.5 with a characteristic Re_1 pattern

¹³C NMR (67.9 MHz, D₂O, DMSO-d₆): see Table 2.42 on page 113

5.5.22 [ReO(L-car)(*syn*-6-O- α -D-Glcp- β -D-Fruf2,3H₂)] · 3 H₂O (**22**)

D-Isomaltulose (684 mg, 2.00 mmol), L-carnosine (226 mg, 1.00 mmol), triethylamine (303 mg, 3.00 mmol) and trichlorido-oxido-*trans*-bis(triphenylphosphane)-rhenium(V) (833 mg, 1.00 mmol) were stirred in methanol (250 mL). The yellow suspension turned into a blue solution over night at room temperature. The solvent was removed *in vacuo* and the remaining blue powder was recrystallized in MeOH/H₂O (10 mL).

Yield, properties: 407 mg (53 %) of a blue solid. A solution of 25 mg in 2.5 mL water (pH 5.8 at 23.4 °C) is stable for more than two months.

Elemental analysis (%)

calc. for C₂₂H₃₈N₄O₁₆Re = [M + MeOH]: C 33.00, H 4.78, N 7.00

found: C 32.82, H 4.91, N 7.01

MS (FAB⁺, glycerine) *m/z*

calc. for C₂₁H₃₅N₄O₁₅Re = [M + H]⁺: 770.2

found: 769.6 with a characteristic Re₁ pattern

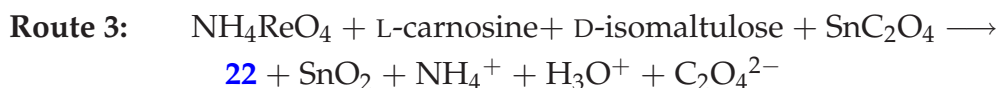
UV/VIS: λ_{\max} = 604 nm

¹³C NMR (67.9 MHz, D₂O): see Table 2.44 on page 117

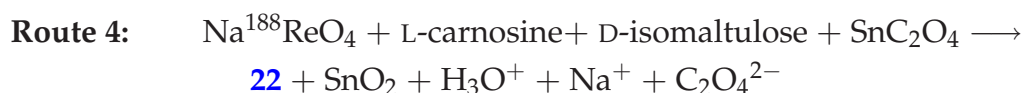


The rhenium(V) compound [ReO(L-his)(ox)] (444 mg, 1.00 mmol, see section 5.5.9 on page 170) was stirred with D-isomaltulose (684 mg, 2.00 mmol) in water (10 mL). After 30 min at room temperature the suspension was heated to 60 °C within one minute and filtrated. The blue solution was stored at room temperature and within 1 day blue crystals of **22** were formed. The cell data of X-ray analysis and ¹³C NMR data were consistent with the data of Route 1.

5 Experimental Part



Ammonium perrhenate (268 mg, 1.00 mmol), L-carnosine (226 mg, 1.00 mmol) and D-isomaltulose (684 mg, 2.00 mmol) were stirred at room temperature in water (5 mL). A suspension of tin(II) oxalate (827 mg, 4.00 mmol) in water (5 mL) was added. After stirring over night the suspension was filtered and a ^{13}C NMR spectrum of the blue solution was recorded, the results were consistent with the data of Route 1.



As given in the following table, the respective amounts of L-carnosine, D-isomaltulose and tin(II) oxalate were stirred under argon at 60 °C with degassed water and eluate (0.9 % saline) taken from a $^{188}\text{W}/^{188}\text{Re}$ generator containing the rhenium isotope with an activity of 1.0 GBq. After filtration the solution still contained 97 % of the total activity. It was purified and analyzed by HPLC. The radiochromatogram of the third experiment is depicted on page 119.

L-carnosine	226 mg (1.00 mmol)	23 mg (0.10 mmol)	2.3 mg (0.01 mmol)	0.7 mg (0.003 mmol)
D-isomaltulose	513 mg (1.50 mmol)	50 mg (0.15 mmol)	50 mg (0.15 mmol)	1.0 mg (0.003 mmol)
tin(II) oxalate	412 mg (2.00 mmol)	41 mg (0.20 mmol)	41 mg (0.20 mmol)	0.7 mg (0.003 mmol)
solvent (total)	7.0 mL	0.9 mL	0.5 mL	1.8 mL
time	85 min	90 min, 120 min	130 min	60 min
HPLC result	26 %	62 %, 82 %	86 %	4 %

5.5.23 (HNEt₃)[ReO(ox)₂(PPh₃)] (23)

A suspension of oxalic acid (360 mg, 4.00 mmol), triethylamine (405 mg, 4.00 mmol) and trichlorido-oxido-*trans*-bis(triphenylphosphane)-rhenium(V) (833 mg, 1.00 mmol) was stirred in methanol (100 mL) for 3 h at 60 °C. The mixture was evaporated to 20 mL and over night at ambient temperature violet crystals of **23** were obtained.

Yield: <1 % of violet crystals

5.5.24 [Re(NPh)(ox)(PPh₃)₂Cl] · MeOH (24)

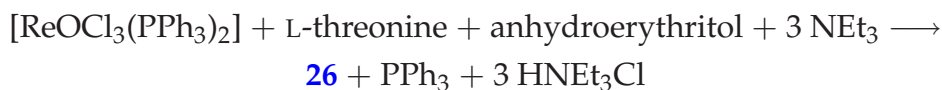
Oxalic acid disodium salt (268 mg, 2.00 mmol) was stirred with trichlorido-phenyl-imido-*trans*-bis(triphenylphosphane)-rhenium(V) (908 mg, 1.00 mmol) in methanol (250 mL) for 3 h at 60 °C. Within this period of time the green suspension turned into a brown solution. Then the volume was reduced *in vacuo* to 30 mL. Over night at room temperature green crystals of **24** were obtained.

Yield: <1 % of green crystals

5.5.25 [ReO(*syn*-AnErytH₋₂)(MeOH)(PPh₃)Cl] (25)

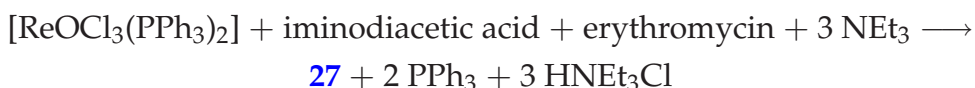
Anhydroerythritol (5.00 mL, 6.35 g, 61.0 mmol) was heated with trichlorido-oxido-*trans*-bis(triphenylphosphane)-rhenium(V) (416 mg, 0.50 mmol) without any further solvent for 3 min at 100 °C. The hot mixture was cooled to room temperature and heated once again with methanol (20 mL) to 60 °C. Over night at ambient temperature violet crystals of **25** were obtained.

Yield: <1 % of violet crystals

5.5.26 [ReO(L-thr)(*syn*-AnErytH₋₂)(PPh₃)] (26)

Anhydroerythritol (208 mg, 2.00 mmol), L-threonine (155 mg, 1.00 mmol), triethylamine (303 mg, 3.00 mmol) and trichlorido-oxido-*trans*-bis(triphenylphosphane)-rhenium(V) (833 mg, 1.00 mmol) were stirred under reflux in methanol (100 mL). After 3 h at 60 °C the yellow suspension turned into a violet solution. The solvent was removed *in vacuo* and the remaining brown precipitate recrystallized in boiling methanol (10 mL). At room temperature green crystals of **26** formed within 1 day.

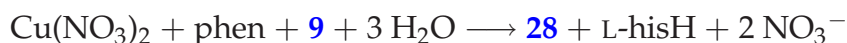
Yield:	<1 % of green crystals
Elemental analysis (%)	
calc. for C ₂₆ H ₂₉ NO ₇ Pre, 684.70:	C 45.61, H 4.27, N 2.05
found:	C 45.59, H 4.14, N 2.00
MS (FAB⁺, NBA) <i>m/z</i>	
calc. for C ₂₆ H ₃₀ NO ₇ Pre = [M + H] ⁺ :	686.1
found:	686.3 with a characteristic Re ₁ pattern

5.5.27 [ReO(*fac*-ida)(Emy_{11,12}H₋₂)] · MeOH · H₂O (27)

Erythromycin (1.101 g, 1.50 mmol), iminodiacetic acid (133 mg, 1.00 mmol), triethylamine (405 mg, 4.00 mmol) and trichlorido-*trans*-oxido-bis(triphenylphosphane)-rhenium(V) (833 mg, 1.00 mmol) were refluxed in methanol (250 mL). After 3 h at 60 °C the yellow suspension turned into a brown solution. The volume was reduced *in vacuo* to 30 mL and violet crystals of **27** were obtained over night at room temperature from this solution.

Yield:	<1 % of violet crystals
Elemental analysis (%)	
calc. for $C_{41}H_{69}N_2O_{17}Re =$	
[M + MeOH + 0.4 H ₂ O]:	C 46.39, H 6.84, N 2.58
found:	C 46.39, H 6.85, N 2.59
MS (FAB⁺, NBA) <i>m/z</i>	
calc. for $C_{41}H_{70}N_2O_{17}Re = [M + H]^+$:	1049.4
found:	1049.8 with a characteristic Re ₁ pattern

5.5.28 [Cu₂(phen)₂(ox)(ReO₄)₂]_{*n*} (**28**)



The rhenium(V) compound [ReO(L-his)(ox)] (444 mg, 1.00 mmol, see section 5.5.9 on page 170) was stirred with 1,10-phenanthroline (180 mg, 1.00 mmol) and Cu(NO₃)₂ · 3 H₂O (241 mg, 1.00 mmol) in acetonitrile (50 mL). After stirring for 30 min at 60 °C the suspension was filtered. From the remaining green-blue solution green crystals of **28** formed within one week at room temperature.

Yield:	<1 % of green crystals
---------------	------------------------

6 Appendix

6.1 Packing diagrams of the crystal structures

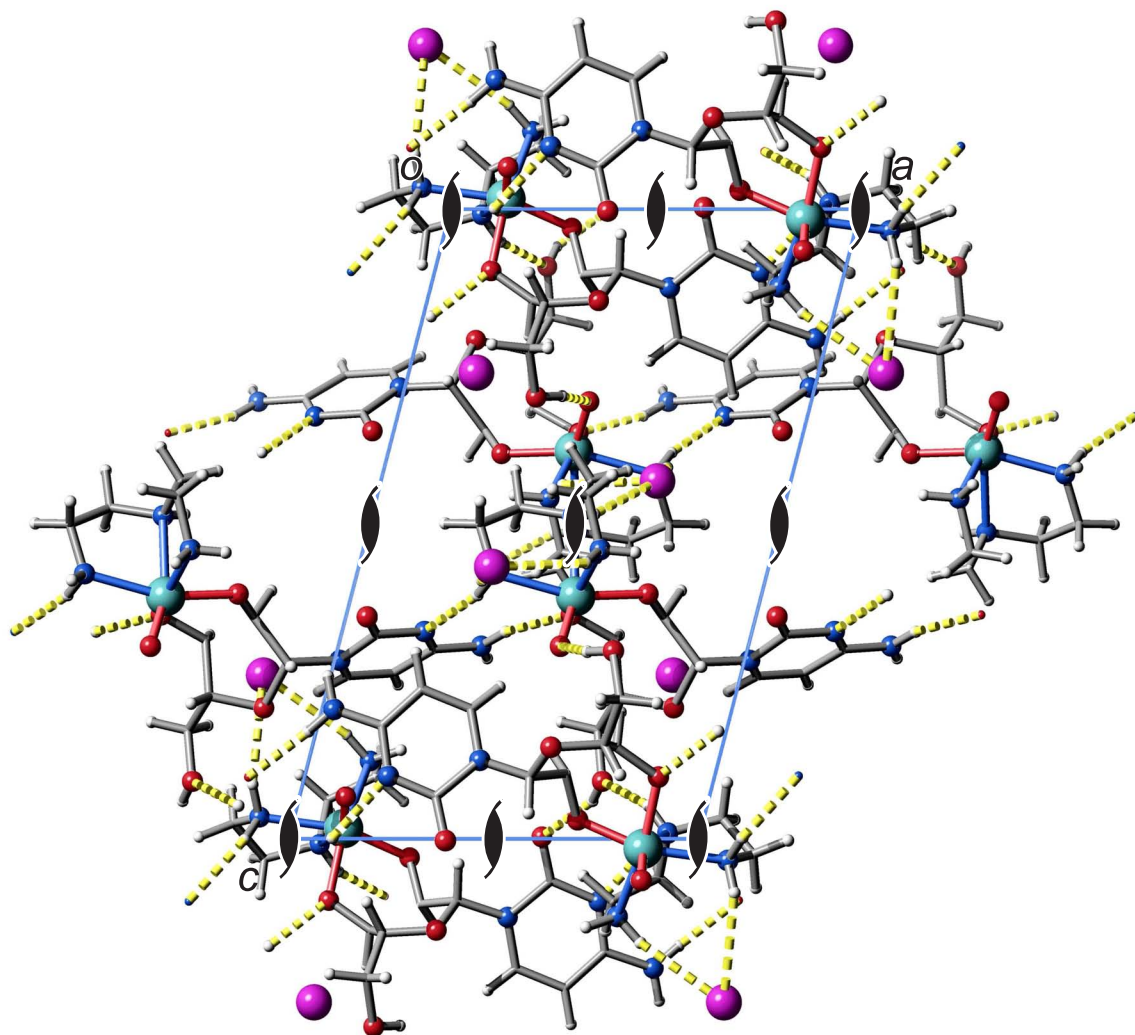


Figure 6.1 SCHAKAL packing diagram of **1** viewed along $[0\bar{1}0]$. Hydrogen bonds are indicated by yellow dashed lines. The symmetry elements of the space group $P2_1$ are overlaid. Atoms: carbon (grey, wireframe), hydrogen (light grey, small), nitrogen (blue, large), iodine (purple, large), oxygen (red, large), rhenium (dark cyan, large).

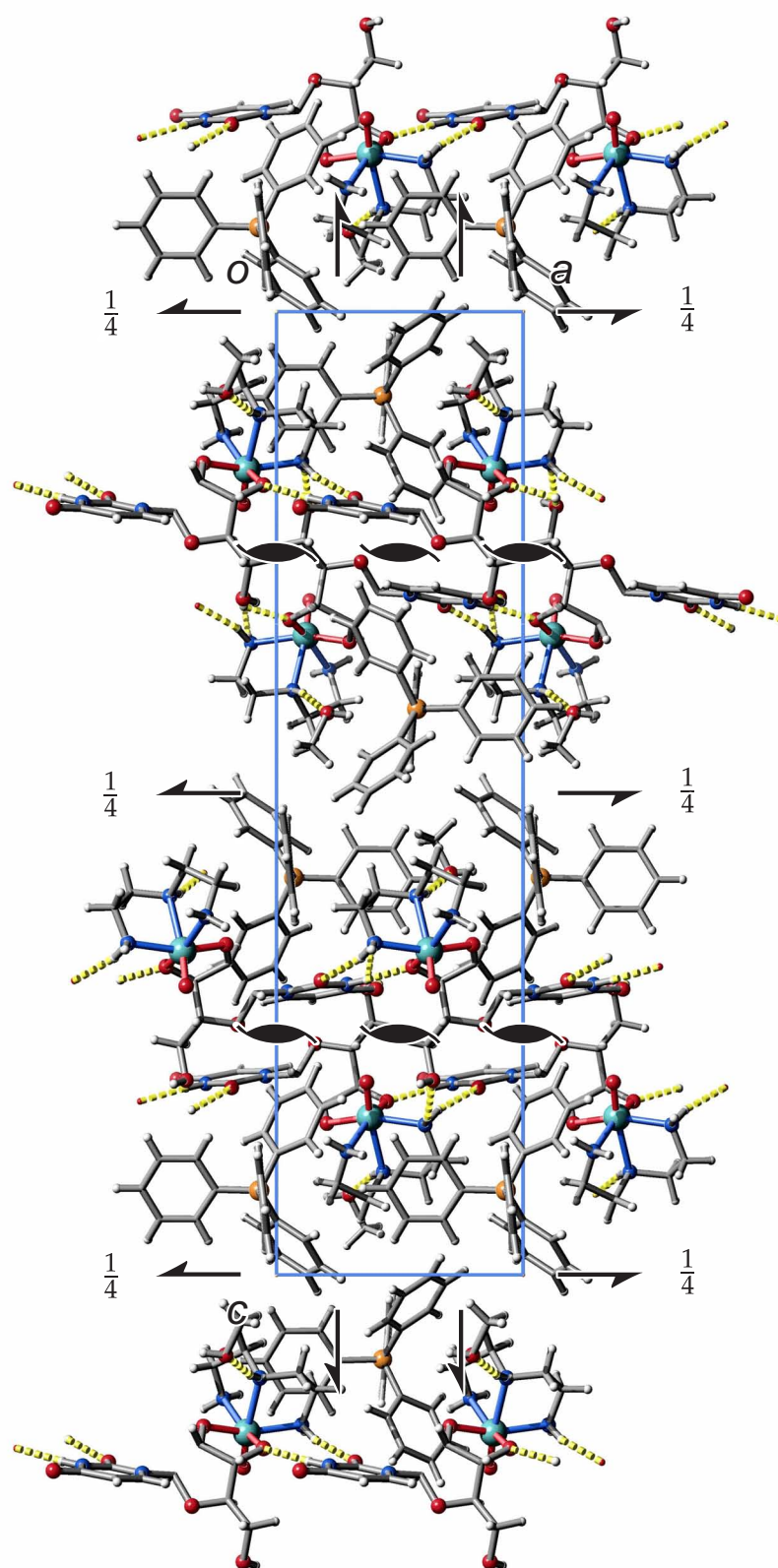


Figure 6.2 SCHAKAL packing diagram of **2** viewed along $[0\bar{1}0]$. Hydrogen bonds are indicated by yellow dashed lines. The symmetry elements of the space group $P2_12_12_1$ are overlaid. Atoms: carbon (grey, wireframe), hydrogen (light grey, small), boron (orange, large), nitrogen (blue, large), oxygen (red, large), rhenium (dark cyan, large).

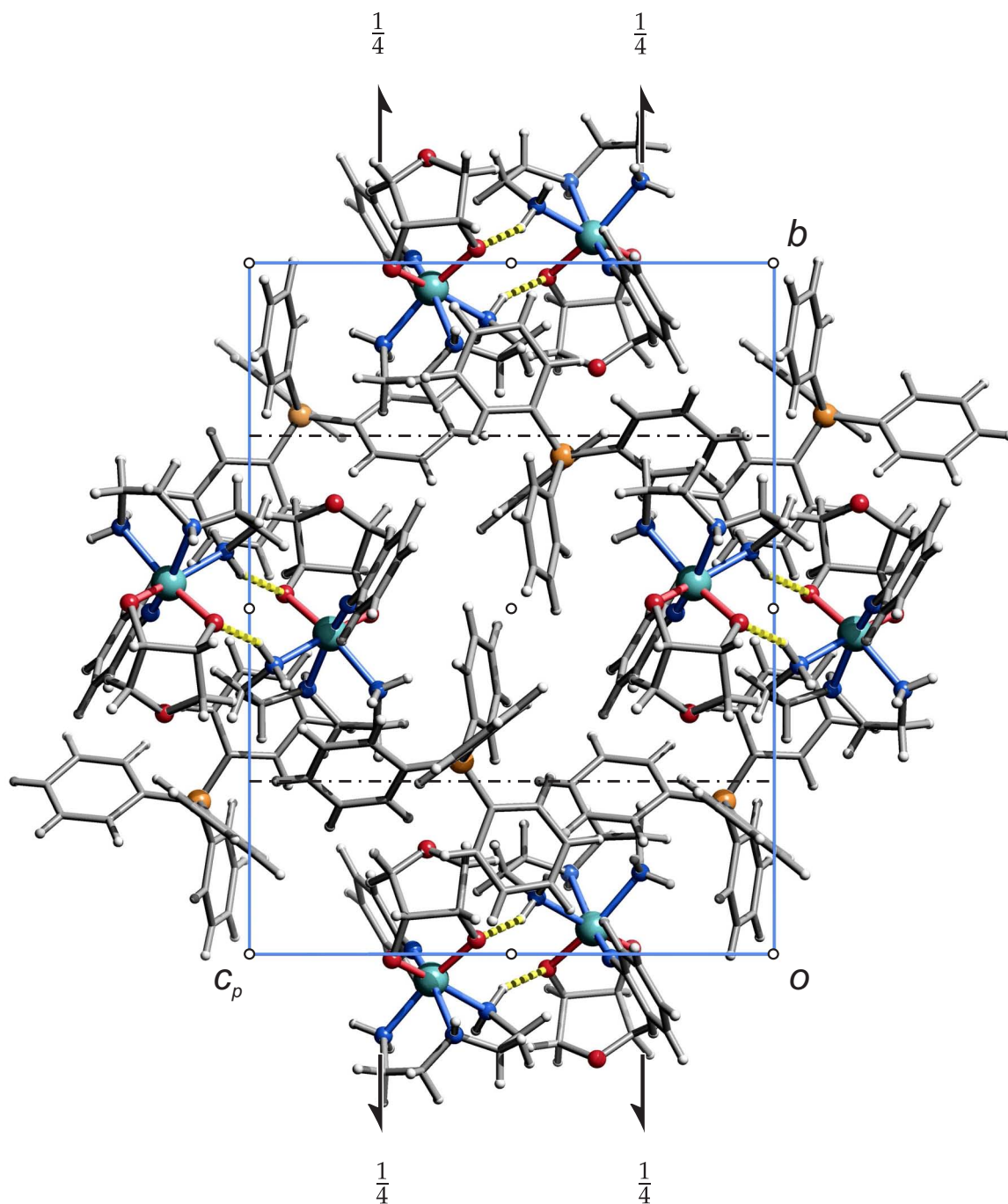


Figure 6.3 SCHAKAL packing diagram of **3** viewed along $[\bar{1}00]$. Hydrogen bonds are indicated by yellow dashed lines. The symmetry elements of the space group $P2_1/n$ are overlaid. Atoms: carbon (grey, wireframe), hydrogen (light grey, small), nitrogen (blue, large), oxygen (red, large), boron (orange, large), rhenium (dark cyan, large).

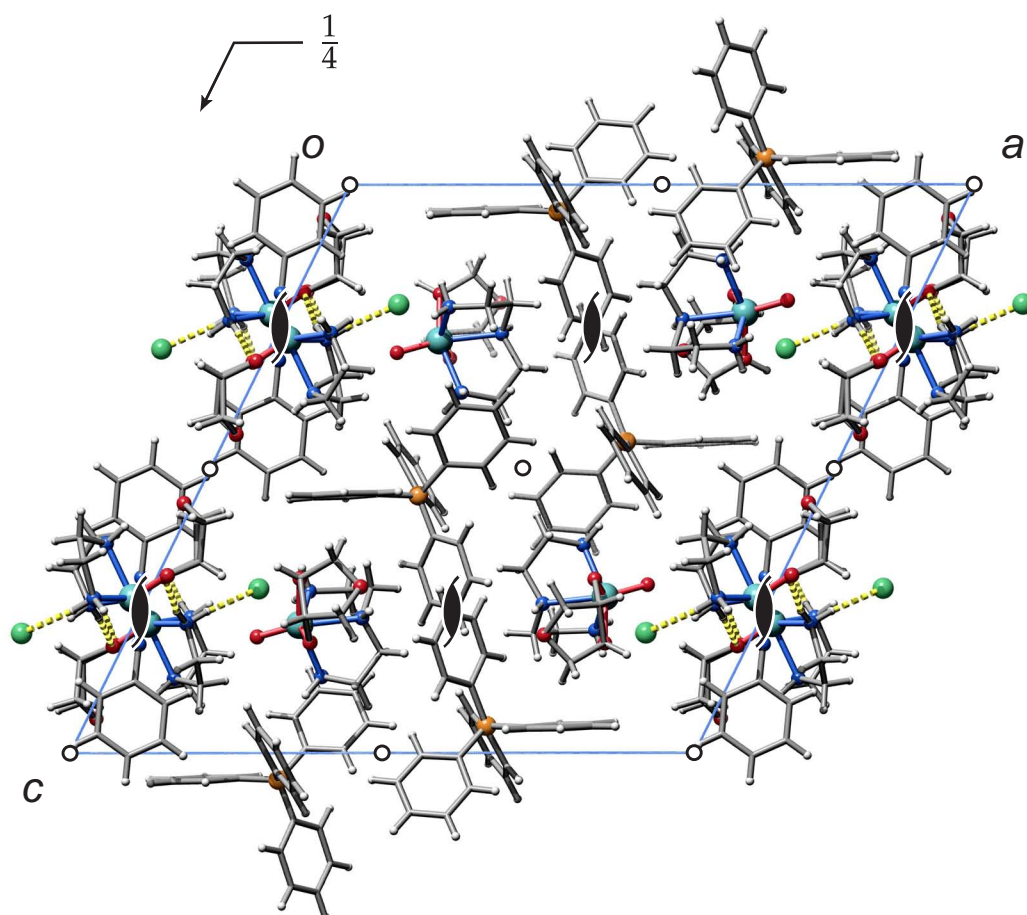


Figure 6.4 SCHAKAL packing diagram of **4** viewed along $[0\bar{1}0]$. Hydrogen bonds are indicated by yellow dashed lines. The symmetry elements of the space group $P2_1/c$ are overlaid. The atoms of the minor part of disordered diethylenetriamine are not shown. Atoms: carbon (grey, wireframe), hydrogen (light grey, small), boron (orange, large), chlorine (green, large), nitrogen (blue, large), oxygen (red, large), rhenium (dark cyan, large).

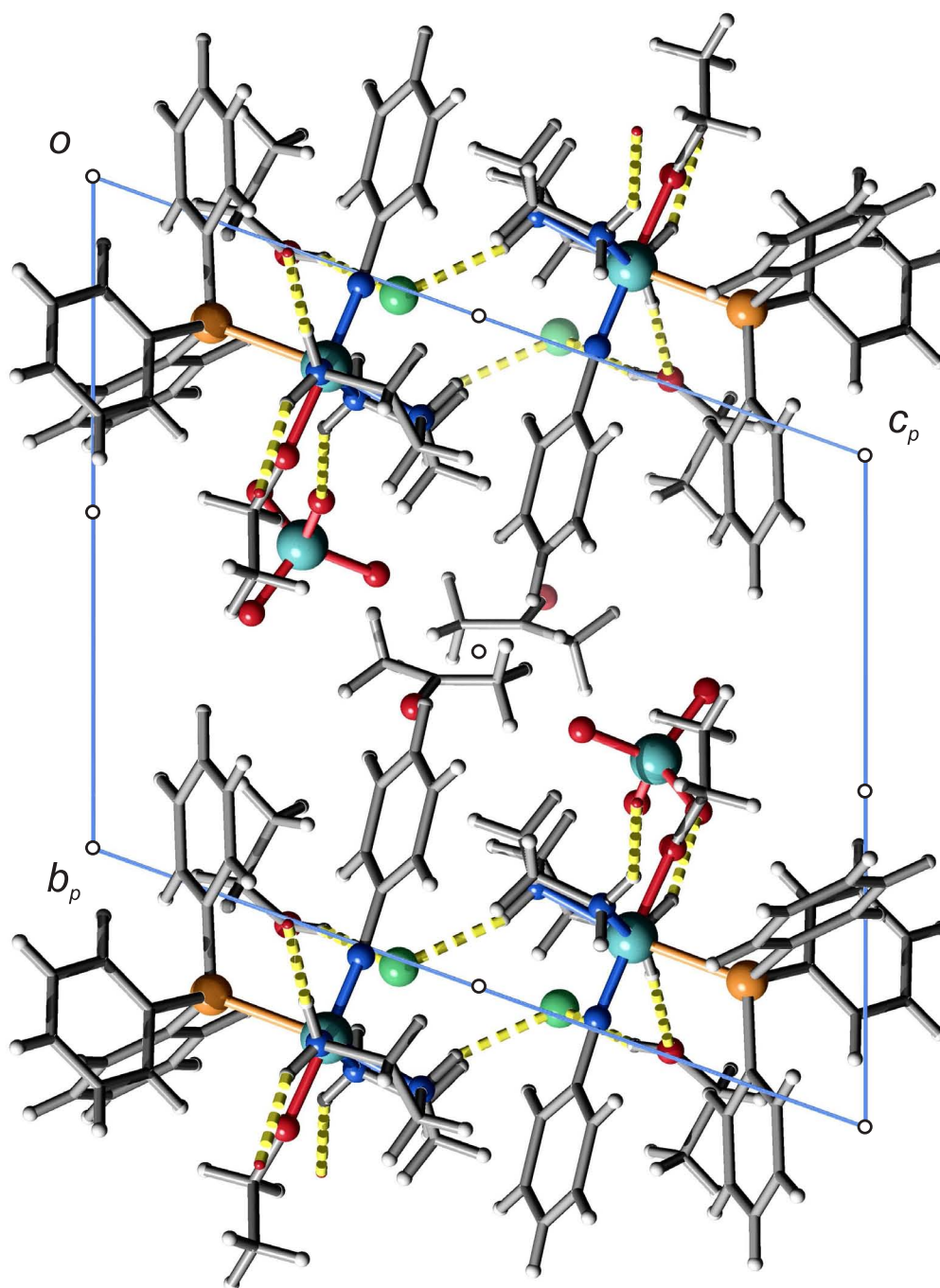


Figure 6.5 SCHAKAL packing diagram of **5** viewed along $[\bar{1}00]$. Hydrogen bonds are indicated by yellow dashed lines. The symmetry elements of the space group $P\bar{1}$ are overlaid. The atoms of the minor part of disordered ethanol are not shown. Atoms: carbon (grey, wire-frame), hydrogen (light grey, small), chlorine (green, large), nitrogen (blue, large), oxygen (red, large), phosphorus (orange, large), rhenium (dark cyan, large).

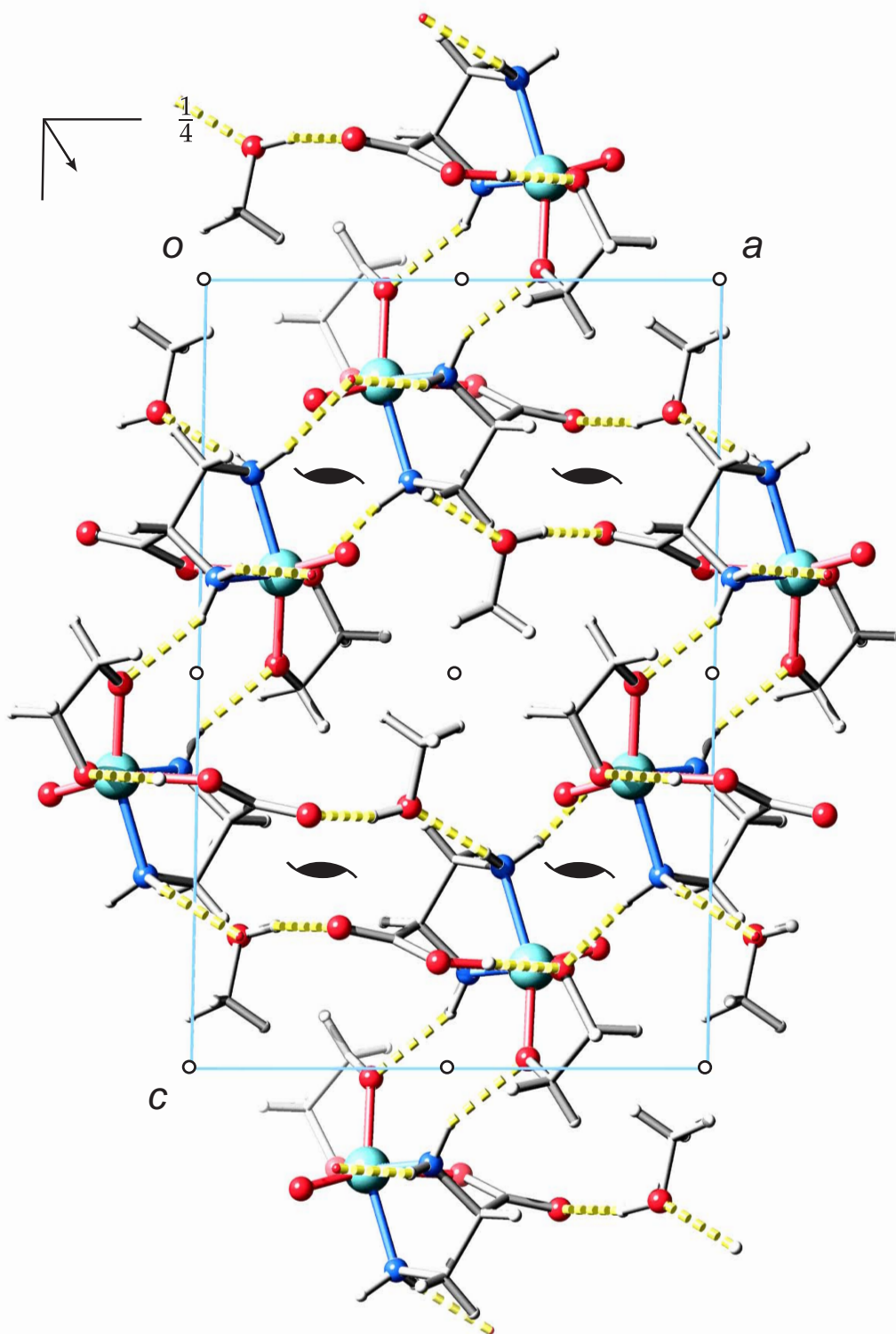


Figure 6.6 SCHAKAL packing diagram of **6** viewed along $[0\bar{1}0]$. Hydrogen bonds are indicated by yellow dashed lines. The symmetry elements of the space group $P2_1/n$ are overlaid. The atoms of the minor part of disordered diaminopropionic acid are not shown. Atoms: carbon (grey, wireframe), hydrogen (light grey, small), nitrogen (blue, large), oxygen (red, large), rhenium (dark cyan, large).

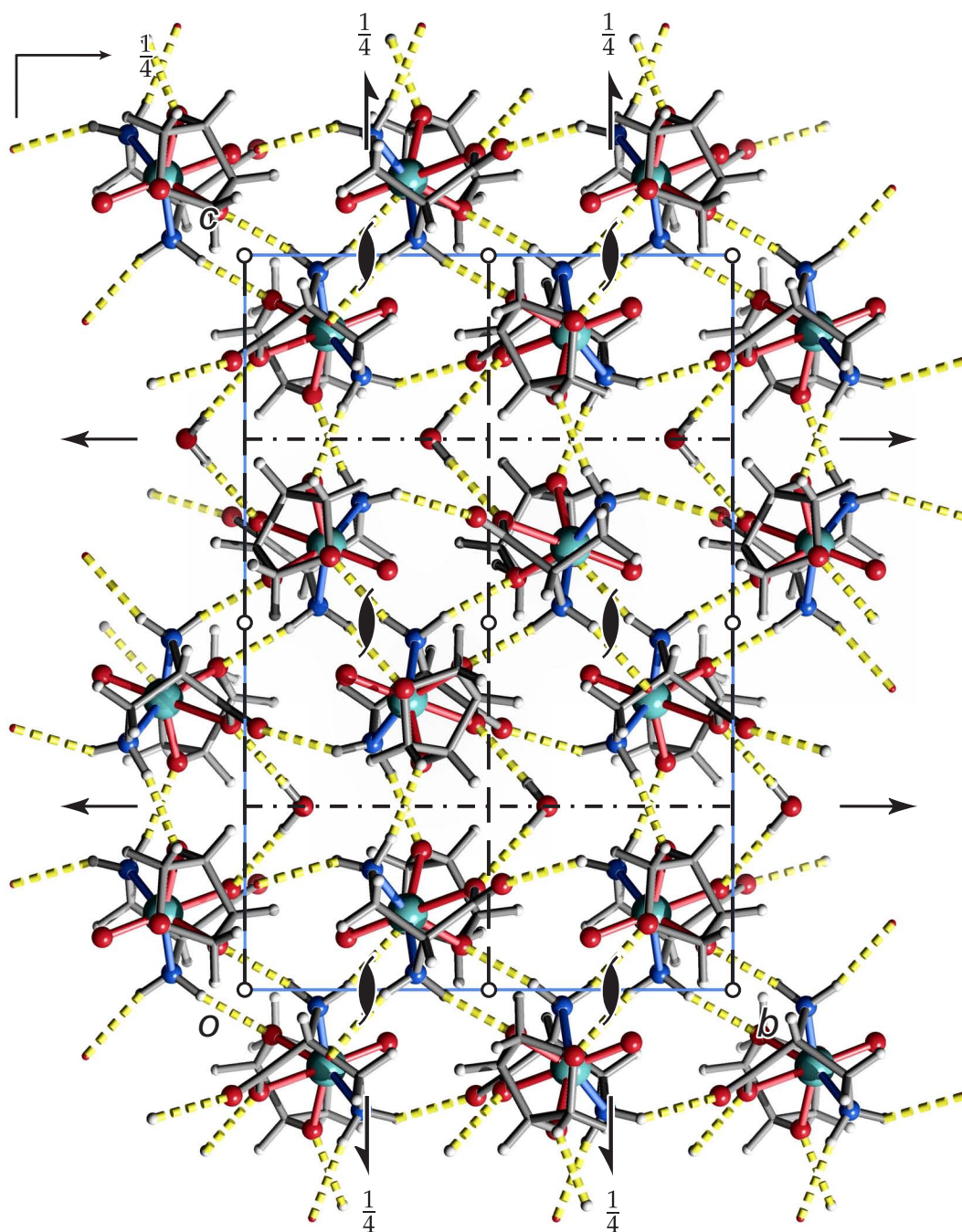


Figure 6.7 SCHAKAL packing diagram of **7** viewed along $[100]$. Hydrogen bonds are indicated by yellow dashed lines. The symmetry elements of the space group $Pbcn$ are overlaid. The atoms of the minor part of disordered diaminopropionic acid are not shown. Atoms: carbon (grey, wireframe), hydrogen (light grey, small), nitrogen (blue, large), oxygen (red, large), rhenium (dark cyan, large).

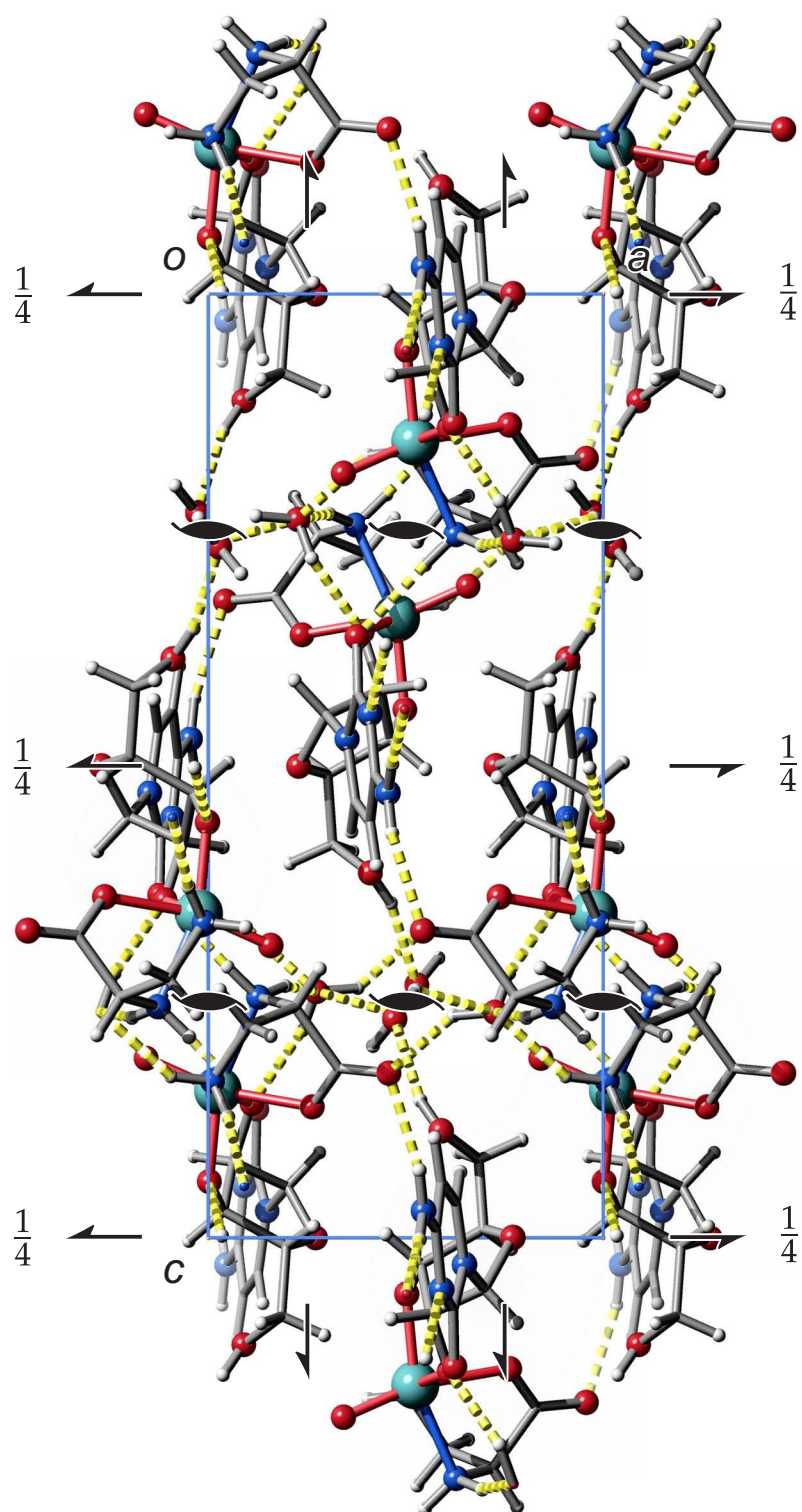


Figure 6.8 SCHAKAL packing diagram of **8** viewed along $[0\bar{1}0]$. Hydrogen bonds are indicated by yellow dashed lines. The symmetry elements of the space group $P2_12_12_1$ are overlaid. The atoms of the minor parts of disordered diaminopropionic acid and water are omitted. Atoms: carbon (grey, wireframe), hydrogen (light grey, small), nitrogen (blue, large), oxygen (red, large), rhenium (dark cyan, large).

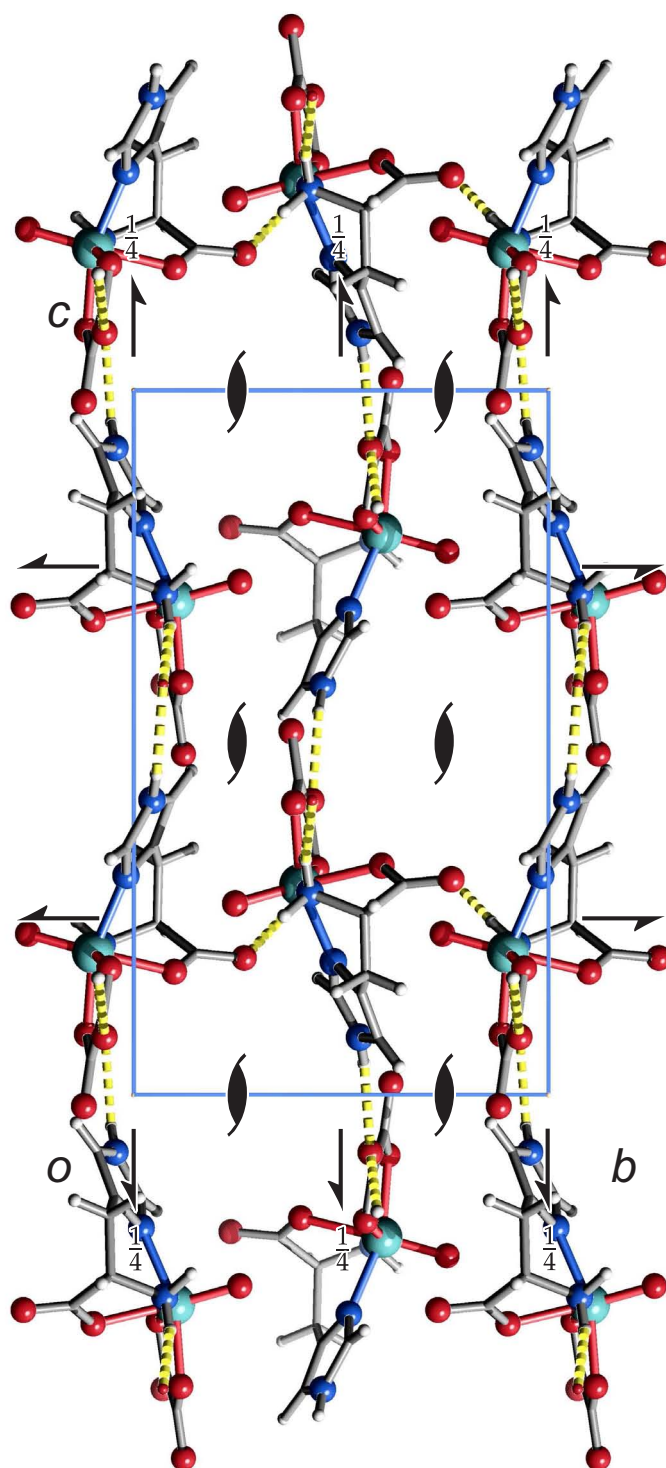


Figure 6.9 SCHAKAL packing diagram of **9** viewed along $[\bar{1}00]$. Hydrogen bonds are indicated by yellow dashed lines. The symmetry elements of the space group $P2_12_12_1$ are overlaid. Atoms: carbon (grey, wireframe), hydrogen (light grey, small), nitrogen (blue, large), oxygen (red, large), rhenium (dark cyan, large).

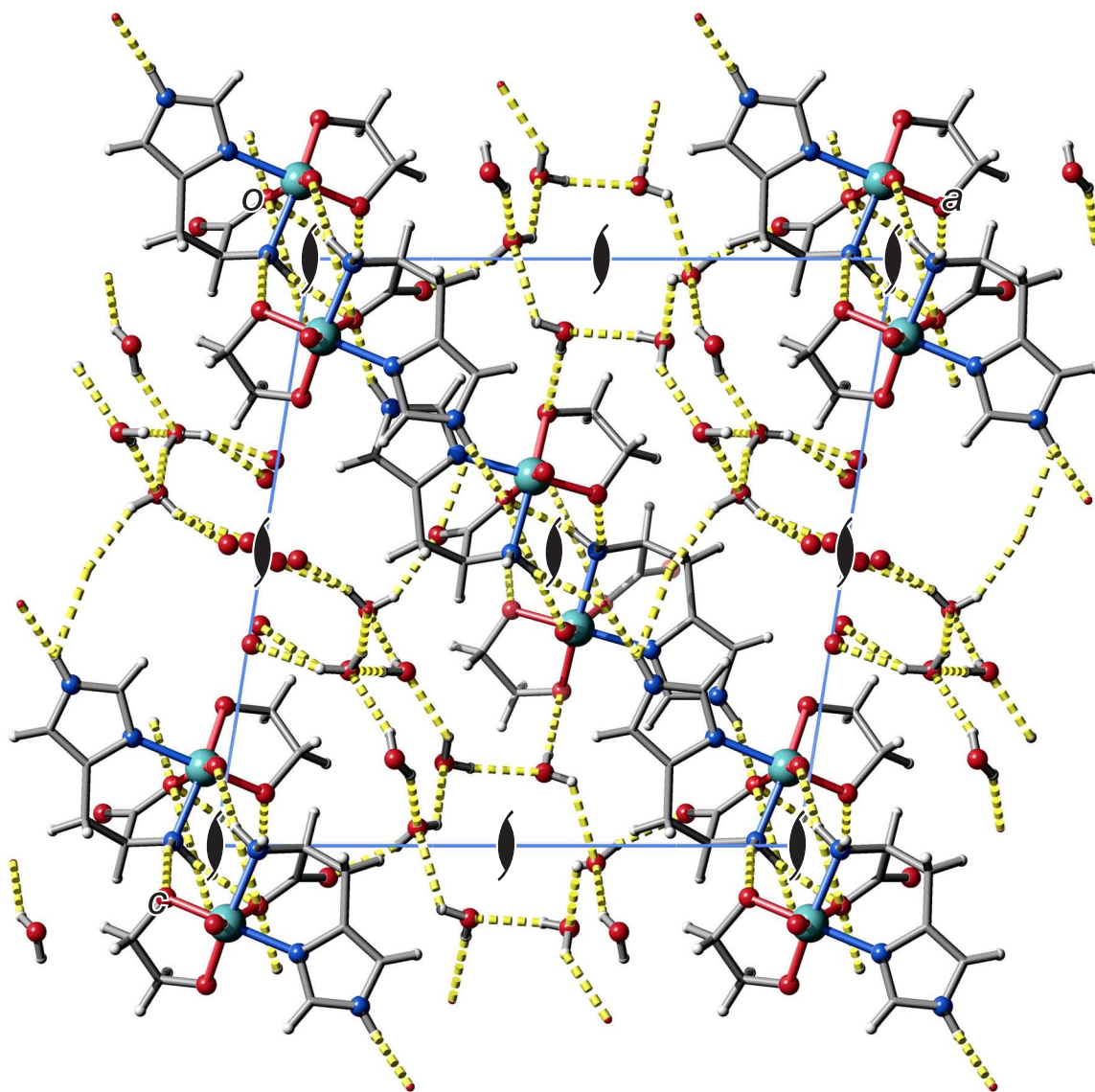


Figure 6.10 SCHAKAL packing diagram of **10** viewed along $[0\bar{1}0]$. Hydrogen bonds are indicated by yellow dashed lines. Two disordered molecules of water were calculated without hydrogen atoms. The symmetry elements of the space group $P2_1$ are overlaid. Atoms: carbon (grey, wireframe), hydrogen (light grey, small), nitrogen (blue, large), oxygen (red, large), rhenium (dark cyan, large).

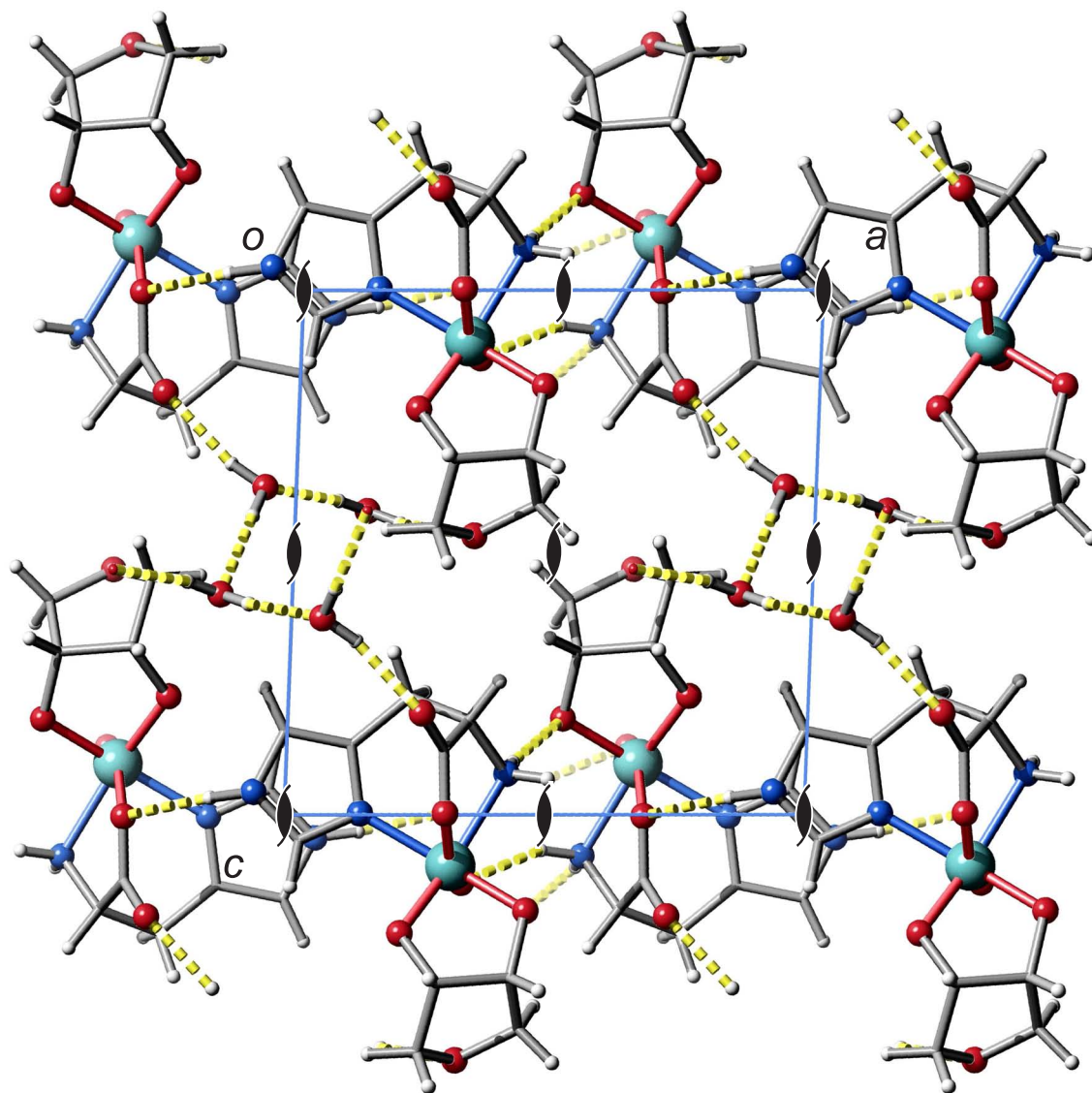


Figure 6.11 SCHAKAL packing diagram of **11** viewed along $[0\bar{1}0]$. Hydrogen bonds are indicated by yellow dashed lines. The symmetry elements of the space group $P2_1$ are overlaid. Atoms: carbon (grey, wireframe), hydrogen (light grey, small), nitrogen (blue, large), oxygen (red, large), rhenium (dark cyan, large).

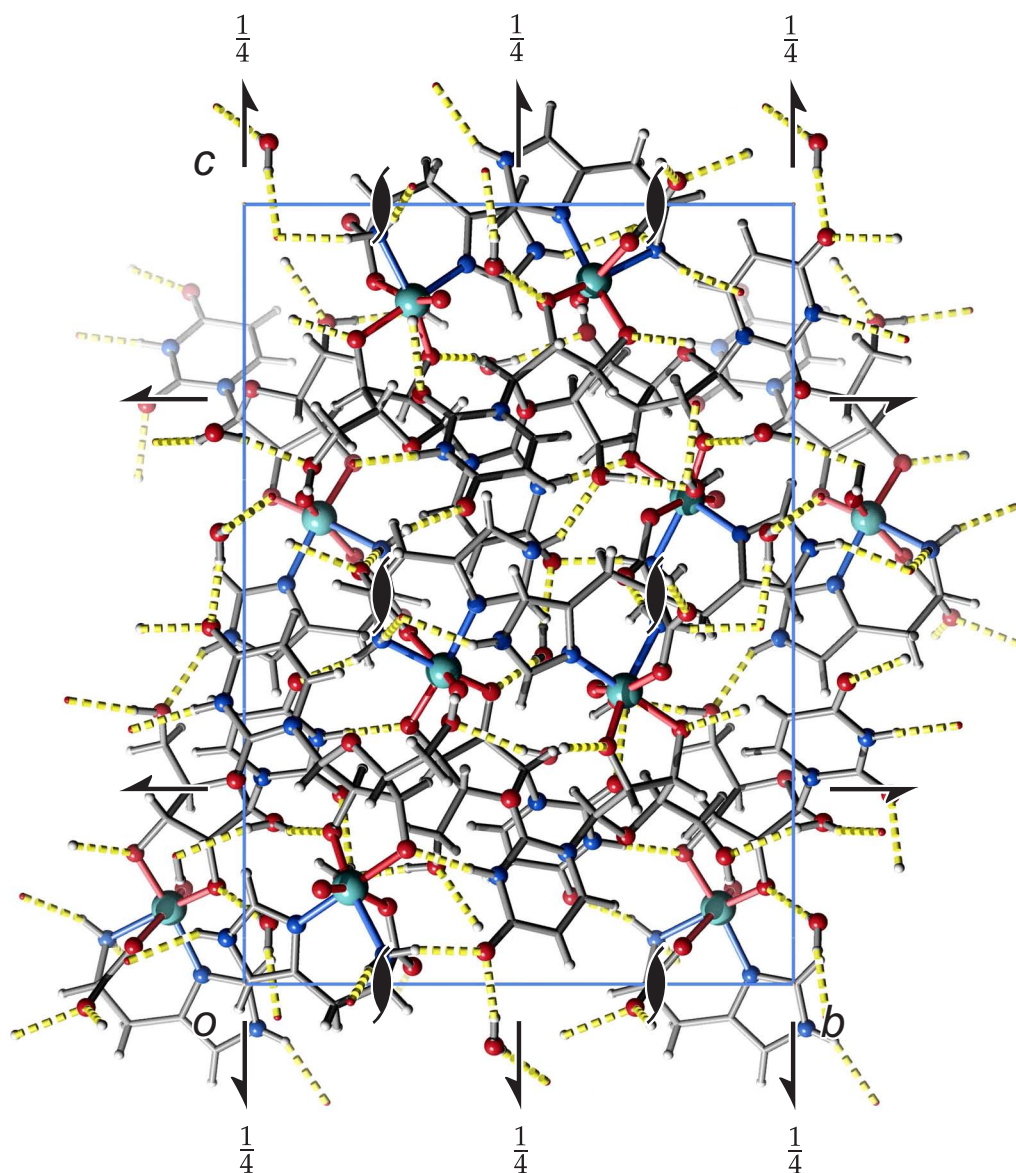


Figure 6.12 SCHAKAL packing diagram of **12** viewed along $[100]$. Hydrogen bonds are indicated by yellow dashed lines. The symmetry elements of the space group $P2_12_12_1$ are overlaid. Atoms: carbon (grey, wireframe), hydrogen (light grey, small), nitrogen (blue, large), oxygen (red, large), rhenium (dark cyan, large).

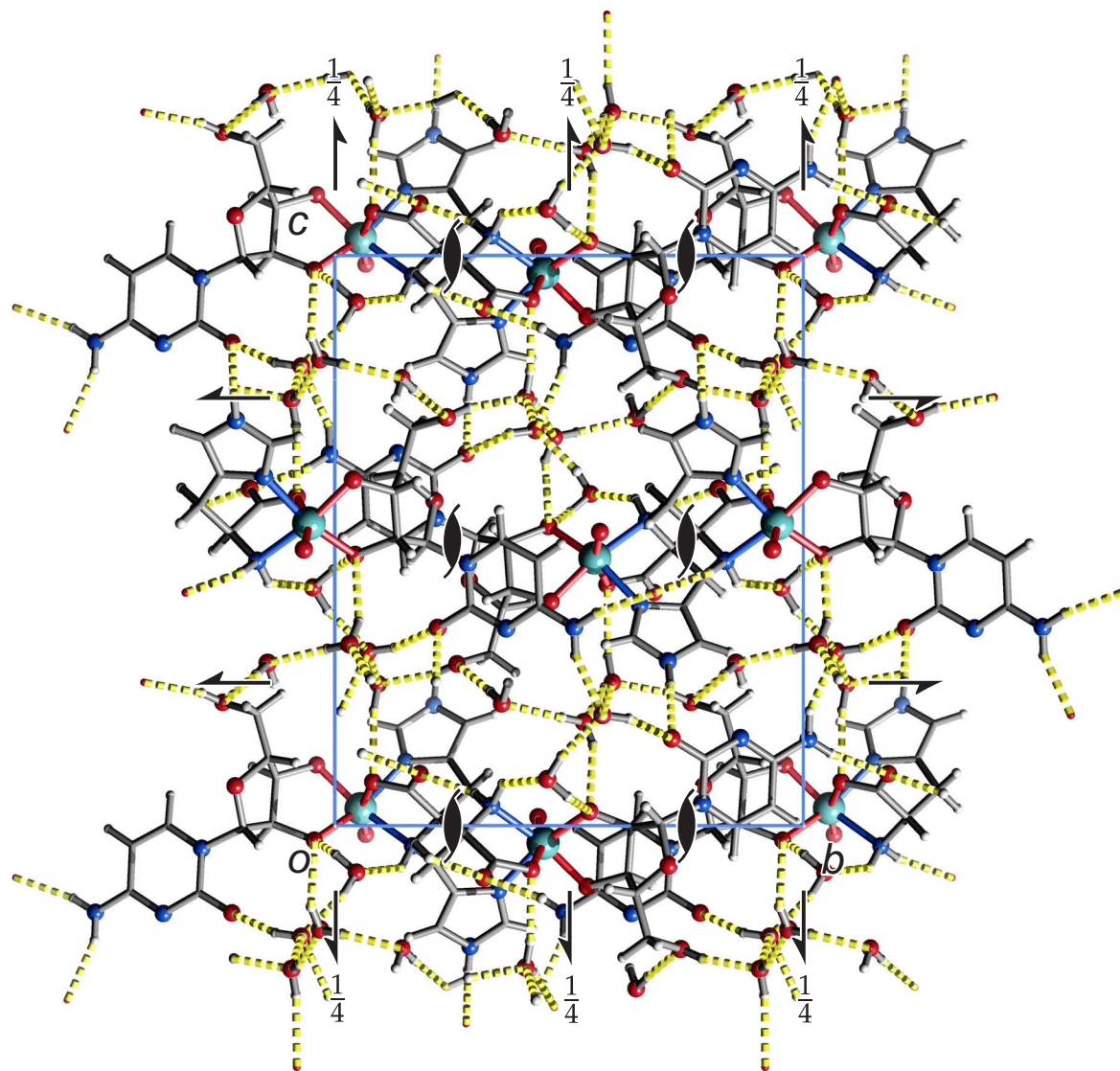


Figure 6.13 SCHAKAL packing diagram of **13** viewed along $[\bar{1}00]$. Hydrogen bonds are indicated by yellow dashed lines. The symmetry elements of the space group $P2_12_12_1$ are overlaid. Atoms: carbon (grey, wireframe), hydrogen (light grey, small), nitrogen (blue, large), oxygen (red, large), rhenium (dark cyan, large).

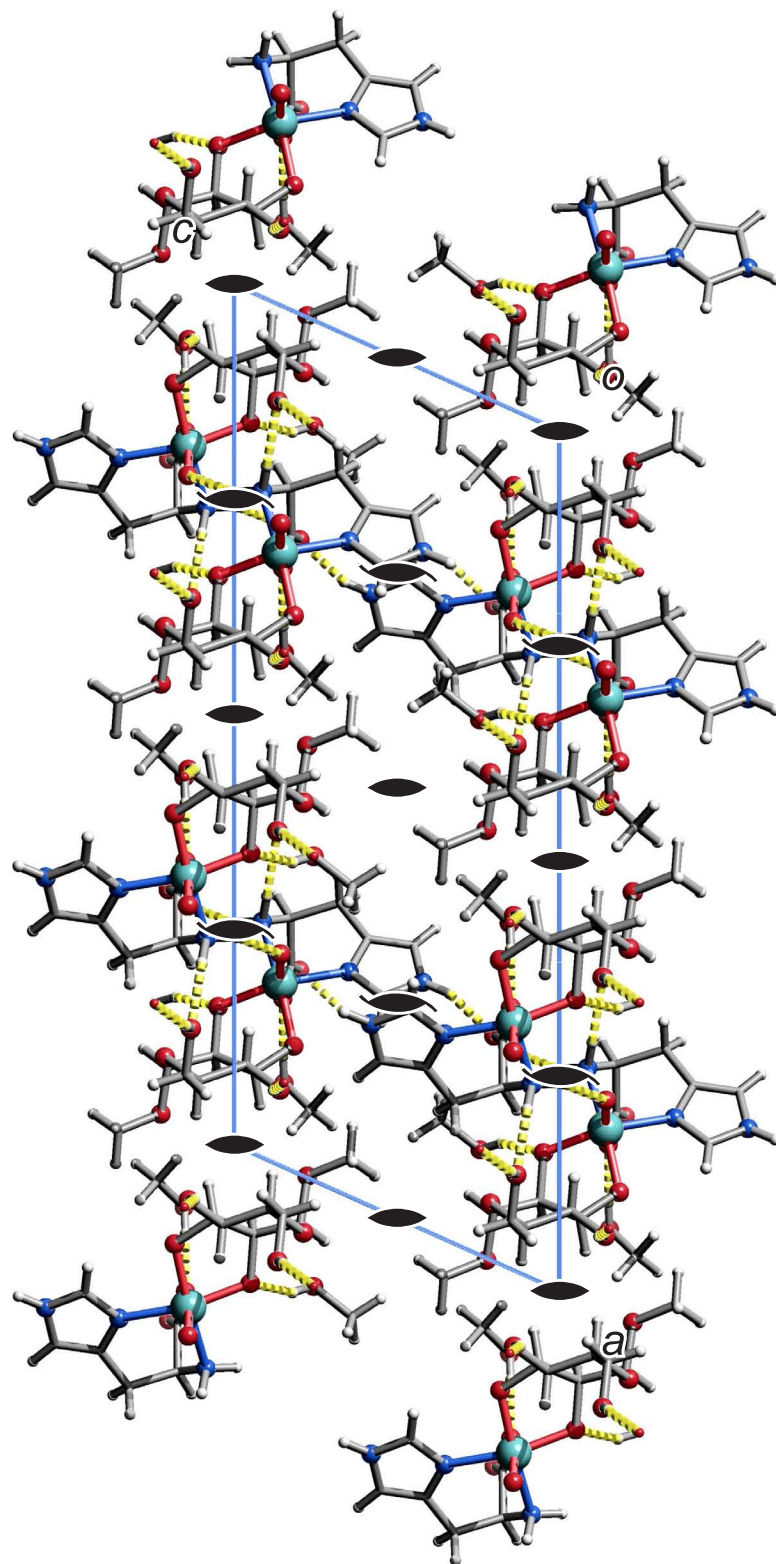


Figure 6.14 SCHAKAL packing diagram of **14** viewed along $[0\bar{1}0]$. Hydrogen bonds are indicated by yellow dashed lines. The symmetry elements of the space group $C2$ are overlaid. Atoms: carbon (grey, wireframe), hydrogen (light grey, small), nitrogen (blue, large), oxygen (red, large), rhenium (dark cyan, large).

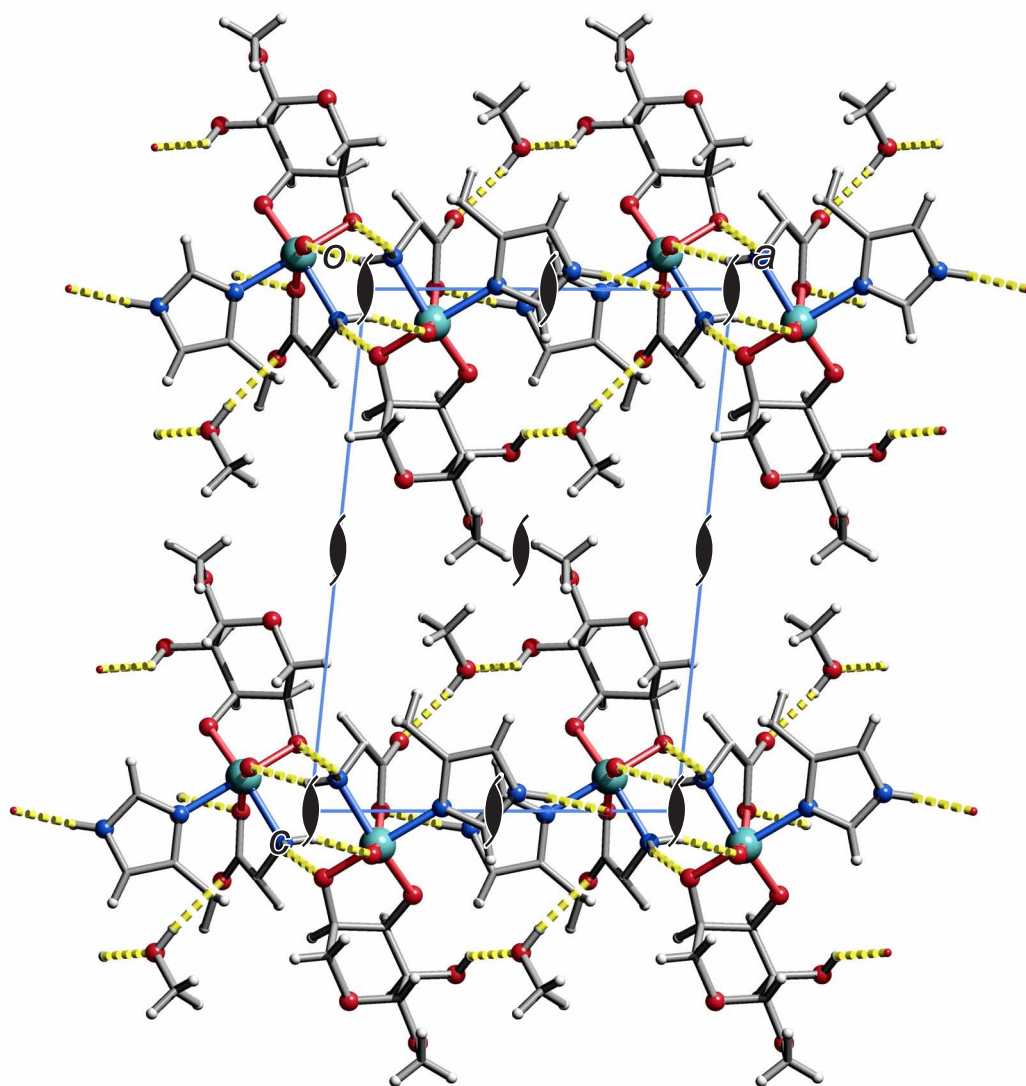


Figure 6.15 SCHAKAL packing diagram of **15** viewed along $[0\bar{1}0]$. Hydrogen bonds are indicated by yellow dashed lines. The symmetry elements of the space group $P2_1$ are overlaid. Atoms: carbon (grey, wireframe), hydrogen (light grey, small), nitrogen (blue, large), oxygen (red, large), rhenium (dark cyan, large).

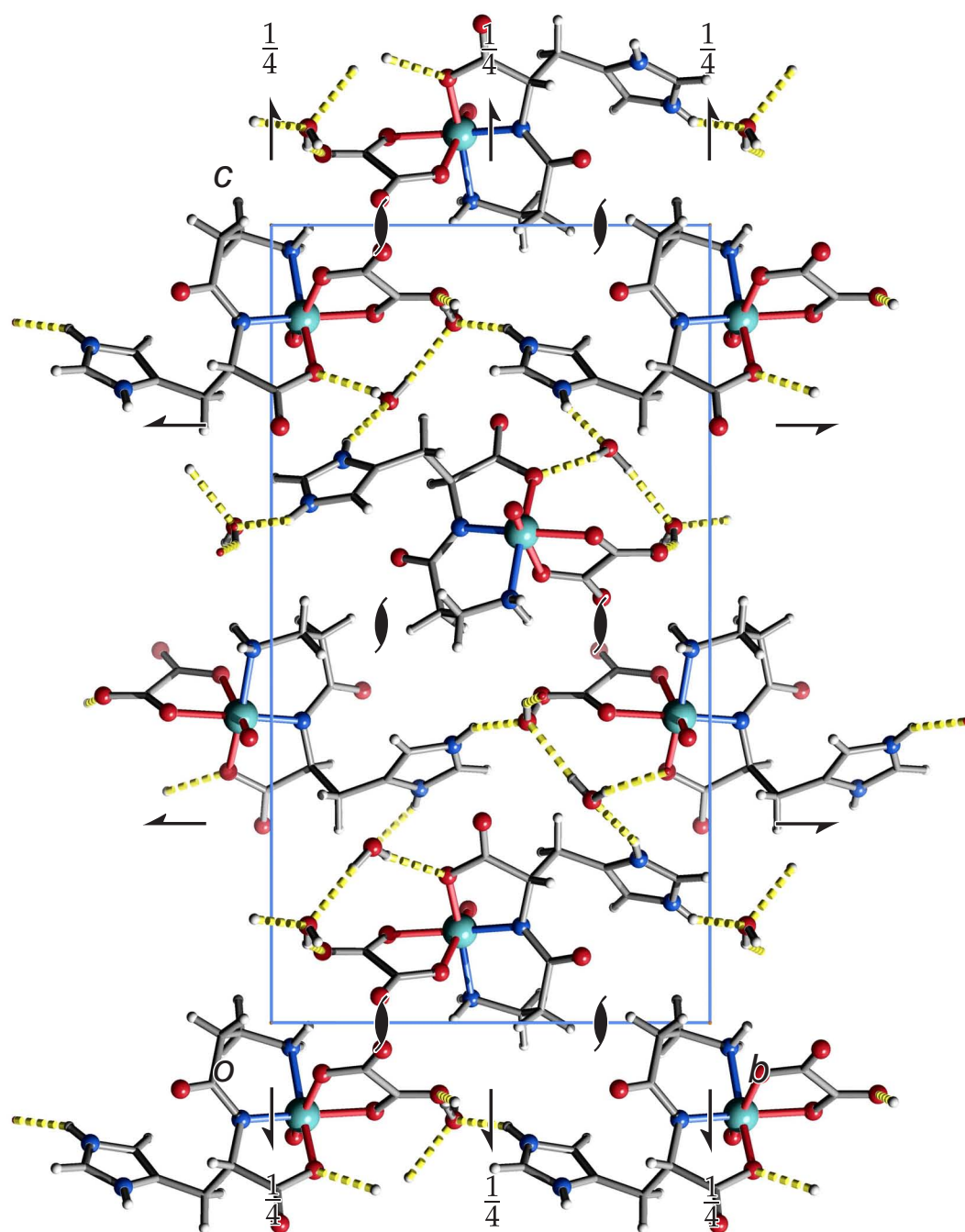


Figure 6.16 SCHAKAL packing diagram of **16** viewed along $[100]$. Hydrogen bonds are indicated by yellow dashed lines. The symmetry elements of the space group $P2_12_12_1$ are overlaid. The minor part of disordered water is not shown. Atoms: carbon (grey, wireframe), hydrogen (light grey, small), nitrogen (blue, large), oxygen (red, large), rhenium (dark cyan, large).

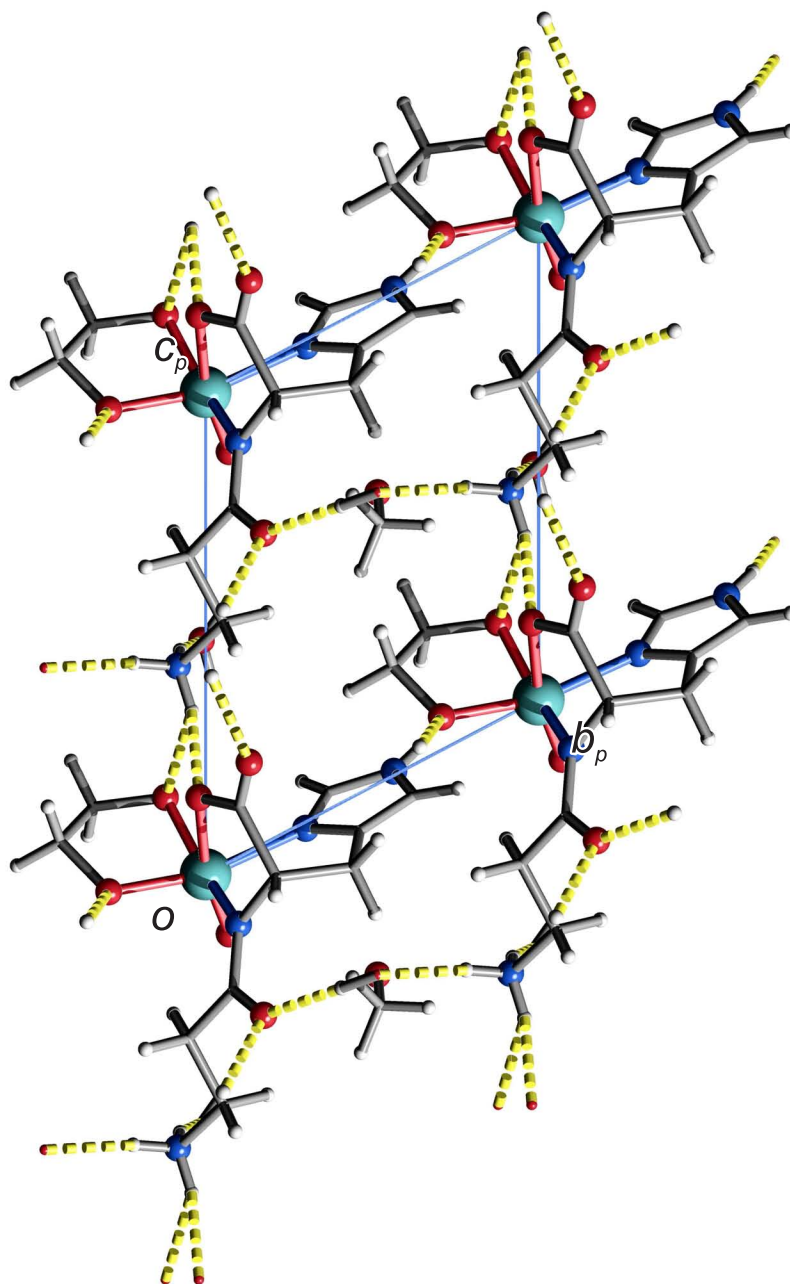


Figure 6.17 SCHAKAL packing diagram of **17** viewed along $[100]$. Hydrogen bonds are indicated by yellow dashed lines. The space group is $P1$. Atoms: carbon (grey, wireframe), hydrogen (light grey, small), nitrogen (blue, large), oxygen (red, large), rhenium (dark cyan, large).

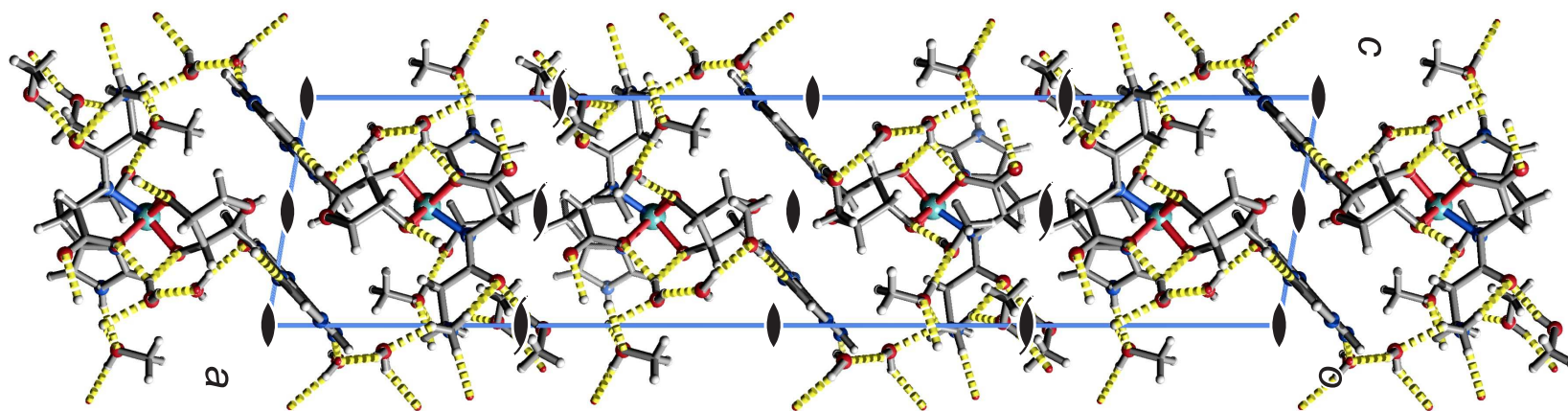


Figure 6.18 SCHAKAL packing diagram of **18** viewed along $[0\bar{1}0]$. Hydrogen bonds are indicated by yellow dashed lines. The symmetry elements of the space group $C2$ are overlaid. The atoms of the minor part of disordered adenine and the CH_2OH group of ribose are not shown. Atoms: carbon (grey, wireframe), hydrogen (light grey, small), nitrogen (blue, large), oxygen (red, large), rhenium (dark cyan, large).

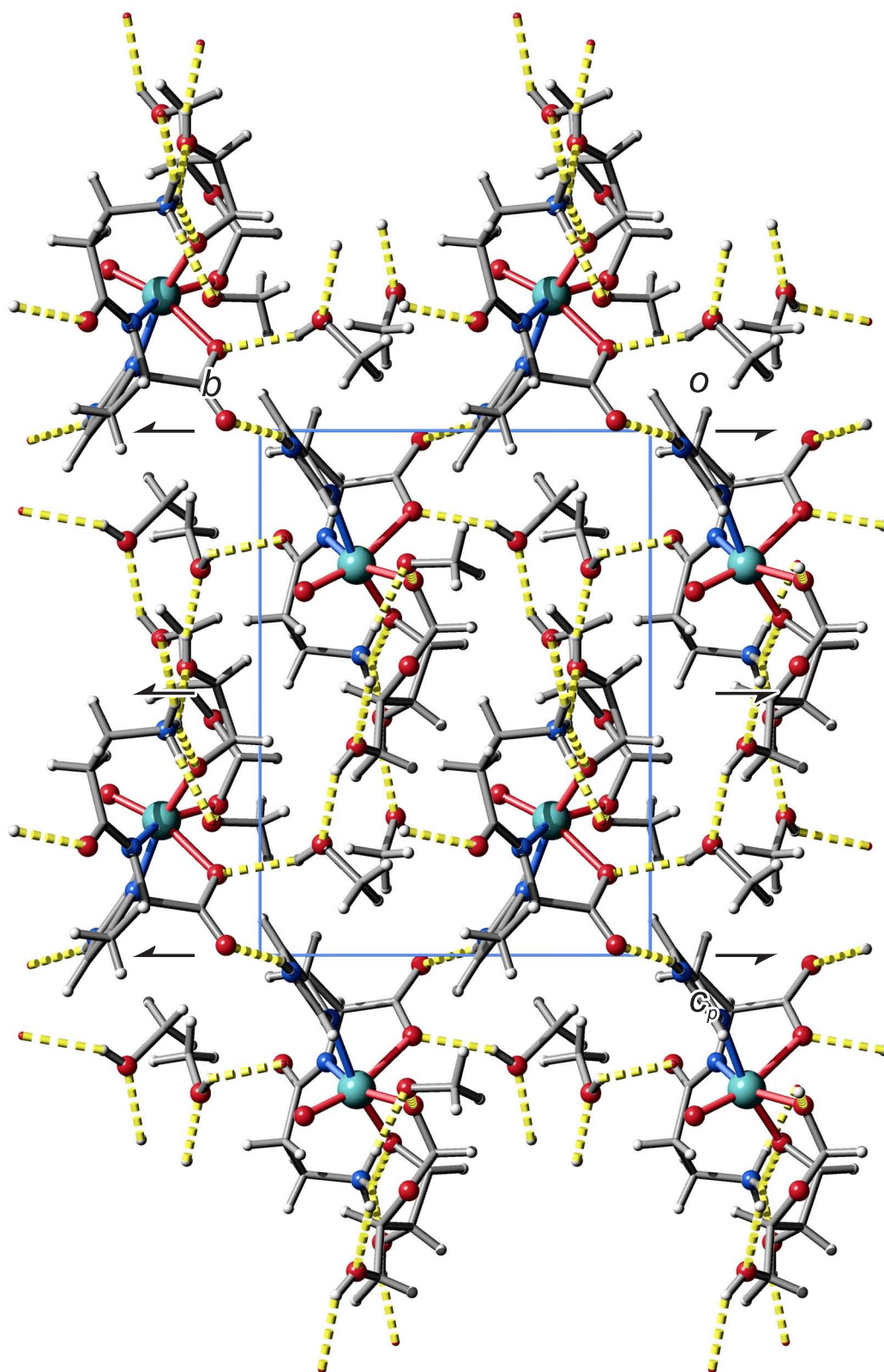


Figure 6.19 SCHAKAL packing diagram of **19** viewed along $[\bar{1}00]$. Hydrogen bonds are indicated by yellow dashed lines. The symmetry elements of the space group $P2_1$ are overlaid. Atoms: carbon (grey, wireframe), hydrogen (light grey, small), nitrogen (blue, large), oxygen (red, large), rhenium (dark cyan, large).

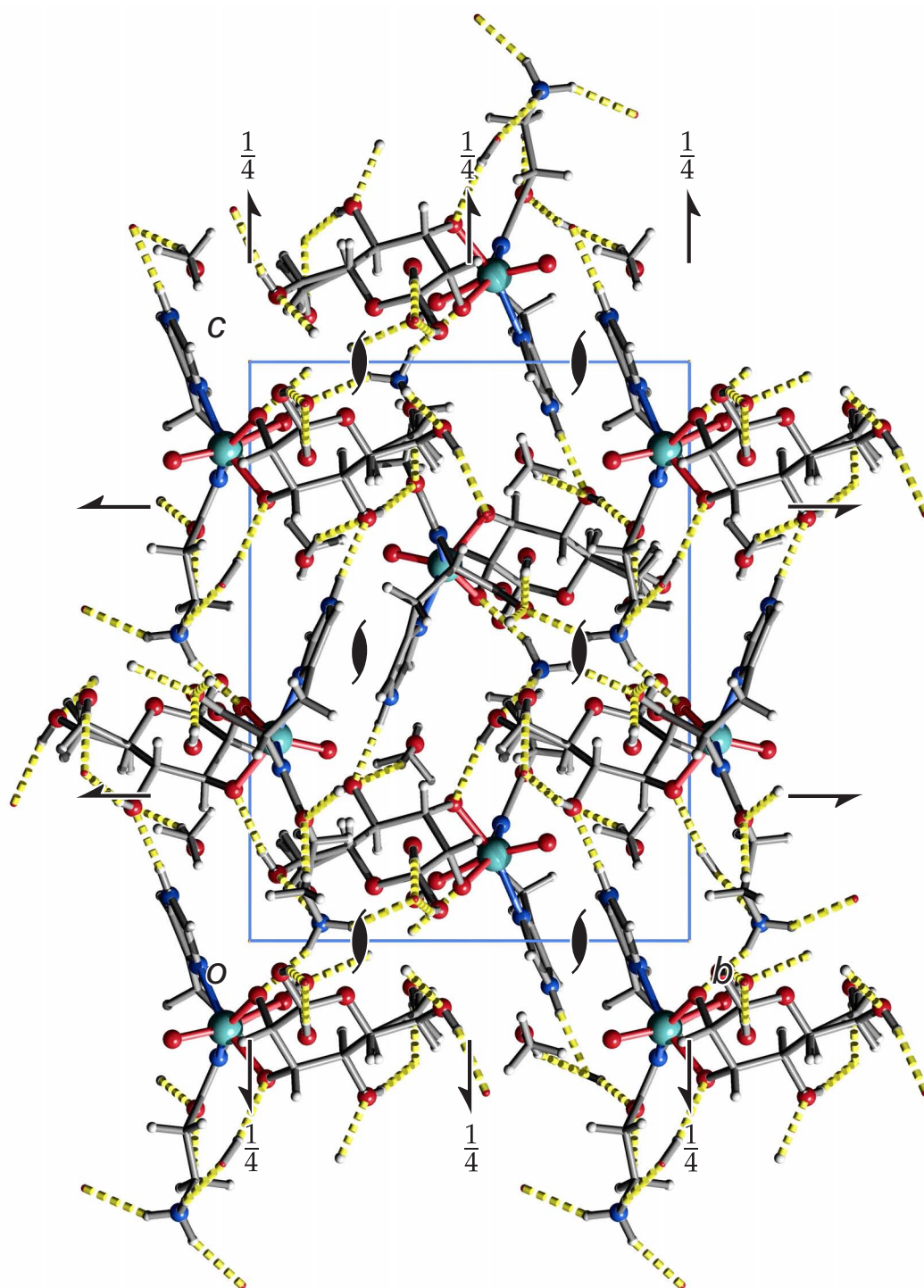


Figure 6.20 SCHAKAL packing diagram of **20** viewed along $[\bar{1}00]$. Hydrogen bonds are indicated by yellow dashed lines. The symmetry elements of the space group $P2_12_12_1$ are overlaid. Atoms: carbon (grey, wireframe), hydrogen (light grey, small), nitrogen (blue, large), oxygen (red, large), rhenium (dark cyan, large).

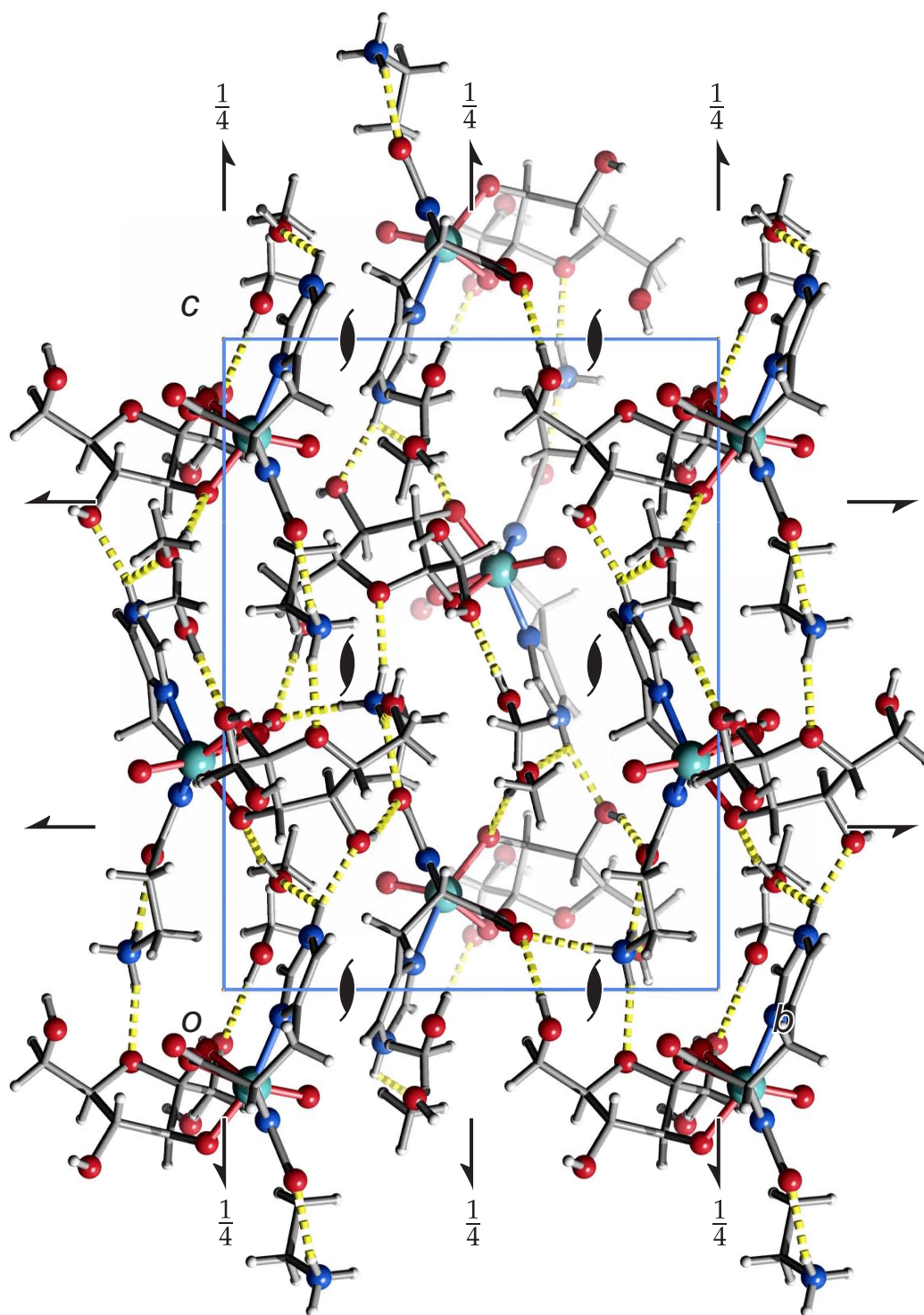


Figure 6.21 SCHAKAL packing diagram of **21** viewed along $[\bar{1}00]$. Hydrogen bonds are indicated by yellow dashed lines. The symmetry elements of the space group $P2_12_12_1$ are overlaid. The atoms of the minor parts of disordered methanol and the hydroxy-function on C1 of fructose are not shown. Atoms: carbon (grey, wireframe), hydrogen (light grey, small), nitrogen (blue, large), oxygen (red, large), rhenium (dark cyan, large).

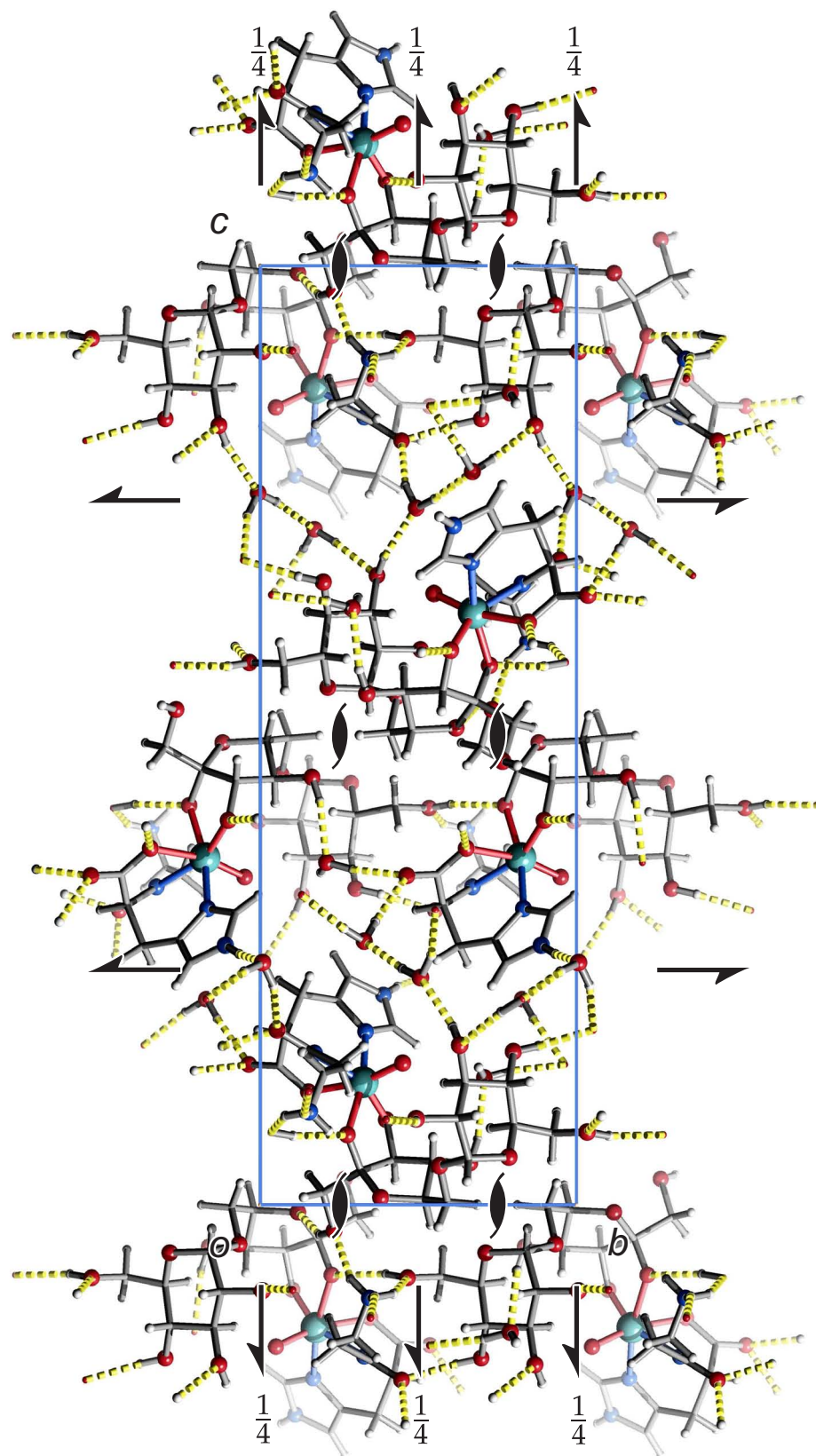


Figure 6.22 SCHAKAL packing diagram of **22** viewed along $[\bar{1}00]$. Hydrogen bonds are indicated by yellow dashed lines. The minor part of disordered N_{β} of alanine is not shown. The symmetry elements of the space group $P2_12_12_1$ are overlaid. Atoms: carbon (grey, wire-frame), hydrogen (light grey, small), nitrogen (blue, large), oxygen (red, large), rhenium (dark cyan, large).

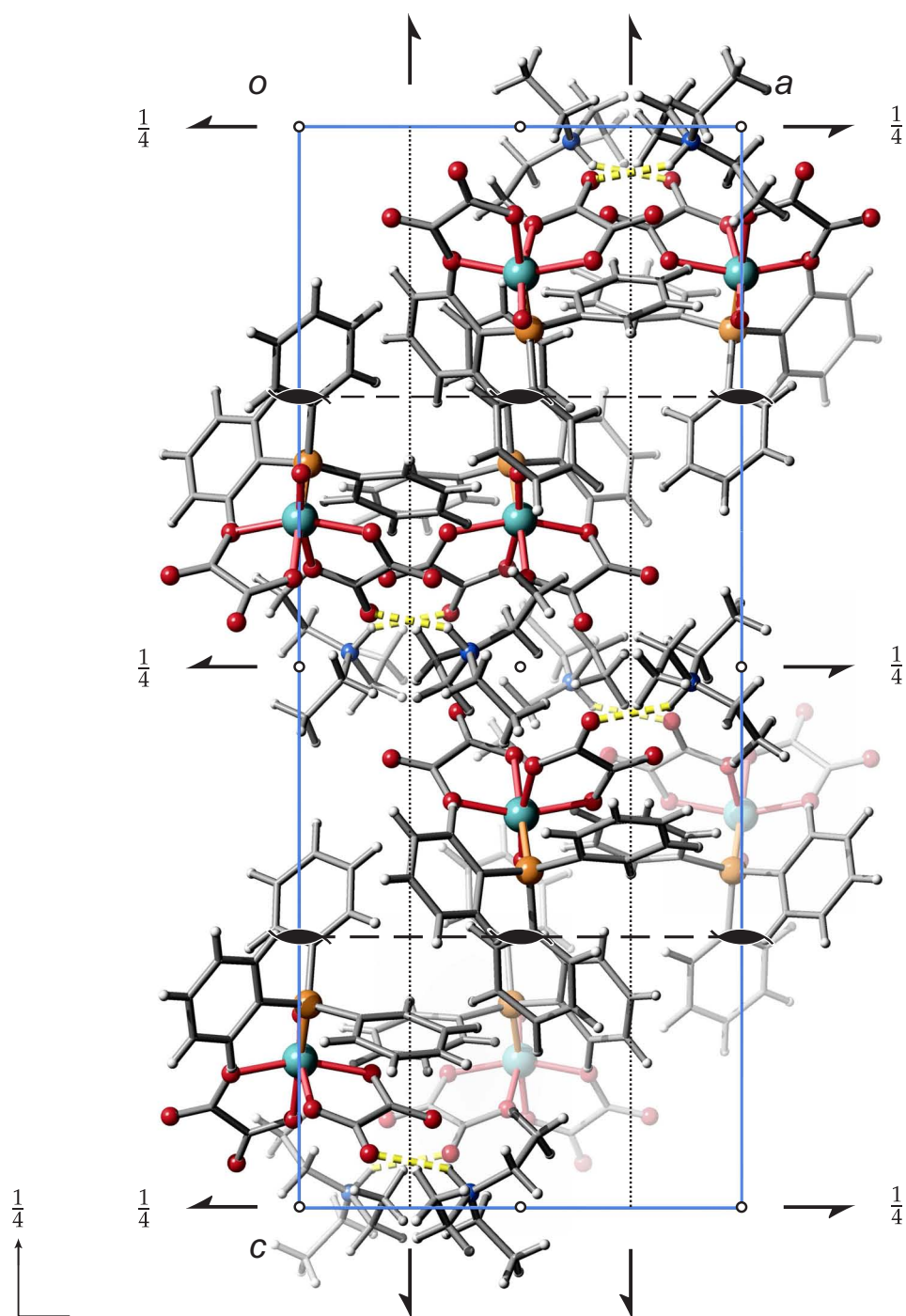


Figure 6.23 SCHAKAL packing diagram of **23** viewed along $[0\bar{1}0]$. Hydrogen bonds are indicated by yellow dashed lines. The symmetry elements of the space group $Pbca$ are overlaid. Atoms: carbon (grey, wireframe), hydrogen (light grey, small), nitrogen (blue, large), oxygen (red, large), phosphorus (orange, large), rhenium (dark cyan, large).

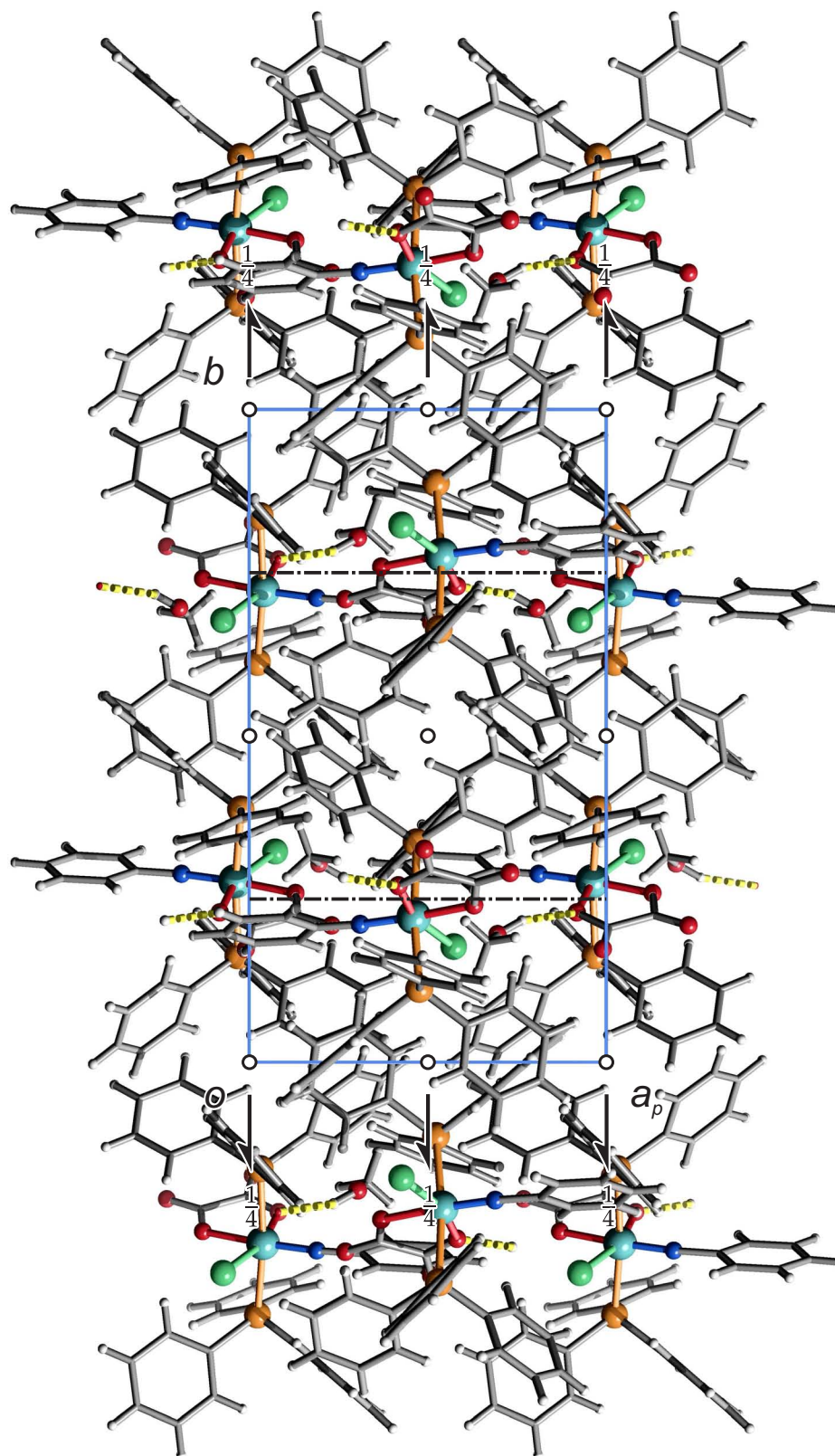


Figure 6.24 SCHAKAL packing diagram of **24** viewed along $[00\bar{1}]$. Hydrogen bonds are indicated by yellow dashed lines. The symmetry elements of the space group $P2_1/n$ are overlaid. The minor part of disordered methanol is not shown. Atoms: carbon (grey, wireframe), hydrogen (light grey, small), chlorine (green, large), nitrogen (blue, large), oxygen (red, large), phosphorus (orange, large), rhenium (dark cyan, large).

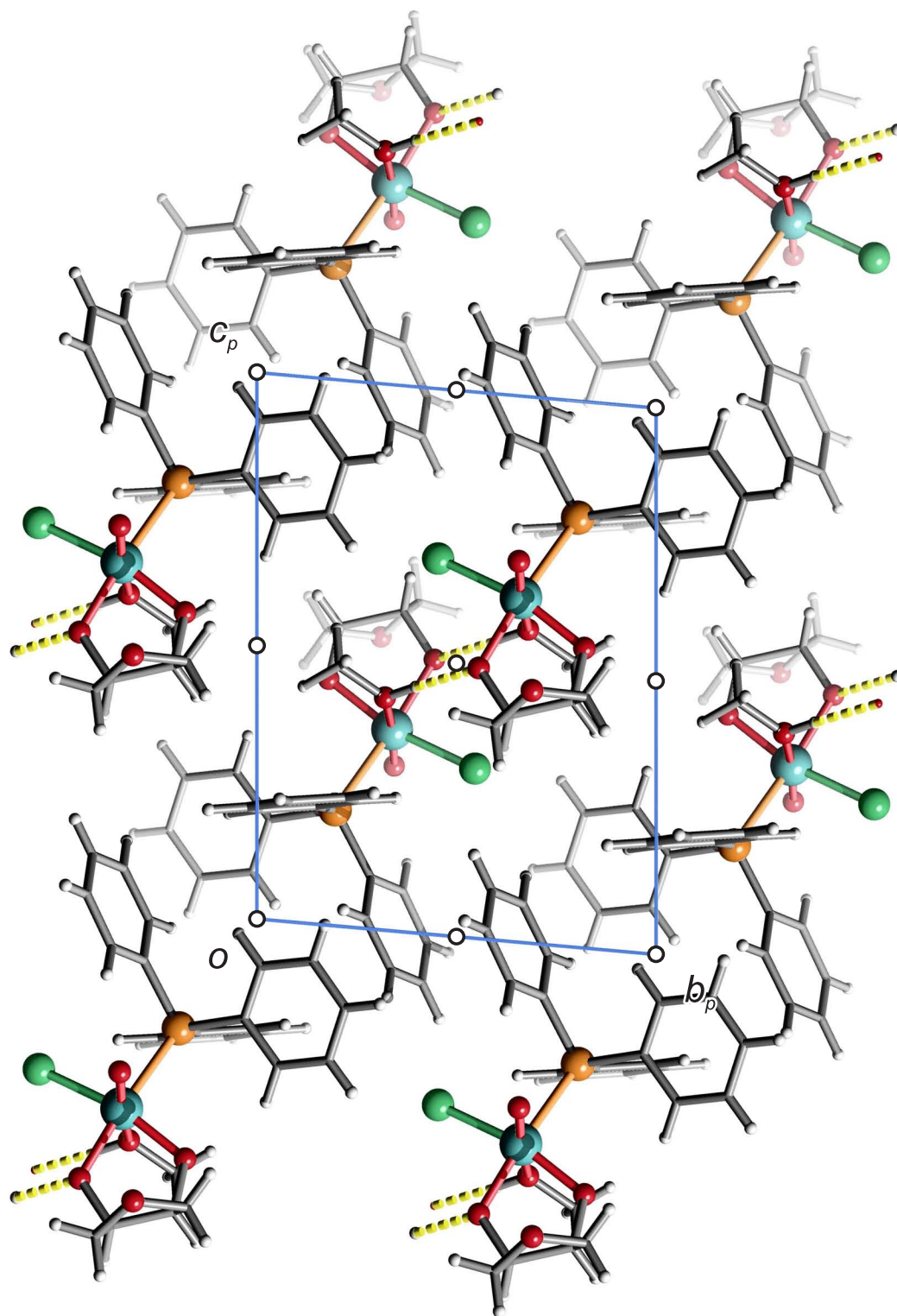


Figure 6.25 SCHAKAL packing diagram of **25** viewed along $[100]$. Hydrogen bonds are indicated by yellow dashed lines. The symmetry elements of the space group $P\bar{1}$ are overlaid. Atoms: carbon (grey, wireframe), hydrogen (light grey, small), chlorine (green, large), oxygen (red, large), phosphorus (orange, large), rhenium (dark cyan, large).

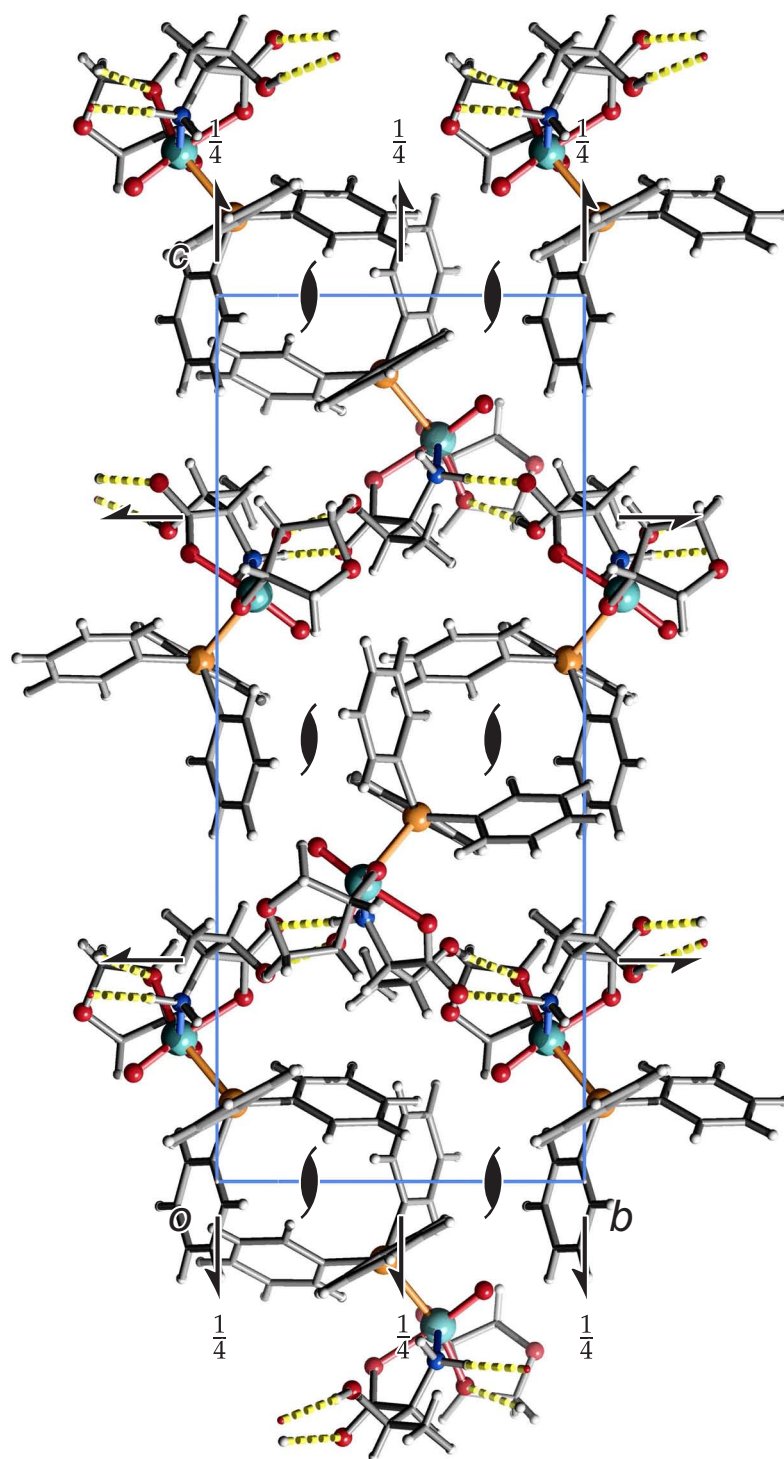


Figure 6.26 SCHAKAL packing diagram of **26** viewed along $[\bar{1}00]$. Hydrogen bonds are indicated by yellow dashed lines. The symmetry elements of the space group $P2_12_12_1$ are overlaid. Atoms: carbon (grey, wireframe), hydrogen (light grey, small), nitrogen (blue, large), oxygen (red, large), phosphorus (orange, large), rhenium (dark cyan, large).

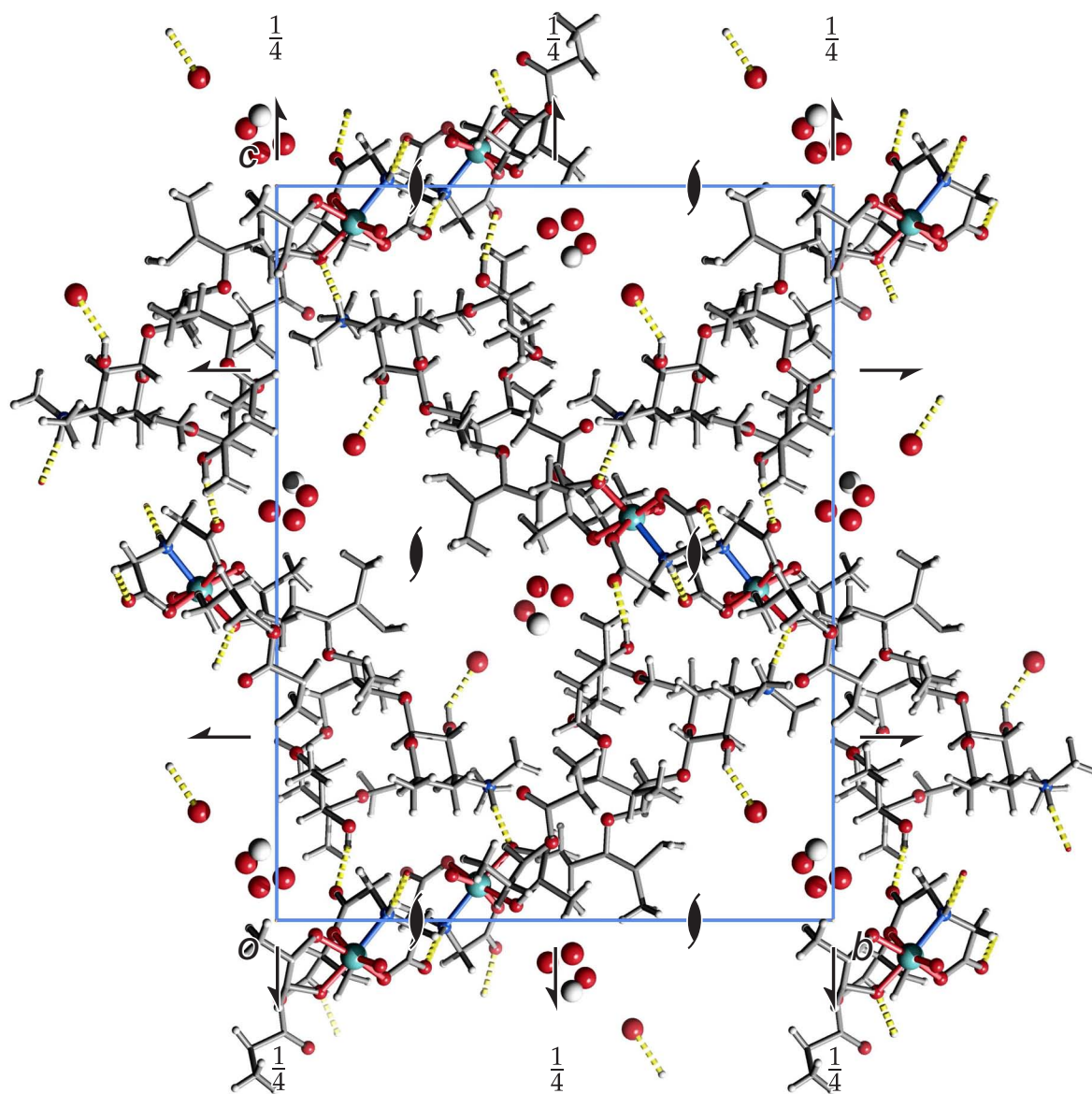


Figure 6.27 SCHAKAL packing diagram of **27** viewed along $[100]$. Hydrogen bonds are indicated by yellow dashed lines. The symmetry elements of the space group $P2_12_12_1$ are overlaid. Atoms: carbon (grey, wireframe), hydrogen (light grey, small), nitrogen (blue, large), oxygen (red, large), rhenium (dark cyan, large). The atoms of disordered water and methanol are depicted in large style without hydrogen atoms.

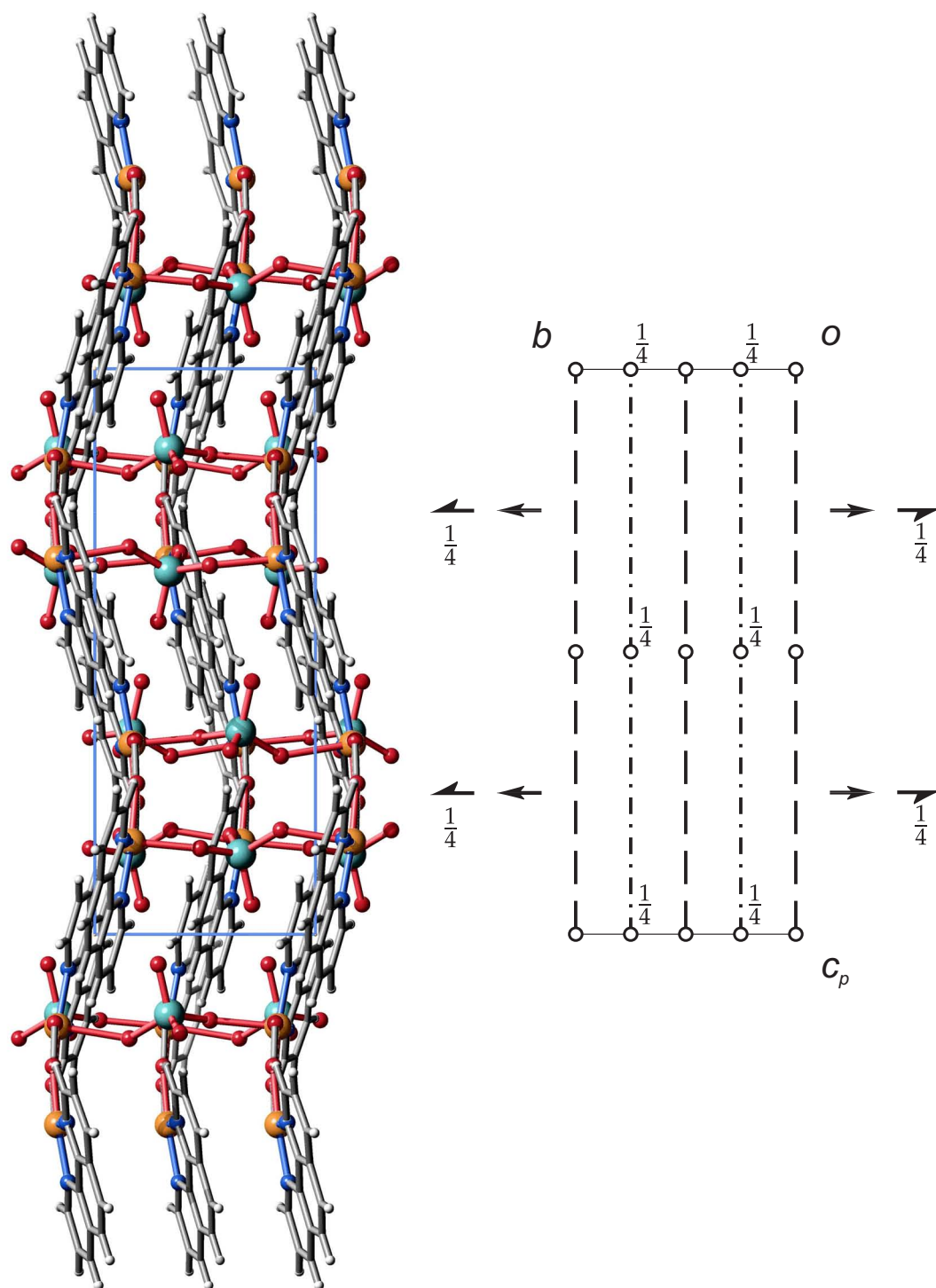


Figure 6.28 SCHAKAL packing diagram of **28** viewed along $[\bar{1}00]$. Hydrogen bonds are indicated by yellow dashed lines. The symmetry elements of the space group $C2/c$ are overlaid. Atoms: carbon (grey, wireframe), hydrogen (light grey, small), copper (orange, large), nitrogen (blue, large), oxygen (red, large), rhenium (dark cyan, large).

6.2 Crystallographic tables

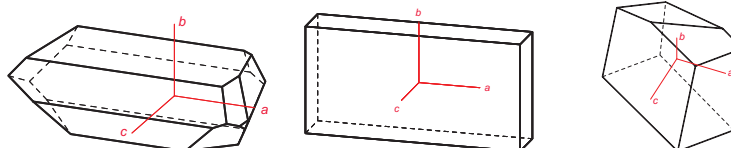
Table 6.1 Archive codes of the compounds in this work. Lower-quality measurements are given in brackets.

Compound	Archive code
1	i078
2	jn121 (in401)
3	i076
4	kn626
5	jn099
6	jn276
7	jn120
8	kn306 (kn114)
9	jn384
10	jn208
11	kn274 (jn179)
12	jn265
13	jn466
14	jn213
15	ln077
16	kn354 (ln106)
17	ln037 (ln023)
18	jn240 (ko012)
19	jn324
20	kn151 (kn104, kn105)
21	jn485
22	jn325 (kn457)
23	kn056
24	jn407
25	kn499
26	jn449
27	kn179
28	lo142

6 Appendix

Table 6.2 Crystallographic tables of [ReO(*fac*-dien)(*syn*-Cyd2',3'H₋₂)]I (**1**), [ReO(*fac*-dien)-(*syn*-Urd2',3'H₋₂)]BPh₄ · MeOH (**2**) and [Re(NPh)(*fac*-dien)(*syn*-AnErytH₋₂)]BPh₄ (**3**).

	1	2	3
empirical formula	C ₁₃ H ₂₄ IN ₆ O ₆ Re	C ₃₈ H ₄₇ BN ₅ O ₈ Re	C ₃₈ H ₄₄ BN ₄ O ₃ Re
M_r /g mol ⁻¹	673.48	898.82	801.78
crystal system	monoclinic	orthorhombic	monoclinic
space group	<i>P</i> 2 ₁	<i>P</i> 2 ₁ 2 ₁ 2 ₁	<i>P</i> 2 ₁ / <i>n</i>
$a/\text{Å}$	10.6867(11)	9.44440(10)	12.1087(9)
$b/\text{Å}$	14.4725(12)	10.6915(2)	19.8809(15)
$c/\text{Å}$	16.9558(18)	36.9230(6)	15.4707(11)
$\alpha/^\circ$	90	90	90
$\beta/^\circ$	104.450(12)	90	102.691(9)
$\gamma/^\circ$	90	90	90
$V/\text{Å}^3$	2539.5(4)	3728.29(10)	3633.3(5)
Z	4	4	4
$\rho/\text{g cm}^{-3}$	1.762	1.601	1.466
μ/mm^{-1}	6.034	3.319	3.385
crystal size/mm	0.371 × 0.200 × 0.114	0.2 × 0.1 × 0.04	0.158 × 0.128 × 0.121
temperature/K	200(2)	200(2)	293(2)
diffractometer	Stoe IPDS	KappaCCD	Stoe IPDS
radiation	MoK α	MoK α	MoK α
anode	fine-focus sealed tube	rotating anode	fine-focus sealed tube
rated input/kW	2.75	4.125	2.75
θ -range/ $^\circ$	1.88–23.92	3.31–27.46	1.69–22.37
reflections	5000	135910	5000
absorption correction	numerical	numerical	numerical
transmission factor range	0.1927–0.5380	0.6193–0.8222	0.6166–0.7221
reflections measured	14269	31344	16964
observed reflections	7765	8394	4642
R_{int}	0.1265	0.0808	0.1094
mean $\sigma(I)/I$	0.1449	0.0753	0.1441
reflections with $I \geq 2\sigma(I)$	5438	7298	2208
x, y (weighting scheme)	0.0725, 0	0.0099, 6.6625	0.0286, 0
refinement	a,b	b	b
Flack parameter	–0.015(15)	0.005(9)	–
parameters	240	482	425
restraints	1	0	0
$R(F_{\text{obs}})$	0.0637	0.0436	0.0408
$R_w(F^2)$	0.1509	0.0828	0.0876
S	0.953	1.104	0.755
shift/error _{max}	0.001	0.001	0.001
max. electron density/e Å^{-3}	1.443	1.556	0.871
min. electron density/e Å^{-3}	–1.742	–1.500	–0.777



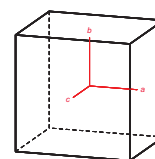
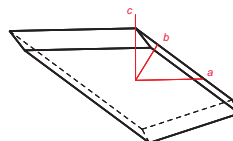
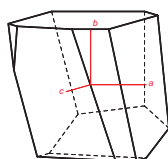
^a All atoms were refined isotropic except for the heavy atoms (rhenium and iodide).

^b All H atoms were calculated in idealized positions riding on their parent atoms.

6 Appendix

Table 6.3 Crystallographic tables of [Re(NPh)(*fac*-dien)(*anti*-AnErytH₋₂)] [ReO(*fac*-dien)(*anti*-AnErytH₋₂)] [BPh₄]Cl (**4**), [Re(NPh)(*mer*-dien)(OEt)(PPh₃)] [ReO₄]Cl · EtOH · 0.5 Me₂CO (**5**) and [ReO(*rac*-dap)(EthdH₋₂)] · MeOH (**6**).

	4	5	6
empirical formula	C ₄₆ H ₆₃ BClN ₇ O ₇ Re ₂	C _{33.5} H ₄₇ ClN ₄ O _{6.5} PRe ₂	C ₆ H ₁₅ N ₂ O ₆ Re
M_r /g mol ⁻¹	1244.69	1048.57	397.40
crystal system	monoclinic	triclinic	monoclinic
space group	$P2_1/c$	$P\bar{1}$	$P2_1/n$
$a/\text{Å}$	23.0247(3)	10.1983(2)	10.7818(3)
$b/\text{Å}$	10.03540(10)	13.9450(2)	5.8322(2)
$c/\text{Å}$	23.3793(3)	16.0432(4)	16.4924(4)
$\alpha/^\circ$	90	70.9763(9)	90
$\beta/^\circ$	116.2546(6)	88.8968(10)	91.0526(10)
$\gamma/^\circ$	90	70.1703(10)	90
$V/\text{Å}^3$	4844.77(10)	2018.35(7)	1036.89(5)
Z	4	2	4
$\rho/\text{g cm}^{-3}$	1.706	1.725	2.546
μ/mm^{-1}	5.104	6.143	11.732
crystal size/mm	0.15 × 0.12 × 0.12	0.06 × 0.05 × 0.02	0.08 × 0.07 × 0.06
temperature/K	200(2)	200(2)	200(2)
diffractometer	KappaCCD	KappaCCD	KappaCCD
radiation	MoK α	MoK α	MoK α
anode	rotating anode	rotating anode	rotating anode
rated input/kW	3.025	4.125	3.025
θ -range/ $^\circ$	3.25 – 27.51	3.14 – 27.47	3.71 – 27.50
reflections	59026	18048	11937
absorption correction	multi-scan/sadabs	numerical	numerical
transmission factor range	0.3756 – 0.542	0.6346 – 0.8820	0.2424 – 0.6043
reflections measured	77855	28925	11571
observed reflections	11085	9154	2373
R_{int}	0.0398	0.0655	0.1319
mean $\sigma(I)/I$	0.0291	0.0727	0.0702
reflections with $I \geq 2\sigma(I)$	9475	6597	2206
x, y (weighting scheme)	0.0233, 5.4231	0.0283, 3.6492	0.0404, 1.6428
refinement	a	a	a
Flack parameter	–	–	–
parameters	597	420	150
restraints	0	0	0
$R(F_{\text{obs}})$	0.0264	0.0405	0.0351
$R_w(F^2)$	0.0589	0.0889	0.0897
S	1.062	1.017	1.103
shift/error _{max}	0.002	0.001	0.001
max. electron density/e Å^{-3}	1.365	1.441	2.921
min. electron density/e Å^{-3}	–1.240	–1.324	–2.717 ^b



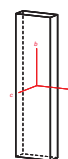
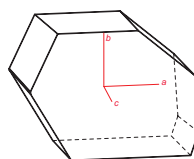
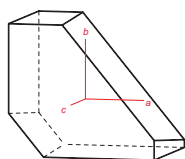
^a All H atoms were calculated in idealized positions riding on their parent atoms.

^b The maximum electron density is located at a distance of 0.90 Å to rhenium.

6 Appendix

Table 6.4 Crystallographic tables of [ReO(*rac*-dap)(*syn*-AnErytH₋₂)] · H₂O (**7**), [ReO(*rac*-dap)-(*anti*-Urd2',3'H₋₂)] · 2 H₂O (**8**) and [ReO(L-his)(ox)] (**9**).

	7	8	9
empirical formula	C ₇ H ₁₄ N ₂ O _{6.5} Re	C ₁₂ H ₂₂ N ₅ O ₁₀ Re	C ₈ H ₈ N ₃ O ₇ Re
M_r /g mol ⁻¹	416.40	582.55	444.37
crystal system	orthorhombic	orthorhombic	orthorhombic
space group	<i>Pbcn</i>	<i>P2₁2₁2₁</i>	<i>P2₁2₁2₁</i>
$a/\text{Å}$	10.0745(2)	8.3369(2)	7.25780(10)
$b/\text{Å}$	12.0837(3)	10.7135(2)	10.2442(2)
$c/\text{Å}$	18.1921(5)	19.9382(4)	17.4025(3)
$\alpha/^\circ$	90	90	90
$\beta/^\circ$	90	90	90
$\gamma/^\circ$	90	90	90
$V/\text{Å}^3$	2214.66(9)	1780.83(6)	1293.88(4)
Z	8	4	4
$\rho/\text{g cm}^{-3}$	2.498	2.173	2.281
μ/mm^{-1}	10.996	6.890	9.424
crystal size/mm	0.18 × 0.16 × 0.15	0.20 × 0.16 × 0.09	0.20 × 0.05 × 0.02
temperature/K	200(2)	200(2)	200(2)
diffractometer	KappaCCD	KappaCCD	KappaCCD
radiation	MoK α	MoK α	MoK α
anode	rotating anode	rotating anode	rotating anode
rated input/kW	4125	3.025	2.250
θ -range/ $^\circ$	4.05–27.48	3.19–27.53	3.44–27.48
reflections	8795	35582	11996
absorption correction	numerical	multi-scan/sadabs	numerical
transmission factor range	0.1491–0.3305	0.338–0.538	0.3125–0.8943
reflections measured	15861	19877	15114
observed reflections	2532	4072	2915
R_{int}	0.0743	0.0427	0.1674
mean $\sigma(I)/I$	0.0442	0.0376	0.0837
reflections with $I \geq 2\sigma(I)$	1864	3960	2860
x, y (weighting scheme)	0.0217, 0	0, 1.0888	0.0396, 2.3984
refinement	a	b	c
Flack parameter	–	0.010(7)	0.018(19)
parameters	178	316	173
restraints	2	9	0
$R(F_{\text{obs}})$	0.0266	0.0199	0.0408
$R_w(F^2)$	0.0557	0.0441	0.0929
S	1.020	1.081	1.045
shift/error _{max}	0.001	0.001	0.001
max. electron density/e Å^{-3}	1.449	1.232	1.509
min. electron density/e Å^{-3}	–1.513	–1.255	–2.724



^a All H atoms were calculated in idealized positions except that one belonging to a half-occupied molecule of water. This hydrogen atom was located in a difference Fourier map and refined as riding on its parent atom (the other hydrogen atom is symmetry-generated). The distance for O-H was refined to 0.77759 Å and the H-H distance for H-O-H was fixed to the 1.57fold (forcing H-O-H to 105°).

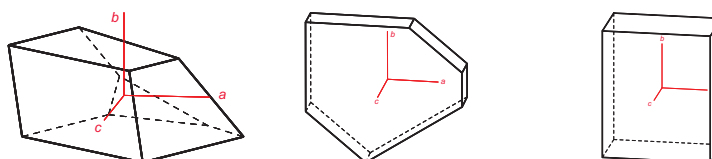
^b All H atoms were calculated in idealized positions except those of two molecules of water. These hydrogen atoms were located in a difference Fourier map and refined as riding on their parent atoms. The distances for O-H were refined to 0.94140 Å and the H-H distances for H-O-H were fixed to the 1.57fold (forcing H-O-H to 105°).

^c All H atoms were calculated in idealized positions riding on their parent atoms.

6 Appendix

Table 6.5 Crystallographic tables of [ReO(L-his)(EthdH₋₂)] · 4.5 H₂O (**10**), [ReO(L-his)(*syn*-AnErytH₋₂)] · 2 H₂O (**11**) and [ReO(L-his)(*syn*-Urd2',3'H₋₂)] · 1.5 H₂O (**12**).

	10	11	12
empirical formula	C ₈ H ₂₁ N ₃ O _{9.5} Re	C ₁₀ H ₁₈ N ₃ O ₈ Re	C ₁₅ H ₂₁ N ₅ O _{10.5} Re
M_r /g mol ⁻¹	497.48	494.47	625.57
crystal system	monoclinic	monoclinic	orthorhombic
space group	<i>P</i> 2 ₁	<i>P</i> 2 ₁	<i>P</i> 2 ₁ 2 ₁ 2 ₁
$a/\text{Å}$	15.6835(3)	10.4052(3)	11.45650(10)
$b/\text{Å}$	6.4703(2)	6.5733(3)	15.5288(2)
$c/\text{Å}$	16.0002(3)	10.5129(3)	22.0816(3)
$\alpha/^\circ$	90	90	90
$\beta/^\circ$	99.2032(17)	92.181(2)	90
$\gamma/^\circ$	90	90	90
$V/\text{Å}^3$	1602.75(6)	718.52(4)	3928.44(8)
Z	4	2	8
$\rho/\text{g cm}^{-3}$	2.062	2.285	2.115
μ/mm^{-1}	7.630	8.502	6.257
crystal size/mm	0.13 × 0.08 × 0.05	0.20 × 0.14 × 0.03	0.06 × 0.05 × 0.03
temperature/K	200(2)	200(2)	200(2)
diffractometer	KappaCCD	KappaCCD	KappaCCD
radiation	MoK α	MoK α	MoK α
anode	rotating anode	rotating anode	rotating anode
rated input/kW	4125	3.025	3.025
θ -range/ $^\circ$	3.38–27.43	3.66–27.53	3.17–27.47
reflections	23280	12902	99629
absorption correction	numerical	multi-scan/sadabs	numerical
transmission factor range	0.4488–0.7286	0.3937–0.775	0.7109–0.8093
reflections measured	21889	11638	42700
observed reflections	7096	3165	8972
R_{int}	0.0523	0.0495	0.0527
mean $\sigma(I)/I$	0.0525	0.0450	0.0397
reflections with $I \geq 2\sigma(I)$	6600	3054	8217
x, y (weighting scheme)	0.0529, 1.4642	0.0095, 0.4048	0.0149, 4.9247
refinement	a	b	c
Flack parameter	–0.025(12)	0.027(9)	–0.015(5)
parameters	431	213	622
restraints	22	7	15
$R(F_{\text{obs}})$	0.0388	0.0218	0.0260
$R_w(F^2)$	0.0960	0.0501	0.0507
S	1.084	1.072	1.071
shift/error _{max}	0.001	0.001	0.001
max. electron density/e Å^{-3}	3.318 ^d	1.144	1.536
min. electron density/e Å^{-3}	–2.102	–1.678	–0.792



^a All H atoms were calculated in idealized positions except those of seven water molecules. These atoms were located in a difference Fourier map and refined as riding on their parent atoms. The distances for O-H were refined to 0.79548 Å and the H-H distances for H-O-H were fixed to the 1.57fold (forcing H-O-H to 105°). Two further water molecules are disordered, these hydrogen atoms were not considered.

^b All H atoms are calculated in idealized positions except those of two molecules of water. These hydrogen atoms were located in a difference Fourier map and refined as riding on their parent atoms. The distances for O-H were refined to 0.82741 Å and the H-H distances for H-O-H were fixed to the 1.57fold (forcing H-O-H to 105°).

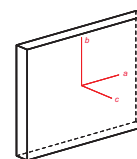
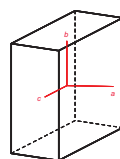
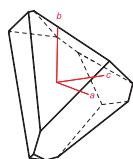
^c All H atoms were calculated in idealized positions except those of three water molecules. These atoms were located in a difference Fourier map and refined as riding on their parent atoms. The distances for O-H were refined to 0.80230 Å and the H-H distances for H-O-H were fixed to the 1.57fold (forcing H-O-H to 105°).

^d The maximum electron density is located at a distance of 0.89 Å to C24.

6 Appendix

Table 6.6 Crystallographic tables of [ReO(L-his)(*anti*-Cyd2',3'H₋₂)] · 5 H₂O (**13**), [ReO(L-his)(*syn*-Me- α -D-Manp2,3H₋₂)] · 2 MeOH (**14**) and [ReO(L-his)(*syn*-Me- β -D-Ribp3,4H₋₂)] · 0.5 MeOH (**15**).

	13	14	15
empirical formula	C ₁₅ H ₂₉ N ₆ O ₁₃ Re	C ₁₅ H ₂₈ N ₃ O ₁₁ Re	C _{12.5} H ₂₀ N ₃ O _{8.5} Re
M_r /g mol ⁻¹	687.64	612.60	534.52
crystal system	orthorhombic	monoclinic	monoclinic
space group	<i>P</i> 2 ₁ 2 ₁ 2 ₁	<i>C</i> 2	<i>P</i> 2 ₁
$a/\text{\AA}$	9.0100(2)	25.2622(4)	10.3763(3)
$b/\text{\AA}$	14.6011(3)	9.0735(2)	6.4665(2)
$c/\text{\AA}$	17.7754(3)	10.4724(2)	14.8657(5)
$\alpha/^\circ$	90	90	90
$\beta/^\circ$	90	114.2054(9)	96.0005(19)
$\gamma/^\circ$	90	90	90
$V/\text{\AA}^3$	2338.46(8)	2189.40(7)	992.00(5)
Z	4	4	2
ρ /g cm ⁻³	1.953	1.859	1.789
μ /mm ⁻¹	5.274	5.610	6.168
crystal size/mm	0.15 × 0.13 × 0.06	0.13 × 0.11 × 0.05	0.18 × 0.13 × 0.02
temperature/K	200(2)	200(2)	200(2)
diffractometer	KappaCCD	KappaCCD	KappaCCD
radiation	MoK α	MoK α	MoK α
anode	rotating anode	rotating anode	rotating anode
rated input/kW	2.250	4.125	3.025
θ -range/ $^\circ$	3.22–27.46	3.28–27.48	3.22–27.56
reflections	64961	14780	22898
absorption correction	numerical	numerical	multi-scan/sadabs
transmission factor range	0.4372–0.6772	0.4851–0.7705	0.58583–0.884
reflections measured	30823	19131	17624
observed reflections	5309	4946	4490
R_{int}	0.0574	0.0367	0.0504
mean $\sigma(I)/I$	0.0376	0.0372	0.0477
reflections with $I \geq 2\sigma(I)$	4933	4702	4112
x, y (weighting scheme)	0.0296, 10.1781	0.0172, 1.8116	0.0879, 0
refinement	a	b	b
Flack parameter	0.001(12)	–0.021(7)	0.043(15)
parameters	348	279	228
restraints	15	1	1
$R(F_{\text{obs}})$	0.0357	0.0207	0.0452
$R_w(F^2)$	0.0896	0.0486	0.1192
S	1.205	1.106	1.062
shift/error _{max}	0.001	0.001	0.001
max. electron density/e \AA^{-3}	1.581	1.167	6.282 ^c
min. electron density/e \AA^{-3}	–1.614	–0.794	–1.935



^a All H atoms were calculated in idealized positions except those of five water molecules. These atoms were located in a difference Fourier map and refined as riding on their parent atoms. The distances for O-H were fixed to 0.83 \AA and the H-H distances for H-O-H were fixed to 1.31 \AA .

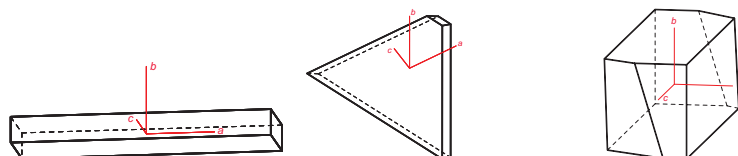
^b All H atoms were calculated in idealized positions riding on their parent atoms.

^c The maximum electron density is located at a distance of 1.457 \AA to O41.

6 Appendix

Table 6.7 Crystallographic tables of [ReO(L-car)(ox)] · 2 H₂O (**16**), [ReO(L-car)(EthdH₋₂)] · MeOH · H₂O (**17**) and [ReO(L-car)(*syn*-AdoH2',3'H₋₂)] · 3 MeOH · 2 H₂O (**18**).

	16	17	18
empirical formula	C ₁₁ H ₁₇ N ₄ O ₁₀ Re	C ₁₂ H ₂₃ N ₄ O ₈ Re	C ₂₂ H ₄₀ N ₉ O ₁₃ Re
M_r /g mol ⁻¹	551.49	537.54	824.83
crystal system	orthorhombic	triclinic	monoclinic
space group	<i>P</i> 2 ₁ 2 ₁ 2 ₁	<i>P</i> 1	<i>C</i> 2
$a/\text{Å}$	5.53010(10)	7.1892(2)	40.8880(8)
$b/\text{Å}$	12.6054(3)	8.0406(2)	8.2436(2)
$c/\text{Å}$	22.9235(6)	9.2764(3)	9.3392(2)
$\alpha/^\circ$	90	64.6911(16)	90
$\beta/^\circ$	90	88.8074(16)	99.8561(10)
$\gamma/^\circ$	90	64.1544(15)	90
$V/\text{Å}^3$	1597.98(6)	427.14(2)	3101.45(12)
Z	4	1	4
$\rho/\text{g cm}^{-3}$	2.292	2.090	1.766
μ/mm^{-1}	7.670	7.162	3.995
crystal size/mm	0.10 × 0.03 × 0.01	0.13 × 0.10 × 0.07	0.30 × 0.15 × 0.13
temperature/K	200(2)	200(2)	200(2)
diffractometer	KappaCCD	KappaCCD	KappaCCD
radiation	MoK α	MoK α	MoK α
anode	rotating anode	rotating anode	rotating anode
rated input/kW	3.025	3.025	4.125
θ -range/ $^\circ$	3.23–27.83	3.18–27.51	3.24–27.47
reflections	41522	5145	49346
absorption correction	multi-scan/sadabs	multi-scan/sadabs	numerical
transmission factor range	0.5479–0.926	0.41184–0.606	0.3913–0.6882
reflections measured	28457	7248	17621
observed reflections	3696	3341	6525
R_{int}	0.1219	0.0197	0.0409
mean $\sigma(I)/I$	0.0799	0.0421	0.0428
reflections with $I \geq 2\sigma(I)$	2929	3341	6115
x, y (weighting scheme)	0.0323, 0	0, 0	0.0345, 18.2127
refinement	a	b	c
Flack parameter	0.011(15)	0.001(7)	0.012(10)
parameters	254	237	472
restraints	9	6	7
$R(F_{\text{obs}})$	0.0418	0.0140	0.0341
$R_w(F^2)$	0.0825	0.0364	0.0822
S	1.049	0.919	1.063
shift/error _{max}	0.001	0.001	0.001
max. electron density/e Å^{-3}	1.301	0.349	1.666
min. electron density/e Å^{-3}	-1.063	-0.918	-1.156



^a All H atoms were calculated in idealized positions except those of two water molecules. These atoms were located in a difference Fourier map and refined as riding on their parent atoms. The distances for O-H were fixed to 0.83 Å and the H-H distances for H-O-H were fixed to 1.31 Å.

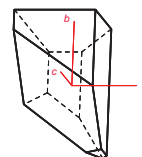
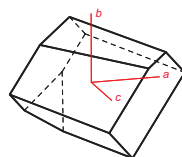
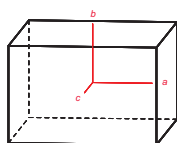
^b All H atoms were calculated in idealized positions except those of one molecule of water. These hydrogen atoms were located in a difference Fourier map and refined as riding on their parent atom. The distances for O-H were refined to 0.82817 Å and the H-H distance for H-O-H was fixed to the 1.57fold (forcing H-O-H to 105°).

^c All H atoms were calculated in idealized positions except those of two water molecules. These atoms were located in a difference Fourier map and refined as riding on their parent atoms. The distances for O-H were refined to 0.83381 Å and the H-H distances for H-O-H were fixed to the 1.57fold (forcing H-O-H to 105°).

6 Appendix

Table 6.8 Crystallographic tables of [ReO(L-car)(*syn*- α -D-Ribf1,2H₋₂)] · 3 MeOH (**19**), [ReO(L-car)(*anti*- α / β -D-Manp2,3H₋₂)] · MeOH (**20**) and [ReO(L-car)(*anti*- β -D-Fruf2,3H₋₂)] · MeOH (**21**).

	19	20	21
empirical formula	C ₁₇ H ₃₃ N ₄ O ₁₂ Re	C ₁₆ H ₂₇ N ₄ O ₁₁ Re	C ₁₆ H ₂₇ N ₄ O ₁₁ Re
M_r /g mol ⁻¹	671.67	637.62	637.62
crystal system	monoclinic	orthorhombic	orthorhombic
space group	<i>P</i> 2 ₁	<i>P</i> 2 ₁ 2 ₁ 2 ₁	<i>P</i> 2 ₁ 2 ₁ 2 ₁
$a/\text{Å}$	8.3488(2)	9.9316(2)	10.0300(2)
$b/\text{Å}$	10.2430(3)	12.6902(2)	12.8684(3)
$c/\text{Å}$	13.7972(4)	16.7231(3)	16.9287(4)
$\alpha/^\circ$	90	90	90
$\beta/^\circ$	93.9294(11)	90	90
$\gamma/^\circ$	90	90	90
$V/\text{Å}^3$	1177.12(6)	2107.68(7)	2184.99(8)
Z	2	4	4
$\rho/\text{g cm}^{-3}$	1.895	2.009	1.938
μ/mm^{-1}	5.230	5.833	5.627
crystal size/mm	0.12 × 0.12 × 0.08	0.07 × 0.05 × 0.04	0.18 × 0.11 × 0.07
temperature/K	200(2)	200(2)	200(2)
diffractometer	KappaCCD	KappaCCD	KappaCCD
radiation	MoK α	MoK α	MoK α
anode	rotating anode	rotating anode	rotating anode
rated input/kW	2.200	3.025	2.250
θ -range/ $^\circ$	3.15–27.50	3.18–29.58	3.15–27.47
reflections	44537	3334	2830
absorption correction	numerical	multi-scan/sadabs	numerical
transmission factor range	0.1681–0.6351	0.51448–0.792	0.1322–0.3865
reflections measured	19331	28513	19146
observed reflections	5367	5909	4972
R_{int}	0.1145	0.0503	0.0989
mean $\sigma(I)/I$	0.0689	0.0552	0.0636
reflections with $I \geq 2\sigma(I)$	5132	5192	4433
x, y (weighting scheme)	0, 10.8648	0.0303, 0.4326	0.0396, 2.7110
refinement	a	a	a
Flack parameter	0.006(15)	0.014(9)	0.009(12)
parameters	291	310	322
restraints	1	0	0
$R(F_{\text{obs}})$	0.0441	0.0330	0.0394
$R_w(F^2)$	0.1101	0.0706	0.0971
S	1.102	1.054	1.076
shift/error _{max}	0.001	0.001	0.001
max. electron density/e Å^{-3}	1.825 ^b	1.250	1.649
min. electron density/e Å^{-3}	-1.922	-1.295	-1.402



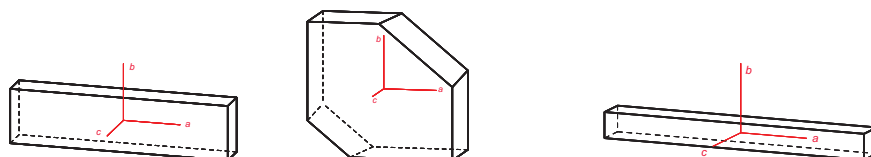
^a All H atoms were calculated in idealized positions riding on their parent atoms.

^b The maximum electron density is located in between two molecules of methanol at a distance of 1.812 Å to C98 and 1.414 Å to O97.

6 Appendix

Table 6.9 Crystallographic tables of [ReO(L-car)(*syn*-6-O- α -D-Glcp- β -D-Fruf2,3H₂)] · 3 H₂O (**22**), (HNEt₃)[ReO(ox)₂(PPh₃)] (**23**) and [Re(NPh)(ox)(PPh₃)₂Cl] · MeOH (**24**).

	22	23	24
empirical formula	C ₂₁ H ₃₉ N ₄ O ₁₈ Re	C ₂₈ H ₃₁ NO ₉ PRE	C ₄₅ H ₃₉ ClNO ₅ P ₂ Re
M_r /g mol ⁻¹	821.76	742.71	957.36
crystal system	orthorhombic	orthorhombic	monoclinic
space group	<i>P</i> 2 ₁ 2 ₁ 2 ₁	<i>Pbca</i>	<i>P</i> 2 ₁ / <i>n</i>
$a/\text{\AA}$	9.00600(10)	12.4146(2)	10.7762(2)
$b/\text{\AA}$	10.29090(10)	15.3531(2)	19.7020(4)
$c/\text{\AA}$	30.6272(3)	30.3448(5)	18.5788(4)
$\alpha/^\circ$	90	90	90
$\beta/^\circ$	90	90	91.0589(9)
$\gamma/^\circ$	90	90	90
$V/\text{\AA}^3$	2838.52(5)	5783.80(15)	3943.84(14)
Z	4	8	4
$\rho/\text{g cm}^{-3}$	1.923	1.706	1.612
μ/mm^{-1}	4.373	4.310	3.278
crystal size/mm	0.14 × 0.035 × 0.02	0.14 × 0.10 × 0.06	0.21 × 0.03 × 0.02
temperature/K	200(2)	200(2)	200(2)
diffractometer	KappaCCD	KappaCCD	KappaCCD
radiation	MoK α	MoK α	MoK α
anode	rotating anode	rotating anode	rotating anode
rated input/kW	2.200	2.250	2.250
θ -range/ $^\circ$	3.29–27.48	3.15–27.65	3.29–27.51
reflections	49980	7243	9233
absorption correction	numerical	multi-scan/sadabs	numerical
transmission factor range	0.6866–0.9130	0.6312–0.772	0.5474–0.9057
reflections measured	28884	60925	55432
observed reflections	6382	6646	9002
R_{int}	0.0592	0.0859	0.1430
mean $\sigma(I)/I$	0.0383	0.0502	0.0992
reflections with $I \geq 2\sigma(I)$	6190	3895	5662
x, y (weighting scheme)	0.0239, 1.5920	0.0284, 5.1510	0.0265, 20.9597
refinement	a	b	b
Flack parameter	–0.016(5)	–	–
parameters	435	365	500
restraints	9	0	2
$R(F_{\text{obs}})$	0.0228	0.0334	0.0637
$R_w(F^2)$	0.0521	0.0790	0.1373
S	1.033	1.021	1.060
shift/error _{max}	0.001	0.001	0.001
max. electron density/e \AA^{-3}	0.796	1.084	2.052 ^c
min. electron density/e \AA^{-3}	–1.144	–0.566	–0.917



^a All H atoms were calculated in idealized positions except those of three water molecules. These atoms were located in a difference Fourier map and refined as riding on their parent atoms. The distances for O-H were refined to 0.90200 \AA and the H-H distances for H-O-H were fixed to the 1.57fold (forcing H-O-H to 105°).

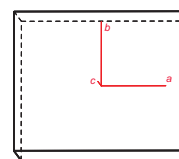
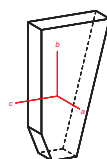
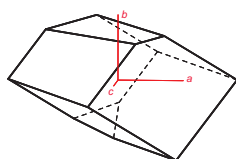
^b All H atoms were calculated in idealized positions riding on their parent atoms.

^c The maximum electron density is located at a distance of 0.99 \AA to rhenium.

6 Appendix

Table 6.10 Crystallographic tables of [ReO(*syn*-AnErytH₋₂)(MeOH)(PPh₃)Cl] (**25**), [ReO-(*L*-thr)(*syn*-AnErytH₋₂)(PPh₃)] (**26**) and [ReO(*fac*-ida)(Ery11,12H₋₂)] · MeOH · H₂O (**27**).

	25	26	27
empirical formula	C ₂₃ H ₂₅ ClO ₅ Pre	C ₂₆ H ₂₉ NO ₇ Pre	C ₄₂ H ₇₅ N ₂ O ₁₉ Re
M_r /g mol ⁻¹	634.05	684.67	1098.24
crystal system	triclinic	orthorhombic	orthorhombic
space group	$P\bar{1}$	$P2_12_12_1$	$P2_12_12_1$
$a/\text{\AA}$	9.2143(2)	10.1324(2)	9.25580(10)
$b/\text{\AA}$	9.5063(2)	10.21270(10)	21.9502(3)
$c/\text{\AA}$	12.9866(4)	24.6530(4)	28.9555(4)
$\alpha/^\circ$	95.0705(14)	90	90
$\beta/^\circ$	93.6892(16)	90	90
$\gamma/^\circ$	90.3853(17)	90	90
$V/\text{\AA}^3$	1130.66(5)	2551.07(7)	5882.79(13)
Z	2	4	4
ρ /g cm ⁻³	1.862	1.783	1.240
μ /mm ⁻¹	5.595	4.872	2.127
crystal size/mm	0.07 × 0.05 × 0.04	0.13 × 0.05 × 0.02	0.12 × 0.1 × 0.1
temperature/K	200(2)	200(2)	200(2)
diffractometer	KappaCCD	KappaCCD	KappaCCD
radiation	MoK α	MoK α	MoK α
anode	rotating anode	rotating anode	rotating anode
rated input/kW	3.025	2.250	3.025
θ -range/ $^\circ$	3.16–27.53	3.18–27.49	3.19–25.06
reflections	14027	3306	197984
absorption correction	multi-scan/sadabs	numerical	multi-scan/sadabs
transmission factor range	0.5508–0.799	0.4363–0.8526	0.6325–0.808
reflections measured	20676	25304	62298
observed reflections	5160	5834	10326
R_{int}	0.0395	0.1022	0.0685
mean $\sigma(I)/I$	0.0413	0.0580	0.0629
reflections with $I \geq 2\sigma(I)$	4574	5457	8564
x, y (weighting scheme)	0.0131, 2.8024	0.0143, 2.7975	0.0812, 0.4218
refinement	a	a	a,b
Flack parameter	–	–0.013(8)	0.025(9)
parameters	283	328	584
restraints	0	0	0
$R(F_{\text{obs}})$	0.0291	0.0297	0.0475
$R_w(F^2)$	0.0582	0.0685	0.1289
S	1.046	1.035	1.086
shift/error _{max}	0.001	0.001	0.001
max. electron density/e \AA^{-3}	1.596	1.469	1.024
min. electron density/e \AA^{-3}	–1.258	–1.592	–0.544



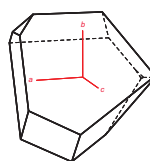
^a All H atoms were calculated in idealized positions riding on their parent atoms.

^b The H atoms of one molecule of disordered water were not considered.

6 Appendix

Table 6.11 Crystallographic table of $[\text{Cu}_2(\text{phen})_2(\text{ox})(\text{ReO}_4)_2]_n$ (28).

28	
empirical formula	$\text{C}_{13}\text{H}_8\text{CuN}_2\text{O}_6\text{Re}$
$M_r/\text{g mol}^{-1}$	537.95
crystal system	monoclinic
space group	$\text{C2}/c$
$a/\text{\AA}$	20.514(3)
$b/\text{\AA}$	7.372(3)
$c/\text{\AA}$	18.973(4)
$\alpha/^\circ$	90
$\beta/^\circ$	93.040(15)
$\gamma/^\circ$	90
$V/\text{\AA}^3$	2865.2(14)
Z	8
$\rho/\text{g cm}^{-3}$	2.494
μ/mm^{-1}	9.959
crystal size/mm	$0.31 \times 0.24 \times 0.09$
temperature/K	200(2)
diffractometer	Oxford XCalibur
radiation	$\text{MoK}\alpha$
anode	fine-focus sealed tube
rated input/kW	2.00
θ -range/ $^\circ$	4.06–27.50
absorption correction	numerical
transmission factor range	0.1630–0.2100
reflections measured	13605
observed reflections	3237
R_{int}	0.0355
mean $\sigma(I)/I$	0.0301
reflections with $I \geq 2\sigma(I)$	2553
x, y (weighting scheme)	0.0312, 0
refinement	a
Flack parameter	–
parameters	208
restraints	0
$R(F_{\text{obs}})$	0.0228
$R_w(F^2)$	0.0535
S	1.021
shift/error _{max}	0.003
max. electron density/ e \AA^{-3}	1.011
min. electron density/ e \AA^{-3}	–1.298



^a All H atoms were calculated in idealized positions. They are riding with $U(\text{H}) = 1.2 \cdot U(\text{C})$ for CH.

6.3 Summary of rhenium coordination geometries

Table 6.12 Selected geometrical parameters of the compounds with rhenium(V) in this work. Re=O, Re=N: Distances [Å] of the oxido and phenylimido ligands to the metal core. Re-O, Re-N: Distances [Å] of the alkoxido and amino ligands to the metal core in *trans* or *cis* position. X-Re-Y, O-C-C-O: angles [°] of the main axes and torsion angles of the diolato moieties.

	Re=O	Re=N	Re-O _{cis}	Re-N _{cis}	Re-O _{trans}	Re-N _{trans}	X-Re-Y	O-C-C-O
Compounds with dien:								
1a	1.658(16)	–	1.936(12), 1.928(12)	2.197(15), 2.18(2)	–	2.29 (2)	160.1(7)	24(2)
1b	1.624(17)	–	1.931(14), 1.945(13)	2.219(15), 2.193(17)	–	2.257(16)	155.8(7)	4(2)
2	1.684(4)	–	1.936(4), 1.965(4)	2.159(6), 2.189(5)	–	2.279(5)	160.7(2)	15.9(7)
3	–	1.720(8)	1.961(6), 1.937(8)	2.075(9), 2.144(10)	–	2.239(10)	163.8(4)	–20.8(18)
4	–	1.723(3)	1.964(2), 1.962(2)	2.157(3), 2.185(3)	–	2.240(3)	162.8(1)	5.4(4)
5	–	1.733(5)	–	2.165(5), 2.148(5), 2.158(5)	1.935(4)	–	178.2(2)	–
mean	1.66 ± 0.03	1.73 ± 0.01	1.95 ± 0.02	2.17 ± 0.10	–	2.26 ± 0.03	164 ± 15	14 ± 10*
Compounds with dap:								
6	1.686(4)	–	1.976(4), 1.943(3)	2.151(5), 2.186(5)	2.118(3)	–	161.0(2)	–40.7(6)
7	1.677(4)	–	1.938(3), 1.939(3)	2.150(4), 2.164(4)	2.167(3)	–	161.0(1)	10.8(5)
8	1.677(3)	–	1.952(2), 1.938(2)	2.169(3), 2.151(3)	2.131(3)	–	162.7(1)	24.5(4)
mean	1.68 ± 0.01	–	1.95 ± 0.03	2.16 ± 0.02	2.14 ± 0.03	–	162 ± 1	25 ± 15*

Continued on next page

Table 6.12 – continued from previous page

	Re=O	Re=N	Re-O _{cis}	Re-N _{cis}	Re-O _{trans}	Re-N _{trans}	X-Re-Y	O-C-C-O
Compounds with L-histidine:								
9	1.676(5)	–	2.034(5), 2.019(6)	2.128(7), 2.071(5)	2.113(6)	–	163.7(3)	–4.4(11)
10a	1.689(6)	–	1.950(5), 1.945(6)	2.143(6), 2.105(6)	2.187(5)	–	163.6(2)	43.5(10)
10b	1.685(6)	–	1.954(5), 1.958(6)	2.151(6), 2.115(6)	2.198(5)	–	163.4(2)	44.1(9)
11	1.682(3)	–	1.924(3), 1.959(3)	2.169(3), 2.102(3)	2.205(3)	–	162.6(2)	28.2(5)
12a	1.676(3)	–	1.962(3), 1.972(3)	2.156(3), 2.117(3)	2.142(3)	–	160.1(1)	28.6(5)
12b	1.688(3)	–	1.934(3), 1.971(3)	2.170(4), 2.092(4)	2.139(3)	–	163.2(2)	1.6(5)
13	1.704(5)	–	1.979(5), 1.936(5)	2.179(6), 2.073(6)	2.198(5)	–	163.7(2)	30.0(7)
14	1.688(3)	–	1.955(2), 1.937(3)	2.179(4), 2.098(3)	2.183(3)	–	161.8(1)	–40.8(5)
15	1.684(7)	–	1.926(6), 1.960(5)	2.179(6), 2.115(7)	2.194(5)	–	162.5(3)	41.3(10)
mean	1.69 ± 0.02	–	1.96 ± 0.07	2.13 ± 0.06	2.17 ± 0.06	–	164 ± 3	29 ± 28*
Compounds with L-carnosine:								
16**	1.660(6)	–	2.082(5), 2.004(7)	1.968(7), 2.111(7)	2.131(6)	–	164.9(3)	6.2(11)
17	1.679(4)	–	1.946(3), 1.946(4)	2.105(3), 2.120(4)	2.171(3)	–	167.7(2)	–36.7(5)
18	1.646(8)	–	1.977(4), 1.947(7)	2.066(5), 2.131(8)	2.177(7)	–	167.4(3)	–32.1(7)
19	1.689(7)	–	2.003(8), 1.951(6)	2.073(7), 2.158(8)	2.165(7)	–	163.4(3)	–18.7(10)
20	1.679(4)	–	1.982(4), 1.972(3)	2.075(4), 2.139(4)	2.166(4)	–	164.8(2)	–46.0(5)
21	1.680(5)	–	1.985(5), 1.944(5)	2.090(5), 2.112(5)	2.226(5)	–	165.3(2)	–28.4(8)
22	1.678(2)	–	1.984(2), 1.968(2)	2.073(3), 2.120(3)	2.198(2)	–	166.2(1)	–32.1(3)
mean	1.68 ± 0.03	–	1.97 ± 0.04	2.11 ± 0.05	2.18 ± 0.04	–	166 ± 2	32 ± 14*

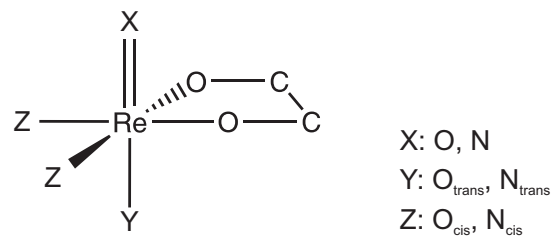
Continued on next page

Table 6.12 – continued from previous page

	Re=O	Re=N	Re-O _{cis}	Re-N _{cis}	Re-O _{trans}	Re-N _{trans}	X-Re-Y	O-C-C-O
other compounds:								
23	1.685(3)	–	2.003(3), 2.031(3), 2.046(3)	–	2.092(3)	–	166.2(1)	1.4(6), 4.4(5)
24	–	1.709(7)	2.090(5)	–	2.059(5)	–	170.2(3)	2.6(10)
25	1.670(3)	–	1.928(3), 1.955(3)	–	2.255(3)	–	168.1(1)	7.3(5)
26	1.680(3)	–	1.948(4), 1.965(3)	2.196(4)	2.117(3)	–	161.2(2)	–20.4(5)
27	1.671(5)	–	2.069(5), 1.949(5), 1.955(5)	2.185(6)	2.101(5)	–	161.0(2)	41.3(7)

*the mean torsion angles were calculated with the absolute values of the torsion angles.

****16** was excluded for mean value calculation due to a different coordination mode.



Bibliography

- [1] F. W. Lichtenthaler, S. Peters, Carbohydrates as green raw materials for the chemical industry, *Comptes Rendus Chimie* **2004**, 7(2), [65–90](#).
- [2] G. Banfalvi, Why Ribose Was Selected as the Sugar Component of Nucleic Acids, *DNA and Cell Biology* **2006**, 25(3), [189–196](#).
- [3] R. Apweiler, H. Hermjakob, N. Sharon, On the frequency of protein glycosylation, as deduced from analysis of the SWISS-PROT database, *Biochimica et Biophysica Acta* **1999**, 1473(1), [4–8](#).
- [4] R. Raman, S. Raguram, G. Venkataraman, J. C. Paulson, R. Sasisekharan, Glycomics: an integrated systems approach to structure-function relationships of glycans, *Nature Methods* **2005**, 2(11), [817–824](#).
- [5] K. F. Aoki-Kinoshita, An Introduction to Bioinformatics for Glycomics Research, *PLoS Comput. Biol.* **2008**, 4(5), [e1000075](#).
- [6] H.-J. Gabius, H.-C. Siebert, S. André, J. Jiménez-Barbero, H. Rüdiger, Chemical Biology of the Sugar Code, *ChemBioChem* **2004**, 5(6), [740–764](#).
- [7] J. D. Marth, A unified vision of the building blocks of life, *Nature Cell Biology* **2008**, 10, [1015–1016](#).
- [8] T. Allscher, P. Klüfers, P. Mayer, Carbohydrate-Metal Complexes: Structural Chemistry of Stable Solution Species, *Glycoscience* **2008**, 4, [1077–1139](#).
- [9] K. J. Waldron, N. J. Robinson, How do bacterial cells ensure that metalloproteins get the correct metal?, *Nature Reviews Microbiology* **2009**, 7, [25–35](#).
- [10] K. Severin, R. Bergs, W. Beck, Bioorganometallic Chemistry - Transition Metal Complexes with α -Amino Acids and Peptides, *Angew. Chem. Int. Ed.* **1998**, 37(12), [1634–1654](#).
- [11] E. Farkas, I. Sóvágó, Metal Complexes of Amino Acids and Peptides, *Amino Acids, Peptides and Proteins* **2007**, 36, [287–345](#).

Bibliography

- [12] N. Wiberg, E. Wiberg, A. F. Holleman, *Lehrbuch der Anorganischen Chemie*, Vol. 101, deGruyter, **1995**.
- [13] S. Szabó, I. Bakos, Electroreduction of rhenium from sulfuric acid solutions of perrhenic acid, *J. Electroanalyt. Chem.* **2000**, 492(2), [103–111](#).
- [14] D. Colodner, J. Sachs, G. Ravizza, K. Turekian, J. Edmond, E. Boyle, The geochemical cycle of rhenium: a reconnaissance, *Earth Planetary Sci. Lett.* **1993**, 117(1–2), [205–221](#).
- [15] Y. Xiong, S. A. Wood, Experimental determination of the solubility of ReO_2 and the dominant oxidation state of rhenium in hydrothermal solutions, *Chem. Geology* **1999**, 158(3–4), [245–256](#).
- [16] Y. Xiong, Solubility and speciation of rhenium in anoxic environments at ambient temperature and applications to the Black Sea, *Deep-Sea Res. Part I* **2003**, 50(5), [681–690](#).
- [17] U. Abram, Rhenium, *Compr. Coord. Chem. II* **2004**, 5, [271–402](#).
- [18] F. A. Cotton, S. J. Lippard, Chemical and Structural Studies of Rhenium(V) Oxyhalide Complexes, *Inorg. Chem.* **1966**, 5(1), [9–16](#).
- [19] B. Nock, T. Maina, F. Tisato, M. Papadopoulos, C. P. Raptopoulou, A. Terzis, E. Chiotellis, Novel Six-Coordinate Oxorhenium “3 + 2” Mixed-Ligand Complexes Carrying the SNS/PO Donor Atom Set: Synthesis and Characterization, *Inorg. Chem.* **1999**, 38(19), [4197–4202](#).
- [20] B. Nock, T. Maina, F. Tisato, M. Papadopoulos, C. P. Raptopoulou, A. Terzis, E. Chiotellis, Synthesis and Characterization of Six-Coordinate “3 + 2” Mixed-Ligand Oxorhenium Complexes with the *o*-Diphenylphosphinophenolato Ligand and Tridentate Coligands of Different N and S Donor Atom Combinations, *Inorg. Chem.* **2000**, 39(10), [2178–2184](#).
- [21] W. A. Herrmann, D. Marz, E. Herdtweck, A. Schäfer, W. Wagner, H.-J. Kneuper, Glycolate and Thioglycolate Complexes of Rhenium and Their Oxidative Elimination of Ethylene and of Glycol, *Angew. Chem. Int. Ed.* **1987**, 26(5), [462–464](#).
- [22] G. Böhm, K. Wiegardt, B. Nuber, J. Weiss, The Re–Re Bond in Binuclear Di- μ -oxorhenium Complexes Containing the 1,4,7-Triazacyclononane Ligand, *Angew. Chem. Int. Ed.* **1990**, 29(7), [787–790](#).

Bibliography

- [23] M. Oßberger, PhD thesis, Rhenium(V/VI)-Kohlenhydrat-Verbindungen, LMU München, [2003](#).
- [24] P. Grimminger, Rhenium(V)-Pyranosid-Komplexe, Diploma thesis, LMU München [2004](#).
- [25] A. Paulo, A. Domingos, A. P. de Matos, I. Santos, M. F. N. N. Carvalho, A. J. L. Pombeiro, Synthesis, Characterization, and Study of the Redox Properties of Rhenium(V) and Rhenium(III) Compounds with Tetrakis(pyrazol-1-yl)borate, *Inorg. Chem.* **1994**, 33(21), [4729–4737](#).
- [26] M. Porchia, G. Papini, C. Santini, G. G. Lobbia, M. Pellei, F. Tisato, G. Bandoli, A. Dolmella, Novel Rhenium(V) Oxo Complexes Containing Bis(pyrazol-1-yl)acetate and Bis(pyrazol-1-yl) Sulfonate as Tripodal *N,N,O*-heteroscorpionate Ligands, *Inorg. Chem.* **2005**, 44(11), [4045–4054](#).
- [27] G. Papini, PhD thesis, New metal complexes supported by scorpionate and macrocyclic ligands: chemistry and biological studies, Università di Camerino, [2008](#).
- [28] J. A. Thomas, A. Davison, High oxidation state technetium and rhenium complexes of hydrotris(1-pyrazolyl)borate, *Inorg. Chim. Acta* **1991**, 190(2), [231–235](#).
- [29] P. R. Lassen, L. Guy, I. Karame, T. Roisnel, N. Vanthuyne, C. Roussel, X. Cao, R. Lombardi, J. Crassous, T. B. Freedman, L. A. Nafie, Synthesis and Vibrational Circular Dichroism of Enantiopure Chiral Oxorhenium(V) Complexes Containing the Hydrotris(1-pyrazolyl)borate Ligand, *Inorg. Chem.* **2006**, 45(25), [10230–10239](#).
- [30] S. N. Brown, J. M. Mayer, Photochemical generation of a reactive rhenium(III) oxo complex and its curious mode of cleavage of dioxygen, *Inorg. Chem.* **1992**, 31(20), [4091–4100](#).
- [31] P. Klüfers, O. Krotz, M. Oßberger, Oxorhenium(V) Complexes of Carbohydrate Ligands, *Eur. J. Inorg. Chem.* **2002**, 8(8), [1919–1923](#).
- [32] O. Labisch, PhD thesis, Offenkettige Monosaccharide als Liganden, LMU München, [2006](#).
- [33] H. Sugimoto, Y. Sasaki, A Series of Oxorhenium(V) Complexes Containing Tridentate Tris(2-pyridylmethyl)amine Bearing One Free 2-Pyridylmethyl Arm, *Chem. Lett.* **1997**, 26(6), [541–542](#).

Bibliography

- [34] J. M. Botha, K. Umakoshi, Y. Sasaki, G. J. Lamprecht, Chelation Processes to an Oxorhenium(V) Center by *N,N,N,O*-Tetradentate and *N,N,O*-Tridentate Ligands As Verified by Structural and Mechanistic Studies of Intermediate Species, *Inorg. Chem.* **1998**, 37(7), 1609–1615.
- [35] A. Abrahams, G. Bandoli, S. Gatto, T. I. A. Gerber, J. G. H. du Preez, A synthetic and structural study of oxorhenium(V) complexes with mixed didentate (*O,O*)-terdentate(*O,N,N*) ligands, *J. Coord. Chem.* **1998**, 43(4), 297–307.
- [36] T. I. A. Gerber, P. Mayer, Z. R. Tshentu, Synthesis and structure of oxorhenium(V) complexes containing a terdentate imidazole ligand. A route to mixed “3 + 2” complexes, *J. Coord. Chem.* **2005**, 58(11), 947–953.
- [37] R. Chiozzone, R. González, C. Kremer, G. de Munno, J. Faus, Oxalato complexes of Re(V). Synthesis and structural characterization of [ReO(OCH₃)(ox)-(L)] (L = bipy, dppe and dppee), *Inorg. Chim. Acta* **2001**, 325(1–2), 203–207.
- [38] J. W. Faller, A. R. Lavoie, Diastereoselective Synthesis and Electronic Asymmetry of Chiral Nonracemic Rhenium(V) Oxo Complexes Containing the Hydrotris(1-pyrazolyl)borate Ligand, *Organometallics* **2000**, 19(19), 3957–3962.
- [39] C. Melian, C. Kremer, L. Suescun, A. Mombru, R. Mariezcurrena, E. Kremer, Re(V) complexes with amino acids based on the “3 + 2” approach, *Inorg. Chim. Acta* **2000**, 306(1), 70–77.
- [40] S. Kirsch, R. Jankowsky, P. Leibnitz, H. Spies, B. Johannsen, Crystal and solution structure of oxo rhenium(V) complexes with cysteine and cysteine methyl ester, *J. Biol. Inorg. Chem.* **1999**, 4(1), 48–55.
- [41] C. Tessier, F. D. Rochon, A. L. Beauchamp, Binding of the Oxo-Rhenium(V) Core to Methionine and to N-Terminal Histidine Dipeptides, *Inorg. Chem.* **2004**, 43(23), 7463–7473.
- [42] C. Tessier, F. D. Rochon, A. L. Beauchamp, Oxorhenium(V) Complexes with the Non-Sulfur-Containing Amino Acid Histidine, *Inorg. Chem.* **2002**, 41(24), 6527–6536.
- [43] S. Liu, Bifunctional coupling agents for radiolabeling of biomolecules and target-specific delivery of metallic radionuclides, *Adv. Drug Delivery Rev.* **2008**, 60(12), 1347–1370.

Bibliography

- [44] J. R. Dilworth, S. J. Parrott, The biomedical chemistry of technetium and rhenium, *Chem. Soc. Rev.* **1998**, 27(1), 43–55.
- [45] S. R. Banerjee, K. P. Maresca, L. Francesconi, J. Valliant, J. W. Babich, J. Zubieta, New directions in the coordination chemistry of ^{99m}Tc : a reflection on technetium core structures and a strategy for new chelate design, *Nucl. Med. Biol.* **2005**, 32(1), 1–20.
- [46] G. Ferro-Flores, C. A. de Murphy, Pharmacokinetics and dosimetry of ^{188}Re -pharmaceuticals, *Adv. Drug Delivery Rev.* **2008**, 60(12), 1389–1401.
- [47] U. Abram, R. Alberto, Technetium and Rhenium - Coordination Chemistry and Nuclear Medical Applications, *J. Braz. Chem. Soc.* **2006**, 17(8), 1486–1500.
- [48] J. Schmaljohann, H.-J. Biersack, S. Guhlke, Radiotherapeutika: Herstellung und therapeutische Anwendung von Radiopharmaka, *Pharm. Unserer Zeit* **2005**, 34(6), 498–504.
- [49] A. Manka-Waluch, PhD thesis, Radionuklidtherapie mit Rhenium-188-HEDP beim hormonrefraktären, ossär metastasierten Prostatakarzinom, Universität Bonn, **2006**.
- [50] D. E. Milenic, E. D. Brady, M. W. Brechbiel, Antibody-targeted radiation cancer therapy, *Nature Rev. Drug Disc.* **2004**, 3, 488–499.
- [51] E. García-Garayoa, R. Schibli, P. A. Schubiger, Peptides radiolabeled with Re-186/188 and Tc-99m as potential diagnostic and therapeutic agents, *Nucl. Sci. Techniques* **2007**, 18(2), 88–100.
- [52] H. M. Bigott-Hennkens, S. Junnotula, L. Ma, F. Gallazzi, M. R. Lewis, S. S. Jurisson, Synthesis and in Vitro Evaluation of a Rhenium-Cyclized Somatostatin Derivative Series, *J. Med. Chem.* **2008**, 51(5), 1223–1230.
- [53] E. Pohl, A. Heine, G. M. Sheldrick, Z. Dauter, K. S. Wilson, J. Kallen, W. Huber, P. J. Pfäffli, Structure of octreotide, a somatostatin analogue, *Acta Crystallogr., Sect. C*, **1995**, 51(1), 48–59.
- [54] C. Saint-Jore-Dupas, L. Faye, V. Gomord, From planta to pharma with glycosylation in the toolbox, *Trends in Biotechnol.* **2007**, 25(7), 317–323.
- [55] P. Niederhafner, J. Šebestík, J. Ježek, Glycopeptide dendrimers, *J. Peptide Sci.* **2007**, 14(1), 2–43.

Bibliography

- [56] S. A. Wunneda Gruner, PhD thesis, Carbohydrate-Based Mimetics in Drug Design: Sugar Amino Acids as Structural Templates and Key Residues of Bioactive Peptidomimetics, TU München, **2002**.
- [57] T. K. Chakraborty, P. Srinivasu, S. Tapadar, B. K. Mohan, Sugar amino acids and related molecules: Some recent developments, *J. Chem. Sci.* **2004**, *116*, **187–207**.
- [58] J. Gancheff, C. Melian, C. Kremer, S. Dominguez, A. Mederos, O. N. Ventura, E. Kremer, Synthesis, characterization and solution chemistry of new Re(V) dioxo complexes, *J. Coord. Chem.* **2001**, *54*(3–4), **285–296**.
- [59] D. Cremer, J. A. Pople, A General Definition of Ring Puckering Coordinates, *J. Am. Chem. Soc.* **1975**, *97*(6), **1354–1358**.
- [60] D. L. Ward, β -Cytidine, $C_9H_{13}N_3O_5$, *Acta Crystallogr., Sect. C*, **1993**, *49*(10), **1789–1792**.
- [61] IUPAC-IUB Joint Commission on Biochemical Nomenclature, Abbreviations and Symbols for the Description of Conformations of Polynucleotide Chains, *Pure Appl. Chem.* **1983**, *55*(8), **1273–1280**.
- [62] A. Bondi, van der Waals Volumes and Radii, *J. Phys. Chem.* **1964**, *68*(3), **441–451**.
- [63] L. Kozerski, H. Sierzputowska-Gracz, W. Krzyzosiak, M. Bratek-Wiewiorowska, M. Jaskolski, M. Wiewiorowski, Comparative structural analysis of cytidine, ethencytidine, and their protonated salts III. 1H , ^{13}C and ^{15}N NMR studies at natural isotope abundance, *Nucleic Acids Res.* **1984**, *12*(4), **2205–2223**.
- [64] C. A. G. Haasnoot, F. A. A. M. de Leeuw, C. Altona, The relationship between proton-proton NMR coupling constants and substituent electronegativities – I An empirical generalization of the Karplus equation, *Tetrahedron* **1980**, *36*(19), **2783–2792**.
- [65] H. Gottlieb, V. Kotlyar, A. Nudelman, NMR Chemical Shifts of Common Laboratory Solvents as Trace Impurities, *J. Org. Chem.* **1997**, *62*(21), **7512–7515**.
- [66] E. A. Green, R. D. Rosenstein, R. Shiono, D. J. Abraham, B. L. Trus, R. E. Marsh, The crystal structure of uridine, *Acta Crystallogr., Sect. B*, **1975**, *31*(1), **102–107**.
- [67] H. H. Mantsch, I. C. P. Smith, Fourier-Transformed ^{13}C NMR Spectra of Polyuridylic Acid, Uridine, and Related Nucleotides — the Use of $^{31}POC^{13}C$

Bibliography

- Couplings for Conformational Analysis, *Biochem. Biophys. Res. Commun.* **1972**, 46(2), 808–815.
- [68] J. Uzawa, M. Uramoto, Assignment of Indirect ^{13}C , ^1H Couplings in the ^{13}C NMR Spectra of Some Purine and Pyrimidine Nucleosides and their Analogues by Long-range Selective ^1H Decoupling, *Org. Magn. Resonance* **1979**, 12(11), 612–615.
- [69] L. G. Marzilli, B. de Castro, C. Solorzano, Nucleoside Complexing: A ^{13}C NMR Spectroscopic Study of Binding of Metal Ions to Guanosine and Related Nucleosides in Solution. Evidence for O-6 Binding under Basic Conditions, *J. Am. Chem. Soc.* **1982**, 104(2), 461–466.
- [70] E. Forsellini, U. Casellato, R. Graziani, M. C. Carletti, L. Magon, Trichloro(phenylimido)bis(triphenylphosphine)rhenium(V) Dichloromethane (1/1), *Acta Crystallogr., Sect. C*, **1984**, 40(11), 1795–1797.
- [71] F. Ikegami, A. Yamamoto, Y. Kuo, F. Lambein, Enzymatic Formation of 2,3-Diaminopropionic Acid, the Direct Precursor of the Neurotoxin β -ODAP, in *Lathyrus sativus*, *Biol. Pharm. Bull.* **1999**, 22(7), 770–771.
- [72] R. W. Hay, P. J. Morris, The Interaction of D,L-2,3-Diaminopropionic Acid and its Methyl Ester with Metal Ions. Part 1. Formation Constants, *J. Chem. Soc. A* **1971**, 3562–3569.
- [73] A. de Bruyn, D. V. Haver, F. Lambein, B. M. Abegaz, Chemical properties of the natural neurotoxin of *Lathyrus sativus* 3-N-oxalyl-2,3-diamino-propanoic acid (β -ODAP), its nontoxic 2-N-oxalyl isomer, and its hydrolysis product 2,3-diamino-propanoic acid (DAPRO) by ^1H - and ^{13}C -NMR spectroscopy, *Natural Toxins* **1993**, 1(6), 328–340.
- [74] Y. Liu, J. K. Pak, P. Schmutz, M. Bauwens, J. Mertens, H. Knight, R. Alberto, Amino Acids Labeled with $[^{99\text{m}}\text{Tc}(\text{CO})_3]^+$ and Recognized by the L-type Amino Acid Transporter LAT1, *J. Am. Chem. Soc.* **2006**, 128(50), 15996–15997.
- [75] H. Liu, H. Ishida, Y. Yoshikawa, Potential propelling and rotating functions of propeller-type complexes. I. Preparation and molecular dynamics simulation of tris(S-2,3-diaminopropionato)cobalt(III), *J. Coord. Chem.* **2005**, 58(4), 343–354.
- [76] J. Chapman, N. L. Pickett, G. Kolawole, M. Motevalli, P. O'Brien, *trans*-Bis[2,3-diamino-(R,S)-propionato-N,N']diaquacopper(II) dihydrate, *Acta Crystallogr., Sect. C*, **2000**, 56(11), e501–e502.

Bibliography

- [77] X. Kästele, P. Klüfers, F. Kopp, J. Schuhmacher, M. Vogt, Silicon Chelation in Aqueous and Nonaqueous Media: The Furanoidic Diol Approach, *Chem. Eur. J.* **2005**, *11*(21), [6326–6346](#).
- [78] J. C. Lee, R. R. Gutell, Diversity of Base-pair Conformations and their Occurrence in rRNA Structure and RNA Structural Motifs, *J. Mol. Biol.* **2004**, *344*(5), [1375–1381](#).
- [79] IUPAC-IUB Joint Commission on Biochemical Nomenclature, Nomenclature and Symbolism for Amino Acids and Peptides, *Pure Appl. Chem.* **1984**, *56*(5), [595–624](#).
- [80] U. Krämer, J. D. Cotter-Howells, J. M. Charnock, A. J. M. Baker, J. A. C. Smith, Free histidine as a metal chelator in plants that accumulate nickel, *Nature* **1996**, *379*, [638–638](#).
- [81] P. Deschamps, P. P. Kulkarni, M. Gautam-Basak, B. Sarkar, The saga of copper(II)–L-histidine, *Coord. Chem. Rev.* **2005**, *249*(9–10), [895–909](#).
- [82] T. Sakurai, H. Iwasaki, T. Katano, Y. Nakahashi, Bis(L-histidinato)nickel(II) monohydrate, *Acta Crystallogr., Sect. B*, **1978**, *34*(2), [660–662](#).
- [83] L. Wang, X.-L. Feng, J. Cai, (Diethylenetriamine-*N,N',N''*)(DL-histinato-*N,N',O*)nickel(II) iodide monohydrate, *Acta Crystallogr., Sect. E*, **2002**, *58*(5), [m209–m211](#).
- [84] W. T. Pennington, A. W. Cordes, D. Kyle, E. W. Wilson, Structure of bis(L-histidinato-*O,N,N'*)chromium(III) nitrate, $[\text{Cr}(\text{C}_6\text{H}_8\text{N}_3\text{O}_2)_2]\text{NO}_3$, *Acta Crystallogr., Sect. C*, **1984**, *40*(8), [1322–1324](#).
- [85] R. Herak, B. Prelesnik, B. Kamberi, M. B. Celap, Investigation of the reactions of hexanitrocobaltate(III) with amino acids. XIII. The structure and absolute configuration of $(-)_589\text{-ab}(\text{histidinato-}N,N')\text{-cdf}(\text{histidinato-}O,N,N')\text{-e}$ -nitrocobalt(III) monohydrate, *Acta Crystallogr., Sect. B*, **1981**, *37*(11), [1989–1992](#).
- [86] P.-F. Wu, D.-S. Li, X.-G. Meng, X.-L. Zhong, C. Jiang, Y.-L. Zhu, Y.-G. Wei, Di- μ -oxo-bis[(histidinato- κ^3N,N,O)oxomolybdenum(V)] trihydrate, *Acta Crystallogr., Sect. E*, **2005**, *61*(8), [m1553–m1555](#).
- [87] M. K. Islam, C. Tsuboya, Y. Miyashita, K. Okamoto, K. Kanamori, (L-Histidinato- κ^3N,N,O) (L-histidine- κ^2N,O)oxidovanadium(IV) perchlorate monohydrate, *Acta Crystallogr., Sect. E*, **2007**, *63*(4), [m1052–m1054](#).

Bibliography

- [88] R. Alberto, R. Schibli, R. Waibel, U. Abram, A. P. Schubiger, Basic aqueous chemistry of $[M(OH_2)_3(CO)_3]^+$ (M=Re, Tc) directed towards radiopharmaceutical application, *Coord. Chem. Rev.* **1999**, 190–192, [901–919](#).
- [89] M. T. Averbuch-Pouchot, Crystal structure of L-histidinium phosphite and a reinvestigation of the monoclinic form of L-histidine, *Z. Kristallogr.* **1993**, 207, [111](#).
- [90] S. H. Kim, H. Miyatake, T. Ueno, T. Nagaob, K. Mikia, Development of a novel ampholyte buffer for isoelectric focusing: electric charge-separation of protein samples for X-ray crystallography using free-flow isoelectric focusing, *Acta Crystallogr., Sect. D*, **2005**, 61(6), [799–802](#).
- [91] B. Henry, P. Tekely, J.-J. Delpuech, pH and pK Determinations by High-Resolution Solid-State ^{13}C NMR: Acid-Base and Tautomeric Equilibria of Lyophilized L-Histidine, *J. Am. Chem. Soc.* **2002**, 124(9), [2025–2034](#).
- [92] G. A. Jeffrey, R. K. McMullan, S. Takagi, A neutron diffraction study of the hydrogen bonding in the crystal structures of methyl α -D-mannopyranoside and methyl α -D-glucopyranoside, *Acta Crystallogr., Sect. B*, **1977**, 33(3), [728–737](#).
- [93] E. Breitmaier, W. Voelter, G. Jung, C. Tänzer, Konfigurations-, Konformations- und Substituenteneinflüsse auf die ^{13}C -chemischen Verschiebungen von Glykosiden, *Chem. Ber.* **1971**, 104(4), [1147–1154](#).
- [94] V. J. James, J. D. Stevens, F. H. Moore, Precision X-ray and neutron diffraction studies of methyl β -D-ribose, *Acta Crystallogr., Sect. B*, **1978**, 34(1), [188–193](#).
- [95] IUPAC-IUB Joint Commission on Biochemical Nomenclature, Nomenclature of Carbohydrates, *Pure Appl. Chem.* **1996**, 68(10), [1919–2008](#).
- [96] W. Gulewitsch, S. Amiradžibi, Ueber das Carnosin, eine neue organische Base des Fleischextractes, *Ber. Dt. Chem. Ges.* **1900**, 33(2), [1902–1903](#).
- [97] H. Abe, Role of Histidine-Related Compounds as Intracellular Proton Buffering Constituents in Vertebrate Muscle, *Biochemistry (Moscow)* **2000**, 65(7), [757–765](#).
- [98] M. S. Horning, L. J. Blakemore, P. Q. Trombley, Endogenous mechanisms of neuroprotection: role of zinc, copper, and carnosine, *Brain Res.* **2000**, 852(1), [56–61](#).

Bibliography

- [99] A. A. Boldyrev, Problems and Perspectives in Studying the Biological Role of Carnosine, *Biochemistry (Moscow)* **2000**, 65(7), [751–756](#).
- [100] A. R. Hipkiss, Carnosine and Protein Carbonyl Groups: A Possible Relationship, *Biochemistry (Moscow)* **2000**, 65(7), [771–778](#).
- [101] V. P. Reddy, M. R. Garrett, G. Perry, M. A. Smith, Carnosine: A Versatile Antioxidant and Antiglycating Agent, *Sci. Aging Knowl. Environ.* **2005**, 18, [pe12](#).
- [102] E. J. Baran, Metal Complexes of Carnosine, *Biochemistry (Moscow)* **2000**, 65(7), [789–797](#).
- [103] H. C. Freeman, J. T. Szymanski, Crystallographic Studies of Metal-Peptide Complexes. V. (β -alanyl-L-histidinato)copper(II) Dihydrate, *Acta Crystallogr.* **1967**, 22(3), [406–417](#).
- [104] C. M. Murdoch, M. K. Cooper, T. W. Hambley, W. N. Hunter, H. C. Freeman, Three chromium(III) complexes with dipeptide ligands, *J. Chem. Soc., Chem. Commun.* **1986**, 17, [1329–1331](#).
- [105] K. Okamoto, T. Yasui, H. Kawaguchi, T. Ama, J. Hidaka, Unusual Coordination Mode of Carnosine (β -Alanyl-L-histidine) in a Cobalt(III) Complex, *Chem. Lett.* **1988**, 17(2), [335–338](#).
- [106] C. E. Brown, W. E. Antholine, W. Froncisz, Multiple Forms of the Copper(II)-Carnosine Complex, *J. Chem. Soc., Dalton Trans.* **1980**, 4, [590–596](#).
- [107] H. Itoh, T. Yamane, T. Ashida, M. Kakudo, Carnosine (β -Alanyl-L-histidine), *Acta Crystallogr., Sect. B*, **1977**, 33(9), [2959–2961](#).
- [108] A. Calcagni, P. G. Ciattini, A. D. Stefano, S. Duprè, G. Luisi, F. Pinnen, D. Rossi, A. Spirito, $\Psi(\text{SO}_2\text{NH})$ transition state isosteres of peptides. Synthesis and bioactivity of sulfonamido pseudopeptides related to carnosine, *Il Farmaco* **1999**, 54(10), [673–677](#).
- [109] C. Pearson, A. L. Beauchamp, Binding of Amino-Dialkylated Adenines to Rhenium(III) and Rhenium(IV) Centers, *Inorg. Chem.* **1998**, 37(6), [1242–1248](#).
- [110] F. Zobi, B. Spingler, R. Alberto, Structure, reactivity and solution behaviour of $[\text{Re}(\text{ser})(7\text{-MeG})(\text{CO})_3]$ and $[\text{Re}(\text{ser})(3\text{-pic})(\text{CO})_3]$: nucleoside-mimicking complexes based on the $\text{fac-}[\text{Re}(\text{CO})_3]^+$ moiety, *Dalton Trans.* **2005**, 17, [2859–2865](#).

Bibliography

- [111] W. T. Klooster, J. R. Ruble, B. M. Craven, R. K. McMullan, Structure and thermal vibrations of adenosine from neutron diffraction data at 123 K, *Acta Crystallogr., Sect. B*, **1991**, 47(3), 376–383.
- [112] Y. Lu, G. Deng, F. Miao, Z. Li, Sugar complexation with calcium ion. Crystal structure and FT-IR study of a hydrated calcium chloride complex of Image D-ribose, *Inorg. Biochem.* **2003**, 96(4), 487–492.
- [113] P. Klüfers, F. Kopp, M. Vogt, Monosaccharides as Silicon Chelators: Pentacoordinate Bis(diolato)(phenyl)silicates with the *cis*-Furanose Isomers of Common Pentoses and Hexoses, *Chem. Eur. J.* **2004**, 10(18), 4538–4545.
- [114] P. Klüfers, T. Kunte, Palladium(II) Complexes of the Reducing Sugars D-Arabinose, D-Ribose, *rac*-Mannose, and D-Galactose, *Chem. Eur. J.* **2003**, 9(9), 2013–2018.
- [115] Y. Lu, G. Deng, F. Miao, Z. Li, Metal-ion interactions with sugars. Crystal structures and FT-IR studies of the LaCl₃-ribopyranose and CeCl₃-ribopyranose complexes, *Carbohydr. Res.* **2004**, 339(10), 1689–1696.
- [116] L. Yang, Y. Zhao, Y. Xu, X. Jin, S. Weng, W. Tian, J. Wu, G. Xu, Complexation of trivalent lanthanide cations by D-ribose in the solid state. The crystal structure and FT-IR study of PrCl₃ · α-D-ribopyranose · 5 H₂O, *Carbohydr. Res.* **2001**, 334(2), 91–95.
- [117] Y. Lu, G. Deng, F. Miao, Z. Li, Metal ion interactions with sugars. The crystal structure and FT-IR study of the NdCl₃-ribose complex, *Carbohydr. Res.* **2003**, 338(24), 2913–2919.
- [118] Y. Lu, J. Guo, Metal-ion interactions with carbohydrates. Crystal structure and FT-IR study of the SmCl₃-ribose complex, *Carbohydr. Res.* **2006**, 341(5), 610–615.
- [119] K. N. Drew, J. Zajicek, G. Bondo, B. Bose, A. S. Serianni, ¹³C-labeled aldopentoses: detection and quantitation of cyclic and acyclic forms by heteronuclear 1D and 2D NMR spectroscopy, *Carbohydr. Res.* **1998**, 307(3–4), 199–209.
- [120] Y. Zhu, J. Zajicek, A. S. Serianni, Acyclic Forms of [1-¹³C]Aldohexoses in Aqueous Solution: Quantitation by ¹³C NMR and Deuterium Isotope Effects on Tautomeric Equilibria, *J. Org. Chem.* **2001**, 66(19), 6244–6251.

Bibliography

- [121] F. Longchambon, D. Avenel, A. Neuman, Structure cristalline de l' α -D-mannopyranose, *Acta Crystallogr., Sect. B*, **1976**, 32(6), 1822–1826.
- [122] P. Klüfers, T. Kunte, Polyol-Metall-Komplexe.47 Kristalline D-Mannose-Kupfer(II)-Komplexe aus Fehlingscher Lösung, *Z. Anorg. Allg. Chem.* **2004**, 630(4), 553–557.
- [123] D. C. Craig, N. C. Stephenson, J. D. Stevens, An X-ray crystallographic study of β -D-mannofuranose- $\text{CaCl}_2 \cdot 4\text{H}_2\text{O}$, *Carbohydr. Res.* **1972**, 22(2), 494–495.
- [124] B. Schneider, F. W. Lichtenthaler, G. Steinle, H. Schiweck, Distribution of Furanoid and Pyranoid Tautomers of D-Fructose in Water, Dimethyl Sulfoxide, and Pyridine via ^1H NMR Intensities of Anomeric Hydroxy Groups in $[\text{D}_6]\text{DMSO}$, *Liebigs Ann. Chem.* **1985**, 12, 2443–2453.
- [125] J. A. Kanters, G. Roelofsen, B. P. Alblas, I. Meinders, The crystal and molecular structure of β -D-fructose, with emphasis on anomeric effect and hydrogen-bond interactions, *Acta Crystallogr., Sect. B*, **1977**, 33(3), 665–672.
- [126] A. E. Flood, M. R. Johns, E. T. White, Crystal growth rates and dispersion for D-fructose from aqueous ethanol, *AIChE J.* **2000**, 46(2), 239–246.
- [127] J. Guo, X. Zhang, Metal-ion interactions with sugars. The crystal structure and FTIR study of an SrCl_2 -fructose complex, *Carbohydr. Res.* **2004**, 339(8), 1421–1426.
- [128] W. J. Cook, C. E. Bugg, Effects of calcium interactions on sugar conformation: crystal structure of β -D-fructose-calcium bromide dihydrate, *Acta Crystallogr., Sect. B*, **1976**, 32(2), 656–659.
- [129] Y. Arendt, PhD thesis, NMR-spektroskopische und röntgenkristallographische Untersuchungen von ein- und zweikernigen Palladium(II)-Kohlenhydratkomplexen, LMU München, **2008**.
- [130] P. E. Pfeffer, K. M. Valentine, F. W. Parrish, Deuterium-Induced Differential Isotope Shift ^{13}C NMR. 1. Resonance Reassignments of Mono- and Disaccharides, *J. Am. Chem. Soc.* **1979**, 101(5), 1265–1274.
- [131] R. Weidenhagen, S. Lorenz, Ein neues bakterielles Umwandlungsprodukt der Saccharose, *Angew. Chem.* **1957**, 69(20), 641.

Bibliography

- [132] B. A. R. Lina, D. Jonker, G. Kozianowski, Isomaltulose (Palatinose®): a review of biological and toxicological studies, *Food Chem. Toxicol.* **2002**, *40*(10), 1375–1381.
- [133] F. W. Lichtenthaler, S. Peters, Carbohydrates as green raw materials for the chemical industry, *C. R. Chimie* **2004**, *7*(2), 65–90.
- [134] F. W. Lichtenthaler, S. Rönninger, α -D-Glucopyranosyl-D-fructoses: distribution of furanoid and pyranoid tautomers in water, dimethyl sulphoxide, and pyridine. Studies on ketoses. Part 4, *J. Chem. Soc., Perkin Trans. 2* **1990**, *8*, 1489–1497.
- [135] J. B. Lambert, G. Lu, S. R. Singer, V. M. Kolb, Silicate Complexes of Sugars in Aqueous Solution, *J. Am. Chem. Soc.* **2004**, *126*(31), 9611–9625.
- [136] W. Dreissig, P. Luger, Die Strukturbestimmung der Isomaltulose, $C_{12}H_{22}O_{11} \cdot H_2O$, *Acta Crystallogr., Sect. B*, **1973**, *29*(3), 514–521.
- [137] J. Thompson, S. A. Robrish, A. Pikis, A. Brust, F. W. Lichtenthaler, Phosphorylation and metabolism of sucrose and its five linkage-isomeric α -D-glucosyl-D-fructoses by *Klebsiella pneumoniae*, *Carbohydr. Res.* **2001**, *331*(2), 149–161.
- [138] M. Kohlíccaronková-Koudelková, V. Jedináková-Krcaronízcaronová, Z. Deyl, Study of perrhenate reduction by capillary electrophoresis, *Electrophoresis* **2002**, *23*(2), 245–248.
- [139] P. Grimminger, P. Klüfers, Triethylammonium bis(oxalato)oxido(triphenylphosphane)rhenate(V), *Acta Crystallogr., Sect. E*, **2007**, *63*(12), m3188.
- [140] P. B. Kettler, Y.-D. Chang, J. Zubieta, Synthesis and characterization of oxorhenium(V)-catecholate complexes. Crystal and molecular structures of $(CH_3)_4N[ReO(O_2C_6H_4)_2]$ and $(CH_3)_4N[ReO(PPh_3)(O_2C_6H_4)_2] \cdot CH_3OH$, *Inorg. Chim. Acta* **1994**, *218*(1–2), 157–165.
- [141] J. R. Dilworth, S. K. Ibrahim, S. R. Khan, M. B. Hursthouse, A. A. Kauraulov, The synthesis, characterization and redox properties of oxo-complexes of rhenium(V) and (VII) with catechol ligands. The x-ray crystal structure of $[ReO_2(O_2C_6H_4)_2]^-$, *Polyhedron* **1990**, *9*(10), 1323–1329.
- [142] R. Chiozzzone, A. Cuevas, R. Gonzalez, C. Kremer, D. Armentano, G. de Munno, J. Faus, Ligand substitution reactions of the $[ReX_6]^{2-}$ (X = Cl, Br) anions. Syn-

Bibliography

- thesis and crystal structure of novel oxalato complexes of rhenium(IV), *Inorg. Chim. Acta* **2006**, 359(7), 2194–2200.
- [143] J. Y. K. Cheng, K.-K. Cheung, M. C. W. Chan, K. Y. Wong, C. M. Che, Rhenium(VII) and -(V) imido and oxo complexes containing 1,4,7-triazacyclononane; synthesis, electrochemistry and crystal structures, *Inorg. Chim. Acta* **1998**, 272(1–2), 176–187.
- [144] M. Porchia, F. Tisato, F. Refosco, C. Bolzati, M. Cavazza-Ceccato, G. Bandoli, A. Dolmella, New Approach to the Chemistry of Technetium(V) and Rhenium(V) Phenylimido Complexes: Novel $[M(\text{NPh})\text{PNP}]^{3+}$ Metal Fragments (M = Tc, Re; PNP = Aminodiphosphine) Suitable for the Synthesis of Stable Mixed-Ligand Compounds, *Inorg. Chem.* **2005**, 44(13), 4766–4776.
- [145] C. F. Edwards, W. P. Griffith, A. J. P. White, D. J. Williams, New catecholato oxorhenium(V) complexes, *J. Chem. Soc., Dalton Trans.* **1992**, 6, 957–962.
- [146] G. F. Ciani, G. D'Alfonso, P. Romiti, A. Sironi, M. Freni, Rhenium(V) Oxide Complexes. Crystal and Molecular Structures of the Compounds *trans*- $\text{ReI}_2\text{O}(\text{OR})(\text{PPh}_3)_2$ (R = Et, Me) and of their Hydrolysis Derivative $\text{ReIO}_2(\text{PPh}_3)_2$, *Inorg. Chim. Acta* **1983**, 72, 29–37.
- [147] N. Marti, B. Spingler, F. Breher, R. Schibli, Comparative Studies of Substitution Reactions of Rhenium(I) Dicarbonyl-Nitrosyl and Tricarbonyl Complexes in Aqueous Media, *Inorg. Chem.* **2005**, 44(17), 6082–6091.
- [148] J. M. McGuire, R. L. Bunch, R. C. Anderson, H. E. Boaz, E. H. Flynn, H. M. Powell, J. W. Smith, Ilotycin: a new antibiotic, *Schweiz. Med. Wochensch.* **1952**, 82(41), 1064–1065.
- [149] I. Kanfer, M. F. Skinner, R. B. Walker, Analysis of macrolide antibiotics, *J. Chromatogr. A* **1998**, 812(1–2), 255–286.
- [150] J. Hansen, J. Ippolito, N. Ban, P. Nissen, P. Moore, T. Steitz, The Structures of Four Macrolide Antibiotics Bound to the Large Ribosomal Subunit, *Molecular Cell* **2002**, 10(1), 117–128.
- [151] D. N. Wilson, J. M. Harms, K. H. Nierhaus, F. Schlünzen, P. Fucini, Species-specific antibiotic-ribosome interactions: implications for drug development, *Biol. Chem.* **2005**, 386(12), 1239–1252.

Bibliography

- [152] F. Schlünzen, R. Zarivach, J. Harms, A. Bashan, A. Tocilj, R. Albrecht, A. Yonath, F. Franceschi, Structural basis for the interaction of antibiotics with the peptidyl transferase centre in eubacteria, *Nature* **2001**, *413*, 814–821.
- [153] W. E. Steinmetz, B. L. Shapiro, J. J. Roberts, The Structure of Erythromycin Enol Ether as a Model for Its Activity as a Motilide, *J. Med. Chem.* **2002**, *45*(22), 4899–4902.
- [154] S. A. Terespolsky, I. Kanfer, Stability of erythromycin and some of its esters in methanol and acetonitrile, *Int. J. Pharm.* **1995**, *115*(1), 123–128.
- [155] H. Muranaka, M. Suga, K. Sato, K. Nakagawa, T. Akaike, T. Okamoto, H. Maeda, M. Ando, Superoxide Scavenging Activity of Erythromycin-Iron Complex, *Biochem. Biophys. Res. Commun.* **1997**, *232*(1), 183–187.
- [156] J. D. Oliver, L. C. Strickland, Structure of a Dihydrated, Di-tert-butyl Alcohol Solvated Zinc Acetate Complex with Erythromycin A at 188 K, *Acta Crystallogr., Sect. C*, **1986**, *42*(8), 952–956.
- [157] T. Cachet, G. van den Mooter, R. Hauchecorne, C. Vinckier, J. Hoogmartens, Decomposition kinetics of erythromycin A in acidic aqueous solutions, *Int. J. Pharm.* **1989**, *55*(1), 59–65.
- [158] A. Hassanzadeh, J. Barber, G. A. Morris, P. A. Gorry, Mechanism for the Degradation of Erythromycin A and Erythromycin A 2'-Ethyl Succinate in Acidic Aqueous Solution, *J. Phys. Chem. A* **2007**, *111*(40), 10098–10104.
- [159] Y. H. Kim, T. M. Heinze, R. Beger, J. V. Pothuluri, C. E. Cerniglia, A kinetic study on the degradation of erythromycin A in aqueous solution, *Int. J. Pharm.* **2004**, *271*(1–2), 63–76.
- [160] H. K. Chepkwony, P. Dehouck, E. Roets, J. Hoogmartens, Isocratic Separation of Erythromycin, Related Substances and Degradation Products by Liquid Chromatography on XTerra RPx8, *Chromatographia* **2001**, *53*(3–4), 159–165.
- [161] J. Paesen, K. Khan, E. Roets, J. Hoogmartens, Study of the stability of erythromycin in neutral and alkaline solutions by liquid chromatography on poly(styrene-divinylbenzene), *Int. J. Pharm.* **1995**, *113*(2), 215–222.
- [162] A. Hempel, M. Bogucka-Ledóchowska, Z. Dauter, E. Borowski, Z. Kosturkiewicz, Crystal and molecular structure of anhydroerythromycin A cyclic carbonate *N*-methyl iodide, *J. Chem. Cryst.* **1975**, *5*(6), 387–401.

Bibliography

- [163] N. N. Greenwood, A. Earnshaw, *Chemie der Elemente*, Wiley-VCH, **1990**.
- [164] CSD, Cambridge Structural Database, Version 5.29, **2008**.
- [165] G. A. Stephenson, J. G. Stowell, P. H. Toma, R. R. Pfeiffer, S. R. Byrn, Solid-state investigations of erythromycin a dihydrate: Structure, NMR spectroscopy, and hygroscopicity, *J. Pharm. Sci.* **1997**, *86*(11), [1239–1244](#).
- [166] A. Hassanzadeh, M. Helliwell, J. Barber, Determination of the stereochemistry of anhydroerythromycin A, the principal degradation product of the antibiotic erythromycin A, *Org. Biomol. Chem.* **2006**, *4*(6), [1014–1019](#).
- [167] R. Chiozzone, R. Gonzalez, C. Kremer, G. de Munno, D. Armentano, J. Cano, F. Lloret, M. Julve, J. Faus, Heterobimetallic Oxalato-Bridged $\text{Cu}^{\text{II}}\text{Re}^{\text{IV}}$ Complexes. Synthesis, Crystal Structure and Magnetic Properties, *Inorg. Chem.* **2001**, *40*(17), [4242–4249](#).
- [168] G. Kramer, PhD thesis, Deprotonierte Zuckersäuren als Liganden in Kohlenhydrat-Metall-Komplexen, LMU München, **2003**.
- [169] M. Korth, MSc thesis, Rhenium(V)-Komplexe mit Glycylhistidin, LMU München, **2007**.
- [170] A. M. Kirillov, M. Haukka, A. J. L. Pombeiro, Synthesis, characterization and molecular structures of the trichloro- η^1 -benzoyldiazenido $[\text{ReCl}_3\{\eta^1\text{-NNC}(\text{O})\text{Ph}\}(\text{PPh}_3)_2]$ and oxorhenium $[\text{ReOCl}_2(\text{OMe})(\text{PPh}_3)_2]$ complexes derived from reactions of $[\text{ReCl}_2\{\eta^2\text{-NNC}(\text{O})\text{Ph}\}(\text{PPh}_3)_2]$ with a peroxide or dioxygen, *Inorg. Chim. Acta* **2006**, *359*(13), [4421–4426](#).
- [171] R. Graziani, U. Casellato, R. Rossi, A. Marchi, Structure of *trans*-dichlorooxobis-(triphenylphosphine)rhenium(V), $\text{ReCl}_2\text{O}(\text{OEt})(\text{Ph}_3\text{P})_2$, *J. Crystallogr. Spectrosc. Res.* **1985**, *15*(6), [573–579](#).
- [172] J. Chatt, G. A. Rowe, Complex compounds of tertiary phosphines and a tertiary arsine with rhenium(V), rhenium(III), and rhenium(II), *J. Chem. Soc.* **1962**, [4019–4033](#).
- [173] T. I. A. Gerber, P. Mayer, Z. R. Tshentu, Synthesis and structure of bis(triphenylphosphino)dichlorohydroxooxorhenium(V), *J. Coord. Chem.* **2007**, *60*(6), [641–645](#).

Bibliography

- [174] D. E. Grove, G. Wilkinson, Oxo-complexes of rhenium(V), *J. Chem. Soc. A* **1966**, 1224–1230.
- [175] J. C. Bryan, R. E. Stenkamp, T. H. Tulip, J. M. Mayer, Oxygen atom transfer among rhenium, sulfur, and phosphorus. Characterization and reactivity of $\text{Re}(\text{O})\text{Cl}_3(\text{Me}_2\text{S})(\text{OPPh}_3)$ and $\text{Re}(\text{O})\text{Cl}_3(\text{CNCMe}_3)_2$, *Inorg. Chem.* **1987**, 26(14), 2283–2288.
- [176] F. E. Kühn, W. A. Herrmann, Rhenium-Oxo and Rhenium-Peroxo Complexes in Catalytic Oxidations, *Structure and Bonding* **2000**, 97, 213–236.
- [177] M. M. Abu-Omar, S. I. Khan, Molecular Rhenium(V) Oxotransferases: Oxidation of Thiols to Disulfides with Sulfoxides. The Case of Substrate-Inhibited Catalysis, *Inorg. Chem.* **1998**, 37(19), 4979–4985.
- [178] J. B. Arterburn, M. C. Perry, Selective Rhenium-Catalyzed Oxidation of Secondary Alcohols with Methyl Sulfoxide in the Presence of Ethylene Glycol, a Convenient One-Pot Synthesis of Ketal, *Org. Lett.* **1999**, 1(5), 769–771.
- [179] J. B. Arterburn, M. Liu, M. C. Perry, Polystyrene-Supported (Catecholato)oxorhenium Complexes: Catalysts for Alcohol Oxidation with DMSO and for Deoxygenation of Epoxides to Alkenes with Triphenylphosphine, *Helv. Chim. Acta* **2002**, 85(10), 3225–3236.
- [180] J. J. Kennedy-Smith, K. A. Nolin, H. P. Gunterman, F. D. Toste, Reversing the Role of the Metal-Oxygen π -Bond. Chemoselective Catalytic Reductions with a Rhenium(V)-Dioxo Complex, *J. Am. Chem. Soc.* **2003**, 125(14), 4056–4057.
- [181] B. Royo, C. C. Romão, Reduction of carbonyl groups by high-valent rhenium oxides, *J. Mol. Catal. A: Chem.* **2005**, 236(1–2), 107–112.
- [182] K. A. Nolin, R. W. Ahn, F. D. Toste, Enantioselective Reduction of Imines Catalyzed by a Rhenium(V)-Oxo Complex, *J. Am. Chem. Soc.* **2005**, 127(36), 12462–12463.
- [183] J. J. Kennedy-Smith, L. A. Young, F. D. Toste, Rhenium-Catalyzed Aromatic Propargylation, *Org. Lett.* **2004**, 6(8), 1325–1327.
- [184] A. M. Santos, F. M. Pedro, A. A. Yogalekar, I. S. Lucas, C. C. Romão, F. E. Kühn, Oxorhenium Complexes as Aldehyde-Olefination Catalysts, *Chem. Eur. J.* **2004**, 10(24), 6313–6321.

Bibliography

- [185] B. E. Ledford, E. M. Carreira, Synthesis of unsaturated esters from aldehydes: An inexpensive, practical alternative to the Horner-Emmons reaction under neutral conditions, *Tetrahedron Lett.* **1997**, 38(47), [8125–8128](#).
- [186] B. D. Sherry, R. N. Loy, F. D. Toste, Rhenium(V)-Catalyzed Synthesis of 2-Deoxy- α -glycosides, *J. Am. Chem. Soc.* **2004**, 126(14), [4510–4511](#).
- [187] T. Fietz, H. Spies, H.-J. Pietzsch, P. Leibnitz, Synthesis and molecular structure of chloro(3-thiapentane-1,5-dithiolato)oxorhenium(V), *Inorg. Chim. Acta* **1995**, 231(1–2), [233–236](#).
- [188] B. Tremaggi, graduate thesis, Hydroxycarboxylato- und Polyolato-Rhenium(V)-Komplexe mit L-Histidin als Hilfsligand, LMU München, **2008**.
- [189] A. Filser, graduate thesis, Polyolato- und Hydroxycarboxylato-Komplexe am Oxidorhenium(V)-Carnosin-Fragment, LMU München, **2008**.
- [190] V. Mazzoni, P. Bradesi, F. Tomi, J. Casanova, Direct Qualitative and Quantitative Analysis of Carbohydrate Mixtures Using ^{13}C NMR Spectroscopy: Application to Honey, *Magn. Reson. Chem.* **1997**, 35(13), [S81–S90](#).
- [191] M. S. Papadopoulos, I. C. Pirmettis, M. Pelecanou, C. P. Raptopoulou, A. Terzis, C. I. Stassinopoulou, E. Chiotellis, Syn-Anti Isomerism in a Mixed-Ligand Oxorhenium Complex, $\text{ReO}[\text{SN}(\text{R})\text{S}][\text{S}]$, *Inorg. Chem.* **1996**, 35(25), [7377–7383](#).
- [192] M. Pelecanou, K. Chryssou, C. I. Stassinopoulou, Trends in NMR chemical shifts and ligand mobility of $\text{TcO}(\text{V})$ and $\text{ReO}(\text{V})$ complexes with aminothiols, *J. Inorg. Biochem.* **2000**, 79(1–4), [347–351](#).
- [193] M. Kaupp, V. G. Malkin, O. L. Malkina, D. R. Salahub, Calculation of ligand NMR chemical shifts in transition-metal complexes using ab initio effective-core potentials and density functional theory, *Chem. Phys. Lett.* **1995**, 235(3–4), [382–388](#).
- [194] C. Kremer, M. Rivero, E. Kremer, L. Suescun, A. W. Mombrú, R. Mariezcurrena, S. Domínguez, A. Mederos, S. Midollini, A. Castiñeiras, Synthesis, characterization and crystal structures of rhenium(V) complexes with diphosphines, *Inorg. Chim. Acta* **1999**, 294(1–2), [47–55](#).
- [195] S. Bolaño, J. Bravo, R. Carballo, E. Freijanes, S. García-Fontán, P. Rodríguez-Seoane, Oxorhenium(V) complexes with bis-phosphinite chelating coligands, *Polyhedron* **2003**, 22(13), [1711–1717](#).

Bibliography

- [196] J. M. Mayer, Metal-oxygen multiple bond lengths: a statistical study, *Inorg. Chem.* **1988**, 27(22), [3899–3903](#).
- [197] P. Pyykkö, S. Riedel, M. Patzschke, Triple-Bond Covalent Radii, *Chem. Eur. J.* **2005**, 11(12), [3511–3520](#).
- [198] A. Neuhaus, A. Veldkamp, G. Frenking, Oxo and Nitrido Complexes of Molybdenum, Tungsten, Rhenium, and Osmium. A Theoretical Study, *Inorg. Chem.* **1994**, 33(23), [5278–5286](#).
- [199] F. A. Cotton, S. J. Lippard, Chemical and Structural Studies of Rhenium(V) Oxyhalide Complexes, *Inorg. Chem.* **1966**, 5(3), [416–423](#).
- [200] R. J. Doedens, J. A. Ibers, Studies of Metal-Nitrogen Multiple Bonds, *Inorg. Chem.* **1967**, 6(2), [204–210](#).
- [201] A. Chiotellis, C. Tsoukalas, M. Pelecanou, A. Papadopoulos, C. Raptopoulou, A. Terzis, I. Pirmettis, M. Papadopoulos, E. Chiotellis, Synthesis and Characterization of novel “3 + 2” oxorhenium complexes, $\text{ReO}[\text{SNO}][\text{NN}]$, *Inorg. Chem.* **2006**, 45(14), [5635–5640](#).
- [202] D. Papagiannopoulou, I. Pirmettis, M. Pelecanou, D. Komiotis, M. Sagnou, D. Benaki, C. P. Raptopoulou, A. Terzis, M. S. Papadopoulos, Synthesis and structural characterization of neutral “3 + 2” oxorhenium and oxotechnetium complexes of the 2-mercaptoethyl-*N*-glycine (SNO)/2,2'-bipyridine (NN) mixed ligand system, *Inorg. Chim. Acta* **2007**, 360(11), [3597–3602](#).
- [203] L. Wei, J. Babich, J. Zubieta, Complexes of the $\text{Re}^{\text{V}}\text{OX}_2^+$ (X = Cl, Br) core with single amino acid chelate derivatives, *Inorg. Chim. Acta* **2005**, 358(7), [2413–2421](#).
- [204] B. J. Coe, S. J. Glenwigh, Trans-effects in octahedral transition metal complexes, *Coord. Chem. Rev.* **2000**, 203(1), [5–80](#).
- [205] M. F. Cerdá, E. Méndez, L. Malacrida, C. F. Zinola, C. Melián, M. E. Martins, A. M. C. Luna, C. Kremer, Redox Behavior of Re(V)-Amino Acid Containing Complexes, *J. Colloid and Interface Sci.* **2002**, 249(2), [366–371](#).
- [206] Jeol USA Inc., Delta NMR Processing and Control Software v. 4.3.4, **1990–2005**.
- [207] A. Altomare, M. C. Burla, M. Camalli, G. L. Cascarano, C. Giacovazzo, A. Guagliardi, A. G. G. Moliterni, G. Polidori, R. Spagna, *SIR97*: a new tool

Bibliography

- for crystal structure determination and refinement, *J. Appl. Cryst.* **1999**, 32(1), 115–119.
- [208] G. M. Sheldrick, A short history of *SHELX*, *Acta Crystallogr., Sect. A*, **2008**, 64(1), 112–122.
- [209] A. L. Spek, *PLATON*, A Multipurpose Crystallographic Tool, **1999**.
- [210] C. F. Macrae, P. Edgington, P. McCabe, E. Pidcock, G. P. Shields, R. Taylor, M. Towler, J. van de Streek, Mercury: visualization and analysis of crystal structures, *J. Appl. Cryst.* **2006**, 39(3), 453–457.
- [211] L. J. Farrugia, *ORTEP-3* for Windows—a version of *ORTEP-III* with a Graphical User Interface (GUI), *J. Appl. Cryst.* **1997**, 30(5), 565.
- [212] E. Keller, Some Computer Drawings of Molecular and Solid-State Structures, *J. Appl. Cryst.* **1989**, 22(1), 19–22.
- [213] F. H. Otey, C. I. Mehlretter, A Simple Preparation of 1,4-Anhydroerythritol, *J. Org. Chem.* **1961**, 26(5), 1673.
- [214] K. G. Childers, S. D. Dreher, J. Lee, J. M. Williams, A Practical and Scaleable Preparation of 1,4-Anhydroerythritol, *Org. Process Res. Dev.* **2006**, 10(5), 934–936.

Danksagung

Herrn Prof. Dr. Peter Klüfers danke ich für die interessante und anwendungsbezogene Themenstellung, die ausgezeichneten Arbeitsbedingungen und den gewährten wissenschaftlichen Freiraum.

Frau Lida Holowatyj-den Toom danke ich für ihre Hilfe bei allen organisatorischen Dingen, ihre herzliche, offene Art und besonders für das Korrekturlesen dieser Arbeit!

Frau Christine Neumann danke ich für die Hilfe im Laboralltag, von der Ausstattung bis hin zur Messung von zahlreichen NMR Spektren.

Herrn Xaver Kästele danke ich für die wichtigen Hinweise zur Laborsicherheit, der Hilfe bei nicht funktionierenden Geräten und bei der Einhaltung von Sicherheitsvorschriften.

Ich danke Sandra Albrecht für Chemikalienbestellungen, die Messung von Kristallen und die energische Einforderung von Auftragszetteln (½ Wo is da Zeddl?).

Großer Dank gilt auch Peter Mayer, Christine Neumann, Prof. Dr. K. Karaghiosoff und allen Mitarbeitern der Analytik für die vielen Messungen und auch allen Mitarbeitern der Röntgenabteilung für die Mühe beim Aufsetzen der Kristalle.

Ich danke allen Mitarbeitern des AK-Klüfers für die angenehme Atmosphäre und eine schöne Zeit: Sandra Albrecht, Thorsten Allscher, Richard Betz, Dr. Hans-Christian Böttcher, Natascha Ghaschghaie, Helene Giglmeier, Kathrin Gilg, David Heß, Sarah Illi, Xaver Kästele, Tobias Kerscher, Phillipp Lorenz, Dr. Peter Mayer, Tobias Mayer, Christine Neumann, Maximilian Pfister, Moritz Reichvilser, Felix Roefßner, Johanna Schulten, Thomas Schwarz, Martin Steinborn, Xaver Wurzenberger, Anna Zangl und allen Ehemaligen, die ich noch kennenlernen konnte.

Ich danke meinen F-Praktikanten und Bachelorstudenten Tatas H. P. Brotosudarmo,

Silvia Zimdars, Klaus Engelke, Angela Wochnik und Stephanie Neumair für ihr Interesse und ihre wertvolle Mitarbeit.

Herrn Dr. F. J. Gildehaus danke ich für den fachlichen Austausch mit der nuklearmedizinischen Abteilung des Klinikums Großhadern, welcher diese Arbeit noch interessanter gemacht hat. An dieser Stelle bedanke ich mich auch bei Milan Coporda für die Hilfe bei den Markierungsexperimenten.

Nochmal herzlichen Danke an die Korrekturleser: Lida, Kathrin, Anna, Richard.

Ein besonderes Dankeschön geht an meine Familie sowie an meine Beatrice und ihre Familie für die bedingungslose Unterstützung, die Geduld, die Aufmunterung und das Vertrauen. Ohne Euch wäre das alles nicht möglich gewesen!

Lebenslauf

Name	Philipp Grimminger
Geburtsdatum	1. 6. 1975
Geburtsort	München
Staatsangehörigkeit	deutsch
Familienstand	ledig

Schulbildung

09.1986–07.1996	Maristenkolleg Mindelheim LK: Mathematik, Physik Abschluss: Allgemeine Hochschulreife
-----------------	---

Zivildienst

07.1996–07.1997	DJH Schönberg/Ostsee
-----------------	----------------------

Hochschulausbildung

10.1997–04.2000	TU München Grundstudium im Fach Chemie
04.2000–05.2003	LMU München Hauptstudium im Fach Chemie Nebenfach: Informatik
07.2003–01.2004	Diplomarbeit unter Anleitung von Prof. Dr. P. Klüfers Abschluss: Diplom-Chemiker
seit 04.2004	Anfertigung der vorliegenden Dissertation unter Anleitung von Prof. Dr. P. Klüfers

berufliche Erfahrungen

07.2003–01.2004	Studentische Hilfskraft am Department Chemie und Biochemie der LMU München
seit 04.2004	Wissenschaftlicher Angestellter am Department Chemie und Biochemie der LMU München